THERMOCHEMICAL CONVERSION AND UPGRADING OF WHEAT STRAW BIOMASS INTO SOLID FUEL

A Thesis submitted by

Bidhan Chandra Nath
BSc., MSc.

For the award of

Doctor of Philosophy

2023

ABSTRACT

Herbaceous biomass is a typical agricultural waste produced from leftover crops. Biomass straw has limited uses due to its unfavourable physical characteristics, including bulkiness, varying sizes, varied compositions, and low energy content, but its availability is abundant. This study investigated the wheat straw's (WS) potential fuel properties and the methods to improve their qualities. Different additives (sawdust: SD, biochar: BioC and bentonite clay: BC) were used to identify optimal pelleting composition. A small-scale pellet mill was used for WS pellet development, and five types of combinations were first investigated (T_1: 100% WS, T_2: 90% WS + 10% SD, T_3: 90% WS + 10% BC, T_4: 90% WS + 10% BioC, and T_5: 70% WS + 10% BC + 10% BioC + 10% SD).

To compare and improve pellet quality, seven types of pellets (T_1, T_5 plus T_6, T_7, T_8, T_9, and T_{10}) were further considered and analysed with different combinations of additive materials (now including starch and crude glycerol also). Most of these treatments could improve the pellet durability to ≥ 92%, bulk density to ≥ 600 kg/m^3 and heating value to ≥18.5 MJ/kg, which meets the pellet ISO 17225-8 standard specification requirements, where the inorganic ash content was all higher than the ISO standard level.

The WS pellet pyrolysis process was studied in a laboratory-scale kiln. The maximum pyrolysis temperature of 600°C was obtained at 60 min for slow pyrolysis. The pyrolysis results demonstrated that additive mixing was particularly useful for pellet (T_5) making, resulting in an increased conversion rate, achieving a gas yield of 43.52%, thermal conversion efficiency of 75.67% and syngas production of 46%.

The thermokinetic behaviour of WS pellets (T_1 and T_5) for both combustion and pyrolysis was determined by thermogravimetric analysis (TGA). The additives, especially biochar added with WS (T_5), considerably changed the thermokinetic behaviour of the pellets compared to pellets without additives (T_1). Both pellets followed a multistage reaction and the equilibrium chemical reaction behaviour, but the T_5 pellet reaction results (*Eα and lnA*) were significantly higher in pyrolysis and combustion cases.

A CFD model was developed using the ANSYS Fluent 2021R2 for gasification simulation. The study was also performed at a steady state regime considering the non-premixed combustion and species transport models. At the same time, biomass and air flow rates were initially set as 9.0 kg/h and 37.78 Nm^3/h, respectively. The model could predict the gasifier's temperature and the composition of the produced gas. With an equivalence ratio (ER) of 0.35 during gasification, the proportions of CO, CO_2, H_2, and CH_4 gas produced were 19.8%, 11.6%, 14.2%, and 0.2% v/v, respectively.

Furthermore, the techno-economic analysis indicated that the cost of pellet production ranged from \$232 to \$360 per tonne. Compared with the current market price, the profit from pellet production was about 42%. Drying a one-tonne wheat crop (moisture removed from 20 to 12%) would require 20 kg of pellets.

Overall, it was concluded that upgrading the WS biomass into pellets and conversion into energy could provide an efficient alternative fuel source. Additional research is needed to explore alternative additives for reducing ash reduction. Furthermore, modifications are required for the developed CFD model to examine ash and tar production and its validation against data obtained from large-scale gasification.

CERTIFICATION OF THESIS

I, Bidhan Chandra Nath, declare that the PhD Thesis entitled *Thermochemical conversion and upgrading of wheat straw biomass into solid fuel* is not more than 100,000 words in length including quotes and exclusive of tables, figures, appendices, bibliography, references and footnotes. The thesis contains no material that has been submitted previously, in whole or in part, for the award of any other academic degree or diploma. Except where otherwise indicated, this thesis is my own work.

Date: 22 April 2023

Endorsed by:

Associate Professor Guangnan Chen
Principal Supervisor

Dr Les Bowtell
Associate Supervisor

Student and supervisors' signatures of endorsement are held at the University.

ACKNOWLEDGEMENTS

DEDICATION

To My Parents

STATEMENT OF CONTRIBUTION

Published paper

Nath, B, Chen, G, Bowtell, L & Mahmood, RA 2022, 'Assessment of Densified Fuel Quality Parameters: A Case Study for Wheat Straw Pellet', *Journal of Bioresources and Bioproducts*. Volume 8, Issue 1, February 2023, Pages 45-58, https://doi.org/10.1016/j.jobab.2022.10.001

https://www.sciencedirect.com/science/article/pii/S236996982 2000585?via%3Dihub

- *Candidate contributed 70%: developed the concept, conducted all lab experiments, analysed the data, and wrote the manuscript.*
- *Co-Author 1 contributed 15%: assisted with the concept and lab experiments and revised the manuscript.*
- *Co-Author 2 contributed 10%: assisted with the concept and lab experiments and revised the manuscript.*
- *Co-Author 3 contributed 5%: revised the manuscript.*

Unpublished papers

(Paper drafted and ready to submit)

1. Nath, B, Chen, G, Bowtell, L & Graham, E 2023, "Kinetic mechanism of wheat straw pellets combustion process with a thermogravimetric analyser".

   - *Candidate contributed 70%: developed the concept, conducted all lab experiments, analysed the data and wrote the manuscript.*
   - *Co-Author 1 contributed 15%: assisted with the concept and lab experiments and revised the manuscript.*
   - *Co-Author 2 contributed 10%: assisted with the concept and lab experiments and revised the manuscript.*
   - *Co-Author 3 contributed 5%: analysed the data.*

2. Nath, B, Chen, G, & Bowtell, L 2023, "Upgrading of physical and elemental quality of wheat straw pellets the effect of additive blends".

   - *Candidate contributed 75%: developed the concept, conducted all lab experiments, analysed the data and wrote the manuscript.*
   - *Co-Author 1 contributed 15%: assisted with the concept and lab experiments and revised the manuscript.*
   - *Co-Author 2 contributed 10%: assisted with the concept and lab experiments and revised the manuscript.*

3.   Nath, B, Chen, G, & Bowtell, L 2023, "Pyrolysis of wheat straw pellets in a laboratory scale fixed bed reactor: Effect of temperature and residence time on pyrolysis product".

- *Candidate contributed 75%: developed the concept, conducted all lab experiments, analysed the data and wrote the manuscript.*
- *Co-Author 1 contributed 15%: assisted with the concept and lab experiments and revised the manuscript.*
- *Co-Author 2 contributed 10%: assisted with the concept and lab experiments and revised the manuscript.*

4.   Nath, B, Chen, G, Bowtell, L & Mahmood, RA 2023, "CFD model of wheat straw pellet gasification in 10 KW downdraft gasifier".

- *Candidate contributed 70%: developed the concept, conducted all lab experiments, analysed the data, and wrote the manuscript.*
- *Co-Author 1 contributed 10%: assisted with the concept and lab experiments and revised the manuscript.*
- *Co-Author 2 contributed 10%: assisted with the concept and lab experiments and revised the manuscript.*
- *Co-Author 3 contributed 10%: reviewed the modelling data and revised the manuscript.*

TABLE OF CONTENTS

LIST OF TABLES

List OF FIGURES

ABBREVIATIONS

2D	Two Dimensional
ADF	Acid Detergent Fibre
ANN	Artificial Neural Networks
ar	As Received
ASTM	American Society for Testing and Materials
BC	Bentonite Clay
BD	Bulk Density
BioC	Biochar
CFD	Computational Fluid Dynamics
CG	Crude Glycerol
C:N	Carbon-to-Nitrogen Ratio
db	Dry Basis
DPM	Discrete Phase Model
DTG	Derivative Thermal Analysis
Du	Durability
EBC	European Biochar Certificate
ER	Equivalence Ratio
ENplus	European Pellet Council
FC	Fixed Carbon
FDM	Finite Difference Method
FEM	Finite Element Method
FVM	Finite Volume Method
GC	Gas-Chromatograph
GCV	Gross Calorific Value
GHGs	Greenhouse Gasses Emissions
HHV	Higher Heating Value
ICTAC	International Confederation for Thermal Analysis and Calorimetry
ISO	International Standard Organisation
LHV	Lower Heating Value
M	Mass
MC	Moisture Content
NDF	Neutral Detergent Fibre
S	Corn Starch
SD	Sawdust
SEM	Scanning Electron Microscope
TA	Thermal Analysis
TCD	Thermal Conductivity Detector
TGA	Thermogravimetric Analyser
TG	Thermogravimetric
TOC	Total Organic Carbon
TS	Tensile Strength
V	Volume
VM	Volatile Matters
wb	Wet Basis
WG	Weight Gain
WI	Wettability Index
WL	Weight Loss
WS	Wheat Straw
WSP	Wheat Straw Pellet
UDF	User Defined Function

LIST OF SYMBOLS

Symbol	Unit	Designation
i	-	i^{th} species
j	-	Number of specific reaction steps
α	%	Degree of conversion
E_α	kJ/mol	Activation of energy
a	-	Absorption coefficient
β	°C/min	Heating rate
D_E	m	Particle diameter
h	m^2.kg/s	Planck constant ($6.626*10^{-34}$)
m	kg	Mass
M	kg/kmol	Molar mass
n	-	Number of moles
P	bar	Pressure
Q	W/m^3	Heat source
R	-	Gas constant
S	kJ/kmol.K	Molar entropy
t	s	Time
T	K or °C	Temperature
H	kJ/kmol	Molar enthalpy change
e	%	Efficiency
f	-	Porosity
A/lnA	1/s	Pre-exponential factor
K	-	Reaction rate constant
k_{cat}	-	Catalytic rate constant
K_β	m^2.kg/s^2.k	Boltzman constant ($1.38 *10^{-23}$)
n	-	Reaction order
σ_s	5.669×10^{-8} W/m^2.K^4	Stefan-Boltzmann constant
ΔG	kJ/mol	Gibbs free energy
ΔH	kJ/mol	Enthalpy/latent heat enthalpy
ΔS	kJ/mol.K	Entropy
T	K	Absolute temperature
T_i	K/°C	Ignition temperature
T_b	K/°C	Burnout temperature
T_m	K/°C	The maximum temperature at which maximum decomposition occurred

CHAPTER 1: INTRODUCTION

1.1. Background

Agricultural production frequently produces a significant amount of biomass as waste, residue and byproducts (De Corato et al. 2018). Typical biomass residues from farm fields include straw, grasses, crop stubble, tree fruits and trash (Nhuchhen, Basu & Acharya 2014). These wastes and residues can be classified as either woody or nonwoody biomass (Widjaya et al. 2018). Herbaceous straw is one kind of nonwoody biomass obtained from plants with no woody stems that wither when the growing season ends (Picchio et al. 2020). Straw biomass is typically abundant, globally accessible and readily available (Zeng, Ma & Ma 2007). Various agricultural cereal crop parts (barley, wheat, oat, rice, corn, sorghum, millet, canola, etc.) are the most common sources of this straw biomass (Wang, L. et al. 2020).

Wheat is the dominant crop of the Australian grain industry. In 2021/22, the average wheat yield in Australia was 2.6 tonnes/ha (1.14 tonnes/ha over the last 15 years), producing 36.3 million tonnes of wheat grain(https://www.statista.com/statistics/631611/australia-wheat-yield/). These crops are estimated to have generated around 45 million tonnes of wheat residue as crop waste (grain and straw ratio = 1:1.3). Only two million tonnes of wheat straw (WS) have currently been used to produce cardboard, fuel, and cow fodder. The remaining quantity was left in the field.

Straw is commonly used or value added as animal bedding, garden mulch, cattle forage, heating fuel, for ethanol production and also building construction materials (Ren, Yu & Xu 2019). However, field crop straw management remains challenging in many countries, including Australia. For example, windrow burning (crop straw burning) is one tool commonly implemented for weed seed destruction/control (Walsh & Newman 2007). In Australia, straw is widely incorporated into the soil (Kingwell & Abadi 2014). This increases soil fertility and soil organic carbon for subsequent crop cultivation (Hanafi et al. 2012). However, straw is fibrous, so decomposition in the soil is often problematic and can cause considerable problems for land preparation and seed germination (Wang, L. et al. 2020). Another common straw management practice is composting. However, market demand for this management method is generally low (Sommer & Møller 2000). Hence, it may be suggested that farmers need a more practical alternative for managing crop straws.

Alternatively, crop residues could be utilised as a potential source of biomass for bioenergy (Cherubini & Ulgiati 2010; Giuntoli et al. 2013; Parajuli et al. 2014; Weiser et al. 2014). Of late, the thermochemical conversion of agricultural residue to bioenergy at the on-farm level has

been gaining popularity, especially in developing countries (Solarin et al. 2018). Zhang et al. (2013) advocated crop straw (lignocellulosic) as a techno-economical viable option for generating heat and electricity. Calabi-Floody et al. (2018) mentioned that reusing crop straws is becoming more popular for various green technologies and applications, including biofuel, biochar, biogas, compost fertiliser, polymers, biotechnological issues and more. One of the possibilities is a thermochemical conversion from biomass into environmentally sustainable bioenergy (Kandasamy et al. 2022). Kingwell and Abadi (2014) also suggested that biofuel production in Australia has strong economic growth potential and should be explored further. Based on current estimates, the annual average energy potential from WS residue alone is 147.23 TJ.

As a solid fuel, nonwoody straw biomass has a low bulk density, uneven shape, varying size, poor lignin content and low quality (Adapa, Tabil & Schoenau 2009). According to Park, Lee and Kim (2018), desirable higher quality solid fuel may be indispensable for conversion into bioenergy. Several techniques are commonly used for upgrading biomass fuel quality as well as efficient biomass-to-bioenergy conversion processes. Based on the biomass's physical characteristics, selecting a suitable conversion method is needed for efficient energy transformation. Among the upgrading approaches, the biochemical (fermentation) and thermochemical are two major routes for biomass-to-bioenergy (Adams et al. 2018). The biological process can convert biomass into ethanol or methane gas through fermentation (Chandra, Takeuchi & Hasegawa 2012). However, this method may be slower and require external energy for fermentation (Datta, Hossain & Roy 2019). In comparison, there is greater efficiency in the feedstock thermochemical process (Singh et al. 2016). The thermochemical process mainly converts solid fuel into gas, liquid or higher energy solid fuel (Pandey et al. 2015). It refers to using heat to carry out chemical reactions, either with or without oxygen (Ong et al. 2020).

Thermochemical pathways can be further categorised into pyrolysis, combustion and gasification based on their temperature, pressure and duration of heating (Kundu et al. 2018). In the pyrolysis system, the primary output is solid (char) rather than gas or liquid, but it can produce valuable chemicals. Furthermore, fast pyrolysis is suitable for bio-oil and slow pyrolysis is mainly used for solid carbon (biochar). In comparison, the combustion process is mainly used for heat and power generation and has been applied widely in heat related industries (Akhtar, Krepl & Ivanova 2018). Finally, gasification is a partial oxidation process and an effective way of converting lignocellulosic materials into energy (via gas). This is because of its simplicity and higher solid fuel conversion capability (>50%) (Gómez-Barea et al. 2013).

Thermochemical conversion of agricultural residue into energy can increase the value of agricultural output and reduce dependence on fossil

fuels (Chan et al. 2019). Overall, nonwoody biomass conversions have more technological challenges than woody biomass conversions (Shrivastava et al. 2021). This is because nonwoody biomass gasification often faces the problem of ash sintering, higher tar content and bed bridging (Widjaya et al. 2018). A sticky melted material can obstruct a gasifier's grate, gas lines, air ducts, etc. High ash content frequently results in high particle output and a low melting point of particulate matter (Mahdavi 2020). An unstable thermochemical conversion process is typically the result of the low density issue. Therefore, nonwoody biomass must be upgraded into high quality solid fuel.

Upgrading the physiochemical characteristics of biomass is an important pathway to efficient energy generation (Zhang, Y. et al. 2020). Densification, particularly pelleting, has been studied to solve the problem of low quality biomass (Picchio et al. 2020; Brand et al. 2021). Pellets are more desirable in industrial, commercial and residential heating systems because they create a uniform feeding system and allow easier flow control (Carvalho et al. 2013).

Furthermore, it is noted that agricultural straw has less lignin content than wood biomass. Lignin acts as a binding material and is, thus, important for pelleting (Theerarattananoon et al. 2011). Several researchers have used coal blending with biomass for pelleting to reduce the tar problem during combustion and gasification due to its low cost and available supply (Guo & Zhong 2018; Li, Y.-H. et al. 2018; Yuan et al. 2022). Coal containing higher carbon could also produce additional heat, which assists in the breakdown of tar components into gases. However, coal use is of concern due to its environmental emissions (Nelson et al. 2010). Interestingly, nonwoody biomass contains more K, Ca, Mg and Na than woody biomass, which may act as a natural catalyst during thermal conversion (Pedroso et al. 2022). The improvement of tar breaking by heat (coal/biochar) or catalyst activities is known as the synergistic conversion effect.

Thermochemical conversion can be influenced by chemical reactions, feedstock composition and conversion reactors (Gil, M. V. et al. 2010; Mian et al. 2020). Further, quality pellet production and energy conversion may require three types of additive/blending materials: structural materials, binding materials, and heating materials (Gilbert et al. 2009; Berghel et al. 2013; Gageanu et al. 2018; Ahmmad et al. 2020; Anukam et al. 2021). However, knowledge about the types of additives, the amount needed, etc., is lacking. Some research has also considered adding binding materials but no heating value upgrading materials (Adapa, Tabil & Schoenau 2009; Theerarattananoon et al. 2011). Others have considered both biomass and coal based blending materials (Guo & Zhong 2018). The third group tried to develop pellets without blending materials (Tabil 1996; Ríos-Badrán et al. 2020).

The present study considered the combination of biomass-based additives and three basic types of additive materials: biochar, sawdust and bentonite clay. High carbon-enriched biochar originates from woody/nonwoody biomass pyrolysis or gasification (Fahmy et al. 2020). The renewably sourced biochar acts as a heating material for WS pellet production, with characteristics similar to coal (Xing, Fan & Jiang 2018; Mohammadi 2021). In addition, there were limited studies on the synergistic effects of biochar blending with biomass (Amalina et al. 2022). Alternatively, sawdust has been used as the structural material for pellets. Also, bentonite clay is a natural product, low cost and suitable binding material for pellet production (Bueno et al. 2021).

1.2. Research goal and objectives

This study aims to develop and evaluate the methods for converting agricultural straw biomass into a valuable fuel source. This research assessed the materials' (pellets) physical, chemical, and thermal properties for use in small scale plants. The scope of this research included both technological development and cost estimation.

WS is an agricultural herbaceous biomass produced in the field. For this study, the pellet was first made from WS with varying concentrations of additives. This research also investigated the WS pellets' thermokinetic behaviour, thermodynamic properties and kinetic triple in a laboratory and small scale pilot plants.

This study further developed a computational fluid dynamics (CFD) computer model to simulate the gasification process of a small scale plant. The final part of this work then assessed how much it would cost to produce WS pellets and use them as a source of alternative energy. The following figure (Figure 1.1) describes the scope of this investigation.
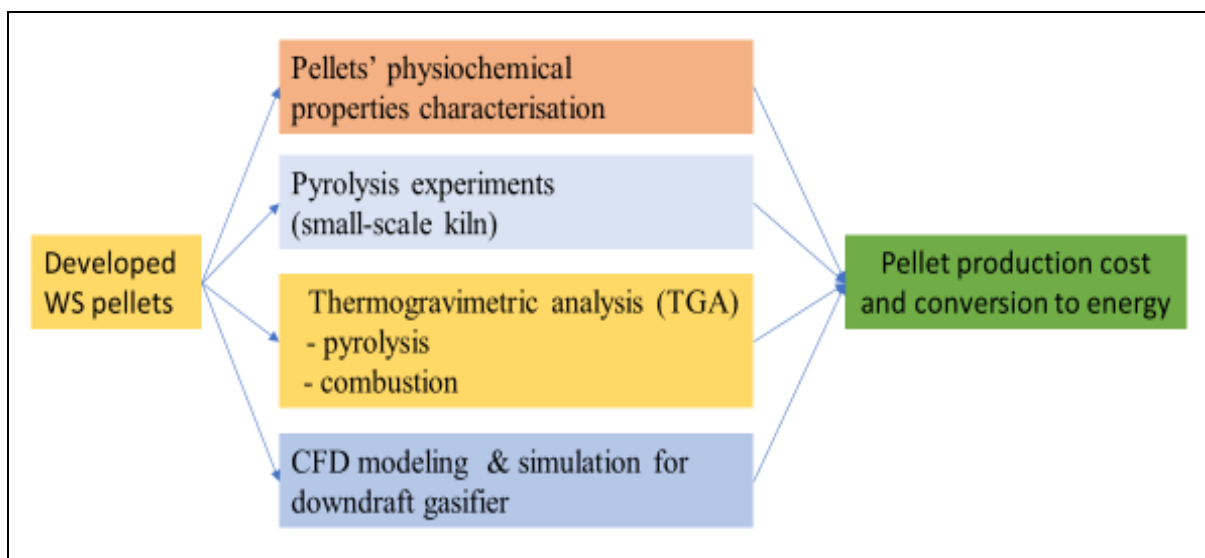
Figure 1.1: Conceptual framework of the study

The specific objectives of this research are as follows:

1. *Develop a suitable quality wheat straw pellet (WSP)*

    This study first investigated manufacturing suitable WSPs' with varied additive combinations. The impacts of different additives on WSPs pellets' properties were then examined.

2. *Experimental investigation of WSP pyrolysis process using oven test*

    This study examined the pyrolysis of WS pellets in a laboratory scale kiln and identified the pyrolysis yield (char, bio-oil, and syngas).

3. *Thermal conversion of WSP and investigation of the kinetic properties*

    This study investigated the developed WSPs' thermochemical conversion (pyrolysis and combustion) behaviour. The thermal decomposition profile and thermokinetic properties were obtained through the thermogravimetric analysis (TGA) method.

4. *CFD model development and simulation of the WSP fuel gasification performances*

    This study developed a computational fluid dynamics (CFD) model to simulate the produced WSP gasification performance in a fixed bed gasifier. After that, the model simulation results were verified with the available gasification experimental output.

5*. Economic analysis of turning WS into fuel pellets and the impact of energy generation*

    This research evaluated the effects of producing and using WSPs' as a source of alternative energy. This assessment further considered energy and cost estimation for pellet production.

1.3. Outline of the thesis

This work is presented in ten chapters. The following is a description of the thesis outline:

Chapter 1. Introduction: The research background guiding this work is presented in this chapter. It also describes the study motivation, aims and general research outline.

Chapter 2. Review literature: This chapter starts with a descriptive analysis of WS availability and energy production potential. In addition, it discussed biomass and thermal energy conversion methods (pyrolysis). The current research on thermogravimetric analysis (TGA) of WSPs' pyrolysis and combustion was also presented. The development and performance of various types of gasifiers were further discussed.

Chapter 3. WS pellet development: Discussed the manufacturing methods of pellets from WS incorporating different additives/binding materials.

Chapter 4. Pellet quality improvement: This chapter discussed in depth techniques for improving the pellets' physical and chemical properties. It also described the pellet properties assessment (including a published paper).

Chapter 5. Oven test of WS pellets: A small scale laboratory kiln was used to study the pyrolysis of WSPs'.

Chapter 6. Thermokinetic behaviour of WS pellets combustion: The experimental work of this chapter was conducted using a Thermogravimetric Analyser (TGA). This section described the WSP combustion behaviour, the additive blends' effect on performance, thermodynamic properties and thermokinetic parameters.

Chapter 7. WS pellets thermokinetic behaviour by pyrolysis: This chapter examined the WS pellet pyrolytic behaviour and the impact of fuel blends and kinetic triple.

Chapter 8. CFD modeling and simulation: This chapter was studied to develop a comprehensive CFD model to study the gasification at a laboratory scale downdraft gasifier. The created model was then applied to simulate and validate the WSP gasification performance.

Chapter 9. Techno-economic analysis of WSPs into energy: This chapter explored the techno-economic properties and circular use of WSPs' for wheat grain drying.

Chapter 10. Conclusion and recommendations: This chapter summarised the main findings and suggested applications for further study.

CHAPTER 2: LITERATURE REVIEW

2.1. Introduction

2.1.1. Overview of this chapter

This chapter reviewed the available research literature. The review has six main themes: (i) pellet fuel development by adding suitable additives, (ii) pellet quality improvement, (iii) laboratory scale pyrolysis tests, (iv) the thermokinetic behaviour of combustion and pyrolysis, (v) gasification modelling and (vi) the economic impact of pellet development.

Section 2.1 discusses the suitability of WS biomass as a pellet fuel. In addition, it examined the possible approaches to upgrading the qualities of raw materials for transformation into high-quality fuel. Finally, WS pellet characteristics were investigated and compared to the ISO densified fuel standards.

Section 2.2 reviews the energetic use of biomass and the conversion process. This section discussed the pyrolysis process of biomass and the method used to obtain the particular yields of gas, both solid (biochar) and liquid (bio-oil). This section also discussed the gas composition and biochar quality traits related to temperature and reaction times.

Section 2.3 covers the thermochemical conversion phase of biomass fuel. It discussed the thermal conditions required for biomass thermal conversion to biofuel. This also included discussions about identifying kinetic characteristics and the chosen thermogravimetric (TG) analysis for pyrolysis and combustion.

Gasification is intricate, and the results vary significantly with operating parameters. Hence, section 2.4 discussed the gasifier's design, operation, and performance. Working conditions optimisation using the CFD model was also addressed.

Section 2.5 focused on the economic influence of WSP development on the energy required and energy cost.

2.1.2. Candidate biomass - wheat straw

Global cereal crop production totalled 2.7 billion tonnes in 2018. This will rise by about 50% by 2050 to meet increasing worldwide demand (FAO 2017). This increased production will increase harvesting residue (e.g., straw, stubble). The world's most-grown cereal crop is wheat, and it is produced in more than 115 countries under various conditions (Talebnia, Karakashev & Angelidaki 2010). In 2020/21, worldwide wheat production was around 776.0 million tonnes (FAO 2022). Pan and Sano (2005)

reported that the WS and grain yield ratio is about 1.3:1, producing approximately 1000 million tonnes of WS globally.

Wheat is also the dominant crop in Australia. The wheat cultivating states of Australia are New South Wales, Queensland, Victoria, South Australia and Western Australia (Wang, B. et al. 2018). Australia's wheat is mostly grown in rain-fed environments. However, climate change impacts may reduce rainfall, which might substantially decrease productivity (Anwar et al. 2015). Australia also exports over 65% of its agricultural production (Grundy et al. 2016), contributing significantly to the global food market (ABARES 2019).

In 2021/22, Australia produced 36.3 million tonnes of wheat grain (https://www.statista.com/statistics/631611/australia-wheat-yield/), which generated around 38.0 million tonnes of wheat residues (Table 2.1). Cardboard, fuel and cattle feeding have all been produced using only two million tonnes of WS. A significant surplus of WS biomass was wasted and abandoned in the field. Consequently, these WS residues possess an annual average energy potential of 147.23 TJ. Considering this, WS biomass exhibits an extraordinary opportunity for bioenergy production.

Table 2.1: Wheat straw energy potential in Australia

Total /average production (1000 tonnes) (Mundi 2020)	Residue production rate (Liu, H. et al. 2008)	Moisture (%) (Di Blasi, Tanzi & Lanzetta 1997)	Dry residue generated (1000 tonnes)	Calorific value (MJ/kg) (El-Sayed & Khairy 2017)	Residue energy potential (TJ)	Energy availability factor (Al-Hamamre et al. 2017)	Available residue energy potential (TJ)
36.3	1.30	10~20	37.57	15.6	588.93	0.25	147.23

Note; Conversion efficiency = 20~30% (Al-Hamamre et al. 2017)

It has been widely advocated for crop straw to be returned to the soil and incorporated with soil to increase crop yields, soil fertility and soil organic carbon (Hanafi et al. 2012). The common straw utilisation practice is shown in Figure 2.1, varying significantly according to geographic location. In Australia, straw decomposition and incorporation with soil are the two widely adopted methods of straw use (Kingwell & Abadi 2014). However, WS degrades slowly under natural conditions due to being relatively chemically stable, fibrous, and high carbon-to-nitrogen ratio (C: N) (Chen 2014). Therefore, when WS is left on the soil surface for nutrient recycling, it may negatively affect the growth of the subsequent crop (Kimber 1973). The unused crop portion (residue) is sometimes mixed with soil as a traditional conservation method (Singh & Sidhu 2014). However, leftover straw in the field poses challenges for developing countries as it obstructs intensive (year-round crop production) agriculture due to issues such as seed germination problems and the extended time required for straw decomposition.
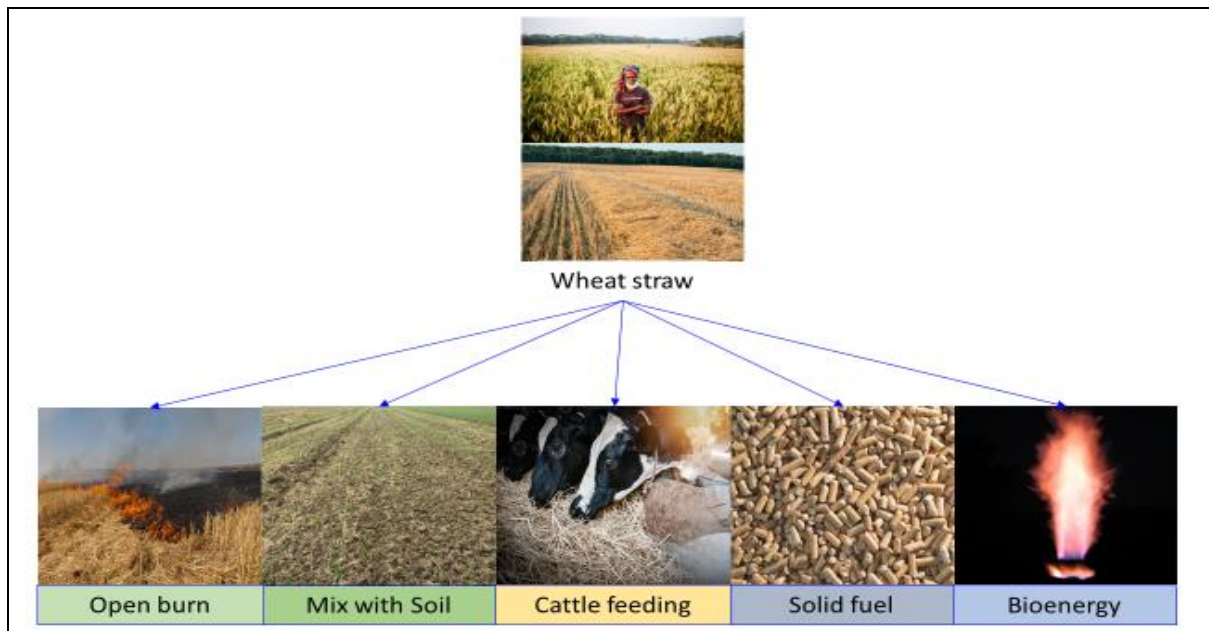
Figure 2.1: Typical use of wheat straw

In situ, straw burning is common (Gupta, Agarwal & Mittal 2016) in many countries, especially China, India and Bangladesh. However, this open-field burning activity is a significant source of air pollution with adverse effects on atmospheric chemistry, climate change and poses severe risks to human health (Figure 2.2) (Udeigwe et al. 2015; Quayle 2016; Montero et al. 2018). Li et al. (2016) noted that burning straw after harvesting maize and wheat is a common practice that can lead to 30 days of smog in Beijing, China. According to Dobermann and Fairhurst (2002), burning rice straws could cause damage to N by up to 100%, P: ~25%, K: ~20%, and S: 5~60%. Similarly, *Biederbeck et al. (1980)* measured Saskatchewan, Canada's soil properties and grain yields. They found that total biological activity had permanently fallen, and more than 50% of the bacterial population was destroyed by repeated burning. Hence, farmers need a more practical alternative method to manage the agricultural residues to reduce emissions, promote "carbon offset" and fit with farm operations.
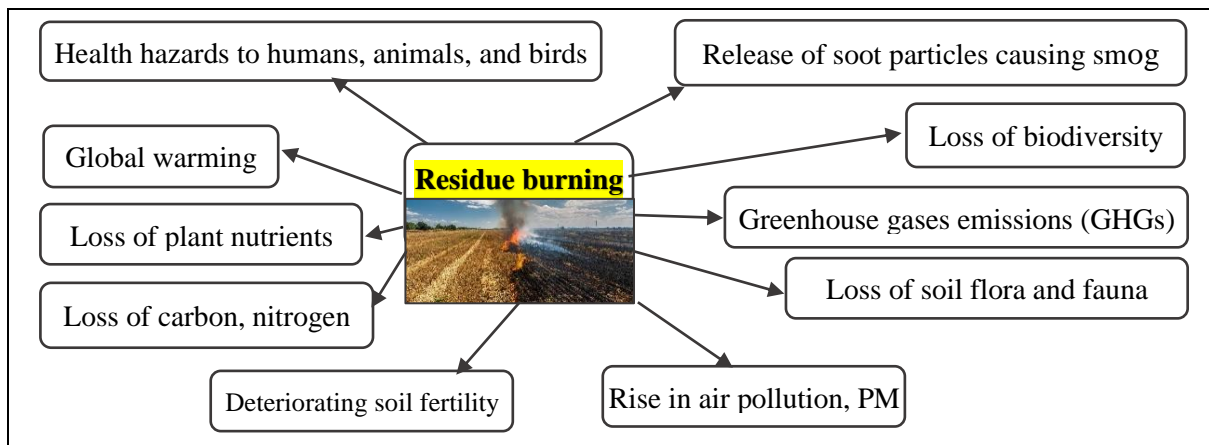
Figure 2.2: Crop residue on field burning consequences

Research has found that crop residues could be employed as a viable source of biomass for bioenergy (Cherubini & Ulgiati 2010; Giuntoli et al. 2013; Parajuli et al. 2014; Weiser et al. 2014). Recently, there has been a growing popularity in developing countries for the on-farm thermochemical conversion of agricultural residue to bioenergy (Siemons 2001; Solarin 2017; Solarin et al. 2018). According to Zhang et al. (2013), utilising crop straw (a type of lignocellulosic feedstock) for heat and electricity production is a viable option techno-economically. Calabi-Floody et al. (2018) also reported that reusing crop straws is becoming more popular for various green technologies and applications. Kingwell and Abadi (2014) claimed that biofuel production in Australia has great economic growth potential and should be emphasised.

2.2. Properties of biomass

2.2.1. Biomass

Biomass is a biodegradable fraction of products, waste and residues from agriculture, forestry, industry, and municipal sources. In a broader sense, biomass refers to all currently existing or recently extinct species of plants and animals (Basu 2010). *B*iomass is an organic carbonaceous material comprised of carbon and hydrogen. The CO_2 generated during biomass combustion is nearly the same amount of CO_2 used for plant growth (Al-Hamamre et al. 2017).

Humans have relied on biomass as a significant energy source. An enormous amount of biomass is produced yearly, of which 200 billion tonnes are available for energy conversion globally (McKendry 2002). It was estimated that the world's 10% of main energy currently comes from biomass resources (Dwyer & Teske 2018). Worldwide, biomass is broadly recognised as a potentially renewable resource (Kim & Dale 2004).

2.2.2. Biomass types/classification

Biomass can be categorised into various distinct groups according to the ecology and biological applications, energy and chemical use (organic material stored) (Cuadros et al. 2013; Yacout et al. 2020):

- Natural biomass: Biomass that occurs naturally without human interference (i.e., forest, some wood, herbaceous biomass, etc.)

- Residual biomass: This biomass is produced as the byproduct of artificial human activities. It happens in resources developed on agricultural actions, forestry/wood activities, urban and industrial wastewater/solids, and livestock wastes.

- Energy crops: This crop is typically grown in short rotations for energy production. Tropical energy crops include sunflower, sugar cane, corn,

beet, willow, poplar, switchgrass, etc. They are also divided into woody and nonwoody (herbaceous) types.

▪ Marine or freshwater algae, macroalgae: The popular aquatic biomass is algae or microalgae, seaweed, water hyacinth, etc.

▪ Industrial biomass and contaminated wastes: Refuse-derived fuel (RDF), sewage and municipal sludge, waste papers, paperboard waste, chipboard, fibreboard, plywood, wood pallets and boxes, railway sleepers, tannery waste, etc. are included in this group.

In addition, biomass can be separated into primary, secondary and tertiary sources (Table 2.2) (Osman et al. 2019). Primary biomass is formed through photosynthesis and harvested directly from the land. On the other hand, secondary biomass sources are derived from the chemical processing of primary resources. Lastly, tertiary biomass resources refer to post-consumer residue stem.

Table 2.2: Biomass types: based on sources

Biomass type	Comments	Example
Primary	▪ Directly via photosynthesis ▪ Directly taken from the land	▪ Herbaceous ▪ Woody biomass ▪ Residues after the harvesting of forest trees ▪ Crops (oil crops, corn stover and WS)
Secondary	▪ Processing of the primary biomass	▪ Physical processing (sawdust) ▪ Chemical processing (black liquor) ▪ Biological processing (manure production by animals)
Tertiary	▪ Post-consumer byproducts	▪ Animal fat ▪ Used vegetable oil ▪ Construction and demolition debris ▪ Packing byproducts

2.2.3. Selection of biomass

Biomass can be used as feedstock for thermal conversion (combustion, gasification and pyrolysis). The fuel's properties (physical and chemical), desired output and intended application influence the potential methods of biomass selection and bioenergy conversion (Vaezi et al. 2012). This study focuses on producing energy for farm-level heat and power generation.

2.2.4. Herbaceous biomass

Herbaceous biomass is a plant with nonwoody stems and undergoes a complete die-back at the end of the growing season. Woody biomass produces a hard woody stem above the ground, whereas herbaceous plants have soft, flexible green stems above the ground. Also, secondary growth is often found in woody plants but not herbaceous ones. The herbaceous biomass typically contains parts of crops like seeds, cones, leaves, and

stems (Table 2.3). Common herbaceous crops include WS, rice straw, sugarcane bagasse, and switchgrass (Naimi & Sokhansanj 2018). The uneven shape of herbaceous waste usually necessitates an additional step of size reduction as a post-harvest handling procedure. This pretreatment will increase bulk density, making herbaceous waste easier to store and transport. The particle size reduction also influences the biodegradability of biomass through the depolymerization of plant cells as well as improves the chemical and biochemical reactions process.

Table 2.3: Herbaceous and agricultural residues

Source	Specific feedstock
Straw	Rice, wheat, barley, bean, flax, corn, mint, oat, rape, rye, sesame, sunflower, sorghum, soybean, millet, hemp and others
Grasses	Alfalfa, miscanthus, switchgrass, bamboo, banana, Cynara, miscanthus, switchgrass and others
Crop residues	Fruits, pips, grains, cobs, bagasse, cakes, cassava stalk, coconut frond, cotton stalks, corn stoves, husks, oil palm fronds and others
Agriculture residues from industrial processing	Cacao pods, coconut husk and shell, coffee shell/husk, cotton hulls, groundnut husk, maize cob and husk, olive pruning/pressing residue, rice husk, sugar cane bagasse, nutshells

Biomass waste materials can be considered as both opportunities and challenges simultaneously (Osman et al. 2019). Typically, herbaceous biomass contains a high level of silica, ash and inorganic content compared to woody biomass (Kaknics, Michel & Poirier 2016). During thermal decomposition, these components often cause several issues. The high ash content is particularly challenging because it catalyses thermochemical reactions (Pham et al. 2018). It also impacts pyrolysis and gasification yields and their subsequent composition. Therefore, it is suggested that the typical method used to maximise the energy contained in herbaceous biomass is blending with other types of wood fuel or coal (Forbes et al. 2014).

Further, the higher moisture content (up to 80%) and lower HHV are also the main disadvantages of straw biomass when considered for energy applications (Gilbert et al. 2009). Biomass-to-bioenergy transformation is more complex due to straw biomass's low bulk density, wet nature, and seasonal variability. Different pretreatments can be applied to lower the moisture content and raise the HHV.

2.2.5. Biomass composition and its decomposition

Plant biomass comprises complex cell walls through cellulose and hemicellulose microfibers networks (Ravindranath & Hall 1995). Typically, biomass material contained lignin (15~25%), cellulose (30~40%) and hemicellulose (20~25%) (Snelders et al. 2014). Unlike starch or carbohydrate, the plant biomass element is difficult for humans to digest.

Consequently, its usage in energy production does not directly threaten the world's food supply (Peng et al. 2015).

The cellulose's numerous molecular units (monomeric: anhydro-D-glucose) comprise a linear polysaccharide crystalline polymer (Table 2.4). This polymer develops the microfibril structure to create stronger intramolecular hydrogen bonds (Mohan, Pittman Jr & Steele 2006; Pasangulapati et al. 2012). Therefore, cellulose (usually around 30% for WS) degrades at a modest temperature from 240~350°C during thermal conversion and produces volatile matter, tar and char (Robbins et al. 2012).

Table 2.4: Biomass compositional function

Primary components of biomass	Function	References
Cellulose	▪ Linear polymer with complex carbohydrate ▪ High molecular weight ▪ Most abundant organic compounds ▪ Structural function in plant cell walls	(Fromm et al. 2003; Shen et al. 2013; Carpenter et al. 2014; Bonechi et al. 2017)
Hemicellulose	▪ Significant elements of plant cell walls ▪ Between 180~350°C, thermally decomposed ▪ Producing noncondensable gas, and a variety of ketones, aldehydes, acids and furans	
Lignin	▪ Contained in plant cell wall ▪ Function of binding, cementing, and putting the fibers together to enhance the compactness and resistance of the plant structure ▪ Content varies according to plant species (15~30%) ▪ Elemental composition is about 61~65% carbon, 5~6% hydrogen, and the remaining is oxygen	

Hemicellulose is a major component of plant cell walls, mainly used in biofuels and bioproducts. The hemicellulose extracted from different plant sources and locations have different microstructures and molecules. Wheat straw is an important biomass raw material for the extraction of hemicellulose. In comparison, hemicelluloses have crystalline regions due to less branched chain polymerisation. Hence, chemical reagents can quickly attack this polysaccharide because the hydrogen bonds in hemicellulose are weaker. Consequently, hemicellulose is thermochemically unstable and promptly decomposes between 200 and 260°C. This component produces additional volatiles and less char and tar than cellulose (Robbins et al. 2012).

According to (Basu 2018), lignin can generate polyaromatic compounds that act as a binding agent, holding the fibres' cells together. Accordingly, lignin's activities contribute to biomass's elasticity and mechanical strength (Lu et al. 2021). Although lignin is relatively stable, it

undergoes degradation across a wide temperature range, typically 280 to 500°C, producing more char than cellulose and hemicellulose (Serapiglia et al. 2013). Further, Gilbert et al. (2009) suggest that lignin can potentially improve pellet durability and quality.

The relative amounts of cellulose and lignin often determine biomass's suitability for further thermal conversion processing (Bhavanam & Sastry 2011). In general, the proportion of lignin and cellulose in biomass is 40/60. In addition, water, and organic solvent, two soluble and insoluble secondary components, are also found in biomass. Ash, starches, proteins, etc., are insoluble, while fatty acids, alcohols, phenols, etc., are soluble in water or other organic solvents (Basu 2010).

One of the most significant issues with biomass gasification is tar production and condenses, which often block and clog processing equipment. WS may contain less than 15% lignin (Table 2.5) which is significantly lower than wood, resulting in less durable pellets (Lee et al. 1998; Woolf et al. 2010; StelteClemons, et al. 2011; Lehmann et al. 2012). Some form of external binding agent would often need to be used to improve both composition and suitable pellet quality.

Table 2.5: Composition of agricultural residues

Composition, Dry wt, %	Straw biomass						Wood biomass		
	Wheat straw	Oat straw	Barley straw	Canola straw	Rice straw	Switch grass	Birch wood	Scots pine	Eucalyptus
Hemicellulose	23.68	23.34	20.36	16.41	27.2	7.43	25.7	28.5	19.2
Cellulose	34.2	37.60	33.25	42.39	34.0	44.34	40.0	40.0	45.0
Lignin	13.88	12.85	17.13	14.15	14.2	30.0	15.7	27.7	31.3
References	(Adapa, Tabil & Schoenau 2009)				(Tumuluru et al. 2011)	(Mani, Tabil & Sokhansanj 2006)	(Tumuluru et al. 2011)		

2.2.6. Biomass chemical elements

Biomass chemical composition is an inherent trait and significantly affects biofuel's characteristics and potential uses (Tumuluru & Wright 2010). Several researchers have discussed the effect of biomass compositions on produce gas quality. Li et al. (2016), Solarin (2017) and Bajwa et al. (2018) noted that biomass materials display diverse physical and chemical characteristics and compositions (Table 2.6). This material composition is also required for theoretically calculating the process reactions, energy release and absorption (Sharma et al. 2021).

Table 2.6: Chemical composition of agricultural residues

Features	Agricultural residue				Wood		Charcoal		
	Wheat straw	Grass reed canary	Sugarcane bagasse	Cotton gin waste	Pinus punning	Spruce wood	Wood charcoal	Bituminous coal*	Lignite coal*
Proximate analysis (% weight, db)									
Moisture	7.4	60.0	9.4	11.80	-	-	-	3~10	25~75
Volatile matters	56.7	-	65.0	68.7	82.10	70.20	8~25	14~45	>45.0
Fixed carbon	31.5	17.65	31.0	20.8	13.98	29.30	70~89	69~86	<69.0
Ash	4.4	8.85	3.6	10.5	2.8	1.50	2~5	5.0	10.0
Ultimate analysis (% weight, db)									
Carbon	44.1	49.6	49.4	45.14	50.55	46.90	70~90	59~81	40~52
Hydrogen	6.0	6.16	6.3	4.93	6.12	5.08	1.7~3	5~5.8	6.2~6.9
Nitrogen	0.4	0.61	0.3	1.16	0.45	-	0.5~1.3	1.1~1.4	0.7~1.0
Sulphur	0.01	0.07	0.07	0.29	<0.01	-	0	1.5~3.5	0
Oxygen	45.1	43.5	43.9	43.66	40.20	40.17	4~18	5~20.6	4~18
Heating value									
HHV, MJ/kg	15.6	18.37	18.9	16.6	19.99	-	18~19	25~36	6.7~25
References	(Nanda et al. 2018)	(Elita 2018)	(Elita 2018)	(Sadaka 2013)	(Sarkar et al. 2014)	(Demirbaş 1997)	(Elita 2018)		

*Note; * as received*

The proximate analysis is often used to assess the biomass's water, ash, volatiles and fixed carbon content (García et al. 2013). The varied composition, moisture content, ash concentration, heavy metals, sulphur, nitrogen, and chlorine content are typical characteristics of straw biomass. Generally, the biomass's physical form is heterogeneous, and the moisture content varies from 40 to 50% when harvested. The biomass with higher moisture matter requires more heat or energy to ignite. Rupar-Gadd and Forss (2018) recommended that an optimum moisture content (8 to 10%) for solid biomass might improve mechanical durability and heat value. The high volatility of the biomass material will result in several advantageous conditions, including low ignition temperatures and retained ignition for lengthy periods. In addition, typical crop residue contains 20% fixed carbon and 80% volatiles (Hong et al. 2020). Based on proximate analysis data plotted in a ternary diagram (Figure 2.3), WS has high volatile matter (>70 %) and fixed carbon contents which are desirable properties for gasification (Basu 2010).
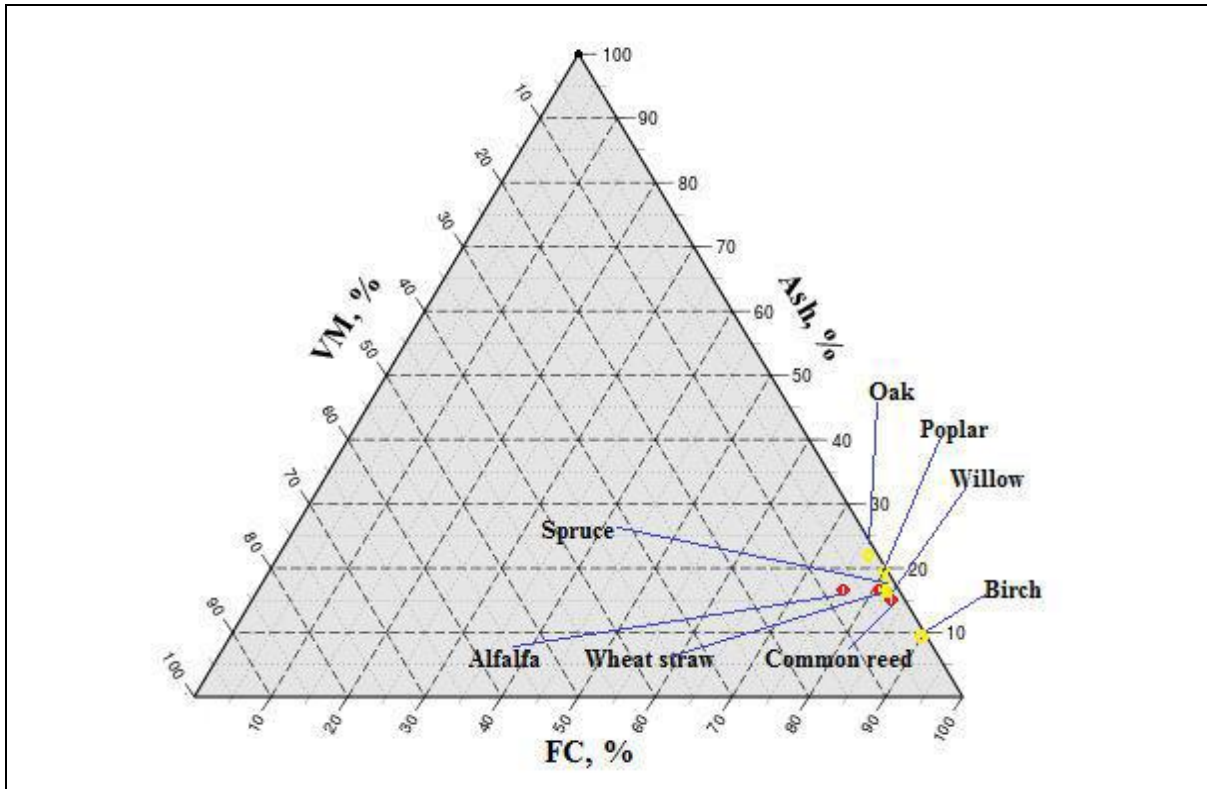
Figure 2.3: Ternary diagram for agricultural residues [modification from (Sarker 2016)]

Note; Red dots: Agricultural straw (WS); FC: Fixed carbon; VM: Volatiles matters

It is well known that ash is the principal inert material accumulating in the gasifier or combustor bed, reducing the reactor's feedstock energy value and effectiveness (Zainal et al. 2001). Unfortunately, WS has a higher ash concentration than other herbaceous biomass (often approximately 10%) (Table 2.7). Therefore, some additives would usually be added to increase the synergistic effect and raise the ash melting temperature.

Table 2.7: Chemical composition of different types of straw

Biomass materials	Proximate analysis (% by mass, dry basis)			Ultimate analysis (% by mass, dry basis)			References
	FC	VM	Ash	C	H	O	
Wheat straw	23.50	63.0	13.5	45.50	5.10	34.10	(Demirbaş 1997)
	18.10	74.80	7.10	49.4	6.1	43.60	(Moilanen 2006; Nutalapati et al. 2007)
Rice straw	18.30	77.30	3.40	47.10	6.00	43.30	(Parikh, Channiwala & Ghosal 2007)
Rape straw	17.90	77.40	4.70	48.5	6.40	44.50	(Masiá et al. 2007)
Oat straw	19.53	74.48	5.99	42.27	5.98	5012	(Mani, Murugan & Mahinpey 2011)
Jawar straw	15.15	75.97	8.88	42.10	5.60	43.38	(Channiwala & Parikh 2002)
Millet straw	16.45	78.28	5.27	43.71	5.85	45.16	(Channiwala & Parikh 2002)
Alfalfa straw	20.15	72.60	7.25	46.76	5.40	40.72	(Parikh, Channiwala & Ghosal 2007)
Barley straw	13.29	82.41	4.30	45.47	5.61	44.57	(Parikh, Channiwala & Ghosal 2007)
Rye straw	15.10	83.02	1.97	46.63	5.62	45.85	(Channiwala & Parikh 2002)
Corn Stover	14.50	78.10	7.40	46.50	5.81	39.67	(Parikh, Channiwala & Ghosal 2007)
Mint straw	19.50	69.70	10.80	50.60	6.20	40.10	(MILES et al. 1995)
Flax straw	21.30	44.57	1.11	45.24	6.25	46.32	(Mani, Murugan & Mahinpey 2011)

Note; FC: Fixed carbon; VM: Volatiles matters; C= Carbon; H= Hydrogen and O= Oxygen

The ultimate analyses measure the biomass Carbon (C), Sulphur (S), Hydrogen (H_2), Oxygen (O_2) and Nitrogen (N_2) concentration (Kumar, Jones & Hanna 2009). Herbaceous and agricultural biomass typically contain C: 42.2~58.4%, H:3.2~9.2%, N:0.1~3.4%, S:0.01~0.60 and O: 34.2~49% (Vassilev et al. 2010). Moreover, agricultural straw biomass has a significant amount of oxygen, contributing to its high thermal instability (Brown 2013).

Biomass's key components (C, H, O, N, S) and minor components (Na, K, Ca, Mg, Si, Al, Fe, P, Cl, Ti, Mn, etc.) influence the thermal reactions directly and indirectly (Vassilev et al. 2010; Molino, Chianese & Musmarra 2016). Most of these mineral matters may be transformed into slag and then melted ash at high temperatures, which can cause significant operational difficulties for gasifiers. Particularly, the mineral substances combine with silica at high temperatures to generate silicates. Silicon concentration is relatively high in WS. Additionally, some biomass types include high levels of alkaline metals (Na, K, Ca, Mg), which lower the melting temperature and cause more significant ash deposition and fouling (obstruction) of boiler equipment (Vassilev & Vassileva 2019). However, some alkali (Na, K) and alkaline earth (Ca, Mg) might also help catalyse the conversion process.

Most biomass has a sulphur content of less than 0.2%, while certain biomass fuels may have a sulphur content of up to 0.5%~0.7% (Sivabalan et al. 2021). The higher N and S will produce hazardous gases (nitrogen oxides: NO_x and sulphur oxides: SO_x) during combustion, which are the main contributors to acid rain and particulate matter (PM) (GummertHung, et al. 2020).

The heat generated by burning "1 kg" of biomass is known as the heating value of biomass. This value depends on fixed carbon and the volatile matter of biomass. An increase in any of these components will increase the heating value. The heating value of biomass typically ranges between 14 and 19 MJ/Nm^3. Sarker, Arauzo and Nielsen (2015) reported that during WS gasification, the producer gas often has a lower heating value (LHV) and produces less char, but the amount of dust released may be higher. In comparison, in the case of softwood gasification, the yield gas can have a much higher LHV and char while emitting the lowest amount of dust (Tumuluru et al. 2011).

2.2.7. Upgrading straw biomass into solid fuel

According to the design and application aims, downdraft gasifiers may be the best well-matched gasifiers for solid fuel conversion (Beohar et al. 2012). However, herbaceous biomass, especially straw, has low bulk densities (Fu et al. 2021). Therefore, straw handling is challenging during conversion as it is difficult to achieve a uniform fuel flow rate (Wang, T. et al. 2020). Thus, upgrading the raw material into high-quality fuel becomes vital (Ibrahim 2018). Typically, two possible approaches are available to convert straw to solid feedstock into energy. The first is to change the raw material shape by making densified solid fuel consistent with the selected reactor. The second approach is to upgrade the feedstock composition for better fuel quality and reactor performance.

2.2.8. Feedstock pretreatment

Developing a WSP that meets the International Standard Organization (ISO) criteria necessitates improving straw biomass properties, so the biomass converts into high quality solid fuel. This section discusses upgrading WS into solid fuel, assessing WSP quality and exploring the fuel's effectiveness for thermochemical conversion.

2.2.8.1. Size reduction

Size reduction is the primary pretreatment for densified fuel production and is necessary for uniform shape because straw varies in size, shape and composition (Bajwa et al. 2018). Uniform size improves conversion or further treatment procedures such as pelleting. Smaller particles have larger surface areas enabling better heat transfer and faster reactions (La Villetta, Costa & Massarotti 2017). Ahmad et al. (2016) have

shown that gasification efficiency is significantly related to biomass particle size. The typical particle size of feedstock ranges from 0.2 mm to 1 cm (Table 2.8) (Souza-Santos 2010; Jiang et al. 2018). A study conducted by Carone, Pantaleo and Pellerano (2011) for pellet production from the olive tree found that particle size is the third most important parameter after temperature and moisture. A similar finding was obtained in Caribbean pine pellets, with pressure, moisture content and particle size (0.63 mm) being the first, second and third most influential factors *(*Relova et al. 2009*)*. Peng et al. (2015) identified that as particle size decreases, the durability of pellets increases.

Table 2.8: Biomass particle size and optimum results

Gasifier type	Feedstock size	Optimum results and remarks	Reference
Fluidised bed	0.3~0.5 mm	▪ Optimum gas composition and highest LHV ▪ Maximum gas yield, low char and heavy tar	(Mohammed et al. 2011)
	0.2~0.3 mm	▪ Maximum gas yield ▪ Optimum gas composition, highest LHV	(Lv et al. 2004)
Fixed bed	2~5.0 mm	▪ Maximum gas yield and H_2 yield ▪ Optimum gas composition ▪ Highest LHV value	(Li et al. 2009)
	0.45~0.9 mm	▪ Maximum total gas yield	(Yan et al. 2010)
Entrained flow	>0.2 mm	▪ Optimum gas composition	(Wu et al. 2019)

During densification, the biomass is chopped, crushed or ground using equipment such as a crusher, grinder, hammer mill or rotary knife cutters (Mani, Tabil & Sokhansanj 2006; Kaliyan & Morey 2009). The extent of grinding/chopping required depends on the feedstock moisture content, size reduction ratio and biomass characteristics like fibre content. These factors also determine the energy necessary for operating these machines (Pradhan, Arora & Mahajani 2018). Souza-Santos (2010) recommended using knife cutters instead of grinders for fibrous materials, which may tangle and clump together in the feeding mechanism (Van der Drift et al. 2004).

The required feedstock size for gasification also depends on the reactor type. For instance, the fluidised bed reactor generally needs feedstock that can easily fluidise and interact with the oxidant (Yang et al. 2020). The entrained-bed type gasifier needs finer particles. On the other hand, fixed bed gasifiers need larger particle sizes when a feedstock chunk is applicable (Wu et al. 2019*)*.

2.2.8.2. Drying

Drying is an energy-intensive pretreatment step for converting biomass to bioenergy. Bioenergy plants' sustainability relates to biomass drying efficiency and quality (Yi et al. 2020). Vassilev et al. (2010) noted that most biomass resources are unsuitable for direct biofuel production due to their high moisture content (MC). Therefore, bioenergy plants commonly use pre-drying to achieve lower MC (8~10% w.b.) (Kaliyan & Morey 2009). The drying system removes water from the biomass through evaporation, usually at temperatures 100 to 120°C. Each kilogram of moisture requires a minimum of 2,300 kJ of energy for vaporisation (Basu 2018). However, in the case of an indirect rotary dryer, the energy needed was 3.2 to 3.6 MJ/kg of evaporated water wood chips or bark. Thus, the dryer's efficiency depends upon the energy demands of the dryer. Overall, the biomass drying plant (dryer) efficiency is around 30% depending on size. However, drying involves smoke and pollutant emissions and reduced production efficiency (Das et al. 2022). Hamelinck et al. (2004) noted that gasification efficiency increases with dried biomass and lower emission. Ståhl et al. (2004) also stated that for pellet manufacturing, the suitable moisture needed about 8~12% w.b. During thermal conversion, biomass moisture must be brought below 15% (Basu 2010), particularly for rain-fed WS (MC up to 35% while harvesting). Alternatively, drying is unnecessary for low-moisture biomass such as winter straw.

2.2.8.3. Torrefaction

Torrefaction is a slow "roasting" thermochemical biomass upgrading technique that occurs at 200~300°C temperatures in an oxygen-free atmosphere, with a 10 to 30 min or more extended residence period (Figure 2.4) (Medic et al. 2010). This biochar processing method is commonly used in converting lower value (energy) biomass into high energy density biomass (Yue et al. 2017). Torrefaction is often a vital pretreatment technology for thermochemical biorefinery applications like pyrolysis, gasification, and liquefaction.

According to Sarkar et al. (2014), the torrefaction process decreases the biomass's moisture and volatiles while increasing its hydrophobicity and energy content. Due to the smaller MC, biomass brittleness increases, thus enhancing downstream grindability (Tumuluru et al. 2011). Overall, torrefaction favours pelletisation, increasing the devolatilisation rates (Van der Drift et al. 2004; Uslu, Faaij & Bergman 2008; Sarkar et al. 2014). Pelletisation of torrefied biomass could upgrade its specific bulk density and energy densities; however, the production cost is also increased (Chen et al. 2021).
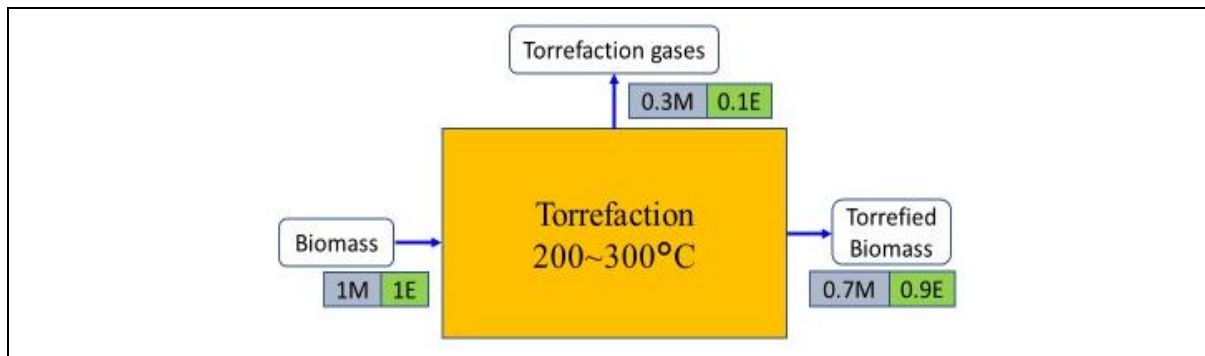
Figure 2.4: Torrefaction process: energy and mass balance of biomass (Teh et al. 2021)

Note; M= Mass and E= Energy and
Energy and mass (biomass) = energy and mass (torrefied gases and biomass)

2.2.9. Solid fuel quality improvement (adding binder)

WS contains lower lignin, high potassium and silica, making the straw pellet less durable and producing more ash and tar during the conversion process (Younis et al. 2018). There are several techniques to improve the straw's quality (Obernberger & Thek 2004; Jezerska et al. 2014). Firstly, combining straw biomass with other low ash content solid fuels can reduce the ash problem (Kulokas, Praspaliauskas & Pedišius 2021). The second method is to mix the biomass with another high grade fuel or catalyst to improve the feedstock quality. However, using a chemical catalyst to strengthen solid fuel quality is costly and requires more care (Li et al. 2009). Therefore, blending feedstock (straw biomass) with solid fuel may be preferred (Collot et al. 1999; Lapuerta et al. 2008; Ataei et al. 2012; Xu et al. 2012; Habibi 2013; Rizkiana et al. 2014).

Several experiments have examined the use of binders in pellet manufacturing (Appendix A, Table A1). Cost, environmental friendliness and acceptance of international standards are the key factors influencing the choice of binders (Nirmale, Kale & Varma 2017). Lehmann et al. (2012) reported that additive materials (binders) could also increase pellet strength. Lu et al. (2014) also showed WS mixed with some additives (5% glycerol, 2% bentonite and 2% lignin) significantly enhanced pellet strength and durability. Ståhl, Berghel and Williams (2016) further suggested that additives could help reduce the net GHG emission and decrease the pelleting process's energy requirements. Furthermore, it has been found that binders also strengthen the fuel's resilience to abrasion and lessen the wear on manufacturing equipment (Jezerska et al. 2014).

2.2.10. Additives (binding) materials for biomass pellet making

Many additives have been used for pellet manufacture, including starchy (corn, potato flour), sugary (sugar, molasses, cassava), and oily (proteins, vegetable oils, lignin, cellulose) (Handbook 2013). Carbohydrate is a very popular binder because it is low cost, contains organic molecules,

and is free of ash, sulphur and nitrogen (Solarin 2017). Also, its hygroscopic properties can absorb more moisture during pelletisation (Jiang et al. 2018). Murugan and Sekhar (2017) showed that including molasses and fructose with feedstock improves pellet quality at low pelleting temperatures.

In addition, several research projects have been performed to improve WS pellet strength, storage time and transport capability and minimise ash and tar formation. Bentonite (Lu et al. 2014), starch (Kuokkanen et al. 2011; Pradhan, Arora & Mahajani 2018) and sawdust (Serrano et al. 2011; Peng et al. 2015) are the binding materials frequently used for the improvement of pellet durability. Bentonite is a water soluble and viscous compound that improves pellet durability (Lu et al. 2014) through strong bonds between particles. Tabil (1996) showed that using bentonite (at a 2.6% rate) can reduce the dust generation of feed pellets. Hence, bentonite clay is often the first choice among binding materials because of its low cost, environmental friendliness (Thomas, Van Vliet & Van der Poel 1998) and wide availability in the market.

Oily materials have also been successfully demonstrated as lubricants to minimise the wear between the pellet dies of the pellet mill. An oil such as kraft lignin (Kuokkanen et al. 2011), lignosulfonate (Mediavilla, Esteban & Fernández 2012; Berghel et al. 2013), rapeseed cake (StelteClemons, et al. 2011; Cao et al. 2015), vegetable oils or glycerol can be used for reducing the energy requirement for pellet production. It has been found that wheat, barley, oat and canola straw blended with glycerol has a lower ash level and higher heating value (Emami, Tabil & Adapa 2015). Moreover, using glycerol with biomass for pelletisation also increases the heating value (Johnson & Taconi 2007; Pagliaro et al. 2007), the flowability of feedstock (Adapa et al. 2010) and works as a good energy source (Yang, Hanna & Sun 2012).

Herbaceous biomass such as WS also contains high K, Cl, P and low S. This usually leads to ash formation (Kupka et al. 2008) and corrosion of energy conversion equipment (Nunes, Matias & Catalão 2016). Additive mixing is one of the possible methods for increasing ash fusion temperature, thereby reducing ash formation. In addition, additive mixing with solid fuel can further upgrade fuel quality and reduce other technical problems related to biomass thermal conversion (Rizkiana et al. 2014). In this case, the solid fuel (sawdust, coal, biochar, etc.) or chemical element (dolomite, NaCl, CaO, ZnO, NiO) acts as a "synergistic" or catalytic for ash reduction and tar melting (Mohammed et al. 2011). Among various additives, sawdust is becoming an increasingly popular alternative material because of its low cost and widespread availability in the market. The sawdust also has lower ash (0.47%) (Lu et al. 2013) and sulphur content (<0.05%) than low-rank coals. Ståhl and Berghel (2011) analysed the results of adding sawdust and rapeseed cake for pellet production and

noted a proportional increase in the durability of rapeseed cake pellets mixed with sawdust. Despite these contributions to ash reducing strategies, the understanding of sawdust related studies remains limited.

Several researchers used coal and biochar to improve the heating value of pellet fuels (Xing, Fan & Jiang 2018; García et al. 2021). The calorific value is nearly the same for both materials, but biochar is available and has less environmental pollution. On the other hand, charcoal needs a lot more heat to break down and decompose. Mohammed et al. (2011) reported that biochar combined or blended with additive materials could lessen tar production. Furthermore, it could destroy the tar structure and convert it into volatile materials. Also, Xu, Pang and Levi (2011) noted that biochar has synergistic effects that may be especially relevant for blended fuel. Therefore, this research used available and low cost additives such as biochar, sawdust and bentonite clay to upgrade the straw quality and pellet standard.

2.2.11. Densification

Handling, transporting, storing, managing and using biomass in its original form is challenging because of its low bulk density, varying size and uneven shape (Kizuka et al. 2019). These problems may be overcome by densification or compaction to increase energy density (Tumuluru & Wright 2010).

Densification is a process to achieve denser and more consistent characteristics than raw biomass (Mani 2005; StelteClemons, et al. 2011). However, the densification process varies depending on biomass type, storage requirements and intended applications. There are generally two methods of feedstock densification: (i) mechanical densification and (ii) pyrolysis (heat application). Mechanical densification is done by applying pressure to the material (LisowskiOlendzki, et al. 2019). Commonly used mechanical densification methods are bales, pellets, cubes, briquettes, pucks and wood chips (Bajwa et al. 2018). A number of densification systems or equipment are commonly used, including: (i) pellet mills, (ii) cubers, (iii) screw extruders, (iv) briquette presses, (v) roller presses, (vi) tablet presses and (vii) agglomerates (Tumuluru et al. 2011).

2.2.11.1. Advantages of densification/pelletising

Agricultural biomass, particularly straw, frequently forms entangled "clumps" in the feeding system due to its varying size and shape (Rahmani et al. 2022). In addition, the irregular feeding system and the unstable combustion or gasification of straw may produce more emissions and overall inefficiency. Thus, industrial heating systems require a uniform feeding operation, so a pelleted form of biomass is often preferable. Holt, G. A., Blodgett, T. L. and Nakayama, F. S. (2006) noted that the residue biomass pellet combustion could produce less ash than raw material.

Pelleting primarily aims to produce homogeneous formation and even physical features (such as size and shape, bulk and unit density, and durability) (Kuranc et al. 2020). Generally, a pellet should have a uniform size (length: 13~19 mm and diameter: 6.3~6.4 mm) and shape (cylindrical) (Tumuluru et al. 2011). Pokhrel, Han and Gardner (2021) reported that the wood pellet's bulk density varies from 700 to 750 kg/m^3.

Pellets provide a homogenous feedstock with particular properties for bioenergy production (Dragutinovic et al. 2019). However, various biomass factors could affect a pellet's density, durability, and quality (Table 2.9). For instance, Shaw (2008) found that process variables (die temperature, pressure and geometry), feedstock variables (MC and particle size/shape) and feedstock composition all have a significant impact on the pelleting biomass quality. According to StelteClemons, et al. (2011), wood-based biomass produces more durable pellets under the same circumstances as straw-based biomass.

Table 2.9: Densification system variables (Puig-Arnavat et al. 2016; Pradhan, Arora & Mahajani 2018)

Biomass	Densified fuel	
	Factors	Methods
▪ Moisture content ▪ Calorific value ▪ Proportions of fixed carbon ▪ Volatile substances ▪ Ash content ▪ Alkali metal content ▪ Cellulose/lignin ratio	▪ Moisture content ▪ Pressure ▪ Temperature ▪ Additives (Binding materials)	▪ Densification methods (pelleting, briquetting)

2.2.12. Pelleting process

The pelleting process follows several basic steps: drying, grinding, pelleting, cooling and screening (Karkania, Fanara & Zabaniotou 2012) (Figure 2.5). The initial comminution is carried out before drying (especially in the case of a straw). After drying, the material is cut into small pieces using a cutting/chopping or hammer mill. A pellet mill consists of a circular die with perforated holes and rollers. The rollers help to force the biomass; consequently, biomass is consistently fed into the pellet mill, producing the pellets (Jackson et al. 2016). The commonly used pellet mills are screw extruders, roller plates, and die pellet mills.

Pellet production capacity and efficiency depend on several factors, such as the mill's features (die temperature, die capacity, roller configuration, pressure), biomass moisture and feedstock feeding rate (Holt, G. A., Blodgett, T. L. & Nakayama, F. S. 2006; Uslu, Faaij & Bergman 2008). The key pelleting factor is the pressure applied with the high temperature for material compaction (Pradhan, Arora & Mahajani 2018). Both temperature and pressure make the biomass polymer soften and transform a glassy form into a plastic form for pelleting.
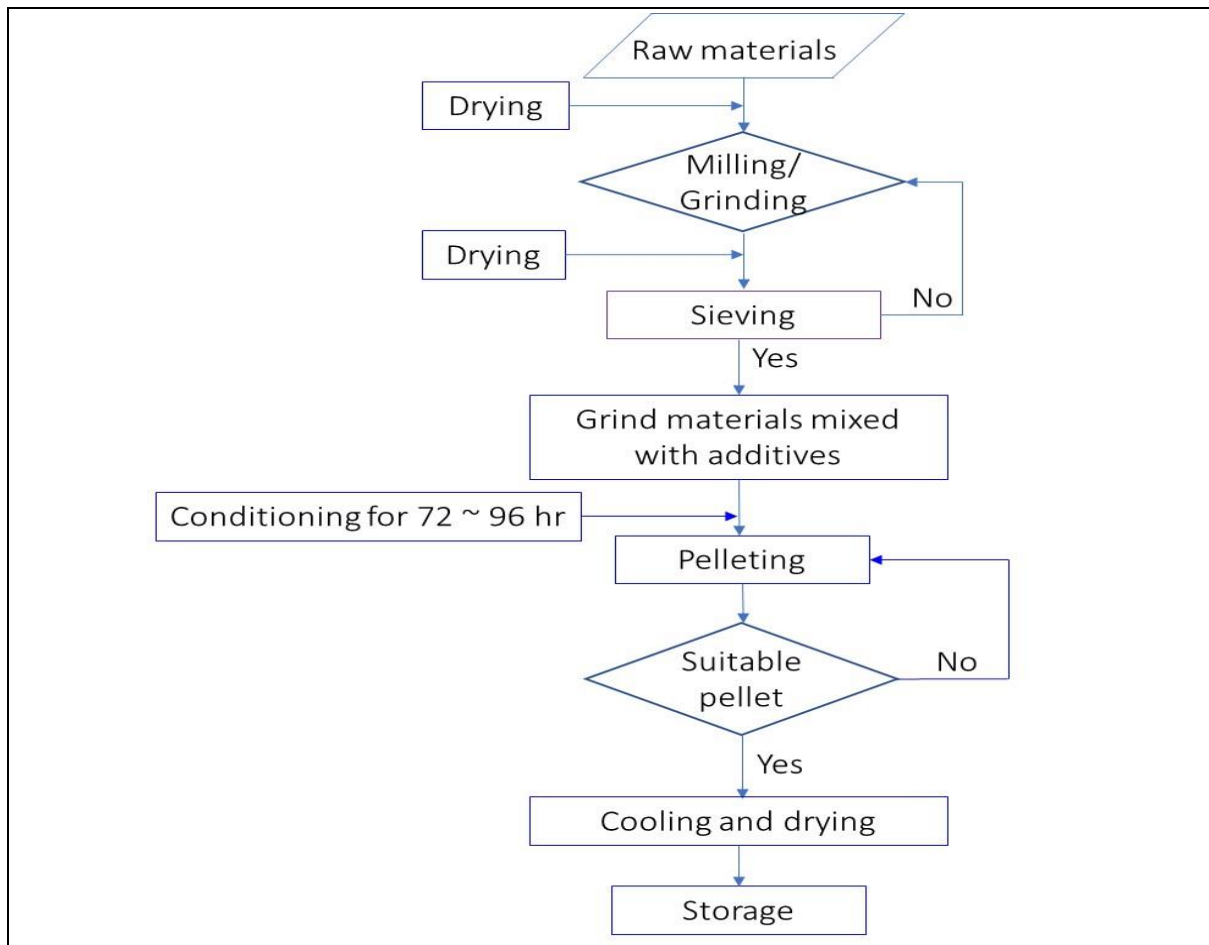
Figure 2.5: Flow chart for pellet processing

Each straw biomass has a distinct lignocellulosic content and bonding structure. As a result, a pretreatment (pressing or compressing) is also necessary to release the lignin bonds that hold cellulose and hemicellulose together. Steam, acid/alkali and biological fermentation processes are common possible pretreatments for modifying bonds (Agbor et al. 2011). The steam treatment is frequently used on an industrial basis where steam is applied at 180~240°C to break up the cellular structure (Shahrukh et al. 2016). Alternatively, biological fermentation is also encouraging, but this method is challenging in large scale industries to achieve colder process efficiency (Agbor et al. 2011). Sultana and Kumar (2012) noted that biological methods might be economically inefficient for nonwoody biomass pelleting. Overall, most researchers suggest mixing binders or additives to increase the pellet's durability, longevity and thermal properties (Wang, T. et al. 2020). Tarasov, Shahi and Leitch (2013) also examined the different biomass sources for pellet improvement and found a positive impact on pellet strength and heating value.

More information is available on recent studies on WS pellet-making objectives and findings in Table A2 (Appendix A). The extensive investigation was mainly limited to additives' impact on pellet qualities and establishing suitable pelleting methods.

2.2.13. Standard quality of a pellet

Pellet quality is usually assessed by its durability, ash content, heating value, density, etc. (García et al. 2019). A quality pellet ensures a uniform feeding system, fewer dust emissions, and minimises the risk of fire and explosions during handling, storage and transportation (Jangam, Karthikeyan & Mujumdar 2011). Pellet quality is particularly important for small-scale boilers and stoves designed for household use. These domestic stoves/boilers have a significantly lower tolerance than boilers with higher capacities (García et al. 2019). In comparison, the larger industrial pellet boilers use lower-quality pellets without causing the same issues because of their more advanced combustion, process control and flue gas cleaning systems. Therefore, two pellet qualities, one for industrial and one for small scale, are available (Obernberger & Thek 2004).

The United States and Europe have developed the quality standard for wood pellets for household heating (Holt, G. A., Blodgett, T. L. & Nakayama, F. S. 2006; Toscano et al. 2013; Duca et al. 2014). The ISO and EN*plus* have also published pellet quality guidelines (based on market requirements and international trade) to assess pellets' physiomechanical and chemical properties threshold values (Zeng et al. 2017). In particular, ISO 17225-2 defined the wood pellets' specifications for industrial and nonindustrial use (ISO 2014). EN*plus* is a global certification programme that evaluates pellet quality for nonindustrial use and establishes the requirements for pellets following the ISO guidelines (Table 2.10) (Jelonek et al. 2020).

The recommended guidelines (EN*plus*) have three subclasses, A1, A2 and B standards (ENplus 2015). Untreated wood or raw biomass pellets (A1) are used in residential, small commercial, public buildings and industrial energy generation applications. Most non-industrial pellets traded are of A1 quality, while A2 quality pellets are used in larger installations (>50 kW) and B quality pellets in large CHP or district heating units. Further, the commercial (A) and residential (B) applications of solid biofuels are characterised under the ISO 17225-8-2014: Part-6: graded nonwoody Pellet standard (ISO 2014). More information on pellet quality standards is available in Tables A3 and A4 (Appendix A).

Table 2.10: Standard quality threshold values for pellets

Property class	Unit	Nonindustrial use (ENplus 2015)			Industrial use (ISO 2014)		
		ENplus A1	ENplus A2	ENplus B	I1 industrial	I2 industrial	I3 industrial
Diameter	Mm	6, 8 (±1)	6,8 (±1)	6, 8 (±1)	6, 8 (±1)	6, 8, 10 (±1)	6, 8, 10, 12 (±1)
Length	Mm	3.15~45	3.15~45	3.15~45	3.15~40	3.15~40	3.15~40
Moisture content	w %, ar	≤10	≤10	≤10	≤10	≤10	≤10
Ash content	wt %, db	≤0.7	≤1.2	≤2.0	≤1.0	≤1.5	≤3.0
Durability	wt %	≥98.0	≥97.5	≥97.5	≥97.5	≥97.0	≥96.5
Fines	wt %	≤1.0	≤1.0	≤1.0	≤ 2.0	≤ 2.0	≤ 2.0
Net energy value	MJ/kg, ar	≥16.5	≥16.5	≥16.5	≥16.5	≥16.5	≥16.5
Bulk density	kg/m^3, ar	600~700	600~700	600~700	≥600	≥600	≥600
Additives	w %, ar	≤2.0			-	-	-
Nitrogen	w %, db	≤ 0.3	≤ 0.5	≤1.0	≤0.3	≤0.3	≤ 0.6
Sulphur	w %, db	≤ 0.04	≤ 0.05	≤0.05	≤ 0.05	≤ 0.05	≤0.05
Chlorine	w %, db	≤0.02		≤0.03	-	≤ 0.10	≤ 0.20
Ash deformation temperature	°C	≥1200	≥1100		-	-	-

Note --- ar: as received; db: dry basis;
Grade A1: Premium pellets - for use in any residential heater or commercial boiler.
Grade A2: Large premium pellets - for use in selected boilers.
Grade B: Commercial grade pellets for use in selected boilers subject to resource and boiler manufacturer consents.
Grade I: Industrial grade.

2.2.14. Energy application of biomass

Biomass is a popular bioenergy energy source with benefits regarding availability, sustainability and diversity (Tezer et al. 2022). Several approaches convert biomass into bioenergy (Fatma et al. 2018; Alam & Tanveer 2020). The conversion method or process is mainly determined based on biomass physicochemical characteristics (Narnaware & Panwar 2022b). The thermochemical conversion processes are outlined in Figure 2.6.
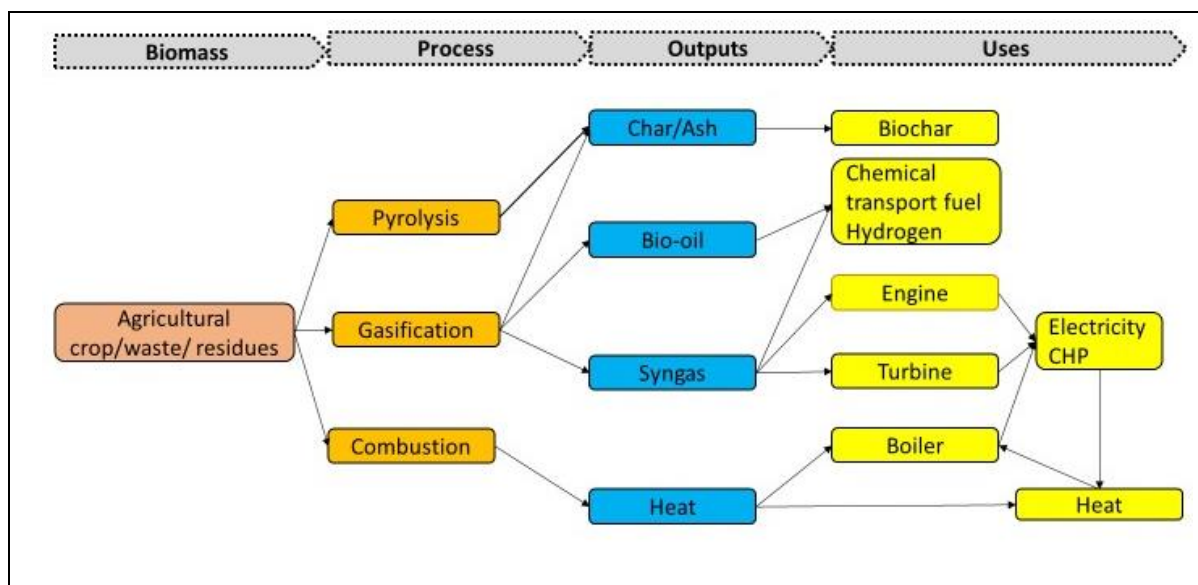
Figure 2.6: Biomass energy production pathway

The present work investigated biomass-to-bioenergy conversion through densification and thermochemical conversion pathways like pyrolysis, combustion, and gasification. The following subsections provide an overview of these processes only.

2.2.14.1. Combustion

Combustion is a complex process where a group of chemical reactions occur in which substances (solid, liquid or gas) react rapidly with oxidizing agents (air, nitrogen and mixture) and produce exhaust and heat (Bhoi et al. 2018). Inadequate combustion releases environmental polluters such as NO_X, SO_2 and PM (particulate matter) (Yang et al. 2021). Exhaust usually occurs as a gas, but there can be liquid or solid exhaust products (soot). Generally, heat is generated during combustion because fuel and oxidisers are turned into exhaust products. Heat resources are also necessary to initiate combustion (e.g., gasoline burning). Therefore, three conditions must be fulfilled for combustion: a fuel (to be burned), an oxidising agent source and heat (Jenkins, Baxter & Koppejan 2019). The combustion process can be controlled or stopped by regulating the above factors. In addition, once combustion begins, it does not need to supply an additional heat source because the heat from the combustion will keep things going. It just keeps burning.

$$\text{Substances + Oxidising agents + (heat)} \xrightarrow{Combustion} \text{Exhaust + heat}$$
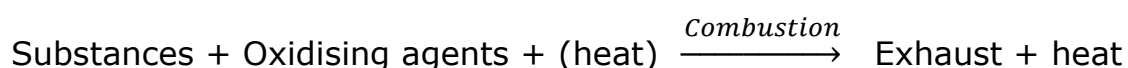
The combustion process usually occurs at 700 to 1000°C, where heat is the main product (Shah et al. 2018). Ullah et al. (2015) described that combustion is not an economically efficient way to use biomass because it is difficult to recover the total stored energy. Also, it has been noted that direct biomass combustion accounts for about 95~97% of the world's

bioenergy output (Fouilland, Grace & Ellis 2010). In contrast, some residual gas is produced due to hydrocarbons' complete or partial combustion (Zhang, Y. et al. 2019).

2.2.14.2. Pyrolysis

A thermal process known as pyrolysis turns biomass into liquid, gas and solid in an oxygen free environment at 250~550°C (Collard & Blin 2014). Osman et al. (2021) reported that the pyrolysis system is a favourable route for biomass-to-bioenergy conversion because it operates at lower temperatures than a gasifier (800~1300°C). The pyrolysis process decomposes the polymeric components (cellulose, hemicellulose, lignin, extractives) into volatile vapours consisting of O- and H- comprising forms and producing bio-oil (Teh et al. 2021). During the pyrolysis, the volatile vapour becomes gas, and the remaining residue is carbon enriched ash (Sharma et al. 2021).

The pyrolysis process is categorised into three groups: flash pyrolysis, fast pyrolysis and slow pyrolysis, based on several operational conditions (time and temperature) and desired outcomes (Table 2.11) (Al-Rumaihi et al. 2022). A reactor's operating conditions (temperature and residence time, pressure, inert gas type and flow), reactor configuration and the chemical composition of biomass can strongly influence product yield (Fahmy et al. 2020). Overall, pyrolysis process selection depends on the expected results.

Table 2.11: Working modes of the various pyrolysis process (Bridgwater 2012)

Pyrolysis mode of thermal conversion	Factors		Yield, %		
	Temperature, °C	Residence time	Liquid	Solid (Char)	Gas
Slow	~400	Hours to days	75	12	13
Intermediate	~500	~10~30 s	50 (In two phases)	25	25
Fast	~500	~1 s	30	35	35
Flash	~500	Very short (< 0.5 s)	75	<13	<12
Gasification	750~900	Long	5	10	85
Torrefaction	~290	~10~60 min	5	-	-

2.2.14.3. Pyrolysis processes and yields

Generally, biomass is pyrolysed through the subsequent steps:

▪ The transfer of heat from the source to the biomass initiates decomposition at temperatures below 200°C (Singh et al. 2020). At this point, the biomass moisture is evaporated and has no chemical source, termed chemically inert.

- Devolatilisation is the second stage, where most of the volatile matter leaves the biomass, which helps to give it high reactivity. This reactivity is closely related to the ignition temperature (Mishra & Mohanty 2020). In this stage, the hemicellulose thermal breakdown occurs because of temperature, and the weak polymeric structure follows at 390°C of pellet temperature (Cen et al. 2019).

- Carbonisation is the third step. It occurs when secondary volatiles transform into gas and the reaction rate slows. In this stage, the autocatalytic secondary pyrolysis reactions occur conjugate with the pyrolytic primary response (Demirbas 2009). At the same time, tar is produced due to secondary reactions and volatile condensation. Finally, most biomass components (cellulose, hemicellulose and lignin) decompose and are converted into light gases (CO, CO_2, CH_4), water and char (Mishra & Mohanty 2018).

Pyrolysis products can be categorised into solids, liquids and gases (Akhtar, Krepl & Ivanova 2018). The pyrolysis yield depends on the operational mode of the process (Chen, X. et al. 2019). For instance, catalytic pyrolysis is gaining popularity due to a decrease in the operating temperature and an increase in the product yield. This process maximises biomass conversion to liquid fuels through better physicochemical qualities (Cai et al. 2019). In addition, a novel thermochemical process called microwave-assisted pyrolysis converts the feedstock of biomaterials into liquid oil (Ingole et al. 2016). In this method, microwave input heat energy is more efficient and can be better controlled than the traditional approaches (slow/fast pyrolysis) (Ethaib et al. 2020). Furthermore, CO_2-assisted pyrolysis uses reactive CO_2 rather than inert N_2 to increase the syngas output, decrease the generated oil, and lower glasshouse gas emissions (Kwon, Kim & Lee 2019). However, the abovementioned pyrolysis method is used for a specific purpose, and the operation is sophisticated.

The additive-assisted pyrolysis includes the addition of inorganic additives like zeolites and charcoal as well as metal salts including sodium, potassium and calcium salts (Yuansheng, He & Shenghua 2007). This method offers several benefits over traditional pyrolyses, such as minimising operational temperature requirements, significantly increasing waste cracking efficiency, shortening cracking times, and improving the pyrolysis products' output (Liu, Y. et al. 2021). Moreover, solar pyrolysis is a technique that increases biofuel production and lowers CO_2 emissions by using sustainable solar energy as a thermal input source rather than electrical energy (Zeng et al. 2017).

One form of pyrolysis where biomaterial feedstock breaks down is hydropyrolysis. It can produce more hydrocarbons with better structural

qualities (Oh et al. 2021). Alternatively, fast pyrolysis (flash and ultrarapid) takes milliseconds or seconds, primarily maximising bio-oil and gas production (Nzihou et al. 2019). According to Bridgwater (2012), fast pyrolysis liquid yields up to 75% by mass and involves rapid heating to temperatures of between 450~600°C. Materials are heated slowly at a heating rate between 5 to 50 °C/min with the longest residence time (Park et al. 2014; Das & Tiwari 2018). In comparison, carbon is the main product (about 80%) of the slow pyrolysis process. Therefore, slow pyrolysis is frequently used due to its simple operating conditions and low cost.

2.3. Thermal analysis

Thermal analysis (TA) is a series of methods for examining a material's characteristics as they change with temperature and time (Aslan et al. 2018). Generally, thermal analysis determines conversion efficiency, mass changes and reaction rate (Weidenkaff et al. 2000). Various thermal analysers with specific functions are shown in Table 2.12.

Table 2.12: Thermal analysis methods and measured properties (Balat & Ayar 2005)

Sl. no.	Methods	Measured property
1	Thermogravimetric analysis (TGA)	Mass/weight change at a controlled temperature
2	Differential thermal analysis (DTA)	Temperature difference
3	Differential scanning calorimetry (DSC)	Heat difference between the sample and the reference
4	Pressurised TGA (PTGA)	Mass changes as a function of pressure
5	Thermomechanical analysis (TMA)	Deformations and dimension
6	Dilatometry (DIL)	Volume
7	Evolved gas analysis (EGA)	Gaseous decomposition products
8	Combined methods	Combined properties

2.3.1. Thermogravimetric analysis

Thermogravimetry (TG) is a branch of thermal analysis that measures the sample mass change (Zhou et al. 2006). These measurements can be done concerning temperature or time in nitrogen, oxygen, argon, helium, air and another gaseous atmosphere (Olatunji et al. 2018). A thermogravimetric analyser (TGA) is used for kinetic data measurement (Cai et al. 2018). TGA measures changes in weight (mass loss curves) with temperature changes that give detailed information such as sample composition, thermal stability, materials purity and kinetics for chemical reactions (Aslan et al. 2018). In addition, a derivative weight loss (DTG) curve can be applied to determine the weight loss rate (Table 2.13).

Table 2.13: Details mass change phenomena (Zhang, Xu & Champagne 2010; Olatunji et al. 2018).

Mass/weight changes mechanism	Phase
▪ Gas adsorption *(WG)* ▪ Gas desorption *(WL)* ▪ Phase transitions *(WL)* 　‑ Fusion 　‑ Vaporisation 　‑ Sublimation ▪ Reduction: Interaction of sample to a reducing atmosphere *(WL)* ▪ Evaporation*: Loss of volatiles with elevated temperature (WL)*	Physical
▪ Decomposition: Breaking apart chemical bonds *(WL)* ▪ Breakdown reactions *(WL)* ▪ Gas reactions *(WG/L)* ▪ Combustion *(WG/L)* ▪ Oxidation: Interaction of the sample with an oxidising atmosphere *(WG)* ▪ Chemisorption: adsorption employing chemical instead of physical forces *(WG)*	Chemical

Note; WG: Weight gain steps; WL: Weight loss steps

2.3.2. Thermogravimetric analyser

In-depth knowledge of biomass TGA is important for the design, scale of industrial operations and evaluations of reactors (Grønli, Várhegyi & Di Blasi 2002). A number of research studies have used TGAs to study the pyrolysis and combustion of coal and woody biomass (Gil, María Victoria et al. 2010; Idris et al. 2010; Boukaous et al. 2018; Mureddu et al. 2018; Barzegar et al. 2020; Singh, Patil & Sawarkar 2020; Wang, T. et al. 2020). However, fewer studies have examined agricultural biomass's combustion and pyrolysis properties and thermal decomposition using TGA (Quesada et al. 2018; Xu et al. 2018; Liu et al. 2020).

A significant amount of research has been done on TG of different biomass feedstock and these studies are listed in Table A5 (Appendix A). TGA studies on WS pellets pyrolysis and combustion are minimal (Gil, María Victoria et al. 2010; Mian et al. 2020; Sher et al. 2020). Based on the TGA analysis, White, Catallo and Legendre (2011) concluded that a range of variables, including process conditions, heat and mass transfer restrictions, the physical and chemical heterogeneity of the sample, and systematic mistakes, could influence the sample kinetic parameters. Saddawi et al. (2010) focused on the data analysis methods for determining kinetic data and reported that TGA provides more reliable data than experimental results. Liu, L. et al. (2021) recently investigated the pyrolysis and combustion properties of maize straw powder, poplar wood chips and rice husk, highlighting their energy conversion processes. Jia (2021) studied the TG analysis of five pellet fuels (Masson pine, Chinese fir, Willow, Slash pine and Poplar) and found good combustion and kinetic characteristics. Therefore, this study's comprehensively calculated reactivity, activation energy, heat flow, and mass transfer rates were enabled by a complete kinetic analysis of WS pellets. Regarding this aim, the study focused on: (i) WSP pyrolysis in a laboratory kiln and (ii) TGA for pyrolysis and combustion.

2.3.3. TG and DTG profile

Kinetic parameters are important for understanding a fuel's thermal behaviour and the chemical impact of physical properties on the reaction (Ding et al. 2017). Fuels' thermal stability and overall kinetic decomposition are guided by TG and DTG profiles (Pis et al. 1996). These curves estimate pyrolysis or combustion characteristics such as average weight loss, reaction rate and peak temperature (Figure 2.7) (Munir et al. 2009; Yuzbasi & Selçuk 2011). The empirical data from the curves (TG/DTG) helps in designing and developing reactors as well as the kinetic model and simulations (Figure 2.7) (Sher et al. 2020).

A significant amount of research has been conducted on biomass decomposition investigation through the TG/DTG profile. Therefore, thermogravimetry (TG/DTG) analyses and TGA data have been used to determine reaction areas, ignition and burnout temperatures at various heating rates. Thermal decomposition and combustion characteristics of biomass materials using TG/DTG at different high heating rates and sizes in the air were investigated by Ismail and El-Salam (2017). They reported that heating rate, lignocellulosic composition and types of gas flow influence materials' thermal decomposition mechanisms and kinetic parameter values. A recent study was conducted by Vuppaladadiyam et al. (2021) on thermogravimetric and kinetic examination of the effect of microalgae on synergism during co-pyrolysis with organic waste biomass.

TG and DTG curve (Zhai et al. 2016)	TG (a) and DTG (b) curves on the heating rate (Al-Moftah, Marsh & Steer 2021)
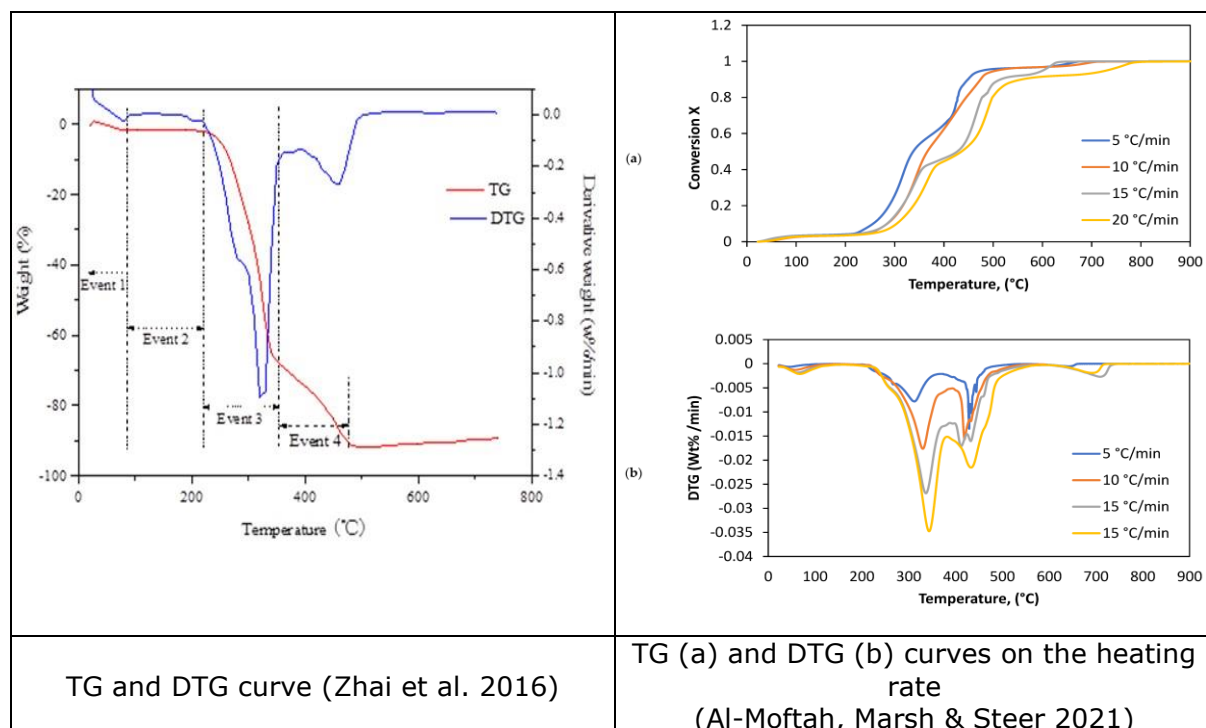
Figure 2.7: Thermogravimetric and Derivative Thermogravimetric profile

2.3.3.1. Thermal conversion phase of biomass

The thermochemical process involves complex chemical and physical functions. During the thermochemical conversion process, solid biomass runs through different phases as (i) volatilisation/drying, (ii) devolatilisation, (iii) oxidation and (iv) reaction (Figure 2.8) (Puig-Arnavat, Bruno & Coronas 2010). Each phase has its particular chemistry and operational conditions summarised as follows.
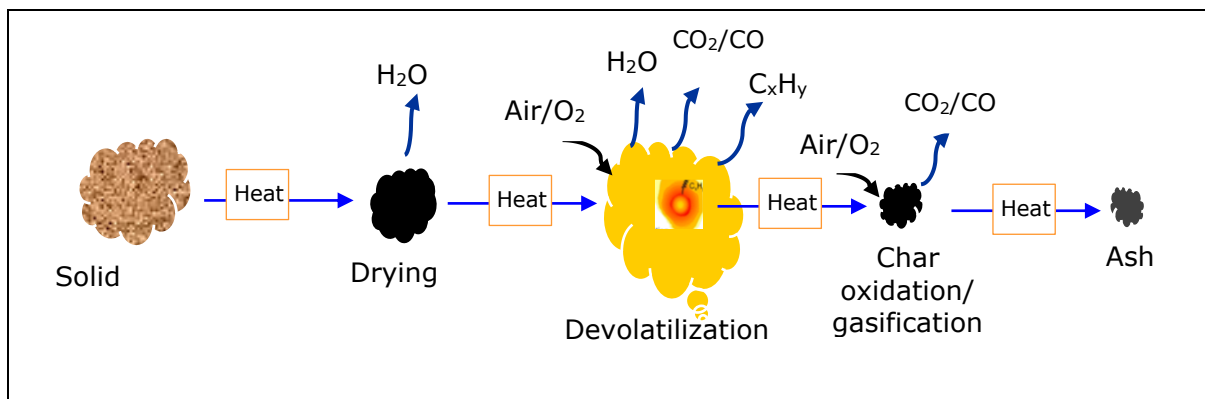
Figure 2.8: Thermochemical conversion of solid biomass fuel

- Vaporisation phase: The initial heating stage is when the water content is vaporised (Singh, Patil & Sawarkar 2020).

- Devolatilisation/pyrolysis phase: The devolatilisation stage commences when the biomass temperature reaches a crucial point. Char and volatiles are the end products in this stage. The volatiles condenses into a thick liquid while a small amount of fumes escape (Natarajan, Nordin & Rao 1998). The pyrolysis process is set up to achieve high devolatilisation, which results in high conversion efficiency for char generation or bio-oil production (Mandal et al. 2022).

- Tar cracking phase: The condensable hydrocarbon combination creates tar. Tar may crack when heated, resulting in homogeneous reactions (gas phase) and heterogeneous reactions on the surface of solid fuel or char particles (Kumar, Mishra & Upadhyay 2020). The heat ignites char and releases volatiles (Sharma et al. 2021). The oxidant and other species undergo homogeneous reactions with the devolatilisation and cracking of gas species.

- Reduction/gasification phase: Char will interact with the gas species in heterogeneous reactions as the residue after devolatilisation (Souza-Santos 2010; Mendiburu, Carvalho & Coronado 2014). The gasification aim is a high conversion of combustible gases to produce combustible gases (CO, CH_4, H_2 and small amounts of hydrocarbons), including tar cracking. On the other hand, the combustion's primary intention is to produce heat energy (with a rich oxidant/fuel mix) and transform fuel into CO_2 and H_2O.

2.3.3.2. *Chemical reactions and produced gas*

The biomass thermal conversion process undergoes several activities where the primary output is liquid, solid or gas (Figure 2.9). The process can also be expressed as (i) particles decompose to char, tar and gaseous products, (ii) reactions among the gaseous products and (iii) tar cracking and char gasification (Lü et al. 2008; Nikoo & Mahinpey 2008; Puig-Gamero et al. 2021). Overall, some chemical reactions happen among the biomass elements such as C, H_2 and O_2, which produce the gaseous product (Table 2.14) (Widjaya et al. 2018). Also, the gasifying agents react with the biomass elements and create a mixture of the permanent gases CO, CO_2, H_2, and CH_4 (Murgia, Vascellari & Cau 2010).
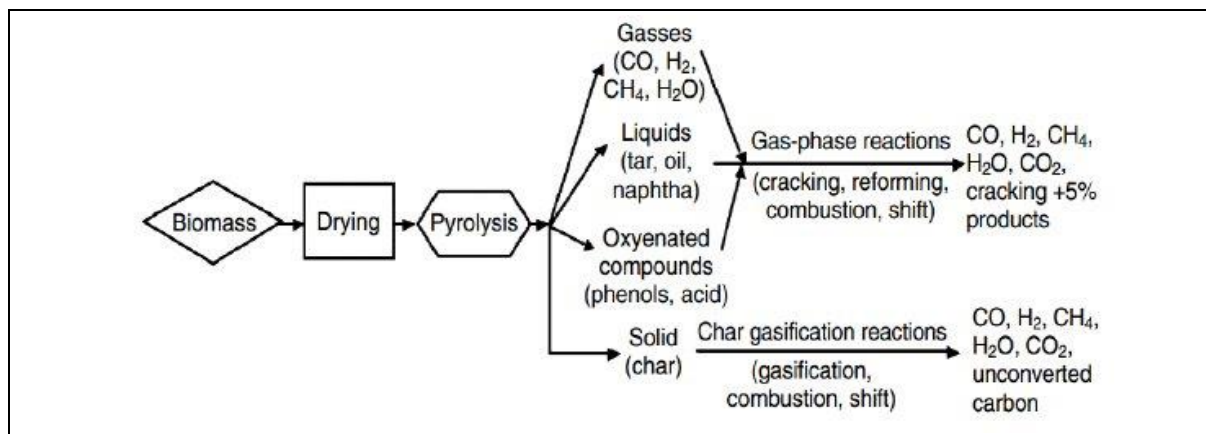
Figure 2.9: Schematic steps of biomass gasification (Pradana & Budiman 2015)

Table 2.14: List of reactions and gasses produced during thermal reactions (Van der Drift et al. 2004; Knoef 2005; Higman et al. 2008; Doherty, Reynolds & Kennedy 2009)

Reaction type	Gasification zone	Reaction and heating value (MJ/kmol)	Name of reaction
Heterogeneous reactions	Oxidation zone	$C + \frac{1}{2}O_2 = CO$ -111	Char partial combustion
	Reduction zone	$C + CO_2 \rightleftharpoons 2CO$ +172	Boudouard reaction
		$C + H_2O \rightleftharpoons CO + H_2 + 131$	Water gas reaction
		$C + 2H_2 \rightleftharpoons CH_4 + H_2O$ - 75	Methane production
		$CO_2 + 4H_2 \rightleftharpoons CH_4 + H_2O$ - 223	
Hydrogen sulfide and ammonia formation reaction	Reduction zone	$H_2 + S \rightleftharpoons H_2S$	H_2S formation
		$\frac{1}{2}N_2 + 1\frac{1}{2} H_2 \rightleftharpoons NH_3$	NH_3 formation
Homogeneous reactions	Oxidation zone	$CO + \frac{1}{2}O_2 = CO_2$ - 283	CO partial combustion
		$H_2 + \frac{1}{2}O_2 = H_2O$ – 242	H_2 partial combustion
	Reduction zone	$CO + H_2O \rightleftharpoons CO_2 + H_2$ – 41	CO shift
		$CH_4 + H_2O \rightleftharpoons CO + H_2$ -206	Steam methane reforming

Note; Negative sign indicates an exothermic reaction and a positive sign shows an endothermic reaction

2.4. Gasification and gasifier types

Gasification is an old art developed over 150 years ago (Bridgwater 1995). The predominant gasification technology aims to efficiently convert feedstock/biomass stored energy into syngas (El-Emam, Dincer & Naterer 2012) and solid fuel (Molino, Chianese & Musmarra 2016). The gasifier is classified based on design, gasifying agents, temperature, pressure, heat supply method and heat sources (Motta et al. 2018). The available gasifier types are summarised in Table A6 (Appendix A).

Ahmad et al. (2016) state that the gas produced, and emission levels are related to gasification types and design. Three types of gasifiers can be used for biomass gasification (Molino et al. 2018; Watson et al. 2018). These include fixed bed, moving bed/fluidised bed (bubbling, circulating and twin bed), and entrained flow (Tezer et al. 2022). Gasifiers have many designs, benefits and drawbacks when used to produce syngas (Appendix A, Table A7). However, each type of gasifier needs specific operating conditions and feedstock characteristics.

The fluidised bed gasifier is suitable for stationary use. Therefore, it is commonly applied for medium to significant scales (up to 1 MW or even higher) (La Villetta, Costa & Massarotti 2017; Sezer & Özveren 2021). This gasifier's main disadvantage is that the produced gas contains a relatively high temperature (800~900°C), alkaline vapours and tar. The feedstock particles of the fluidised bed gasifier must be very small so that they can be mixed with other solids. Also, a cyclone separator is needed to remove high particle content from the outlet gas (2~20%) (Mansaray et al. 1999). Therefore, this gasification method is generally expensive and unsuitable for small to medium scale farm applications.

An entrained flow gasifier needs finer particles (Roberts & Harris 2015). This type of gasifier often operates with a high temperature and pressure, resulting in rapid conversion (residence time of a few seconds). It allows high throughput (98~99.5%) with large capacities (>1 MW) (Knoef 2005; Puig-Arnavat, Bruno & Coronas 2010). However, the entrained flow gasifiers' thermal efficiency is low because water is mixed with syngas. One of the other main disadvantages is that the high temperature tends to shorten the lifespan of system components. Overall, relatively complex construction, operation and costly feed preparation are the main drawbacks of this gasifier (Beenackers 1999).

Among the different reactors, a fixed bed gasifier is the oldest and most straightforward to construct (Hoque, Rashid & Aziz 2021). Generally, this reactor type includes carbon transformation, prolonged heating time, and minimal ash residue (Reed & Das 1988; Lucas 2005). Downdraft gasification technology has attracted increased interest due to its suitability for small scale (~200 kW) operation at an affordable price (Reed & Das 1988; Puig-Arnavat, Bruno & Coronas 2010; Beohar et al. 2012). For

instance, a review of gasifier producers in Europe, the US and Canada revealed 50 manufacturers selling commercial gasification facilities; 75% of which used fixed bed downdraft systems, 20% used fluidised bed techniques, 2.5% used updraft systems, and 2.5% used a variety of alternative designs (Knoef 2005).

2.4.1. Downdraft gasifier

A fixed bed gasifier is a conventional technology for the gasification process and can be classified as updraft, downdraft, and crossflow according to the airflow direction (Yucel & Hastaoglu 2016; Sharma et al. 2021). An auto heating system (*pyrocoil*) provides the heat for a downdraft fixed bed gasifier, which can be cost effective for small to medium sized capabilities (Chen 2014; Zhang et al. 2018). Therefore, researchers often consider it the most sustainable way of generating direct heat at the on-farm level (Pradhan, Mahajani & Arora 2018).

In the downdraft gasifier, the feedstuff flows downward, allowing all pyrolytic products to pass through the hot combustion zone and thermally split some tar into noncondensable tar and water (Soomro et al. 2018). The producer gas from this system will have less tar in it. Moreover, regarding the tar and particulate issues, the downdraft gasifier is more suitable than the updraft, fluidised bed and entrained flow gasifier (Susastriawan, Saptoadi & Purnomo 2017). More information regarding the comparative advantages of the gasifiers is listed in Tables A8 and A9 (Appendix A).

Downdraft gasifiers usually have two designs: the Imbert gasifier (throated or closed top) and the stratified gasifier (throat less or open core) (Watson et al. 2018) (Appendix A, Table A10). An open top or throat less gasifier forces air to move downwards to prevent hot spot formations. This small sized gasifier facilitates high flexibility and efficiency in processing certain solid materials (Martínez et al. 2012). It is also easier to construct and has good scaleup properties (Bhavanam & Sastry 2011). However, tar content is high, and the process can be unstable. Alternatively, the throat increases gas turbulence and raises the combustion zone temperature, affecting the tar cracking thermally (Reed & Das 1988). The Imbert gasifier has a throat, resulting in a lack of oxygen in the oxidization zone for higher temperature reactions. Typically, the Imbert gasifier requires a low moisture content (less than 20%) and a uniform blocky fuel (densified fuel) to allow gravity to feed through the constricted hearth.

Gasification research has been carried out at a medium to large scale in a fluidised bed and entrained bed reactors (Pinto et al. 2003; Xu 2013; Howaniec & Smoliński 2014; Mahapatro, Kumar & Mahanta 2020; Martínez et al. 2020). Only a few studies have been conducted on a small scale (Kumabe et al. 2007), not counting the small laboratory scale.

2.4.2. Factors influencing the gasification

Gasification efficiency and output depend upon several factors, including temperatures, feedstock and reactor (Ismail & El-Salam 2017) (Table 2.14). The following section discusses several important gasification factors.

Table 2.15: Gasification operating parameters and yield products

Gasification factors	Gasification products
▪ *Operating condition:* temperature, pressure	▪ *Gaseous products:* CO, H_2O, CO_2, H_2, CH_4
▪ *Gasification agent:* air, stream, water, CO_2	▪ *Solids:* char, ash
▪ *Bed materials:* CaO, Nickle, sand	▪ *Condensable:* tars, oils
▪ *Feedstock:* types, particle size, moisture content, flow rate	▪ *Noncombustible gas:* CO_2, H_2O
	▪ *Combustible gas:* CO, H_2, CH_4
▪ *Gasification types:* fixed bed, moving bed	▪ *Emissions:* NO_x, So_x, PM_{10}, PM_5, $PM_{2.5}$, ozone, lead
▪ *Others:* equivalence ratio, steam to biomass ratio, superficial velocity, lower heating value, higher heating value	▪ *Environmental issues:* CO_2, S_2O, N2, dust
▪ *Cost:* operation	▪ *Emissions:* CO_2, SO_2, NO_x, O_2

- *Gasification temperature*

The gasification temperature significantly impacts the syngas composition, carbon conversion and overall efficiency (Watson et al. 2018). Gil et al. (1999) stated that the temperature limit for biomass gasification is between 550 and 900°C. It has been reported that the maximum temperature for coal gasification in fluidised bed gasifiers is between 750 and 1000°C (Lee et al. 1998). Moreover, several experimental results have shown that temperature increases to 1100°C influence gas composition (Pinto et al. 2003; Luo et al. 2018). Generally, a higher temperature is preferred for hydrogen production (Lv et al. 2004). The advantages of higher temperatures are increasing the H_2 and CO production whilst decreasing the CH_4 and CO_2 concentration and lowering the char and heavy tars (Ciferno & Marano 2002; Skoulou et al. 2009).

When a reaction occurs, it absorbs or releases energy from its surroundings. In addition, gasification reactions are firming up due to temperature. These two thermodynamic reactions are exothermic or endothermic (Narnaware & Panwar 2022a). Most gasification reactions inside gasifiers are endothermal, apart from the combustion zone (Udomsirichakorn & Salam 2014). High temperatures also favour endothermal reactions, producing more tar cracking and H_2 and CO (Chen et al. 2015). Hence, the temperature of this investigation was kept at 600~1200°C to optimise the downdraft gasifier output.

- *Gasification agent*

The gasification agent also impacts gas composition and heating value (Habibollahzade, Ahmadi & Rosen 2021). The agent-to-fuel ratio is one of the key factors influencing the process temperature. For gasification, steam, CO_2, air, oxygen, or a combination are often used as agents *(Xu, Pang & Levi 2011; Widjaya et al. 2018; McCaffrey et al. 2019)*. Air gasification is cheap, widely used, and ideal for small scale applications *(Zhang et al. 2015)*. However, it comprises a high proportion of nitrogen, resulting in syngas with a low LHV *(Pinto et al. 2003)*. Conversely, oxygen increases the LHV because of nitrogen removal, but pure oxygen use can increase plant operating costs as well as safety problems (Pinto et al. 2003). In addition, air separation units and distribution systems are needed for this approach. While applying steam can produce high quality syngas, it needs an external heating system for steam production (Karl & Pröll 2018). Therefore, this research applies to air as the gasification agent.

- *Equivalence ratio*

The difference between the actual air-fuel ratio (used in gasification) and the stoichiometric air-fuel ratio for combustion is known as the equivalence ratio (ER) (Guo et al. 2020). ER values significantly influence gasification products (Park et al. 2020). For instance, if ER is lower than 0.2, pyrolysis dominates gasification. Conversely, combustion governs gasification if ER is higher than 0.4 (Olgun, Ozdogan & Yinesor 2011). For complete combustion to occur, ER should equal 1 (Mevissen et al. 2009). Meng, Meng and Zhang (2018) recommend that the typical ER for effective gasification varies between 0.2~0.4.

2.4.3. Modelling and simulation

The thermochemical conversion of fuel depends on several interacting elements such as fuel mix, operating conditions and converter design (Xue, Zhong & Zhang 2019). Laboratory research on fuel thermokinetic behaviour is frequently used to determine the kinetic changes in the material phase. Sometimes, the laboratory study can differ from the upscale situation and change in an upscale setting. Equipment design, however, impacts the outcomes of the more complicated gasification process considerably. Typically, computer modelling can solve enormous thermal conversion issues and act as a virtual plant.

Overall, a gasification model can be employed to:

- investigate reactor geometry influence (Tinaut et al. 2008)
- investigate gasifier design optimisation (Jarungthammachote & Dutta 2007)
- investigate forces of operational behaviour (Baruah, Baruah & Hazarika 2017)

- investigate the optimisation of the gasifier process (Mendiburu, Carvalho & Coronado 2014)
- assess the impact of input factors' (Kumabe et al. 2007)
- predict gasification performance (La Villetta, Costa & Massarotti 2017)
- forecast the emission and byproducts (La Villetta, Costa & Massarotti 2017).

Mathematical modelling can help to understand gasification principles and operational behaviour (La Villetta, Costa & Massarotti 2017). Various numerical models and simulation tools have been proposed as virtual laboratory simulations for gasification plant design (Jarungthammachote & Dutta 2007). Several models and simulations are currently being used to characterise and optimise gasification performance (Gagliano et al. 2016; Vithanage et al. 2017; Li, Y. et al. 2018). But, biomass gasification modelling is still a developing topic within the various features of biomass (Wang & Yan 2008). Typically, biomass gasification modelling can be categorised as thermodynamic equilibrium, kinetics, and computational fluid dynamics (CFD) (Patra & Sheth 2015; Basu 2018; Dhanavath et al. 2018).

2.4.3.1. Equilibrium model

Thermodynamic equilibrium is the condition where the reactant's concentrations and products do not change significantly over time due to chemical reactions (Valente 2021). The thermodynamic equilibrium hypothesis is predominantly used (Babu & Sheth 2006) because of its simplicity but limited accuracy (La Villetta, Costa & Massarotti 2017). This model forecasts the tendency of influencing parameters rather than the relative experiment value (Ferreira et al. 2019). Also, this equilibrium model considers the ultimate composition of the gasses (Zainal et al. 2001; Mendiburu, Carvalho & Coronado 2014). Two general methods, stoichiometric and nonstoichiometric, could be used in the equilibrium model (Safarian, Unnthorsson & Richter 2020). The stoichiometric technique describes chemical reactions and their products. In contrast, the nonstoichiometric approach relies solely on Gibbs's free energy without mentioning the feed reactions (García et al. 2021). During the calculation of the equilibrium model, considered simplifications/assumptions, resulting in various important chemical reactions, are generally left out, which provides misleading or inaccurate results (Wong & Gunawardena 2020).

The thermodynamic equilibrium model predicts the composition of the products in the theoretical value prediction by using the mole ratios of the specified gas composition (Antonopoulos, I.-S. et al. 2012). The thermodynamic equilibrium model is better suited to predicting feedstock gasification performance (Patra & Sheth 2015). With an approximate composition finding, thermodynamic equilibrium calculates the gas composition. The results of experiments and equilibrium models frequently diverge, especially regarding hydrogen and methane (Prins, Ptasinski &

Janssen 2007). Methane is higher than anticipated, while hydrogen is typically lower. However, some attempts have been made to enhance the model, and it now incorporates the residual chars, tar, equivalent ash, and a model corrected value in the global gasification reaction (Babu & Sheth 2006; Jarungthammachote & Dutta 2007; Barman, Ghosh & De 2012; Simone et al. 2013).

The equilibrium model can better predict the downdraft gasifier's gas composition than the fluidised gasifier's (Torres, Urvina & de Lasa 2019). This is because the gasification temperature is higher in the downdraft type, where the combustion zone is located between the pyrolysis and reduction zones. Additionally, the longer the residence period of the downdraft fuels relative to the fluidised fuels, the closer the condition to the equilibrium state (Baruah & Baruah 2014). Table A11 (Appendix A) summarises the various studies on biomass gasification modelling using equilibrium models.

2.4.3.2. Kinetic model

The Kinetic models depend on evaluating the chemical reactions' kinetic constants k(T) that are used to simulate the thermochemical conversion processes. Kinetic modelling is useful for better understanding reaction mechanisms (Yang, Liu & Wang 2020).

The kinetic model has been applied in several kinds of gasification to determine a reactor's profiles, temperatures and gas compositions (Di Blasi 2000; Kaushal, Abedi & Mahinpey 2010). Particles' dynamic phase change over time is also included in some models. These come in four components: zero stirred tank dimension, one plug flow dimension, two dimensions and three dimensions (Baruah & Baruah 2014). In addition, the kinetic model forecasts yield at a finite period or a finite volume in contrast to the equilibrium model, which predicts yields at an infinite duration (Baruah & Baruah 2014). For operating circumstances and gasifier configuration, the kinetic model can easily forecast the profiles of the reactors (Smith et al. 2019). The predictions made by this model are more precise than those made by the equilibrium model. However, precision depends on the operation parameters, requiring more empirical data and much more computing.

The biomass gasification kinetic model is best suited for char determination as the char conversion rate via kinetic rate expressions (Jayah et al. 2003; Babu & Sheth 2006). The gas composition is expressed by simulating the char reactions, which require empirical kinetic data for precision (Zhang, Xu & Champagne 2010; Xu, Pang & Levi 2011). A volumetric, random pore or decreasing core model can be the foundation for the expression of a kinetic model (Zhang, Xu & Champagne 2010).

Many kinetic models for biomass gasification consider kinetics, hydrodynamics, particle distribution, etc., and these are listed in Table A12 (Appendix A). This model provides more precise predictions (Rizkiana et al.

2014), but the accuracy is specific to the design parameters. Also, this model uses the kinetic data obtained by the TGA, which is questionable because of information variation between the experiment and actual gasification processes (Fernandez et al. 2020). Additionally, kinetic models do not consider several important reactor design considerations, such as the influence of turbulence on the effect of wall reactor design. These elements might have a significant impact on how well gasification works.

2.4.3.3. Computational fluid dynamics model

Computational fluid dynamics (CFD) is a technique of flow predictions by numerically solving governing equations of fluid flows (Bhatti et al. 2020). Governing equations are conservation of mass, momentum, heat and mass transfer. Numerical methods are used to convert partial differential equations into an algebraic set of equations.

The most powerful model is a CFD run by available commercial software (e.g., ANSYS, CFX) (Janajreh et al. 2021). This model can act as a virtual laboratory analysis of the plant (Shiehnejadhesar et al. 2017). The CFD model applies a finite mass, mass-energy balance, and dynamic mass transform chemical reactions, which can predict the temperature profile along the zone (Figure 2.10) (Xiong et al. 2016; Chogani et al. 2020). This model embeds a reactor design in which the finite mass/volume is carried within a mesh structure. Additionally, it considers turbulence, which cannot be considered in the kinetic equilibrium model (González et al. 2018). The CFD models have a significant advantage: they can accurately predict the temperature and gas yield in the reactor (Vidian, Dwi Sampurno & ail 2018).
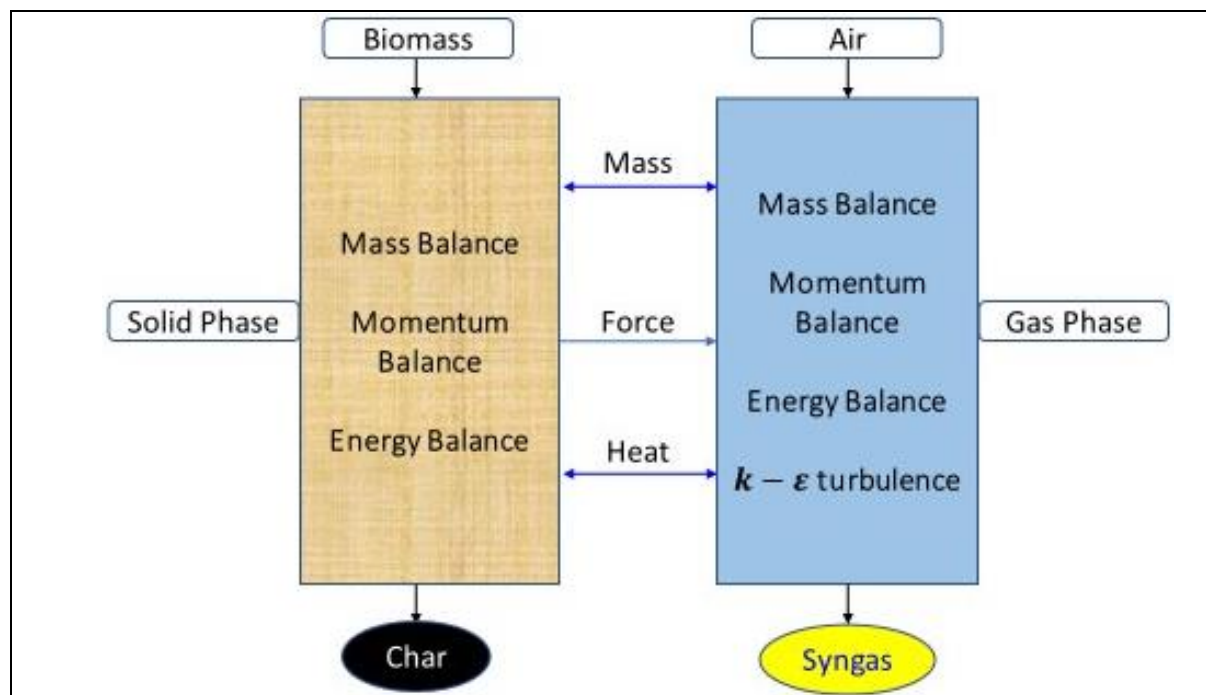
Figure 2.10: Schematic of the CFD model (modified from (Wu et al. 2013))

The temperature profile, the gas compositions across the zones, and the flow pattern of solid and liquid particles inside the reactor can be predicted using CFD simulation (Di Blasi 2000; Jaojaruek 2014). These results can be used to assess the effectiveness and efficiency of the gasification process (Kumar & Paul 2019). Studies of improvements, modifications or performance optimisation for a particular gasification process can also be conducted. This model can allow for the simulation analysis of the conditions in an actual plant (Ismail et al. 2018).

CFD models are suitable for dense particulate (pellets) and vary in specific chemistry (Pepiot, Dibble & Foust 2010). Because of biomass's complex composition and structure, biomass gasification process modelling still presents significant difficulties (Wang & Yan 2008). Several researchers use CFD for different purposes (Table A13 of Appendix A). Murugan and Sekhar (2017) simulated a downdraft gasifier (40 kW) utilising a feedstock of rice husks. Their results showed that a gasification process would produce syngas and a composition of 1.7% CH_4, 22% CO, 8% CO_2, and 13% H_2, where the equivalence ratio (ER) is 0.30. They also found a maximum heating value of 5.19 MJ/Nm^3. However, CFD approaches are often very challenging in predicting tar and reduction issues. Researchers are currently attempting to build a multiphase model heading to different zones of the gasifier reactor. The prediction accuracy depends on the empirical data for the necessary inputs, just like the kinetic technique (Liu et al. 2017).

Limited gasification research with various feedstock has been carried out with CFD modelling (Gao et al. 2012; Jakobs et al. 2012; Janajreh & Al Shrah 2013). Murugan and Sekhar (2017) developed a computational model for an Imbert type downdraft biomass gasifier using CFX. They reported that the CFD modelling approach is helpful for numerical studies on pyrolysis and gasification in a downdraft gasifier. Also, Kumar and Paul (2019) reported that an advanced CFD based model might play a valuable function in the biomass gasification method and its design requirements. The major advantage of the CFD models is a very accurate temperature and gas yield prediction in the whole reactor (Wu et al. 2013). Gupta, Jain and Vyas (2017) simulated a 10 KWE biomass downdraft gasifier for woody biomass. They found that the average gasification temperature was 800.3K and the maximum temperature was at the char reduction zone. They also mentioned that the pressure varies with gasifier heights. Pandey, Prajapati and Sheth (2021) recently studied the 2D axisymmetric CFD model of an Imbert downdraft gasifier for Ecoshakti biomass pellets. The increases in equivalence ratio (ER) tended to increase the temperature inside the gasifier.

The downdraft gasification CFD models reported two primary factors: temperature distribution and syngas composition. Therefore, it is necessary to investigate various operating conditions (such as inlet velocity,

temperature, pressure, feedstock flow rate, oxidising agent, etc.). The current research project conducts the CFD modelling for the downdraft gasifier of a WS pellet using ANSYS Fluent software. The model optimises the WS characteristics and gasification operation parameters to forecast gas yield and composition.

2.5. Techno-economic analysis

A techno-economic analysis of any product is a study that combines technical and economic aspects of the production process (Yang, Y. et al. 2018). It aims to evaluate the feasibility and profitability of the production process, considering factors such as the cost of raw materials, labour, equipment and energy, as well as revenue generated from the product's sale (Kwan, Hu & Lin 2018).

The Techno-economic analysis plays a vital role in determining the viability and profitability of the product within the industry. The investigation would also consider market conditions such as product demand, industry competition, and future market trends (Zetterholm et al. 2020). Additionally, the analysis would consider any government regulations or incentives that may affect the production process. The analysis would also consider the return on investment.

Many stakeholders and the researcher conducted the economic analysis of bioenergy production (Sultana & Kumar 2012; Zhang et al. 2013; Martinez-Hernandez, Amezcua-Allieri & Aburto 2021). However, most articles related to life cycle analysis compared to the cost benefit investigation (Faber, Mangin & Sick 2021). Therefore, studying the economic feasibility and fundamental information related to bioenergy production from biomass is needed.

2.6. Summary of the literature review

The wheat industry is one of the leading agricultural sectors in Australia. In 2021-2022, the wheat yield was about 2.6 tonnes/ha and WS was 3.4 tonnes/ha. Also, wheat straw is an abundant and readily available herbaceous biomass worldwide. However, WS is bulky and has a lower density, which creates significant management issues. Current WS management in Australia often converts it into open field composting or mixes it with soil for nutrient conservation. Due to the low market value for composting and on-field management difficulties, the transformation into energy may be more desirable. This study examines the alternative approach to WS utilisation through pelleting (high quality solid fuel), pyrolysis and gasification.

Improving herbaceous biomass (WS) material properties to a good quality fuel requires one or a combination of several processes such as size reduction, drying, additive adding and densification. The available literature

reported that densification could increase the density as well as thermal efficiency but requires an additive blend for WS. Together with pelleting, this study also proposed different biomass-based additives mixing with WS. The blend can also potentially create a synergy between fuel components to improve conversion efficiency.

A laboratory scale kiln is suitable for pyrolytic WS and WS pellets analysis and can help to estimate the WS pellets output as biochar, bio-oil and gas. However, a kiln is unsuitable for measuring mass degradation rate, mass loss and kinetic parameters. Hence, a TG analysis may provide the kinetic information for WSPs' in pyrolysis and combustion. Recently, a CFD model with commercial software (ANSYS Fluent) has been used for accurate and practical gasification performance prediction and optimisation of actual plant activities. Also, a CFD model can be a virtual laboratory to simulate fuel properties, operational conditions, reactor design and the profile picture along the zone. Therefore, the pyrolysis yield, TGA data, and model information were used for gasification performance evaluation.

CHAPTER 3: WHEAT STRAW PELLET PRODUCTION AND QUALITY ASSESSMENT

Abstract

Densification (pelleting) is essential for managing biomass as a feedstock for biofuel. The suitable use of binders can improve the straw pellets' strength and efficiency. The present study investigates the effect of the binder on pellet quality. The pellets were made with different levels of binders (WS with bentonite clay, sawdust, and biochar) in a laboratory type pellet mill. The density, dimensional stability, tensile strength, mechanical durability, chemical composition, abrasive resistance, and wettability index were measured. According to the results, the heating value increased with added binders. Adding binders to the WSPs also increased their tensile strength. The addition of the binder also helped to reduce the generation of fines from 8.58 to 1.92%. Further, the addition of binders decreased the wettability index. Finally, this study compared the produced pellet quality with the ISO 17225-8 standard. The results demonstrated that, except for ash content and bulk density, the binder improved pellet quality to the requirements of the ISO standard.

3.1. Introduction

Global energy demand has steadily increased due to the rising population (Dayoub et al. 2021) and industrialisation (Al-Hamamre et al. 2017). There is a growing need to develop alternative economically and ecologically friendly technologies and shift to renewable energy sources from traditional fossil fuels.

A form of renewable energy is biomass. It has an advantage over other renewable sources (wind, hydro, solar, etc.) as it is less affected by geography and climate (Nanda et al. 2018). In addition, it is often widely available, particularly in rural and regional areas (Sedighi & Salarian 2017; Abdelhady, Borello & Shaban 2018; Ríos-Badrán et al. 2020).

This research investigates using cereal crop straw, particularly WS, as a source of feedstock for energy generation. Each year, the agricultural sector produces huge surpluses of cereal straw (Auersvald et al. 2019). For instance, in 2010, global straw production from cereal crops was approximately 1.5 Gt. Assuming a 10~20% conversion rate, this is a valuable resource of potential feedstock for bioenergy production (Sun et al. 2015).

As a solid fuel, cereal straw has poor characteristics such as high porosity, high O_2 content and low bulk density. Bulkiness might reduce conversion efficiency or even fail to convert biomass to bioenergy.

Moreover, varying biomass sizes and shapes can also lead to difficulties with storage, transport, management, and conversion processes.

Densification can enhance calorific value, improve physical properties and use efficiency. Biomass pellets have a particularly high application potential compared to other techniques such as bale, cube, puck, briquette, etc. A pellet is more suitable for handling, transport and storage (Adapa, Tabil & Schoenau 2009). However, the production of pellets usually needs the addition of a certain proportion of binding materials to hold the materials together and increase durability while decreasing fines and dust. Binding materials in common use are starch, lignin, and protein. A range of pretreatment methods (applications of various chemicals, additives, temperatures, pressures, steam exploration, etc.) has also been commonly used to improve pellet durability and strength.

Some research on low-cost pellet production from agricultural straw is available (Shahram Emami 2014); however, little specific research has been conducted on optimising WS pelletising processes. Lu et al. (2014a) explored the WSP-making process. Lu et al. (2014b) investigated the compression load and binder relation to WSP production. They found that binding materials (bentonite clay and wood residue) and compression load can significantly influence pellet density, tensile strength and specific energy consumption. Furthermore, a recent investigation studied rice husk and WS mixed pellets (Ríos-Badrán et al. 2020).

This chapter is divided into three sections. The first section focuses on examining the characteristics of raw materials. Subsequently, pellet fuel manufacturing methods are discussed, followed by an exploration of the features of the produced fuel pellets. A comparison is made using the relevant ISO standard to assess the pellet quality.

3.2. Development of pellet

3.2.1. Raw materials

The present study used four different raw materials (WS, sawdust (SD), bentonite clay and activated carbon/biochar). Table 3.1 shows the raw materials' physical appearance, collection source and purpose.

Table 3.1: Description of raw materials used for pellet manufacturing

Typical appearance of raw materials		Purpose	Collection source
Ground WS		Base materials of pellet	Wheat (*Triticum aestivum* L.) straw used in this research was collected from the UniSQ Centre for Agricultural Engineering (CAE) farm field, Toowoomba, Australia. The WS was harvested at an average height of 105 mm above the ground by a combine harvester in December 2020.
Sawdust		Structural binders (increase pellet strength and density)	The SD was obtained from Pollards SD Suppliers, 130 Yan Yean Road, Plenty, Victoria. The source of SD is nontreated plantation softwood radiate pine (*Pinus Radiata*). The uniformity, specific gravity and flammability were 100%, 1(one) and low.
Coconut shell biochar		Energy additives (increase heating value)	The activated carbon (coconut shell biochar) was obtained from commercial sources in Australia (http://www.clearwaterfilters.com.au).
Bentonite clay		Binding agent (increases pellet strength)	Bentonite clay is an absorbent swelling clay consisting mainly of montmorillonite. The bentonite clay in this study was purchased from a Queensland commercial reseller.

Note; WS: Wheat straw; SD: Saw dust

3.2.2. Experimental design

This study aimed to develop a suitable WSP by measuring and comparing the effect of different combinations of binder treatments (Table 3.2). According to Pradhan, Mahajani and Arora (2018), to make a good quality pellet, the moisture range should be 15 to 23% and particle size should be less than 6.5 mm. In addition, Kaliyan and Vance Morey (2009) suggested using 20% of SD. Also, binders in the value from 0.5 ~ 5% (fraction to mass basis) could improve pellet quality (Kashaninejad & Tabil 2011). Therefore, the present research considered the raw material moisture content to be around 20% by ≤ 2 mm particle size. Moreover, the bentonite clay, SD and biochar ratios were 10%, respectively.

Table 3.2: Experimental design

Treatment	Materials Composition (% = fraction of total mass basis)
T_1	WS (100%)
T_2	WS (90%): SD (10%)
T_3	WS (90%): Bentonite clay (10%)
T_4	WS (90%): Biochar (10%)
T_5	WS (70%): SD (10%): Bentonite clay (10%): Biochar (10%)

Note; SD, biochar and bentonite clay are available and low cost compared to other additives, T_1: Wheat straw, T_2: Wheat straw and Saw dust, T_3: Wheat straw and Bentonite clay, T_4: Wheat and Biochar, T_5: Wheat straw, Saw dust, Bentonite clay, Biochar.

3.2.3. Pelleting process

The pellet production method follows the raw materials collection, size reduction, mixing additives with the ground WS, homogenisation (mixing all materials), pelleting and drying steps (Figure 3.1).
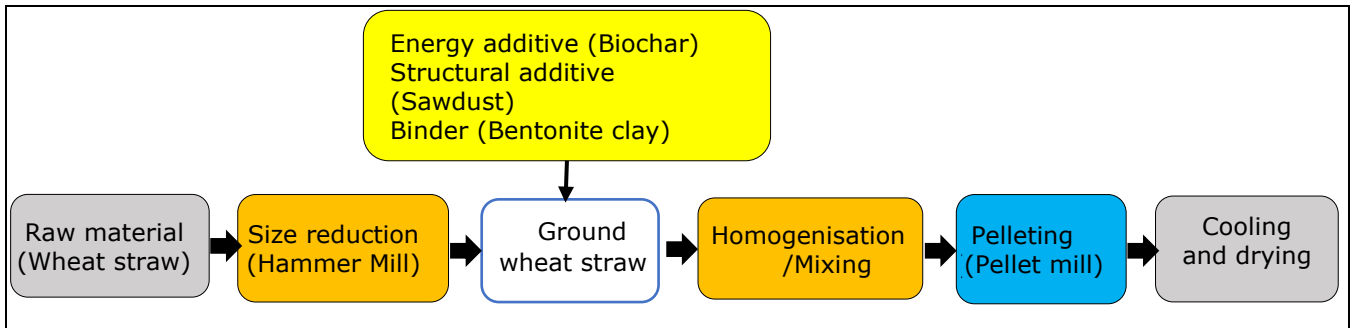
Figure 3.1: Schematic block diagram of the pellet production process

3.2.3.1. Size reduction of wheat straw

A hammer mill (*MKHM 198, Meelko CO-United States, Agricultural Machinery*) was used for size reduction (chopping) and mixing of the WS (Figure 3.2). The mill was powered by a 4.0 kW (446 V and 2865 rpm) three phase electric motor. The chopper mill had a feed hopper and a pair of rollers to feed the material to the chopping blades. The biomass feed rate was dependent on the roller speed. A shaft consisted of 16 swinging knives for chopping purposes. In addition, a cyclone separator (dust collector) was connected to the outlet of the hammer mill to collect and control the dust.

Figure 3.2: Hammer mill and ground wheat straw

The screen size and diameter of the particles were correlated. For size reduction, the screen size of the hammer mill should not be larger than the diameter of the pellet making dies. Too large size particles are difficult to pass through the die. Conversely, too small or powder needs excessive energy. This study also used a 3.2 mm screen size for WS grinding to less than 2 mm particle sizes. The screen size was exchangeable. The sample was milled to ground particles less than 7 mm (Figure 3.2); however, during this process, fine powders were also produced.

3.2.3.2 *Particle size distribution*

The particle size analysis method separates the sample into defined size fractions expressed in the weight percentage. This procedure was adopted from ASTM E 828-81 "designating the size of refuse derived fuel-3 from its sieve analysis"(ASTM 2004).

The material was sieved to determine the particle size distribution. For particle size analysis, a sieve shaker (*Civilab Australia*) and a sieve (*Impact Laboratory Test Sieve*) were used (Figure 3.3). The sieve numbers 031…86, 47, 50 and 70 (sieve opening sizes: 6.7, 4.75, 2.36, 1.8 and 0.7 mm, respectively) were used. A 100 g sample was placed on a stack of sieves and shaken for 10 minutes, and a replicated particle size analysis was undertaken three times. The particle size distribution of WS grinds and SD is shown in Figure 3.4. The particle size of WS was larger than the SD. Therefore, for this experiment, less than 2 mm particle size of WS was chosen to achieve a reasonably uniform particle size mixture (WS and SD).

Sieve shaker	Sieve

Figure 3.3: Sieve analysis of wheat straw and saw dust
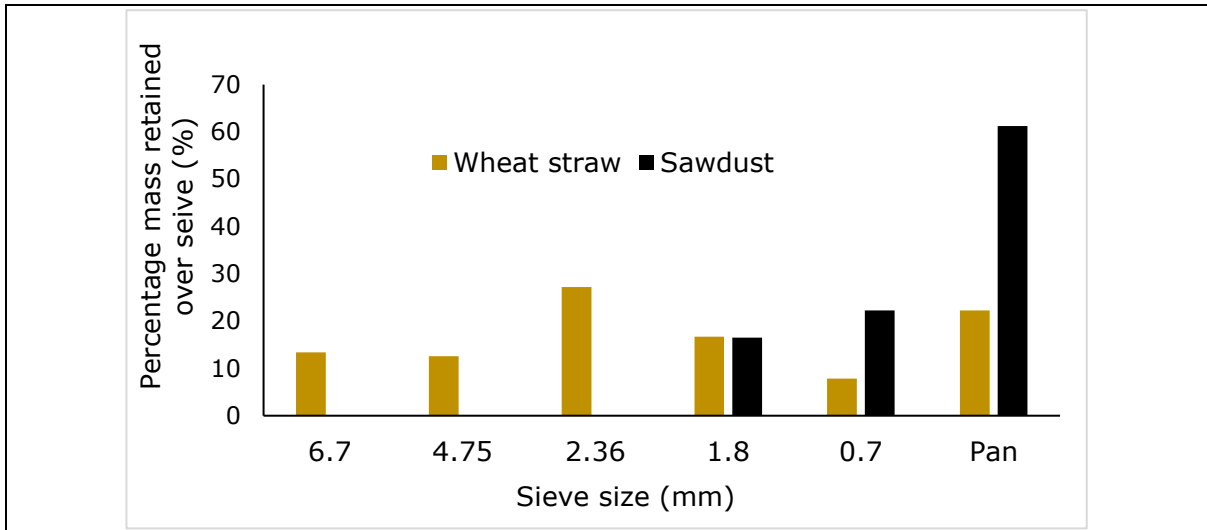
Figure 3.4: Particle size distribution of the WS grinds and SD

3.2.3.3. Sample preparation

Uniform mixing (additives and raw materials) and the condition (weathering) are important factors for quality pellet production. This research produced five different types of pellets. Additives were directly mixed into the WS grinds. For conditioning, the desired sample moisture content was adjusted to 20% (w.b.). A mass balance between the original ground sample and the desired sample moisture calculated the optimum water required. Then, the sample was remoisture by spraying water and kept in an air-tight container (Figure 3.5). The materials were conditioned at room temperature for 72 to 96 hours before the experiments were conducted. Subsequently, during the conditioning, all materials were mixed every 12 hours to achieve uniform distribution of each material and equilibrium moisture content (Emami et al. 2014).

| Raw material mixtures stored in a container | Raw materials after mixing |
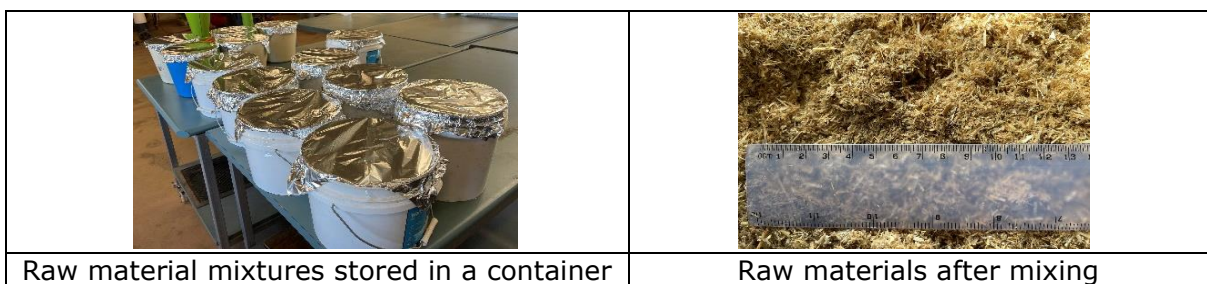
Figure 3.5: Sample preparation for pellet

3.2.3.4. Pellet mill and pellet preparation

The WSPs were produced at the University of Southern Queensland, Toowoomba, Australia. A Roller Turned Flat Die pellet mill (GEMCO China, Model: ZLSP200B R Type) was used (Figure 3.6). The wood pellet production capacity of this machine was 80~120 kg/hour. The pellet mill consisted of a feeding hopper, a barrel, a cylindrical steel roller, a plate-type flat die with a hole, and an electrical motor (3 phase, 7.5 kW). The

corrugated roller (diameter 85.0 mm) was connected to an electric motor moving crosshead, which provided the circular movement of the roller. The pellet ejection hole had an internal diameter of 8 mm and a length of 40 mm. The pellet mill had no heating facilities. The pellet production chamber was wrapped with a heating element to maintain the pellet production temperature at around 80°C (Adapa et al. 2007).

	Instrument: Roller Turned Flat Die pellet mill
	Manufacturer: GEMCO China
	Model: ZLSP200B R Type
	Type: Flat plate die & rollers
	Power: 7.5 kW Electric motor
	Electricity: 415 V, 50Hz, 3 phases
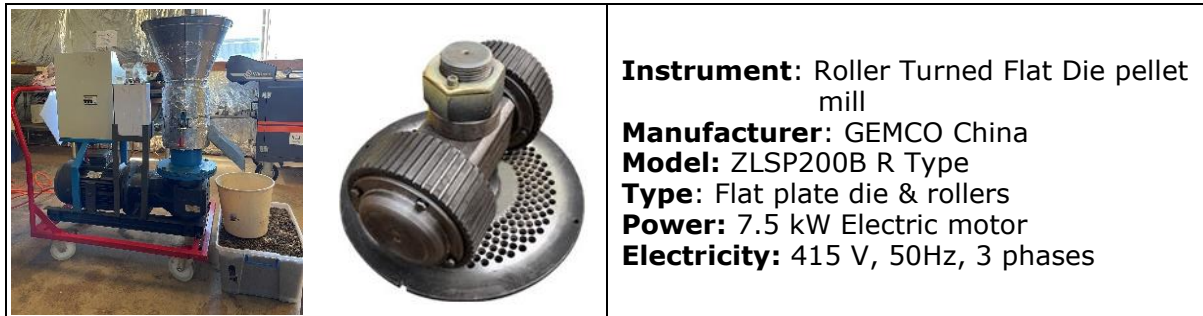
Figure 3.6: Pellet mill

The best clearance range between the die and roller was kept at 0.1 to 0.3 mm as clearance could significantly influence pellet quality (http://www.pelletmillequipment.com/). The roller's weight produced friction and load to compress the biomass samples and pass the biomass into a die. The roller rotated on the die plate surface, which helped to discharge the densified sample. As the materials were fed into the mill, the rotating roller (50 rpm) created a friction load between the roller and the die plate to compress the materials and eject them from the die as a pellet. Initially, these discharged pellets often needed refeeding to achieve good physical quality, thus reducing production capacity. The refeeding of materials into the pellet mill was done 3~5 times (taking about 5 to 10 minutes) until a smooth, nonabrasive and relatively dry pellet product was achieved. Then, as the barrel temperature reached 70~80°C, the pellet could be formed directly without refeeding.

In this study, the produced pellets were cool and dry under ambient conditions in the open air. As a result, their moisture content reached approximately 12% after one day. However, the moisture was ≤10% within three days after pellet production due to Toowoomba's QLD low humidity. The low moisture content promoted good storage quality (free of mould, fungal growth, hydrolytic breakdown, etc.).

3.3. Measurement procedures

3.3.1. Moisture content (mass fraction of water) of biomass

Moisture content (MC) expedites natural binding and lubricant in biomass (Kaliyan & Vance Morey 2009). The pellet mill continuously clogs without optimum MC due to ground straw's low bulk density and poor flowability. Pradhan, Mahajani and Arora (2018) observed that the production of high-quality pellets is possible only if the moisture content of

the feed/raw materials is between 15 to 23%. Therefore, spraying water adjusted the biomass moisture content to around 20%.

This study measured the moisture content of raw materials and produced products using the "Ohaus moisture analyser mb23 lab infrared heating grain moisture tester meter" and oven dry method in three replicates. Ground straw, SD and biochar's mean preliminary MC was 9.12%, 9.05% and 7.88%, respectively. However, these moisture values cannot densify biomass in pelleting machines (Ríos-Badrán et al. 2020). Therefore, the remoistened biomass was modified and kept in an air tight plastic container for three to four days.

3.3.2. Measurement of pellet physical properties

The physical characteristics of the WSPs represent size (diameter, length and weight), density, durability and hardness.

3.3.2.1. Pellet dimension and density

This study used 33 pellets from each treatment to measure physical properties, including pellet diameter, length, weight and density (individual and bulk). Two data sets were used to calculate and compare each pellet's dimensional expansion and density (apparent and relaxed). The first set of data measurements was recorded after one day of pellet extrusion, while the second set was taken on the 14th day of storage. A digital calliper was used to measure the size (length and diameter), while the pellet weight was measured by digital balance (Figure 3.7).

Figure 3.7: Pellet size, weight and density measurement equipment

The actual material density of a single pellet is vital for stability analysis. The apparent density of a single pellet is the weight-to-volume ratio, but bulk density is the mass-to-volume ratio (Souza-Santos 2010).

After one day of extrusion, a single pellet density is defined as the initial apparent density (Lu et al. 2014a). Subsequently, storage, the apparent density, is called the apparent relaxed density (Emami et al. 2014). Finally, the difference between initial apparent density and apparent relaxed density is termed relax density.

3.3.2.2. Pellet dimensional stability

Density is a fundamental property of a material and is defined as mass divided by volume. It was described in ASTM E 873-82 as "bulk density of densified particulates biomass fuels" (ASTM 2013). Most agricultural residues have low bulk densities, such as loose WS bulk having a density of about 18 kg/m^3. This is compared with coal density which is 700 kg/m^3.

A standard cylindrical container (volume: one liter) was used to measure the bulk density of the experimental materials (ground WS, SD, bentonite clay and biochar). For bulk density measurement, three repeats were made.

$$\text{Bulk density, (kg/m}^3) \; BD = \frac{M}{V}$$ ……………………………………..*3.1*

Where: *V*= volume of the materials, m^3
   M= Mass of the materials, kg

The possible deformation/shrinkage in pellet size is termed dimensional stability, and it accounts for length and diameter. Therefore, the pellet needs to be dried and stored for the measurement of both types of stability (diametric and longitudinal). According to the literature, 14 days is an acceptable duration for pellet stability (do not change to any longer) (Shahram Emami 2014; Lu et al. 2014a). The pellet was therefore dried at room temperature and kept in a container for 14 days. Then, the dimension measurement was retaken to determine expansion (length and diameter). A negative increase indicates that the object's size has shrunk, while positive growth is named expansion.

3.3.3. Measurement of elemental composition

The chemical analysis of the WS, SD, biochar, bentonite clay and produced pellets was performed in the Feed Central Laboratory, Toowoomba, Queensland, Australia. Triplicate measurements were undertaken for each sample.

- *Component analysis*

The primary component of biomass is lignin, cellulose and hemicellulose. These were determined from acid detergent fibre (ADF) and neutral detergent fibre (NDF). Lignin and ADF were determined using the Association of Official Analytical Chemists (AOAC) standard method 973.18 - Fiber (Acid detergent) (AOAC 1990b). NDF was determined using AOAC standard method 992.16 (AOAC 1990a). The proportion of cellulose and hemicellulose was estimated ultimately from the ADF and lignin as % Hemicellulose= % NDF - % ADF and % Cellulose = % ADF - % ADL (Mani, Tabil & Sokhansanj 2006).

- *Proximate analysis*

Proximate analysis is a broad measurement to determine the volatile matter content (VM), moisture content (M), ash content and fixed carbon content (FC). These are all typically measured on a mass basis. Moisture is driven off at 105~110°C (just above the boiling point of water), representing physically bound water only. In contrast, a slow heating rate drives volatile compounds off in an inert atmosphere at 950°C.

First, the reported Hach methods determined the moisture content and volatile compound (AOAC 2002). Next, the AOAC standard method 942.05 was used to calculate the total ash content, where 2~3 g of the sample was burned in a furnace at above 700°C in oxygen (AOAC 1990c). Next, it took the remaining material (after VM loss). Finally, the fixed carbon content was calculated from 100% reduced by moisture, ash and volatile matters by

$$FC = 1 - M - Ash - VM \text{ (ASTM 1998)} \quad …………………....3.2$$

- *Ultimate analysis*

Total organic carbon (TOC) and nitrogen were determined by CN628 Carbon/Nitrogen Determinator followed by AOAC 990.03 - Protein (Crude) in Animal Feed (AOAC 2006). In addition, the sulphur was determined by the CEM Application Notes for Acid Digestion method (ASTM 2008). Finally, the difference of elements decided was oxygen.

- *Heating value (HV)*

Solid materials' gross energy (gross heating value) is expressed as calories per gram (Cal/g). The HV was calculated by an IKA C2000 basic oxygen bomb calorimeter using the standard ASTM D5865-03 (ASTM 2003). The instrument was set to IKA's dynamic mode with an outer vessel temperature of 25ºC. The calorimeter was standardised using 1.00 g of Parr standard benzoic acid. About 0.50 g of the sample was put in the metal combustion capsule and placed in the sample holder in the bomb head for gross energy determination.

3.3.4. Measurement of physical quality

A pellet quality assessment compared the experiment's pellets with the commercially prescribed standard (ISO/TS 2016). The pellet fuel quality was typically evaluated by density, durability, water absorption index and fines (Zafari & Kianmehr 2014). Therefore, a specific qualitative analysis of five different pellet types (treatments) was carried out (Figure 3.8). First, all samples were handled and chosen to ensure a certain homogeneity. Then, weight, diameter, length, bulk density, water absorption and dust content were all tested in the laboratory on the selected samples (Mani, Tabil & Sokhansanj 2006; Jiang, L.-b. et al. 2016; Pampuro, Busato & Cavallo 2018).
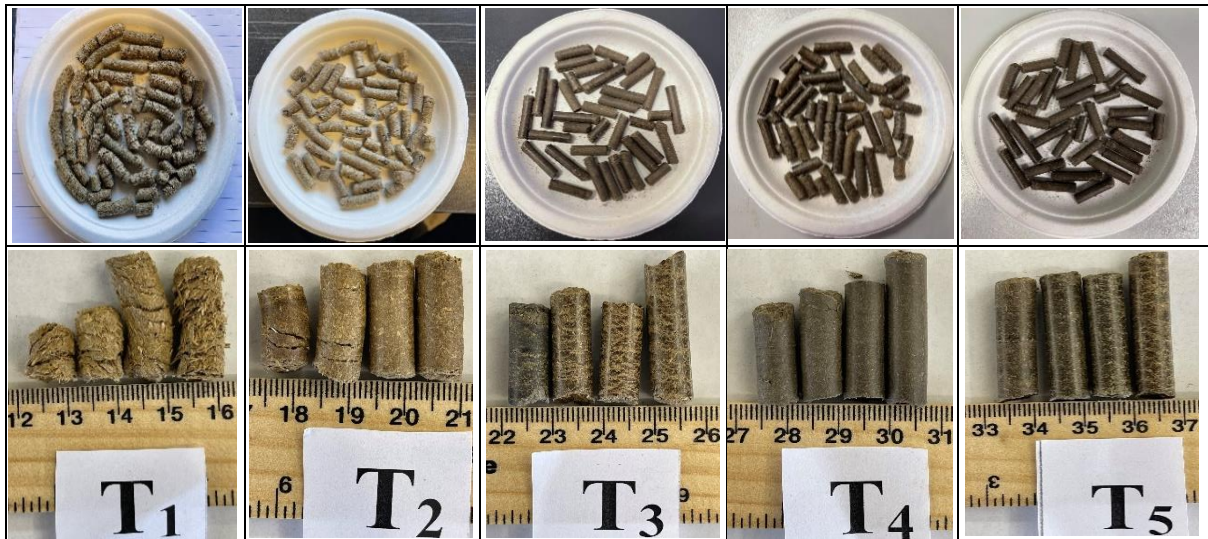
Figure 3.8: Physical appearance of pellet samples

3.3.4.1. Tensile strength

The pellet diametric compression test represents the tensile strength (Shaw, Karunakaran & Tabil 2009). Therefore, this research evaluated the pellet tensile strength through diametral compression. Using a diamond cutter wheel bit in an automatic precision cutting machine (Struers Minitom, Pederstrupvej 84, Denmark), pellets were cut into around 2 mm diametrically thick tablets (Shaw, Karunakaran & Tabil 2009) (Figure 3.9).

$$\text{Tensile strength } (\sigma) = \frac{2F}{\Pi dl} \quad\text{...}\textit{3.3}$$

Where: σ = Tensile (horizontal) stress (Pa),
    F = load at fracture (N),
    d = Compact diameter/Pellet diameter (m),
    l = Compact thickness (m).

| Cutting machine | Cutting pellets |
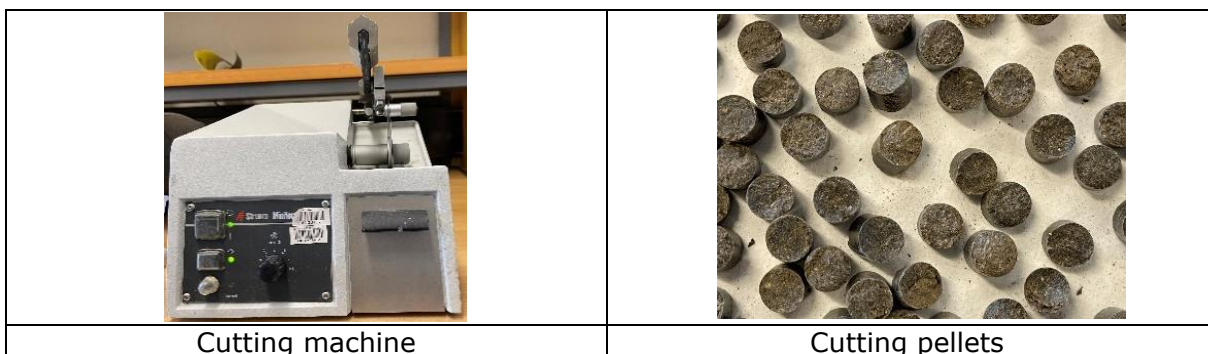
Figure 3.9: Pellet cutting machine and cut pellet specimens

3.3.4.2. Hardness test

The hardness test is usually considered to check the stability of the pellet, which is essential to transport, storage, and handling. The practical

application of the hardness test is evaluating fines/dust generation during handling. The commonly used hardness tester is the "Individual Pellet Hardness Tester". The hardness of the pellet was determined using the compression test (Tilay et al. 2015). The test was intended to imitate the effect of pressure that may be present in the lower layers of pellets during handling, transporting and storage due to the weight of the upper layers. A Hounsfield testing machine was employed in this experiment (Figure 3.10). A single pellet was placed between two bases. The load was gradually increased until a fracture occurred. The minimum load capacity for the Hounsfield testing machine was 25000 N, and the crosshead speed was 10 mm/min. The pellet hardness was defined as the maximal load before fracturing. Ten replicates of each pellet type were tested for each treatment sample.
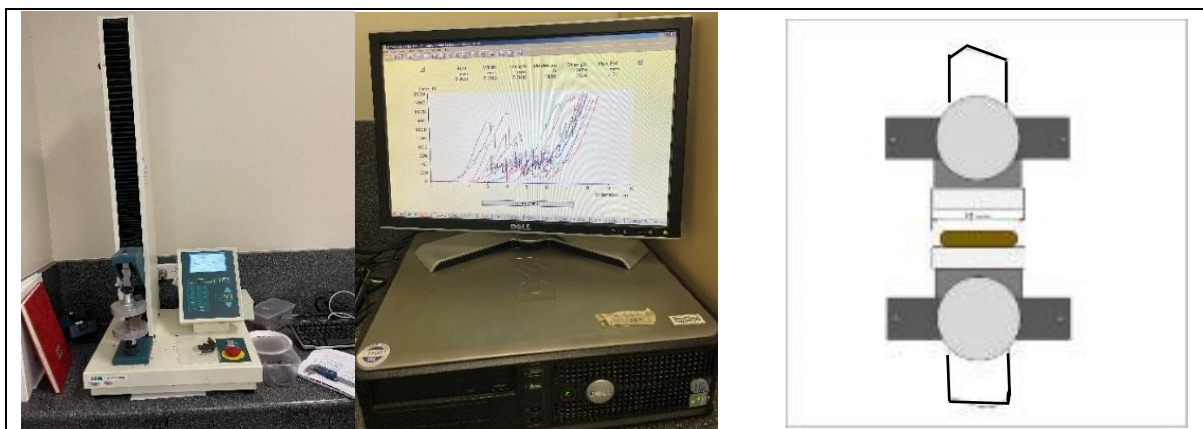
Figure 3.10: Load testing machine for pellet hardness

3.3.4.3. Mechanical durability

Durability represents the pellet's impact resistance to breaking due to handling, distribution, and transportation. In this study, durability was used to indicate impact resistance. The impact resistance study measured the durability after 14 days of storage using the single drop test method (Al–Widyan 2001; Iroba et al. 2014; Tilay et al. 2015). The durability test was determined following ASTM D3038's procedures (ASTM 2013). The test was done by tumbling a single pellet into a stainless steel pan from a height of 1.85 m (Figure 3.11). The pellet was then weighed before and after the drop. This practice was repeated four times. Furthermore, durability is the final weight of pellets (large fragments) to the initial weight multiplied by 100. Thirty three (33) replicates were made for each treatment.

$$\text{Pellet durability (\%)} = \frac{weight\ of\ biggest\ broken\ pellet\ piece}{weight\ of\ the\ original\ pellet} \times 100 \quad \text{...............}3.4$$
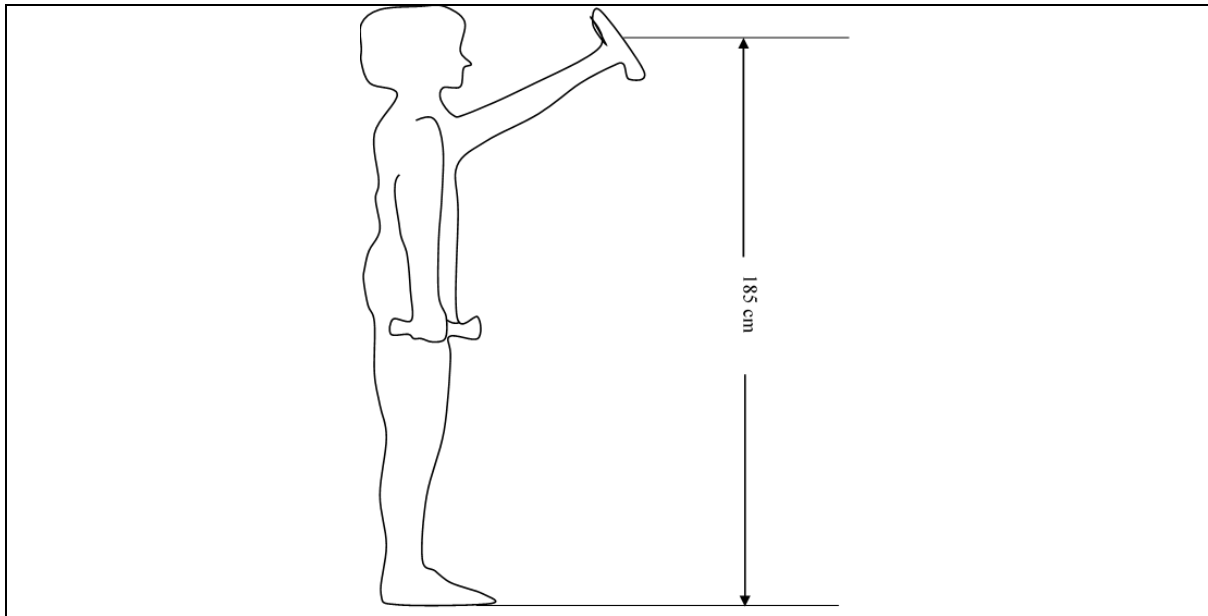
Figure 3.11: Pellet single drop test

3.3.4.4. Abrasive resistance

The ASABE 269.4 techniques were used to conduct the durability test following CEN/TS 15210:2005 standard (CEN 2004). The abrasive resistance test applies stress to the pellet to demonstrate its resistance to shocks and abrasions (Papandrea et al. 2021). The abrasive stress has implications for pellet handling and storage and the related loss of a significant portion of the material (Ramírez-Gómez 2016; Ilic et al. 2018). Thus, due to poor abrasive resistance, pellet length reduction correlated to the small particle quantity making (ASTM 2008). Furthermore, pellet breakup and the creation of small particles reduced the bulk density.

$$\% \text{ of particle type } = \frac{M_i}{M_t} \times 100 \quad \text{………………………………………. } 3.5$$

Where: M_t= total mass of pellet/sample before tumbling (g) and
M_i= final mass of particles after sieve (g)

The particles generated by the pellets during the tumbling process were measured using a 5.60 mm mesh sieve. Henceforth, "fines and dust" are denoted ≤3.15 mm particles according to ISO 18846 (ISO/TS 2016), and "small particles" are those with a diameter of less than 6.5 mm. This procedure was performed three times. First, the particles were considered with the equation:

$$\% \text{ of small particles } = \frac{(W_i - W_f)}{W_i} \times 100 \quad \text{…………..…………… } 3.6$$

Where: W_i = pellet initial weight before tumbling (g) and
W_f = pellet final weight after tumbling (g)

3.3.4.5. Wettability index

Short term rain (high humidity) conditions may damage the quality of the densified materials when transporting and storing (Kaliyan & Vance Morey 2009). Therefore, moisture resistance is an essential parameter of pellet evaluation using the wettability index (Papandrea et al. 2021). This index measures the quantity of water absorbed by the pellet.

Craven et al. (2015) used an environmental chamber to maintain temperatures from 10 to 40°C and relative humidity of 70~90% for the moisture resistance assessment test. However, Lindley and Vossoughi (1989) measured the briquette's water resistance capacity. The method was to immerse the briquette in water for 30 s at 27°C temperature. Papandrea et al. (2021) and Yoshida et al. (2021) followed the same procedure to record pellet water absorption. Therefore, this research followed the Papandrea et al. (2021) method to measure water resistance.

Five sets of samples were prepared with around 50 g of weight for each treatment for this test. The pellet samples were immersed in water for 30 s in ambient conditions (26°C and RH 51%) (Kaliyan & Vance Morey 2009). Then, the water was removed, and the pellet was placed in ambient conditions for one hour and weighed again. The percentage of pellet weight variance before and after water immersion was expressed in the wettability index (Papandrea et al. 2021).

$$\text{Wettability index (WI)} = \frac{(W_f - W_i)}{W_f} \times 100 \quad \text{..............................} \quad \textit{3.7}$$

Where: W_i = initial pellet weight before submerging in water (g)
W_f = final pellet weight after (30 s) submerging in water (g)

3.3.5. Statistical analyses

Statistical analysis was conducted using the IBM SPSS software version 27 (IBM crop., Armonk, New York). The impact of different binder mixing ranges on size, density, durability, and hardness was compared by the ANOVA (one-way analysis of variance). Duncan's multiple range tests examined significant variations in mean at a 5% significance level.

3.4. Results and discussion

The experimental data, statical analysis and discussion on pellet characteristics (density, durability, wettability index, fines) are presented in this section. The factors affecting pellet quality are also presented and discussed here.

3.4.1. Chemical composition

The chemical analysis of the elemental composition of pellets is useful for thermochemical conversion modelling and predicting the solid and gas phase. Major and minor components comprise the pellet's element characteristics. Ultimate analyses were used to examine the major elements. Table 3.3 presents the analytical composition of WS, SD and pellets with different treatments. The fixed carbon, moisture, ash and volatile matter were determined using proximate analysis (Table 3.4).

Table 3.3: Composition of wheat straw, binder, and pellets

Treatment	Dry wt, %		
	Hemicellulose	Cellulose	Lignin
T_5 (WS+SD+BC+BioC)	23.30	30.00	10.60
T_4 (WS+Bioc)	23.00	29.30	13.90
T_3 (WS+BC)	33.20	27.20	5.40
T_2 (WS+SD)	27.80	32.20	8.50
T_1 (WS)	22.40	41.30	7.00
WS	23.0	40.5	7.30
SD	13.66	45.38	26.66

Note; WS: Wheat Straw, BC: Bentonite Clay, SD: Saw Dust, BioC: Biochar

Table 3.4: Chemical composition of raw materials and pellets

Features	Sawdust	Wheat straw	Coconut shell biochar	Pellets				
				T_1	T_2	T_3	T_4	T_5
Proximate analysis (wt % as received, db)								
Moisture	6.60	9.62	7.40	6.20	6.00	4.00	3.70	3.50
Volatile matters	76.80	72.78	7.40	75.61	56.8	59.3	43.4	53.03
Fixed carbon	16.27	10.30	81.30	11.10	22.60	19.40	41.50	31.60
Ash	0.33	7.30	3.90	7.09	14.60	17.30	11.40	11.87
Calorific value, HHV (MJ/kg)	20.95	17.6	30.75	17.02	18.23	18.14	20.21	19.06
Ultimate analysis (wt % as received, db)								
Carbon	51.8	46.06	83.8	44.32	44.32	44.89	45.25	45.87
Hydrogen	6.14	5.0	0.90	4.90	4.9	4.5	5.78	6.30
Nitrogen	0.26	0.53	0.50	0.56	0.56	0.74	0.74	0.72
Sulphur	0.02	0.11	0.10	0.11	0.11	0.17	0.21	0.21
Oxygen (by difference)	41.78	48.3	14.70	50.11	50.11	49.7	48.02	46.9

Note; HHV: Higher Heating Value, T_1: Wheat straw, T_2: Wheat straw and Saw dust, T_3: Wheat straw and Bentonite clay, T_4: Wheat and Biochar, T_5: Wheat straw, Saw dust, Bentonite clay, Biochar.

Lignin, hemicellulose and cellulose are significant components of biomass as well as WS (Lu et al. 2014a). The lignin content of SD (26.66%) was higher than WS (7.30%) (Table 3.3). Many researchers have noted that lignin acts as a binder which positively affects the strength of the densified product. However, the straw's low lignin content may not be able

to bind the particles well (Thomas, Van Vliet & Van der Poel 1998). Therefore, SD was mixed with WS (for example, T_2 and T_5) to increase the lignin content and help particle bonding. Ultimately, lignin was increased from raw WS by 7~7.3% to treatment T_2 (8.5%) and T_5 (10.60%). The densified product's strength and durability improved as a result.

In the thermochemical conversion, nitrogen and sulphur convert to form NOx and SOx. These features are included in the commercial pellet standard for small pellet stoves or burners that do not have emission controls. WS may contain more nitrogen and sulphur than wood. All pellets generated in this study met the nitrogen standard set by ISO 17225-8: N≤1.5% for grade A and N≤2.0 % for grade B. The pellets may also fulfill the sulphur content requirements set at S≤0.2 % for Grade A and S≤0.3 % for Grade B, respectively (Appendix A, Tables 3 and 4). Furthermore, producing pellets from straw increases nitrogen concentration with additives *(Duca et al. 2014)*.

3.4.2. Pellet dimension, density and dimensional stability

The pellet mean size (length and diameter) and weight before and after storage are shown in Table 3.5. The length of the pellet depends on the material's bonding capacity. In this study, the initial diameter of a WSP (T_1) was 8.2 mm, but the WSP with additives (T_2 to T_5) ranged from 8.01 to 8.48 mm. Regarding the pellet standard (EPC 2013; ISO/TS 2016), the pellet diameter supports the figures, where the pellet length must be 6 to 8.0 mm. In addition, the pellet diameter was immediately expanded because the pellet production die's hole diameter was 8.0 mm.

Table 3.5: Pellet dimension and weight before and after storage

Treatment	Length, mm		Diameter, mm		Weight, g	
	Before storage	After 14 days of storage	Before storage	After 14 days of storage	Before storage	After 14 days of storage
T_1	22.69 ± 7.36[a]	22.67 ± 7.35[a]	8.20 ± 0.15[ad]	8.21 ± 0.16[ad]	1.38 ± 0.25[ae]	1.34 ± 0.23[a]
T_2	22.79 ± 9.19[a]	22.75 ± 9.18[b]	8.27 ± 0.15[ad]	8.32 ± 0.16[b]	1.20 ± 0.49[be]	1.18 ± 0.52[a]
T_3	26.89 ± 6.01[b]	26.52 ± 6.20[c]	8.38 ± 0.33[b]	8.32 ± 0.28[a]	1.53 ± 0.46[a]	1.45 ± 0.49[ac]
T_4	35.82 ± 4.64[cf]	35.45 ± 4.50[a]	8.17 ± 0.08[acd]	8.13 ± 0.11[ad]	2.22 ± 0.33[ce]	2.12 ± 0.33[bc]
T_5	37.38 ± 3.56[df]	37.44 ± 3.68[d]	8.13 ± 0.12[acd]	8.10 ± 0.10[c]	1.32 ± 0.18[ade]	1.37 ± 0.18[ad]

Note; Average and standard deviation of 33 replicates at a 95% confidence interval

Figures following the "±" were the standard deviation of samples

Superscript letters of the alphabet indicate that means with the same letter designation in a column were insignificantly different at $p = 0.05$

T_1: Wheat straw, T_2: Wheat straw and Saw dust, T_3: Wheat straw and Bentonite clay, T_4: Wheat and Biochar, T_5: Wheat straw, Saw dust, Bentonite clay, Biochar.

The initial pellets length from WS with binders (T_2 to T_5) varied from 22.79 to 37.38 mm, longer than the pellets from WS only (22.69 mm). According to the pellet standard (ISO/TS 17225-8:2016), the produced pellets supported the data where the pellet length needs to be 3.15 to 40.0 mm. It was found that both biochar (10%) and a combination of additives (SD, biochar, and bentonite clay) blended with WS resulted in pellets of considerably longer lengths and smaller diameters than nonblended pellets (T_1). This was likely because the biochar particle improved the pellet's compaction quality, allowing it to remain a more stable pellet shape when it exited from the plate die. This study supports other research results like Serrano et al. (2011), who made pellets from barley straw mixed with pine SD to improve the quality and observed increased pellet length by adding additional ingredients. Serrano et al. (2011) showed that pellet length increased with the addition of pine meal (12%), woody biomass, like our study with biochar to straw biomass. Also, the research results were consistent with another work (Lu et al. 2014a), where pellets were 40 mm long and 13 mm in diameter. Overall, binders increase WSPs' physical quality (length).

Furthermore, the individual pellet weight was more or less the same for all pellets, except T_4 (WS and biochar), where the average weight was almost two times (2.22 g). The T_4 pellets' individual weight was higher because biochar has more bulk density. Thus, the mean apparent density values were not proportional to the pellet's biochar amount. Therefore, the finding of this study was comparable to Serrano et al. (2011). They also discovered that the increased pine SD in the barley pellets did not correlate with the mean apparent densities. Finally, it is concluded that individual pellet weight increase was not a simple proportion of higher density.

In this research, a one-way ANOVA test was used to examine the influence of blending on the sizes of pellets after storage, followed by a Duncan posthoc test (Appendix B, Table B1). After 14 days, pellet storage was considered as a stable pellet, and the size and density were measured. Table 3.6 shows the initial pellet density, diameter, and longitudinal expansion, as well as relaxed density.

Table 3.6: Mean size expansion and density change after storage

Treatment	Initial apparent density, kg/m^3	Apparent relax density, kg/m^3	Average expansion, %		
			Relax	Longitudinal	Diametrical
T$_1$	1214.02 ± 229.71[a]	1181.38 ± 229.27[a]	32.64[a]	0.026	0.00[ac]
T$_2$	972.00 ± 96.22[bd]	934.85 ± 80.88[bef]	37.15[a]	0.039	-0.04[bc]
T$_3$	1041.57 ± 244.75[bd]	1003.68 ± 256.34[cef]	37.88[a]	0.37	0.07[a]
T$_4$	1189.24 ± 147.37[a]	1163.54 ± 152.64[a]	25.70[a]	0.37	0.04[a]
T$_5$	683.03 ± 96.7[6c]	713.39 ± 104.32[d]	-30.36[a]	-0.06	0.03[a]

Note; Average and standard deviation of 33 replicates at a 95% confidence interval
Figures following the "±" were the standard deviation of samples
Superscript letters of the alphabet indicate that means with the same letter designation in a column were insignificantly different at p = 0.05

The initial apparent density values for pellets without binders were significantly higher than the WSPs with binders. For example, the initial average pellet density of WS (T$_1$) with no binder was 1214.02 kg/m^3 and was as low as 683.03 kg/m^3 for a WSP with binders (T$_5$) due to being less compact. Similarly, the pellets made of WS had higher apparent relax densities than those made with binders. Generally, adding a binder did not significantly increase the pellets' density, and there was no significant difference in pellet density related to the varying binders.

When bentonite (T$_3$) and biochar (T$_4$) were added to the WS, the pellet density was higher than that when SD was added (T$_2$). Because bentonite particles are so small, they can fill the spaces between WS grind particles. Furthermore, they may have formed films around the biomass particles during pelleting due to water and high pressure, resulting in particle bonding. In addition, because bentonite and charcoal are heavy (higher specific gravity), the particle density is higher than SD.

During stabilisation, the change in pellet dimension is referred to as dimensional stability (Appendix B, Table B1). The ANOVA test findings in Table 3.6 show an insignificant difference in size before and after storage. Furthermore, the standard deviation values for the additives were quite similar, although the changes were relatively significant.

The apparent relaxed density (a set of 33 single pellets after 14 days of storage) and percentage of mean size expansions relative to the initial density are shown in Table 3.6. The pellets tended to expand in length, although they were statistically insignificant. The diameter fluctuates with no clear trend. During 14 days of equilibration, the overall impact decreased in apparent density.

All pellets decreased their relaxed densities throughout the 14 day storage period, excluding T_5, indicating unstable mobility inside the particle structure. The relaxing of compressed WS fibres, seen by the expansion of all pellet lengths, is a feature of the reduction in relaxed density. The relaxed density and longitudinal expansion were negative in the case of T_5. This might have occurred due to the possible moisture released during storage. Moreover, the diametrical expansion of T_2 (WS and SD) pellets was negative because SD has a water holding capacity, which was released after storage.

Overall, this study confirmed the other studies' results. During storage, woody and nonwoody pellets expanded longitudinally and either shrank or expanded radially (Lu et al. 2014a). However, compared to Lu et al. (2014a)'s work, the pellets produced in this study showed a more significant proportion of longitudinal expansion. For example, the longitudinal expansion in this study was 3.7%. In contrast, the longitudinal increase of WS pelleting was only 2% in the analysis (Lu et al. 2014a).

3.4.3. Effect of binders on heating value and ash content

The bulk density of WS, SD, biochar and pellets of various treatments are shown in Table 3.7. The lowest and highest bulk density was 107.26 and 890.0 kg/m^3 for WS and bentonite clay, respectively. Generally, adding SD increased the WSP density (Lu et al. 2014a). However, pellet density was significantly different. Similarly, the bulk density of the wheat pellet (T_1) without binders was considerably lower than that of the WSP with binders. However, adding biochar and bentonite clay resulted in higher pellet density than using SD, primarily due to a gap between the particles of the WS grind. In addition, a combination of additives with WS (T_5) could increase pellet density (427.45 kg/m^3) because of its multiple effects as a binding material during the pellet. However, in this study, all pellet bulk density was lower than 600 kg/m^3 and lower than the ISO/TS bulk density standard for commercial nonwoody pellets (ISO/TS 2016) (Toscano et al. 2013; Duca et al. 2014).

Table 3.7: Higher heating value, ash content and bulk density

Features	Saw dust	Wheat straw	Coconut shell biochar	Bentonite clay	Pellets				
					T_1	T_2	T_3	T_4	T_5
Bulk density, kg/m^3	208.09	107.26	583.48	890.0	244.79	322.45	521.6	505.75	607.4
Ash, (%)	0.33	7.3	3.90	89.63	7.09	14.60	17.30	11.40	11.87
Calorific value HHV (MJ/kg)	20.95	17.6	30.75	0.0	17.02	18.23	18.14	20.21	19.06

Note; HHV: Higher Heating Value, T_1: Wheat straw, T_2: Wheat straw and Saw dust, T_3: Wheat straw and Bentonite clay, T_4: Wheat and Biochar, T_5: Wheat straw, Saw dust, Bentonite clay, Biochar.

The quantity of ash WSPs depended on several parameters, including the pelleting procedure. The ash content (0.33%) of SD was far lower than all treatments, ranging from 7.30 to 17.30%. In the case of WS, the ash content comprised up to 7.30% of the weight, more significant than that of SD. This disparity could be due to a combination of dust present in the original WS material. On the other hand, the ash level of all treatment (T_1 to T_5) samples increased significantly, particularly in the T_3 treatment (WS and bentonite clay) samples. The pellet T_3 had the highest ash content (17.30), which was bentonite containing 89.63% ash. Likewise, the pellets of T_5 had a higher ash percentage than WS due to a blend of 10% bentonite with other additives. According to the statistical study, introducing binders affects the ash content of the WSPs.

This study found that biochar blending might improve the WS's performance as a fuel pellet, bringing it closer to the ash level limit of commercial nonwoody pellets. The nonwoody pellets ash percentage was graded based on ISO 17225-8 and was limited to less than 10% of Grade B. (Table A4, Appendix A). In contrast, the ash content of pellets from solely WS was the lowest (7.09%) of the pellets.

The HHV of WS, SD, charcoal and pellets of various treatments are listed in Table 3.7. WS, SD and biochar had average HHVs of 17.6, 20.95 and 30.75 MJ/kg, respectively. WS had a lower HHV than the other samples. At the same time, ash content was higher (Table 3.7), indicating no correlation between ash content and heating value. Other researchers (Shaw, Karunakaran & Tabil 2009) and (Mani, Tabil & Sokhansanj 2006) reported similar findings.

Biochar has a substantially larger energy potential than SD, with a 30.75 MJ/kg heating value, whereas bentonite has no heating value. As a result, adding additives to WS can significantly enhance the pellets' HHV, but adding biochar was the most significant. In comparison, barley straw had a 17.02 MJ/kg calorific value (Serrano et al. 2011), and WS had 17.74 MJ/kg (Lu et al. 2014a). Wood pellets are in the market in heating values ranging from 16 to 20 MJ/kg (Toscano et al. 2013; Duca et al. 2014). This study supported previous research findings, demonstrating that using bentonite clay, biochar, and a combination of additives achieved excellent performance in terms of higher heating value and bulk density.

3.4.4. Effect on durability

Several factors can affect the durability of pellets, such as pressure, pelleting temperature, volume reduction and material composition (Tilay et al. 2015). This research produced the pellet through the rollers' constant spinning and friction between the plate die and the rollers. As a result, the production pressure was fixed. As previously indicated, excellent quality pellet results from the barrel's operating temperature of 60~80°C.

Table 3.8 shows the drop test results for each treatment. Table B2 of Appendix B contains a sample data measurement for the pellet durability test. Moreover, the ANOVA test was performed to investigate the additive treatment on pellet durability effect. From the statistical analysis, it was found that there was no significant difference in durability among the treatments. In contrast, the individual pellet weight was statistically varied.

Table 3.8: Single drop test for durability measure

Treatment	Pellet weight, Mean (g)	Durability as single drop test, Mean (%)
T_1	0.88 ± 0.16^a	83.22 ± 14.40^a
T_2	1.37 ± 0.5^b	86.75 ± 18.72^a
T_3	1.75 ± 0.39^{cf}	80.85 ± 17.45^a
T_4	2.03 ± 0.34^{de}	84.45 ± 16.80^a
T_5	1.97 ± 0.36^{efe}	82.51 ± 16.75^a

Note; Average and standard deviation of 15 replicates at a 95% confidence interval
Figures following the "±" were the standard deviation of samples
Superscript letters of the alphabet indicate that means with the same letter designation in a column were insignificantly different at $p = 0.05$

The ANOVA test revealed that pellet weight did not significantly impact pellet durability. Moreover, average pellet weight and standard deviation refer to homogeneity, resulting in an insignificant influence on durability. The durability of pellets was roughly the same whether they were blended with additives or not.

In this study, pellet durability ranged from 97 to 99%, with a standard variation of 10%, similar to other research (Iroba et al. 2014). Iroba et al. (2014) investigated the manufacture of ground barley straw pellets using pretreatment radio frequency and temperature change during compaction compared to other nonwoody biomass pellets. The single drop test revealed that the durability of the generated pellet could reach 99.17%, meeting the ISO standard.

3.4.5. Effect of pellet hardness

Compression tests of pellets were carried out until they broke, and ten pellet samples from each treatment were measured. Firstly, the pellet sizes were measured and recorded. Table 3.9 summarises the mean average of hardness test findings.

Table 3.9: Hardness as compression test

Treatment	Sample pellet length, mean (mm)	Hardness as max compressive, mean (N)
T_1	22.67 ± 7.35^a	249.40 ± 267.90^a
T_2	22.75 ± 9.18^a	1352.10 ± 229.81^b
T_3	26.52 ± 6.20^a	950.10 ± 181.99^c
T_4	35.45 ± 4.50^b	2193.10 ± 306.01^{df}
T_5	37.44 ± 3.6^{ac}	2300.60 ± 139.29^{ef}

Note; Average and standard deviation of 10 replicates at a 95% confidence interval
Figures following the "±" were the standard deviation of samples
Superscript letters of the alphabet indicate that means with the same letter designation in a column were insignificantly different at p = 0.05

The pellets had a mean hardness ranging from 249 to 2300 N (Table 3.9). The hardness of the pellets without additives (T_1) was significantly low (249 N), which means the compaction was not good enough for ISO pellet quality. The compressive testing (Tilay et al. 2015) revealed that pellet hardness was less than 100 N, using a canola meal to make the pellets. The pellets were softer than the pellets produced in this experiment. The pellets that result have no hardness. One of the reasons might be that the lignin content was lower in the WS, which exhibited less binding action.

The statistical ANOVA test was used to determine the influence of additive treatments on average hardness values. The mean lengths of the pellet samples indicate that the pellets utilised in these comparisons were relatively nonuniform (Table 3.9). As a result, the influence of particle length on hardness was noticed. Overall, it was found that the pellet length and covariate length with treatment significantly affect the pellet's hardness. From the summarised results in Table 3.9, it is noticed that the additive mixing increased the hardness, especially biochar (T_4), and combined additives (T_5) had a significant impact on the pellet hardness (Sig. p = 0.05). In comparison, pellets made from coconut fibre, rice husk, and SD had hardness ranging from 1049 to 1867 N (Lu et al. 2014a). Overall, it was demonstrated that the additives increased the pellet hardness.

3.4.6. Tensile strength of pellet

Tensile strength reflects pellet quality concerning pellet strength and hardness and its resistance to breaking and dust generation through transportation and handling. Table 3.10 presents WSP fracture load and tensile strength with and without binder. The pellet diameter and thickness ranges are 8.12 to 8.33 and 2.35 to 3.30 mm. The average fracture load of WSPs with binders varied between 21.64 to 37.23 N. In contrast, the average fracture load was 13.37 N for pellets without binders (T_1). With the addition of a binder, pellets' tensile strength and fracture load were much higher than no binder pellets. As a result, the tensile strength of WS binder pellets ranged from 0.52 to 1.22 MPa. The significant tensile strength was

for pellet made WS with bentonite clay (1.22 MPa). Kashaninejad and Tabil (2011) reported that the fracture load and tensile strength of WSPs were 19.10 N and 0.81 MPa, individually, near this paper's WSP information (Table 3.10). Table B3 of Appendix B contains samples detail raw and statical analysis data of tensile strength.

Table 3.10: Tensile strength and fracture load

Treatment	Observation No	Mean		Facture load, N	Tensile strength (MPa)
		Diameter, mm	Thickness, mm		
T_1	10	8.31	2.95	13.37	$0.36 \pm .4^a$
T_2	10	8.33	3.30	21.64	$0.52 \pm .12^a$
T_3	10	8.20	2.41	37.23	$1.22 \pm .21b^e$
T_4	10	8.17	2.35	35.26	$1.19 \pm .27^{ce}$
T_5	10	8.12	2.38	33.16	$1.09 \pm .41^{de}$

Note; Average and standard deviation of 15 replicates at a 95% confidence interval
Figures following the "±" were the standard deviation of samples
Superscript letters of the alphabet indicate that means with the same letter designation in a column were not significantly different at p = 0.05

3.4.7. Fines/dust content of pellet

One quality indicator is the amount of fines coming directly from the pellet. Fines/small particles are generated during transportation, handling and storage through attrition and breakage due to the fragile nature of the pellet (Boac, Casada & Maghirang 2008; Oveisi et al. 2013). This has implications including an increased risk of dust explosion, fire, segregation, arching, equipment fouling, health issues for people inhaling the dust, and the loss of a significant portion of the material (Ramírez-Gómez 2016; Ilic et al. 2018).

Table 3.11 presents the total small particle categories. The particles produced from the abrasive test were in the following order: $T_1>T_2>T_4>T_3>T_5$. It was observed that WSPs without additives had more fine particles. In contrast, pellets with bentonite clay had fewer fines. According to the sieving analysis, the particle was sieved to determine the particle size distribution and presented in Table 3.11.

Table 3.11: Produced particle types from pellets

Treatment	Small particles (%)	3.15 mm < lumps < 5.6 mm (%)	1 mm < fines < 3.15 mm (%)	Dust <1 mm (%)
T_1	44.32 ± 3.34^a	30.87 ±1.49^a	8.58±2.56^a	4.86±.73^a
T_2	34.96 ± 3.45^b	26.75±3.69^a	5.46±.48^a	2.74±2.16^a
T_3	9.76 ± 1.73^{cf}	6.89±1.44^{be}	1.92±.08^{be}	.94±.24^b
T_4	17.03 ± 4.10^{df}	14.39±2.33^c	1.97±.30^{ce}	.63±.62^c
T_5	7.52 ± 2.37^{efg}	4.51±2.39^{de}	1.93±.04de	1.07±.11^d

Note; Average and standard deviation of 3 replicates at a 95% confidence interval
Figures following the "±" were the standard deviation of samples
Superscript letters of the alphabet indicate that means with the same letter designation in a column were not significantly different at $p = 0.05$

As can be seen in Figure 3.12, the sample containing the highest quantity of fines (1 mm < fines < 3.15 mm) was T_1 and the lowest was T_3 (1.92%). The visual observation of particles produced from pellets is presented in Figure 3.13. It can be seen that all particles retain their cylindrical shape. The detailed raw and statical analysis data of the finesse test can be found in Table B4 in Appendix B.
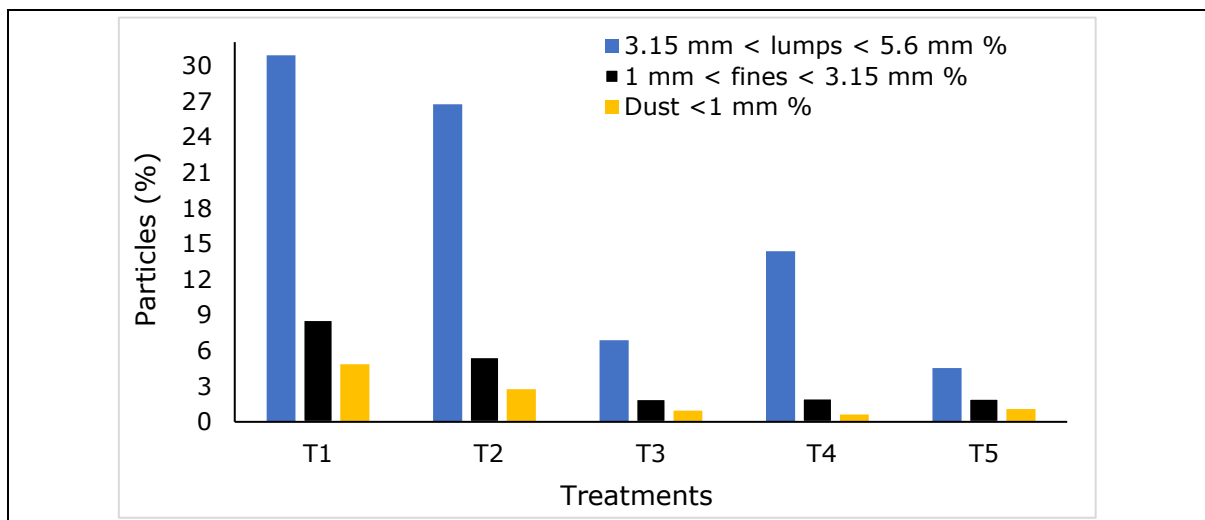
Figure 3.12: Categories of particles
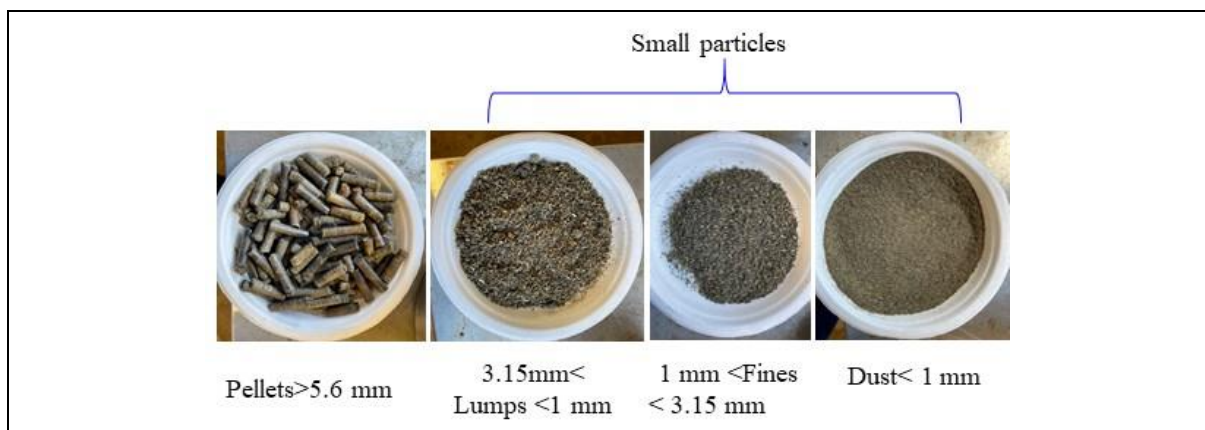
Figure 3.13: Small particles size classified after sieving

3.4.8. Water resistance impact

The visual observation of the pellet shape after weathering is presented in Table 3.12. Observing the pellet shape after being submerged in water revealed that the T_1 and T_2 pellets had almost entirely lost their shape, while the T_3 pellets showed partial swelling and collapse. In contrast, no visual disintegration was observed in the T_4 and T_5 pellets, indicating that a slight bump might be preventing water from penetrating them. T_4 pellets had a superior waterproof capacity, leading to advantages for storage in small scale usage. Table B5 in Appendix B contains detailed raw and statical analysis data of the wettability index.

Table 3.12: Visual observation of the pellet before and after weathering

Condition	Treatment				
	T_1	T_2	T_3	T_4	T_5
Before watering					
After watering					
% WI	78.64	115.68	26.29	24.04	27.17

The maximum water absorption for T_2 was 147% and the second highest was T_1, which is not within the ISO/TS 17225-8 (ISO/TS 2016). Therefore, the T_2 results indicate that SD enhanced water penetration. Moreover, theoretically, the water absorption capacity of T_3 to T_5 was within the ISO limit and could enable combustion. However, the lowest moisture content was ~24% for the T_4 pellets. This indicates that the increase in moisture content was much lower for these pellets than for the other group.

The average diameter of pellets after weathering indicated swelling. For example, the pellet diameter for T_3, T_4 and T_5 was slightly changed, meaning it penetrated the pellets (Table 3.13). Kubojima and Yoshida (2015) and Ghiasi et al. (2014) examined the dimensional change of various pellets that were swollen in water. They showed that the changes in post-torrefied pellets were small, supporting a similar result in this study. In this current study, pellets produced from binders, especially biochar, showed very little change in diameter means, i.e., they were slightly swollen. As a result, pellets retained their outer layer, preventing water from penetrating them. Therefore, the results demonstrate that avoiding water uptake needs additives like bentonite, biochar, or a combination.

Table 3.13: Weathering effect on moisture content and pellet diameter

Treatment	Moisture content (%)		Diameter (mm)	
	Initial	Final	Initial	Final
T_1	6.27	29.44	8.21	n. a.**
T_2	6.01	n. a.*	8.23	n. a.**
T_3	4.4	5.97	8.27	8.58
T_4	3.70	4.87	8.07	8.13
T_5	3.82	5.32	8.11	8.22

Note; * Not available and uncountable;
    ** Not available for determination due to lost shape

3.5. Morphology of wheat straw pellets

The morphology of the material structures of pellets made with various additives using a scanning electron microscope (SEM) is shown in Figure 3.14. Here, the SEM pictures of the WS after adding the binders were used to examine the structure of those fibres (size 50 µm X 400). Mechanical interlocking is the most common binding mechanism for pellets, followed by solid bridging, interparticle attraction and short range physical forces induced by the binder (Valdés et al. 2018).
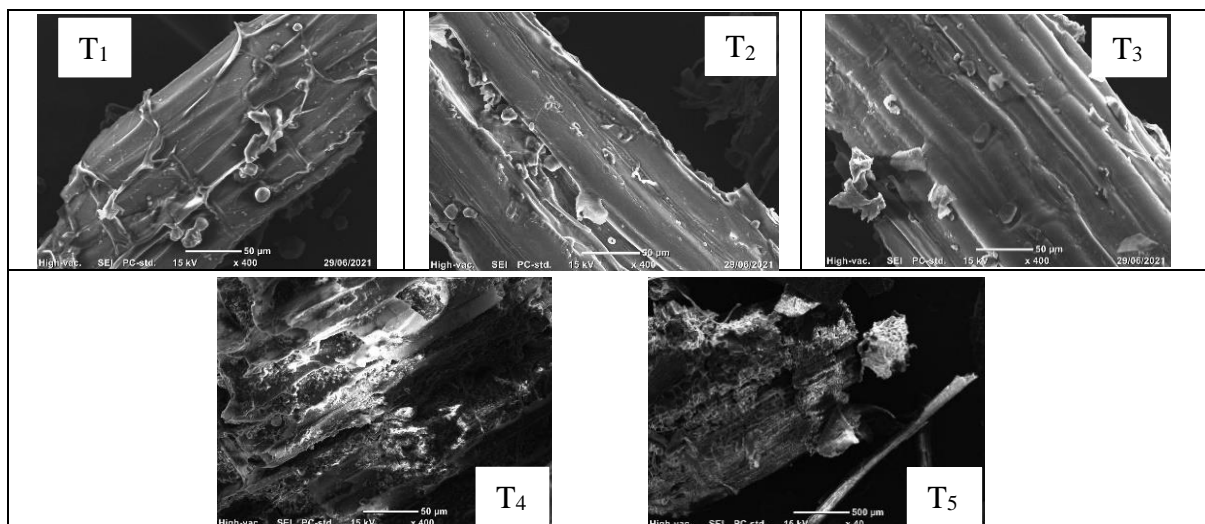
Figure 3.14: Scanning electron microscope (SEM) images of pellet

By observing the apparent morphology, it can be seen that the WSPs (T_1) had a prominent fibrous structure similar to most biomass (Cui et al. 2012). Furthermore, the pellet structures were crystallised, forming solid bonds to increase the hardness and solidification properties following cooling (Zaini, Nurdiawati & Aziz 2017). Moreover, the lignin present in the mixtures created solid bridges that guaranteed the physical quality of the pellets in terms of durability, even without the additives (Zanetti et al. 2017; Fusi et al. 2021).

Figure 3.14 shows fewer fibres exploded open with increasing temperature and friction in treatments T_1, T_2 and T_3. In contrast, the number of long fibres decreased while short fibres increased, resulting in

71

pelleted WS being destroyed into fibres or fibres bundles through pelleting (T_4 and T_5) with biochar. Furthermore, it was observed that there were many clusters of treatments in T_4 and T_5 compared to the others (T_1, T_2 and T_3). This is because biochar application produces high temperatures, creating a more compact and robust structure. In addition, high temperatures during pelletisation can lead to the development of solid bridges through the interaction of molecules (Kaliyan & Morey 2009).

3.6. *Pellet quality comparison*

Table 3.14 highlights the suitability of the produced pellets based on the ISO 17225-8 standard (ISO/TS 2016) for nonwoody/herbaceous/straw biomass pellet quality standards. All pellets fitted into both application categories (A and B) of the average based on diameter, length, moisture content, durability, and net calorific value. Conversely, the pellet bulk density was outside the ISO standard.

Table 3.14: Pellet properties comparison with ISO 17225-8:2016 standard*

ISO 17225-8	D (mm)	L (mm)	MC (%)	Ash (%)	HV (MJ/kg)	Du (%)	FC (%)	BD (kg/m³)
A	6~25	3.15~40	≤ 10	≤ 5	≤ 18	≤ 97.5	≤ 2.0	≥ 600
B	6~25	3.15~40	≤ 10	≤ 10	≤ 17	≤ 96.5	≤ 2.0	≥ 600
Treatment								
T_1	A - B	A - B	A - B	B	A - B	A - B	X	X
T_2	A - B	A - B	A - B	X	A - B	A - B	X	X
T_3	A - B	A - B	A - B	X	A - B	A - B	A - B	X
T_4	A - B	A - B	A - B	X	A - B	A - B	A - B	X
T_5	A - B	A - B	A - B	X	A - B	A - B	A - B	A - B

Note; A = Household use; B = Commercial use; X= Treatment does not fit into any category; D= Diameter; L = Length; MC = Moisture content; Du = Durability; FC = Fines content (<3.15 mm); NCV = Net calorific value; BD = bulk density.
*Classification parameters of nonwoody/herbaceous biomass/straw biomass

When pellet properties were examined according to the ISO standards, the additives blend with WS (T_2 to T_5) failed to meet the standard's use specifications for ash content criteria. Therefore, regarding the same quality standards, pellets made solely with WS (T_1) could only be considered for commercial use (B) but did not fulfil other qualification criteria. Similarly, pellets made solely with wheat residues (T_1) and T_2 (WS and SD), did not meet the requirements of the minimum fine to be classified in categories A and B. However, the T_3, T_4 and T_5 pellets produced less than 2% fines and met the ISO standards. Moreover, the produced pellets containing the additive did not reach the minimum bulk density to be included in the same category according to the ISO 17225-8 standard.

Additive inclusion with WS increased the ash content and the net calorific value, meeting the quality criteria of the straw pellet standard. As a result, the pellets containing additives (T_3, T_4 and T_5) presented the most significant potential for pellet production and mostly complied with the ISO 17225-8 standard (ISO/TS 2016). In addition, they had the highest net calorific value, the highest mechanical durability, and less dust.

3.7. Summary and conclusion

Five pellet types were made with or without binders (WS only) to examine the quality attributes. The results revealed that the binder added pellets possessed the standard value of bulk density, abrasive resistance, heating value and lower moisture absorption than WSPs. Overall, the binder contributed to the making of straw based pellets. However, more study is needed to minimise ash content in the developed pellet. The main conclusions that emerged from the present research are summarised below:

- For homogenisation, a size reduction procedure was required first. After mechanical comminution, the material was pretreated by wetting and left with its binders for at least three days. The wetting acted as a medium for enzymatic activities that softened the component linkages and functioned as a binder.

- It has been found that the pellet mill's barrel temperature should reach 60-80 °C to create smooth, non abrasive, and dry pellets. Furthermore, the raw material moisture level should be around 20% w.b. for pellet production and 10% for optimum storage quality. However, binder added pellets possessed a more uniform apparent density than those without a binder.

- Due to densification, the bulk density of WSPs increased from 205.41 kg/m^3 to more than 500 kg/m^3. Therefore, binder mixes resulted in a longer and heavier pellet. This study also found that biochar blends lower ash concentration (11.40%) and creates a higher heating value by 20%.

- In a single drop test, the pellet's durability varied from 97 to 99%, revealing that additive mixing did not encourage durability.

- The pellets of WS with binder tensile strength varied from 0.52 to 1.22 MPa, revealing that additives, especially biochar and bentonite clay, increased the strength of the pellets considerably.

- In the abrasive test, pellets showed that small particles varied from 7.52 to 44.32% and observed the order $T_1>T_2>T_4>T_3>T_5$. Moreover, the percentage of fines followed the same trend, where pellets with binders complied with the ISO standard (fines <2.0%).

- The wettability test revealed less water absorption capability in the pellet for binding materials and the dimension was unchanged.

- The results demonstrated that the binder could improve pellet quality, meeting the requirements of the relevant ISO standards except for ash content and bulk density. All pellets generated in this study also met the nitrogen standard set by ISO 17225-8: N≤1.5% for grade A and N≤ 2.0% for grade B. The pellets also fulfilled the sulphur content requirements, set at S≤0.2% for Grade A and S≤0.3% for Grade B, respectively.

CHAPTER 4: UPGRADING OF PELLETS QUALITY: EFFECT OF ADDITIVE BLENDS

Abstract

Agricultural residues like straw contain less lignin and other natural binders, which is challenging when producing suitable quality pellets. This research aimed to improve pellet quality by mixing different wheat straws (WS), saw dust (SD), bentonite clay (BC), corn starch (CS), crude glycerol (CG), and biochar (BioC). Seven treatments were analysed to identify suitable pellet quality, and ISO 17225-8 standards were used to evaluate the results. The results showed that additives improved the pellets' physical and elemental properties and quality. An additive could improve pellet durability by ≥92%, bulk density by ≥600 kg/m³ and heating value by ≥18.5 MJ/kg, meeting the pellet ISO standard specification requirements. However, the inorganic ash content was higher than the ISO standard level, suggesting further research on alternative additive use for ash reduction.

4.1. Introduction

The previous chapter reported making WSPs using suitable binders. This chapter discusses upgrading the physical and chemical quality of WS pellets.

The available pellet production work has reported on fuel properties (Kaliyan & Vance Morey 2009), a different combination of biomass (Demirbas 2004; Bilal et al. 2017), varied binder use (Shahram Emami 2014), and pellet durabilities (Shaw 2008; Kumar, Jones & Hanna 2009) among other things. Until now, little information has been available regarding the quality improvement of straw pellets. Lu et al. (2014a) conducted a detailed experiment on the thermochemical conversion of binders and wood wastes added to WSPs. Another attempt has been made to quantify oat, wheat, barley and canola straw densification properties. They concluded that handling, transport and use significantly correlated with density (Adapa, Tabil & Schoenau 2009). In addition, Lu et al. (2014b) investigated the additives admixing and densification load for WS pelletisation. They found that binding materials (BC and wood waste) and compact load (4000 N) positively impacted density and tensile strength.

Different additives and pretreatment processes (steam exploration, microwave irradiation and enzymatic hydrolysis) have been investigated to improve pellet quality (Zhu et al. 2006; Yang, Hanna & Sun 2012; Ríos-Badrán et al. 2020; Brand et al. 2021). The pretreatment process often involves significant energy requirements, a complex system, and sophisticated steps that can increase pellet production costs. For example, stream exploration needs a temperature of 180~230ºC for 2~10 minutes

(Harmsen et al. 2010). Hence, the present study focused only on different additive mixing and the size reduction of WS for pellet production to avoid the additional cost. Also, the proposed method is suitable for farm-level pellet production due to the relatively simple process involved.

The objectives of this chapter are as follows: (a) to explore the utilisation of various additive combinations for enhancing the chemical and physical characteristics of pellets; (b) to assess the influence of additives on fuel properties; and (c) to compare the fuel properties with the standard values specified by ISO 17225-8.

4.2. Materials and methods

In this study, pellet making used five different additives: SD, BC, CG, CS and activated BioC (Table 4.1). The pellet-making process and testing procedures were the same as reported in Chapter 3. Figure 4.1 illustrates seven distinct types of pellets.

Table 4.1: Experimental design for pellet production

Treatment	Mixing materials	Percentage in the mix, %
T_1	WS	100
T_5	WS: SD: BC: BioC	70: 10: 10: 10
T_6	WS: SD: BC	80: 10: 10
T_7	WS: SD: CS	80: 10: 10
T_8	WS: SD: BC: CG	70: 10: 10: 10
T_9	WS: SD: CS: BioC	70: 10: 10: 10
T_{10}	WS: SD: CS: BC: BioC	60: 10: 10: 10: 10

Note; % = fraction of total mass basis

T_6 and T_7: WS with binding additives

T_8 and T_5: WS with energy materials

T_9: WS with both binding and energy additive

T_{10}: All combinations with WS.

WS: Wheat Straw, BC: Bentonite Clay, SD: Saw Dust, BioC: Biochar, corn starch (CS)
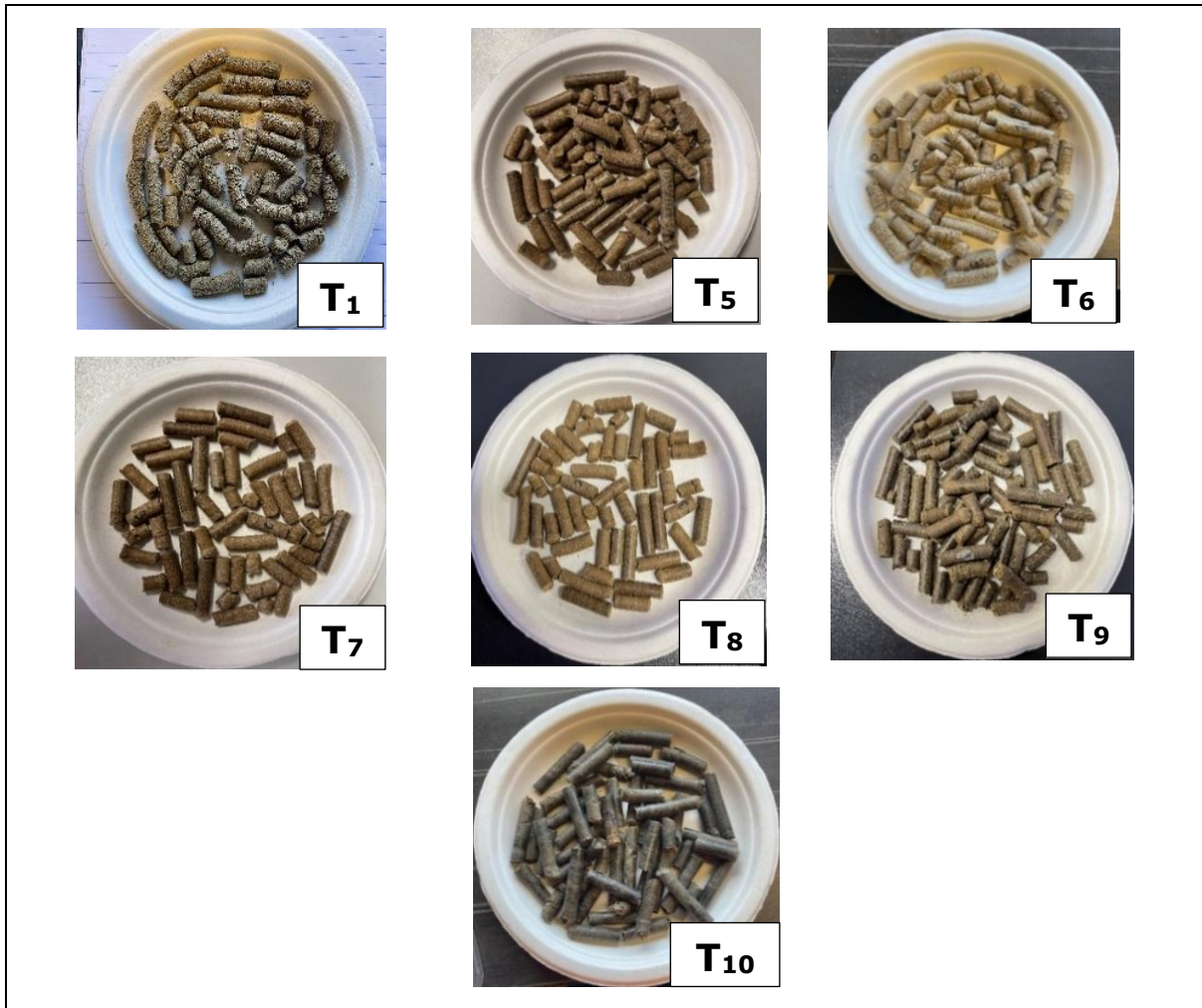
Figure 4.1: Pellets with different additive blends and WS

4.3. Results and discussion

4.3.1. Pellet composition

The primary components of biomass as well as WS, are lignin, cellulose and hemicellulose (Lu et al. 2014a). Hemicelluloses and lignin are all amorphous polymers that act as binders. They are activated (softened) with temperature and moisture to create particle-to-particle solid bonding. In addition, based on the moisture content, the glass transition temperature of lignin is 60~200ºC (Olsson & Salmén 1997). Furthermore, StelteHolm, et al. (2011) noted that the WS's lignin softening glass transition was about 53ºC. However, in this study, the pellet development temperature reached around 80ºC due to particle friction in the pelletising machine.

Many research studies have noted that enhancing lignin is essential for densification and pellet quality improvement. WS has a low lignin content and may not bind the particles well (Thomas, Van Vliet & Van der Poel 1998). However, in this research, the lignin content of SD (26.66%) was significantly higher than WS (7.30%) (Table 4.2).

Treatment	Dry wt, %		
	Hemicellulose	Cellulose	Lignin
T_1	22.40^a	41.30^a	7.0^a
T_5	23.30^e	30.0^b	10.60^c
T_6	27.30^b	30.70^b	8.10^b
T_7	29.00^c	28.80^c	10.50^c
T_8	24.80^d	30.20^b	9.60^d
T_9	20.0^f	31.10^b	13.10^e
T_{10}	20.6^g	28.20^d	12.10^f

Note; N = 3 replications

Superscript letters of the alphabet indicate that means followed the same letter were insignificantly different at p = 0.05

T_1: Wheat straw, T_5: Wheat straw, Sawdust, Bentonite clay, Biochar; T_6: Wheat straw, Sawdust, Bentonite clay; T_7: Wheat straw, Sawdust and Corn starch; T_8: Wheat straw, Sawdust, Bentonite clay and Glycerol; T_9: Wheat straw, Saw dust, Corn starch, Biochar and T_{10}: Wheat straw, Sawdust, Corn starch, Bentonite clay and Biochar.

From Table 4.2, the hemicellulose content did not vary significantly. The physical process (temperature change) did not change the amount of hemicellulose. Instead, the cellulose content decreased through additive mixing. Hence, the pelleting temperatures broke down the structure and changed the cellulose content (Pradhan, Mahajani & Arora 2018). Therefore, different additives were mixed with WS to increase the lignin content and help it bond with the WS particles. Among the treatments, the lignin and cellulose content had an inverse relationship. Overall, cellulose decreased by 41% to 28%, and lignin varied from 7 to 13.10% (Table 4.2).

4.3.2. Chemical configuration

The chemical analysis of the elemental composition of pellets is useful for thermochemical conversion modelling, predicting the solid and gas phase and reactant ratio. The pellet's element characteristics are determined by both major and minor chemical components. The proximate analysis focuses on the major elements, while the ultimate analysis reveals few features in comparison.

The proximate analysis of pellets involves determining the content of various components, including moisture, volatile matter, fixed carbon and ash (Table 4.3). This analysis provides insights into the fuel's combustion properties, such as its heating value, reactivity and potential for emissions. Furthermore, the ultimate analysis determined the minor elements of a WSP (Table 4.4).

Table 4.3: Proximate analysis of pellets

Treatments	MC, %	VM, %	FC, %	Ash, %	GCV, MJ/kg
T_1	6.20[a]	75.61[a]	11.10[a]	7.09[a]	17.02[a]
T_5	3.50[c]	53.03[e]	31.60[e]	11.87[e]	19.06[e]
T_6	4.20[b]	58.9[b]	20.70[b]	16.20[b]	18.67[b]
T_7	3.45[c]	61.88[c]	21.80[c]	12.87[c]	18.89[c]
T_8	7.20[d]	60.30[d]	18.60[d]	13.90[d]	18.49[d]
T_9	5.70[e]	53.50[f]	32.60[f]	8.20[f]	19.12[f]
T_{10}	3.70[f]	56.60[g]	30.90[g]	8.80[g]	20.36[g]

Note; MC: Moisture content; VM: Volatile materials; FC: Fixed carbon; HV: Heating value; GCV = Gross calorific value; N = 3 replications
Superscript letters of the alphabet indicate that means following the same letter insignificantly different at p = 0.05
T_1: Wheat straw, T_5: Wheat straw, Sawdust, Bentonite clay, Biochar; T_6: Wheat straw, Sawdust, Bentonite clay; T_7: Wheat straw, Sawdust and Corn starch; T_8: Wheat straw, Sawdust, Bentonite clay and Glycerol; T_9: Wheat straw, Saw dust, Corn starch, Biochar and T_{10}: Wheat straw, Sawdust, Corn starch, Bentonite clay and Biochar.

Table 4.4 represents the minor components of the pellets according to the ultimate analysis. The treatments showed slight differences in carbon, hydrogen, nitrogen, and oxygen. These chemical characteristics help promote clean combustion (Vamvuka & Sfakiotakis 2011). A higher oxygen level in biomass will be more thermally reactive but reduce the heating value (Haykiri-Acma & Yaman 2008). As observed in Table 4.4, the oxygen content variation levels were not remarkable (43~50%).

Table 4.4: Ultimate analysis of pellets

Treatments	Dry wt, %				
	Carbon	Hydrogen	Nitrogen	Sulphur	Oxygen*
T_1	44.32[a]	4.90[a]	0.56[a]	0.11[a]	50.11[a]
T_5	45.87[eh]	6.30[dg]	0.72[e]	0.21[eg]	46.90[e]
T_6	45.48[bh]	5.20[b]	0.81[b]	0.21[bg]	48.30[b]
T_7	46.57[c]	5.00[a]	0.66[c]	0.17[c]	47.60[cg]
T_8	45.31[di]	6.20[cg]	0.68[d]	0.13[dh]	47.68[dg]
T_9	44.89[fi]	4.40[e]	0.59[f]	0.12[ah]	50.00[a]
T_{10}	50.44[g]	5.60[f]	0.77[g]	0.19[f]	43.00[f]

Note; *Determined by a difference; N = 3 replications
Superscript letters of the alphabet indicate that means following the same letter were insignificantly different at p = 0.05

4.3.3. Moisture content

The moisture content of pellets directly impacts their combustion efficiency (Gil, M. V. et al. 2010). Initially, the raw material moisture content was maintained at around 20% for pellet production. However, the generated pellets' moisture content was significantly lower when compared to pelletising moisture because water evaporated due to the temperature produced by die and roller friction (LisowskiPajor, et al. 2019). Huangfu et al. (2014) found that lowering the biomass moisture content from 20% (initial) to 5% (final) boosted combustion efficiency by 50%. In conclusion, the additives improved pellet quality by minimising the moisture content.

4.3.4. Inorganic ash content

The inorganic ash content of WS, SD, BioC and BC showed considerable variation, ranging from 7.09 to 13.90% (Table 4.3). Dick et al. (2007) noted that additive composition and source fuel elements influence biomass pellets' inorganic ash presence. Therefore, the ash content of pellets varies (Table 4.3). For example, among the treatments, the ash percentage was higher in the T_6 pellets, possibly due to the addition of BC (89.63% of ash). In addition, the pellets' ash content varied significantly with additive type. However, BioC positively impacted ash reduction, possibly due to a synergetic effect (T_6). In addition, treatment T_7 had lower ash content (8.20%), resulting in an additive combination that reduced the ash content. All pellets' ash content did not meet the ISO pellet fuels standard (ISO/TS 2016). As a result, further research is needed to minimise pellets' ash content by applying additives and using suitable technologies.

4.3.5. Gross calorific value

The gross calorific value (GCV) is an important measure for assessing the burnability of a material. It represents the amount of energy released per unit of fuel burned. Based on analytical techniques, three types of energy were determined from the biomass. In this case, a higher heating value (at constant volume: dry basis), a lower heating value (constant pressure - dry basis), and a GCV (constant pressure - wet basis or as received) are all defined (Telmo & Lousada 2011). The GCV was considered for all pellets in this investigation because it is measured most practically.

Telmo and Lousada (2011) mentioned that the composition of materials significantly impacts pellets' GCV. From this study, it was evident that pellets with additives ($T_5 \sim T_{10}$) had a higher GCV than pellets without additives (T_1) (Table 4.3). Therefore, due to additive blending, the GCV varied (from 17.02 to 20.36 MJ/kg). The analysis data showed that the additive combination positively impacted GCV and was the highest in T_{10} (20.36 MJ/kg). Moreover, all pellets had a GCV of more than 17.0 MJ/kg, which satisfies the ISO standard's minimum value for commercial/domestic pellet production (ISO/TS 2016). In summary, additives mixed with WS are worthwhile for important combustion parameters (GCV).

4.3.6. Minor chemical elements of pellets

According to the ultimate analysis, Table 4.4 represents the pellets' minor components (insignificant amount). The treatments showed slight differences in carbon, hydrogen, nitrogen, and oxygen. These chemical characteristics help promote clean combustion (Vamvuka & Sfakiotakis 2011). A higher oxygen level in biomass means it will be more thermally reactive, but the heating value will be reduced (Haykiri-Acma & Yaman 2008). As observed in Table 4.4, the oxygen content variation levels were not remarkable (43~50%).

In contrast, higher carbon content is essential for good combustion (Munir et al. 2009). Hence, the carbon concentration level should be like oxygen. The hydrogen and nitrogen variation amounts ranged from 4.40 to 6.30% and 0.56 to 0.81%, respectively. In addition, the pellets had varying sulphur content (~21%), which has no influential role in combustion. In conclusion, the additive addition had no significant impact on minor elements.

4.3.7. Measurement of pellet quality attributes

Pellet quality is an important consideration in handling, transportation, and storage. Pellet quality was measured using six criteria: dimension, bulk density, durability, tensile strength, fines content and wettability index.

4.3.7.1. Pellet dimension

Pellet dimensions (diameter and length) are important aspects of combustion. It is well known that, especially in small furnaces, the thinner pellet enables a more uniform burning rate than the thicker one (Liu, Z. et al. 2013). The pellet length also exaggerates fuel-feeding qualities. It is easier to arrange a continuous flow with shorter particles (Lehtikangas 2001).

Table 4.5 illustrates the pellet's length, diameter, and weight. The analysis information showed the mean and standard deviation from 33 pellets. The lowest length was 22.66 mm for the WSP (T_1); however, the highest length was 39.77 mm for the T_{10} treatment (combining additives with WS). Therefore, additive mixing significantly increased pellet length.

Table 4.5: Physical characteristics of pellet

Treatment	Length, mm	Diameter, mm	Unit weight, g	Apparent density, kg/m^3
T_1	22.66 ± 7.34[a]	8.20 ± .16[a]	1.33 ± .22[a]	1181.37 ± 229.26[a]
T_5	37.44 ± 3.67[bd]	8.10 ± .10[ac]	1.36 ± .18[c]	713.38 ± 104.31[e]
T_6	35.26 ± 3.46[b]	8.15 ± .15[ab]	1.64 ± .24[ad]	893.86 ± 103.99[b]
T_7	29.26 ± 7.64[c]	8.12 ± .13[b]	1.40 ± .52[b]	911.37 ± 213.72[cb]
T_8	34.97 ± 7.05[b]	8.25 ± .10[a]	2.36 ± .54[aeg]	1266.51 ± 176.06[d]
T_9	34.01 ± 5.58[bd]	8.02 ± .13[d]	1.85 ± .38[af]	1072.17 ± 123.79[f]
T_{10}	39.77 ± 2.25[be]	8.14 ± .06[ae]	2.34 ± .25[aeg]	1131.27 ± 98.35[ag]

Note; The values are expressed as means ± standard deviation, N = 33 replications
Superscript letters of the alphabet indicate that means following the same letter insignificantly differs at p = 0.05

Pellet diameter varied slightly from 8.0 to 8.20 mm (Table 4.5). The variation observed could be attributed to the movement of water among the particles, which disrupts the bond development during pellet formation (Mahapatra et al. 2010). Thus, additives had no considerable impact on pellet diameter.

Pellets' apparent/unit density is a significant reactor design and modelling factor. Unit density depends on the influence of individual weight, length, and diameter. For instance, T_8 had the highest unit weight (2.36 g) as well as the most excellent apparent density at 1266.51 kg/m^3. Also, the second highest unit density was 1181.37 kg/m^3 for T_1, and the lowest was for T_5 (713.38 kg/m^3). The unit weight varied from 1.33 to 2.34 g but was inconsistent with additive adding (Table 4.5). Accordingly, a similar trend was found for the apparent density, meaning additive adding had no impact.

4.3.7.2. Pellet bulk density

According to several quality standards, particle density is used to evaluate densified fuels such as pellets and briquettes (Filbakk et al. 2011). The pellet's bulk density impacts transportation and storage space requirements. Higher bulk density means better transportation efficiency and less storage space (Liu et al. 2016). The pellets' average density (bulk and unit) from 33 repetitions/treatment is shown in Table 4.6. The pellets from the fewer mixture (T_1) had a low bulk density (244.79 kg/m^3), maybe causing the pellets to be less compact. Accordingly, the density of the $T_5 \sim T_{10}$ pellets was higher, which might indicate a strong bond among the particles. The highest density found in T_{10} was 665.21 kg/m^3 which could be related to additive combinations. Based on the statistical analysis, density varied significantly with additive admixing (Table 4.6).

Table 4.6: Physical properties of wheat straw pellets

Treatment	BD, kg/m^3	DU, %	GCV, MJ/Kg	TS, MPa	FiC, %	WI, %
T_1	244.79[a]	85.22[a]	17.02[a]	0.36[a]	8.58[a]	78.63[a]
T_5	607.40[e]	97.06b[efg]	19.06[e]	1.09[b]	1.93[c]	28.17[c]
T_6	204.69[b]	92.20[bg]	18.67[b]	1.07[b]	5.13[b]	54.84[b]
T_7	567.04[c]	97.17[b]	18.89[c]	1.08[b]	1.92[c]	22.32[c]
T_8	513.97[d]	97.27[cf]	18.49[d]	1.15[b]	1.97[c]	21.61[c]
T_9	610.12[f]	99.66b[g]	19.12[f]	1.25[b]	1.91[c]	15.57[c]
T_{10}	665.21[g]	97.20[d]	20.36[g]	2.09[c]	1.82[c]	24.29[c]

Note; BD = Bulk density; Du = Durability; GCV = Gross calorific value; TS = Tensile strength;
FiC: Fines content and Wi = Wettability index
Superscript letters of the alphabet indicate that means the following the same letter was insignificantly different at p = 0.05

4.3.7.3. Pellet durability

Several factors can affect the durability of pellets, such as pressure, pelleting temperature, volume reduction and material composition (Tilay et al. 2015). This research produced the pellet through the rollers' constant spinning and friction between the plate die and the rollers. As a result, the production pressure was fixed. As previously mentioned, the excellent pellet quality resulted from the barrel's operating temperature of 60~80°C.

Table 4.6 shows the drop test results for each treatment. According to the statistical study, there was no significant variation in durability, excluding the pellets from WS (T_1). Pellet durability increased when the binder was increased with WS, and the maximum (99.66%) was observed in T_9. In this study, the pellet's durability ranged from 97% to 99 % for T_5 to T_{10} (pellets with additives), meeting the ISO standard. Iroba et al. (2014) explored the manufacture of ground barley straw pellets via pretreatment radio frequency and temperature change during compaction compared to other nonwoody biomass pellets. They found that durability was 99.17% (Iroba et al. 2014), similar to this research. This demonstrates that pellet durability can be improved through additives mixed with WS. Conversely, WSP production is challenging without additives, and quality may fall short of expectations.

4.3.7.4. Pellet strength

Tensile strength reflects pellet quality when it comes to pellet strength and hardness. It resists breaking and dust generation from transportation and handling. The pellets' tensile strength ranged from 0.36 to 2.09 MPa (Table 4.6). The highest strength was T_{10}, and the lowest was for T_1 (WSP without binders). Moreover, T_6 to T_9 pellet strength was similar but varied significantly for T_{10}. The T_{10} pellet strength was highest (2.09 MPa), probably due to a better combination of CS and BioC, which made a strong particle bond. Kashaninejad and Tabil (2011) noted that WSPs had a tensile strength of 0.81 MPa, which supported this study's results. In conclusion, additives help to improve pellet tensile strength.

4.3.7.5. Pellet wettability

The moisture absorption characteristics of pellets influence the physical deformation encountered throughout storage and transportation. For example, Yılmaz et al. (2021) mentioned that the formation of loose pellets is caused by increased moisture followed by a decline in bulk density.

The pellet wettability index results in Table 4.6 show the binders that affect the water absorption rate. The T_1 (without additive) and T_9 (BC) pellets absorbed the highest amount of water, i.e., 78.63 and 54.84%, respectively. The causes might be WS and BC, which may have enhanced the water holding ability of the pellets. In contrast, the T_7 to T_{10} pellets had a superior waterproof capacity, leading to storage advantages. Kubojima and Yoshida (2015) and Ghiasi et al. (2014) examined the various pellets' water absorption capacities. They showed that the pellet with blending materials (post-torrefied pellet) protects moisture absorption, supporting a similar result in this research. As a result, the water retains its outer layer, preventing water from penetrating inside the pellets. However, in this current study, the pellets produced from binders showed less water intake than those without binders. Therefore, the results demonstrated that avoiding water uptake demands additives like BioC or a combination of additives.

4.3.7.6. Pellet fines content

Small particles created directly from pellets are one kind of quality indicator. Due to the fragile nature of pellets, fines/small particles are generated during transportation, handling and storage through attrition and breakage (Boac, Casada & Maghirang 2008; Oveisi et al. 2013). This has implications including increased dust explosions, equipment fouling, inhalation problems and the loss of a large amount of material (Ramírez-Gómez 2016; Ilic et al. 2018).

As part of the sieving analysis, the particles were sieved for particle size distribution determination and the results are presented in Table 4.7. The fines produced from the abrasive test were in the subsequent order $T_1>T_6>T_9>T_8>T_5>T_7>T_{10}>$. The T_1 and T_6 pellets produced more fines than the others because of their smaller tensile strength and probably loose particle bonding. The fines from T_5 to T_{10} pellet were nearly 2%, which could be due to the better structural formation of the pellet. In summary, the additives reduced fines generation.

Similarly, dust belonged to treatments and had a similar trend related to the broken percentage. In conclusion, WSPs (T_1) without additives produced more particles than pellets with additives. Hence, additive addition significantly reduced the production of fines.

Table 4.7: Produced particles classification

Treatment	Small particles		
	Slump (<5.6 to >3.15mm), %	Fines (<3.15 mm to > 1 mm), %	Dust (<1 mm), %
T_1	30.88	8.58	4.86
T_5	4.52	1.93	1.07
T_6	4.43	5.13	2.75
T_7	6.68	1.92	0.95
T_8	7.89	1.97	0.60
T_9	4.03	2.01	2.17
T_{10}	5.13	1.82	2.74

4.3.8. Pellet quality comparison according to ISO 17225-8: 2016

The ISO pellet standards specify that pellets in the A and B quality types are used in household and commercial stages. Table 4.8 shows the physical characteristics of different pellets and their comparison with the ISO standard (ISO/TS 2016). The required ash content (%) for the A and B classes were ≤6 and ≤10, respectively. The heating value (MJ/Kg) were ≥18 and ≥17.

From the ISO pellet standards norm, it has been noted that pellet durability should be ≥97.5% in the A quality category, and B class pellets should be ≥ 96.5%. By contrast, produced pellet moisture content should be 10% in the A and B classes. Hence, the produced pellets showed ISO

compliance for WSP durability and moisture content. Moreover, this study's pellet length and diameter were 22 to 40.0 mm and 8 to 8.3 mm, respectively, which meets the ISO standards (Table 4.8).

However, the T_5, T_6, T_7 and T_8 pellets did not meet the ISO ash content range for both categories, but the T_1, T_9 and T_{10} pellets complied with B (commercial use). In contrast, the heating values increased with the added additives and met the ISO standard.

ISO has asserted that pellet bulk density should be 600 kg/m^3 or more (ISO/TS 2016). The treatments T_1, T_6, T_7 and T_8 did not meet the bulk density standards; however, the pellet produced with BioC ($T_5 \sim T_7$) fitted both criteria (A and B). Therefore, the pellets made from T_5 to T_7 could be considered for commercial and household use. It was also found that additive addition enhanced bulk density.

The densification process aims to make biomass easier to handle, transport, store and use (Liu, Z. et al. 2013), which is a vital consideration in this study. Hence, the produced pellets need to meet commercial criteria like ISO 17225-8, EN*plus, etc.* (ISO/TS 2016). Although the pellet characteristics were tested based on ISO pellet values, most physical traits fit standard ranges except for ash and fines content (Table 4.8). Therefore, despite the lack of standard pellet value, it is possible to improve pellet structure by adding various additives, technological applications, etc.

Table 4.8: Comparison of the produced pellets by the ISO 17225-8:2016

| Parameter | Standard value | | T_1 | T_5 | T_6 | T_7 | T_8 | T_9 | T_{10} |
	A	B							
Length, mm	*3.15~40*		**	**	**	**	**	**	**
Diameter, mm	*6~25*		**	**	**	**	**	**	**
Moisture content, %	*≤10*		**	**	**	**	**	**	**
Bulk density, kg/m^3	*≥ 600*		X	**	X	X	X	**	**
Ash content, %	*≤6*	*≤10*	X	X	X	X	X	X	X
Heating value, MJ/Kg	*≥18*	*≥17*	**	**	**	**	**	**	**
Durability, %	*≥97.5*	*≤96.5*	X	**	**	**	**	**	**
[a] Fines, %	*≤2.0*		X	**	X	**	**	**	**

Note; A: **; B: *; X: Out of standard
A = Household use; B = Commercial use; [a] Fines content (<3.15 mm)

In conclusion, this study identified the implications for binders by several physical features of pellets such as length, diameter, density (apparent and bulk), resilience and fines content. The summary in Table 4.8 notes that additives with WS particles improved some physical traits of pellets, which was expected in this study. Additives work as a natural binder, forming a solid bridge between particles (Liu, Z. et al. 2013)*.* Moreover, this improves the mechanical interlocking behaviour amongst the solid particles (WS), enhancing physical traits (Holt, G. A., Blodgett, T.

& Nakayama, F. 2006). Kaliyan and Morey (2010) identified that the binders in the biomass are exposed through the pelletising process and form solid bridges between particles.

4.4. Conclusion

Pellet composition influences important combustion characteristics like gross heating value, moisture content and ash content. However, the raw materials component has an impact on pellet elements. In addition, various additives also affect the pellets' chemical and physical properties (diameter and length, bulk density, durability, fines, tensile strength and wettability).

The different additives' functions are also diverse. For instance, SD works as structural formation, while GC and BioC are energy additives, and CS and bentonite are binding agents. However, SD increased the water absorption capability, and BC raised the ash content. Overall, additives improved the pellet quality traits.

The highest quality pellets were made from T_5, T_9 and T_{10}, with the best physical qualities and energy density. Nevertheless, the standard pellets made from T_6 to T_{10} were blended additives considering the heating value and fines content. One of the characteristics that restricted the use of pellets to either home or commercial use or possibly both was the ash concentration.

The pellets with additives mixing met the pellet ISO standard specification requirements except for inorganic ash content for the Residential/Commercial needs of densified pellets. However, WSPs without additives (T_1) did not fulfil most of the ISO solid fuel standards, such as bulk density, inorganic ash, durability and fines content. The treatments T_1 to T_8 did not meet the bulk density standards; however, the pellet produced with BioC ($T_5 \sim T_{10}$) fitted both criteria (A and B). Therefore, the pellets made from T_5 to T_{10} could be considered for commercial and household use.

As a result, there is research potential for minimising ash content by adding additives with WS particles. This study has also demonstrated that adding different additive materials to optimise the properties of solid biomass fuel is a viable option.

CHAPTER 5: PYROLYSIS OF WHEAT STRAW PELLETS IN A FIXED-BED REACTOR

Abstract

The pyrolysis of two wheat straw (WS) pellets (T_1: 100% WS and T_5: 70% WS, 10% sawdust (SD), 10% biochar (BioC), 10% bentonite clay (BC) was performed in a pilot scale reactor under a nitrogen environment at 20 to 700°C. The aim was to investigate pyrolysis yields and gas composition as a function of temperature and residence time. Experimental data were obtained between 300 and 600°C, residence time 90 min, nitrogen flow rate 50 cm^3/min, and heating rate 20 °C/min. The results indicated that the maximum pyrolysis temperature is 605°C with 60 min of residence time. The product analysis showed that the proportion of gas was higher than biochar and bio-oil. Biomass conversion efficiency increased with higher temperatures and varied between 66% and 76%. The results showed that carbon dioxide was the main component of the produced gas, and the maximum gas concentration was 63.6% at 300°C for T_1. Higher temperatures and longer residence time increased the syngas ($CO+H_2$) composition for the T_1 and T_5 treatments. The produced biochar had high carbon and retained a high calorific value, indicating that slow pyrolysis is the ideal utilisation route from WS pellet biomass to biochar.

5.1. Introduction

Globally, crops generate enormous amounts of residues and often build up in landfills (Hameed et al. 2018; Zulkifli et al. 2019). Along with other residues, this accumulated waste is creating disposal problems. Some countries burn crop straws directly, which causes severe environmental pollution. Australian farmers often mix crop residues with soil. It would be better that these crop residues be used to address energy deficits and replace the consumption of fossil fuels and other nonrenewable resources.

Agricultural waste biomass is the most promising source of energy production among all renewable sources (air, water, and solar) because they act in a carbon-neutral manner (Neves et al. 2011; Naqvi et al. 2020). Wei et al. (2019) noted that biomass could meet about 9.7% of global energy and fuel demand through thermal and biochemical processes. *Wheat straw*, rice straw, rice husk, corncob, bagasse, cotton stalks, perennial grass, etc., are common agricultural residues (De Conto et al. 2016; Naqvi et al. 2019). They are good candidates for bioenergy production due to their low cost, availability, and enormous quantities. These materials are often used for heat generation and electricity production instead of open burning (Demirbas 2004; Wahab et al. 2020). This work chose agricultural straws, particularly WS, because they have great potential for energy production in developed and developing countries (Naqvi et al. 2019). Straw comprises 15~40% of total agricultural residues (Nanda et al. 2018).

Energy (syngas) production from biomass by thermochemical conversion (pyrolysis and gasification) has recently been increasing (Kabir, Chowdhury & Rasul 2015; Tanoh et al. 2020). The yield and pyrolysis product composition depends on the particle gas residence time, heating rate, reactor pressure and temperature (Dufour et al. 2009). However, tar formation during the pyrolysis and gasification processes can degrade the producer's gas quality and restricts its use. Therefore, the main obstacles tend to be related to removing tar and maximising the output of gaseous products from biomass.

A thermal decomposition process is pyrolysis that transforms biomass into bioenergy without additional air (Parthasarathy & Sheeba 2015). Snyder (2019) noted that pyrolysis is a possible thermal conversion route from biomass to energy and offers good advantages. Because of the chemical nature of biomass, pyrolysis has been demonstrated to be a suitable method for converting biomass waste into more valuable materials (Zhang, Xu & Champagne 2010). Biomass pyrolysis can create three products: carbonaceous biochar, bio-oil (a complex mixture of liquid hydrocarbons) and syngas (mainly made of H_2, CO, and CH_4) (Figure 5.1) (Babler et al. 2017; Pichler et al. 2021). Moreover, the reactor related factors influence reactor outputs (Solar et al. 2016).
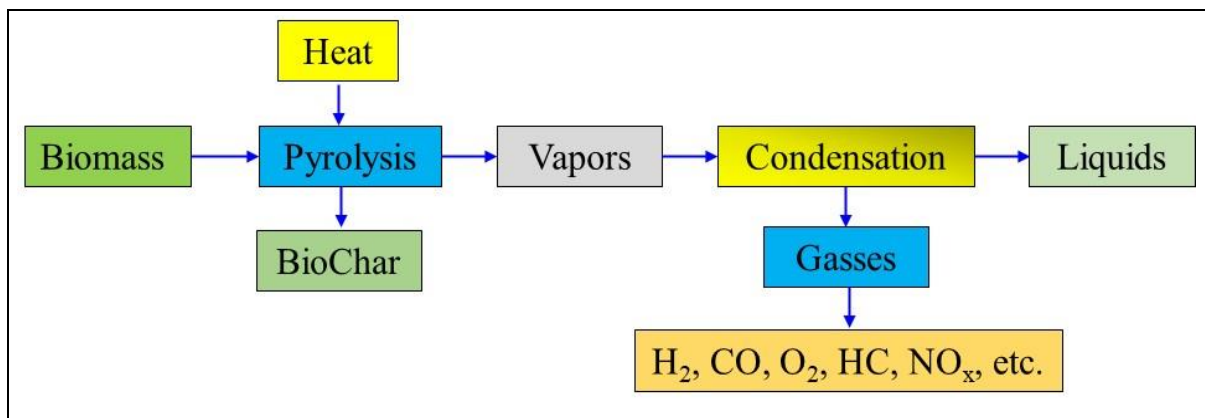
Figure 5.1: Process flow chart of pyrolysis and possible products

The thermal degradation method is linked to the weight loss profile associated with time and temperature. This technique is strongly influenced by thermogravimetric tools or reactors (Magdziarz, Wilk & Wądrzyk 2020). Screw, fixed bed, tubular and rotary kilns have been used to pyrolyse various biomasses (Kern et al. 2012). From the viewpoint of energy transformation, fixed bed pyrolysis is more attractive among the different thermochemical conversion processes because of its simplicity and the higher conversion capability of biomass and solid wastes into a liquid product.

The impact of operating conditions on pyrolysis products has been studied by many authors using experimental and numerical approaches (Njenga et al. 2016; Paredes et al. 2017). The common parameters are residence time and temperature. Numerous researchers have investigated the impact of temperature on biomass pyrolytic products using different reactors (Dufour et al. 2009; Ningbo et al. 2015; De Conto et al. 2016). Hossain, Hasan and Islam (2014) experimented with the design, fabrication and performance study of a biomass solid waste pyrolysis system for alternative liquid fuel production. They used Devdaru (*Cedrus deodara*) seeds in a fixed bed reactor in pyrolytic oil. It was found that the parameters such as reactor bed temperature, running time, and feedstock particle significantly influenced the product yield. The obtained HHV of Devdaru seed oils was 24.22 MJ/kg. Li et al. (1999) examined the effects of temperature (550~850°C) on wood pyrolysis products in a laboratory-scale rotary kiln. They focused mainly on mass yields, proximate and ultimate analysis, and product quality (surface area, biochar pore volume, pH, electric conductivity, cation exchange capacity, etc.). The gas composition and tar content were, however, not examined.

Most current studies concentrate on wood biomass and primarily explore rotary reactors as their preferred type. Some recent research was done on WS pyrolysis (Kern et al. 2012; Greenhalf et al. 2013; Biswas et al. 2017; Sedmihradská et al. 2020b). Straw pyrolysis has also received considerable interest (Table 5.1). No studies were found in the literature about the pyrolysis of WSPs in fixed-bed small-scale kiln reactors. This kiln type is low-cost and highly suitable for on-farm use.

Table 5.1: Past work on WS pyrolysis

Reactor types	Study area	References
• Screw reactor • Continuously fed bubbling reactor • Fluidised bed reactor • Fixed bed tubular reactor • Rotary kiln	Pyrolysis mass yield, proximate and ultimate analysis, higher and lower heating value	(Chun et al. 2004; Kern et al. 2012; Greenhalf et al. 2013; Wang et al. 2013; Aqsha et al. 2017; Biswas et al. 2017; Farooq et al. 2018)
	Surface area pH, and pore volume of the solid product (BioC)	(Bridgeman, T. G. et al. 2008; Fahmi et al. 2008; Min et al. 2011)
	The cation exchange capacity and electrical conductivity of char	(Kloss et al. 2012; Wang et al. 2013)

In order to maximise the syngas yield, this research will analyse the WSP pyrolysis process on a small scale suitable for the on-farm level. The investigation was conducted in a pilot scale fixed bed oven to determine product yields, gas composition, tar, and char characterisation.

Temperature and residence periods (length of time biomass stay in the reactor's active zone) can be used to categorise pyrolysis (Zhao et al. 2018). Fast pyrolysis processes are designed to maximise the portion of gas production (Khosravanipour Mostafazadeh et al. 2018), while

intermediate pyrolysis focuses on the liquid part (Kazawadi, Ntalikwa & Kombe 2021). The fast and intermediate pyrolysis works in high temperatures (over 500°C) and short residence time (<1 min). However, the process is often more complicated and costly. Also, this sophisticated system is typically more suitable for the industrial scale. In addition, slow pyrolysis focuses on biochar production while having opportunities to produce bio-oil and biogas (Yogalakshmi et al. 2022). This pyrolysis operates around 400°C with a long residence time (hours) (Sahoo et al. 2021). Based on the literature review, slow pyrolysis is widely accepted for small-scale reactors. Therefore, this study considered slow pyrolysis in a fixed-bed reactor to investigate the amount of biochar, gas components and bio-oil.

5.2. Materials and methods

5.2.1. Feedstock and biochar analysis

This investigation used two different kinds of WSPs as feedstock. The T_1 pellet was manufactured from 100% WS, whereas the T_5 pellet was made from a 70% WS, 10% BC, 10% charcoal and 10% SD combination. A chemical analysis of the pellets and biochar was conducted. Triplicate measurements were undertaken for each sample. The ultimate and proximate component was also done for elemental analysis (as discussed in Chapter 3).

5.2.2. Reactor description

The pyrolysis experiments were conducted in a Rio Grande PMC (model #703-117) laboratory scale kiln (Figure 5.2). The main parts of the reactor unit included an electric heating system, air or nitrogen gas introduced port, electrical data plate and feedstock burning chamber. The unit also had a measuring facility (gas, temperature). Ceramic-fibre-firing embedded elements covered its inner wall. The firing internal chamber (where the pyrolysis process occurred) had the dimensions of 20 cm, 18.7 cm and 14.6 cm in width, length and height, respectively. The reactor was heated by electrical resistance at 11.4 amps and 110 volts.

| Kiln working view | Process flow of pyrolysis pilot plant |
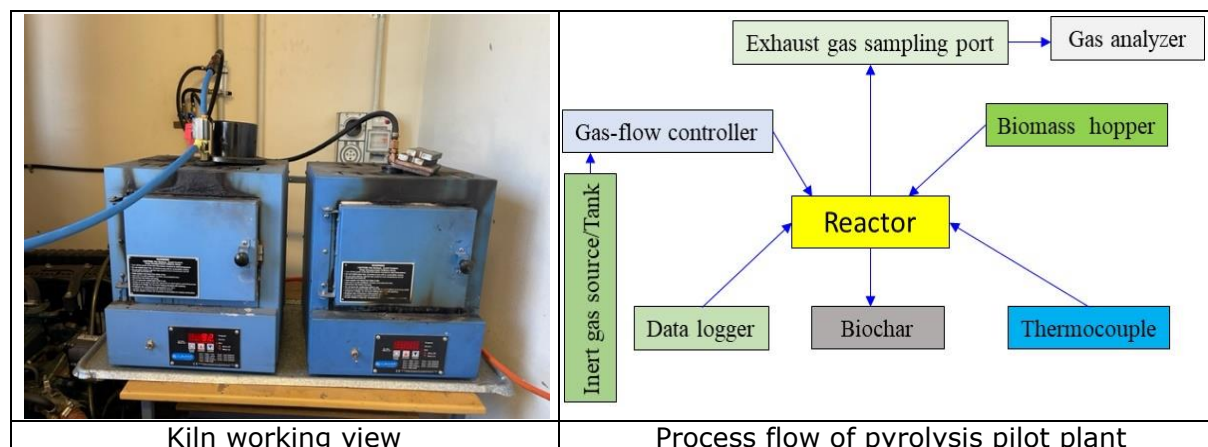
Figure 5.2: Schematic diagram and laboratory scale kiln

The maximum working temperature of the reactor was 1093°C, and the power outputs were 1370 watts. The hopper (where the biomass was fired) had a capacity of 2 kg. This reactor had five programs for firing. The reactor option "PMC+™ slow" was chosen because the research aim was the investigation of WSP under slow pyrolysis conditions. The produced gas left the reactor from the upper part. The gas collection port or gas analyser connection point was also located in the upper part.

5.2.3. Experimental procedures

The WSPs were pyrolysed at various temperatures (Table 5.2). Each WSP sample was approximately 500 g. Nitrogen was introduced to the top of the reactor at a 50 cm^3/min flow rate as carrier inert gas. The experimental temperature and residence time were selected using a controller programming display (P1 for Pyrolysis). All the samples were measured under the same conditions (Tanoh et al. 2020). Each experiment was conducted twice to ensure data repeatability, with a less than 5% relative error.

Table 5.2: Experimental parameters

Particular	Value
Pyrolysis	Slow
Temperature range, °C	25 ~ 700
Data recorded temperature, °C	300, 350, 400, 450, 500, 550, 600
Heating rate, °C/min	20
Nitrogen flow rate, cm^3/min	50
Pellet diameter, mm	7 ~ 8.2
Pellet length, mm	22 ~ 40
Biomass used, g	500
Residence time, min	90

The feedstock (WSPs) was placed in a ceramic hopper inside the pyrolysis chamber. Due to the WSPs' highly inhomogeneous composition and distinctive properties (Ríos-Badrán et al. 2020), the burning process was subject to many disturbances. These disturbances were reflected in process instabilities that could lead to incomplete pyrolysis and other problems. Moreover, the burning agents (nitrogen, air, and steam) impacted the pyrolysis products. Furthermore, the pyrolysis result depended on the WSP's thermal behaviour as thermal conductivity and specific heat were 0.13 W/m.K and 1.63kJ/kg.K at 300 k, respectively (Ahn et al. 2009).

The feedstock's average diameter and length were 35.0 and 8.0 mm, respectively. Correspondingly, the bulk density was 244.79 and 607.40 kg/m^3 for the T_1 and T_5 pellets, respectively.

5.2.4. Temperature and time measurement

The reactor had a temperature measurement facility and a data logger. The biomass bed temperature was recorded inside the reactor as the pyrolysis temperature, which was automatically stored. Pyrolysis began at room temperature (25°C), while 20 °C/min was the heating rate, and the temperature reached its highest level of 600°C at 60 min. Phounglamcheik et al. (2017) recommend keeping residence times under 90 minutes to maximise biomass thermal conversion efficiency.

5.2.5. Pyrolysis yield

The quantity of materials converted into liquid or gaseous products is called conversion in this pyrolysis process (Ethaib et al. 2020). The remaining solid after the reaction left in the reactor is defined as biochar.

Bio-oil is a condensable phase of a substance consisting of water and vapours. Because of the unavailability of bio-oil measurement equipment, reference bio-oil information was obtained from Biswas et al. (2017) and Paul et al. (2020). In a nitrogen environment, they measured the bio-oil at seven temperature levels (300, 350, 400, 450, 500, 550, and 600°C). Several equations (1~4) are used to calculate gas, biochar, bio-oil and conversion (Krishna et al. 2016; Al Afif, Anayah & Pfeifer 2020).

$$\text{Bio-oil yield, wt\%} = \frac{W_4 - W_3}{\text{Weight of feedstock}} \times 100 \text{ ....} 5.1$$

$$\text{Biochar yield, wt\%} = \frac{W_2 - W_1}{\text{Weight of feedstock}} \times 100 \text{ ....} 5.2$$

$$\text{Gas yield, wt\%} = 100 - (\text{Bio} - \text{oil yield} + \text{biochar yield}) \text{.................} 5.3$$

$$\text{Biomass conversion, \%} = 100 - \text{Biochar yield, wt \%} \text{ ....} 5.4$$

Where: W_1 = weight of empty reactor, g
W_2 = weight of reactor after reaction, g
W_3 = weight of the empty measuring cylinder, g
W_4 = weight of measuring cylinder with bio-oil, g

5.2.6. Gas sampling and analysis

Thermal gas is a condensable phase of pyrolysis vapour (Ningbo et al. 2015). The exhaust (gas and vapour) exits the reactor as the pyrolysis process begins. The gaseous products were examined using Agilent 7820A gas chromatography (Agilent Technologies, Santa Clara, CA, USA) (Figure 5.3). The thermal conductivity detector (TCD) for the gas chromatograph was made up of three columns: Ultimetal HayesepQ T 80/100 mesh (H_2, CO, and CH_4), Ultimetal Hayesep T 80/100 mesh (CO_2) and Ultimetal molsieve13 80/100 mesh column (N_2 and O_2) (Li, Zone & Guan 2009). A consistent temperature of 60°C was maintained across all columns, with argon as the carrier gas.

| Flow diagram of pyrolysis product analysis | Agilent 7820A gas chromatography |
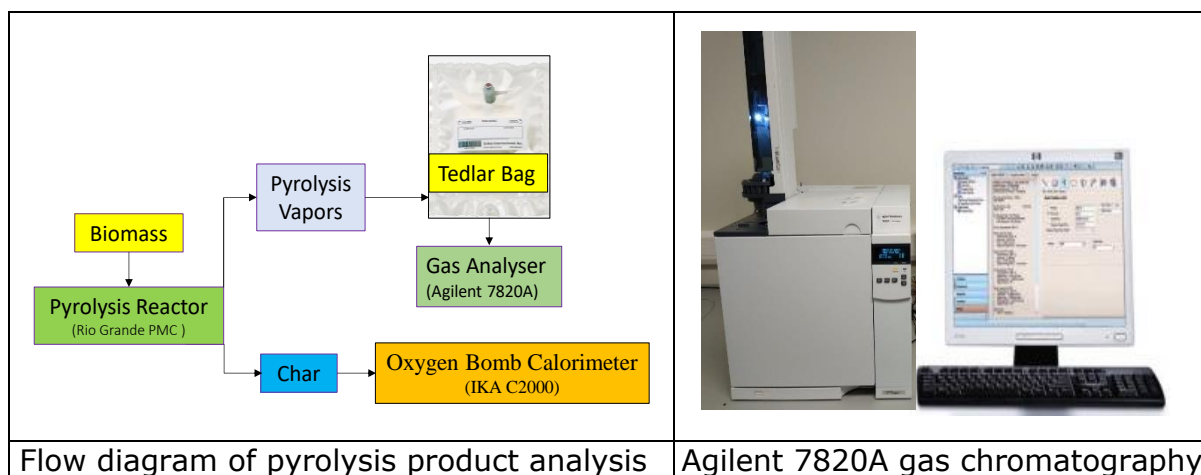
Figure 5.3: Gas analysing flow diagram and the analyser

The top of the pyrolysis reactor contained a gas sample port where the gas exited. For gas analysis, the pyrolysis vapour was collected in a Tedlar bag and analysed using Agilent gas chromatography. This work investigated the gas composition at 300, 350, 400, 450, 500, 550 and 600°C.

5.2.6. Biochar measurement

Biochar is non-volatilised in biomass fraction (Ningbo et al. 2015; de Jesus et al. 2020). This study examined char reactivity at 300, 350, 400, 450, 500, 550 and 600°C. After the pyrolysis process, the reactor was left for at least two hours (oxygen-free environment) the cool down. During this time, the pyrolysis products were released and weighed. The leftover material in the oven was considered biochar or carbon-enriched ash after the pyrolysis process.

An IKA C2000, a basic oxygen bomb calorimeter using the ASTM D5865-03 standard, was employed for the heating value measurement (Yandapalli & Mani 2014). The calorimeter was standardised using 1.00 g of Parr standard benzoic acid, and the mode was dynamic with an outer vessel temperature of 25°C. About 0.50 g of the sample was put in the metal combustion capsule and placed in the sample holder in the bomb head for gross energy determination.

5.3. Results and discussion

5.3.1. Biomass fuel (WS pellet) characterisation

The chemical analysis is important because the mineral matter of biomass, in combination with the organic composition, performs a major role in determining the pyrolysis product allocation and product properties (Raveendran, Ganesh & Khilar 1995). The feedstock pellets (T_1 and T_5) ultimate and proximate analysis were presented in Chapter 3.

Generally, proximate analysis results are used to complete the pyrolysis process energy balance. Feedstocks with a higher volatile fraction and or less ash content produce more syngas during pyrolysis and have a lower biochar yield (Kabir, Chowdhury & Rasul 2015). Therefore, the high ash content of WSP may result in a higher solid product (char) content. In addition, the ultimate analysis indicates the carbon content and the nature of the organic compounds in the feedstock. For both T_1 and T_5, the ultimate analysis components were very similar. Therefore, the pyrolysis yields were very similar for both types of pellets.

5.3.2. Temperature variation with time

A typical set of data (time vs temperature) for WSP (T_1 and T_5) pyrolysis is presented in Figure 5.4. In the current experiments, the heating flow was maintained at 20 °C/min, with a 90 min projected residence period. Pyrolysis began at room temperature. It was noticed that the temperature was raised from the beginning of the experiments and reached 605°C at 60 minutes. After 60 minutes, the temperature did not increase, becoming stable and lasting up to 90 minutes. Thus, it can be summarised that the maximum pyrolysis temperature was 605°C (Figure 5.4). These results are similar to Tanoh et al. (2020), even though the reactor and feedstock (wood pellet) used differed. McBeath, Wurster and Bird (2015) also mentioned that the optimum pyrolysis temperature varied from 500 to 700°C, supported by the present research.
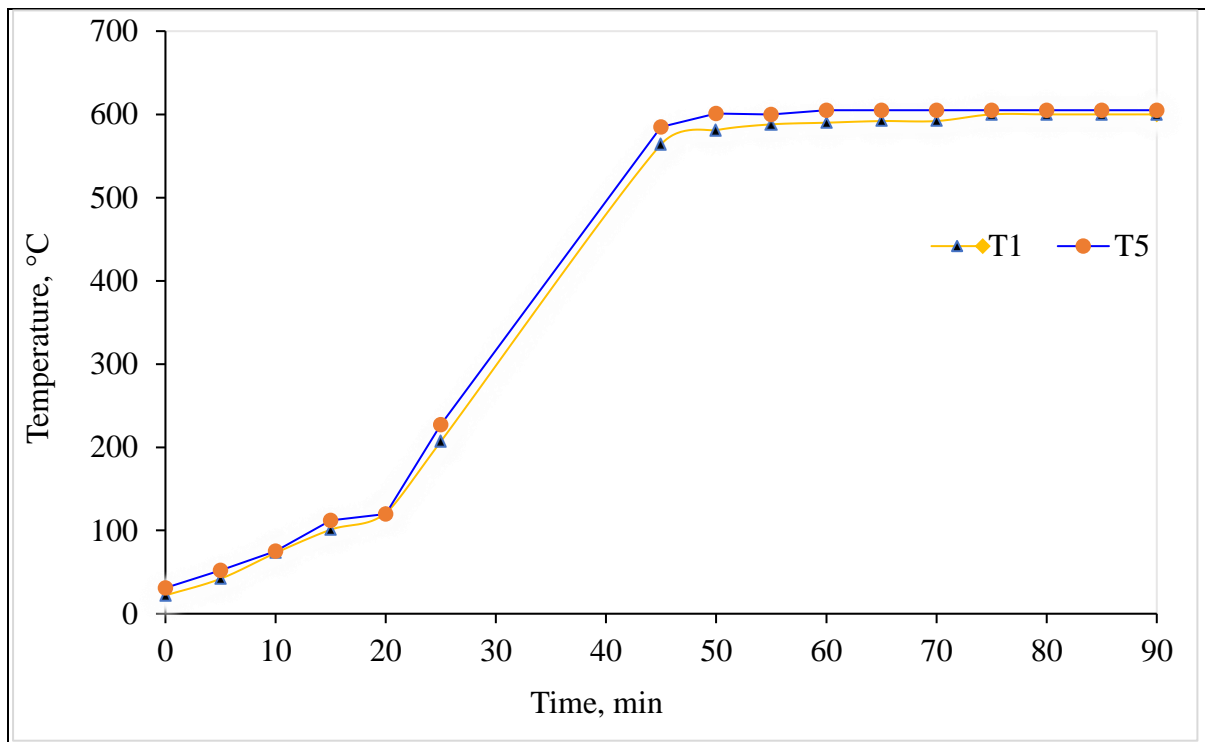
Figure 5.4: Relationship between the pyrolysis time and temperature of wheat straw pellet

Based on the above findings (maximum pyrolysis temperature), all data were only collected and related to the pyrolysis yields (char, gas and bio-oil) at 300, 350, 400, 450, 500, 550 and 600°C. The data sampling continued for 50 min.

5.3.3. Burning mechanism of wheat straw pellets

The bulk density of WSPs T_1 and T_5 were 244.7 and 607.4 kg/m^3, respectively, but the ignition time varied slightly. Figure 5.5 illustrates the burning behaviour of the WSPs as time passes. The WSPs gradually become darkened with time and eventually turn to an ash colour (Figure 5.5). After a few minutes of the burning, the grey smoke was observed due to the release of volatile matter. This stage is also termed the initial gas phase (El-Sayed & Khairy 2017). In this gas stage, drying and devolatilisation were considered the main conversion phase due to temperature gradients and the respective reactions that occurred (De Conto et al. 2016). After that, the surface temperature of the WSPs was raised and the pellets were exposed to a heated environment. The heat is transmitted through conduction and convection processes from the pellet surface to the centre, releasing gas and the remaining solid residues (such as char and ash) (Tanoh et al. 2020). During the burning, cellulose, hemicelluloses, and lignin produced water (vapour) and light gases like CO_2, CO, CH_4 and char (Biswas et al. 2017).

| Before burning | After 25 minutes | End of burning |
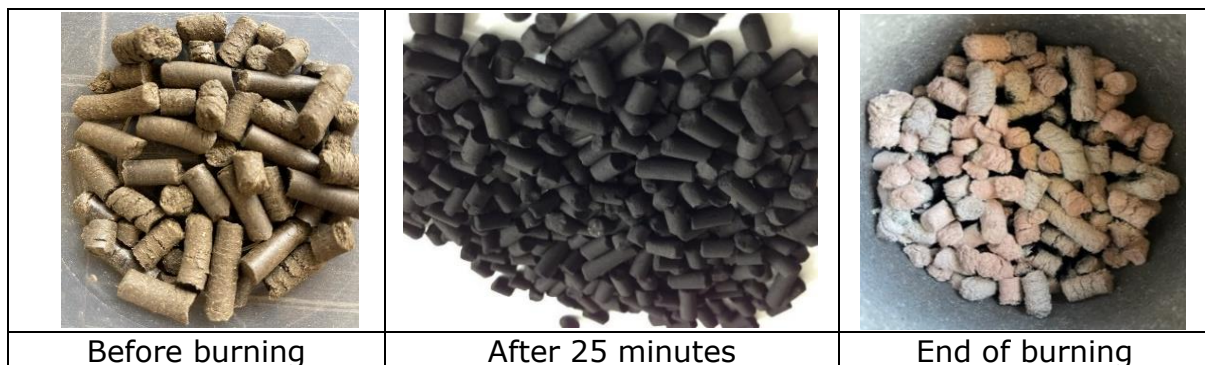
Figure 5.5: Observation of WSPs during burning

5.3.4. Product (yield) distribution

The temperature has a noticeable effect on pyrolysis yields. Experiments were conducted at temperatures 300, 350, 400, 450, 500, 550 and 600°C in a nitrogen environment under atmospheric pressure for the pyrolysis product investigation. Fahmy et al. (2018) and Zhang and Ma (2015) mentioned that the pyrolysis of wood usually begins at 200~300°C. This particular temperature is related to factors such as the type of biomass, type of reactor and type of pyrolysis (Sedmihradská et al. 2020a). Table 5.3 displays the pyrolysis product yield of WSP, where the highest bio-oil (with water) yield was 43.61% obtained at 450°C, while the minimum was 30.24 % at 600°C temperature (Paul et al. 2020).

Table 5.3: Slow pyrolysis product yields

Pellets	Temperature, °C	Bio-oil*, %	Biochar, %	Gas, %	Total, %
T_1	300	32.5	33.9	30.4	96.8
	350	36	32.1	29.93	98.03
	400	36.7	31.8	28.89	97.39
	450	43.61	30.3	23.79	97.7
	500	42.3	28.68	27.23	98.21
	550	35.61	26.81	35.57	97.99
	600	30.24	25.31	41.85	97.4
T_5	300	32.5	32.5	32.79	97.79
	350	36	32.2	29.0	97.2
	400	36.7	30.8	29.39	96.89
	450	39.61	29.6	28.59	97.8
	500	42.3	27.67	26.83	96.8
	550	35.61	25.78	36.58	97.97
	600	30.24	24.33	43.52	98.09

*Reference value collected from Biswas et al. (2017) and Paul et al. (2020) because of the unavailability of bio-oil measurement equipment.
Note; T_1: Wheat straw, and T_5: Wheat straw, Saw dust, Bentonite clay, Biochar.

The maximum biochar yield for T_1 and T_5 treatments found in this reactor was 33.9 and 32.5%, respectively, at 300°C (Table 5.3). The decreased biochar yield with increasing temperature (Parihar et al. 2007) could be due to a more significant decomposition of the primary product (hemicellulose and cellulose) or secondary degradation of char residues (Ronsse et al. 2013; Wang et al. 2013; Aqsha et al. 2017; Jazini, Soleimani & Mirghaffari 2018).

Table 5.3 shows that each biomass can produce a certain amount of gas at a specific pyrolysis temperature. However, the highest amount of gas was found at 600°C for both pellets (T_5 was 43.52% and T_1 was 41.85%). These results agreed with the investigation of Nanda et al. (2018). This indicated an increase in gaseous product yield as the pyrolysis temperature increased. This was because of the secondary cracking of the pyrolysis vapours at higher temperatures (Parihar et al. 2007). The secondary decomposition of the char at higher temperatures may also give noncondensable gaseous products, increasing gas yield by increasing the pyrolysis temperature. Overall, oil and char yield reduced while the gas yield was boosted with the increasing temperature (Onay, Beis & Kockar 2000).

The total sum of all the pyrolysis products ranged between 96.8 and 98.21%, consistent with the results of Sedmihradská et al. (2020a), who used wheat and barley straw as pyrolysis feedstock.

5.3.5. Biomass conversion

This study estimated biomass conversion using Equation 5.4 (Krishna et al. 2016). The proposed formula was based on the remaining biochar after combustion. The conversion rate varied from 67.5 to 75.67% for T_5 pellets within the temperature range of 300 to 600°C, while the conversion rate was 66.1 to 74.69% for T_1. The T_5 pellets' conversion rate was higher than T_1 because of the synergistic effect of the biochar blend pellet. These findings were supported by Biswas et al. (2017). They investigated the agricultural biomass pyrolysis and found the conversion efficiency varied from 64~76 % for all biomass (corn cob, WS, rice straw and rice husk). The conversion rate also increased with the temperature, while biochar decreased primarily because the hemicellulose and lignin decomposed (Krishnamoorthy, Krishnamurthy & Pisupati 2019). Overall, the yield data from the T_1 and T_5 pellets at various temperatures indicated that the compositional variations in the different pellets considerably impacted product distribution (Figure 5.6).
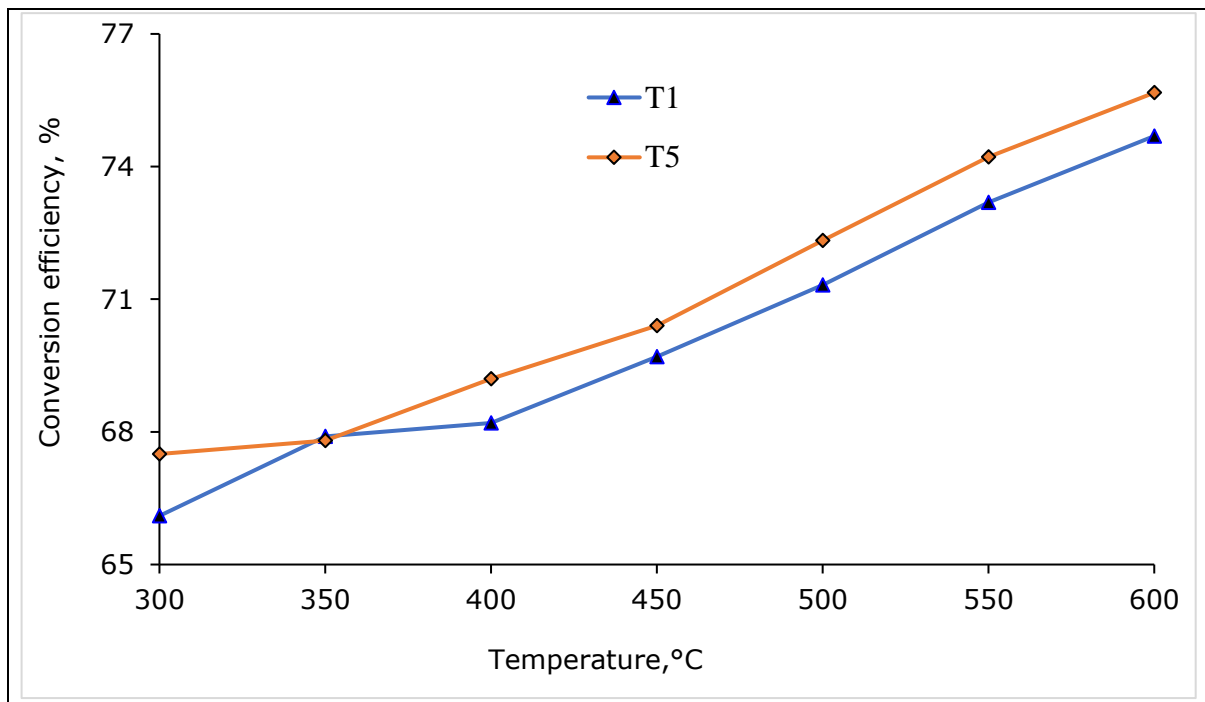
Figure 5.6: Biomass conversion through pyrolysis

5.3.6. Characterisation of produced gas

Burning a material produces gases such as H_2, CO_2, O_2, N_2, CH_4 and CO, which can be measured by an Agilent Gas Chromatograph's thermal conductivity detector (TCD) (Li, Zone & Guan 2009). This study measured only the primary component of the produced gas. Methane (CH_4), carbon monoxide CO), hydrogen (H_2) and water (H_2O) were the primary components of pyrolysis gas, in addition to a small amount of oxygen (O_2) and nitrogen (N_2) (Kern et al. 2012).

5.3.6.1. Relationship between pyrolysis temperature and gas concentration

The gas composition under different temperatures is shown in Figure 5.7. It can be seen that the gas was mainly made up of carbon dioxide because most CO_2 was produced by decarboxylation reaction at relatively low temperatures (Amutio et al. 2012). The CO_2 varied from 63.6 to 50.59% for the T_1 pellets and 60.11 to 47.53% for the T_5 pellets. A pyrolysis study of wheat and barley straw was conducted by Sedmihradská et al. (2020b) and it agreed with the present study's results. They found the CO_2 percentage varied from 61.26 to 39.46% related to the temperature variation 400 to 800°C.
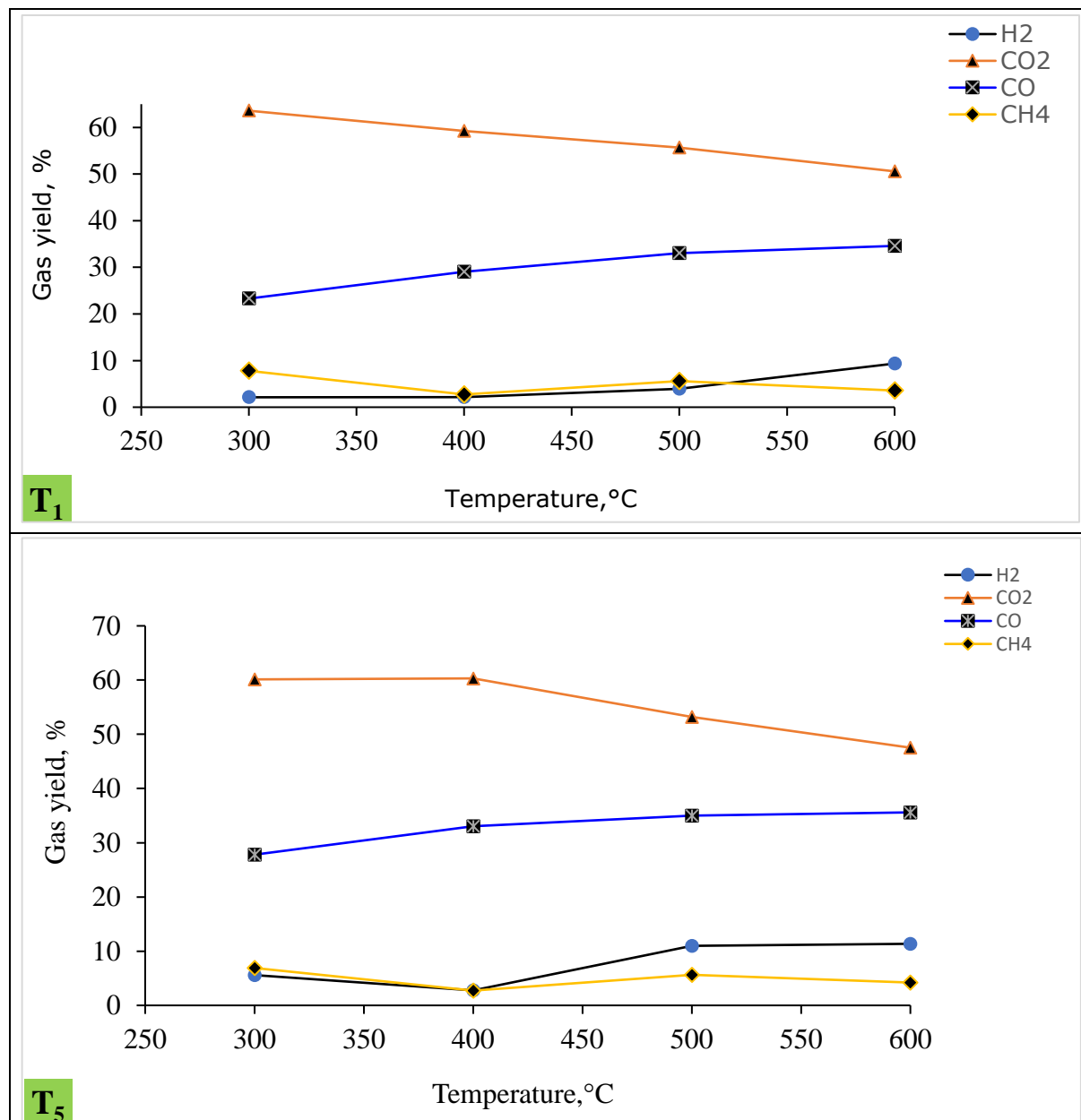
Figure 5.7: Effect of temperature on gas composition

On the other hand, the CO varied from 23.3 to 34.6% for the T_1 pellets, with the increasing pyrolysis temperature resulting from the enhancement of the decarbonylation reaction. In the case of treatment T_5, the carbon monoxide (CO) exhibited a significant increase of 27.8% to 35.6% within the temperature range of 300 to 600°C. These values were comparable with other investigations conducted by Kern et al. (2012) on agricultural straw in rotary kiln pyrolysis, and they observed the CO was 34 vol% with temperature variation from 450~600°C.

The concentration of CH_4 decreased between 300 and 400°C and increased with a higher temperature increase for the T_1 pellet. Alternatively, for the T_5 pellets, the CH_4 variation ranged from 6.9 to 4.2%, with a temperature range of 400 to 600°C. Other authors (Ningbo et al. 2015) confirmed this trend, but the CH_4 concentration (14~17.5%) was higher than this research might be due to different agricultural residues such as pine SD. Moreover, the decline in CH_4 yield might be attributed to the reaction of CH_4 and oxygen to produce acetylene at higher temperatures (Lu & Chen 2015).

The H_2 content increased for T_1 from 2.13% at 300°C to 9.36% at 600°C, produced by the cracking and rearrangement of aromatic bonds at higher temperatures (>500°C) (Aguilar et al. 2015). On the other hand, the H_2 content decreased at 300 to 400°C, whereas it increased between 400 and 600°C by 2.77 to 11.36%. The results agreed with the works of Sedmihradská et al. (2020a), who found the relatively same amount of H_2.

The content variation of gas composition agrees with Fagbemi, Khezami and Capart (2001), who studied the pyrolysis product yield from three biomasses: wood, coconut shell and straw. The present study results were inconsistent with Nanda et al. (2018). They conducted an experimental study on WS catalytic gasification for hydrogen production and found that CO_2, H_2 and CH_4 concentrations increased significantly with higher temperatures, but the CO increasing rate was limited.

5.3.6.2. Relationship between residence time and gas composition

Figure 5.8 illustrates the effect of reaction time on gas composition. The CO_2 concentration decreased sharply from 58.11 to 38.36% for the T_1 pellet, with a 5 to 55 minutes residence time. Similarly, the CO_2 concentration dropped from 46.15 to 40.36% for the T_5 pellets in the same residence time. These findings were coherent with the investigation of Ningbo et al. (2015), even with a different biomass and reactor. However, CO increased from 26.6 to 42.4% within 55 minutes for the T_1 pellets. A similar trend was found for the T_5 pellets, increasing the range from 38.12 to 42.69% for the same duration. This rising trend indicated that long residence time allowed secondary cracking, and more macromolecular compounds were decomposed for CO release (Xu et al. 2020).
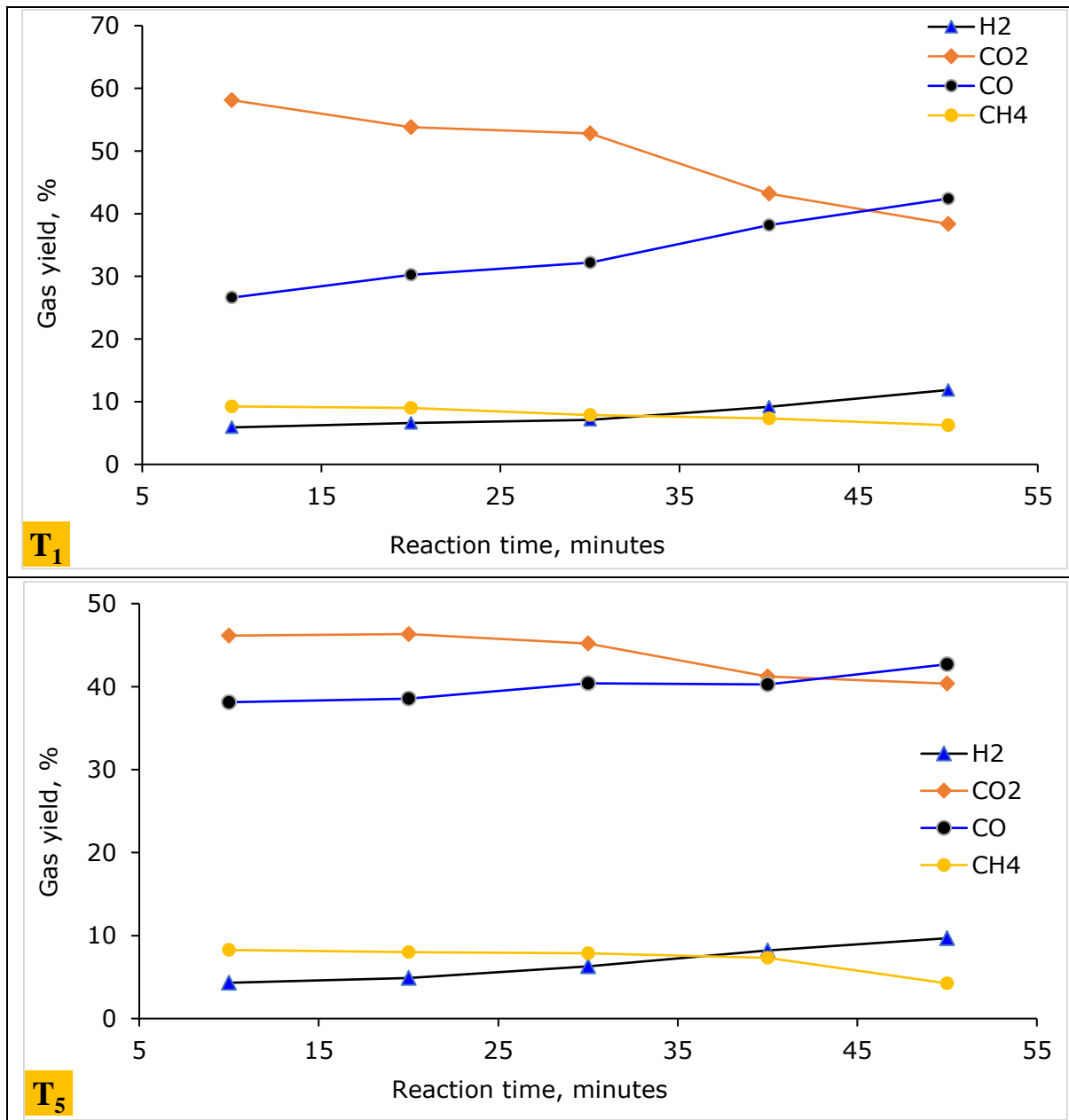
Figure 5.8: Effect of residence time on gas composition

H_2 content gradually increased from 5.9 to 11.87% with prolonged residence time in the case of the T_1 pellets. In the pyrolysis of the T_5 pellets, the H_2 concentration increased from 4.31 to 9.68% for equal residence time. As observed, the CH_4 yield for both treatments had a slightly decreasing trend, indicating that the solid residence time had not influenced the production of CH_4 (Ningbo et al. (2015).

Overall, Figure 5.8 shows that residence time enhanced the generation of H_2 and CO while decreasing the CO_2 and CH_4. According to (Yogalakshmi et al. 2022), pressure, residence time and higher temperature might favour higher CO and H_2 concentrations in the gas mixture.

5.3.5.3. Biochar characterisation

Biochar is a carbon rich material produced by heating (Tomczyk, Sokołowska & Boguta 2020). In this experiment, the temperature for BioC production was set as 300, 450 and 600°C. The biochar and pellets' basic properties are shown in Table 5.4.

Table 5.4: Characteristics of the WSP

Property		T_5				T_1			
		Pellets	Biochar at temperature, °C			Pellets	Biochar at temperature, °C		
			300	450	600		300	450	600
Proximate analysis (% dry basis)	Moisture content	3.5	3.26	2.11	3.03	6.2	3.71	4.28	1.98
	Ash	11.87	11.45	10.39	8.71	7.09	7.02	6.31	5.85
	Volatile matter	53.03	44.51	35.66	32.77	75.61	58.31	45.92	41.39
	Fixed carbon	31.6	40.78	51.84	55.49	11.1	30.96	43.49	50.78
HHV (dry basis, MJ/kg)		19.06	23.06	29.25	28.73	17.02	17.02	25.81	27.07

Note; T_1: 100% WS and T_5: 70% WS, 10% sawdust, 10% BioC, 10% bentonite clay

Typically, biomass contains some water or moisture. The generation of biochar is influenced by moisture concentration (Kloss et al. 2012; Sun et al. 2014). The biomass's moisture raises the energy needed to achieve the pyrolysis temperature and prevents tar development (Tomczyk, Sokołowska & Boguta 2020). The moisture content present in the biochar represents partial burning. The moisture content of the T_1 and T_5 treatments was 6.2 and 3.5%, respectively. However, the biochar moisture content was low compared to the raw materials because water evaporated due to heating (Tauqir, Zubair & Nazir 2019) (Table 5.4). Therefore, low moisture biomass is recommended for biochar production since it substantially reduces the heat energy requirement and time for pyrolysis (Tripathi, Sahu & Ganesan 2016).

The higher lignin concentration in plant biomass encourages carbonisation and raises BioC ash and carbon contents (Sohi et al. 2010). As observed in Table 5.4, the ash content was lower in the BioC than in the raw pellets. This study's results are very close to those reported in the work of Pérez-Maqueda et al. (2014). Rafiq et al. (2016) also reported that an increase in ash content of 5.7~18.7% resulted from higher pyrolysis temperatures. The gradual concentration of inorganic components and OM combustion residues caused the ash level to rise (Zhao, Ta & Wang 2017).

The volatile matter in BioC indicates incomplete thermal degradation during pyrolysis (Yin et al. 2013). It can be observed from Table 5.4 that the pyrolysis temperature increases led to a decrease in volatile content

from 44.51 to 32.77% for T_5 pellets and 75.61 to 42.39% for T_1 pellets. This trend was due to the increasing temperature resulting in volatile fractions being broken into liquids and gases rather than charcoal (Ronsse et al. 2013). The results were consistent with the investigation of Tag et al. (2016). Overall, the pyrolysis temperature influenced the BioC composition due to the release of volatiles (Shaaban et al. 2014).

Depending on pyrolysis temperature and biomass type, the volatile matter of biochar decreased, and fixed carbon increased in a different way (Fuertes et al. 2010). The fixed carbon rose from 31.6 to 55.49% for T_1 pellets and 11.1 to 50.78% for T_5 pellets, while the temperature increased from 300 to 600°C. These might be due to the secondary cracking reaction increasing with the increasing pyrolysis temperature, contributing to the biomass's combustible composition surge (Ningbo et al. 2015). In addition, the high carbon content indicates that biochar likely still contained some plant residues (cellulose and lignin) (Chun et al. 2004). Therefore, this result suggests that the pyrolysis temperature led to lower volatile matter and higher fixed carbon content. The same trends were observed in the work of Gabriela and Cora (2018).

The calorific value of biomass is needed for the technological design of a pyrolysis plant. To determine the heating values of the T_1 and T_5 samples and biochar, a Bomb Calorimeter was used. It was found that the maximum calorific value of biochar for 600°C was 27.73 and 27.07 MJ/kg for the T_5 and T_1 pellets, correspondingly. The HHV of the WSP biochar increased with the pyrolysis temperature. This increasing tendency of HHV can also be seen in the work of Ningbo et al. (2015), where the heating value was 27.54MJ/kg at 900°C.

Overall, biochar quality (heating value, fixed carbon) increases with longer residence time and higher temperature (Sedmihradská et al. 2020a). According to the European biochar Certificate (EBC), standard biochar should contain more than 50% of fixed carbon (EBC 2012). In the present study, the biochar of the T_5 pellets had more than 50% fixed carbon at 450 to 600°C, while T_1 pellets had 50.78% fixed carbon at 600°C.

5.4. Study limitations

The limitations of this study were mainly related to the small sample types and the assumptions within the pyrolysis yield distribution. It was originally planned that five pellets would be manufactured with different combinations of additives materials with ground WS and selected for the pyrolysis experiments. The research work was adversely affected by the COVID-19 pandemic, and only two types of pellets (T_1 and T_5) were considered. Further, detailed work on the different heating rates and the char molecular analysis was not completed. The small scale reactor is also only suitable for biochar production on a limited scale with a lower cost.

Overall, the current pyrolysis gas analysis provided good results but would need a separate analyser for other gases (O_2, N_2). The kiln also had no facility to measure the bio-oil. Therefore, this study had to use some published literature information which could have resulted in differences in total pyrolysis yields.

5.5. Conclusion

In this study, the pyrolysis of two WSPs was performed in a laboratory scale oven in an inert environment of nitrogen. This was done to obtain basic information on pyrolysis products, especially biochar and gas suitable for on-farm uses. The biomass conversion efficiency was higher in the additive blend pellet (T_5) because the additive materials like biochar showed synergistic activity, increasing the decomposition rate.

The study showed that temperature and reaction time significantly influenced the total pyrolysis yields and gas composition. The different pellet combinations (T_1 and T_5) also led to residence time and temperature variations. The results indicated an applied temperature of 300°C for the optimum amount of biochar production, while the maximum gas production temperature was 600°C. The char quality at such a temperature complies very well with the European biochar Certificate (EBC) standards, with the carbon content significantly higher than 50% mass. The results indicate that WSPs could be a promising agricultural crop residue for bioenergy production.

CHAPTER 6: COMBUSTION CHARACTERISTICS OF WHEAT STRAW PELLETS: A THERMOKINETIC STUDY

Abstract

Reaction kinetics is important for transferring small-scale studies into industry scale reactor conditions. This work presents the combustion studies of two types of wheat straw (WS) pellets (T_1: 100% WS and T_5: 70% WS, 10% sawdust (SD), 10% biochar (BioC) and 10% bentonite clay (BC) at 5, 10 and 20 °C/min heating rates. Combustion performance was measured in an air atmosphere range of 25~1200°C to investigate the activation energy, pre-exponential factor, and the reaction model. The combustion of the WSPs was assessed with an STA 449F3 Jupiter TGA (thermogravimetric analyser) and NETZSCH Proteus 8.0 software. The kinetic factors were found for use in the model-free and model-based techniques. Based on the TG/DTG profile, the WSPs thermal decomposition followed in four stages, while the model-based method comprised four consecutive reaction steps. A→B→C→D→E→F. The corresponding result of the WSP TG/DTG curves found that the model-free approach was not suitable for kinetic analysis, whereas model-based techniques like Cn (nth order reaction with autocatalyst), Fn (reaction of nth order), F2 (second order phase interfacial reaction mode) and D3 (diffusion control model) were best fitted.

The average $E\alpha$ for Fn, Cn, D3 and F2 models were 164.723, 189.782, 273.88 and 45.0 kJ/mole, respectively, for the T_1 pellets. For the T_5 pellets, the pre-exponential factor (lnA) was 4.764, 37.405, 54.666 and 7.006 (1/s) for the F2, D3, Cn and Fn models, respectively, at 20 °C/min heating rate. According to thermodynamic properties (ΔH, ΔG and ΔS), an equilibrium reaction for the T_1 combustion was observed. In contrast, the additive blending of WS (T_5) pellets had complex and multipoint reactions. In addition, the ignition temperature for the T_1 and T_5 pellets were 292 and 277°C, respectively, while the burnout point was similar (422°C) for both pellets at a 10 °C/min heating rate. The evaluation of the WSPs' thermal behaviour indicated potentiality as a bioenergy feedstock. For gasification reactor design, the obtained kinetic parameters were also important.

6.1. Introduction

Globally, biomass is a promising source of bioenergy and has attracted increasing attention (Winarno, Alwendra & Mujiyanto 2016). Agricultural waste is primary biomass with poor quality solid fuel characteristics (Liu et al. 2015). Lower density, low calorific value and higher ash content are the main drawbacks of agricultural waste/lignocellulosic straws (Wang, L. et al. 2016). In addition, straw is

usually less expensive and widely available as it is mainly generated from field crops. WS is available globally among the different types of agricultural waste (Kumar & Nandi 2021). This research used WSPs blended with various additives. The additives can change the poor quality WS into a higher value solid fuel (Dragutinovic et al. 2019; Mack et al. 2019).

A large amount of scientific literature is available on WS co-combustion. However, most research has been conducted on coal blended with biomass (Sher et al. 2020; Szufa et al. 2020; Kumar & Nandi 2021). Xinjie et al. (2021) found that co-combustion is a promising method for coal's clean and efficient application with straw. Ren et al. (2011) explored the status of nitric oxide (NO) for four straws (WS, rice straw, cotton stalk and corn stalk) during combustion. They discovered that including limestone encourages NO emission during the combustion of the cotton stalk. The presence of S in the environment inhibits SO_2 produced while burning straw. Zhang and Lu (2013) studied the high ash coal and straw co-combustion and reported that adding straw to coal lowers the burning profile temperatures while increasing the combustion rate.

Due to its high basicity index, WS has a more suitable ignition temperature and more combustion traits indices than coal (Xinjie et al. (2021). Hence, coal could increase WS combustion efficiency (Wang et al. 2009). But coal production and use present an environmental concern. In this context, blending available additives aside from coal with WS could be an alternative for generating thermal energy while sustaining environmental sustainability.

Bridgeman, T. et al. (2008) investigated torrefied reed canary grass, WS and willow's combustion behaviours. They reported that torrefaction biomass enhances ignition and heat transfer. Zhaosheng, Xiaoqian and Ao (2009) studied the catalytic combustion of rice and WS and found that catalysts influence the ignition and combustion. The thermal performance and co-combustion kinetics between WS and sewage sludge and their blends were also studied empirically using TGA. The results showed a substantial synergetic interaction in high temperature zones (Wang et al. 2019). Paniagua, García-Pérez and Calvo (2019) conducted a thermal study of WS and poplar wood blends and found the combination achieved the best combustion characteristics indexes. El-Sayed and Khairy (2017) experimented with the burning and emissions of pelletised WS in high temperature airflows. This study solely examines the decomposition behavior and does not identify the thermokinetic parameter. They suggest that high temperatures quickly increase the initial combustion temperature, reduce the combustion period and boost the total combustion speed. Ríos-Badrán et al. (2020) recently investigated manufacturing and characterising pellets from WS and rice husk. They contended that biomass mixtures enhanced the pellet's quality and combustion properties. Barley

straw, waste wood, WS, willow, miscanthus and wood pellets were studied using thermal and kinetic analyses by Sher et al. (2020). They reported an inverse relationship between activation energy and reactivity.

Overall, the literature review suggests that thermokinetic combustion studies of additive blends WSPs and individual WSPs are still rare. Therefore, research on the combustion of WSPs is essential to address combustion properties for reactor design and biomass-to-energy transformation.

Biomass thermochemical conversion involves intricate physiochemical mechanisms (Hussain et al. 2022). The Thermogravimetric Analyzer (TGA) is an essential laboratory tool used for material thermal characterization. TGA is used to characterise various environmental, food, pharmaceutical, and petrochemical applications. Understanding solid state degradation kinetics and heterogeneous reaction processes is essential for TGA (Vamvuka & Sfakiotakis 2011). TGA is a powerful, commonly used tool for measuring the thermogravimetric (TG) profile based on mass changes in the function of time or temperature (Emiola-Sadiq, Zhang & Dalai 2021). The derivative thermogravimetry curve (DTG) is also helpful in observing the act of temperature and time for reaction rate. The nonisothermal and isothermal models are generally used for the thermal analysis of a TG/DTG profile. The nonisothermal technique has recently been preferred because it has less experimental noise and is less complicated than the isothermal method (Gai, Dong & Zhang 2013). In addition, the activation energy can be precisely calculated using the isoconversional (differential or integral) forms without knowing the reaction model beforehand. Model-free and model-based approaches are the main ways of estimating the nonisothermal solid state kinetic data (Cai et al. 2013). The model-free approach is suitable for a one-step reaction. Alternatively, model fitting is appropriate for complex biomass decomposition with one or multi-point reactions (Soh et al. 2019).

The reaction mechanism is the internal process through the thermal conversion processes that use heat or thermal energy to convert biomass energy into another chemical energy. Several kinetic reaction models frequently used in solid state reaction kinetics are listed in Table 6.1. Therefore, this study used model-based and model-free techniques to investigate and compare thermal decomposition (TG/DTG curves) patterns and determine the most suitable model. The different kinetic approaches, including the model-based (nth order reaction with autocatalysis: Cn, and phase interfacial reaction n^{th} order: Fn) and model-free (Friedman, OFW and KAS) approaches, were also utilised to characterise the kinetic parameters.

Table 6.1: Common reaction models (Khawam & Flanagan 2006; Vyazovkin et al. 2011; Dhyani, Kumar & Bhaskar 2017; Manić, Janković & Dodevski 2021)

Reaction mechanism	Model name	Code	Functions
Chemical reaction	Zero-dimensional phase boundary	R_0	0
	First-dimensional phase boundary	R_1	$f = e$
	Two-dimensional phase boundary	R_2	$f = 2e^{1/2}$
	Three-dimensional phase boundary	R_3	$f = 3e^{2/3}$
Phase interfacial reaction	First-order reaction	F_1	$f = e$
	Contracting cylinder (Second order)	F_2	$f = e^2$
	Contracting sphere (Third order)	F_3	$f = e^3$
	Random nucleation (Fourth order)	F_4	$f = e^4$
	Reaction of nth order	F_n	$f = e^n$
Diffusion models	One-dimensional diffusion	D_1	$f = e^{0.5/p}$
	Two-dimensional diffusion (Valensi model)	D_2	$f = -1/ln(e)$
	Diffusion control (Jander model)	D_3	$f = 1.5e^{2/3}/(1-e^{1/3})$
	Diffusion control (Ginstling model)	D_4	$f = 1.5/(e^{-1/3}-1)$
Nucleation and growth models	Two-dimensional nucleation, according to Avarami-Erofeev	A_2	$f = 2e.[-ln(e)]^{1/2}$
	Three-dimensional nucleation, according to Avarami-Erofeev	A_3	$f = 3e.[-ln(e)]^{2/3}$
	n-Dimensional nucleation according to Avrami–Erofeev	A_n	$f = n.e.[-ln(e)]^{(n-1)/n}$
Auto catalyst reaction	Reaction of 1st order with autocatalysis by product	C_1	$f = e.(1+AutocatOrder.P)$
	Reaction of nth order with autocatalysis by product	C_n	$f = e^n.(1+AutocatOrder.P)$

Note; T_1: 100% WS and T_5: 70% WS, 10% sawdust (SD), 10% biochar (BioC) and 10% bentonite clay (BC)

The present work investigates the WS pellets (with (T_5) and without (T_1) additives) combustion for thermal and kinetic behaviour using TGA. The TG/DTG profile can help derive the WS pellet's thermokinetic properties, which are essential for comprehending solid fuel combustion and designing, developing, and operating large scale industrial reactors (Al-Ayed & Saadeh 2021). Also, CFD (Computational Fluid Dynamics) modelling uses these kinetic parameters as input data.

6.2. Materials and methods

The main intentions of the present work were to (a) use model-free and model-based techniques to examine and contrast the thermal decomposition techniques; (b) determine the burning profile parameters *[Eα, A*, and *f(α)]* and *(*c) determine of thermodynamic parameters.

6.2.1. Test sample and sample preparation

In this study, two WSPs (T_1 and T_5) were manufactured with different material combinations (Table 6.2). The materials' chemical analysis results are shown in the previous study (Chapter 3) followed the standard techniques.

Table 6.2: Pellets' physical characteristics

Pellets	Combinations (Weight proportion)	Average length, mm	Mean diameter, mm	Bulk density, kg/m³	Ash content, %
T_1	WS (100%)	22.0	8.21	244.79	7.09
T_5	WS (70%) + SD (10%) + BC (10%) + BioC (10%)	37.0	8.13	607.40	11.87

Note; WS = Wheat straw, BC = Bentonite clay, SD = Sawdust and BioC = Biochar

The pellet was a cylindrical solid fuel made from WS with and without additives. However, for TGA, the samples needed to be ground to increase their surface area (Duffin et al. 2007) and conversion efficiency (Rioux et al. 2005). After drying for 24 hours at 105°C in an oven, the sample was ground into a powder with an average particle size of 1 mm (Figure 6.1). The crushed sample was sieved to ensure the uniform size of the particles. In addition, a dummy test was done on each heating rate to avoid systematic error and baseline information.

| T₁ pellet | T₅ pellet | Ground pellets |
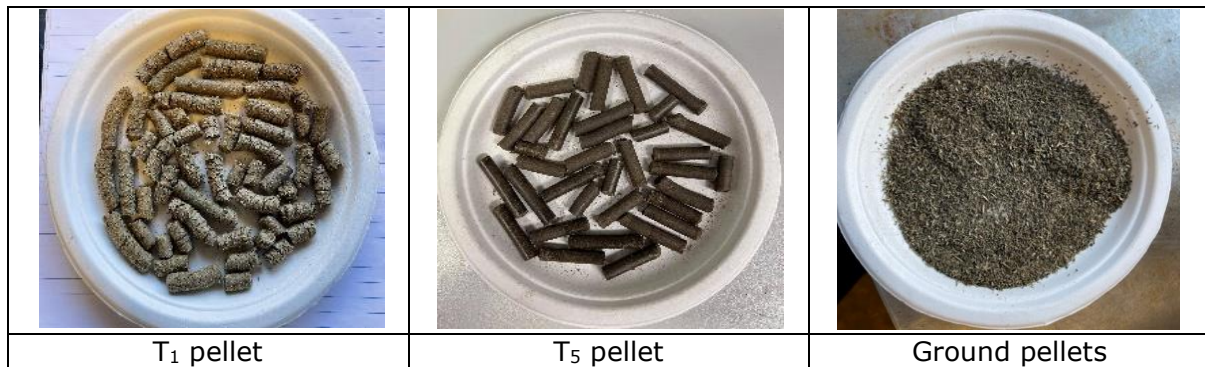
Figure 6.1: Experimental materials photographic illustration

The same sample size (weight) was used for each treatment to ensure accurate experimental results (Grønli, Antal & Varhegyi 1999). Regarding this issue, we considered a 50 mg sample as an initial weight for each run. However, the sample holding capacity of the TGA pan was 8.75~9.75 mg. The sample was burned in an alumina based pan, and a lid has used to create the best possible heat transmission conditions. The experiment was repeated three times to maintain the precision and reproducibility of the analysis. The collected data's mean value was used for the current study.

6.2.2. Thermogravimetric analyser (TGA)

TGA is popular equipment used to investigate fuels' thermal behaviours and the carbonaceous materials' kinetics as a function of temperature (nonisothermal) and time (isothermal) (Jeguirim & Trouvé 2009; Carrier et al. 2011; Ali, Bahaitham & Naebulharam 2017).

The STA 449F3 Jupiter TGA (Erich NETZSCH GmbH & Co. Holding KG, Germany) (Figure 6.2) was used to measure and record the dynamics of the constant mass loss of the samples with increasing temperature and time (Vhathvarothai, N., Ness, J. & Yu, Q. J. 2014). This Jupiter TGA equipment comprised a furnace, sample pan, precision balance, gaseous supply system and data collection system (Rex & Miranda 2020). During the experiment, the feedstock was combusted in the control zone under a pressure of 0.1 MP. Air was used as the carrier gas and maintained at a 50 ml/min steady flow rate.

Model: STA 449F3 Jupiter (Erich *NETZSCH* GmbH & Co. Holding KG, Germany)
Serial no.: 3A-1343-M
Furnace: Platinum
Measure: Mass loss (decomposition, thermal stability, kinetic parameter)
Software: Netzsch Proteus 8.0
Pan: Alumina, 85 ul
Purge gas: Air
Thermocouple: Platinum Rhodium - 10%/Platinum (Type S)
Convenient data: plain text, CSV, XML, Excel®, Word®, PowerPoint®, and image formats
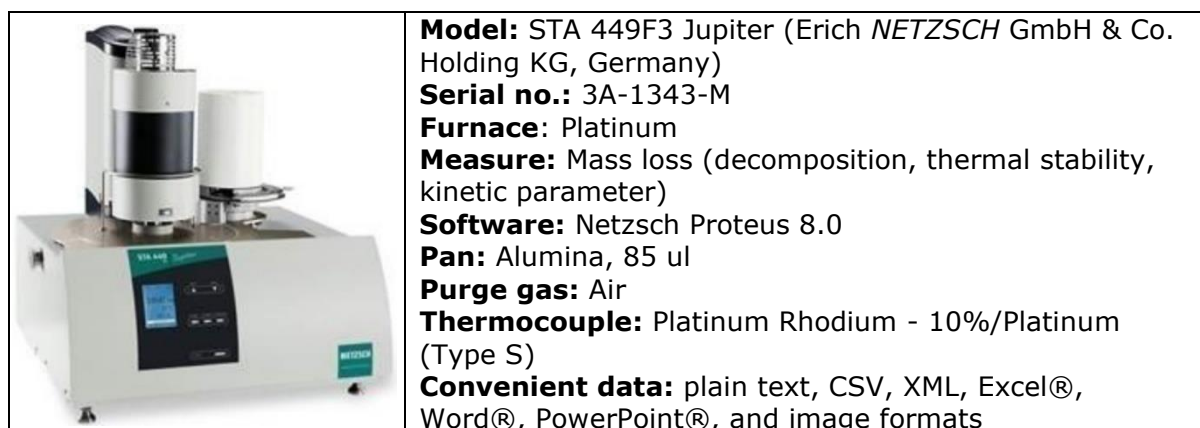
Figure 6.2: Thermogravimetric analyser

In the present study, the kinetic triple was derived using state-of-the-art kinetic software, *NETZSCH* Proteus 8.0 (NETZSCH-Gerätebau GmbH), for WSP combustion with dynamic conditions. *NETZSCH* software allows the analysis of temperature-dependent chemical processes (Manić, Janković & Dodevski 2021). A computer automatically controls the entire process, records the mass changes and draws a weight loss curve; such investigation output in kinetic techniques that defines the experimental results under temperature.

6.2.3. Data analysis and treatments

The samples' reaction rate during combustion was determined using the remaining mass distribution and the mass loss data derivative. In addition, the mass loss (TG curves) was employed to estimate the degradation of the pseudo components (lignin, hemicellulose and cellulose) (Yeo et al. 2019). In contrast, the degradation rate was assessed by DTG profiles (Fonseca et al. 2022). A moving average trend line was also used to reduce the noise data from the TGA. This strategy frequently examines TGA data (Yi et al. 2013; Lu & Chen 2015).

The TGA data were obtained from the built-in computer at the linear heating rates: 5, 10 and 20 °C/min, and the ranges of temperatures were 25 to 800°C. Similar temperatures and heating rates have been employed

in numerous experiments to assess the kinetic properties of different biomasses (Dhyani, Kumar & Bhaskar 2017; Kaur et al. 2018).

6.2.4. Kinetic parameters

Thermokinetic properties of feedstock and operating conditions can significantly influence the efficiency of a reactor and conversion performance (Janković 2015). According to the Arrhenius law, three variables ($E\alpha$, A and (α)), are highly relevant in the study of thermokinetic decomposition. Usually, these three parameters are referred to as "kinetic triple" and represent thermal breakdown (Vyazovkin 2006).

Empirical data studies can estimate the activation energy from the temperature constant of total reaction rates. At the same time, the preexponential component's magnitude also represents a scaling factor for overall reaction rates. This approach has been applied to various materials (inorganic, metals and polymers) to characterise thermal properties (Vyazovkin 2000). Finally, the reaction model described by $f(\alpha)$ is generally used for thermal decomposition.

6.2.5. Kinetic theory

A kinetic modelling study using TG data can explore the feedstock decomposition behaviour and biomass processing mechanism (Mandapati & Ghodke 2021). Generally, with heat application, the biomass is converted into solid as char, liquid as bio-oil and gaseous fraction through the composition degradation. The conversion or thermal decomposition rate is a heterogeneous reaction and can be expressed as a single step kinetic equation (Vyazovkin 2006; Singh, Patil & Sawarkar 2020). This formula represents the mass conversion rate of two functions ($k(T) \text{ and } f(\alpha)$) and can be denoted as (Huang et al. 2018):

$$\frac{d\alpha}{dt} = k(T)f(\alpha) \dots\dots\dots\dots\dots\dots\dots\dots\dots\dots\dots\dots\dots\dots\dots\dots\dots\dots\dots\dots6.1$$

Where $f(\alpha)$ is conversion model depends on the actual reaction mechanism (Chong et al. 2019), $k(T)$ the reaction rate at absolute temperature T and α is the conversion degree.

The fraction (α) data is commonly used for the kinetic model of that material decomposition. The conversion degree (α) was defined as:

$$\alpha = \frac{w_0 - w}{w_0 - w_f} \quad \dots\dots\dots\dots\dots\dots\dots\dots\dots\dots\dots\dots\dots\dots\dots\dots\dots\dots\dots\dots\dots.6.2$$

Whereas:
α = conversion degree or reactant decomposition fraction at the time (t),
w, w_0, w_e, w_f = the sample's initial, actual and final weights (g), respectively, and
n = the reaction order.

Commonly, the Arrhenius law is used to calculate biomass combustion and pyrolysis kinetic parameters. This law is also important in obtaining information about the reaction rate. The Arrhenius law can be expressed mathematically (Ozsin & Putun 2019; Laouge & Merdun 2020):

$$k(T) = A\, e^{(-\frac{E_\alpha}{RT})} \dotfill 6.3$$

Whereas:

K = reaction rate constant, 1/s
E_α = activation of energy, kJ/mol
A = pre-exponential factor, 1/s
R = universal gas constant (8.314), kJ/K.mole
T = absolute temperature, K

The following equation can be expressed using Equations (6.1) and (6.3) for the nonisothermal reaction process with a linear/constant heating rate (Urbanovici, Popescu & Segal 1999):

$$\frac{d\alpha}{dT} = \frac{A}{\beta}\, e^{(-\frac{E_\alpha}{RT})} f(\alpha) \dotfill 6.4$$

Where: the heating rate, $\beta = \frac{dT}{dt}$

Various models have explored the kinetic parameters through a single step equation (Figure 6.3) (Leroy-Cancellieri et al. 2012; Shagali et al. 2023). The two main categories of empirical models (model fitting and model free methods) are commonly used (Moukhina 2012).
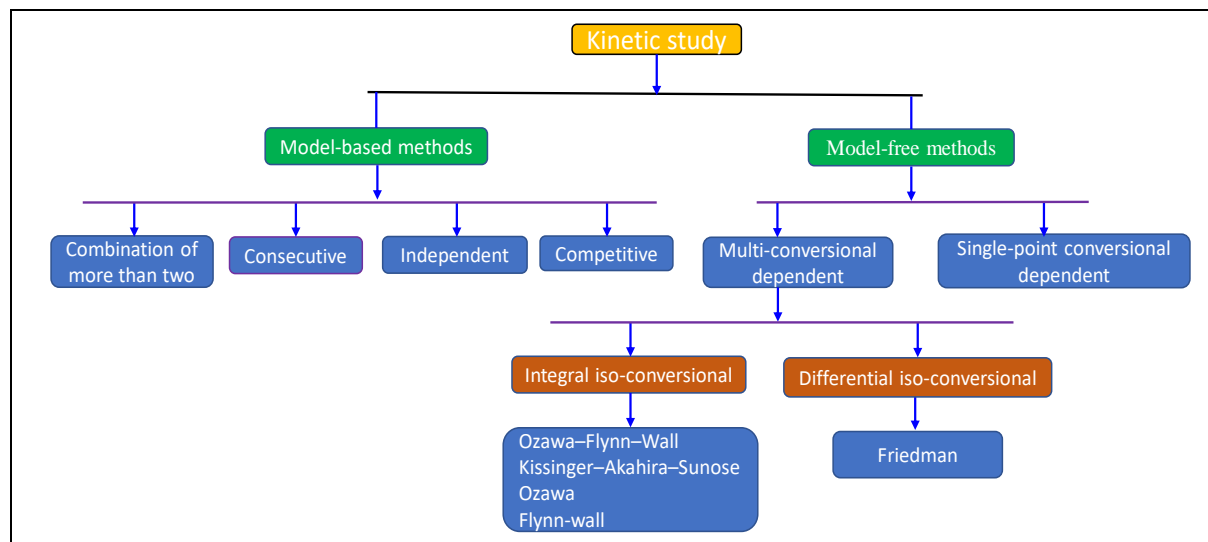
Figure 6.3: Available kinetic model used for thermal analysis (Mandal et al. 2022)

6.2.6. *Model-free analysis*

The kinetic analysis based on an isoconversional technique is usually referred to as "model-free" (Hu et al. 2019). The model-free techniques are straightforward and can more accurately identify multi-step processes. This method gives information only on Reactant (*A*) and Product (*B*) and no

other information on intermediate steps or products. Hence this analytical method can mostly be done on paper or an Excel sheet. However, it only works for mixtures or competitive or highly overlapping steps (Mureddu et al. 2018). The process describes only one chemical equation (Arrhenius equation) (NETZSCH 2021).

$$\frac{d\alpha}{dT} = A(\alpha)\,.f(\alpha).\exp\left(-\frac{E_\alpha}{RT}\right) \quad \dots\dots\dots\dots\dots\dots\dots\dots\dots\dots\dots\dots\dots\dots\dots\dots\dots 6.5$$

Here (α) and $A(\alpha)$ are unknown, while $A(\alpha)$ can be found only with the assumption of $f(\alpha)$.

It is not so easy to describe this equation with one value. Therefore, this method computes E_α from a series of TG data sets via constant heating rate figures or/and temperatures (Vyazovkin 2006; Moukhina 2012; Wang et al. 2017). In addition, the method is based on some assumptions and kinetic reactions and does not depend on specific models (Vyazovkin 2006). The data must satisfy specific assumptions to validate any model by model-free techniques such as (Manić, Janković and Dodevski (2021):

- Only one kinetic equation, for example, Reactants A → Products B
- E_α, and A depends on α (degree of conversion)
- Reaction rate at the same conversion is only a function of temperature

- Total effect (total mass loss or total peak area) must be the same for all curves
- Changes in the mechanism should be at the same conversion value.

There are several model-free methods, including the (i) Kissinger approach, (ii) Kissinger-Akihara-Sunose (KAS), (iii) Friedman techniques, (iv) Flynn-Wall and (v) Flynn-Wall-Ozawa (FWO) (Blaine & Kissinger 2012). Vyazovkin et al. (2011) noted that the most accurate techniques are KAS and FWO for kinetic parameter evaluation. However, the Friedman approach is widely applied using a differential tool. At the same time, the KAS and FWO are the two frequently applied integral techniques (Damartzis et al. 2011). They are widely used for many purposes (Albu et al. 2011; Klimova et al. 2013), but all are based on presumptions.

6.2.6.1. Flynn-Wall model

Flynn-Wall uses conventional approaches such as 5% conversion points or 50% conversion points (half decomposition) (Yuansheng, He & Shenghua 2007). The TGA curves are examined at various heating rates and the remaining mass against temperature. The plot of $\frac{\Delta(\ln \beta)}{\Delta\left(\frac{1}{T}\right)}$ is then used to create the linear regression for the isoconversational points. Finally, the slope can be used to determine how much energy is activated.

$$E_\alpha = -\frac{R}{b} * \frac{\Delta \log(\beta)}{\Delta(\frac{1}{T})} \dots\dots\dots\dots\dots\dots\dots\dots\dots\dots\dots6.6$$

Where:

      b = interactive value

      T = temperature at a point of isoconversion, K

The integration method calculates the conversion of α at temperature T.

$$\int_0^\alpha \frac{1}{f(\alpha)}d\alpha = g(\alpha) = \frac{A}{\beta}exp^{\left(\frac{-E_\alpha}{RT}\right)}dt \dots\dots\dots\dots\dots\dots\dots\dots6.7$$

This integration is approximated:

$$\int_{T_0}^T exp^{\left(\frac{-E_\alpha}{RT}\right)}dt \approx \frac{R}{E_\alpha}T^2 exp^{\left(\frac{-E_\alpha}{RT}\right)} \dots\dots\dots\dots\dots\dots\dots\dots6.8$$

Rearranging this equation in the logarithmic form gives,

$$\frac{\ln\beta}{T_\alpha^2} = \ln\left[\frac{RA}{E_\alpha\, g(\alpha)}\right] - \left(\frac{E_\alpha}{R}\cdot\frac{1}{T_\alpha}\right) \dots\dots\dots\dots\dots\dots\dots\dots6.9$$

Global values of E_α and A calculate the theoretical $g(\alpha)$ curves (Vyazovkin et al. 2011).

6.2.6.2. Kissinger model

The Kissinger approach uses derivative data curves (DTG) for numerous constant heating rates. It investigates the temperature (T_m) at the maximum reactivity rate ($r_{max} = \frac{d\alpha}{dt}$). The reactivity's second derivative at a maximum point equals zero.

$$\frac{d^2\alpha}{dt^2} = \left[\left(\frac{E_\alpha\beta}{RT_m^2}\right) + Aexp^{\frac{-E_\alpha}{RT}}f`(\alpha)\right]\frac{d\alpha}{dt} = 0 \dots\dots\dots\dots\dots\dots6.10$$

The method is as in Equation 6.1 and the linear form is as in Equation 6.6, is the modified form as:

$$\frac{\beta}{T_m^2} = \frac{AR}{E_\alpha}exp^{\frac{-E_\alpha}{RT}}f`(\alpha) \dots\dots\dots\dots\dots\dots\dots\dots\dots\dots\dots\dots6.11$$

$$\ln\left(\frac{\beta}{T_m^2}\right) = \left(\frac{-E_\alpha}{RT_m}\right) + \ln\frac{AR}{E_\alpha} + \ln[n(1-\alpha_m)^{n-1}] \dots\dots\dots\dots\dots6.12$$

The value ($-\frac{E_\alpha}{R}$) is the slope of $\ln\left(\frac{\beta}{T_m^2}\right)$ versus ($\frac{1}{T_m}$).

The drawback of the Kissinger method is that the technique produces a single activation energy value for any reaction's complexity (Liavitskaya & Vyazovkin 2017).

6.2.6.3. Kissinger-Akihara-Sunose (KAS) model

The Kissinger-Akihara-Sunose (KAS) method is suitable for DTG profile evaluation. However, DTG figures select data from the isoconversasional point and a constant rate value (α) at various heating rates. The following is a simplified version of Equation (6.12) for the KAS model (Chen, Jiacong et al. 2017):

$$\ln\left(\frac{\beta}{T^2}\right) = \left(\frac{-E_\alpha}{RTf(\alpha)}\right) + \ln\frac{AR}{E_\alpha} \dots\dots\dots\dots\dots\dots\dots\dots\dots\dots\dots\dots\dots\dots\dots\dots.6.13$$

The content of conversion (α) is selected at several heating rates (β); therefore, the curve of $\ln\left(\frac{\beta}{T^2}\right)$ versus $\left(\frac{1}{T}\right)$ gives the slop value of $\left(\frac{-E_\alpha}{R}\right)$.

6.2.6.4. Friedman (FM) model

Friedman's model applies isothermal data from several constant heating rate curves corresponding to a similar temperature. The FM technique does not require mathematical assumptions (Huidobro et al. 2016). The Equations (6.1) and (6.3), in their natural logarithmic function for the FM model, become:

$$\ln\beta\left(\frac{d\alpha}{dT}\right) = \ln(A).f(\alpha) - \frac{E_\alpha}{RT}\dots\dots\dots\dots\dots\dots\dots\dots\dots\dots\dots\dots\dots\dots..6.14$$

For the kinetic triple at a chosen temperature, the plot of $\ln\beta\left(\frac{d\alpha}{dT}\right)$ versus $\left(\frac{1}{T}\right)$ at various constant heating rates, data gives the slope of $\left(-\frac{E_\alpha}{R}\right)$.

6.2.6.5. Flynn-Wall-Ozawa (FWO) model

The Flynn-Wall-Ozawa (FWO) model is an isoconversional technique. It is predicated on the following approximation by Doyle (Ding et al. 2017):

$$\ln p\left(\frac{E_\alpha}{RT}\right) \cong -3.315 + \frac{E_\alpha}{RT}\dots\dots\dots\dots\dots\dots\dots\dots\dots\dots\dots\dots\dots.6.15$$

The reaction model can be linearly formed by the following equation (Jiang et al. 2015)

$$\ln(\beta) = \ln\left[\frac{AE_\alpha}{Rf(\alpha)}\right] - 2.315 - 0.4567\frac{E_\alpha}{RT}\dots\dots\dots\dots\dots\dots\dots\dots6.16$$

The heating rate constant ($ln(\beta)$) versus the inverse temperature (1/T) graph should provide a linear line with a slope of $-E_\alpha$/R at a constant value. This slope is applied to compute the activation energy.

6.2.7. Model-based analysis methods

The model-based kinetic method analyses complex chemical processes with multiple reaction steps (https://kinetics.netzsch.com/en).

Each reaction step has its kinetic equation and a kinetic triplet (Nebojša, Marija & Kristina 2020). In addition, the model-based approach can display each reactant's reaction rate and concentration for each step (Opfermann, Kaisersberger & Flammersheim 2002). Also, Karaeva et al. (2022) mentioned that 95% of chemical reactions are multistage during thermal conversion. Hence, model-based kinetics is effective for analysing chemical reactions comprehensively. However, before examining the thermal data, the model-based method's prerequisite assumption needs to be acknowledged. The assumptions for model-based kinetic analysis are as follows (Moukhina 2012):

- The reaction comprises several basic reaction steps with their kinetic reaction equations
- All kinetic parameters are constant values
- The signals from all the individual reaction stages, added together with their weight are the total signal.

Kinetics *NETZSCH* Proteus software develops the best kinetic model that precisely captures the heterogeneous process using reliable, cutting-edge mathematical computations to determine kinetic triple. Two and three stage reaction models describe multistage reaction systems (García et al. 2012). Following the International Confederation for Thermal Analysis and Calorimetry (ICTAC) suggestions, one should construct a kinetic model that includes the least number of stages and corresponds to a significant experimental range (Karaeva et al. 2022). The following equation can define the general reaction rate for individual reaction steps (NETZSCH 2021).

$$\text{Reaction rate } (_j) = \frac{d(a \rightarrow b)}{dt} = A_j * f_j\left(e_j p_j\right) * \exp\left(-\frac{E_{Aj}}{RT}\right) \ldots\ldots\ldots\ldots\ldots\ldots\ldots\ldots.6.17$$

Where: $f_j\left(e_j p_j\right)$ = function of reaction type
e_j = initial reactant concentration
p_j = product concentration
A_j = pre-exponential factor
j = number of specific reaction steps.

The literature suggests that kinetic triple estimation depends on the user, as different findings might be found for the same data set (Vyazovkin et al. 2020). It relies on the selection of the model and the reaction types (i.e., independent, consecutive or competitive) (Mandal et al. 2022). This thermal analysis used the Kinetics *NETZSCH* with Proteus 8.0 software multi-step analytical engines, an excellent tool for model-based and model-free analysis. This study used the following theoretical model to perform the multi-step kinetic model (Chrissafis et al. 2012; Parcheta, Koltsov & Datta 2018; Safiullina et al. 2020).

n^{th} order reaction with autocatalysis

$$(C_n),\ \frac{d\alpha}{dt} = Ae^{\frac{E_\alpha}{RT}}(1-\alpha)^n(1+k_{cat}\,a)\ \ldots\ldots\ldots\ldots\ldots6.18$$

$$n^{th}\text{ order reaction }(F_n) = \frac{d\alpha}{dt} = Ae^{\frac{E_\alpha}{RT}}(1-\alpha)^n\ \ldots\ldots\ldots\ldots\ldots\ldots\ldots\ldots\ldots6.19$$

Whereas: n = Reaction order
$\qquad k_{cat}$ = Catalytic rate constant

6.2.8. Model fitting values and kinetic triple estimation

The model-fitting equations have no analytical solution under non-isothermal conditions. It can calculate the kinetic parameters for a single temperature rise (Mandapati & Ghodke 2021). Moreover, this method depends on approximations of algebraic expressions (Fedunik-Hofman, Bayon & Donne 2019). Hence, the model fitting technique is only suitable for evaluating the action order and the frequency factor (Damartzis et al. 2011).

Model fitting approaches are based on fitting experimental data to different solid state reaction models and the results of E_α and A (Khawam & Flanagan 2006). The E_α can be obtained from the slope of the line drawn between $ln\left[\frac{-ln\,(1-\alpha)}{T^2}\right]$ and $\frac{1}{T}$ or $ln\left(\frac{g(\alpha)}{T^2}\right)$ and $\frac{1}{T}$ (Vyazovkin et al. 2011). In brief, E_α can be measured by graphically representing various slopes listed in Table 6.3. However, in all cases, the conversion degree (a) varies from 0.01 to 0.99 (Klimova et al. 2013).

Table 6.3: Kinetic properties estimation for various model-free methods

Model	kinetic properties $(E_\alpha,\ A\text{ and }f(\alpha))$	Reference
Kissinger model	$\left(-\frac{E_\alpha}{R}\right)$ is the slope of $\ln\left(\frac{\beta}{T_m^2}\right)$ versus $\left(\frac{1}{T_m}\right)$	(Vyazovkin et al. 2011)
Kissinger-Akihara-Sunose (KAS) model	$\left(\frac{-E_\alpha}{R}\right)$ is the slope of $\ln\left(\frac{\beta}{T^2}\right)$ versus $\left(\frac{1}{T}\right)$	(Chen, Jiacong et al. 2017)
Friedman model	$\left(-\frac{E_\alpha}{R}\right)$ is the slope of $\ln\beta\left(\frac{d\alpha}{dT}\right)$ versus $\left(\frac{1}{T}\right)$	(Huidobro et al. 2016)
Flynn-Wall model	Global values of E_α and A calculated the theoretical $g(\alpha)$ curves	(Vyazovkin et al. 2011)
Flynn-Wall-Ozawa (FWO) model	$\left(-\frac{E_\alpha}{R}\right)$ is the slope of $\ln(\beta)$ versus $(1/T)$	(Ding et al. 2017)

The degradation of biomass commonly falls into several primary groups. First, the integral form $g(\alpha)$ estimation should be considered into several predefined reaction models (Table 6.1) while fitting the curve (Table 6.3). The best fit model has the maximum correlated coefficient of determination R^2 and the value is close to E_α (Hu et al. 2019). Finally, the optimum value of E_α is determined with one highest R^2 for approximation.

6.2.9. Thermodynamic analysis

Biomass combustion requires information on thermodynamic parameters (Singh et al. 2020). The essential thermodynamic parameters (Enthalpy: ΔH, entropy: ΔS, and Gibbs free energy: ΔG) are often used to characterise thermal behaviour (Dhyani, Kumar & Bhaskar 2017). The thermodynamic parameters depend on the combustion process efficiency and the measurement of heat (Naqvi et al. 2020). Moreover, energy calculation and the process feasibility determination depend on the thermodynamic analysis results. To determine ΔH, ΔG and ΔS from kinetic parameters, the following measures were used (Xu & Chen 2013; Kaur et al. 2018):

$$\Delta H = E_a - RT \text{ ....} 6.20$$

$$\Delta G = E_a + RT_m \ln\left(\frac{K_\beta T}{hA}\right) \text{ ....} 6.21$$

$$\Delta S = \frac{\Delta H - \Delta G}{T_m} \text{ ....} 6.22$$

Whereas:
K_β = boltzman constant ($1.38 *10^{-23}$), m^2.Kg/s^2.k
h = planck constant ($6.626*10^{-34}$), m^2.kg/s
T_m =maximum temperature at which maximum decomposition occurred, K
R = universal gas constant (8.3145), J/mole.K

The A and E_α data were taken from *NETZSCH* Kinetics software at a particular conversion for 20 °C/min for the calculation of ΔH, ΔS and ΔG,. These parameters were estimated according to the highest temperature where the maximum decomposition occurred and was acquired from the DTG profile (Kumar, Mishra & Upadhyay 2020; Singh, Chakraborty & Mondal 2020).

6.2.10. Ignition and burnout temperatures

Investigating fuel qualities is important in evaluating fuel selection, consumption, combustor design and successful application (Du, Chen & Lucas 2007). In this context, the fuels' ignition and burnout temperatures are two fundamental properties of bioenergy production. The ignition temperature is lowest when the fuel spontaneously ignites without an external burning source (Zheng et al. 2020). In contrast, the temperature at which the feedstock will almost be consumed during combustion is known as the burnout temperature (Lu & Chen 2015).

Different methods, such as intersection, conversion and deviation, can determine the fuel's ignition and burnout temperatures (Arias et al. 2008). With a constant heating rate, the intersection technique determines the ignition and burnout temperatures from the TG and DTG combustion

profiles (Tognotti et al. 1985). The primary advantage of this method is the simplicity of description (Morais et al. 2022). Figure 6.4 illustrates the intersection method for ignition and burnout temperature.

Lu and Chen (2015) have reviewed several methods (Figure 6.4). The ignition temperature determines (the intersection method) to follow the steps:

- At Point A, a vertical line is illustrated from the first DTG peak, which is the peak value of the DTG curve (Figure 6.4). The beginning of DTG is the devolatilisation point B

- A tangent from A and a horizontal line through B were sketched on the TGA curve

- The two lines' intersection temperature (T_i) considers the ignition temperature at the).

The single peak of a DTG curve was considered to estimate the biomass burnout temperature (Liu et al. 2012). Several biomass species exhibit two different peaks in their DTG plots when air is the carrier gas (Soh et al. 2019). In this instance, the burnout temperature should be calculated using the second peak rather than the first. Figure 6.4 depicts Point "C" on a TG curve, where a vertical line from the second peak of the DTG curve meets the TG curve. The TG curve readjusts at a location designated as "D". The junction of a tangent of the TG curve at "C" and the horizontal line through "D" is where the burnout temperature (T_b) is found.
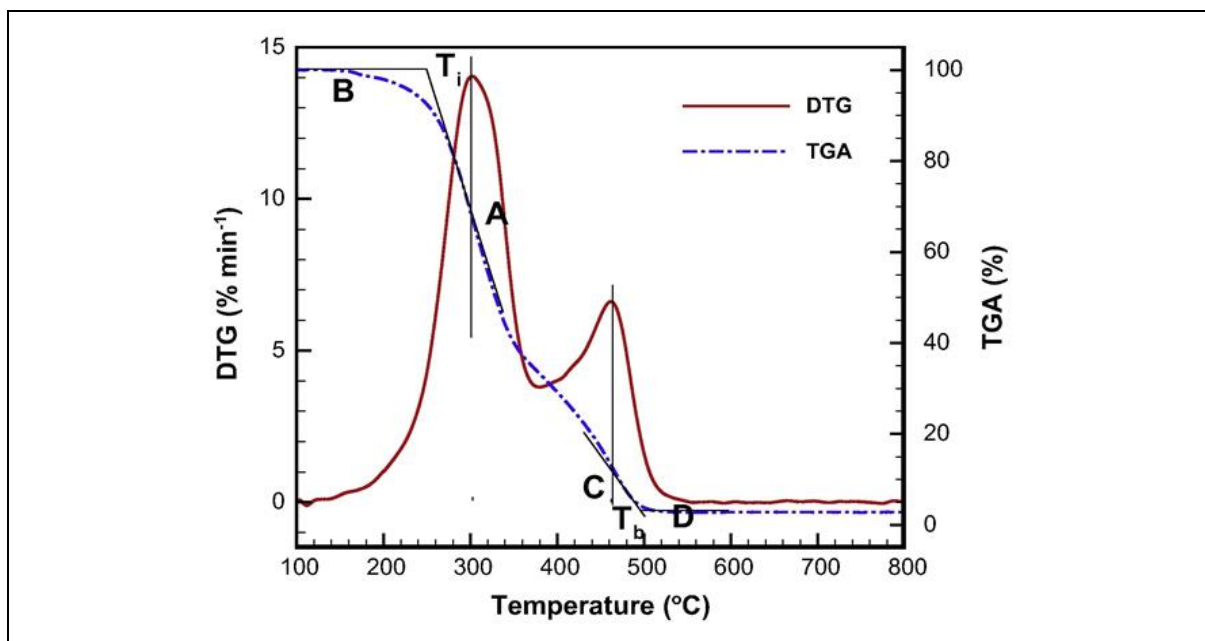
Figure 6.4: Intersection method for determination of ignition (T_i) and burnout (T_b) temperatures (Lu & Chen 2015)

6.3. Results and discussion

6.3.1. Combustion characteristics

The thermal properties of WSPs (T_1 and T_5) combustion processes were carried in a TGA under an air atmosphere. Figures 6.5~6.10 display the TG/DTG curve for the T_1 and T_5 pellets. Thermal degradation of each WSP can be subdivided into four stages, as numbered in Figures 6.4 and 6.5, which is supported by other research (Hu et al. 2019; Rahib et al. 2019; Fonseca et al. 2022). Since the main component of the samples included hemicellulose, cellulose, lignin and extractives (Yao & Ma 2018), the four steps are related to their release and decomposition (Table 6.4). The central peak and many side peaks were visible in the DTG profiles. The side peak was created by hemicellulose, lignin and other substances, while the combustion of the cellulose created the prominent peak (Mishra & Mohanty 2020).

Table 6.4: Combustion profile stages (Zhao et al. 2019)

Stages	I	II	III	IV
Name	Dehydration and desorption stage	Oxidation stage	Combustion stage	Burnout stage/Char combustion
Activities	Removal of moisture from below 110°C	Removal of volatiles and adsorption/ absorption of oxygen, resulting in a mass loss in temperature zone 110~350°C	Combustion of volatiles & carbon content in temperature zone 350~650°C	Combustion of lignin matter or gangues in temperature zone >650°C
Degradation component	Hemicellulose	Hemicellulose and cellulose		Lignin and charring

6.3.1.1. Analysis of TG/DTG profiles for pellet T_1

- *At a heating rate of 20 °C/min*

The TG/DTG profile for 20 °C/min is shown in Figure 6.5. In the first stage (I), the temperature ranged from 25 to 172°C, while the maximum DTG was 2.66 %/min with peak temperatures of 72°C for a 20 °C/min heating rate. In this stage, the highest mass loss was 7% (Table 6.5). The biomass cellular and surface water loss was related to the first combustion stage (I) (Ahmad et al. 2018). The moisture evaporated and escaped when the sample was heated, resulting in a slight mass loss. The second stage (II) temperature range was 172 to 332°C, resulting in a large volatile volume release and significant mass loss. Xu (2013) supported this result. The second stage, named oxidative degradation, was connected to the decomposition of hemicellulose and cellulose. The maximum DTG was

49.45 %/min in the second stage (II). Alternatively, the sample burnt more quickly and thoroughly and achieved the most weight loss (54.15%) at a peak temperature of 297°C (Table 6.5). Due to its most volatile content at this point, the mass loss was at its highest (Hu et al. 2019).

Table 6.5: Combustion characteristics of T_1 pellet

Heating rate, °C/min	Item	Stage I	Stage II	Stage III	Stage IV	Residue, %
	T_{range}, °C	25-172	172-332	332-409	409-1200	
20	T_{peak}, °C	72	297	357	442	6.71
	M_{loss}, %	7	54.15	22.72	9.42	
	DTG_{max}, %/min	2.66	49.45	6.33	11.37	
10	T_{peak}, °C	62	292	347	447	7.86
	M_{loss}, %	6.66	56.64	15.74	13.1	
	DTG_{max}, %/min	1.22	22.99	8.58	3.4	
5	T_{peak}, °C	62	282	367	442	7.6
	M_{loss}, %	6.96	60.13	17.08	8.23	
	DTG_{max}, %/min	0.86	9.02	1.51	1.38	

Note; T_{range} = Temperature range
T_{peak}= Peak/highest temperature
M_{loss}= Mass loss
DTG_{max} = Maximum Differential Thermogravimetric/ maximum reaction rate
Stage I = Mass losses occurred due to the moisture
Stage II = Mass losses due to oxidative degradation (volatile released and then burned)
Stage III = Mass losses oxidative degradation (decompose of cellulose)
Stage IV = Mass losses combustion of the remaining char

In the third stage (III), the overall weight loss was 22.72% with a peak temperature of 357°C; however, the temperature ranged from 332 to 409°C (Figure 6.5). This stage is also called devolatilisation. At this stage, the weight loss was related to the volatile matter and fixed carbon content. Therefore, the third stage can be considered the most significant thermal degradation of lignin and char. The temperature varied from 332 to 409°C, with the highest reaction rate at 6.33 %/min (Table 6.6). The results were similar to those of other authors (Alvarez et al. 2016), even when a different type of biomass was used. The inorganic materials, residual lignin, and char were burned out and stabilised in the final combustion area (IV) (Huang et al. 2018). The final char formation occurred in this division and removed the secondary gases. The temperature at maximum weight loss (9.42%) of lignin was 442°C, while the temperature difference in this stage was 409 to 1200°C.
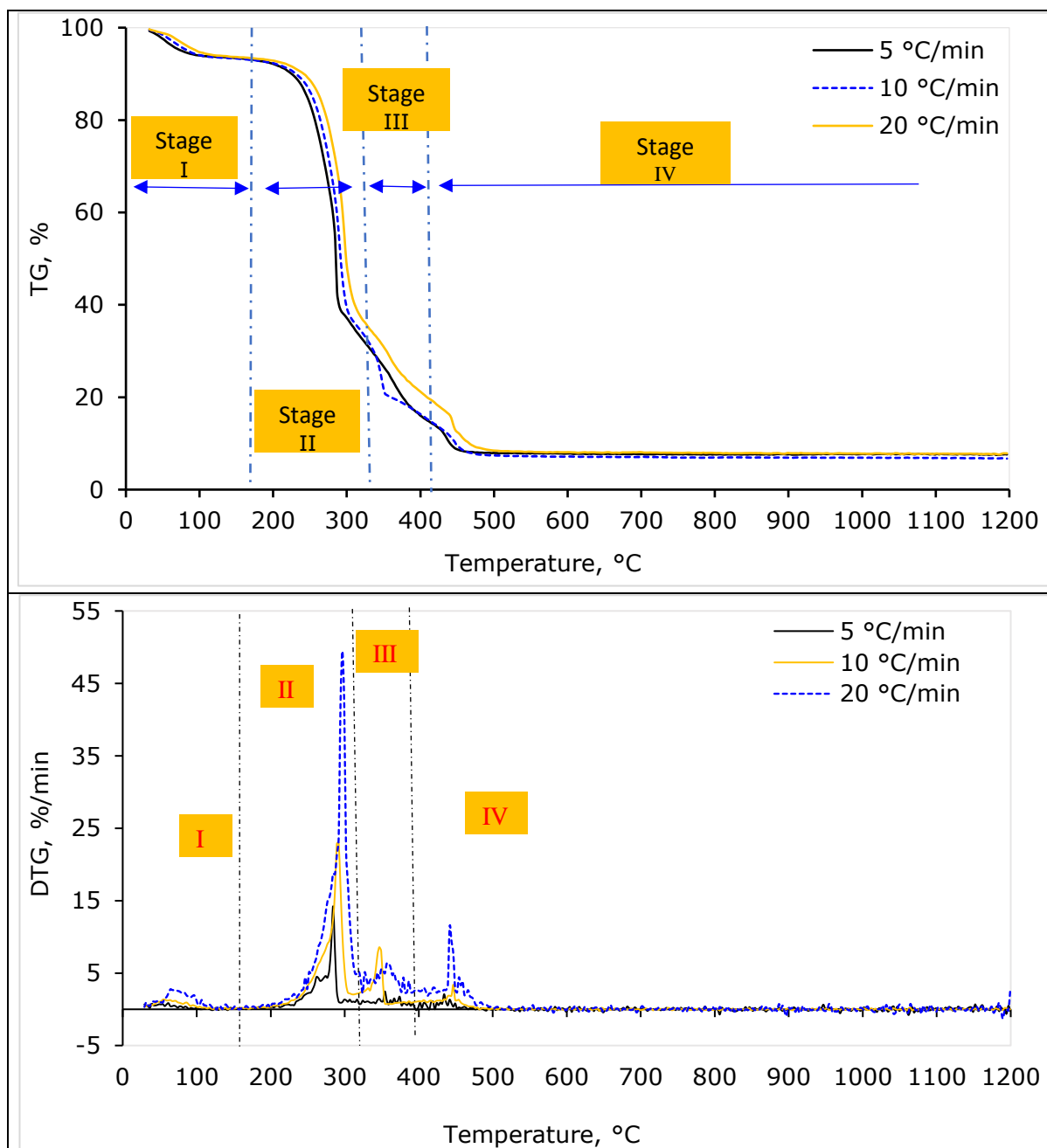
Figure 6.5: Combustion profile of T_1 pellets: (a) TG curve and (b) DTG curves

- *At a heating rate of 10 °C/min*

The TG/DTG curves are displayed in Figure 6.5. In this instance, four regions made up the thermal degradation combustion process. Stage (I) experienced a temperature between 25 and 172°C, with a weight loss of 6.66% because of moisture evaporation from the WSPs. Stage (II), which involved the thermal degradation of hemicellulose and had a mass loss of 56.64%, was visible at temperatures between 172 and 332°C. Region (III) temperature variation of 332~409°C corresponded to the breakdown of cellulose, resulting in a weight loss of 15.74% and the highest reaction rate of 8.58 %/min. Rahib et al. (2019) supported this result using Argan

nutshell as biomass. Stage (IV) involved weight loss of 13.1% and lignin degradation between 409 and 1200°C. Lignin often decomposes slowly in the temperature range because of its complicated structural makeup. At 1200°C, the remaining amount of sample was around 7.86% (Table 6.5).

- *At a heating rate of 5 °C/min*

The TG/DTG profile is shown in Figure 6.5. In this case, the combustion process of biomass thermal degradation consisted of four zones. The mass loss at stage (I) was 6.96%, observed between 25 and 172°C and might have been due to the evaporation of moisture from the WSP. At temperatures between 172 and 332°C, the second region involved the heat breakdown of hemicellulose and had a mass loss of 60.13% and a quick reaction rate (DTG$_{max}$) of 9.02 %/min, as can be found in Figure 6.5. The III stage, corresponding to the cellulose breakdown, caused a DTG$_{max}$ of 1.51 %/min between 332~409°C. Stage (IV) lost 8.23% mass, breaking down lignin between 409 and 1200°C. Liu, L. et al. (2021) supported this finding using different biomass (corn straw powder, poplar wood chip and rice husk). After the combustion, the TG/DTG profiles tended to be flat, and the remaining residue content was around 7.6% (Table 6.5).

6.3.1.2. Analysis of TG/DTG profiles for T$_5$ pellet

- *At a heating rate of 20 °C/min*

For the T$_5$ pellets, the DTG profile was classified into four stages (Figure 6.6). In stage (I), the initial combustion occurred between 25 and 194°C. In this moisture loss zone, the highest DTG was 2.49 %/min, with a 72°C peak temperature and a 6.1% mass loss. The peak of this region represents hemicellulose degradation (Table 6.6). Most decomposition occurs in stage II between the temperatures of 194~297°C, with around 60.11% overall weight loss and a peak temperature of roughly 277°C. The maximum reaction rate of this stage was 54.75 %/min, signifying the decomposition of primary cellulose and partially hemicellulose and lignin at a 20 °C/min heating rate. Therefore, the sample quickly burned in this oxidative region, and this finding agrees with Xie et al. (2020).

Table 6.6: Combustion characteristics of T$_5$ pellet

Heating rate, °C/min	Item	Stage I	Stage II	Stage III	Stage IV	Residue, %
	T$_{range}$, °C	25~194	194~297	297~384	384~1200	
20	T$_{peak}$, °C	72	277	307	407	11.9
	M$_{loss}$, %	6.1	60.11	11.72	10.17	
	DTG$_{max}$, %/min	2.49	54.75	6.69	2.9	
10	T$_{peak}$, °C	57	277	347	457	9.49
	M$_{loss}$, %	6.7	56.59	15.53	11.69	
	DTG$_{max}$, %/min	1.37	32.05	4.38	1.2	
5	T$_{peak}$, °C	62	277	362	442	11.39
	M$_{loss}$, %	6.64	55.08	17.02	9.87	
	DTG$_{max}$, %/min	0.96	38.63	1.82	0.29	
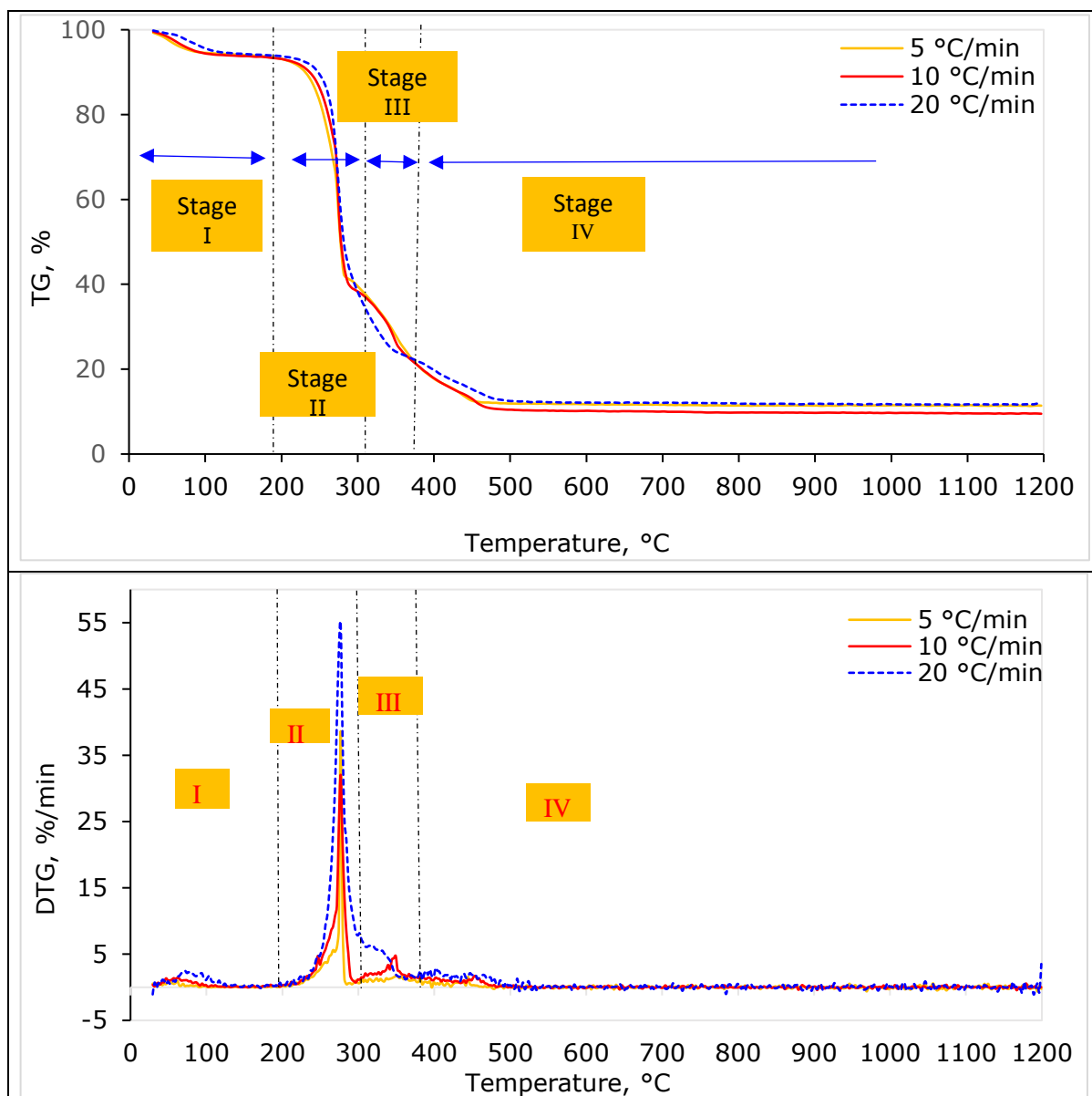
Figure 6.6: Combustion profile of T_5 pellets: (a) TG curve and (b) DTG curve

On the other hand, stage III denotes the sample devolatilisation with a temperature change from 297 to 384°C (Figure 6.6). The maximum reaction rate (6.69 %/min) occurred with a peak temperature of 307°C, while the weight loss was 11.72%. Gao et al. (2016) mentioned that primary combustion occurs in stages II and III. The char formation and removal of secondary gases region signify the char combustion stage (IV), while temperature varied from 384 to 1200°C. In their study, Hameed et al. (2020) and Qureshi et al. (2017) mentioned that lignin decomposed at maximum temperatures of 500~900°C. In this stage IV, the highest decomposition rate was 2.9 %/min, with peak temperatures of 407°C and mass loss of 10.17% (Table 6.6). Also, in the last stage, the combustion of hemicelluloses and cellulose was almost completely burned, while lignin was the main component. Therefore, in the final stage, the sample weight

continued to drop, but with a smaller amplitude than the second and third phases, and the DTG curves tended to be flat which was consistent with Liu, L. et al. (2021). The DTG profiles tended to be flat, consistent with the sample weight continuing to drop but with a smaller amplitude than in the second and third stages. After that, the remaining sample portion was around 11.9% at 1200°C for a 20 °C/min heating rate.

- *At heating rates of 10 °C/min*

The TG/DTG profile for the T_5 pellet at 10 °C/min is shown in Figure 6.6. The maximum reaction rate was 56.59 %/min, while the temperature was 347°C in stage II. Following combustion, the residual mass was 11.39% (Table 6.6). Sait et al. (2012) experimented with an investigation of date palm biomass for combustion and pyrolysis kinetics and found the same TG profile, even with different biomass.

- *At heating rates of 5 °C/min*

Figure 6.6 displays the TG/DTG profile for T_5 pellets regardless of heating rates. As observed from Figure 6.6, the maximum mass loss in stage II was 55.08% for the 5 °C/min heating rate, while the peak temperature was 277°C. After combustion, the remaining residue contents were 11.39% for 5 °C/min (Table 6.6). These values were similar to those of other agricultural waste, such as WS and groundnut stalk (Gajera et al. 2022).

6.3.2. Effect of heating rate on combustion profile

The combustion profile of the WSPs (T_1 and T_5) at 5, 10 and 20 °C/min is shown in Tables 6.6 and 6.7. As observed from the result, there was no effect on temperature variation in the different stages of TG/DTG profiles due to the changing heating rate of 5 to 20 °C/min. However, the rise in heating rate shifted the peak temperature, resulting in mass loss and maximum reaction rate change regardless of all treatment and heating rates. Asadieraghi and Daud (2014) reported that the rising heating speed accelerated the decomposition rate, which agrees with the current study.

In the case of the T_1 pellet, the peak temperatures were 357, 347 and 367°C for the heating rates of 20, 10 and 5 °C/min, respectively, for stage III. Alternatively, for stage (II), the DTG_{max} was 9.02, 22.99 and 49.45 %/min at 5, 10 and 20 °C/min heating rates (Table 6.5). For the T_5 pellets, the average mass loss was 6.1, 6.7 and 6.64% at 5, 10 and 20 °C/min in Zone (I). After the combustion, the remaining residuals were 11.39, 9.49 and 11.9 % for heating charges 5, 10 and 20 °C/min, correspondingly, for the T_5 pellets (Table 6.6). The overall result was consistent with another research (Singh et al. 2020; Açıkalın 2021), which used different biomass. In general, heating rate increases had a relative effect on the combustion profile, suggesting that increasing the conversion's heating rate was not significantly beneficial.

6.3.3. Temperature effect on thermal degradation in the combustion process

The TG curve (Figures 6.7 and 6.8) reveals that the mass loss of WSP was temperature dependent, resulting in mass loss occurring due to temperature. The mass loss was 6.1% and 60.11, 11.72 and 10.27% within the temperature range 25~194°C, 194~297, 397~384 and 384~527°C, respectively, for the T_5 treatment at 20 °C/min heating rate. After 527°C, the TG curve becomes nearly flat, with 11.9% of the remaining mass for the same heating rate. The mass loss of the T_5 pellet followed the same trend for 10 and 5 °C/min heating rates (Figure 6.7). On the other hand, for T_1, the weight loss was 7% and 86.29%, in the variation of temperatures 25~172°C and 172~542°C, respectively, at 20 °C/min heating rate in an air environment. However, average weight loss was negligible after 542°C, indicating that very little volatile material was present, while the remaining mass was 6.71% (Figure 6.8). These findings align with the work of Singh et al. (2020).
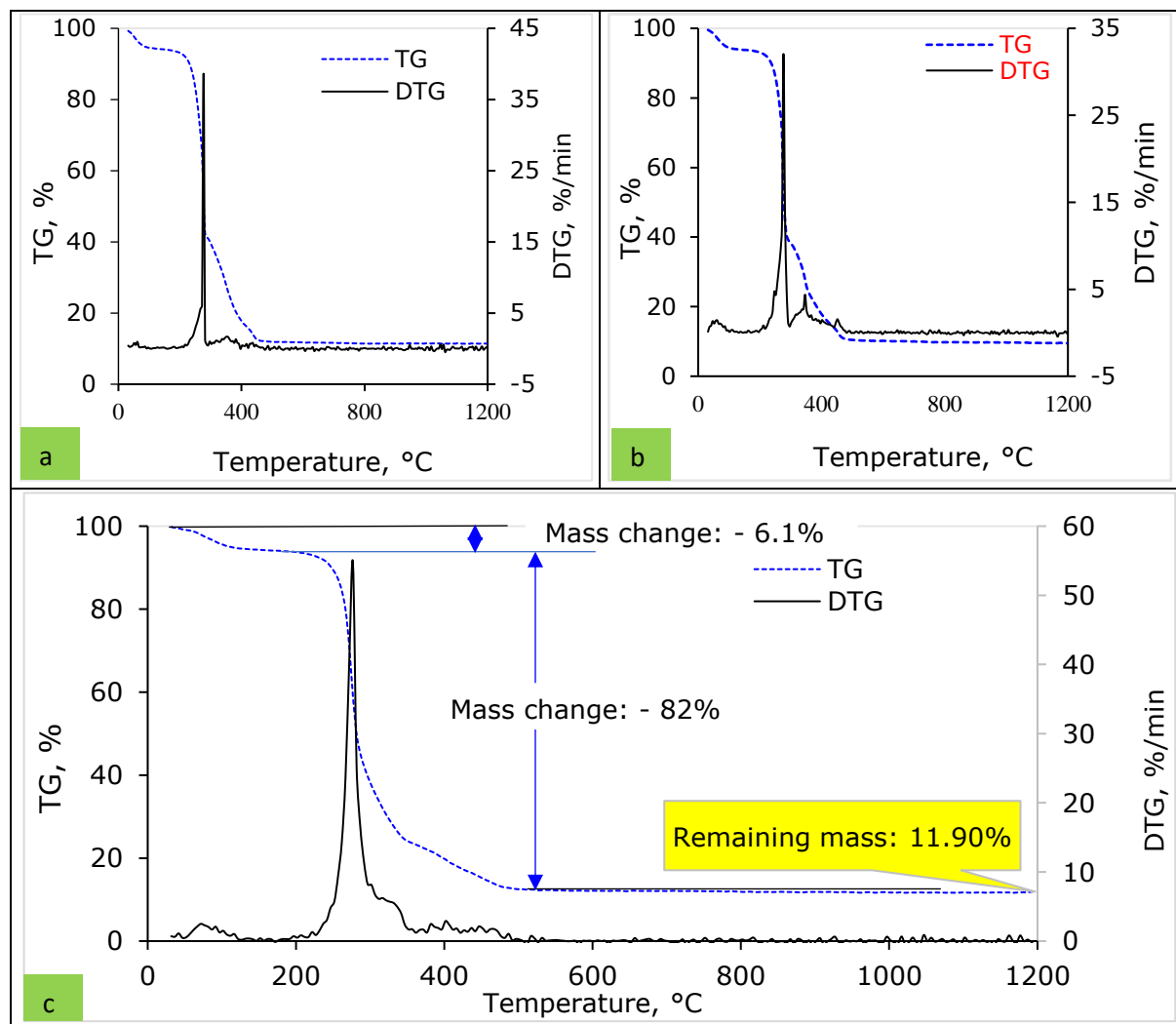
Figure 6.7: TG and DTG curve for T_5 pellet combustion at a constant heating rate: (a) 5 °C/min, (b) 10 °C/min and (c) 20 °C/min

The DTG profile fluctuation represents the component variation of the sample (Punsuwan & Tangsathitkulchai 2014). Considering that the DTG profile had identical peaks and several side peaks for all types of pellets with each heating rate, that could be due to elemental variations (Gupta & Mondal 2019). The highest peak represents the rapid maximum reaction rate which occurred between the temperatures of about 200~325°C. These values are comparable with other studies which used agricultural residues such as castor residue, maize cob, linseed stalks and rice straw (Chen, W.-H. et al. 2019). The decomposition rate was slow at the first stage of combustion, while the conversion rate accelerated when the temperature increased, and after 542°C, the reaction rate gradually ended (Figures 6.7 and 6.8). Overall, all heating rates typically followed the rule that temperature enhances certain decomposition reaction rates with a similar trend.
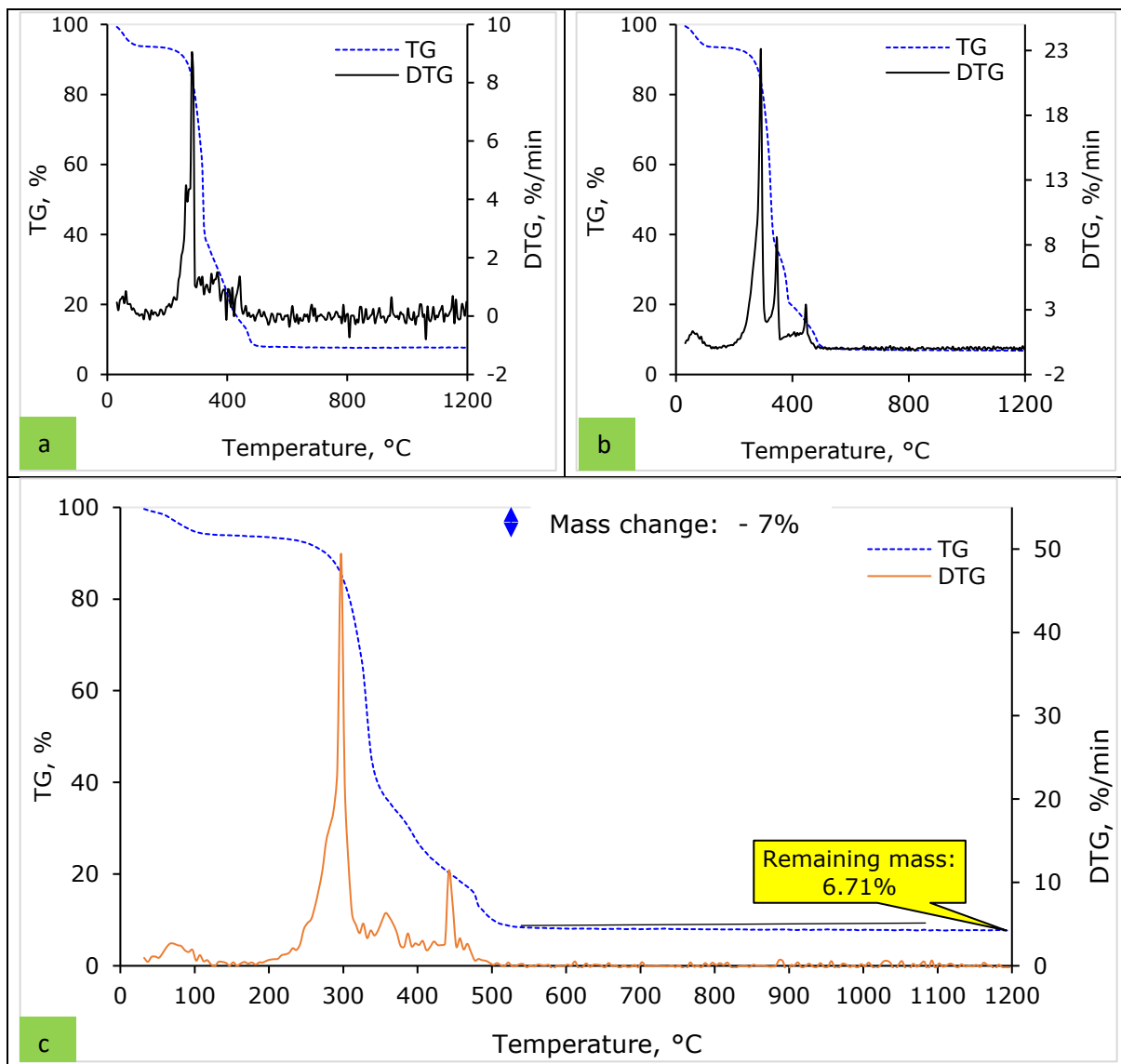
Figure 6.8: TG and DTG curve for T_1 pellet combustion at a constant heating rate: (a) 5 °C/min, (b) 10 °C/min and (c) 20 °C/min

6.3.4. *Effect of additive on thermal combustion of WSPs*

Figure 6.9 illustrates the TG profile of T_1 and T_5 pellets during combustion. Both pellets followed a general trend regardless of heating rates. From the initial temperature to about 207°C, the TG for T_1 and T_5 nearly overlapped regardless of heating rates (Figure 6.9). Between the temperatures 207 to 455°C, the mass loss of the T_5 pellet was high (approximately 8%), but there was no significant difference for all heating rates. Alternatively, after 455°C, the mass loss of T_5 was higher, about 5%. Interestingly, the three heating rates followed the same trend, and the additive blending had no apparent significant effect on thermal properties. Overall, the mass loss for both pellets was very similar, meaning the additive blending did not considerably affect combustion performance. The same finding was observed in the study of Ríos-Badrán et al. (2020). They used rice husk, WS and their blend pellets.
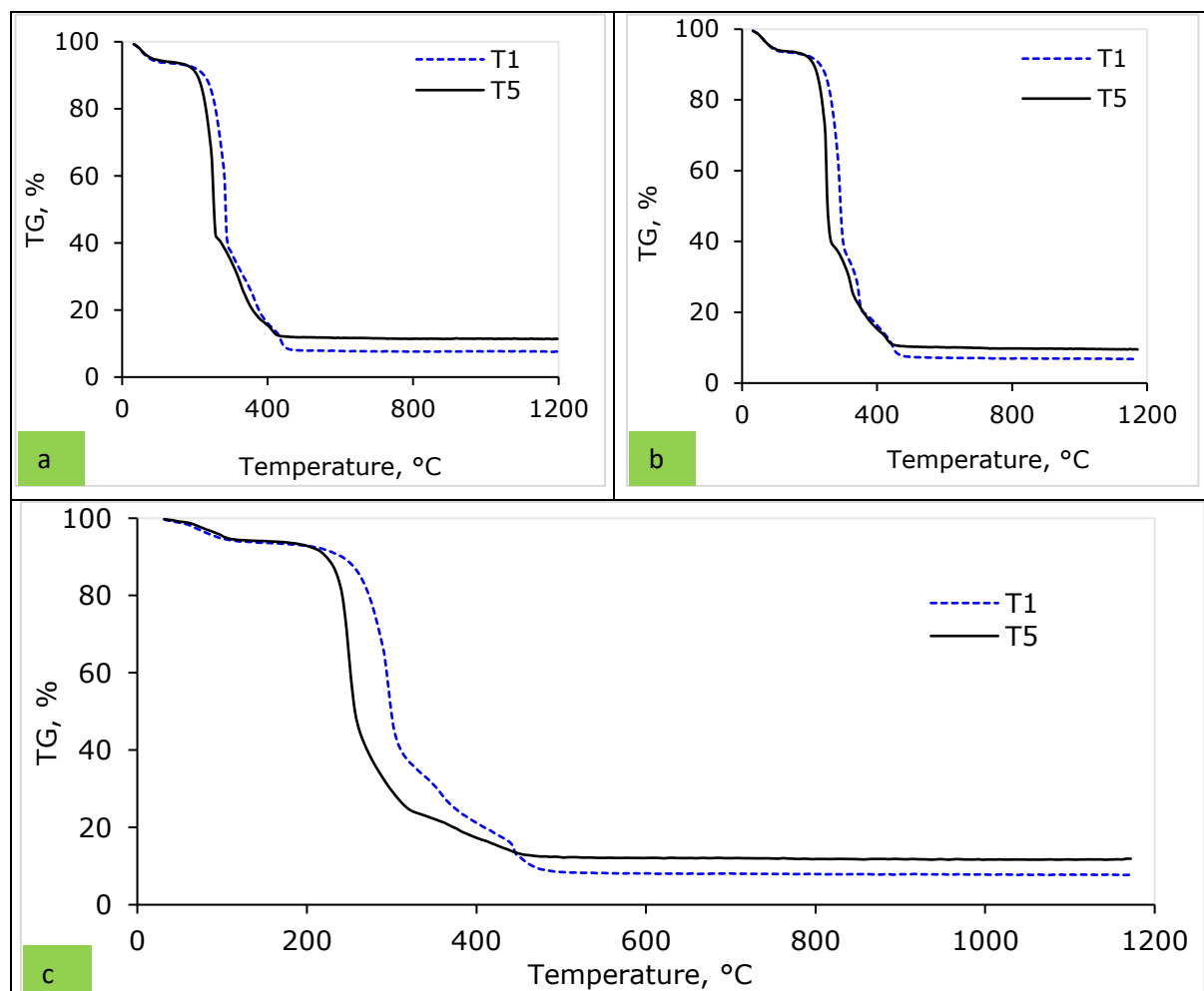
Figure 6.9: T_1 and T_5 pellets comparison based on TG curves at a constant heating rate: (a) 5 °C/min, (b) 10° C/min and (c) 20 °C/min

In the case of the DTG curve, the additive blended effect on thermal combustion is shown in Figure 6.10. From the observation, the DTG profile almost coincided regardless of the heating rates, possibly because the ash

content was similar. Link, Yrjas and Hupa (2018) discovered that ash content substantially impacts the conversion rate. In addition, both pellets followed the same trend, such as the reaction rate being higher in the T_5 pellet than the T_1 pellet in the case of all hating rates. The high conversion rates for T_5 were likely due to the heat transfer from the additive (BioC) blended material and chemical interactions.
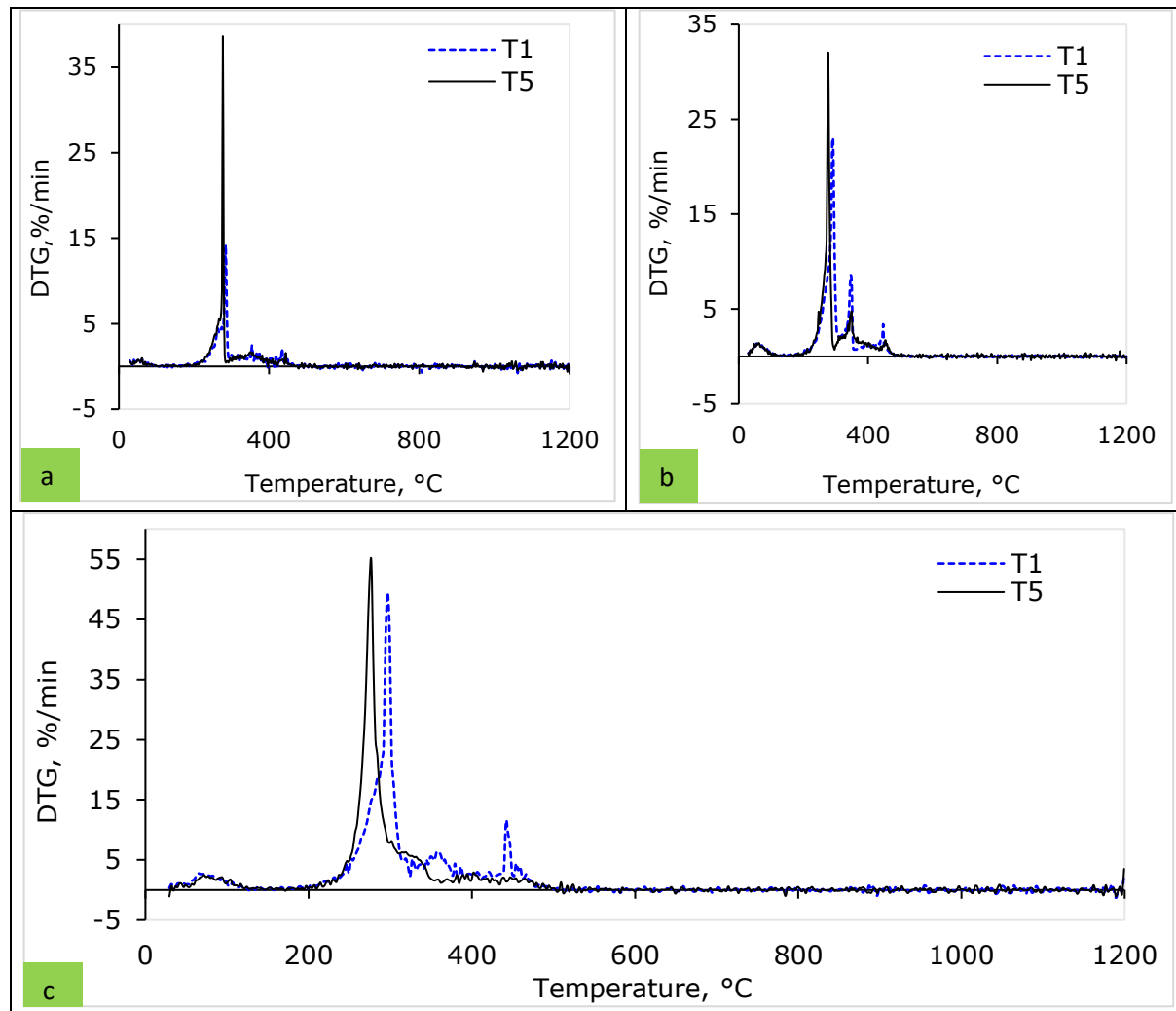
Figure 6.10: T_1 and T_5 pellets comparison based on DTG curves during combustion at a constant heating rate: (a) 5 °C/min, (b) 10 °C/min and (c) 20 °C/min.

Alternatively, the DTG_{max} temperature was comparatively lower for additive blended pellets (T_5) than without additive blended pellets (T_1) at 5 to 20 °C/min heating charges. For instance, at 10 °C/min heating speed, the peak reaction rate was 32.05 %/min at 277°C for the T_5 pellet, while in the case of the T_1 pellet, the DTG_{max} was 22.99 %/min at 292°C (Figure 6.10b). Interestingly, the T_5 pellets' DTG_{max} temperature was the same (277°C) regardless of heating rates, but the peak temperatures varied for T_1 pellets. Further, the T_1 pellet showed different distinct DTG peaks than the T_5 pellet. Therefore, additives mixed into the WS boosted the

128

conversion rate and indicated a synergistic occurrence. The present study's findings were supported by Dhyani, Kumar and Bhaskar (2017), because additives improved the WSPs' physical and compositional characteristics. They suggest that blending materials (coal, biomass and others) improves the fuel composition and boosts thermal properties.

6.3.5. Analysis of thermodynamic parameters

Entropy, Enthalpy, and Gibbs free energy are the thermodynamic properties that help decide a reactor's heating and cooling requirements/arrangement (Coker 2001). Table 6.7 lists the thermodynamic parameters, which were determined using empirical equations. To determine the entropy, enthalpy and Gibbs free energy, the $E\alpha$ and A were taken from the *NETZSCH* program at 20 °C/min heating rates. According to the results (Table 6.7), the average activation energy and enthalpy difference were approximately 5 KJ/mole. This trait was consistent with Kaur et al. (2018). Both pellets in Peak 1 (first zone) gave the lowest value for all thermodynamic parameters. This result agreed with Naqvi et al.'s (2020) and Gajera et al. (2022) research output. The reaction is endothermic and releases energy, as seen by the reaction's negative enthalpy value. In the T_1 pellets, the highest ΔH and ΔG were 268.747 kJ/mole and 308.100 kJ/mole, respectively, for Peak 2.

Table 6.7: Thermodynamic parameter for combustion of WSP at 20 °C/min heating rate

Pellets	Items	Peak 1	Peak 2	Peak 3	Peak 4
T_1	Tm, °K	345.15	570.15	630.15	715.15
	E_α, kJ/mole	45.00	273.488	189.782	164.723
	lnA, 1/s	4.769	22.804	14.245	10.089
	A, 1/s	117.801	8.01E+9	1.53E+6	2.40E+4
	ΔH, kJ/mole	42.130	268.747	184.542	158.776
	ΔG, kJ/mole	116.268	308.100	273.405	285.090
	ΔS, kJ/mole.K	-0.214	-0.069	-0.141	-0.176
T_5	Tm, °K	345.15	550.15	580.15	680.15
	E_α, kJ/mole	45.03	418.94	632.07	115.47
	lnA, 1/s	4.76	37.41	54.67	7.01
	A, 1/s	1.172E+2	1.75E+16	5.509E+23	1.103E+3
	ΔH, kJ/mole	42.16	414.36	627.24	109.81
	ΔG, kJ/mole	116.32	385.38	513.68	247.10
	ΔS, kJ/mole.K	-0.21	0.05	0.20	-0.20

In addition, all negative values for entropy (ΔS) suggest that T_1 pellet combustion experienced minor physical and chemical changes and trends towards thermodynamic equilibrium (Sriram & Swaminathan 2018). Alternatively, for T_5 pellets, the entropy of Peak 1 and Peak 4 was negative; however, the second and third zone values were positive. This finding indicates that the reaction did not reach equilibrium due to the activated complex formation's association reaction mechanism (Naqvi et al. 2018; Açıkalın 2021).

6.3.6. *Measurement of ignition and burnout temperatures*

The biomass ignition temperature is significantly associated with its safety in transportation and storage when used in industry (Jiang et al. 1995). In contrast, a fuel's burnout temperature serves as an indicator of reaction degree. Du, Chen and Lucas (2014) noted the less volatile (inflammable) fuel components have a higher burnout temperature.

The intersection method determines the WSP's ignition and burnout temperatures (Figures 6.11 and 6.12). The WSPs' (T_5) ignition and burnout temperatures were 277°C and 442°C, corresponding to a heat-changing speed of 10 °C/min (Figure 6.11). In a study conducted by Wang et al. (2009), the TG was employed to investigate the ignition temperature of both WS and aspen wood sawdust, revealing an ignition temperature of 279°C. Remarkably, this finding closely aligns with the results obtained in the present study. Another study found that the current research validated the ignition temperature of 256°C for wheat and rice straw (Zhaosheng, Xiaoqian & Ao 2009).
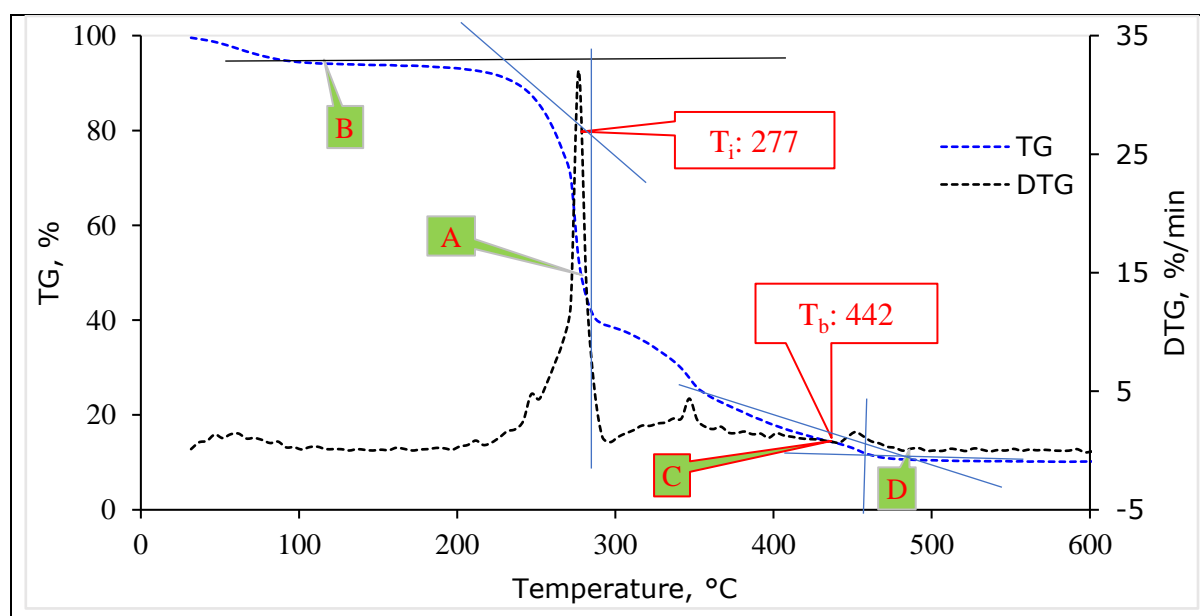
Figure 6.11: TG and DTG curves for T_5 pellets at a constant heating rate of 10 °C/min

Figure 6.12 displays the thermal degradation of the WSP without an additive blend (T_1) and its derivative curve. The ignition and burnout temperatures were 292 and 442°C for the T_1 pellets, and the heating rate was 10 °C/min (Figure 6.12). Recently, Lu and Chen (2015) experiment investigated ignition and burnout temperatures for bamboo and sugarcane in TG. They found burnout temperatures of 492 and 494°C for bamboo and bagasse, respectively. The present investigation's results agree with Lu and Chen (2015). The ignition point of the T_1 pellets was higher for all heating rates than the T_5 pellets, while burnout temperatures were higher for T_5, except at 10 °C/min.
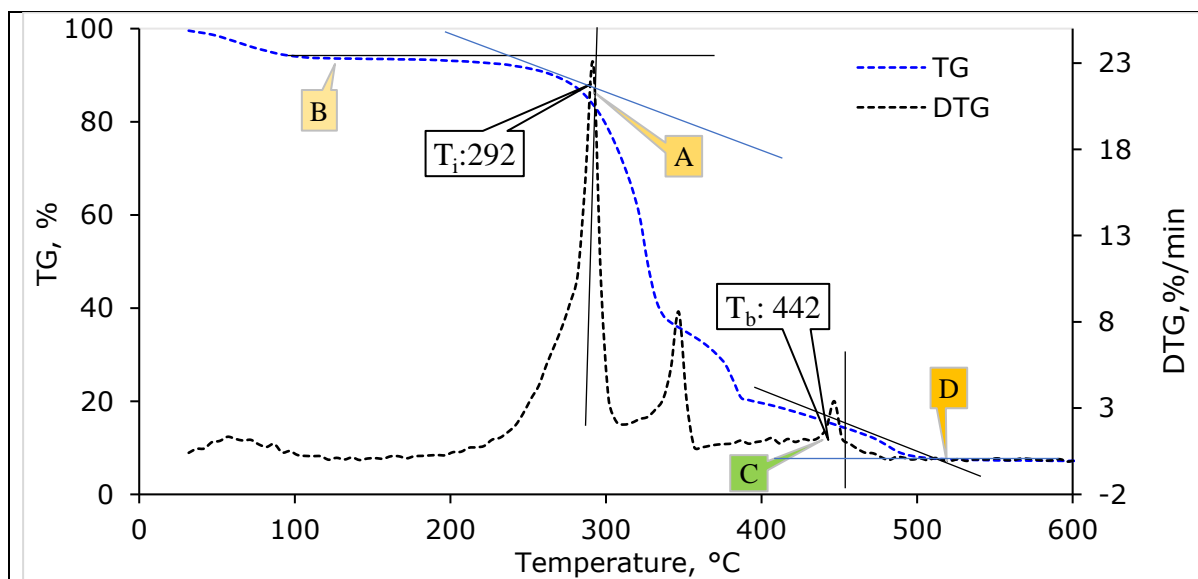
Figure 6.12: TG and DTG curves for T_1 pellets at a constant heating rate of 10 °C/min

Table 6.8 clearly shows the three heating rates' ignition and burnout temperatures for all types of pellets. Among the heating rates, the 10 °C/min heating speed had the highest ignition temperatures for both pellets. The T_1 pellet shows the highest heating rate. To the definition of ignition temperatures, higher heating rates meant the barriers to reaction start (Cao et al. 2019). In this research, the additives mixing with WS could be the ignition barrier, resulting in higher ignition temperatures. Alternatively, the burnout temperature was lowest for the 10 °C/min heating rate. The relationship between ignition and burnout temperatures was inverse (Table 6.8).

Table 6.8: Ignition and burnout combustion temperature of WSPs

Treatment	Heating rates, ºC/min	T_i, ºC	T_b, ºC
T_1	5	251	462
	10	292	442
	20	267	467
T_5	5	233	456
	10	277	442
	20	207	492

Note; T_i = Ignition temperature, T_b = Burnout temperature

6.3.7. Evaluation of WSP profile through kinetic model

Thermal decomposition data are frequently analysed using various kinetic models, including the model free and model based methods (Shi, Gong & Zhai 2022). TG and DTG profiles are typically used to synthesise the thermokinetic properties. Therefore, the primary criteria of the model were used to assess the present WSP combustion results (Figure 6.13.)

Model free techniques data	**Present experimental data**
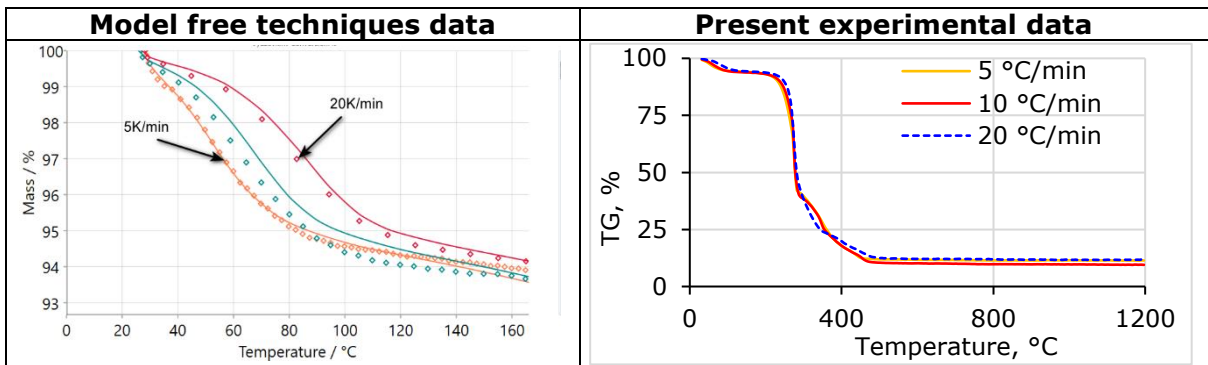
Note: In model free techniques, different heating rates belong to various mass losses, however, the present study showed that the mass was nearly similar regardless of heating rates. As a result, the experimental result was not suitable for model free solutions.
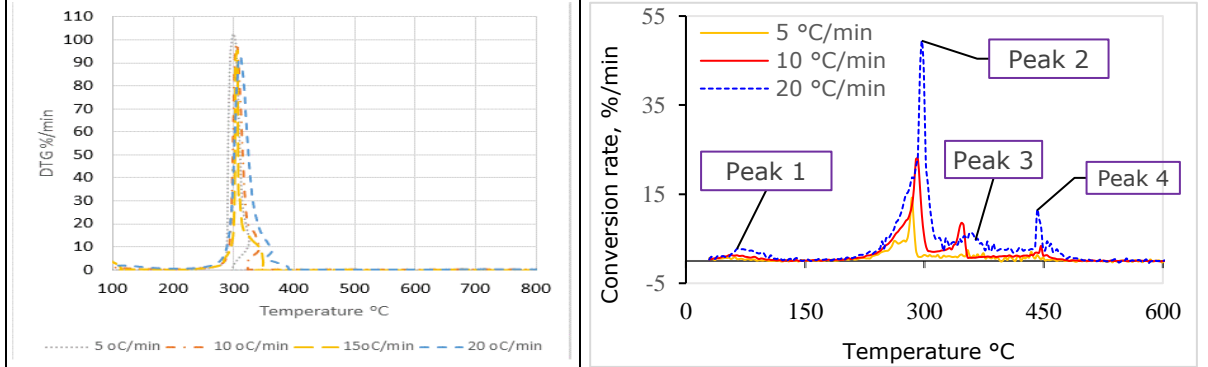
Note: The standard model only counts one peak, but the experimental output had a multistep reaction and different peaks. Hence, the model free analysis method did not fit with WSP kinetic character.
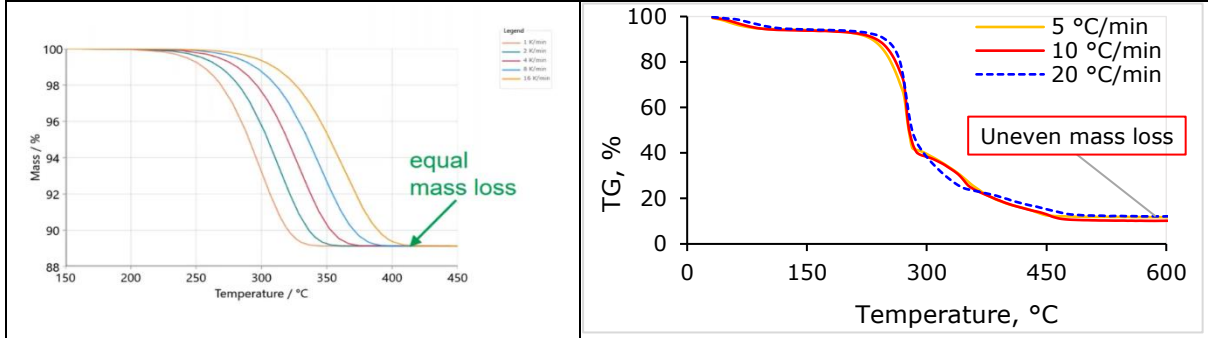
Note: In model free approaches, the total mass loss or peak area must be the same for all curves, but the present research result showed that mass loss was not the same, therefore, the model free approaches were unsuitable.
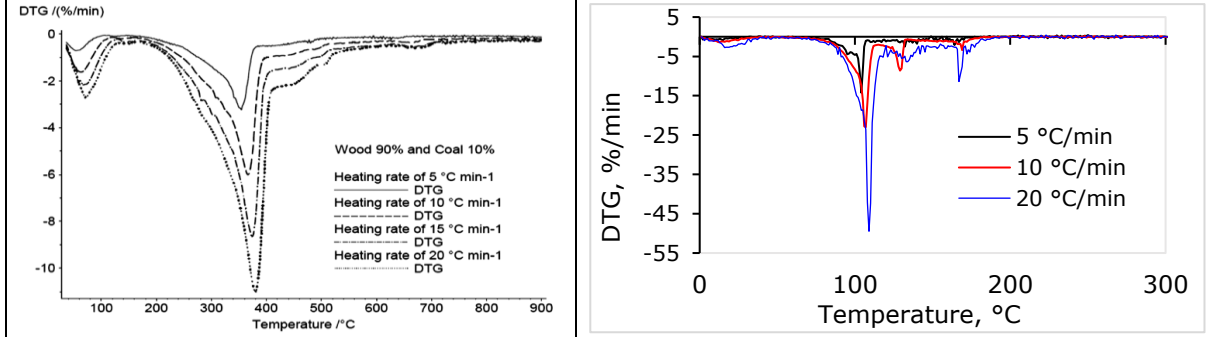
Note: Model free methods need the same peak direction. However, the current study results displayed different signs. As a result, the model free approaches did not apply to WSP.

Figure 6.13: Evaluation of wheat straw pellet combustion characteristics

The model-free approach is best for a single reaction (Moukhina 2012); however, the model-based approach is applicable for both single and multiphase reactions (Vyazovkin et al. 2020). From the review literature, the lignocellulosic biomass transformation process (kinetic mechanism changes) follows complex reactions (Soh et al. 2019). In addition, the conversion of lignocellulosic biomass like WS has filled the multipoint direction (Anca-Couce 2016), where model-free analysis provides ambiguous and misleading results. However, some researchers consider single-step reactions for studying the lignocellulosic biomass (El-Sayed & Mostafa 2020; Singh et al. 2020; Mandapati & Ghodke 2021).

The kinetic results' interpretation for multipoint reactions using various methods varied greatly (Kumar & Nandi 2021). From the observation, the assumptions of the model-free technique did not fit the WSPs' thermal degradation profiles (TG/DTG curves). Instead, the model-free methods produced contradictory kinetic results/misleading values of $E\alpha$ and A due to the continuous changes during reactions. Therefore, this research considered only model-based approaches.

6.3.8. Combustion process analysis by model-based method

The WSPs (T_1 and T_5) are shown to follow the multistep reaction by the DTG curves from Figures 6.14 and 6.15. Therefore, this study considers Kinetics *NETZSCH Proteus 8.0* Software's multistep analytical engines, which allows model free and model based kinetic analyses on thermal measurements (Opfermann, Kaisersberger & Flammersheim 2002).

Within this analysis and simulation, the Kinetics *NETZSCH* software performed a complete estimate of E_a and A and determined the compatible reaction mechanism (Manić, Janković & Dodevski 2021). After the simulation, deep explanations were used to obtain combustion parameters (Table 6.9). The following differential equations could solve a single-phase reaction to a series of subsequent multi-phase combustion reactions, where the balance equation is as follows:

$$\text{Mass = Initial mass} - \text{TotalMassChange} \times \{\text{Contribution } (a \to b)$$
$$\times \int [\frac{d(a \to b)}{dt}]dt + \text{contribution } (c \to d) \times \int [\frac{d(c \to d)}{dt}]dt + \text{contribution } (d \to e) \times$$
$$\int [\frac{d(d \to e)}{dt}]dt\} + \text{contribution } (e \to f) \times \int [\frac{d(e \to f)}{dt}]dt \dots\dots\dots\dots\dots\dots\dots 6.23$$

Table 6.9: Reaction steps and equations during combustion of wheat straw pellets

Model scheme	Reaction steps	Concentration equations
A-B C-D-E-F	A → B (Step 1)	$\frac{da}{dt} = -\frac{d(a \to b)}{dt} = -A_1 \cdot f_1(a.b) \cdot \exp(-\frac{E_{a1}}{RT})$ ....6.24 $\frac{db}{dt} = \frac{d(a \to b)}{dt} = A_1 \cdot f_1(a.b) \cdot \exp(-\frac{E_{a1}}{RT})$ 6.25
	C → D (Step 2)	$\frac{dc}{dt} = -\frac{d(c \to d)}{dt} = -A_2 \cdot f_2(c.d) \cdot \exp(-\frac{E_{a2}}{RT})$ ....6.26 $\frac{dd}{dt} = \frac{d(c \to d)}{dt} - \frac{d(d \to e)}{dt}$ $= A_2 \cdot f_2(c.d) \cdot \exp(-\frac{E_{a2}}{RT}) - A_3 \cdot f_3(d.e) \cdot \exp(-\frac{E_{a3}}{RT})$ 6.27
	D → E (Step 3)	$\frac{de}{dt} = \frac{d(d \to e)}{dt} - \frac{d(e \to f)}{dt}$ $= A_3 \cdot f_3(d.e) \cdot \exp(-\frac{E_{a3}}{RT}) - A_4 \cdot f_4(e.f) \cdot \exp(-\frac{E_{a4}}{RT})$ 6.28
	E → F (Step 4)	$\frac{df}{dt} = \frac{d(e \to f)}{dt} = A_4 \cdot f_4(e.f) \cdot \exp(-\frac{E_{a4}}{RT})$ 6.29

Note; $f_1(a,b) = n_1 a[-ln(a)]^{\frac{(n_1-1)}{n_1}}$; $f_2(c.d) = n_2 c[-ln(c)]^{\frac{(n_2-1)}{n_2}}$;

$f_3(d.e) = n_3 d[-ln(d)]^{\frac{(n_3-1)}{n_3}}$ $f_4(e.f) = n_4 d[-ln(d)]^{\frac{(n_4-1)}{n_4}}$

6.3.8.1. Analysis of reaction model

The TG/DTG curves of the WSP samples for the combustion experiment were divided into four main predominant stages (Table 6.4). Both pellets (T_1 and T_5) showed two distinct reactions: $A \to B$ and $C \to D \to E \to F$ (Table 6.9). The first reaction Step of $A \to B$, where A was the reactant (sample as presented) and B was the product (dehydrated sample). The second reaction Step was as $C \to D \to E \to F$, where C was the starting material, F was the final product, also D and E were the intermediate product (Tables 6.10 and 6.11).

The 1st stage ($A \to B$) was the pore gases releasing phase after the removal of internal moisture from WSP pores, and the second stage ($C \to D \to E \to F$) was the sorption of oxygen within the WSP matrix by increasing mass gain. So, kinetic modeling, was simplified by assuming four different reaction steps, i.e., $A \to B$ corresponds to the dehydration and desorption stage, $C \to D$ represents the oxidation stage, $D \to E$ denotes the combustion stage and $E \to F$ associates the burnout stage. This phase category entirely agreed with the results of Manić, Janković and Dodevski (2021).

Table 6.10: Thermal reactions and kinetic parameter for WSP (T_1)

Reaction step	Reaction type	Equation	E_a, kJ/mole	lnA, 1/s	A, 1/s	Reaction order	Contribution /Slope
1 ($A \rightarrow B$)	F2: Second order	$\dfrac{d(a \rightarrow b)}{dt} = A * a^2 * e^{-\frac{E_\alpha}{RT}}$	45.0	4.769	1.18E+2	-	0.080
2 ($C \rightarrow D$)	D3:3-D diffusion	$\dfrac{d(c \rightarrow d)}{dt} = A * 1.5 * \left[\dfrac{c^{\left(\frac{2}{3}\right)}}{1 - c^{\left(\frac{1}{3}\right)}}\right] * e^{-\frac{E_\alpha}{RT}}$	273.488	22.804	8.01E+9	-	0.573
3 ($D \rightarrow E$)	Cn: n^{th} order	$\dfrac{d(d \rightarrow e)}{dt} = A * d^n * (1 + A_{autocat} * e) * e^{-\frac{E_\alpha}{RT}}$	189.782	14.245	1.54E+9	3.507	0.243
4 ($E \rightarrow F$)	Fn: n^{th} order	$\dfrac{d(e \rightarrow f)}{dt} = A * e^n * e^{-\frac{E_\alpha}{RT}}$	164.723	10.089	2.41E+4	1.194	0.104

Note; $A_{autocat}$:0.010

Table 6.11: Thermal reactions and kinetic parameter for WSP (T_5)

Reaction step	Reaction type	Equation	E_a, kJ/mole	lnA, 1/s	A, 1/s	Reaction order	Contribution /Slope
1 ($A \rightarrow B$)	F2: Second order	$\dfrac{d(a \rightarrow b)}{dt} = Aa^2 e^{-\frac{E_\alpha}{RT}}$	45.034	4.764	1.17E+2	-	0.078
2 ($C \rightarrow D$)	D3:3-D diffusion	$\dfrac{d(c \rightarrow d)}{dt} = A * 1.5 * \left[\dfrac{c^{\left(\frac{2}{3}\right)}}{1 - c^{\left(\frac{2}{3}\right)}}\right] * e^{-\frac{E_\alpha}{RT}}$	418.935	37.405	1.76E+16	-	0.584
3 ($D \rightarrow E$)	Cn: n^{th} order	$\dfrac{d(d \rightarrow e)}{dt} = A * d^n * (1 + A_{autocat} * e) * e^{-\frac{E_\alpha}{RT}}$	632.065	54.666	5.5E+23	9.288	0.197
4 ($E \rightarrow F$)	Fn: n^{th} order	$\dfrac{d(e \rightarrow f)}{dt} = A * e^n * e^{-\frac{E_\alpha}{RT}}$	115.470	7.006	1.1E+3	2.059	0.141

Note; $A_{autocat}$:0.010

Overall, the WSP combustion process followed the four step consecutive reaction process as $A \rightarrow B \rightarrow C \rightarrow D \rightarrow E \rightarrow F$, where *A, B, C, D, E* and *F* represent the decomposition states. The reaction rate for decomposition for each step was given by $\frac{da}{dt}$. In the presented equations, total conversion, $\alpha = 1 = a + b + c + d + e + f$, while the *a, b, c, d, e* and

f represent *A, B, C, D, E* and *F* concentrations in the chemical model kinetics. Moreover, the consecutive mechanism follows: $a = (1- \alpha_1)$, $b = (1- \alpha_2)$, $c = (1- \alpha_3)$, $d = (1- \alpha_4)$, and $A_1, A_2, A_3, A_4, E_{a1}, E_{a2}, E_{a3}$ and E_{a4} signifies *lnA* and E_a quantities linked to the first, second, third and fourth reactions steps. Moreover, n_1, n_2, n_3 and n_4 are reaction orders associated with the autocatalyst's first, second, third and fourth reaction steps.
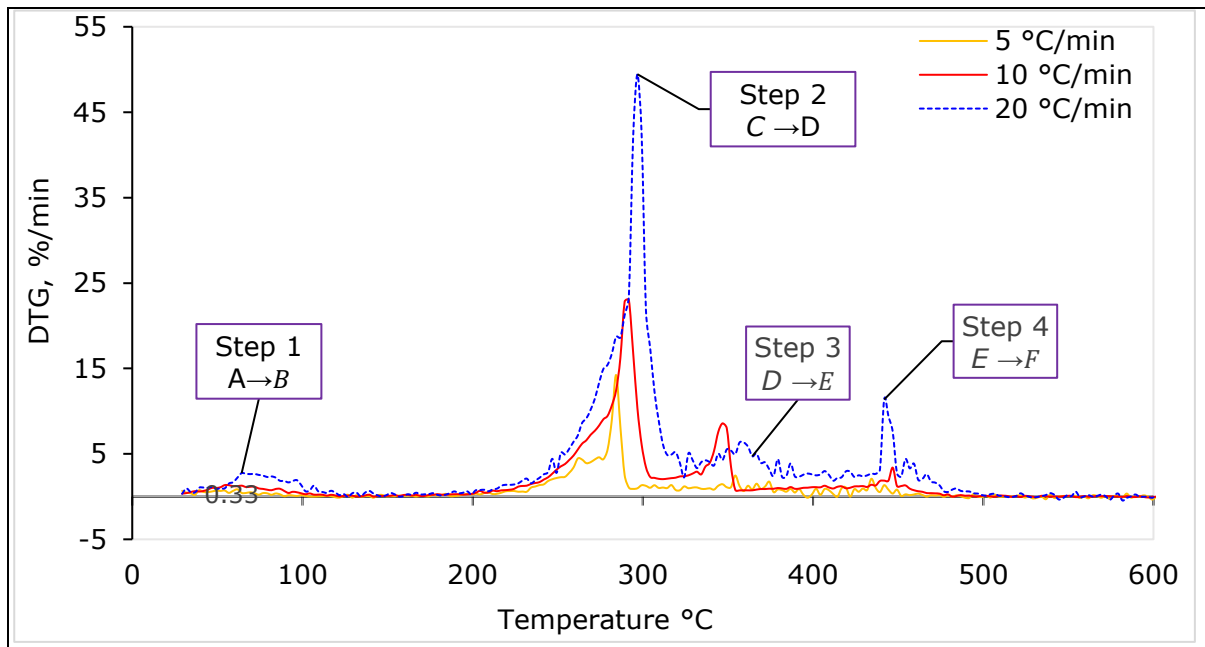
Figure 6.14: TG curve for WSP (T₁)

Note; Four identifiable peaks in the DTG curve suggest four different reaction steps
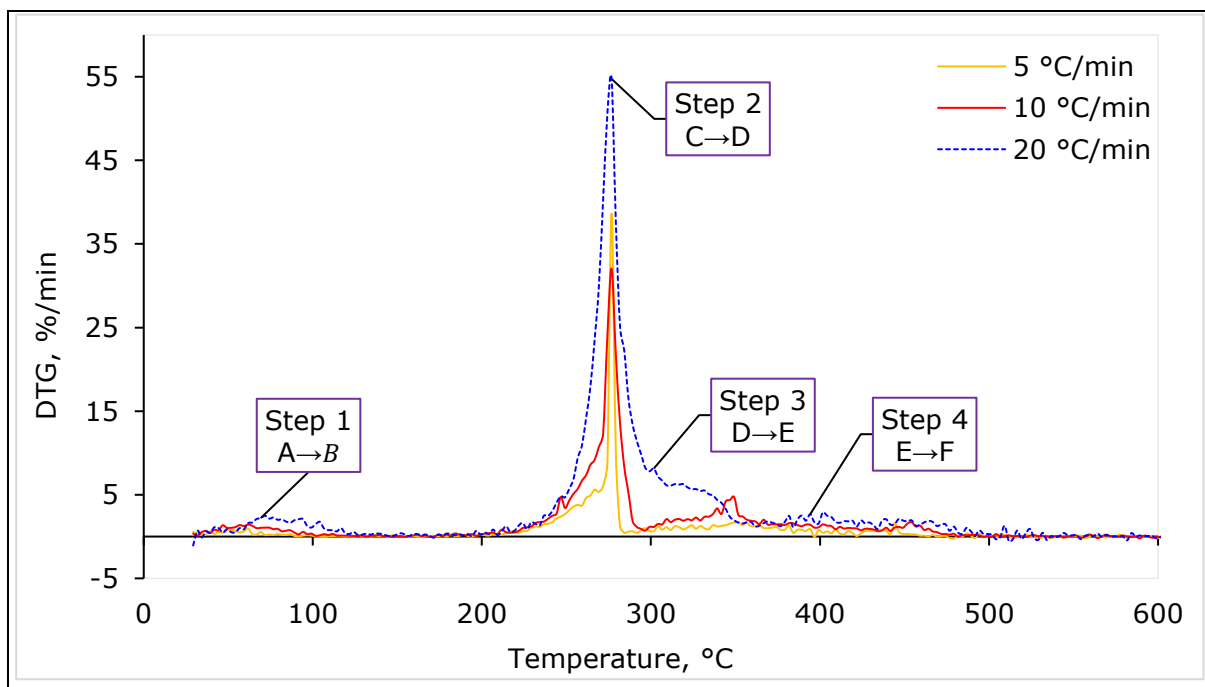
Figure 6.15: DTG curves for WSP (T₅)

Note; Four identifiable peaks in the DTG curve suggest four different reaction steps

6.3.8.2. Analysis of kinetic triple

The kinetic triple are important for optimising industrial reactors and predicting reactions (Chen, Jianbiao et al. 2017; Varma et al. 2021). To find kinetic triplicates, apply the model based approaches assuming the nth order of reaction ($f(\alpha) = e^n$). The four different consecutive reaction steps ($A{\rightarrow}B, C{\rightarrow}D, D{\rightarrow}E, E{\rightarrow}F$) were as shown in Tables 6.10 and 6.11 (Janković et al. 2019; NETZSCH 2021). This thermal process combines or overlaps several mechanisms, including nucleation, diffusion and interface. However, the reaction depends on the sample origin, processing and experimental conditions (Vyazovkin et al. 2020). The E_a and *lnA* derived through *NETZSCH* Proteus 8.0 software for each type of reaction step regarding T_1 and T_5 pellets are shown in Tables 6.10 and 6.11.

In reaction step 1, hemicellulose content boosted the sequential mechanism, where $E\alpha$ was 45.0 kJ/mole (lowest) for the T_1 pellet. The highest $E\alpha$ (273.488 kJ/mole) was observed in step 2, where the cellulose content enhanced the successive mechanism (Table 6.10). Typically, the lower $E\alpha$ value denoted less energy required to start the reaction, while the higher value meant the reaction began gradually (Huang et al. 2019). Alternatively, the $E\alpha$ varied from 45.0 to 273.488 kJ/mole for the T_1 pellets. The $E\alpha$ and *lnA* values fluctuated with the reaction stages, ensuring that a complex combustion reaction occurred during the entire combustion range that successfully decomposed the hemicellulose and cellulose. Lin et al. (2009) reported that the $E\alpha$ varied from 48 to 282 kJ/mole for the reaction mechanism for the primary two step. The present study's results were slightly lower than the experimental reports of Lin et al. (2009), which might be due to the different feedstock, temperature difference and heating rates.

The cellulose mostly decomposed in step 2; however, the cellulose and lignin contribution in the third region (Step 3) was less (Cozzani et al. 1997). The $E\alpha$ and *A* values in step 3 were 272.488 (kJ/mole) and 22.804 (1/s), which noted the second highest value for the T_1 pellet. In Step 4, the activation energy and pre-exponential factors were 164.723 (kJ/min) and 10.089 (1/s), resulting in lignin decomposition with the likelihood of several dissipations of volatile reaction pathways. After step 4, residual ash and tars were found to be the remaining materials.

Table 6.11 shows the $E\alpha$ and *lnA* for each reaction step during the combustion of T_5 pellets obtained from the *NETZSCH* Proteus 8.0 software. The lowest E_a and *lnA* were seen at 45.0 (kJ/mole) and 4.769 (1/see), respectively, in step 1 for the T_5 pellets. These results agreed well with the Fang et al. (2021) research even though the feedstock was different. The highest $E\alpha$ was 632.065 (kJ/mole) in Step 3, while the maximum *lnA* was 54.666 (1/s) during the combustion of the T_5 pellet, which might be due to cellulose and volatile matter decomposition. Overall, the observed results

revealed that the E_a and *lnA* were correlated, which means if *lnA* was higher, *Eα* was also higher (Tables 6.10 and 6.11). In brief, the quantity diversity of kinetic parameters depends on biomass pseudo components' decompositions.

The pre-exponential factor (A) fluctuation occurred due to biomass combustion reaction chemistry, such as a surface reaction or simpler complex. When *lnA*>109 (1/s) occurred in a simpler complex reaction, but *lnA*<109 (1/s), the reaction did not depend on the surface (Maia & de Morais 2016). According to the results for the T_1 pellets, steps 1 and 4 were independent of the surface, while steps 2 and 3 represent simpler complex reactions (Table 6.10). Alternatively, steps 1 and 4 signify no dependent reaction on the surface, while steps 2 and 3 illustrate the activated complex reaction for the T_5 pellet (Table 6.11). Alternatively, the activated complex's limited reactions were termed when *lnA* was between 1010 and 1012 (1/s) (Xu & Chen 2013).

6.3.8.3. Reaction dimensionality

For the assessment of reaction dimensionality (n) based on model-based kinetic expressions, the reaction mechanism was considered according to a 20 °C/min heating rate while the temperature ranged from 25~1200°C. The consecutive reaction mechanism can observe for all steps assessing the dimensionality (n) that the values were higher than the unity (n>1) for steps 3 and 4 (Tables 6.10 and 6.11). Alternatively, steps 1 and 2 were the noninteger dimensionality (less than a unit or equal to zero) that can result from the size and shapes of reaction particles (Barud et al. 2011). Changes in *Eα* values through numerous elemental phases were linked to dimensional variations throughout the steps.

Overall, the results (Tables 6.10 and 6.11) showed that both pellets' reaction types were similar. However, the reaction order value differed. Therefore, the reaction types were not significantly influenced by the additives blend pellets (T_5).

6.3.8.4. Kinetic reactions

The kinetic mechanism evaluated for various reaction models is listed in Table 6.1. The general reaction procedure can be reproduced through a kinetic model act of F2, D3, Cn and Fn models for the observed results (Tables 6.10 and 6.11).

The F2 model best described the primary combustion steps (Peak 1) of both types of pellets. This reflected the decomposition of cellulose (Zhang, D. et al. 2019). In this stage, the reaction type was phase interfacial second order. This result agrees with Huang et al. (2019). In addition, for step 2, the observed diffusion controlled process may be involved and modelled as D3 (3D diffusion), while the function is $f(\alpha)=1.5e^{\frac{2}{3}}$

138

$/(1-e^{\frac{1}{3}})$, which was noted in the combustion complex reaction. These results agree with Várhegyi, Chen and Godoy (2009). As a solid carbonaceous biomass, WSPs decomposed when heated, causing gaseous byproducts to float to the particles' surface.

For step 3, the Cn kinetic model is the best presentation technique for the combustion process by the autocatalyst model. This reaction process significantly reduced the growth rate because of fragmentation and volatile emission (Moukhina 2013). These types of reactions accelerated the reaction mechanism. The final step (Peak 4) was the carbonisation region, where the leftover residue was biochar or carbon enriched ash. This step was titled phase interfacial nth order reaction. The differential function was $f(\alpha) = e^n$ *(Table 6.1).* Overall, the reaction order models were well suited to describe the combustion reaction mechanism of lignocellulosic biomass (WSP). Therefore, it can be concluded that several steps occurred due to the decomposition of biomass components and complex reaction effects.

6.3.8.5. Relationship between degree of conversion and kinetic parameters

Various biomass compositions might suggest a complex combustion reaction that results in $E\alpha$ differences. The relationship between activation energy and conversion degree is demonstrated in Figure 6.16. The $E\alpha$ fluctuated in both pellet types regarding the reaction degree α. This fluctuation profile exhibits various endothermic and exothermic picks, resulting in energy absorption and release during different reactions (Kumar & Nandi 2021). Moreover, the $E\alpha$ increases (+value) signify the endothermicity with conversion, while the activation energy decreased (-value) indicates exothermic reactions of the combustion process (Muravyev, Pivkina & Koga 2019). This trend was observed in the study of Baruah et al. (2018), which suggests that a complicated series of processes occurred during the combustion of WSP, and a significantly small amount of cellulose and hemicellulose remained.

The maximum activation energy for T_1 pellets found was 312.23 kJ/mole, attributed to the energy absorbed during the degradation of hemicellulose and cellulose (Figure 6.16a). At the same time, the minimum $E\alpha$ was (-) 34.307 kJ/mole representing energy release in lignin breakdown. Alternatively, the peak $E\alpha$ value was 1573.768 kJ/mole with the conversion degree 0.41 for the T_5 pellets (Figure 6.16b). The maximum negative value of $E\alpha$ was (-) 738.795 kJ/mole at the degree of conversion point at 0.69. Overall, both pellets followed the same fluctuations, but the linear trendline differed (Figure 6.16). In addition, the correlation coefficient (R^2) showed that there was no significant relationship. Sharma, Pandey and Diwan (2019) noted that $E\alpha$ and lnA were correlated, which did not support the present study's results and could be due to a variation in the analysis method.
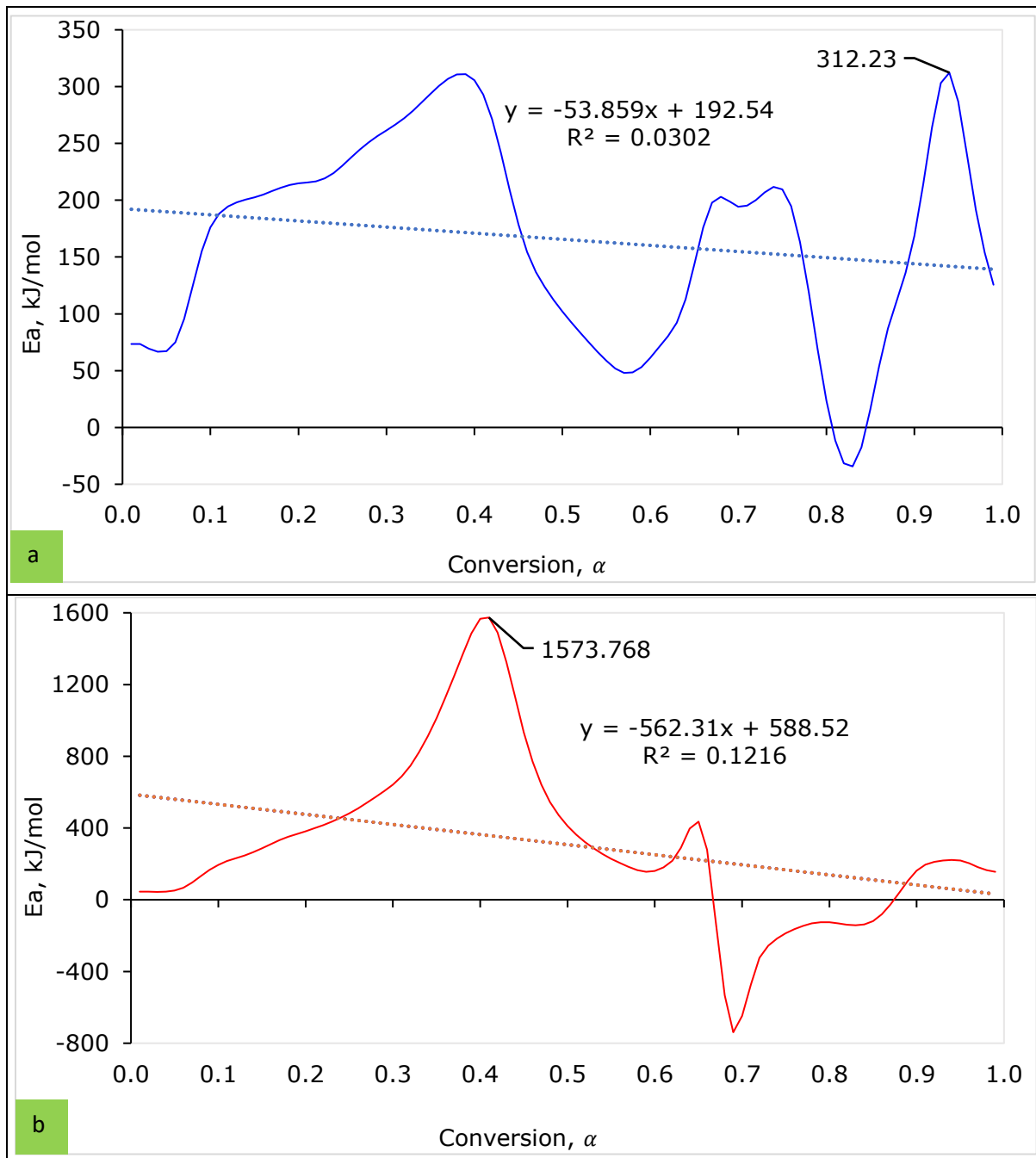
Figure 6.16: Dependence of conversion degree and activation energy for (a) T_1 and (b) T_5 pellet

Figure 6.17 depicts the relationship between the pre-exponential factor (*lnA*) versus the conversion degree (α). As the conversion degree rose between 0.1 to 1.0, the $E\alpha$ fluctuated in both pellets. The highest *lnA* were 2.842 and 148.18 (1/s) for T_1 and T_5, respectively. Conversely, (-) 5.26 and (-) 68.096 (1/s) were the minimum pre-exponential factors for the T_1 and T_5 pellets. The observation indicates that exothermic (-value) and endothermic (+value) reactions occurred during conversion (Koga et al. 2022).
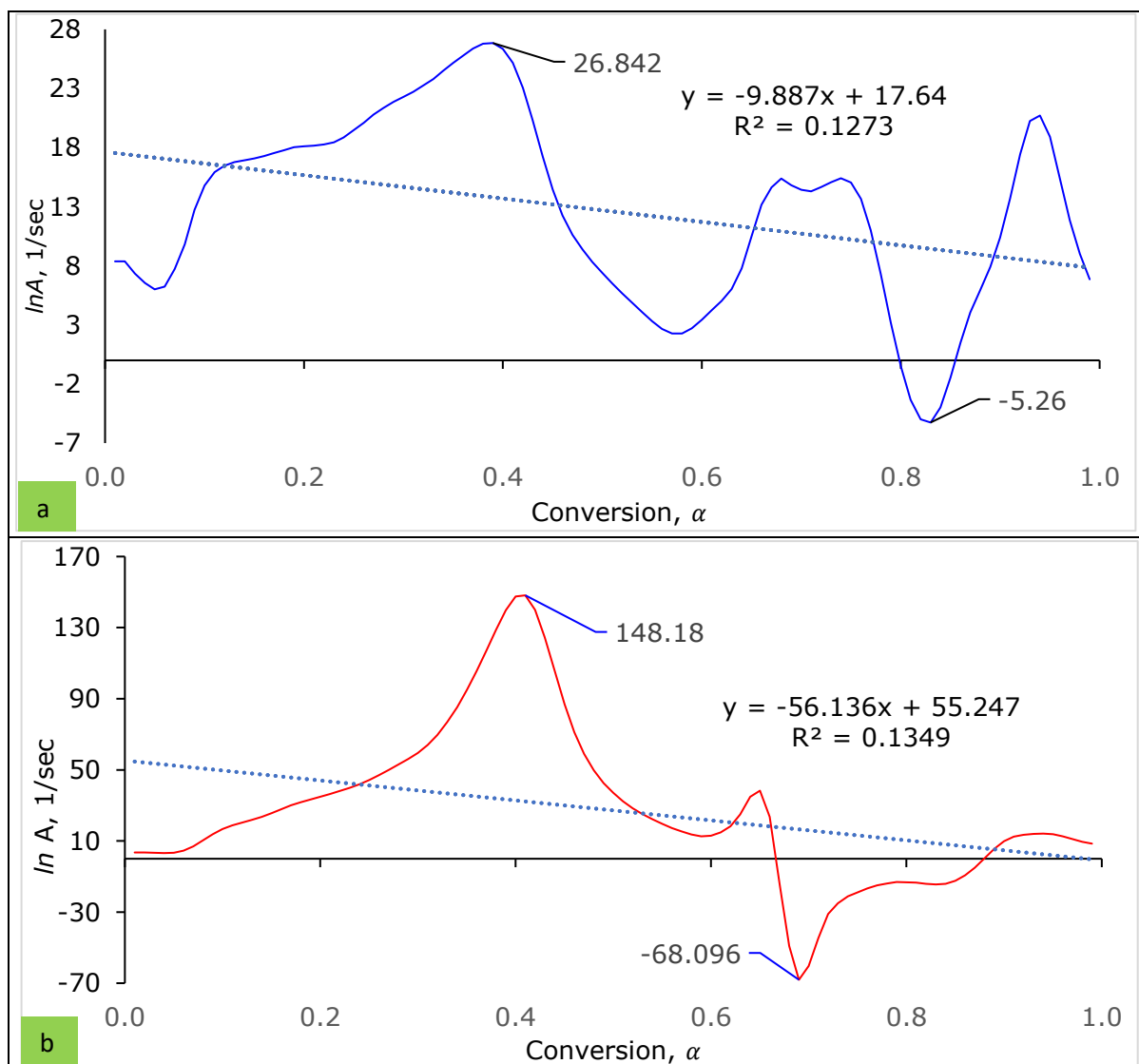
Figure 6.17: Conversion degree vs pro-exponential factor plot for (a) T_1 and (b) T_5 pellet

The profiles and linear trendline of the two pellets (T_1 and T_5) followed the fluctuation, but the trend was not similar. From Figure 6.17, the coefficient of determination (R^2) value was relatively lower ($\sim$0.15). Consequently, there was no significant correlation between the conversion degree and lnA. The lnA dependent on the degree of conversion followed the same trend, which supported the study of Muravyev, Pivkina and Koga (2019). However, the lnA value adversely varied might be due to the different analysis methods.

6.4. Conclusion

This study presents the combustion characteristics of two types of WSPs (T_1 and T_5). The results showed four stages to the thermal degradation of the WSPs. The outcome of the TG analysis suggested that the WSPs' thermal behaviour was similar regardless of heating changes.

The peak mass loss rate (reaction rate) shifted to a higher temperature in the DTG curve without altering the shape of the curves during the heating rate increase. The observed results from DTG showed that the peak reaction rate was 49.45 %/min (297°C), 22.99 %/min (292°C) and 9.02 %/min (282°C) for the T_1 pellet with heating speeds 20, 10 and 5 °C/min. The T_1 pellet's entropy followed the equilibrium reactions, but the T_5 pellet observed the nonequilibrium reaction. Hence, based on the thermodynamic parameter, the additive blended pellets had no significant impact on the reaction process. In addition, evaluation of the thermal behaviour by TG and DTG showed pellet decomposition followed the exothermic and endothermic processes.

The TG/DTG profile has confirmed that the thermal characteristics were unsuitable for model free approaches. The kinetic elements of the WSP combustion process were identified using TGA and model-based techniques. The activation energy for stages I, II, II and IV were 45.0, 273.488, 189.782 and 164.723 kJ/mole, respectively, for the T_1 pellet, and 45.034, 418.935, 632.065 and 115.470 kJ/mole for T_5 pellet. According to model-based techniques, the variation of $E\alpha$ pointed to complex combustion reactions. The $F2$, $D3$, Fn and Cn appeared to be the best fitted models for a four step successive disintegration mechanism for both types of pellets. The $E\alpha$ value thus indicates the auto catalyst as the dominant process for T_5, while diffusion control (Jarden model) was the dominant process for T_1. Furthermore, the pre-exponential factor and reaction dimensionality was positively correlated with activation energy.

CHAPTER 7: PYROLYSIS OF WHEAT STRAW PELLET: THERMOKINETIC BEHAVIOUR

Abstract

To investigate WSPs pyrolysis behaviour, this study used the STA 449F3 Jupiter thermogravimetric analyser (TGA) with NETZSCH Proteus 8.0 software. The pyrolytic kinetic parameters and the reaction mechanism under a nitrogen environment were determined. The temperature ranged from 31 to 800°C. The heating rates were at 5, 10 and 20 °C/min. This study also considered two types of WS pellets (T_1: 100% WS and T_5: 70% WS, 10% SD, 10% BC and 10% BioC). According to the TG/DTG analysis, the WSP thermokinetic decomposition followed three stages: drying, devolatilisation and carbonisation.

The obtained result showed that temperature significantly impacted the mass loss and reaction rates. However, the influences on heating rates were not significant. The model-free and model-based methods' characteristics were used to evaluate TG-DTG profiles. It was found that the model-free approaches were unsuitable for WSP thermodynamic and kinetic properties discussion. Instead, a model-based reaction such as Fn (nth order phase interfacial reaction model) and $F2$ (second-order model) was the most appropriate kinetic technique for explaining thermal degradation and the three-phase consecutive reaction mechanism ($A{\rightarrow}B$, $C{\rightarrow}D$ and $D{\rightarrow}E$). The average $E\alpha$ for phases 2 and 3 (Fn reaction model) were 136.038 and 358.110 KJ/mole for the T_1 pellet. The pre-exponential factor (lnA) varied from 3.647 to 21.802 (1/s) for T_5 pellets at the 20 °C/min heating rate. Based on the thermodynamic properties (ΔH, ΔG and ΔS), equilibrium reactions for both T_1 and T_5 pellets pyrolysis were observed.

7.1. Introduction

Biomass is a biofuel and the fourth most significant energy source after coal, oil and natural gas (Liu, L. et al. 2021). The wide availability of biomass, its clean and low level emissions characteristics and the recent progress of conversion technologies make biomass a growing potential biofuel choice (El-Sayed & Mostafa 2020). The abundant biomass can meet various energy needs, including power generation, heating and liquid fuel production. Pyrolysis, combustion and gasification are the three common biomass thermal conversion pathways to bioenergy (Peacocke & Bridgwater 2001; Basu 2010). Pešenjanski, Miljković and Vićević (2016) stated that pyrolysis is a more complex process than other thermal transformation systems. This is because pyrolysis involves complex reactions influenced by heating rates, biomass properties, operating circumstances and reactor layouts (Sadhukhan et al. 2008; Zhang, Xu & Champagne 2010).

Many researchers have investigated biomass pyrolysis (Idris et al. 2010; Wei et al. 2017; Hoang et al. 2021). Most of this research was carried out on small scale lab equipment and focused on feasibility studies, kinetic behaviour and reactivity values as a function of time and temperature. It was reported that the detailed pyrolysis experimental study is sometimes complicated, challenging and involves a cost (Munir et al. 2009; Ding et al. 2017). As an alternative, the TGA is frequently used for pyrolysis and combustion (Mandapati & Ghodke 2021; Varma et al. 2021; Fonseca et al. 2022). It effectively determines how solid fuels react to heat during pyrolysis and combustion (Lu et al. 2013). Therefore, this study investigated WS pellet pyrolysis with a thermogravimetric analyser (TGA).

The thermokinetic parameters are important for understanding biomass fuel thermal performance and reaction. The kinetic triple, such as activation energy ($E\alpha$), pre-exponential factor (*A*) and the conversion model (*f(α)*), can be defined using the TG/DTG profile (mass change, time and temperature) (López-García et al. 2013). In contrast, the derivative thermogravimetric (DTG) curve illustrates the weight loss as a role of temperature (Vhathvarothai, N., Ness, J. & Yu, Q. J. 2014).

A TGA is a device that determines the TG/DTG profiles of solid fuels (Vhathvarothai, N., Ness, J. & Yu, Q. J. 2014). TGA is a popular tool that provides high precision, rapid data collection rate and excellent repeatability within a well defined kinetic control zone (Várhegyi, Chen & Godoy 2009; Yusuf et al. 2020). Thus, several studies have applied the TGA approach to explore thermal decomposition patterns and kinetics during the pyrolysis of diverse samples, including biomass, coals and their blends (Cheng, Winter & Stipanovic 2012; Burhenne et al. 2013; Anca-Couce et al. 2020). Also, different types of TGA with analysing software have been available for specific utilisation, including SDT650, DMA Q800, HITACHI-STA7200, STA449F3 Jupiter, etc. (Mandapati & Ghodke 2021; Teh et al. 2021). This research used the STA449F3 Jupiter with *NETZSCH Proteus 8.0* software.

The TG studies used thermal analysis models and simulations, including isothermal and nonisothermal approaches with single and multiple heating rates. Nonisothermal multiple heating rates are referred to by the Coats–Redfern integral methods (Kumar et al. 2021; Raza et al. 2022). Moreover, the Friedman, Flynn–Wall–Ozawa (FWO) and Kissinger–Akahira–Sunose (KAS) technique is a model free approach that reaches mathematical models dealing with isothermal and nonisothermal conversion (Mureddu et al. 2018; Hu et al. 2019). Kissinger's modified kinetic equation determines the thermal breakdown kinetics of samples and their mixes. Several other reaction models were also used to investigate kinetic pamperers (Table 6.1, Chapter 6) (Manić, Janković & Dodevski 2021).

Biomass, particularly agricultural straw, is a lower quality (density, heating value) fuel than coal (Grammelis 2010; Wang, Xun et al. 2016). Therefore, coal is often used as a supplementary fuel blended with biomass for energy generation (co-pyrolysis) to increase biomass fuel quality (Al-Mansour & Zuwala 2010; Surono & Saptoadi 2022). Therefore, it was suggested to use available biomass instead of coal as a blending material (Bridgeman, T. et al. 2008; Wang et al. 2019). Consequently, the biomass based co-blending process reduced CO_2 emissions (De & Assadi 2009; Vhathvarothai, N., Ness, J. & Yu, Q. J. 2014). Various scientists have recommended adding additives that changed poor quality WS to a higher value solid fuel (Dragutinovic et al. 2019; Mack et al. 2019). This research used a WS pellet that blended different biomass-based additives.

A number of studies have been conducted on TG pyrolysis of different biomass feedstock (Table 7.1). However, most studies have only partially investigated biomass thermal behaviour and the kinetic reaction process (Liu, L. et al. 2021; Shagali et al. 2023). Xiao et al. (2020) investigated lignocellulosic biomass (rice straw, pine SD, phoenix tree leaves) pyrolysis and explored kinetic characteristics through the Coats-Redfern, DAEM and Doyle methods. They found similar activation energy and pre-exponential factors for all models. However, according to another study (Mulligan, Strezov & Strezov 2010), WS and mallee residue was used to examine the pyrolysis yield. They found that pyrolysis efficiency was 96% at 500°C but did not consider mass losses. Also, the use of the distributed activation energy model (DAEM) for TG/DTG analysis of different types of straw (wheat, oat, barley and *Brassica Carinata*) was investigated by Várhegyi, Chen and Godoy (2009). They found that the sharp DTG peak oriented to cellulose decomposition and much wider $E\alpha$ distribution were related to hemicellulose, lignin and extractive decomposition. Vuthaluru (2004) used TG to study the thermal behaviour of biomass fuels (wood waste and WS) and coal during co-pyrolysis and found no interactions between biomass and coal. Overall, previous studies provide mixed or ambiguous results on thermal behaviour during co-pyrolysis.

Sher et al. (2020) studied the thermal and kinetic analysis of barley straw, waste wood, WS, willow, miscanthus and wood pellet. They found higher activation energy with lower reactivity. Mass losses during the thermal degradation of WS samples were investigated by Pešenjanski, Miljković and Vićević (2016). They identified that heating rates have a significant effect, but moisture content does not impact mass loss. Greenhalf et al. (2013) conducted experimental studies on the thermal behaviour and kinetics of WS, switchgrass, miscanthus, willow and beech wood. They used TGA and a laboratory scale continuous fed bubbling fluidised reactor and observed that WS contains the highest bio-oil with water content than perennial grass. Recently, Fonseca et al. (2022) examined the challenges of the kinetic parameter determination of high ash content WS pyrolysis. They used the model fitting approach and

isoconversional model to identify degradation kinetics and found that degradation depends on potassium content. Overall, a literature review reveals that thermokinetic pyrilysis studies of additive blends of WS pellets and individual WS pellets are rare.

Table 7.1: TG analysis for biomass

Materials	Technology	Findings	Reference
Rice husk	Pyrolysis (TGA)	Thermal stability and thermal degradation process	(Chiang et al. 2009)
Napier grass	Combustion and Pyrolysis (TGA)	Thermal characteristics	(Mohammed et al. 2015)
Corn brakes, wheat straw, and hazelnut shell	Pyrolysis (TGA-MS)	Gas product increase with heating rate	(Manić et al. 2019)
Sugarcane straw	Slow pyrolysis (TGA-FTIR)	Decomposition increases with the heating rate	(Halder et al. 2019)
Corn stover	Combustion and Pyrolysis (TGA)	TGA characteristics depend on heating rates and temperatures	(Kumar et al. 2008)
Rice straw and pine sawdust	Combustion and Pyrolysis (TGA)	Pyrolysis kinetics characteristics depend on analysis models	(Xiao et al. 2020)
Wheat straw and plastic	Combustion and Pyrolysis (TGA)	Synergistic effect on blending materials	(Jin et al. 2019)
Mustard straw	Pyrolysis (TGA)	Biochar, bio-oil, and hydrocarbon gases are influenced by temperature	(Jacob et al. 2022)
Corn straw powder, poplar wood chip, and rice husk	Combustion and Pyrolysis (TGA)	Pyrolysis and combustion characteristics boost heating rates	(Liu, L. et al. 2021)
Sewage sludge and wheat straw	Pyrolysis (TGA)	Mixing ratio has an impact on pyrolysis yield	(Wang, Xuebin et al. 2016)
Empty fruit bunch, rice husk, coconut pulp, sawdust, coconut shell, and sugar cane bagasse	Pyrolysis (TGA)	Hating value and thermal degradation rate rose with operating conditions such as temperature, time, and reactors	(Balasundram et al. 2018)
Biomass wastes and digests biomass wastes	Co-pyrolysis (TGA)	The blending process enhances the gas yield	(Vuppaladadiyam et al. 2021)
Wheat straw	Pyrolysis (TGA-FTIR)	Pyrolysis or DTG changes with temperature	(Yang, X. et al. 2018)
Wheat straw, rape straw, reed canary grass and switch grass	Pyrolysis (TGA)	Perennial grass has more attractive properties for the first pyrolysis	(Greenhalf et al. 2012)

Therefore, WSP and additives' impact on kinetics still needs to be studied. In addition, in depth studies on biomass blends with additives need to be investigated, particularly in agricultural straws (wheat, rice, etc.). Furthermore, the kinetics of the biomass based co-pyrolysis process is unknown. Therefore, WS pellet TG analysis is essential to address pyrolysis

properties for reactor design and biomass-to-energy transformation. These kinetic parameters were later used as input data in Computational Fluid Dynamics (CFD) modeling for designing and analysing the pellets' energy conversion reactor (gasifier).

7.2. Materials and methods

This study used two WSPs (T_1: 100% WS and T_5: 70% WS, 10% SD, 10% BC and 10% BioC) under a nitrogen environment. This study investigated WS pellet pyrolysis behaviour using the STA 449F3 Jupiter TGA with *NETZSCH* Proteus 8.0 software.

The pyrolysis temperatures ranged from 31 to 800°C at 5, 10 and 20 °C/min heating rates. It is noted that the procedures of WS pellet pyrolysis in TGA were similar to the TGA combustion, which was detailed described in Chapter 6. Also, this study applied model based and model free techniques to determine, analyse and present the kinetic parameter.

7.3. Results and discussion

7.3.1. Thermal behaviour of WS pellet pyrolysis

The chemical and elemental composition of WSP needs to be considered to understand the thermal degradation behaviour (Rahib et al. 2019). Available literature suggests that the proportion of biomass cellulose, hemicellulose, lignin and extractives is very important for conversion processes (Shah, Khan & Kumar 2018). Generally, the biomass's cellulose, hemicellulose and lignin concentrations range from 42~49%, 16~23% and 21~39%, respectively (Sannigrahi, Ragauskas & Tuskan 2010). In addition, the hemicellulose, cellulose and lignin degradation temperatures varied from 220~315°C, 315~400°C and 500~900°C, accordingly (Shadangi & Mohanty 2014). Therefore, the varying pyrolysis temperatures depend on the component concentration of the biomass (Zhang et al. 2005). Thus, the WS pellet (T_1 and T_5) pyrolysis temperatures were from 31 to 800°C in the TG furnace, where 5, 10 and 20 °C/min were the heating rates. The temperature increased throughout the pyrolysis, the water evaporated, and the components decomposed, resulting in decreased biomass weight.

7.3.2. Analysis of TG/DTG profiles

Biomass pyrolysis thermal profiles are typically divided into three phases with various reaction mechanisms and decomposition activities (Table 7.2) (Bach & Chen 2017). The previous literature agrees well with the present TG and DTG profile (Singh, Patil & Sawarkar 2020; Liu, L. et al. 2021). Moreover, Jeguirim and Trouvé (2009) categorised the TG and DTG curves into active and passive phases. The passive phase (I and III) includes carbonisation and drying, whereas the active phase (II) includes devolatilisation (Slopiecka, Bartocci & Fantozzi 2012).

Table 7.2: Pyrolysis decomposition phases/stages/zones

Phase	Name	Degradation component	Activities
I (passive)	Drying	Free moisture and a limited amount of volatile matters	▪ Removal of water from below 110°C
II (active)	Devolatilisation	Hemicellulose and cellulose	▪ Removal of volatiles and adsorption/ absorption of oxygen ▪ Mass loss in temperature zone 110~350°C ▪ Produces primary gasses
III (passive)	Carbonisation	Cellulose, lignin, and extractives	▪ Burnout lignin and produces secondary gases ▪ Temperature greater than 350°C ▪ Produces carbon enriched char/ash

- *TG/DTG profile for T_1 pellets*

The first phase (I) of the TG-DTG curve was the dehydration/drying stage, where the temperatures ranged from 31 to 151°C for the T_1 pellet (Figure 7.1). In this passive phase, heating the sample resulted in a certain amount of weight loss due to moisture evaporation. Also, from Figure 7.1, it can be seen that a modest fluctuation occurred in the DTG curves. Xiao et al. (2020) reported similar results using the lignocellulosic biomass for kinetic pyrolysis investigation. In this phase, the unbound moisture was released between 31 to 100°C, while bound water and extractives were removed at 100 and 151°C.
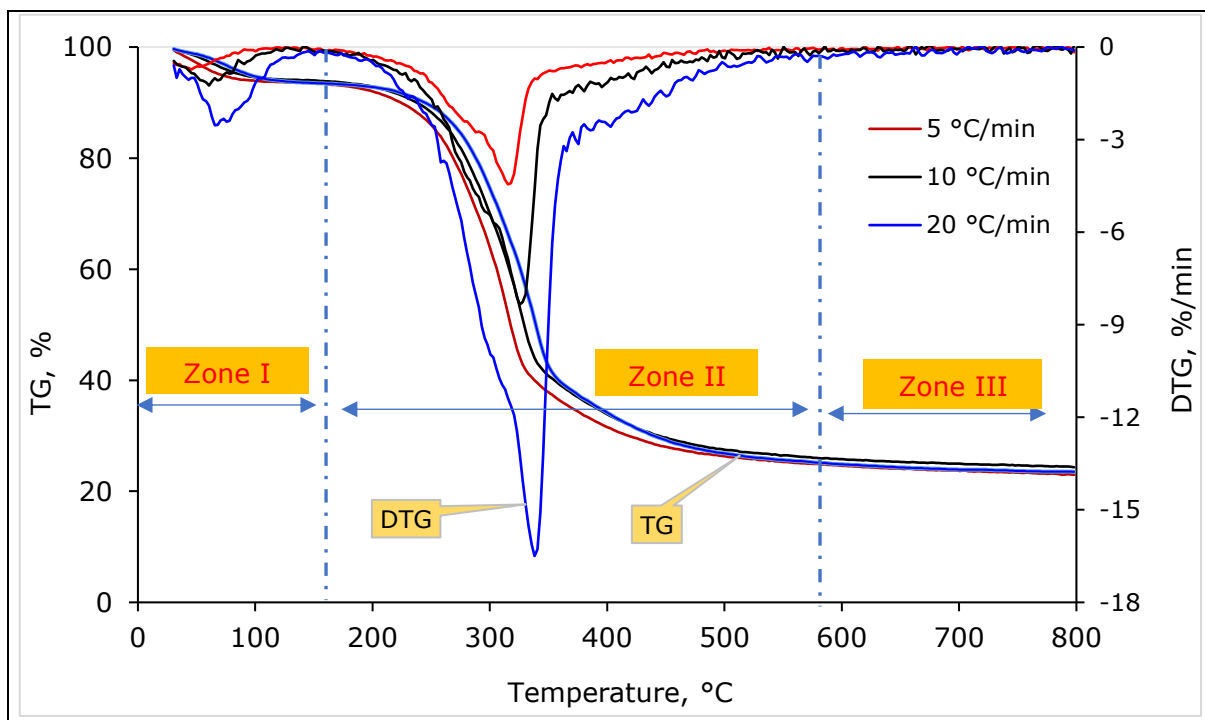
Figure 7.1: Pyrolysis profile (TG/DTG) of T_1 pellets

The second phase (II) is devolatilisation, where biomass depolymerises and "glass transition" occurs. This is the core part of the pyrolysis, and temperatures range from 151 to 553°C. The volatiles were rapidly released, resulting in significant weight loss (Figure 7.1). Alternatively, the DTG profiles presented primary and several side peaks where the major volatile components of WSP were decomposed. The various peaks depended on the biomass's relative hemicellulose and cellulose concentration (Kan, Strezov & Evans 2016). According to Mishra and Mohanty (2020), the prominent peak was formed by cellulose pyrolysis, while the side peak was formed by hemicellulose pyrolysis.

The last phase (III) is carbonisation, where temperatures ranged from 553 to 800°C for the T_1 treatment (Figure 7.1). During this phase, the remaining hemicelluloses and cellulose were nearly solidified into char, and the lignin pyrolysis commenced to be converted into tar (Liu, L. et al. 2021). The slow pyrolysis in the third zone resulted in a smaller weight loss amplitude than in the other zones. A similar trend was reported by Singh et al. (2020). In Figure 7.1, the DTG profiles were relatively flat tended, resulting in a very nominal reaction rate. This finding is consistent with the work of Gani and Naruse (2007).

- *TG/DTG curves for a WS pellet with additives (T_5)*

Figure 7.2 shows the TG curves for T_5 pellets, where the WSP decomposition process was allocated into three phases. The drying phase (passive zones) ranged in temperature from 31 to 158°C, and the maximum reaction rate was 2.33 %/min for a heating rate of 20 °C/min.
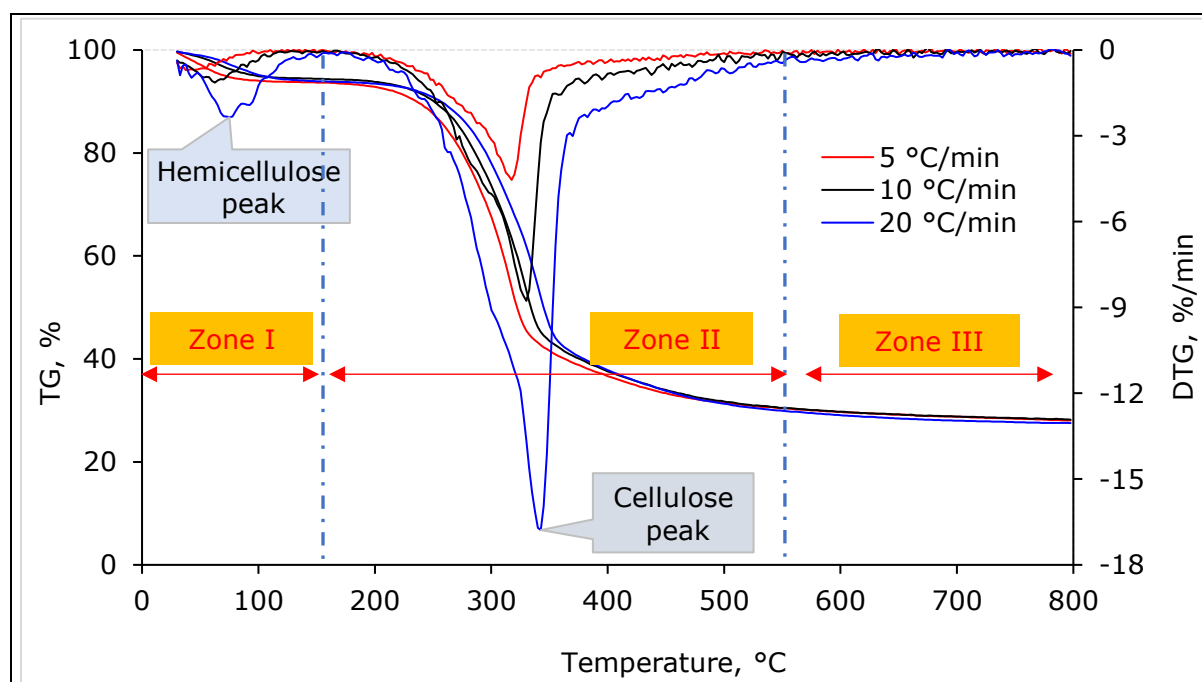
Figure 7.2: Pyrolysis profile (TG/DTG) of T_5 pellets

The TG curve (phase II) shows the WS pellet's major components degradation between 158 and 558°C (Figure 7.2). This second phase (II) was an active zone where cellulose decomposed. The DTG curves also show the maximum peak with a higher reaction rate (16.78 %/min), referring to the cellulose degradation at 20 °C/min heating rate. These results agreed with the literature of Masnadi et al. (2014), who investigated the switchgrass pyrolysis characteristics and found devolatilisation temperatures reaching 600°C.

In addition, the third reaction phase was also the passive zone, where lignin decomposition occurred. In the case of the T_5 pellets, a weight loss of only 2.38% occurred with temperatures varying from 553 to 800°C (Figure 7.2). In T_5 pellets, weight loss low because of the solid-bond than T_1 pellets. Conversely, phase III's reaction rate was less than 0.5 %/min. Huang et al. (2011) investigated the kinetic parameters of biomass, including rice straw, rice hulls, corn leaves, coffee hulls, bamboo leaves, sugarcane bagasse and sugarcane peel. They concluded that most of the biomass provided similar decomposition information. The present study agreed with these results. TG/DTG curve flattened after the maximum reaction where lignin was pyrolysed and burned. This trend was confirmed by other authors (Jeguirim et al. 2014; Mandal et al. 2022).

7.3.3. Effect of temperature on the pyrolysis behaviour

The biomass components' decomposition depends on the temperature and heating rates affecting the pyrolysis behaviour (Ghaffar & Fan 2013). Analysis of the TG curve (Figure 7.3(a)) reveals that the mass loss of WSP was temperature dependent, resulting in weight loss increasing with the temperature. The T_1 and T_5 pellets experienced rapid weight loss at temperatures between approximately 155 and 550°C (Zone II), referred to as the active pyrolysis zone (Mishra & Bhaskar 2014). In comparison, the weight loss in the passive pyrolysis phase (I and III) were milder (Tursunov et al. 2019).

Continuous mass losses and reactions occurred as a result of the applied temperature. The different decomposition phases I, II and III temperature variations were 31~148°C, 148~558°C and 558~800°C for the T_1 treatment at all heating rates. In addition, the mass losses of the T_1 pellets were 6.44, 68.07 and 1.99% for the decomposition of phases I, II and III for a heating rate of 20 %/min (Figure 7.3(c)). The DTG profile fluctuation represents the component variation of the sample (Punsuwan & Tangsathitkulchai 2014). The DTG profile had peaks and several side peaks for both types of pellets with each heating rate which could be related to elemental variations (Gupta & Mondal 2019). Figure 7.3(c) shows that the most effective reaction rate was 16.28 %/min at 341°C. Therefore, the mass loss, decomposition phase and reaction rates was affected by the temperature variation, which agrees with previous research (Balsora et al. 2021; Narnaware & Panwar 2022b).
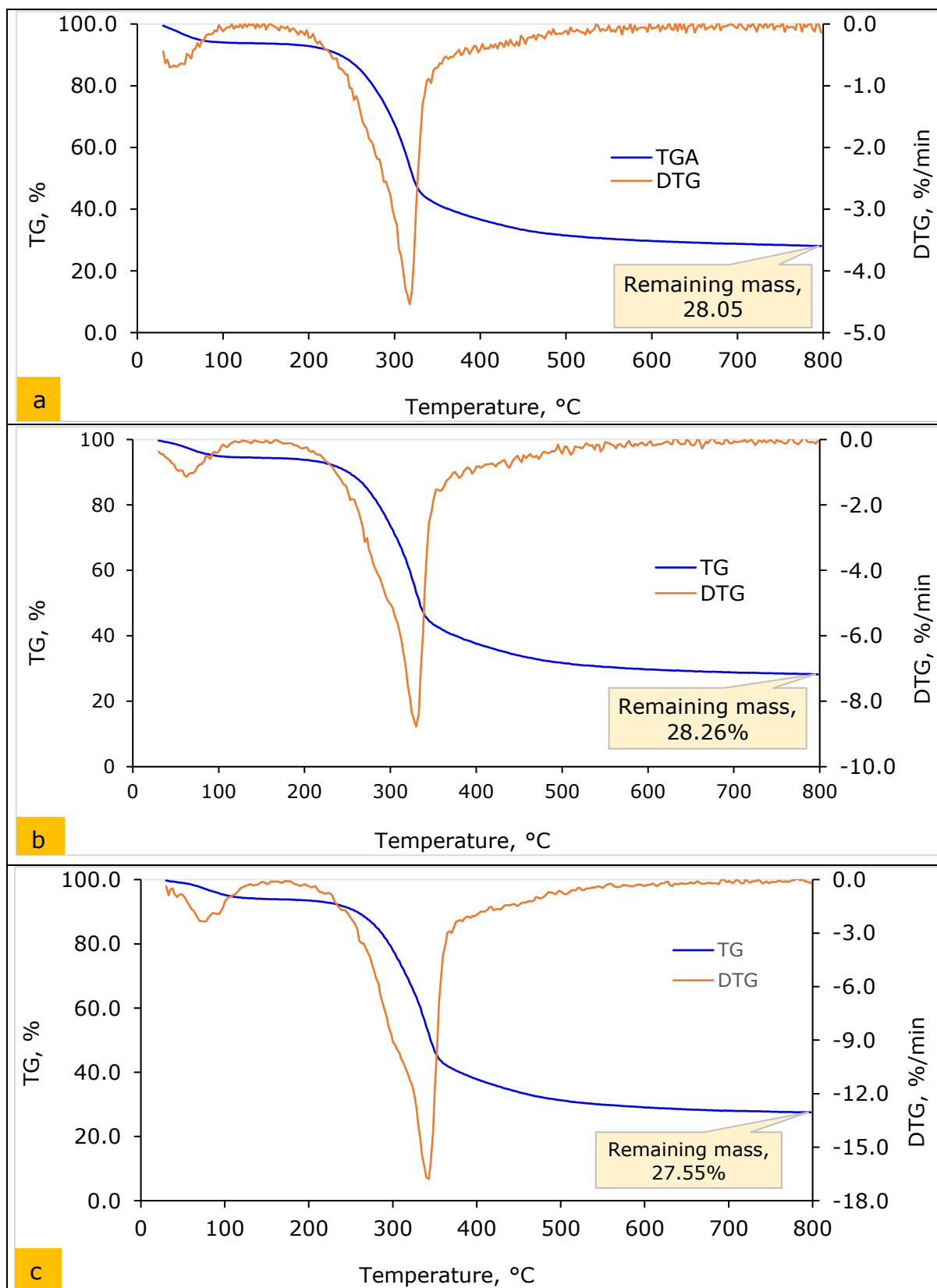
Figure 7.3: TG and DTG curve for T_1 pellets pyrolysis at constant heating rate (a) 5 °C/min; (b) 10 °C/min and (c) 20 °C/min
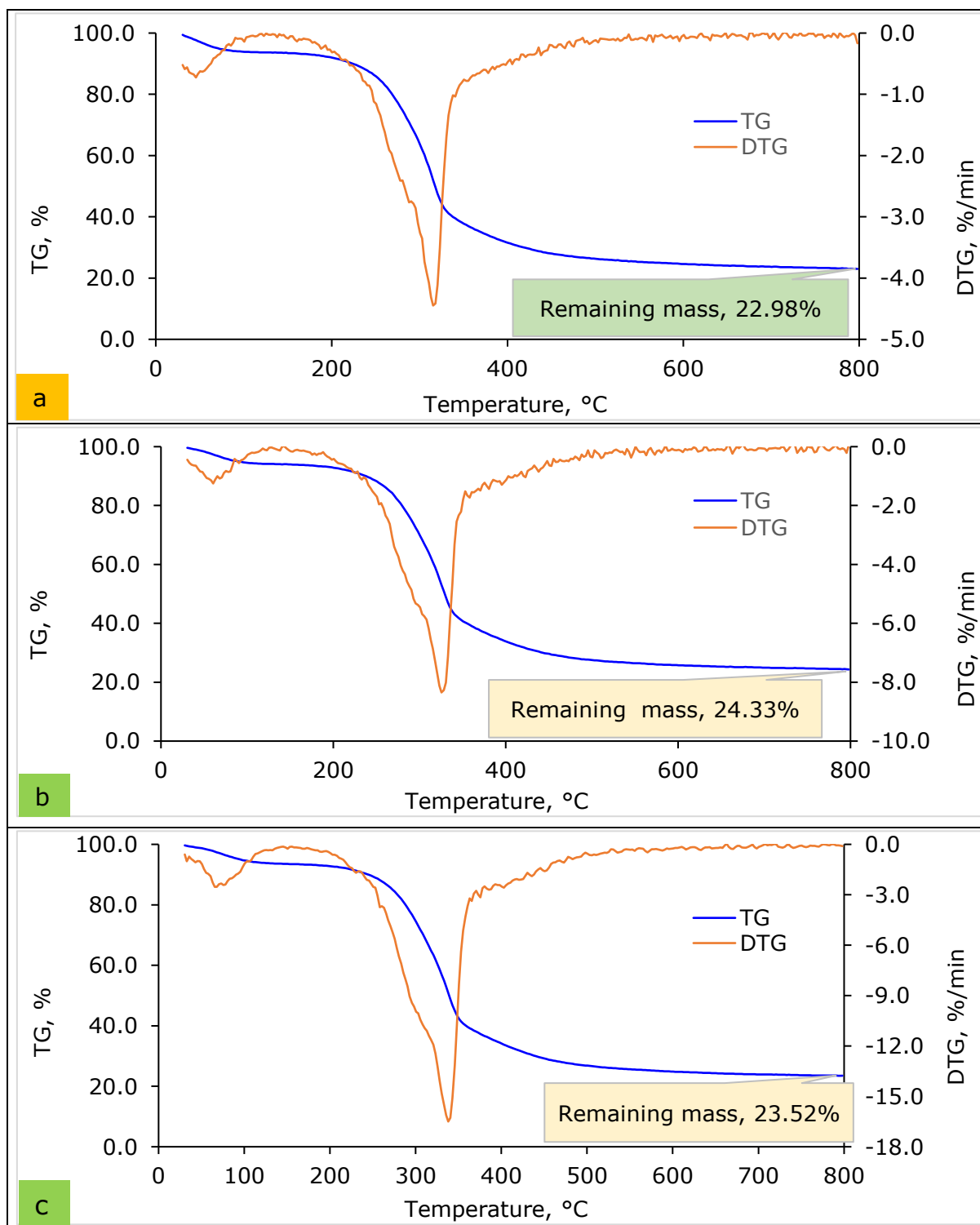
Figure 7.4: TG and DTG profile for T_5 pellets pyrolysis at constant heating rate (a) 5 °C/min; (b) 10 °C/min and (c) 20 °C/min

For T_5, the weight loss was 5.65, 64.44 and 2.38% in temperatures 31~158°C, 158~553°C and 553~800°C (Figure 7.4(a)). However, average weight loss (approximately 2.0%) was negligible after 560°C for both pellets regardless of heating rates, indicating that very few volatile materials were present. At the same time, the fast mass loss occurred

between 158 and 553°C. These findings align with the literature of Singh et al. (2020). They used the garlic husk for the TGA investigation. In comparison, the highest peak represents the rapid maximum reaction rate (8.27 %/min) which occurred between the approximate temperatures of 200~375°C for a 10 %/min heating rate (Figure 4(b). These values are comparable with other studies (Chen, W.-H. et al. 2019). In addition, the decomposition rate was slow in the first and third phases (passive pyrolysis zones). In contrast, the maximum mass loss in the active zone for both pellets means the temperatures significantly influenced pyrolysis rates. The results agreed with other research using rice straw, pine SD, and phoenix tree leave biomass (Shah, Khan & Kumar 2018).

7.3.4. *Effect of heating rate on pyrolysis kinetics*

The impact of the heating rates on WSP (T_1 and T_5) pyrolysis is shown in Table 7.3. As observed from the result, there was no effect on temperature variation in the subdivision of TG/DTG profiles due to the heating rate changes from 5 to 20 °C/min. However, the increase in heating rate shifted the peak temperature, resulting in mass loss and maximum reaction rate change regardless of the treatment and heating rate. Asadieraghi and Daud (2014) also reported that rising heating speed accelerated the decomposition rate, which agrees with the current study.

Table 7.3: Pyrolysis characteristics of T_1 and T_5 pellet

Heating rate, °C/min	Item	Phase I (Drying)	Phase II (Devolatilization)	Phase III (Carbonisation)	Remaining mass, %
	T_{range},°C	31~148	148~558	558~800	
T_1 pellet					
20	T_{peak},°C	68	341	-	23.52
	M_{loss}, %	6.44	68.07	1.99	
	DTG_{max}, %/min	2.52	16.28	-	
10	T_{peak},°C	66	326	-	24.33
	M_{loss}, %	5.99	67.66	2.02	
	DTG_{max}, %/min	1.10	8.55	-	
5	T_{peak},°C	61	318	-	22.98
	M_{loss}, %	6.43	67.41	3.18	
	DTG_{max}, %/min	0.53	4.41	-	
T_5 pellet					
20	T_{peak},°C	78	343	565	23.52
	M_{loss}, %	6.13	67.97	2.38	
	DTG_{max}, %/min	2.33	16.78	0.42	
10	T_{peak},°C	53	333		27.53
	M_{loss}, %	5.65	64.44	2.38	
	DTG_{max}, %/min	1.05	8.38	-	
5	T_{peak},°C	60	320	-	23.58
	M_{loss}, %	6.16	67.82	2.44	
	DTG_{max}, %/min	0.51	4.34	-	

Note; T_{range} = Temperature range
T_{peak} = Peak/highest temperature
M_{loss} = Mass loss
DTG_{max} = Maximum Differential Thermogravimetric/ maximum reaction rate
Zone I = Mass losses due to the moisture evaporation
Zone II = Mass losses devolatilisation (volatile released and then burned)
Zone III = Mass losses carbonisation (decompose of cellulose and char)

Table 7.3 shows the T_1 pellets' pyrolysis behaviour. The drying (phase I) temperatures were the same (from 31 to 148°C) regardless of heating rate, but the peak reaction rate temperature (T_{peak}) was 68, 66 and 61°C for 20, 10 and 5 °C/min heating rates, respectively. Also, the maximum reaction rate (DTG_{max}) was 16.28, 8.55 and 4.41 %/min with the heating rates 20, 10 and 5 °C/min. The pyrolysis was finished with 23.52, 24.33 and 22.98% remaining mass for 20, 10 and 5 °C/min heating rates. These findings were similar to Mishra and Mohanty (2020), who reported a correlation between an increase in heating rate and a rise in DTG peak temperature. The present findings align with Kirubakaran et al. (2009). They noted that a lower heating rate provides better heat transfer in biomass, which means a lower amount of remaining mass after pyrolysis.

The T_5 pellet pyrolysis behaviour based on heating rates of 5, 10, and 20 °C/min is shown in Table 7.3. In the initial phase (I), the mass loss was 6.13, 5.65 and 6.16% for 20, 10 and 5 °C/min heating rates, respectively. In addition, the maximum reaction rates were 16.78, 8.38 and 4.34 %/min for heating rates 20, 10 and 5 °C/min, correspondingly. Similarly, the peak temperature varied with the heating rate increasing from 5 to 20 °C/min. The remaining mass was 23.52, 27.53 and 23.58% for heating rates 20, 10 and 5 °C/min, respectively. Overall, the heating rates influence the peak temperature, mass loss and reaction rates, which is supported by Haykiri-Acma, Yaman and Kucukbayrak (2006) for rapeseed. Also, this results in values consistent with other research (Singh et al. 2020) which used banana leaves for pyrolytic behaviour with TGA.

7.3.5. *Effect of additive addition in the pyrolysis of WS pellets*

Figure 7.5 illustrates the TG profile of the T_1 and T_5 pellets during pyrolysis. From the initial temperature to about 200°C, the TG curves for T_1 and T_5 nearly overlapped (Figure 7.5). After 200°C, it was evident that the weight loss of the T_5 pellet was high, but there was no significant difference for all heating rates. Interestingly, the three heating rates followed the same trend and the mass loss difference was about 5% which remained consistent with the original material's (WS pellet) properties. Therefore, the pyrolysis performance was not considerably affected by additive blending. The same finding was observed in the study of (Ríos-Badrán et al. 2020), which used rice husk, WS and their blended pellets.
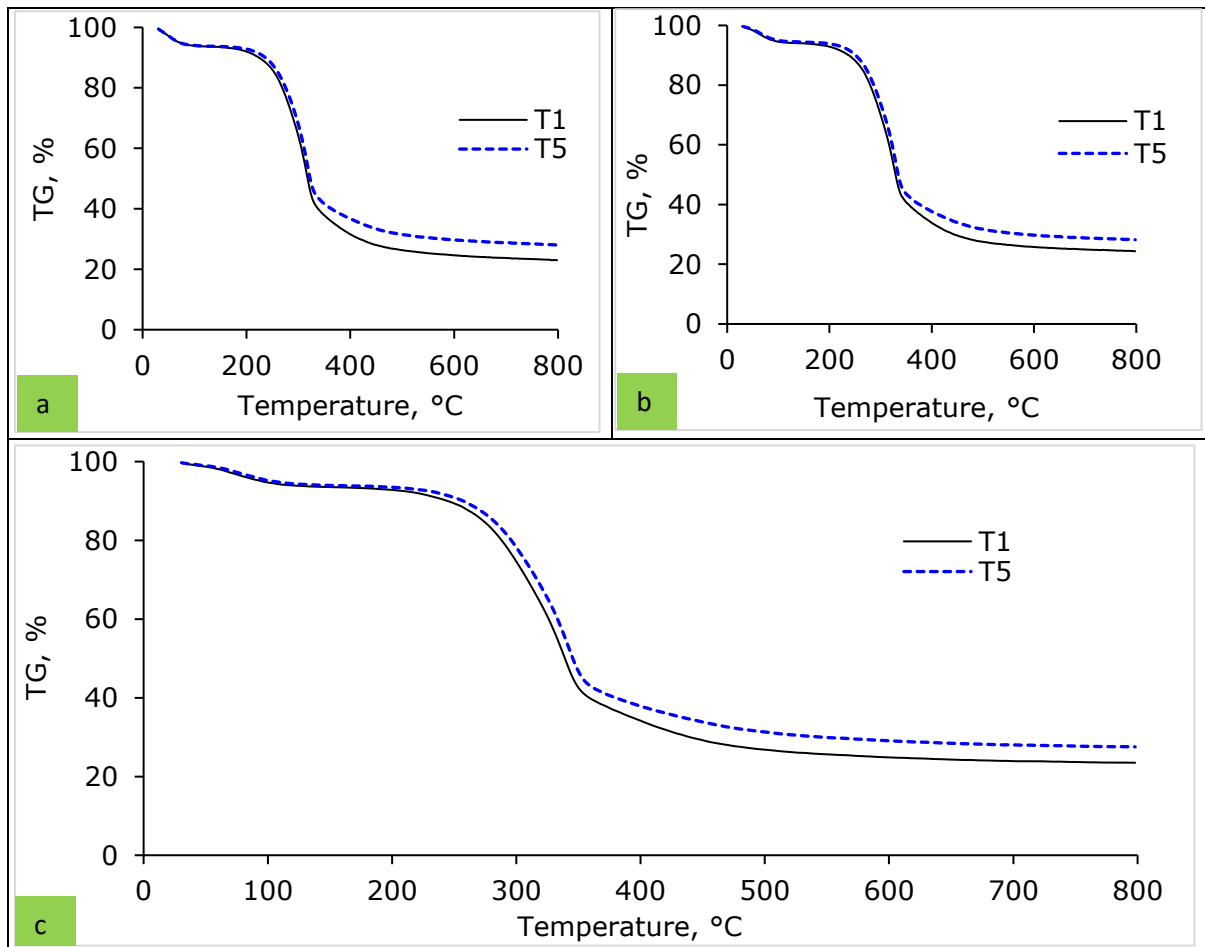
Figure 7.5: TG curves during pyrolysis at a constant heating rate (a) 5 °C/min; (b) 10 °C/min and (c) 20 °C/min for two types of pellets

The DTG curve presents the reaction rate, which varied due to different volatiles and fixed carbon. For all heating rates, the DTG curves had identical peaks that might be changed due to an elemental variation (Figure 7.6). The small peak represents the slow decomposition rate as well as slow pyrolysis, while the highest peak represents the flash pyrolysis. The conversion rate accelerated when the temperature increased. Based on previous research conducted by Link, Yrjas and Hupa (2018), a high ash content significantly impacts the conversion rate, leading to slower conversion processes. According to Yu et al. (2017), cellulose is primarily a condensable product of biomass, indicating the high reactivity of biomass. Also, moisture, hemicellulose and lignin decomposed more slowly, showing slow pyrolysis and a lower reaction rate (Lee et al. 2013).
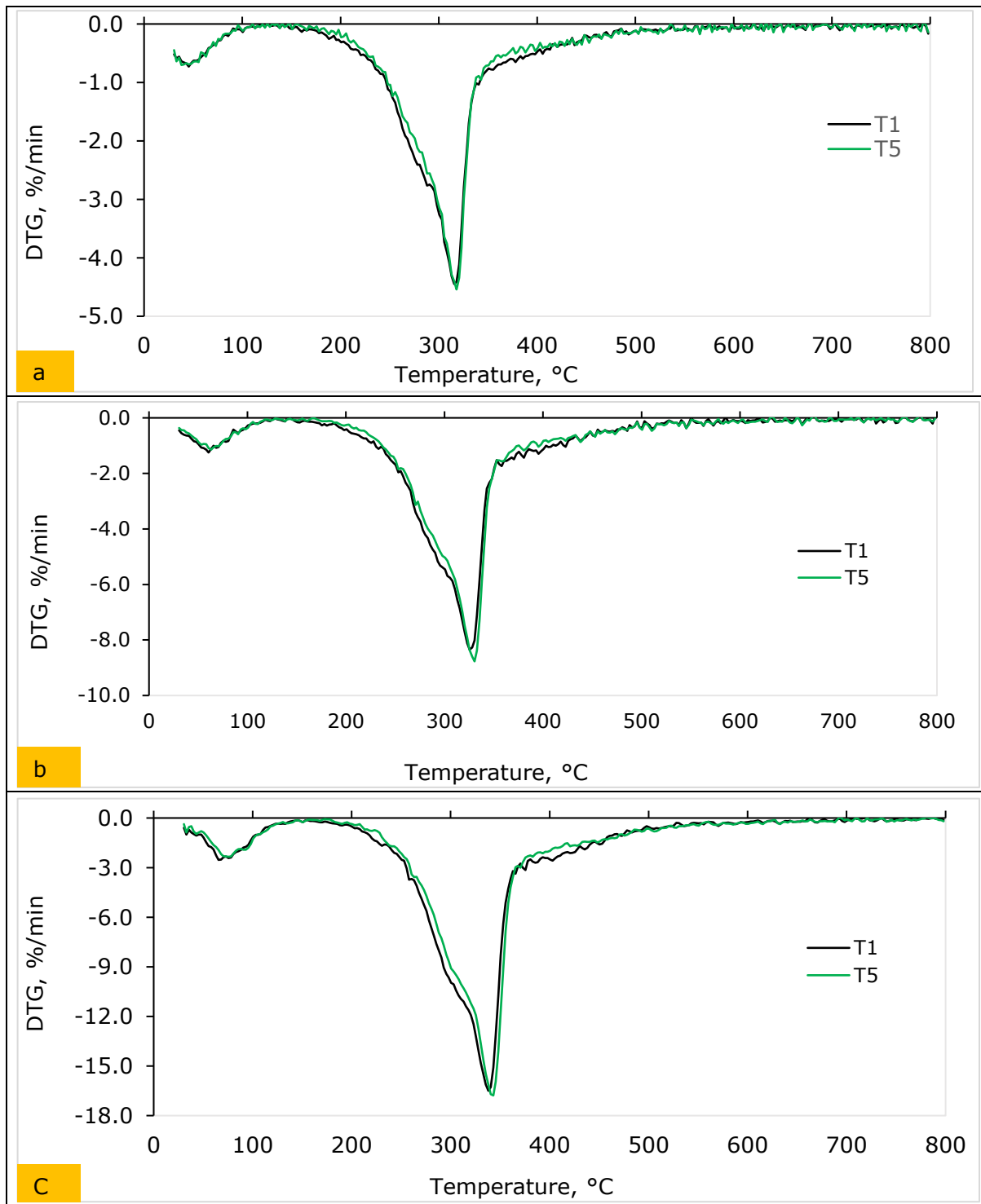
Figure 7.6: DTG curves during pyrolysis at a constant heating rate (a) 5 °C/min; (b) 10 °C/min and (c) 20 °C/min

Interestingly, the conversion rate of T_1 and T_5 nearly overlapped, which could result from similar ash content. However, the conversion rate was slightly higher in T_5 than in the T_1 pellet. The high conversion rates for T_5 were likely due to the heat transfer from the additive (BioC) blended material and chemical interactions. Overall, the additives mixed into WS did not boost the conversion rate or indicate a synergistic occurrence.

7.3.6. WS pellet thermal characteristics evaluation

The thermal characteristics were typically represented by TG and DTG curves. This study evaluated the TG/DTG profile using model free, and model based kinetic features (presented in Chapter 6). The experiment's results showed that the experiments were suitable only for model-based solutions.

The model free approach is best for a single reaction (Moukhina 2012); however, the model-based approach is applicable for both single and multi-phase reactions (Vyazovkin et al. 2020). The literature review revealed that the lignocellulosic biomass transformation process (kinetic mechanism changes) follows multi-step reactions (Soh et al. 2019). The WS pellet is lignocellulosic biomass and follows a multi-point direction (Anca-Couce 2016). Therefore, for thermal analysis, this study only considered the model-based technique. However, some researchers have used single step reactions for studying lignocellulosic biomass (El-Sayed & Mostafa 2020; Singh et al. 2020; Mandapati & Ghodke 2021).

7.3.7. Pyrolysis process analysis by model based technique

Determining pyrolysis parameters is required for a pyrolysis plant's efficient design and better functionality. Model based methods were employed for the pyrolysis kinetic study because the process has a complicated, heterogeneous, multi-step reaction mechanism (Gupta, Gupta & Mondal 2020).

The DTG curves from Figures 7.7 and 7.8 show various peaks in which the WS pellets (T_1 and T_5) follow the multi-step reaction. Kinetics *NETZSCH* is a program that allows model free and model based kinetic analyses on thermal measurements (Opfermann, Kaisersberger & Flammersheim 2002).
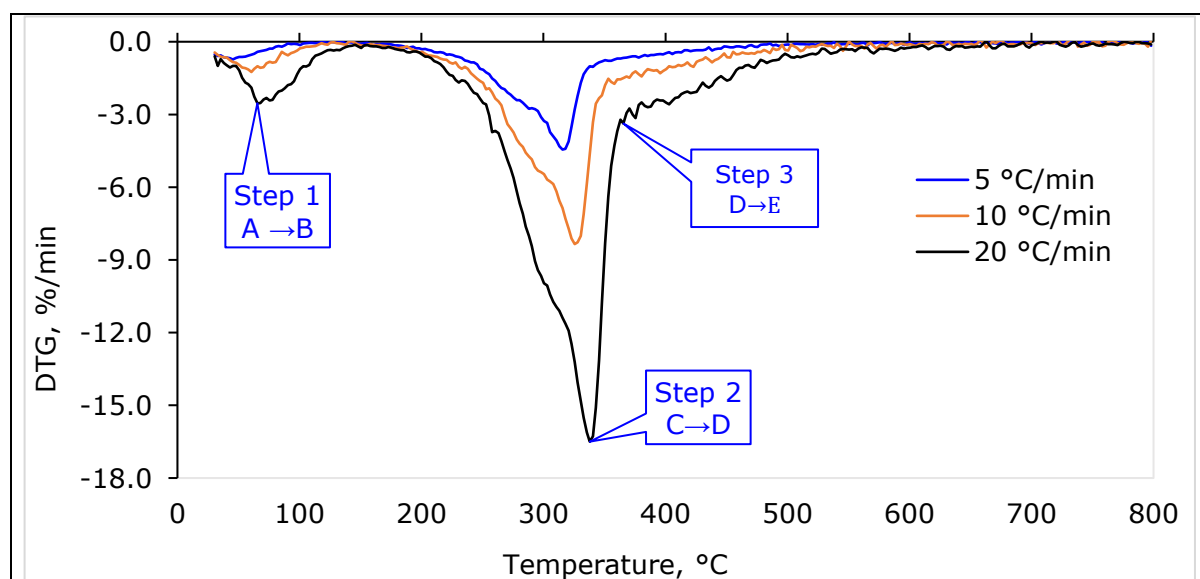
Figure 7.7: DTG curve for WS pellet (T_1) in the nitrogen environment
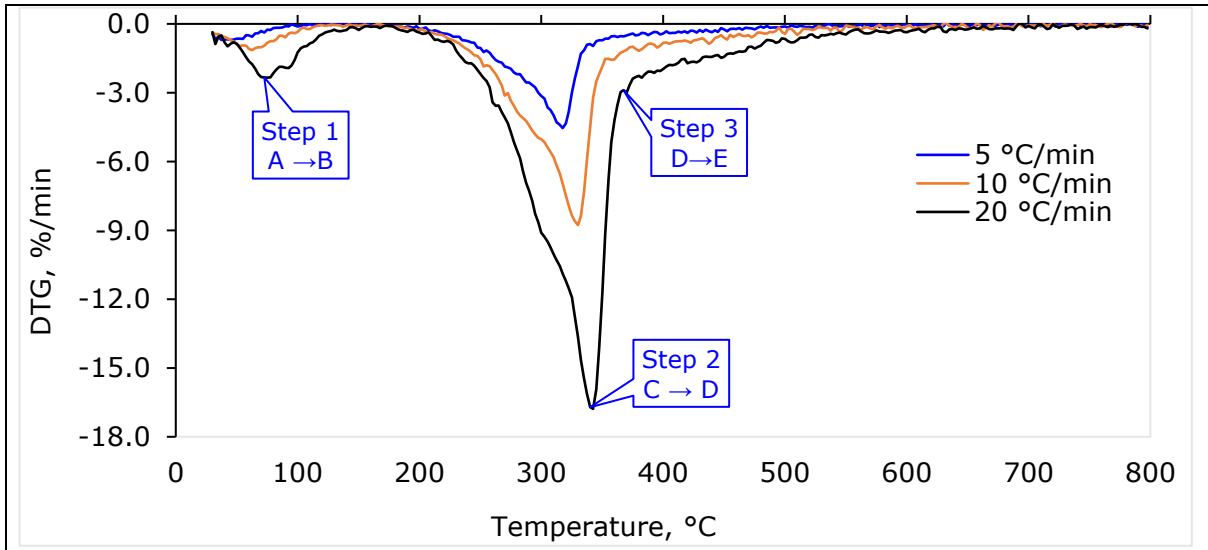
Figure 7.8: DTG curve for WS and additives mixed pellet (T_5)

In this analysis and simulation, the kinetics *NETZSCH Proteus 8.0* software performed a complete estimate of E_α and A and determined the compatible reaction mechanism (Manić, Janković & Dodevski 2021). After the simulation, it used deep explanations to obtain pyrolysis parameters (Table 7.4). The following differential equations could represent a single-phase reaction to a series of subsequent multi-phase pyrolysis reactions where the balance equation is as follows:

Mass = Initial mass– TotalMassChange × {Contribution (a → b)

$\times \int[\frac{d(a \to b)}{dt}]dt$ + contribution (c → d) $\times \int[\frac{d(c \to d)}{dt}]dt$ + contribution (d → e) ×

$\int[\frac{d(d \to e)}{dt}]dt$} *7.1*

Table 7.4: Consecutive reaction steps and equations for WS pellet pyrolysis

Model scheme	Reaction steps	Concentration equations
A–B *C–D–E*	A → B (step 1)	$\frac{da}{dt} = -\frac{d(a \to b)}{dt} = -A_1 . f_1(a.b). \exp(-\frac{E_{a1}}{RT})$ ....*7.2* $\frac{db}{dt} = \frac{d(a \to b)}{dt} = A_1 . f_1(a.b). \exp(-\frac{E_{a1}}{RT})$ *7.3*
	C → D (step 2)	$\frac{dc}{dt} = -\frac{d(c \to d)}{dt} = -A_2 . f_2(c.d). \exp(-\frac{E_{a2}}{RT})$ ....….............*7.4* $\frac{dd}{dt} = \frac{d(c \to d)}{dt} - \frac{d(d \to e)}{dt}$ $\quad = A_2 . f_2(c.d). \exp(-\frac{E_{a2}}{RT}) - A_3 . f_3(d.e). \exp(-\frac{E_{a3}}{RT})$ *7.5*
	D → E (step 3)	$\frac{de}{dt} = \frac{d(d \to e)}{dt} = A_3 . f_3(d.e). \exp(-\frac{E_{a3}}{RT})$ *7.6*

Note; $f_1(a,b) = n_1 a[-ln(a)]^{\frac{(n_1-1)}{n_1}}$; $f_2(c.d) = n_2 c[-ln(c)]^{\frac{(n_2-1)}{n_2}}$ and $f_3(d.e) = n_1 d[-ln(d)]^{\frac{(n_3-1)}{n_3}}$

7.3.7.1. Analysis of the reaction model

The WS pellet samples' decomposition (TG/DTG) curves were split into three predominant zones (Table 7.3). At the same time, the kinetic model was developed based on the various peaks of the DTG profile (Figures 7.7 and 7.8). Both pellets (T_1 and T_5) showed two distinct reactions: $A \rightarrow B$ and $C \rightarrow D \rightarrow E$. The first reaction step was modelled as $A \rightarrow B$, where A is the reactant (raw sample) and B is the product (dehydrated sample). In comparison, the second reaction is due to the breakdown of the sample and comprises two separate steps ($(C \rightarrow D)$ and $(D \rightarrow E)$). This reaction was modelled as $C \rightarrow D \rightarrow E$, where C is the starting material, E is the final product, and D is the intermediate product (Table 7.5).

Table 7.5: Thermal reactions and kinetic parameters for T_1 and T_5 wheat straw pellets

Three-step consecutive mechanism: $A \rightarrow B \rightarrow C \rightarrow D$							
Reaction step	Reaction type	Equation	$E\alpha$, kJ/mol	lnA, 1/s	A, 1/s	Reaction order value	slope
T_1 pellets							
1 ($A \rightarrow B$)	F_2: Second order	$\dfrac{d(a \rightarrow b)}{dt} = A.a^2.exp^{-\frac{E_\alpha}{RT}}$	45.015	4.843	1.2E+2	-	0.092
2 ($C \rightarrow D$)	F_n: n^{th} order	$\dfrac{d(c \rightarrow d)}{dt} = A^2.c^n.exp^{-\frac{E_\alpha}{RT}}$	136.038	10.574	3.9E+4	2.762	0.548
3 ($D \rightarrow E$)	F_n: n^{th} order	$\dfrac{d(d \rightarrow e)}{dt} = A.d^n.exp^{-\frac{E_\alpha}{RT}}$	358.110	33.931	5.45E+14	16.876	0.360
T_5 pellets							
1 ($A \rightarrow B$)	F_2: 2nd order	$\dfrac{d(a \rightarrow b)}{dt} = A.a^2.exp^{-\frac{E_\alpha}{RT}}$	37.298	3.647	38.244	-	0.086
2 ($C \rightarrow D$)	F_n: n^{th} order	$\dfrac{d(c \rightarrow d)}{dt} = A^2.c^n.exp^{-\frac{E_\alpha}{RT}}$	132.868	10.106	2.4E+4	2.346	0.546
3 ($D \rightarrow E$)	F_n: n^{th} order	$\dfrac{d(d \rightarrow e)}{dt} = A.d^n.exp^{-\frac{E_\alpha}{RT}}$	227.105	21.802	2.9E+9	20.0	0.368

Note; E_α = activation of energy, lnA or A = pre-exponential factor,
F_2: Contracting cylinder (Second order), F_n: Reaction of nth order

The first step *(A→B)* was the pore gases releasing zone after removing internal moisture from WSP pores. The second zone ($C \rightarrow D \rightarrow E$) was oxygen sorption within the WSP matrix by increasing mass gloss. So, three different reaction steps can be assumed to simplify the kinetic modelling. For instance, *A→B* corresponds to the dehydration and

desorption zone. *C→D* represents the devolatilisation/pyrolysis zone, while *D→E* denotes the burnout/carbonisation zone. This phase category agreed with Manić, Janković and Dodevski (2021) results.

The WS pellet pyrolysis method followed the three-step consecutive reaction process as *A→B→C→D*, where *A, B, C, D*, and *E* represent the decomposition process. The reaction rate for decomposition for each step was given by $\frac{da}{dt}$. In the presented equations 1 to 6, total conversion, α = *1= a + b + c + d*, while the *a, b, c,* and *d* represent *A, B, C,* and *D* concentrations in the chemical model kinetics. Moreover, the consecutive mechanism follows: *a = (1- α₁), b = (1- α₂), c = (1- α₃),* and *A₁, A₂, A₃,* E_{a1}, E_{a2}, and E_{a3} signifies *lnA* and E_a quantities linked to the first, second and third reactions. Moreover, *n₁, n₂,* and *n₃* are reaction orders associated with the autocatalyst's first, second and third reaction steps.

7.3.7.2. Analysis of kinetic triple

The kinetic triple is important for optimising industrial reactors and predicting reactions (Chen, Jianbiao et al. 2017; Varma et al. 2021). To find the best-fitted kinetic triplicates, we apply the model-based approaches assuming the nth order of reaction (*f(α)= e^n*). The *lnA* and E_a derived by *NETZSCH Proteus 8.0* software for each type of reaction step regarding T₁ and T₅ pellets are presented in Tables 7.6 and 7.7. The three different consecutive reaction steps (*A→B, C→D, D→E*) are shown in Tables 7.6 and 7.7 (Janković et al. 2019; NETZSCH 2021). This thermal reaction process combines or overlaps several mechanisms, including the phase interface reaction as F2 and F*n* (Vyazovkin et al. 2020).

In reaction step 1 (*A→B*), hemicellulose content boosted the sequential mechanism, where *Eα* was 45.015 kJ/mole, the lowest of the reaction steps for the T₁ pellet. Also, the pre-exponential factor (*lnA*) was 4.843 (1/s), and the reaction contribution was 0.092 (Table 7.5). The lower *Eα* value was in Step 1. Gas-phase polymerisation of tar may follow solid-phase pyrolysis chemistry (Cheng, Winter & Stipanovic 2012).

In comparison, in the case of the T₅ pellets, the *Eα, lnA* and slope were lower than T₁, whereas there was the same reaction type (F2) and reaction step. Typically, the lower *Eα* value denoted less energy required to start the reaction, while the higher value meant the reaction began gradually (Huang et al. 2019). The presence of BioC in the T₅ pellets might ignite easily, referred to as the synergistic effect. Also, the result of impurities and higher extractives content in the WSP sample were the causes of lower *Eα* (Janković et al. 2019).

In reaction step *C→D*, the average *Eα* values were 132.868 kJ/mol for T₅ and 136.038 kJ/mol for T₁ pellets. Similar findings were observed by Alves et al. (2019) for the thermal decomposition of microalgae in their study, and the average E*α* values were from 107.1 to 132.6 kJ/mol. Also,

in this step, the reaction order values were 2.762 and 2.346 for the T_1 and T_5 pellets, respectively (Table 7.5). The $E\alpha$, lnA and reaction contribution were lower in the T_5 than in the T_1 pellets in the second zone's consecutive mechanism, which is enriched with cellulose content. This result is supported by Lin et al. (2009). They reported that Ea varies from 48 to 282 kJ/mol for biomass reaction mechanism and depends on the sample origin, processing, and experimental conditions. Also, Radojević et al. (2018) reported that $E\alpha$ is a potential measure of reactivity where high values indicate lower reactivity, meaning that more energy is required for the reactions to proceed.

In addition, the pre-exponential factor for T_1 and T_5 were 33.931 and 21.802 (1/s) at reaction step 3 ($D{\rightarrow}E$), respectively. This observation was similar to the research results of Gupta, Gupta and Mondal (2020), who found the pre-exponential value between 16.11~48.35 (1/s) for TG pyrolysis of a pistachio shell even though they used different isoconversional models. According to a study, lnA could be caused by interparticle diffusion or evaporation restrictions, as well as the latent heat of vaporisation for tars (Banerjee et al. 2021).

7.3.7.3. Reaction dimensionality

Changes in $E\alpha$ values through various elemental phases were linked to dimensional variations throughout the steps. Additionally, the n and $E\alpha$ are likely to vary when basic changes occur in one element as it moves to the next zone. For assessing reaction dimensionality (n) based on model-based kinetic expressions, the reaction mechanism was considered using a 20 °C/min heating rate while the temperature ranged from 31~800°C. The consecutive reaction mechanisms can be observed for all steps assessing the dimensionality (n). Its values were higher than the unity ($n > 1$) for Steps 2 and 3 (Table 7.5). In comparison, Step 1 was the noninteger dimensionality (less than a unit or equal to zero) that can result from the sizes and shapes of reaction particles (Barud et al. 2011).

The overall results (Table 7.5) showed that both pellets' reaction types were similar, while the reaction order values differed. Therefore, it was concluded that the reaction types were not significantly influenced by the additives blends pellet (T_5).

7.3.7.4. Kinetic reactions

Generally, the kinetic mechanism is evaluated for various reaction models (Janković et al. 2019). The total system can be reproduced by a kinetic model function of F2 and Fn models for the observed results (Table 7.5). The second order reaction (F2) model could best describe the primary pyrolysis zones (Peak 1) of both pellets which reflected the decomposition of hemicellulose (Zhang, D. et al. 2019). In this zone, the reaction type

was "phase interfacial reaction" second order. This result agrees with (Huang et al. 2019; Zhang, D. et al. 2019).

The reaction Steps 2 and 3 were titled phase interfacial n^{th} order reaction differential function was $f(a) = e^n$. For Step 2, the Fn kinetic model represents the most suitable pyrolysis process through the reaction n^{th} order and contracting cylinder, significantly reducing the growth rate due to intensified fragmentation and the emission of volatiles. These results agreed with Várhegyi, Chen and Godoy (2009). Therefore, it can be concluded that several steps occurred due to the decomposition of biomass components and the complex reaction effects of WSP.

7.3.8. Dependence of Eα and A on the degree of conversion

7.3.8.1. Relationship between α and Eα

Biomass compositional variations might suggest a complex pyrolysis reaction that results in $E\alpha$ differences. The relationship between activation energy and conversion degree is demonstrated in Figure 7.9. Regarding the reaction degree (α), the $E\alpha$ fluctuated in both pellet types. This fluctuation profile exhibited various endothermic and exothermic picks, resulting in energy absorption and release during different reactions (Kumar & Nandi 2021). Moreover, the $E\alpha$ increased (+value) indicating endothermicity with conversion, while the activation energy decreased (-value) indicating exothermic reactions of the pyrolysis process (Muravyev, Pivkina & Koga 2019). This trend was observed in the study of Thakur et al. (2018), which suggests that a complicated series of processes occurred during the pyrolysis of WSP, and a significantly less amount of cellulose and hemicellulose remained.

As observed in Figure 7.9, $E\alpha$ strongly depended on the degree of conversion (α) for the WSP. The graphic interpretation shows one noticeable peak at 0.9496 degrees of conversion where the $E\alpha$ was around 571.249 kJ/mole, which can be attributed to the maximum energy absorbed during the degradation of hemicellulose and cellulose (Figure 7.9). At the same time, the minimum $E\alpha$ was (-)439.189 kJ/mole, representing the highest energy release in lignin breakdown. The maximum and minimum $E\alpha$ values for T_5 were the same as T_1, with a similar conversion degree (Figure 7.9). Overall, both pellets followed the same fluctuations with the linear trendline (Figure 7.9). In addition, the correlation coefficient (R^2) revealed no significant relationship. Sharma, Pandey and Diwan (2019) observed a correlation between the activation energy ($E\alpha$) and pre-expronential factor (A), which contradicts the findings of the present study. This discrepancy may be attributed to variations in the analysis method.
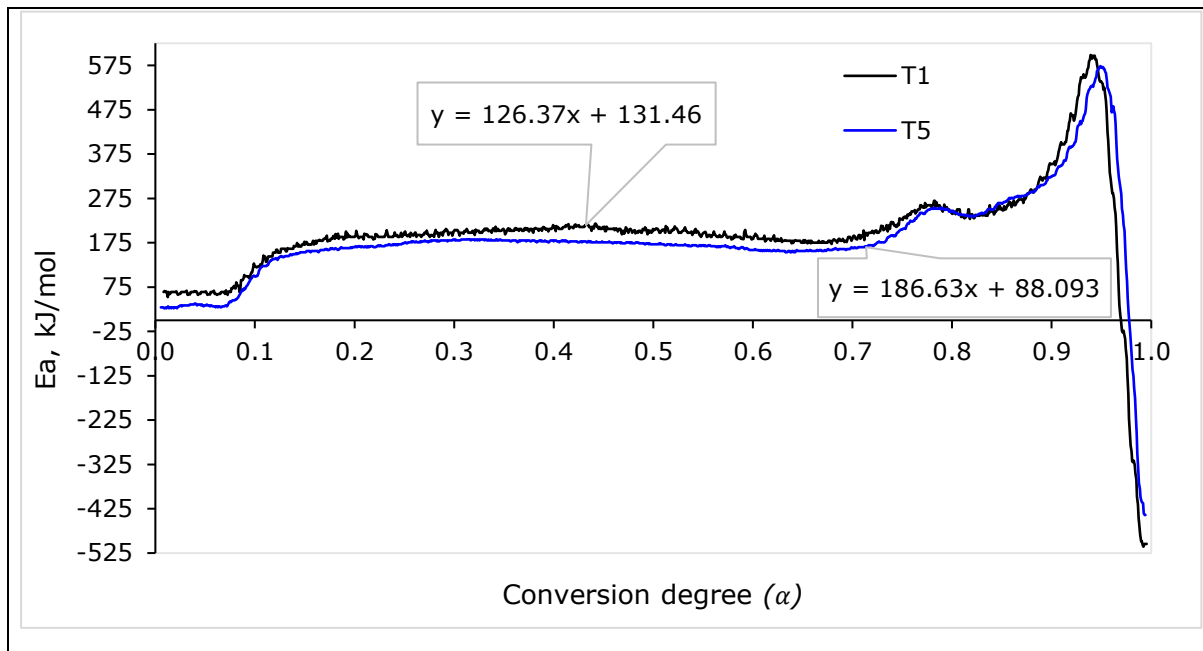
Figure 7.9: Dependence of conversion degree and activation energy for (a) T_5 and (b) T_1 pellet

7.3.8.2. Relationship between α and A

The relationship between the pre-exponential factor (A) and the conversion degree (α) of pellets T_1 and T_5 at 20 °C/min heating rates are shown in Figure 7.10. It can be seen that both pellets followed the same trend, and the values (A and α) were similar. However, the maximum A for T_1 and T_5 were 33.727 and 40.4958 (1/s), respectively. The A increased for the decomposition degree variation between 0.1 and 0.94, suggesting that endothermicity increases with conversion. Further, A decreased for conversion from 0.94 to 1.0, indicating the presence of exothermic reactions for the pyrolysis of WSP in this conversion range. However, the final *lnA* decreased with the conversion, which made pyrolysis more complex (Karaeva et al. 2022).
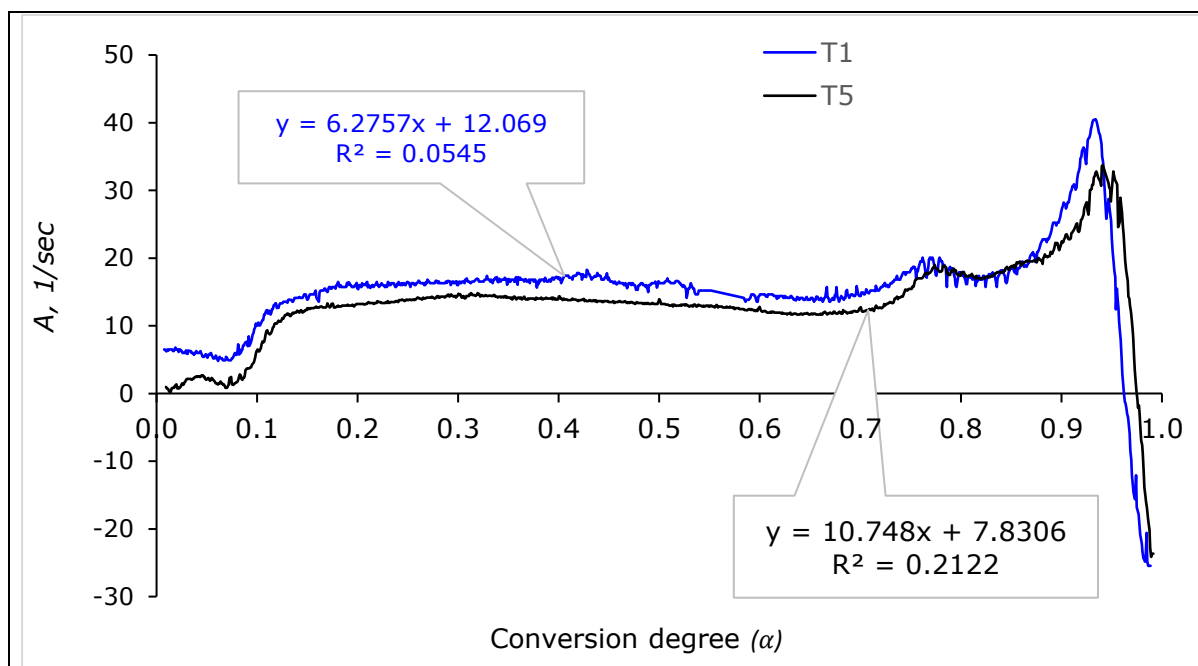
Figure 7.10: Degree of conversion vs pre-exponential factor plot

From Figure 7.10, the coefficient of determination (R^2) value was lower (~0.20). Consequently, there was no significant correlation between the conversion degree and the pre-exponential factor. Also, the linear trendline equations of the two pellets (T_1 and T_5) followed the fluctuation trend, but the fluctuation trend was not similar. Overall, it can be said that the *lnA* value increased with the variation of conversion degree.

7.3.9. *Dependence of temperature on the degree of conversion*

Figure 7.11 shows the relationships between temperature and the conversion degree of both pellets for three heating rates. For pellet T_1, the temperature and degree of conversion were correlated regardless of the applied heating rates and followed the same trend (Figure 7.11). Banerjee et al. (2021) also showed that the heating rates did not affect the degree of conversion and supported the present research findings. In addition, the conversion rate was low at 31°C to 250°C, whereas the conversion rate increased sharply, ranging from 250 to 500°C. The conversion rate increasing patterns indicated that there might be a complex, multi-stage reaction during pyrolysis which agrees with the results of Soria-Verdugo et al. (2018).

On the other hand, for the T_5 pellet, the 5 and 10 °C/min heating rates followed the same direction, while the 20 °C/min heating rate temperature direction was higher (Figure 7.11). Overall, the conversion degree increased with increasing temperature for all heating rates (Luo & Zhou 2022).
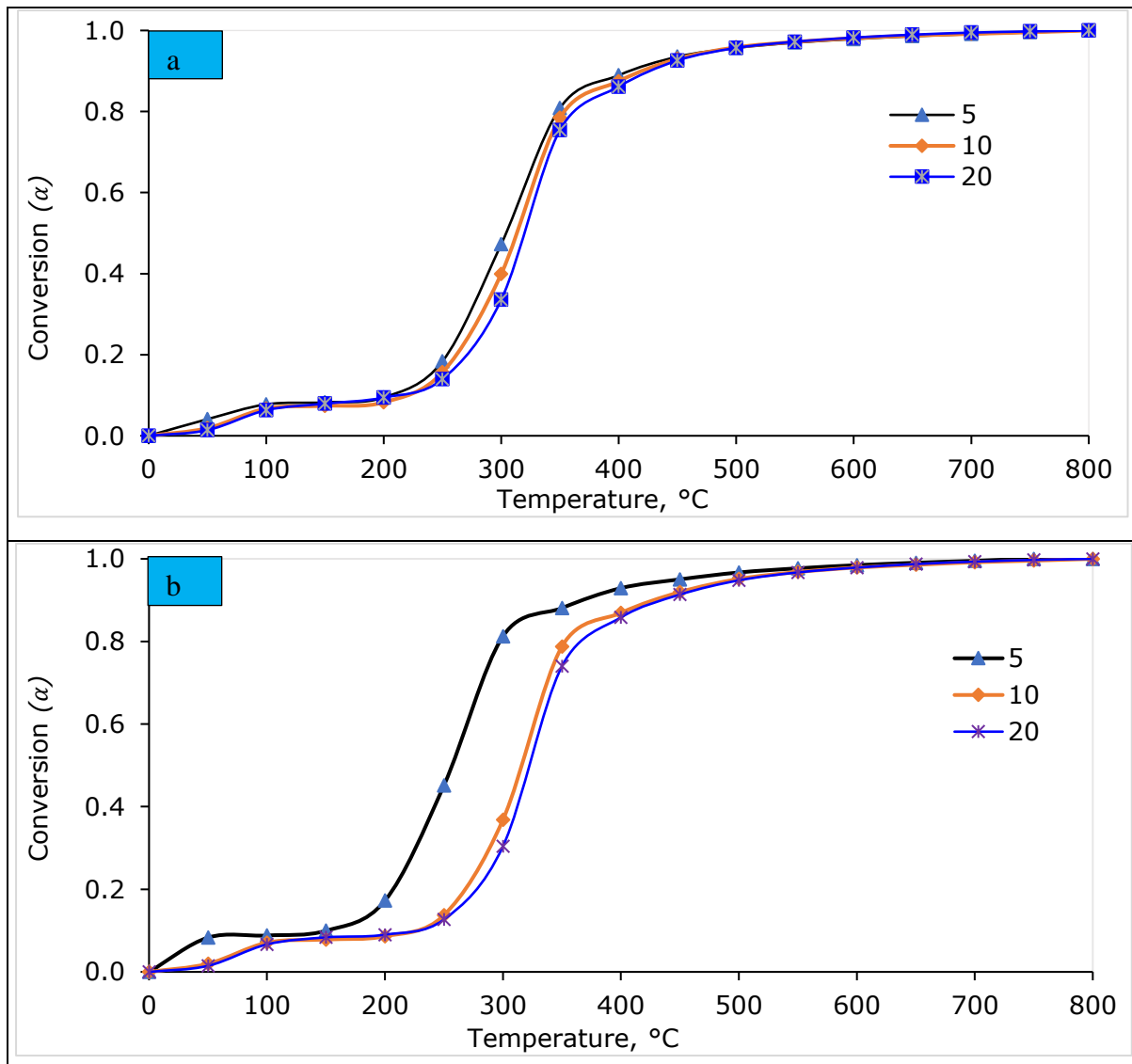
*Figure 7.11: Relationship between degree of conversion vs temperature
for (a) T_1 and (b) T_5 pellet at different heating rates*

7.3.10. Compensation effect (relation between Eα and A)

The model-based technique can determine the different conversion levels for WS pellets. The relationship between the $E\alpha$ and A is shown in Figure 7.12. From the beginning to the end values of the conversion degree, a compensating effect is evident with an excellent fitting factor (Gupta, Gupta & Mondal 2020). Typically, particle vibration increased at the molecular level as the temperature rose, causing molecules degradation and debonding. Furthermore, due to increased biomass, porosity and "phase interfacial reaction" took over at higher temperatures. As observed from the plot, the linear relationship between A and $E\alpha$ followed the Arrhenius type law (Liang et al. 2021). In addition, the linear trend with high fitting accuracy ($R^2 \geq 0.97$) demonstrated the validity of the calculated kinetic factors (Chelouche et al. 2019). The result supported the previous research (Tarchoun et al. 2019; Rasool & Kumar 2020).
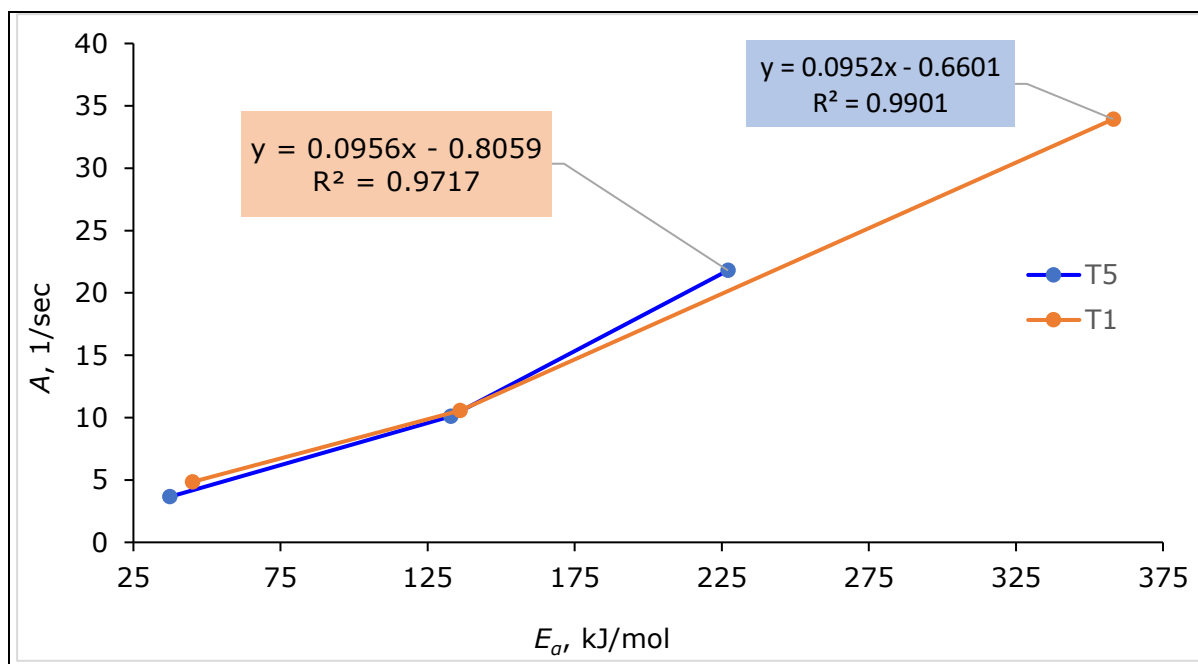
Figure 7.12: Correlation between activation energy (E_α) and pre-exponential factors (A) of pellets

7.3.11 Thermodynamic analysis

Thermodynamic parameters like enthalpy (*ΔH*), Gibbs free energy (*ΔG*) and entropy (*ΔS*) were calculated using activation energy values from the kinetics model-based method due to its accuracy for activation energy calculations. These parameters are critical for designing, scaling and optimising the pyrolysis reactor and parameters (Alves et al. 2019). The *Eα* and *lnA* were taken from the *NETZSCH* program at 20 °C/min heating rates for determining the entropy, enthalpy and Gibbs free energy, as shown in Table 7.6.

Table 7.6: Thermodynamic parameter for WSP at 20 °C/min heating rate

Items	Treatment					
	T_1			T_5		
	Reaction Step1	Reaction Step2	Reaction Step3	Reaction Step1	Reaction Step2	Reaction Step3
Tm, K	591.15	606.15	614.15	591.15	603.15	616.15
E_α, kJ/mol	45.015	136.038	358.110	37.298	132.868	227.105
lnA, 1/s	4.846	10.574	33.931	3.647	10.106	21.802
A, 1/s	1.272E+2	3.910E+4	5.445E+14	38.359	2.449E+4	2.940E+9
ΔH, kJ/mol	40.100	130.998	353.004	32.383	127.853	221.982
ΔG, kJ/mol	169.347	234.782	338.955	167.522	233.445	270.042
ΔS, kJ/mol.K	-0.219	-0.171	0.023	-0.229	-0.175	-0.078

Enthalpy (*ΔH*) relates to the energy transferred between products and reactants during a thermochemical process that reflects the absorbed or released heat at constant pressure (Coker 2001). For the T_5 samples, the activation energy (*Ea*) and enthalpy (*ΔH*) had a low energy barrier,

167

demonstrating the reaction's viability under given parameters and that the chemical reactions can begin quickly. The low energy barrier results agreed with other published studies (Varma & Mondal 2016; Kaur et al. 2018). The ΔH values were 32.0~222.0 kJ/mol for T_5, alternatively 40~353.0 kJ/mol for the T_1 pellet. All the positive values of ΔH in the WS pellet's thermal degradation indicated the endothermicity process. The low values of ΔH favoured the activated complex formation, demonstrating that the products may be readily created with little energy addition (Açıkalın 2021).

Gibbs free energy (ΔG) shows the total energy growth of the process and the reaction's tendency to happen in a specific direction concerning the first and the second laws of thermodynamics (Shagali et al. 2023). The ΔG for the reaction Steps 1~3 presented increasing trends in all pellets at 20 °C/min heating rate, which ranged between around 167.0 and 339.0 kJ/mol, near the observation of Dhyani, Kumar and Bhaskar (2017).

In the case of T_1, the entropy (ΔS) for reaction Steps 1 and 2 was negative, but for Step 3, the ΔS was positive, meaning an inconsistent reaction. The higher ΔS in T_1 suggests that their reactivity was more robust than the other steps, making the system react faster to produce activation energy. For T_5, all entropy values were negative, implying that the extent of disorder in generated products by bond disconnections was lower than that of initial blend samples. The negative (low) entropy (ΔS) value indicates that the pyrolysis of WSP biomass experienced lower physical and chemical changes and was near the thermodynamic equilibrium. As the additive blends (T_5) significantly affected the kinetic triple concerning the T_1 sample, blending the feedstocks also led to changes in the thermodynamic parameters. A similar trend was observed by Yuan et al. (2017).

7.4. Summary and conclusion

This chapter studied the pyrolysis characteristics of a WS pellet with (T_5) and without (T_1) additives using a TGA under a nitrogen environment. A significant mass loss (about 65%) was observed within temperature variation from 150 to 550°C. With the increase in the heating rate, the TG and DTG profiles shifted to the high-temperature side. The maximum mass loss rate during the devolatilisation phase (II) of 4.41 to 16.28 %/min, respectively, for 5 to 20 °C/min at the T_1 pellet. The outcome of the TG analysis suggested that the thermal behaviour of WSPs was similar regardless of heating rate and mixture.

The pyrolysis decomposition of WSP occurred in three stages: drying, devolatilisation and carbonisation, and devolatilisation was a key stage. The WSP kinetic characteristics of the pyrolysis process were determined using the model-based approaches with *NETZSCH* Proteus 8.0 software. The kinetic analysis confirmed the *Fn* (n^{th} order phase interfacial reaction) and

*F*2 (second order chemical reaction) models were the best-fitted analysis technique. Both pellets followed the equilibrium chemical reaction trend. The pre-exponential factor (*lnA*) for the T_5 pellet varied from 3.647~21.802 (1/s). Alternatively, the activation energy ranged from 45.0 to 358.0 kJ/mol for the pellet without additives (T_1). The *Ea* of additive blend pellets (T_5) was lower than WS pellets without additives (T_1) which might be related to BioC's synergistic effect. The WS pellet thermal decomposition mechanism and accurate reaction kinetic models could be used in designing and fabricating pyrolysis reactors and optimising pyrolysis process conditions.

CHAPTER 8: CFD MODEL OF WHEAT STRAW PELLET GASIFICATION IN 10 KW DOWNDRAFT GASIFIER

Abstract

A two-dimensional computational fluid dynamics (CFD) model was developed in this chapter to examine the gasification of wheat straw pellets (WSP) in a 10 kW fixed bed gasifier. The model was created in ANSYS meshing and simulated in the ANSYS Fluent software package with in-house coding via the User-Defined Function (UDF). For this work, the gas and solid phases were defined using an Euler-Euler multiphase technique to describe the transport of mass exchange, momentum and energy terms whilst applying the k-ε turbulence model for the gas phase. The study was also performed at a steady state regime considering the non-premixed combustion and species transport models. The model output was validated with previously collected data from a fixed bed downdraft gasifier for macadamia shell gasification. Biomass and air flow rates were initially set as 9.0 kg/h and 37.78 Nm³/h, respectively. The simulated results exhibited a reasonable agreement with the experimental data. Based on the developed model, the factors affecting the producer gas, such as equivalence ratio, higher heating value and the temperature distribution inside the gasifier, were evaluated. We found that the equivalence ratio (ER) negatively and positively impacts gas production and lower heating value (LHV). The suitable ER value was 0.35 for syngas (H_2+CO) production. The producer gas composition was CO~27.67%, CH_4~3.29%, CO_2~11.09%, H_2~11.09% and N_2~51%, respectively when the ER was 0.35. The reactor temperature positively affected the syngas quantity increase. The contour profile and centreline distribution of temperature, static pressure, velocity, and density were not constant due to the uneven shape of the reactor and various thermal reactions. In contrast, the gas species distribution followed the same trend, but the volume was dissimilar.

8.1. Introduction

Biomass is well known as a reliable alternative bioenergy source for both developed and developing countries (Demirbas 2004). Its contribution significantly impacts the world's power generation (Gupta, Jain & Vyas 2017). It is usually inefficient to use biomass directly for energy or power production (Pandey, Prajapati & Sheth 2021). Therefore, converting biomass to the desired fuel is one of the preferred methods (Ahrenfeldt et al. 2013). Many technologies have been developed to create energy from biomass, such as combustion, gasification and pyrolysis (Bahng et al. 2009). Among the technologies, gasification is commonly used, and with a high conversion efficiency of up to 50% (Caputo et al. 2005). In addition, downdraft gasification is one of the promising thermochemical conversion technologies (Jahromi et al. 2021) that is well suited for small to medium scale power generation (Janajreh & Al Shrah 2013).

Gasification is more complicated than combustion and pyrolysis because it is a pyrolytic process through a series of chemical reactions (Susastriawan, Saptoadi & Purnomo 2017). Therefore, the findings of laboratory scale gasification experiments are frequently indecisive. Designing new gasifiers of suitable size requires enormous effort and resources. Further, it takes a lot of time and requires considerable experimental facilities (Pandey, Prajapati & Sheth 2021). Therefore, a numerical method is an efficient way to obtain an insight into the gasifier and the basic physics involved in biomass gasification.

Various numerical models and simulation tools have been proposed for gasification plant design (Jarungthammachote & Dutta 200). Mathematical modelling can be used to help understand gasification principles and operational behaviour (Baruah & Baruah 2014; La Villetta, Costa & Massarotti 2017). Overall, biomass gasification modelling can be characterised as thermodynamic equilibrium, kinetics, computational fluid dynamics (CFD) and artificial neural networks (ANN) (Patra & Sheth 2015; Dhanavath et al. 2018).

Among the various modelling approaches, the thermodynamic equilibrium model most accurately describes the ultimate composition of gases (Zainal et al. 2001; Mendiburu, Carvalho & Coronado 2014). This model forecasts the tendency of influencing parameters rather than the relative experiment value guess. The thermodynamic equilibrium hypothesis is predominantly preferred (Babu & Sheth 2006) because of its simplicity, but its accuracy is limited (La Villetta, Costa & Massarotti 2017)). In comparison, kinetic models are obtained from experiments and used for char conversion during gasification (Jayah et al. 2003; Babu & Sheth 2006). These models provide more precise predictions, but the accuracy is specific to the design parameters (Antonopoulos, I. S. et al. 2012). Conversely, the ANN model provides a sophisticated and complex numerical process but cannot produce analytical results. Further, this approach requires substantial time and significant processing resources and incurs high costs (Baruah, Baruah & Hazarika 2017).

The CFD model is often run by available commercial software (e.g., ANSYS Fluent). Because of this, CFD is favoured by many for both scientific and engineering applications (Liu, H. et al. 2013). CFD is sufficient for the simulation and prediction of the gasification process in the fixed bed gasifier due to its ease of operation (Ahmed et al. 2012). The CFD model employs mass energy balance and dynamic chemical reactions that can predict the zone's temperature distribution profile (Wang & Yan 2008; Chogani et al. 2020). The significant advantage of CFD models is accurate temperature and gas yield estimation in the whole reactor (Wu et al. 2013). In addition, CFD models are suitable for dense particulate (pellets) (Pepiot, Dibble & Foust 2010).

Several researchers have created two dimensional (2D) CFD simulations in the gasification process for updraft and downdraft gasifiers (Fernando & Narayana 2016; Gupta, Jain & Vyas 2017; Chogani et al. 2020; El-Shafay et al. 2020). Murugan and Sekhar (2017) simulated a 40 kW downdraft gasifier utilising rice husks as fuel. Their results showed that a gasification process would produce syngas and a composition of 22% CO, 13% H_2, 8% CO_2 and 1.7% CH_4, where the equivalence ratio (ER) was 0.30. They also found a maximum heating value of 5.19 MJ/Nm^3.

Wu et al. (2013) employed ANSYS Fluent software in a 2D CFD for a highly preheated air and steam biomass gasification process. They considered a demonstration scale fixed bed downdraft gasifier using the Euler-Euler multiphase approach with chemical reactions. They found that an external heat source necessitates a high temperature gasification system. The 10 kW downdraft gasifier was modelled using CFD for the Euler-Lagrange approach (dispersed two phase flows) (Meenaroch, Kerdsuwan & Laohalidanond 2015). The simulated results revealed that the air flow rate affected the temperature change, the gasifier height, the syngas composition and other factors.

Gupta, Jain and Vyas (2017) also simulated a 10 kW biomass downdraft gasifier for woody biomass. They reported that the average gasification temperature was 800 K, and the maximum temperature was at the char reduction zone. They further reported that pressure varies with gasifier height. Pandey, Prajapati and Sheth (2021) recently studied the 2D axisymmetric CFD model of an Imbert downdraft gasifier for Ecoshakti biomass pellets. They found that the increases in equivalence ratio (ER) tend to increase the temperature inside the gasifier.

The different types of biomasses are comprised of other chemical structures and compositions. During the thermochemical process, various compositions degrade at varying speeds and through varying mechanisms and impact one another. Several scientists approached downdraft gasification technology using wood as feedstock (Zainal et al. 2002; Hsi & Kuo 2008; Vidian, Dwi Sampurno & ail 2018). A few studies have been developed for biomass pellet gasification, especially WSPs.

CFD was also used to simulate a moving bed updraft biomass gasifier by Fernando and Narayana (2016). They found that a specific air flow rate is required for CO production.

This study developed a CFD model for 10 kw gasifying WSPs in a downdraft fixed-bed reactor. Moreover, it examines optimal operating parameters for maximising pellet gasification's syngas yield and conversion efficiency. This research also investigates several operating factors in temperature, pressure and produced gas distribution. The output of this study will provide valuable insights for researchers and practitioners working with other types of biomass and gasifiers.

8.2. Materials and methods

A CFD model for a 10 kW downdraft gasifier was developed in this research. The created CFD model was initially validated using existing macadamia shell gasification experimental data (Elita 2018). After that, the developed model was used to simulate WSP gasification processes. The pellets were made with additive mixtures (T$_5$: 70% WS, 10% SD, 10% BC, 10% BioC). Chapters 3, 4, 5 and 6 presented the detailed characteristics of the T$_5$ pellet.

8.2.1. Feedstock

The WSP was characterised by ultimate and proximate analysis and presented in detail in Chapter 3. Also, a TGA (*NETZSCH* STA 449F3 Jupiter) was used for the kinetic analysis of the WSP and obtained E_α and *lnA* were listed in Chapters 6 and 7. Table 8.1 provides a summary of the chemical composition and thermokinetic parameters used as input data in the CFD model.

Table 8.1: Input data for model simulations

Pellet features		Value
Proximate analysis (wt % as received, db)	Moisture	3.50
	Volatile matters	44.51
	Fixed carbon	36.99
	Ash	15.00
	Calorific value, HHV (MJ/kg)	19.06
Ultimate analysis (wt % as received, db)	Carbon	45.97
	Hydrogen	5.22
	Nitrogen	0.72
	Sulphur	0.21
	Oxygen (by difference)	47.88
Density	Apparent density (kg/m^3)	817.71
	Bulk density (kg/m^3)	427.45
Thermokinetic properties*	*In combustion*	
	Activation of energy, E_α (kJ/mol)	418.935
	Pre-exponential factor, A (1/s)	1.76E+16
	In pyrolysis	
	Activation of energy, E_α (kJ/mol)	132.868
	Pre-exponential factor, A (1/s)	2.4E+4

Note; * = devolatilisation phase and heating rate 20 °C/min

8.2.2. Reactor - the central part of the gasifier

Gasifiers have been used to convert solid fuel (biomass material) into gaseous fuel (Mahinpey & Gomez 2016). The downdraft (co-current flow) and updraft (cross-current flow) approaches are two widely used configurations for fixed bed gasifiers that are distinguished by the relative motion of the feedstock and gasifying agent (Warnecke 2000). The downdraft gasifier has three key work actions: (i) biomass flow on top of

the reactor, (ii) air-flow from the side into the reactor and (iii) combustion/gasification inside the reactor (Siripaiboon, Sarabhorn & Areeprasert 2020). A gasifier (working condition) and a graphical illustration are shown in Figure 8.1.

| Package of gasifier with gas Engine-Genset in working conditions | Schematic diagram of the downdraft reactor (Janajreh & Al Shrah 2013) |
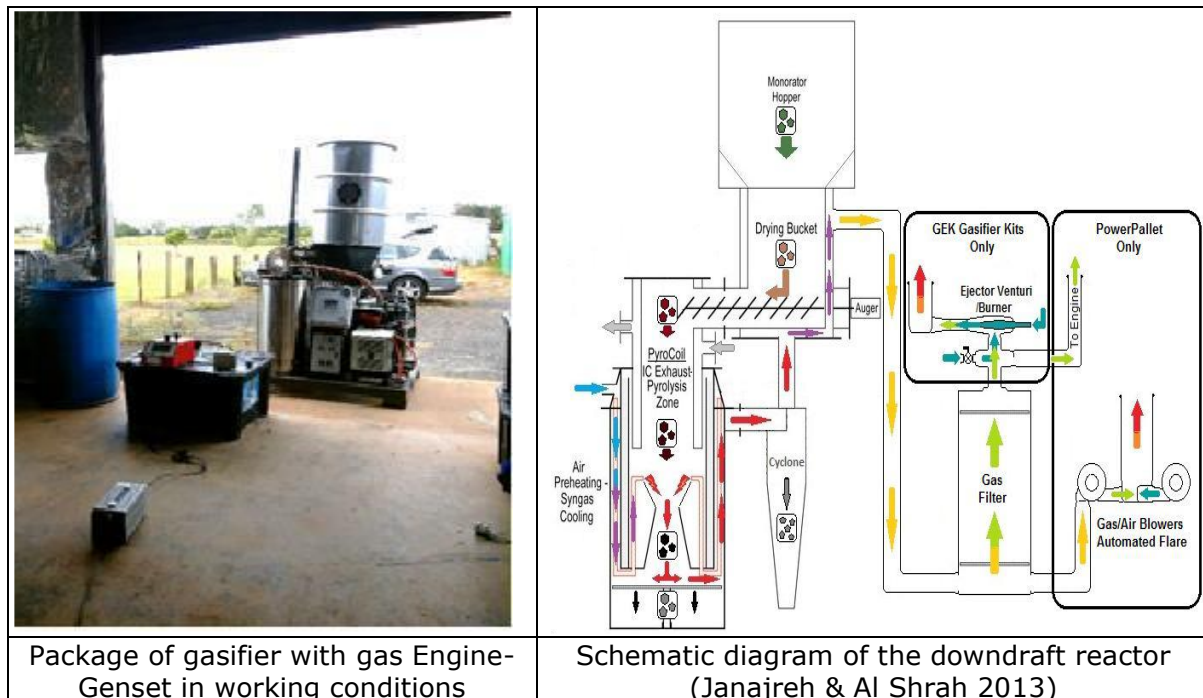
Figure 8.1: Pilot scale experiment using macadamia shell and schematic diagram of Imbert downdraft gasifier

Note; 1. Drying bucket, 2. Auger, 3. Pyrocoll, 4. Insulation, 5. Combustion zone, 6. Reduction zone, 7. Cyclone separator, T/C: Thermocouple and P: Pressure sensor

There are usually two designs of downdraft gasifiers: the Imbert gasifier (throated or closed top) and the stratified gasifier (throat less or open core). The most popular kind of downdraft gasifier is the Imbert gasifier. It is a closed top gasifier with a throat between the zones where deoxidation and reduction reactions occur in the reactor core (Mendonça et al. 2022). The gasifier's throat contributes significantly to lowering the tar concentration in the producing gas by generating a more favourable mixing environment and a uniform temperature field (Martínez et al. 2012). Conversely, the open top gasifier is easier to construct and has good scale-up properties design, but the tar content is high, and the process can be unstable (Bhavanam & Sastry 2011; Martínez et al. 2020). As a result, this study focused on the downdraft gasifier Imbert type's conceptual framework which is shown in Figure 8.1.

The reactor is the principal part of the gasifier which is inbuilt. For gasification, the feedstock is supplied into the reactor from the top while air is injected through nozzles from both sides. The bottom of the reactor releases outlet syngas and char rich ash. A sketch of the reactor with zones and immediate production formation is shown in Figure 8.2.

| Schematic of reactor zones | Reaction intermediate production formation |
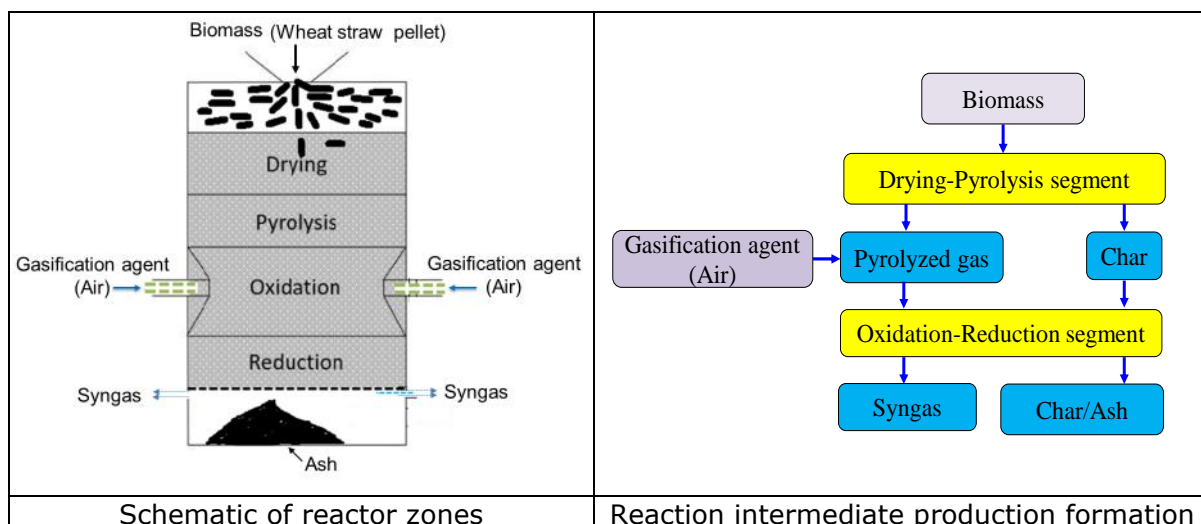
Figure 8.2: Reactor zone and transitional product formation

The dimension is needed and done in the laboratory to present the reactor graphical profile. The overall height and diameter of the reactor were 660 mm and 375 mm, respectively (Table 8.2).

Table 8.2: Dimension and specifications of the reactor (10 kW downdraft gasifier)

Parts	Dimension (mm)
Total height of the reactor	660
Reactor outer shell diameter	375
Reactor inner shell diameter	295
Reduction zone (height)	150
Char oxidation/gasification/combustion zone (height)	210
Devolatilisation/pyrolysis zone (height)	200
Drying zone (height)	100
Air inlet tube diameter	12.7
Air nozzle diameter	17.5
Ash gate diameter	353
Ash deposition part	100
Ash deposition hole diameter	4.76
Gas release part	50
Wall/insulation thickness	3
Reactor walls (interior and exterior walls)	Stainless steel

8.2.3. Modelling theory - thermochemical conversion of solid fuel

The principal activity of gasification modelling is the movement of particles in two ways: gas and solid phases (Dupont et al. 2007). Solid particles and gases move in the downdraft gasifier in the same direction. Heat and mass are exchanged between the solid particles and gas on a single continuous surface during gasification. The sum of solid and gas surface areas equals the total surface area. However, the total particle area varies with bed height. Also, gas and solid composition move and change all over the bed. Therefore, the reactor bed of the model has both solid and gas phases moving through it. Figure 8.3 represents the particles involved in the plug flow regime.
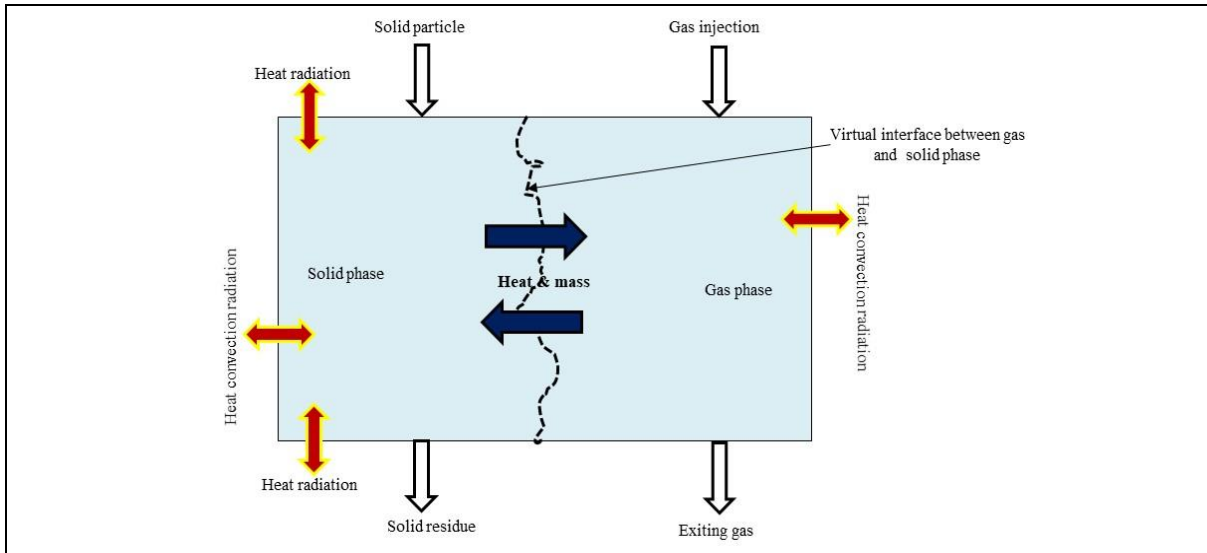
Figure 8.3: Modelling scheme of solid fuel in the fixed bed downdraft gasifier (Souza-Santos 2010)

8.2.4. CFD model development

The downdraft gasifier model was constructed in a 2D planner configuration applying ANSYS Fluent 2021 R2. The procedure of the CFD simulations is shown in Figure 8.4.
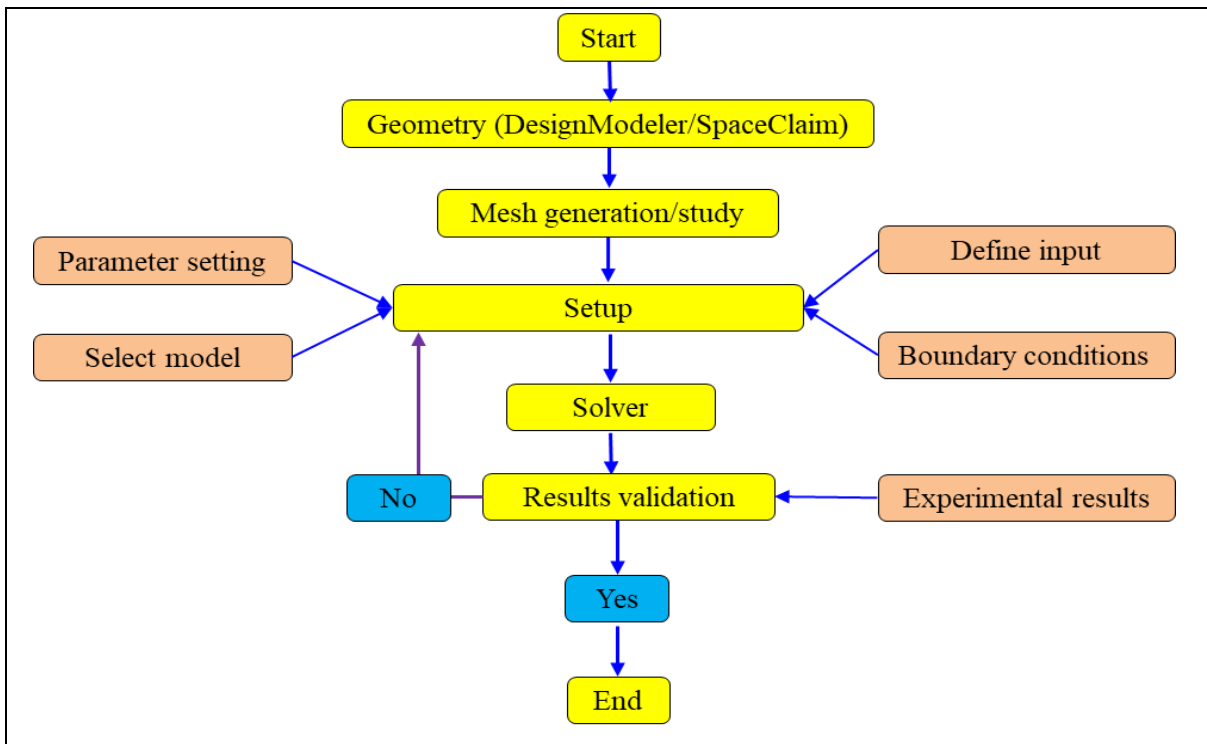
Figure 8.4: Flowchart of gasification numerical simulation using CFD

The five steps such as i) Geometry designing, ii) Meshing, iii) Setting up, iv) Solution and v) Post-processing must be followed for model development (Nørregaard et al. 2019). Pre-processing was the first step,

176

defining the geometry. The meshing requirements were set to confirm the geometry's independence test. At the same time, it was constructing the probability density functions (PDF) that would reflect the mixture of products in the syngas. Next, the main boundary conditions were defined, where WSP was the fuel input and air were the gasification agent. Finally, analysis and interpretation specified the post-processing technique.

1) Geometry construction

Geometry is the important, elementary part of the simulation (Abele & Fujara 2010). First, the geometry was generated based on an in-built downdraft gasifier reactor. The present work used the Design Modeler Programme (DMP) of the ANSYS Workbench 2021.1R2 to create the geometry domain. The 2D planner of geometry is shown in Figure 8.5.

| Reactor dimension (mm) | Geometry (2D Planner) |
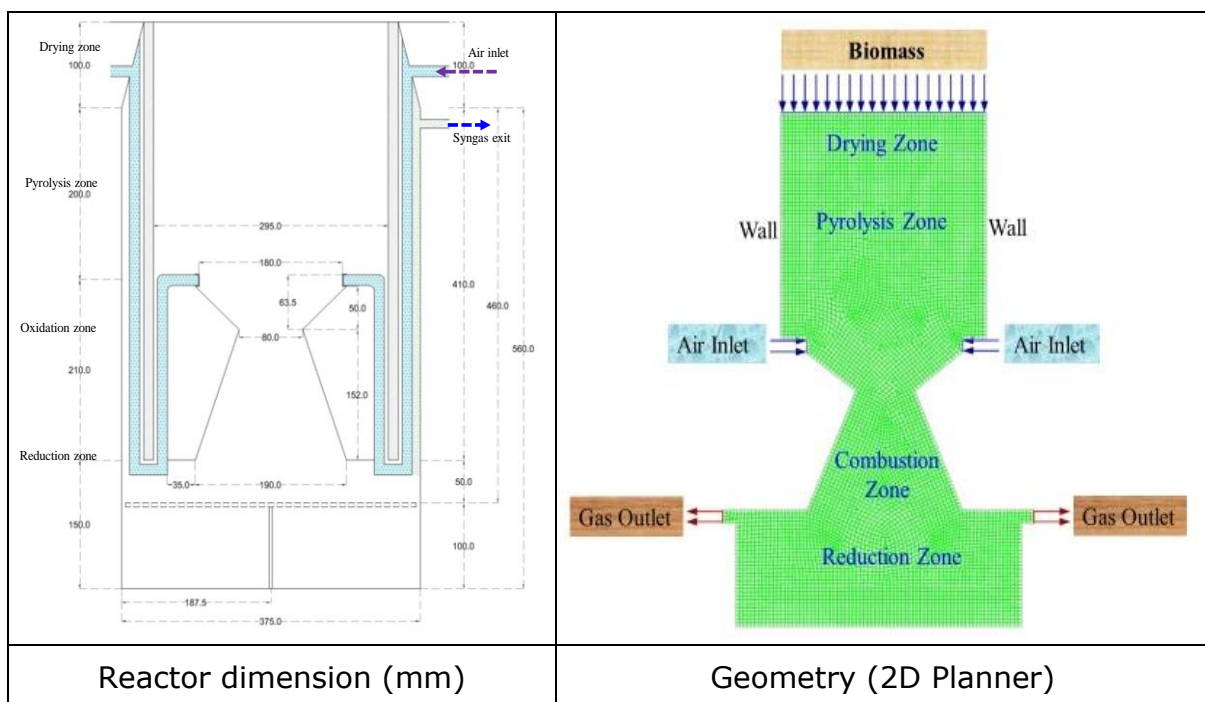
Figure 8.5: Reactor and 2D geometry

2) Mesh generation

High quality meshes are important for CFD simulation's accurate and fast convergence (ANSYS 2015). The ANSYS Meshing package was used to generate and optimise the mesh, where an unstructured grid was obtained using a global tool. A series of tests were applied to local sizing parameters to achieve good mesh quality. Figure 8.6 represents the generated model meshing.
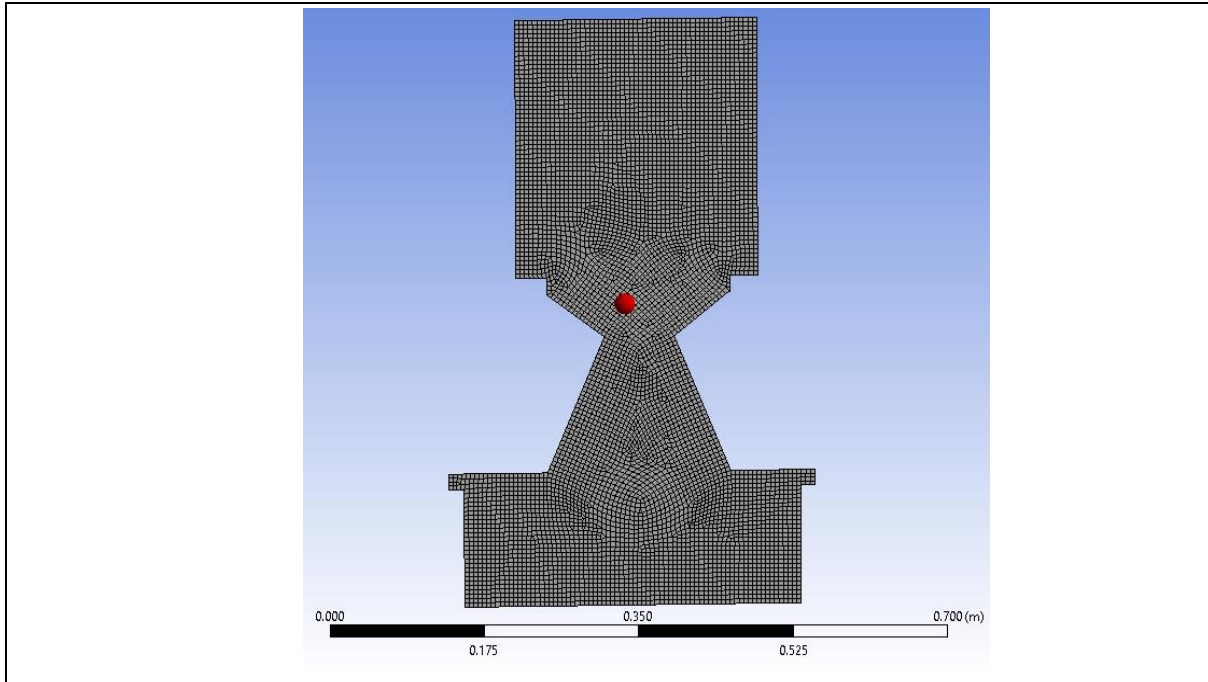
Figure 8.6: Mesh details of a 2D model: black represents the insulation

To choose the optimum mesh number, various mesh quality criteria were considered. Typically, two methods (orthogonal and skewness) were used to quantify the recommended mesh quality, ranging from 0 to 1 (Table 8.3). The skewness value, inversely related to solution accuracy, should be small enough to minimise error in the solution. Generally, it is recommended to keep the minimum orthogonal quality of >0.10 and maximum skewness <0.95. These values may differ depending on all cells' physics and location. In addition, if the mesh contains degenerated cells, the cell volumes might be negative.

Table 8.3: Recommended mesh metrics (ANSYS 2015)

Approaches	Excellent	Very good	Good	Acceptable	Bad	Unacceptable
Skewness	0.0~0.25	0.25~0.50	0.50~0.80	0.80~0.94	0.95~0.97	0.98~1.0
Orthogonal quality	0.95~1.0	0.70~0.95	0.2~0.69	0.15~0.20	0.001~0.14	0.0~0.001

Refinement is a technique better to capture the steep flow gradients in highly turbulent regions (Yang et al. 2019). Therefore, the mesh in the combustion, reduction, and air nozzle outlet areas was refined.

3) Model setting

- *Model selection*

During gasification, different types of physiochemical (decomposition) phenomena occurred. These decomposition factors were water release, volatile flammable gases release, heat conduction, fissuring,

shrinkage and the fragmentation of solid particles (Kumar, Jones & Hanna 2009). However, inside the reactor, the input biomass and air interacted with each other and followed various activities described in different models (Table 8.4). Also, the interaction between heat and particle mass occurred within the reactors and generated different chemical kinetic reactions specified by the governing equations.

Table 8.4: Represented (air, biomass and reactor) model during gasification

Components	Computational model
Biomass	- Discrete phase model (DPM) - $k\text{-}\varepsilon$ turbulence - P-1 for radiation model
Air	- Resistance flow - Turbulence flow model - Porous media model
Gasification	- Lagrangian discrete phase model - Turbulence-chemistry interaction model - Energy and species transport equations

- *Model simplifications*

Gasification involves several complex processes involving homogeneous and heterogeneous reactions. Therefore, some simplifications were made to create a suitable model for a downdraft gasifier. Generally, simplification depends on model intentions. An appropriate model optimises gasification parameters as well as saves time and cost to avoid the complexity of the operation, feedstock and equipment. The following general assumptions were made to simplify the model (Souza-Santos 2010; Janajreh & Al Shrah 2013; Gupta, Jain & Vyas 2017):

- Flow is symmetric, i.e., 2D
- Flow is a steady state
- Numerical calculations, the governing equations were nonlinear partial differential equations
- Reactor wall surfaces and separator/insulation bulk materials were at the no slip condition
- Chemical reactions were faster than the time scale of the turbulence eddies
- A discrete phase model was used to give the small particle size and compare it to the reactor volume
- All chemical reactions were considered to be in the inner shell of the gasifier
- Particles have uniform distribution and spherical shapes; however, the particle size is much smaller (0.1 mm)
- Oxidiser is an air.

8.3. Solution of model based equation

The ANSYS Fluent CFD software package uses in house C coding via a User Defined Function (UDF) (Barone & Martelli 2014). Therefore, the partial differential equations are easily transformed into a discrete form using CFD, solving the conservation equations. Also, CFD is based on a set of simultaneous calculations for governing equations and species conservation. However, Finite Element Method (FEM) can be used for discretisation, while ANSYS Fluent customises the Finite Volume Method (FVM) (Wu et al. 2022). A pressure velocity coupling technique is also employed to solve the governing equation.

8.3.1. Governing equation: pressure velocity coupling method

The CFD model incorporates governing equations with species transfer (fluid flow). The species were divided into two phases: gas (primary flow) and solid (secondary flow), which employed an Euler-Euler multiphase technique to solve the phases, including exchange terms (ANSYS 2018). The equations are also solved numerically under steady state and turbulent flow conditions with finite rate reaction kinetics (Pandey, Prajapati & Sheth 2021).

The Navier-Stokes equations, which describe fluid flow, can be written as follows using the tensor notation:

$$\frac{\partial(\rho\mu_i)}{\partial t} + \frac{\partial(\mu_i\mu_j)}{\partial x_i} = -\frac{\partial\rho}{\partial x_j} + \frac{\partial\tau_{ij}}{\partial x_i} + p\sum_{k=1}^{N} Y_k f_{kj} \quad \text{............................}8.1$$

Where: ρ = the density of the fluid mixture
t = time
p = pressure
$\mu_i\mu_j$ = the velocity components
τ_{ij} = the viscus stress tensor
Y_k = the mass fraction of species K in the fluid mixtures
f_{kj} = the volume force acting on species k in the j direction
$x_i\,x_j$ = the coordinates axes

To solve Equation 8.1, a further equation associated with the viscous stress tensor is required. Equation 8.2 can then be used to determine the stress tensor while assuming that the mixture is a Newtonian fluid (Valdés et al. 2020).

$$\tau_{ij} = -\frac{2}{3}\mu\frac{\partial u_k}{\partial x_k}\partial_{ij} + \mu\left(\frac{\partial\mu_i}{\partial x_j} + \frac{\partial\mu_j}{\partial x_i}\right) \text{..................................}8.2$$

Where: μ is the dynamic viscosity of the mixture and ∂_{ij} is the tensor unit

According to the rule of mass conservation, there cannot be any creation or destruction of mass. The overall mass and elemental compositions consequently follow the formula:

$$\frac{\partial \rho}{\partial t} + \frac{\partial(\rho \mu_i)}{\partial x_i} = 0 \quad \text{...} 8.3$$

The species' mass depends on the chemical reaction arising at a given time because thermochemical conversion involves several chemical processes. As a result, the mass conservation equation is rewritten as (Zawawi et al. 2018):

$$\frac{\partial(\rho Y_k)}{\partial t} + \frac{\partial}{\partial x_i}[\rho Y_k(\mu_i + V_{ki})] \quad \text{...................................} 8.4$$

Where: $V_{ki} =$ the *i*-component of the diffusion velocity of species *K*

$\omega_k =$ the reaction rate of species *k*

The empirical Arrhenius equation was determined using E_α and *lnA* input data can define reaction rates. The energy conservation equation is written as follows:

$$\frac{\partial(\rho e_t)}{\partial t} + \frac{\partial}{\partial x_i}(\rho \mu_i e_t) = -\frac{\partial q_i}{\partial x_i} + \frac{\partial}{\partial x_j}[(\tau_{ij} - \rho \delta_{ij})u_i] + \dot{Q} + \rho \sum_{k=1}^{N} Y_k f_{ki}(\mu_i + V_{ki}) \quad \text{......} 8.5$$

Whereas: $q_i =$ energy flux in the mixture

$e_t =$ total energy from chemical, potential and kinetic energies

$\dot{Q} =$ energy flux from the outer heating source

The mixture's energy flux can be defined as (Portarapillo et al. 2020)

$$q_i = -k\frac{\partial T}{\partial x_i} + \rho \sum_{k=1}^{N}(h_k Y_k V_{ki}) \quad \text{.......................................} 8.6$$

Heat conduction via Fourier's law is the first term on the right hand side, while energy flux via species diffusion in the mixture is the second term.

8.3.2. *Turbulence model*

Turbulence is caused by velocity, pressure, energy and mixture composition changes (Ngadi & Lahlaouti 2021). The governing equation divides each variable "*f*" into a time averaged value ($\bar{f}$) and a fluctuating component (f'):

$$f = \bar{f} + f'' \text{...} 8.7$$

Where: $f =$ Favre-average value variation

$\bar{f} =$ mass weighted average

$f'' =$ fluctuating component around the mean

When the velocity (u_i) used to replace the variables in the governing equations, the Reynolds decompositions for this are:

$$u_i = \bar{u}_\iota + u_i' \quad \text{...} 8.8$$

Whereas: $\mu_i =$ velocity

$\bar{u}_\iota =$ average velocity

$u_i' =$ fluctuating component of velocity

181

The Reynolds-averaged Navier-stokes equations (RANS) are produced by substituting the variable of the governing equation (Maia et al. 2022). The RANS equations are obtained by the Cartesian tensor (Equations 8.1).

$$\frac{\partial}{\partial t}(\rho u_i) + \frac{\partial}{\partial x_j}(\rho \mu_i u_j) = -\frac{\partial p}{\partial x_i} + \frac{\partial}{\partial x_j}[\mu(\frac{\partial u_i}{\partial x_j} + \frac{\partial u_j}{\partial x_i} - \frac{2}{3}\partial_{ij}\frac{\partial u_i}{\partial x_i}] + \frac{\partial}{\partial x_j}(-\rho\overline{u_i}\overline{u_j}) \dots\dots\dots8.9$$

The Reynolds stress $(-\rho\overline{u_i}\overline{u_j})$, is a characteristic of the turbulence model. ANSYS Fluent offers numerous estimates, including $k-\varepsilon$ models, $k-\omega$ models, and the Eddy Simulation Model. In industrial engineering, commonly used the standard $k-\varepsilon$ model based on turbulence kinetic energy (k) and dissipation rate (ε) model transport equations (Phapatarinan, Bumrungthaichaichan & Wattananusorn 2018). The theoretical handbook for ANSYS Fluent (ANSYS 2018) has more information on the equations of those turbulence models.

8.3.3.1. *Turbulence flow model: k-ε*

In this study, WSP fuel is stacked in a packed mode inside a downdraft reactor. The air passes through the pack bed fuel as a turbulent flow. In the gas phase, the standard k-ε turbulence model was applied. The kinetic turbulence energy (k) and its dissipation rate (ε) were obtained from the following equations (Lu et al. 2018).

$$\frac{\partial}{\partial x_i}(\rho k \mu_i) = \frac{\partial}{\partial x_j}\left[\left(\mu + \frac{\mu_t}{\sigma_k}\right)\frac{\partial k}{\partial x_j}\right] + G_k + G_b - \rho\varepsilon - Y_m + S_k \dots\dots\dots\dots\dots8.10$$

$$\frac{\partial}{\partial x_i}(\rho \varepsilon \mu_i) = \frac{\partial}{\partial x_j}\left[\left(\mu + \frac{\mu_t}{\sigma_\varepsilon}\right)\frac{\partial \varepsilon}{\partial x_j}\right] + C_{1\varepsilon}\frac{\varepsilon}{k}(G_k + C_{3\varepsilon}G_b) - C_{2\varepsilon}\rho\frac{\varepsilon^2}{k} + S_\varepsilon \dots\dots\dots\dots\dots8.11$$

Where: G_b = turbulence kinetic energy due to buoyancy
Y_m= fluctuation dilation in compressible turbulence
S_k= user defined source terms for k
S_ε= user defined source term for ϵ
σ_k= turbulent Prandtl numbers for k
σ_ε = turbulent Prandtl numbers for ϵ

G_k represents the production of kinetic turbulence energy, which is associated with the average velocity gradient, while μ_t is the Turbulence viscosity (or eddy) is obtained from the product of k and ε:

$$\mu_t = \rho C_\mu \frac{k^2}{\varepsilon} \dots\dots\dots\dots\dots\dots\dots\dots\dots\dots\dots\dots\dots\dots\dots\dots\dots\dots\dots8.12$$

The constants of the experimental model are equal to $C_{1\varepsilon}$ = 1:44, $C_{2\varepsilon}$ = 1:92, $C_{3\varepsilon}$ = 0:09, σ_k = 1:0, σ_ε=1:3 (Launder & Spalding 1972).

8.3.3. Turbulence-chemistry interaction model

Gas turbulence can induce chemical reactions to interact with one another. When the mass conservation (Equation 8.4) is considered, the balance equation for species k is as follows.

$$\frac{\partial(\bar{\rho}\tilde{Y}_k)}{\partial t} + \frac{\partial}{\partial x_i}\left(\bar{\rho}\tilde{\mu}_i\tilde{Y}_k\right) = -\frac{\partial}{\partial x_i}\left(\overline{V_{k,\iota}Y_k} + \bar{\rho}\widetilde{u_\iota''}\widetilde{Y_k''}\right) + \bar{\omega}_k \quad \ldots\ldots\ldots\ldots\ldots\ldots\ldots..8.13$$

Where: $\tilde{Y}_k$ = *the species k's average mass fraction*

The right-hand side of this equation has three key variables:
 (i) $\overline{V_{k,\iota}Y_k}$ = the diffusion variable in laminar flows
 (ii) $\bar{\rho}\widetilde{u_\iota''}\widetilde{Y_k''}$ = diffusion in turbulent flows
 (iii) $\bar{\omega}_k$ = the reaction rates

ANSYS Fluent uses an equation including the Schmidt number and turbulence viscosity to calculate turbulence mass diffusion. The ANSYS Fluent theory guide provides more detailed equations for mass diffusion by laminar and turbulent flow (ANSYS 2018).

One of the three models in ANSYS Fluent calculates the reaction rates $\bar{\omega}_k$ (Dahms 2018):

- Laminar finite-rate model
- Eddy-dissipation model
- Eddy-dissipation concept (EDC).

The Arrhenius kinetic expression determines the reaction rates in the laminar finite rate model, which ignores turbulence fluctuations. In comparison, the Eddy dissipation model proposes that reaction rates control by turbulence, allowing Arrhenius chemical kinetic computations to be avoided. In turbulence flames, detailed Arrhenius chemical kinetics can be added for EDC. These three models use only the mixture fraction (f) variable to describe chemistry. Statistical methods were required for mixture fraction models. A measure called mixture fraction variance, f'' is utilised to link the mixture fraction interaction with turbulence *(ANSYS 2015)*.

The mixture fraction obtained from a non-premixed combustion model is used in this study. These phenomena could be related to the downdraft gasification stage of combustion.

ANSYS Fluent has a template for non-premixed combustion computations that includes a coal calculator and can also be used with biomass as a fuel source. This possibility has been taken into account in this research and its calculations. The coal calculator has been used to calculate the source term for reacting particles using the biomass factors

(proximate and ultimate). The species mixes were determined using these parameters based on chemical reactions with an oxidiser preselected under thermodynamic equilibrium circumstances.

The PDF method is based on the relationship between three scalar variables: species fractions, density and temperature (Lipatnikov & Sabelnikov 2020). Fuel and oxidisers go through the reaction zone separately in non-premixed combustion. Thus, the local mass portion of the fuel stream that is burned and unburned for all species $i = 1…………..N$ is given by f (Equation 8.14). In chemical reactions, the technique also ensures that atomic elements are conserved. As a result, there is no source term in the governing transport equation (Keshtkar, Eslami & Jafarpur 2020). Thus, combustion is reduced to a simple mixing problem.

$$f_i = \frac{Z_i - Z_{i,ox}}{Z_{i,fuel} - Z_{i,ox}}$$ 8.14

Where: Z_i = element of mass fraction for i
ox = value at the oxidiser stream inlet
$fuel$ = value at the fuel stream inlet

The mixture fraction takes into account a simple combustion system with a fuel stream (F), an oxidant stream (O) and a product stream (P) (Schluckner et al. 2020). Therefore, it can be stated as follows under stoichiometric conditions:

$$F + rO \rightarrow (1 + r)P$$ 8.15

Where r is the air-to-fuel ratio on a mass basis or the equivalence ratio $\emptyset$ as (Otchere et al. 2020):

$$\emptyset = \frac{(fuel/air)_{actual}}{(fuel/air)_{stoichiometric}}$$ 8.16

Under non-premixed combustion, the mixture percentage permits the computation under the following conditions (http://www.ansys.fem.ir/ansys_fluent_tutorial.pdf):

- Stoichiometric condition: $\phi=1$
- Fuel-rich condition: $\phi>1$
- Fuel-lean conditions: $\phi<1$.

There are two types of flow in nature: adiabatic and nonadiabatic. Radiation, heat transfer through barriers and heat transfer to/from discrete phase particles are a few circumstances where the nonadiabatic is used (Rahn et al. 2018). Because heat transmission happens between the continuous and discrete phases, particle combustion is supplied from discrete phase particles, and nonadiabatic conditions apply. Therefore, the local thermochemical energy relates to f and H in nonadiabatic states. Figure 8.7 illustrates the system's logical model calculation (http://www.ansys.fem.ir/ansys_fluent_tutorial.pdf).
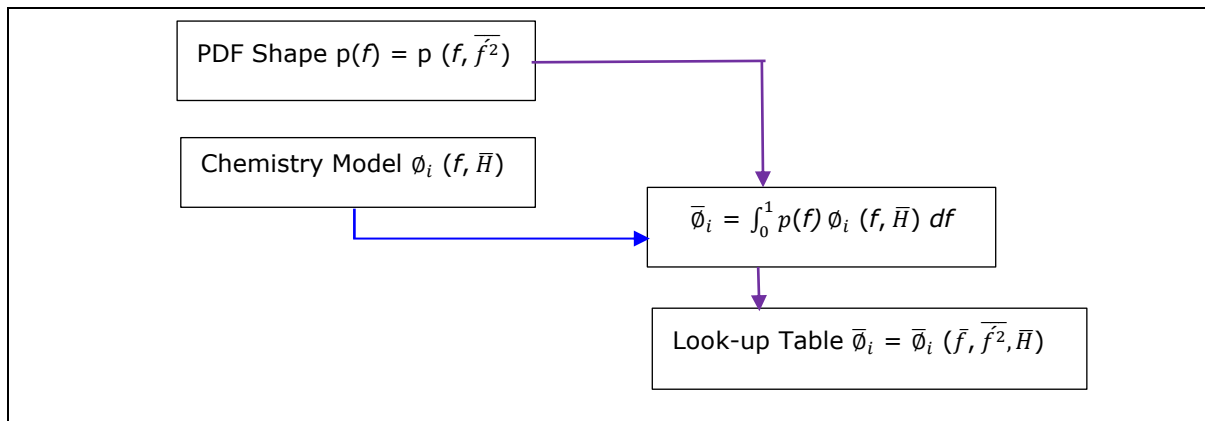
Figure 8.7: Logical dependence of Averaged Scalars

8.3.4. Energy and species transport equation

The species model is the best way to simulate biomass gasification, where chemical reactions are important. This model is also used to investigate the chemical reaction inside the gasifier while determining the composition of various species such as CO, CO_2, N_2, H_2 and CH_4 (Keshtkar, Eslami & Jafarpur 2020). Therefore, the species transport equations and the enthalpy formations can be used to compute the chemical reactions (Magnussen & Hjertager 1977).

Enthalpy, H = h + ΔH ……………………………………………………..*8.17*

$h = h_{ref} + \int_{T_{ref}}^{T} c_p dT$ …………………………………………..…………*8.18*

Species transport equation, $\frac{\partial}{\partial t}(\rho Y_i) + \nabla.(\rho \vec{\mu} Y_i) = -\nabla.\vec{J_i} + R_i + S_i$ ……*8.19*

Energy balance equation, $\rho C_p \frac{\partial T}{\partial t} = k\nabla^2 T + qv$ …………………..…………*8.20*

Where: h = sensible enthalpy
  ΔH = latent heat enthalpy
  h_{ref} = reference enthalpy
  T_{ref} = reference temperature
  C_p = specific heat at constant pressure
  R_i = net rate of production of species, i
  S_i = source term for the ith (x, y, z) momentum equation
  Y_i = species i's average mass fraction
  R_i = net rate of production of species "i" by chemical reaction

8.3.5. Particle combustion model

Euler-Lagrange and Euler-Euler approaches can solve particle interaction. While the Euler-Euler approach is multiphase, the Euler-Lagrange system is also known as the Discrete phase (Zhu et al. 2020). This study used the Discrete phase.

The WSP is converted into a gaseous product and ash in the gasification and combustion processes. The process occurs continuously, so the Discrete-Lagrangian phase was appropriate in this study.

During the combustion, the particle first reaches vaporisation temperature, where the non-volatile mass is less than the particle mass. In ANSYS Fluent, there are four devolatilisation models available (Zhang, J. et al. 2020):

(i) Constant rate model: The devolatilisation material follows a constant value linear rate
(ii) Single kinetic rate model: The kinetic rate input data requires a practical value of E_a and A to avoid heat effects
(iii) Two competing rates model (Kobayashi model): Regulates devolatilisation over two temperature ranges while needing two kinetic rates
(iv) Chemical percolation devolatilisation model: This model was designed for coal and is not utilised in this study.

The WSPs pyrolysis properties (Chapter 6) reveal that all created pellets undergo a multi-step reaction. As a result, the kinetic rate of devolatilisation was used rather than the constant rate. The WSPs' experiential data of E_α and A (Chapters 6 and 7) were used in the model to predict their decomposition rate. In comparison, the discrete Lagrangian approaches consist of various heat mass transfer calculation models. This work considered the particle force balance equation, heat balance equation and the devolatilisation law balance equation (Pandey, Prajapati & Sheth 2021).

- *Force balance equation*

$$\frac{\partial}{\partial t}(\vec{\mu}_\rho) = F_D(\vec{\mu} - \overrightarrow{\mu_\rho}) + \frac{\vec{g}(\rho_p - \rho)}{\rho_p}$$ *8.21*

Where $F_D(\vec{\mu} - \overrightarrow{\mu_\rho})$ is drag force per unit particle mass.

$$\text{Drag force } F_D = \frac{18\mu C_D R_e}{24\rho_p d^2{}_p}$$ *8.22*

- *Particle heat balance equation*

$$m_p C_p \frac{\partial T_p}{\partial t} = hA_p(T_\infty - T_p) + \varepsilon_p A_p \sigma(T^4{}_R - T^4{}_p)$$ *8.23*

- *Heat transfer during the devolatilisation process*

When the particle temperature reaches the vaporisation temperature (T_{vap}) then devolatilisation law is applied to the combusting particle mass (m_p) (Siripaiboon, Sarabhorn & Areeprasert 2020). It is written as:

$$m_p C_p \frac{\partial T_p}{\partial t} = hA_p\left(T - T_p\right) + \frac{\partial m_p}{\partial t} h_{fg} + \varepsilon_p A_p \sigma(T^4{}_R - T^4{}_p) \quad \text{...........................8.24}$$

$$-\frac{\partial m_p}{\partial t} = Ae^{-\left(\frac{E}{RT}\right)}\left[m_p - \left(1 - f_v{}^0\right)m_p{}^0\right] \text{...8.25}$$

Where: f_v = volatile fraction and $m^0{}_p$ = initial mass

The particle mass (m_p) has the effect of volatile particles. When the particle is non-volatile, the limit is exceeded.

- *Heat transfer during the char conversion process*

Convection, radiation and heat loss contribute to heat transfer to the particle during devolatilisation (Lian & Zhong 2022). It is written as:

$$m_p C_p \frac{\partial T_p}{\partial t} = hA_p\left(T_\infty - T_p\right) + f_h \frac{\partial m_p}{\partial t} h_{fg} + \varepsilon_p A_p \sigma(T^4{}_R - T^4{}_p) \text{.................8.26}$$

Where: C_p, h_{fg}, A and σ are specific heat, latent heat of evaporation, particle surface area and Stefan constant, respectively.

8.3.6. Radiation model

In the radiation model, the radiative conversion equation for position "*r*" in the direction "*s*" can be derived according to Habibi, Merci and Heynderickx (2007).

$$\frac{dI(\vec{r},\vec{s})}{ds} + (\alpha + \sigma_s)I(\vec{r},\vec{s}) = an^2\frac{\sigma T^4}{\pi} + \frac{\sigma_s}{4\pi}\int_0^{4\pi} I\left(\vec{r},\vec{s}'\right)\emptyset(\vec{s},\vec{s}')d\Omega' \text{...........8.27}$$

Where: $\vec{r}$ = position vector
$\vec{s}$ = direction vector
$\vec{s}'$ = scattering direction vector
S = path length
α = absorption coefficient
n = refractive index
σ_s = scattered coefficient
σ = Stefan-Boltzmann constant (5.669×10^{-8} W/m^2.K^4)
I = radiation intensity which depends on $\vec{r}$ and $\vec{s}$ direction
T = local temperature
$\emptyset$ = phase function
Ω' = solid angle

There were five common radiation models in ANSYS Fluent: the P-1 model, the Rosseland model, the Discrete ordinates model, the Discrete transfer model and the Surface-to-Surface Model (Gupta, Jain & Vyas 2017). The P-1 model typically works better in combustion applications with large optical thickness, complex geometries with curved coordinates and radiation heat transfer (Luan, Chyou & Wang 2013). The P-1 radiation

model is based on expanding the radiation intensity I into an orthogonal series of spherical harmonics (Siegel & Howell 1992). The radiation flux (q_r) is calculated based on the P-1 model, and the equation is (Wang & Yan 2008):

$$q_r = -\frac{1}{3(\alpha+\sigma_s)-C\sigma_s}\nabla G \quad\text{..}8.28$$

$$-\nabla q_r = \alpha G - 4\alpha\sigma T^4 \quad\text{...}8.29$$

Where: α = absorption coefficient,
σ_s = Stefan-Boltzmann constant,
G = incident radiation, and
C = linear-anisotropic phase function coefficient (ANSYS 2018).

8.4. Chemical Reaction model

Devolatilisation is the principal decomposition process during biomass gasification. However, devolatilisation involves homogeneous and heterogeneous approaches, including the chemical reaction model (Gupta, Jain & Vyas 2017). The reaction model undertakes downdraft gasification in four stages: drying, pyrolysis, combustion and reduction (Gerun et al. 2008). The feedstock pyrolysis rate was modelled using a straightforward one-step reaction model (Di Blasi & Branca 2013). On the other hand, the three primary oxidation zone reactions were considered (R_g2, R_g3 and R_s8, as shown in Table 8.5) for combustion. The oxidation and pyrolysis zones products were transformed into noncondensable gases in the reduction zone by both heterogeneous and homogeneous processes (R_g4, R_s5, R_s6, R_s7, R_s8 and R_s9, as shown in Table 8.5).

Table 8.5: Solid particle surface reactions (Di Blasi 2000)

Gas phase reactions		Solid particle surface reactions	
Reaction	Reaction order	Reaction	Reaction order
Volatile decomposition	R_g1	Char decomposition	R_s5
CO Combustion: $2CO + O_2 \rightarrow 2CO_2$	R_g2	$C_{(s)} + O_2 \rightarrow CO_2$	R_s6
H$_2$ Combustion: $2H_2 + O_2 \rightarrow 2H_2O$	R_g3	$C_{(s)} + O_2 \rightarrow 2CO$	R_s7
Water-gas shift: $CO + H_2O \rightarrow CO_2 + H_2$	R_g4	$C_{(s)} + 2H_2 \rightarrow CH_4$	R_s8
		$C_{(s)} + H_2O \rightarrow CO + H_2$	R_s9

8.4.1. Devolatilisation/volatile decomposed

During devolatilisation, the fuel chemical structure disintegrates and emits tars, hydrocarbons and gaseous components (H_2, CO, CH$_4$, CO$_2$ and light hydrocarbons). Finally, only residual porous materials (char) remain, consisting of carbon residue and inorganic compounds (ash) (Basu 2018). The biomass devolatilisation model is given:

$$Biomass \overset{k}{\rightarrow} Char\ (C_s) + Ash + Moisture + Volatile + Tar$$
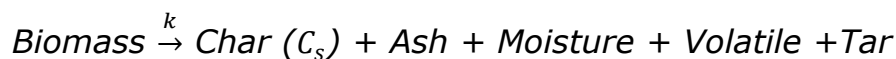
8.4.2. *Volatile reduction/release*

The volatile represented by $C_nH_mO_xN_yS_z$ is decomposed into gas components. Chemical reaction (R_g-1) holds a precise balance of heat and mass basis (Janajreh & Al Shrah 2013).

$$C_{0.84922}\,H_{2.0304}\,O_{1.04319}\,N_{0.01464}$$
$$\rightarrow 0.84922\,CO + 0.19397\,H_2O + 0.82123\,H_2 + 0.00732\,N_2$$
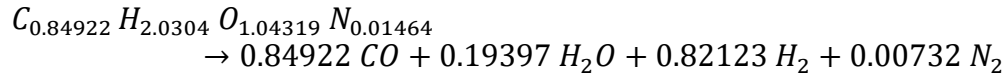
Devolatilisation reduction: $Volatile \rightarrow Gass_1(CO, CO_2, H_2, CH_4, \text{etc.})$

Char combustion: $Char \rightarrow Gass_2(CO, CO_2)$

The mathematical formula for biomass and volatiles was created based on proximate and ultimate analyses. The ANSYS (2018) designed scheme for species prediction was used and assumed that the volatiles elemental analysis distribution was CO, CH_4, H_2, H_2O, H_2S and tar.

8.4.3. *Gas phase reactions*

The finite rate (eddy dissipation) model accurately represents the interaction between chemistry and turbulence because there is a significant kinetics gap between the gas phase and solid particle reactions (Janajreh & Al Shrah 2013). The following global processes are considered for reactions: CO combustion (R_g2), H_2 combustion (R_g3) and water gas shift (R_g4) (Table 8.5).

8.4.4. *Particle surface reactions*

The combustion and gasification of biomass particles are modelled using a multiple surface reactions model. Char combustion and char reduction of CO_2, H_2 and H_2O were the considered reactions. Table 8.5 provides a summary of their kinetic data.

8.5. Boundary and operating conditions setup

This study set primary and secondary steps depending on the two phase flow pattern. The solid was identified as the primary and the gas as the secondary phase. The operating and boundary conditions were important to generate reliable simulations, where we first need to select the reaction phase.

The boundary and operating conditions for the gasification of WSPs in downdraft reactors were based on the experimental operations and literature data (Siripaiboon, Sarabhorn & Areeprasert 2020; Pandey, Prajapati & Sheth 2021). Table 8.6 summarises the operating conditions.

Table 8.6: Boundary and operating conditions

	Parameter	References
Gasification agent (air)	Air flow rate: 54 kg/h (37.87 Nm³/h)	-
	Air velocity: 3.2 ~7.2 m/s (average 5.2)	(Gupta, Jain & Vyas 2017)
	Air fuel ratio: 6:1 v/m	(Janajreh & Al Shrah 2013)
	Air inlet temperature: 300K	(Gupta, Jain & Vyas 2017)
Pressure	Gasification pressure: 1 atm = 101325 pascal	(Jahromi et al. 2021)
	Outlet gauge pressure: 0	(Siripaiboon, Sarabhorn & Areeprasert 2020)
	Pressure outlet: 249 Pa (min) and 747 Pa (max)	-
Biomass	Input: Biomass (WSP) inject (Gravity feed)	-
	Gravitational acceleration: - 9.8 m/s²	-
	Biomass inlet temperature: 300K	(Pandey, Prajapati & Sheth 2021)
	Biomass flow rate: 9 kg/hr	(Gupta, Jain & Vyas 2017)
	Biomass moisture content: 3.5%	-
Temperature	Temperature-Atmospheric condition: 300K	(Siripaiboon, Sarabhorn & Areeprasert 2020)
	Operating temperature: 300 ~ 2500K	-
Reactor wall	Motion: stationary	(Siripaiboon, Sarabhorn & Areeprasert 2020)
	Wall shear condition: No slip	
	Wall roughness: standard	
	Inlet species mass fraction of O_2: 0.23	(Siripaiboon, Sarabhorn & Areeprasert 2020)
	Inlet velocity magnitude: 0.056 m/s	-
	Wall (interior and exterior walls): Stainless steel	-
	Wall thickness: 3 mm	-
Others	Equivalence ratio: 0.2 ~ 0.6	(Zainal et al. 2002)
	Turbulence intensity: 5%	(Siripaiboon, Sarabhorn & Areeprasert 2020)
	Particle-specific heat: 2.5 kJ/kg.K	(Siripaiboon, Sarabhorn & Areeprasert 2020)
	Particle size in the discrete phase: 0.1 mm	(Pandey, Prajapati & Sheth 2021)
	Uniform porosity: 0.5	(Muilenburg, Shi & Ratner 2011)
	For simulation time setup: 10 s	(Siripaiboon, Sarabhorn & Areeprasert 2020)
	Model run: 0 to 7200 s	

8.6. Input data for simulations

The simulation input data were obtained from the experimental results and previous literature in Tables 8.6 and 8.7. First, the particle combustion of the pellet fuels was specified by ultimate and proximate analysis, which was done in Chapter 3. In biomass gasification modelling, the chemical reaction was set as an equilibrium to operate in non-adiabatic conditions. In addition, the devolatilisation temperature was taken from pyrolysis experiments during the devolatilisation rate (Table 8.6, pyrolysis

zone temperature). Also, the apparent density of the pellet was specified as the particle density and used in the material input. In addition, the shrinkage coefficient was 0.6 in a downdraft gasifier, estimated based on experimental results of empty fruit bunch pellets (Erlich & Fransson 2011). The ANSYS Fluent template used the swelling coefficient opposite the shrinkage coefficient.

Table 8.7: Summary of the model used for the WSPs gasification

	Parameters	Conditions/Assumptions
1	General	✓ Double precision: Two phase flow (gas and solid) simulation ✓ Solver type: Pressure based ✓ Velocity formulation: Absolute ✓ Steady state ✓ Axisymmetric/Planner ✓ Gravitational effect on biomass feeding
2	Radiation	P1: Radiation reflection at the surface is isotropic
3	Turbulence	$SST\ k\omega$-intermittency: Include the effect of share stress transport, kinetic and its dissipation rate and the change in velocity
4	Reactions	Nonpremix combustion-non-adiabatic
5	Particle interaction	Euler-Lagrange (discrete phase) Particle devolatilisation model: Single kinetic rate Particle combustion: Kinetic/diffusion-limited rate

In the downdraft gasification simulation, the air was injected from the side nozzle and defined as velocity (m/s). In comparison, the feedstock fuel mass was specified by distinct material that was injected from the top. The feedstock material pellet was cylindrical rather than spherical. Therefore, the equivalent diameter was determined by the pellet volume as follows (Erlich & Fransson 2011):

$$D_E = 2 * \sqrt[3]{\frac{3}{4\pi} V_p} \quad\text{...}8.30$$

Where: D_E = Particle diameter (m)
V_p = Average volume of a particle (m^3)

The equivalence ratio (*ER*) is the proportion of the gasification model (AF_{model}) air-to-fuel ratio to the stoichiometric air-fuel ratio for complete combustion ($AF_{stoichiometric}$) (Hwang et al. 2021).

$$ER = \frac{Actual\ air\ to\ biomass\ ratio}{Stoichiometric\ air\ to\ biomass\ ratio} = \frac{AF_{model}}{AF_{stoichiometric}} \quad\text{...............}8.31$$

The $AF_{stoichiometric}$ can be calculated based on the empirical formula, which is based on the ultimate fuel analysis data.

$$CH_hO_oN_n + kO_2 \rightarrow CO_2 + \frac{h}{2}H_2O + \frac{n}{2}N_2 \quad\text{.................................}8.32$$

191
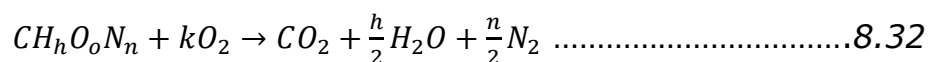
$$k = \frac{h}{4} + 1 - \frac{O}{2} \quad \text{...8.33}$$

Where: k = number of moles of oxygen for complete combustion
h = mole fraction of hydrogen in fuel
O = mole fraction of oxygen in fuel

In gasification, air was used as the oxidising agent to provide oxygen, with a mole ratio of 4.76 of air to oxygen (Barco-Burgos et al. 2021). The stoichiometric air-to-fuel ratio ($AF_{stoichiometric}$) can determine as follows:

$$\text{Stoichiometric air-to-fuel ratio } (\frac{A}{AF_{stoichiometric}}) = \frac{4.76 * k * mw_{ox}}{mw_{fuel}} \quad \text{.................8.34}$$

Where: k = the number of moles of oxygen for complete combustion
mw_{ox} = molecular weight of oxygen in the air, g/mol
mw_{fuel} = molecular weight of fuel, g/mol

The primary characteristics of the current model and gasification reactor are outlined in Table 8.7. The reactor wall was stationary with no slip conditions, while the gasifier wall was set at consistent values. The air opening temperature was adjusted to nearly oxidise the bed's temperature (ANSYS 2015). In reality, the crawling generated gas warms the air pipe before it leaves the fuel bed.

8.7. Numerical calculation

There are two approaches within an ANSYS Fluent solver programme: pressure and density based. This study used the pressure-based technique as the default solver in the non-premix combustion model (Table 8.8) (ANSYS 2019).

Table 8.8: Particulars of model solver

Variable	Discretisation Scheme	Information
Pressure staggering option	PRESTO!	Pressure based Navier-Stokes solution algorithm (the default)
Pressure velocity coupling	SIMPLE	Governing equation
Gradient option	Least Squares Cell based	-
Pressure	Second Order Upwind	Spatial discretisation
Momentum	Second Order Upwind	Spatial discretisation
Turbulent Kinetic Energy	Second Order Upwind	Spatial discretisation
Energy	Second Order Upwind	Spatial discretisation
Mean mixture fraction	First Order Upwind	Spatial discretisation
Mixture fraction variance	Second Order Upwind	Spatial discretisation
Soot	Second Order Upwind	Spatial discretisation
Others	First order Upwind	-
Discrete ordinates	Second Order Upwind	Spatial discretisation
Formulation	Implicit	-
Velocity formulation	Absolute	default setting
Porous formulation	Superficial velocity	-
Initialisation	Hybrid	-

Two pressure-based solver techniques that are accessible in ANSYS fluent is the segregated and coupled algorithms. As a result, convergence was improved and reached convergence much faster in the separated algorithm. On the other hand, the separated algorithm takes nearly twice as much memory as the segregated method. A SIMPLE pressure velocity coupling was applied to work out the equations in this model, which uses a coupled algorithm technique (Table 8.8).

8.8. Results and discussion

8.8.1. Grid sensitivity analysis

A grid dependency/sensitivity test was conducted to determine optimum mesh elements (Pandey, Prajapati & Sheth 2021). This test allows the evaluation of the influence of the mesh density on the simulation results and helps to estimate the consumption of computational resources (Yepes Maya et al. 2021). Typically, tetrahedron and hexahedral mesh could be produced using ANSYS Fluent. In this study, the hexahedral mesh was created, providing better quality mesh and faster computation times.

Five different computational grid sets were generated with 5000, 10000, 25000, 50000 and 100000 cells for the dependency test. For the grid generation, the test assumed only one boundary condition. The initial conditions considered the gasifier interior a porous medium without chemical reaction. The air was a gasification agent with a mass flow of 54 kg/hr and a pressure outlet to compensate for the boundary condition (Table 8.6). The grid dependency test was based on the velocity measurements in different reactor planes. Figure 8.8 shows velocity distribution along the reactor at 660 mm from the top for five other mesh elements. As shown in Figure 8.9, all mesh cells followed the same trend, where velocity increased with the shifted position.
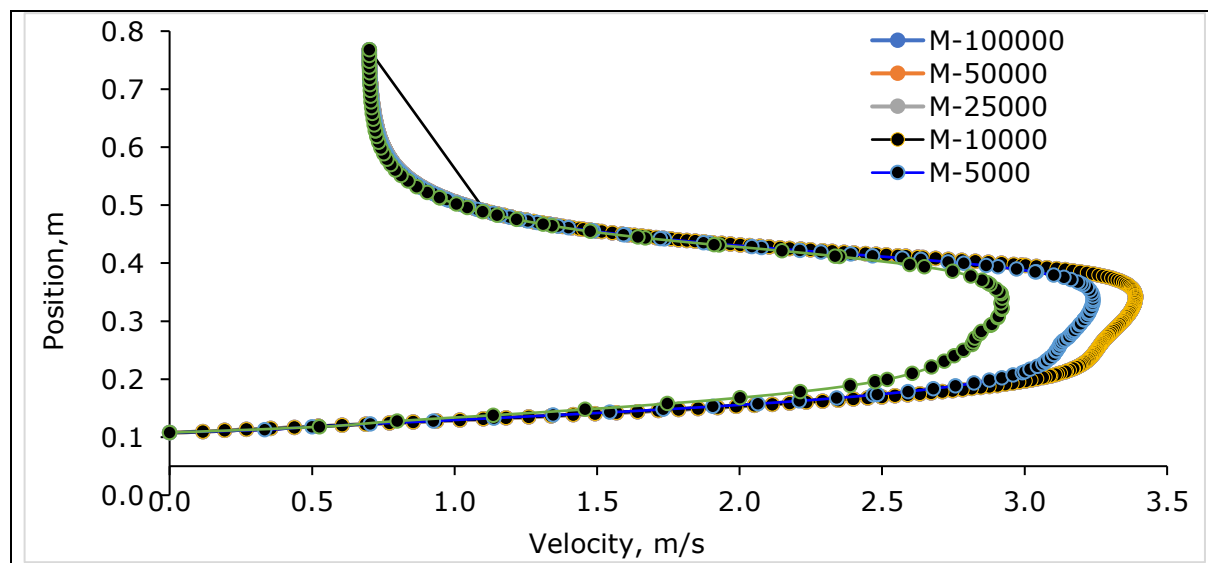
Figure 8.8: Relation between velocity and vertical position of reactor regarding mesh elements

Figure 8.9 shows a minor velocity difference between 25000 and 50000 mesh cells which was less than 2% on average. It can be seen that there was no significant change in the velocity when the mesh number increased beyond 50000. Therefore, the optimum number of mesh elements was considered to be 50000, representing the gasification phenomena with the best combination (Murugan & Sekhar 2017). Hence, all simulations were performed with these mesh cells, and the mesh statistics were:

- Mesh element size (average):1 mm
- No of nodes: 172677
- No of elements: 171558 with a rectangular shape
- Minimum orthogonal quality: 0.38916
- Maximum aspect ratio: 5.27929.
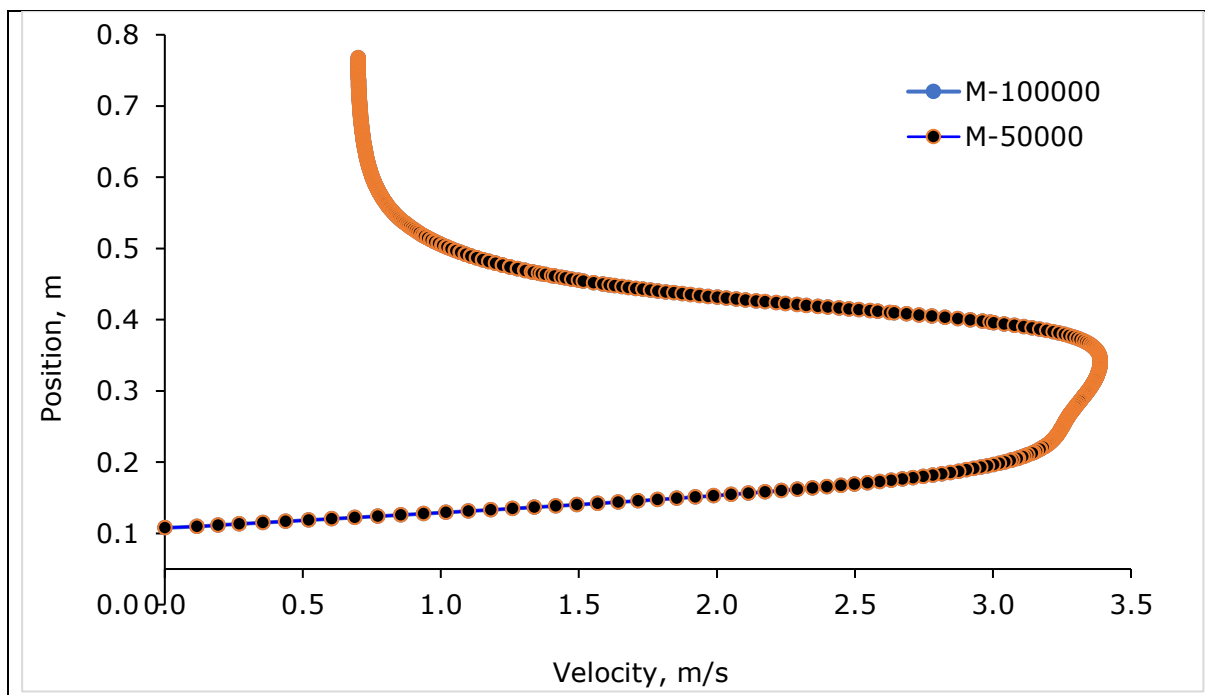
Figure 8.9: Velocity comparison between the grid cells

8.8.2. Model validation and comparison

Validation of the developed model is necessary to assess accuracy. Several researchers have validated the model with experimental data and published results. This study considered experimental data for model validation.

8.8.2.1. Experimental details on macadamia shell gasification

Due to time limitations, a WSP gasification experiment was not conducted to validate the model in this study. Instead, previous data from a gasification experiment using the macadamia shell was considered (Elita 2018). The experiment was done in a GEK 10 kW downdraft gasifier

(http://www.allpowerlabs.com) at UniSQ, Australia. The CFD model was created for the same gasifier reactor. The model can use various fuels; users must input the fuel (feedstock) property data.

The experiment results were used to validate the model by looking at the temperature in the combustion zone and the gas composition. Two thermocouples were used to record the reactor inside bed temperatures. The T_{red} was positioned in the higher portion of the reactor concentric space to represent the temperature of the combustion zone. The thermocouple T_{bred} was placed in the lower part of the concentric space to represent the temperature of the reduction zone. Also, an online gas infrared analyser was mounted to the gas output pipe to monitor CO, CO_2 and total hydrocarbon contents (HC).

The gas composition and temperature data are shown in Figure 8.10. After 70 minutes of gasification running time, the experiment reached a stable state. After that, the combustion zone (Tred) temperature was around 1200~1250 K, and the reduction zone (T_{bred}) temperature was about 1000~1083 K. On the other hand, at a steady state operation, the obtained gas was approximately 9% CO_2 and 23% CO (Figure 8.10).
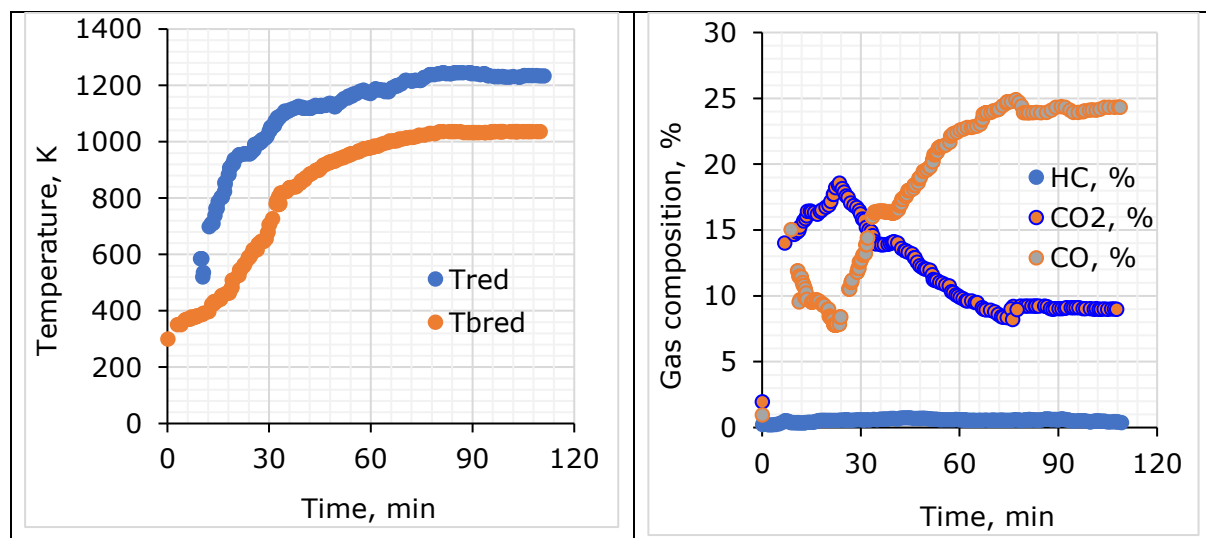
*Figure 8.10: Experiment of macadamia shell gasification (*Elita 2018*)*

In the CFD model for macadamia shell, the data from a previous study was taken (Vhathvarothai et al., 2014b; Vhathvarothai et al., 2014a). The model simulation used the air/fuel ratio of 1.3 (v/m) and equivalence ratio (ER) = 0.25. Also, pyrolysis and combustion TGA's pre-exponential factor and activation energy were considered for simulation (Elita 2018).

Figure 8.11 displays the simulation's output in the reactor's vertical iso surface at *Y=1.5* mm. The iso-surface was built near the central axis of symmetry. The baseline temperature was 1413.22 k.
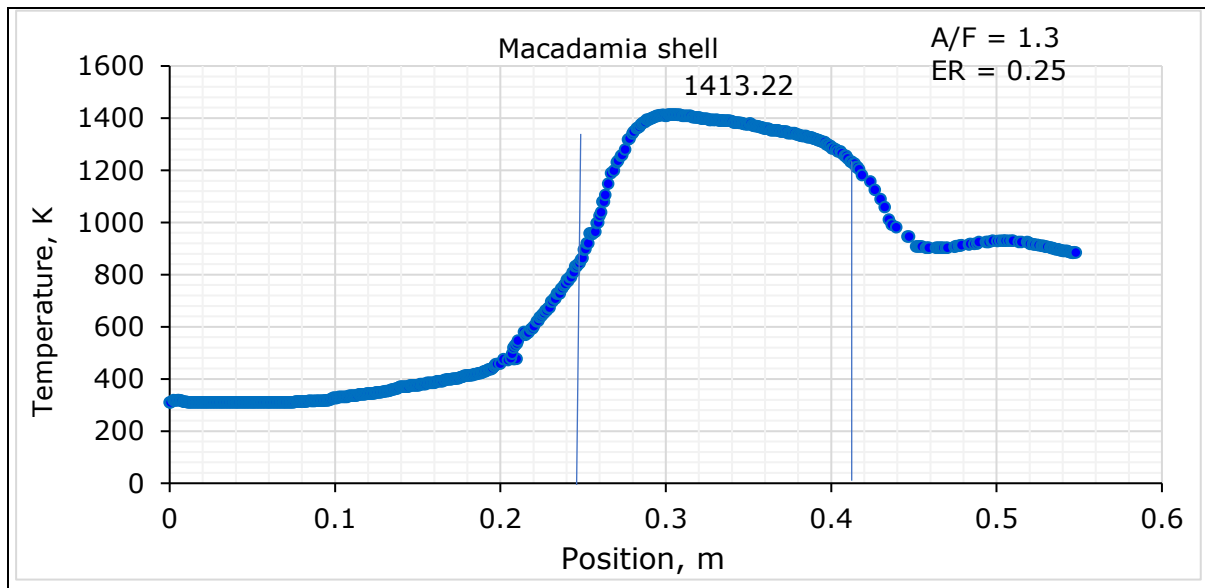
Figure 8.11: Iso-surface of the temperature of CFD model results for macadamia shell gasification

The outline of the experimental data and the modelling result are presented in Table 8.9. The simulated temperature and gas species volume was similar to the experimental measurements. The values of CO_2 and CH_4 were slightly overvalued, whereas the CO concentration was relatively underestimated. However, the high concentration of hydrogen prediction remained unknown. Overall, the simulations fit satisfactorily with the previous experimental data regarding temperature patterns and gas composition. Therefore, the accuracy of this model was acceptable.

Table 8.9: Result comparison: CFD gasification model and macadamia shell gasification

Particulars		Results	
		Model	Experiments
Temperature (k)	Combustion (Upper concentric at x = 0.25 to 0.3 m)	900~1413	1250
	Reduction (Bottom reduction at x = 0.425 m)	1100	1080
Gas species (% v/v)	CO_2	9.99	9.4
	CO	21.60	23.3
	CH_4	0.13	0.051
	H_2	16.81	N/A

8.8.3. Prediction profile and gas distribution

In gasification, biomass initially moves into the pyrolysis zone and enters the combustion zone (Figure 8.12). The combustion zone reaches the neck of the concentric area from beneath the air inlet. Finally, the pressure outlet releases the gas while the remaining particle (char and ash) passes down the grate. These residual char and ash further participate in oxidation and reduction processes (Pandey, Prajapati & Sheth 2021).
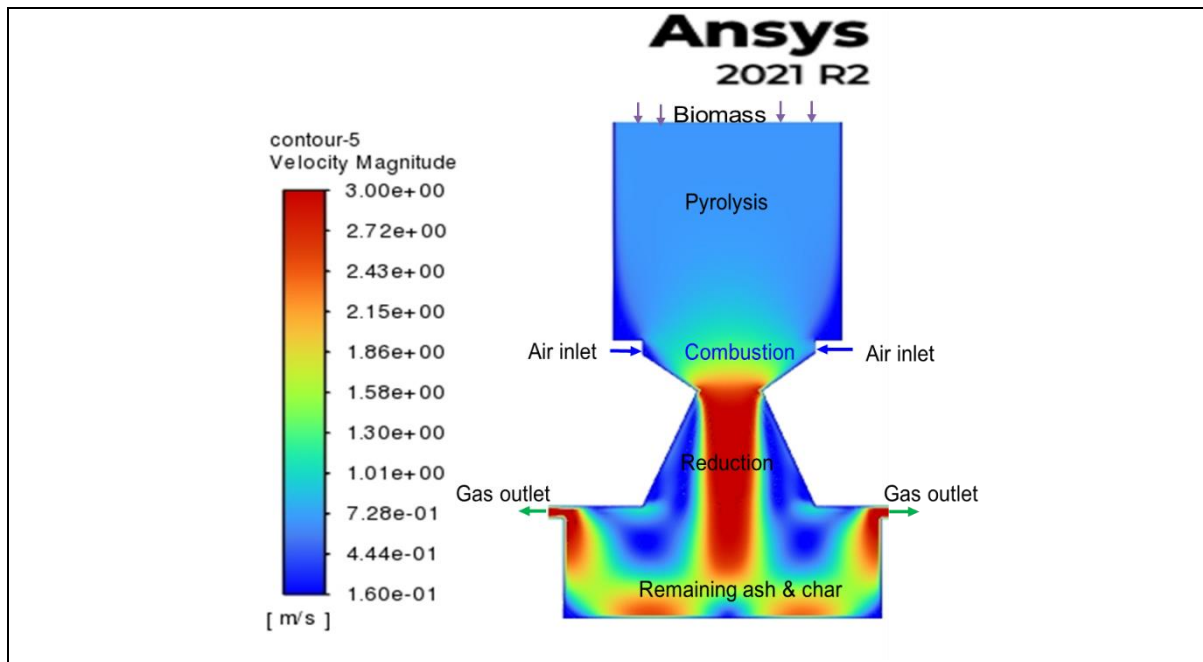
Figure 8.12: Model interpretation of velocity contour

The input biomass initiates the gasification process, producing syngas, which are then distributed throughout the gasifier. As the biomass enters the gasifier, it undergoes thermal decomposition, breaking down into volatile and char. According to the volatile disintegration scheme, volatile decomposes into CO, H_2, CH_4, CO_2 and H_2O. When released, volatile (CO, H_2 and CH_4) meet oxygen, it reacts with it and produces CO_2 and H_2O. But, not all the CO, H_2 and CH_4 participated in the oxidation reactions due to the regulated oxygen supply. Devolatilization also has char which reacts with O_2, CO, CO_2, H_2O and H_2 gas species. Char reaction (heterogeneous reaction) with oxygen is not as effective as CO, H_2 and CH_4 because a homogeneous reaction is far faster than a heterogeneous one. However, char reactions with CO_2 and H_2O significantly contribute to CO and H_2 production.

- Velocity profile

According to the velocity profile pattern, the fastest velocity particles (Figure 8.12) occurred in the central zone of the concentric area. This happened because the middle concentric area had a higher particle velocity. In contrast, the lowest velocity particles appeared in the devolatilisation (pyrolysis) zone. The middle of the pyrolysis zone has a slightly brighter blue colour indicating low velocity in this zone. The maximum turbulence influenced particle velocities inside the reduction zone in the concentric centre. So, particles in the centre moved faster than those along the wall. This demonstrates that particles introduced into the gasifier from the centre moved more quickly than those in the sides closer to it. The particle velocity variation inside the reactor was 0.16 to 3 m/s.

- Temperature profile

Figure 8.13 shows the reactor's temperature distributions for the vertical sections. In the vertical section of the reactor, temperature distribution was not uniform due to the uneven fluid field. Also, the air inlet and gas outlet were geometrically symmetrical, but the reactor shape was irregular.
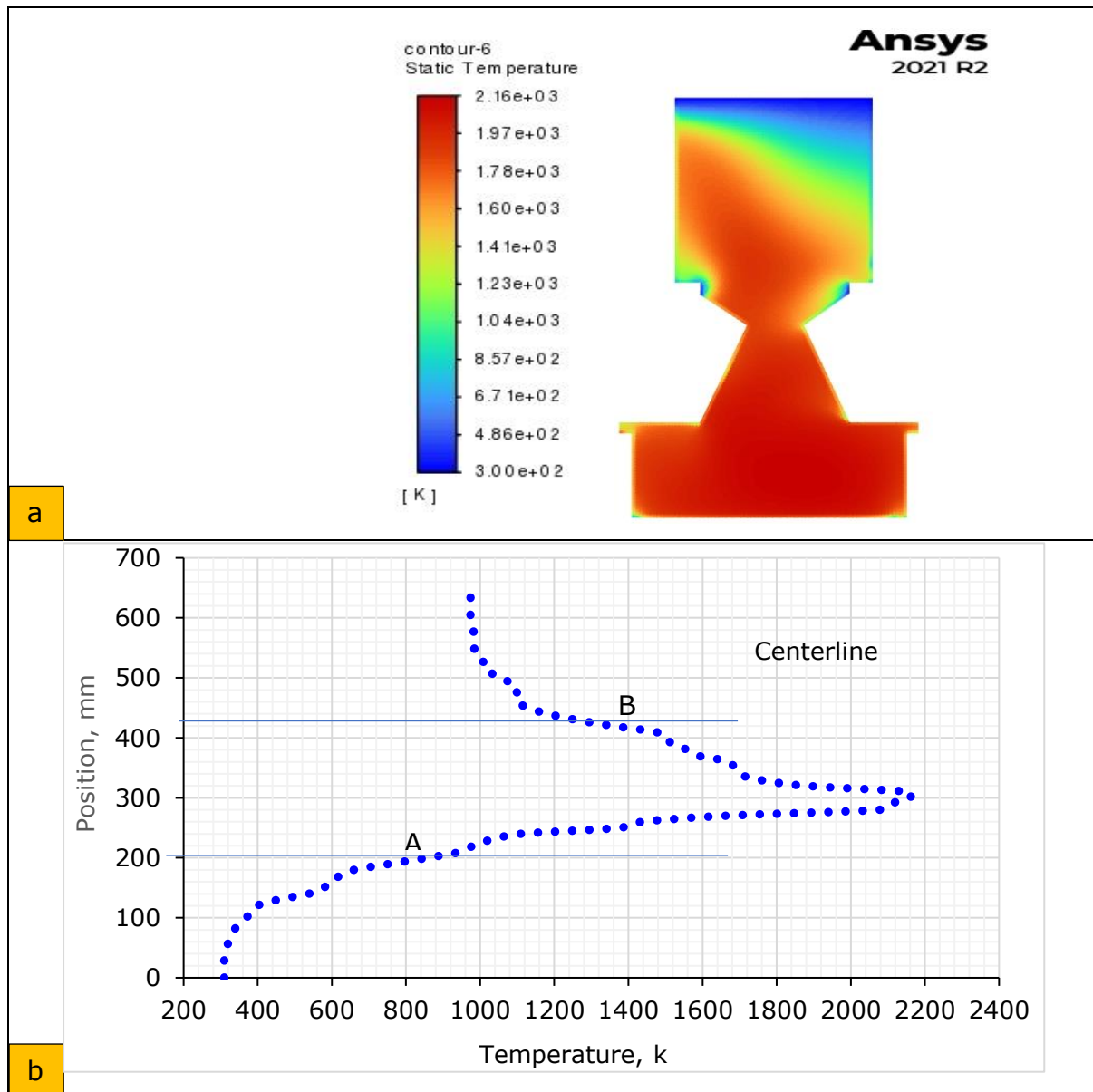
Figure 8.13: Temperature profile: (a) Contour and (b) Centreline

The non-premix combustion technique was used in the developed model as the source term for the reacting particle particles. It applied the area of the diffusive flame where the highest fuel oxidiser mixture turbulence occurred. The mixture fraction was the hottest in this area, while temperature increased with the shortest distance from the flame. Therefore, a rich flame region results from the highest fuel oxidiser mixture

during gasification. A central line was selected along the bed to assess the temperature profile and measure the temperature differential inside the reactor (Figure 8.13).

Figure 8.13 depicts a specific instance of a temperature curve. The flame was dark yellow across the combustion and reduction zone. The particle within the flame varied with temperature and found rich flames even though they existed in the combustion zone. The flame temperature was around 2100K (1827°C) in both the reduction and combustion zone. The cooler area was the pyrolysis area corresponding to the devolatilisation beginning temperature, which was 400~750K (117~470°C) (Janajreh & Al Shrah 2013). The present study results were similar to Gerun et al. (2008). They established a 2D axisymmetric CFD model for the oxidation zone in a downdraft gasifier.

Figure 8.13b presents the centreline temperature inside the reactor, where point A represents the ends of the pyrolysis zone and B is the end point of the combustion zone. Table 8.10 shows that the maximum temperature occurred in the combustion zone due to the exothermic reaction starting (Fang et al. 2021). In contrast, a lower temperature observed in drying and pyrolysis varied from 300 to 856 K because of an endothermic reaction. Similarly, the endothermic reaction also occurred in the bottom zone (reduction zone) (Li et al. 2019). Janajreh and Al Shrah (2013) studied a diverse model (the Species Transport Reaction model) for the same design as our gasifier. They reported a reduction temperature of 1273K, similar to the present study results.

Table 8.10: CFD simulation temperature at air-fuel ratio 6:1 and ER =0.35

Zone	Temperature range, k
Drying and pyrolysis	300~856
Combustion	856~1356 (Max temp. 2160)
Reduction	1356~974

- *Model limitation for temperature*

This model's limitation was that it could not forecast the temperatures in the middle area of the ash residue (under the grate) and the pressure outlet zone (Figure 8.13). The flame and predicted temperature in the char ash residual area (beneath the grate) indicated that further reaction may occur. This would cause the temperature of the gas crawling area (located beneath the pressure exit) to rise dramatically. However, in actual situations, the char and ash are automatically removed from the gasifier, but this model could not simulate this feature.

The current model's further weakness was that continuous burning projected high turbulence in the gas crawling space, resulting in high turbulence. In real situations, this did not happen. Instead, the vacuum

pump sucked the gas products with a moderate temperature of <600k, which was the model prediction of over 1273K.

- Gas density profile

As previously mentioned, this model applied the PDF, which depends on a scalar parameter called the mixing fraction to particle density. This density was the fraction of unburned fuel to the mixture species. The density of unburned fuel would be lower in areas of high turbulence, referred to as high temperature circumstances, than in regions with low turbulence.

According to this theory, the flame has the lowest density and the most turbulence, while the denser particles could move near the wall. Figure 8.14 displays the density contour (a) and centreline mass fraction (b) of the pellet during gasification simulation.
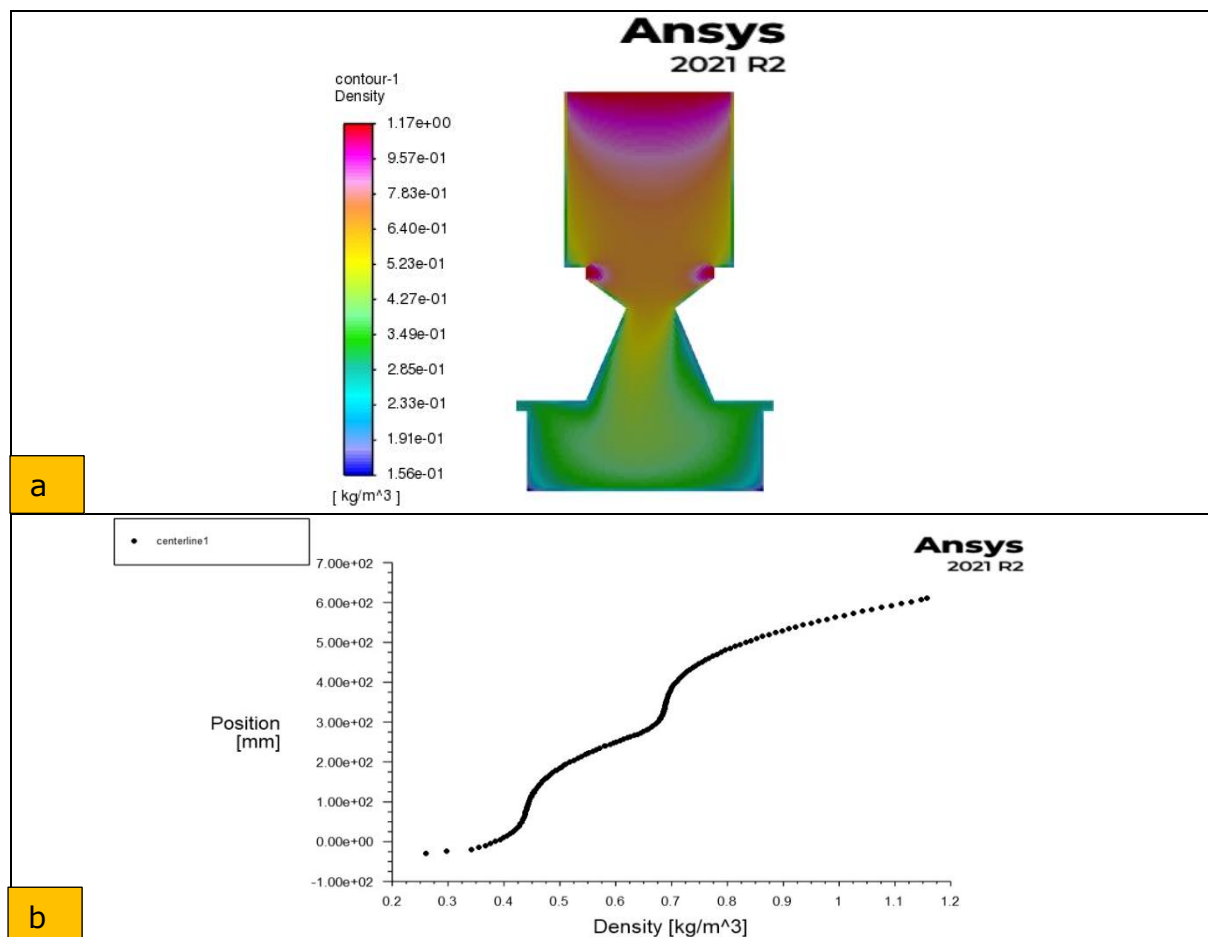
Figure 8.14: Density profile: (a) Contour and (b) Centreline

The mass fraction of solid particles was higher in the pyrolysis zone (dark yellow) than in reduction and char reason (yellow colour). However, the outer wall belongs to the maximum unburned carbon portion. The unburnt carbon mass fraction gradually dropped when reaching the

concentric space. The particle density varied inside the reactor from 0.156 to 1.17 kg/m^3 (Figure 8.14). This result was similar to the coal gasification model study by Patel et al. (2013), which used a comparable non-premix combustion model for the chemical processes.

Janajreh and Al Shrah (2013) developed a CFD model for the downdraft gasifier with a larger capacity with species transport approaches. They reported that the char content was drastically reduced right after the combustion zone and continued to the bottom of the gasifier. They also found a similar trend for unburned carbon profiles, although they employed a different approach to modelling reactions than this study.

- *Pressure profile*

The pressure profile contour presents pressure distribution within the downdraft gasifier inner shell at desired operating conditions (Figure 8.15). The gasifier works at atmospheric pressure, but the gasifier's static pressure changes with the height due to generating a gaseous combustion product. Static pressure varied between 0.766 to 3.53 Pa with the height of the gasifier.
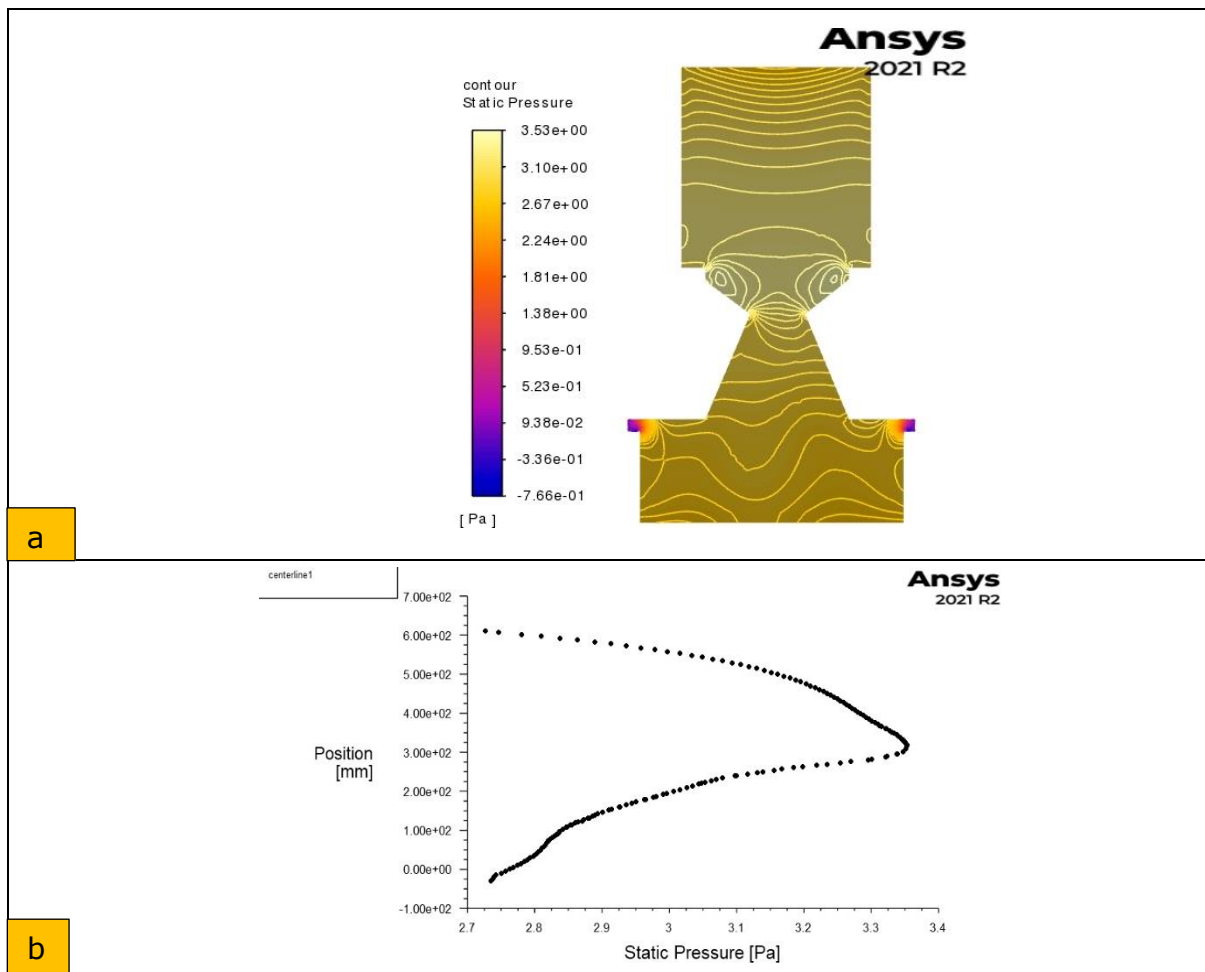
Figure 8.15: Static pressure profile: (a) Contour and (b) Centreline

- Turbulence of Kinetic Energy

The centreline pressure distribution is shown in Figure 8.15b. The pressure in the biomass input (660 mm height from the bottom) was low while biomass went down into the reactor; it increased and reached 2.75 Pa at the bottom. Lastly, the generated gas was released through the outlet with decreased pressure. Therefore, the pressure varied with the gasifier heights, which agrees with Gupta, Jain and Vyas (2017). They modelled a 10 kWE biomass downdraft gasifier for woody biomass for 2D simulation.

Kinetic energy turbulence and flow velocity are shown in Figure 8.16. Inside the reactor, the direction and mechanism of the kinetic energy were very complex. The maximum turbulence was 1.11 m^2/s^2 in the gas outlet area (red colour). Also, the centreline (Figure 8.16b) represents the movement of biomass, increasing the kinetic energy turbulent.
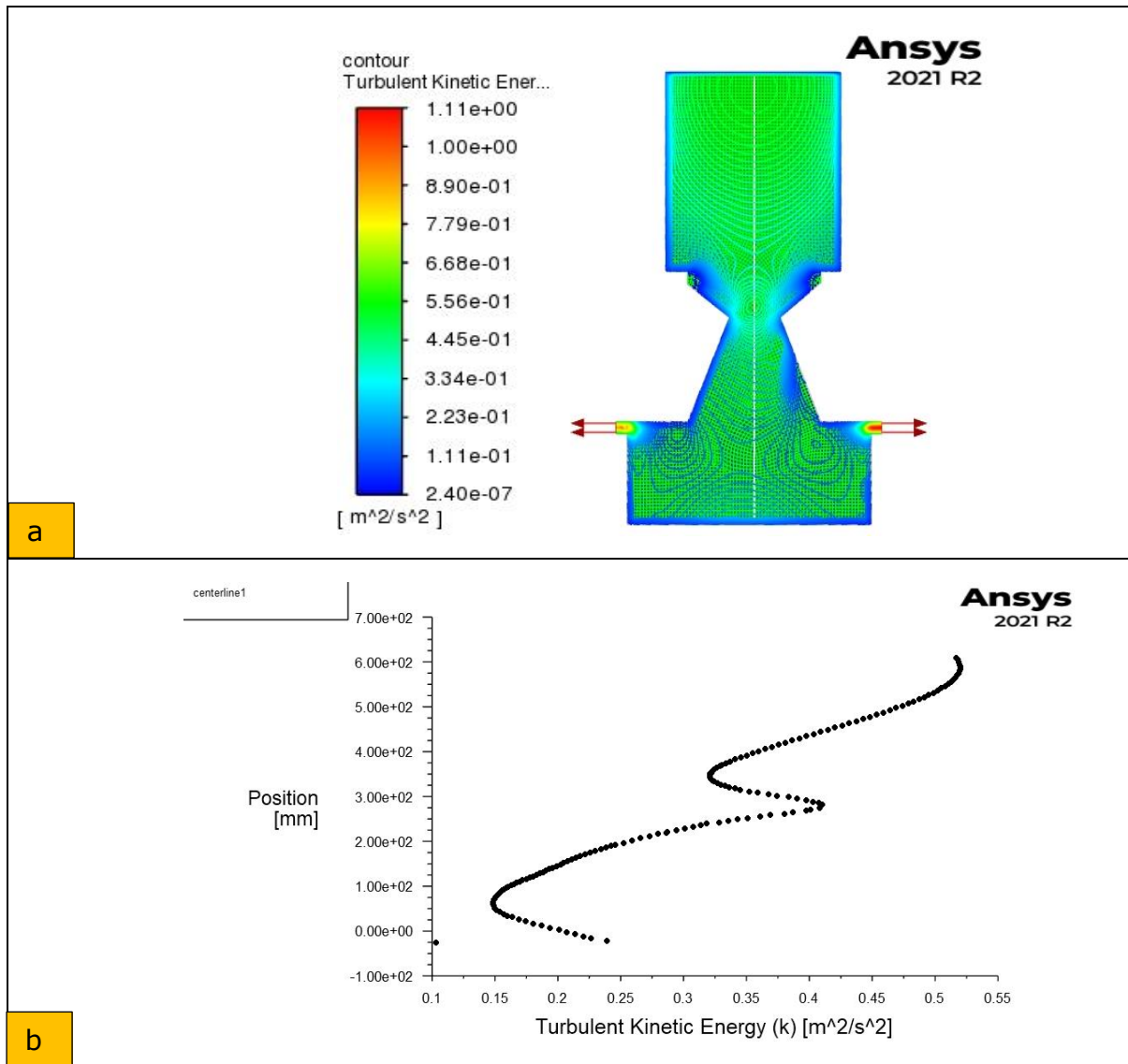
Figure 8.16: Turbulent kinetic energy profile: (a) Contour and (b) Centreline

- *Gas species profile*

A complicated chemical process in biomass gasification produced three fractions: light gases, ashes (chars) and condensates. Gas fraction distributions inside the downdraft gasifier at fixed ER (0.35) are shown in Figure 8.17 and 8.18. The most significant fraction was light gases amounting to more than 70% (w), consisting of CO, H_2, CH_4, CO_2 and N_2 (Monteiro et al. 2017).

- *CO_2 and O_2 profile*

The CO_2 and O_2 contours from a simulation of WSP (T_5) gasification are shown in Figure 8.17. As can be seen, a marginally higher CO_2 level was found in the pyrolysis region, and it peaked in the flame zone region. In comparison, O_2 was shown near the flash combustion zone and increased at the bottom of the reduction zone. The mole or volume fraction of O_2 was at its highest point near the air inlet (red colour), whereas CO_2 was lowest for the same reason. Also, the burning of some volatiles resulted in the creation of CO_2.

In contrast, the consumption of O_2 at higher regions in the gasifier provided the heat required for the endothermic processes. This forecast might be accurate for the downdraft gasification process employing air as the oxidant agent. The behaviour of CO_2 and O_2 contours was similar, but the concentration was dissimilar. These results agree with the literature of Zhou et al. (2005).
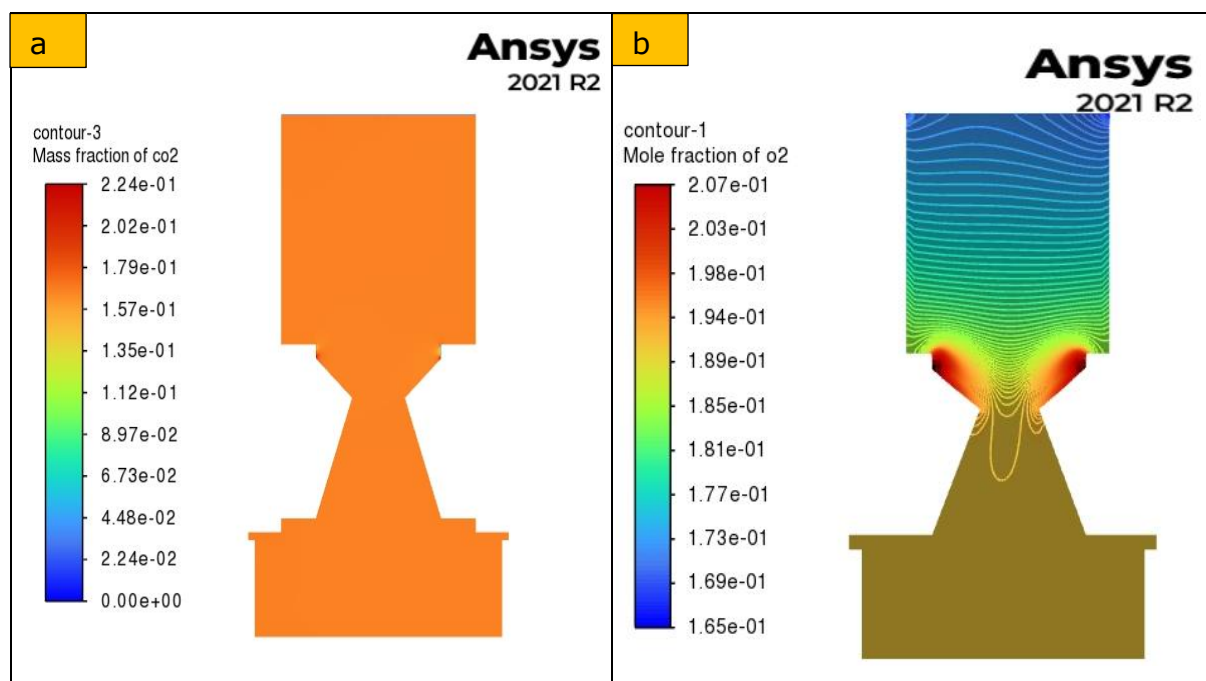
Figure 8.17: Gas species contour: (a) CO_2 and (b) O_2 mole fraction

- *H_2O and N_2 mole fraction profile*

The H_2O and N_2 contours are shown in Figure 8.18. In both profiles, the concentration was higher at the bottom of the gasifier. The H_2O mole fraction inside the reactor was almost similar. In comparison, the N_2 movement was significantly higher (about 0.82%) in the pyrolysis zone. Air entered by the air inlet where the N_2 concentration was lower (Figure 8.18). Janajreh and Al Shrah (2013) reported that N_2 concentration was 25.76% for nonadiabatic and 37.29% for adiabatic equilibrium reactions. The present study results were higher, possibly due to using different feedstock (WSP).
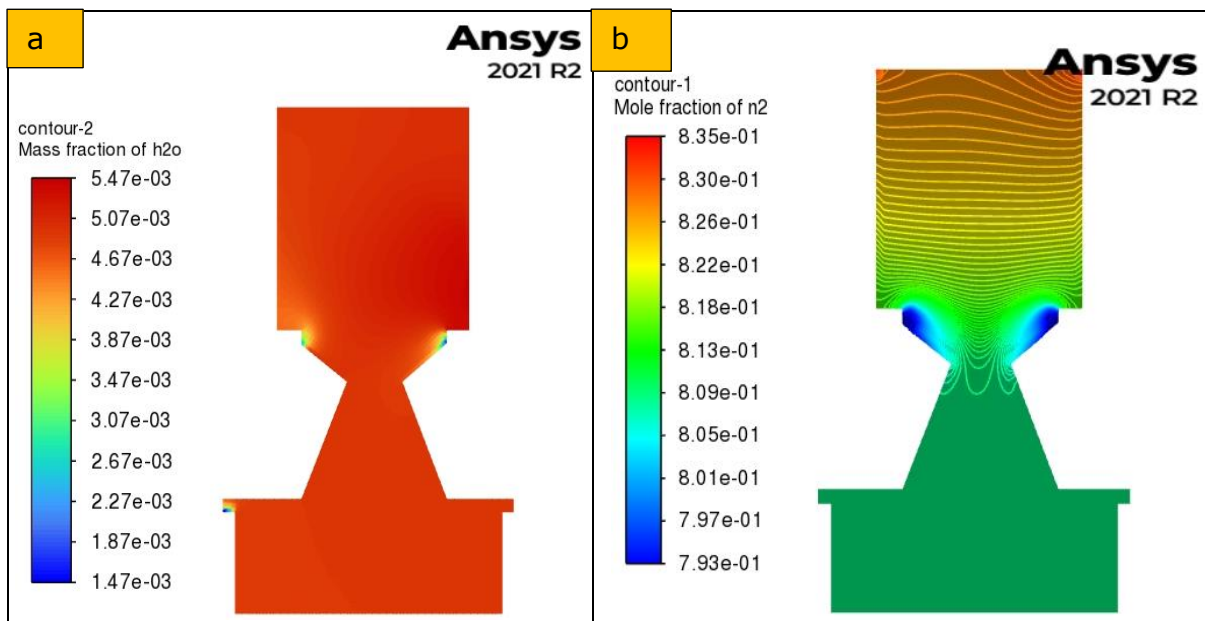
Figure 8.18: Gas species contour: (a) H_2O and (b) N_2 mole fraction

8.8.4. Performance study

The operating conditions directly influence the performance of the gasifier. The study below examined the temperature and equivalence ratio (ER) performance on gas production.

8.8.4.1. Effect of ER on gas composition

The ER influences the behaviour of oxidation and reduction reactions (Monteiro et al. 2017). In reduction reactions, less char was involved, while a large amount of char was involved in oxidation reactions, resulting in decreased CO and H_2 production. ER likewise impacts the distribution of mole fraction inside the gasifier. Higher ER values result in more O_2 and N_2 delivery inside the gasifier, raising the nitrogen concentration level and decreasing the producer gas mole fraction. The mole fraction of the gases determines gas quality in producer gas, and the ER significantly influences it.

The mole fraction of producer gas at various ER is shown in Figure 8.19. ER ranged from 0.25 to 0.60 with a step value of 0.05. A relatively low ER value may occasionally lead to incomplete gasification or produce producer gas with a low heating value and substantial char formation. On the other hand, a high ER value could push gasification into complete combustion, making gas with a high percentage of CO_2 and a low amount of CO and hydrogen. The observation of Figure 8.19 supports the statement that CO, H_2 and CH_4 levels decrease as ER increases as oxidation reactions are favoured (Sheth & Babu 2009). A slight decrease in the hydrocarbons (CH_4) was also seen for a similar reason.

In contrast, CO_2 and N_2 levels rose with increasing ER. These findings agree with the reported literature (Gungor & Yildirim 2013; Couto et al. 2016). Therefore, the ER = 0.35 seemed to be the optimum for syngas production.
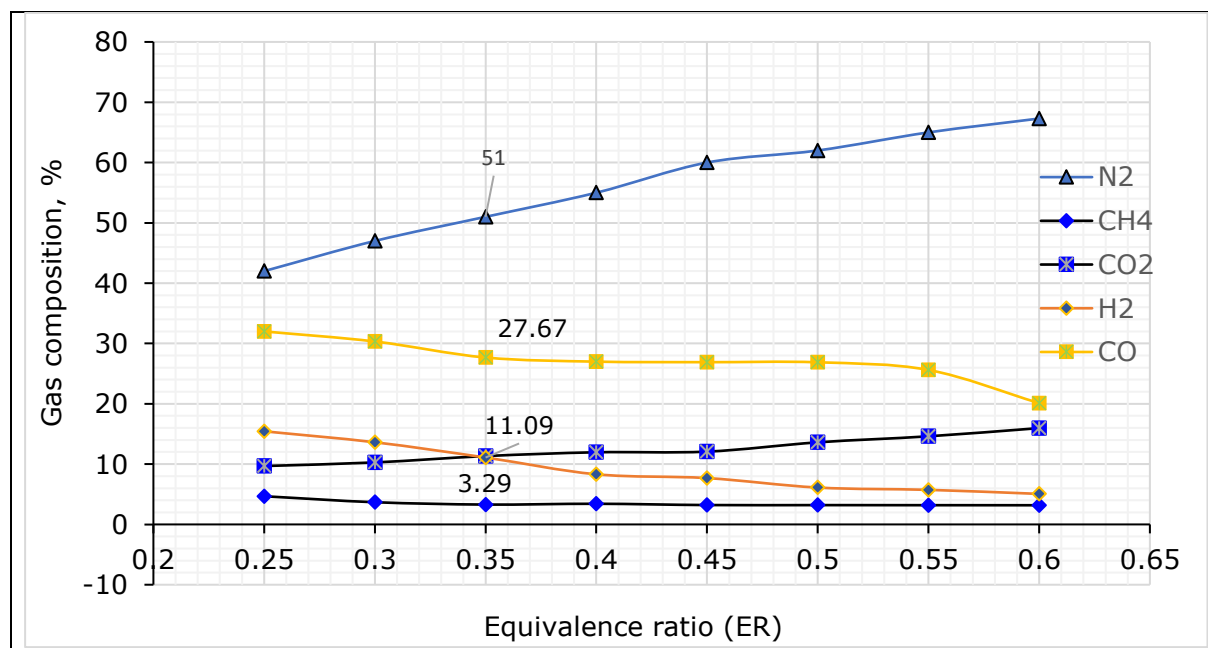
Figure 8.19: Gas composition at different equivalence ratios

8.8.4.2. *Gas production and gas efficiency*

Theoretically, the concentration of carbon containing gases (CO, CH_4, and CO_2) increases with the higher carbon contained feedstock in air gasification processes. Table 8.11 provides the forecast of the generated average gas species fraction. The heating value and produced gas efficiency were calculated as follows:

$$LHV_{gas} = (Y_{CO} \times 13.1) + \left(Y_{CH_4} \times 37.1\right) + \left(Y_{H_2} \times 11.2\right) \text{ ....} 8.35$$

$$E_{ff_{gas}} = \frac{HV_{gas} \times F_{gas}}{HV_{fuel}} \text{ ....} 8.36$$

Where: $E_{ff_{gas}}$ = Production gas conversion efficiency, %

HV_{fuel} = Heating value of fuel, MJ/m^3
LHV_{gas} = Lower heating value of gas, MJ/m^3
F_{gas} = Production gas – fuel feed ratio, m^3/kg
Y = Mole fraction of the gas

Assume a gas yield (F_{gas}) of approximately 1.6~2.5 m^3/kg fuel pellet when determining gas conversion efficiencies. This reference number was calculated based on experimental findings from the gasification of various biomass pellets in a downdraft gasifier with air-to-fuel ratios ranging from 1.1 to 1.4 (Erlich & Fransson 2011). Also, the WSP heating value was 19.06 MJ/m^3 (Table 8.1).

Table 8.11: Species gas composition for ER=0.35

Items	Value							
ER, %	0.25	0.30	0.35	0.40	0.45	0.50	0.55	0.60
LHV, MJ/m^3	7.65	6.86	6.09	5.74	5.57	5.39	5.18	4.38
E_{ffgas}, %	64~100	58~90	51~80	48~75	47~73	45~71	43~68	37~57

Note; ER= Equivalence ratio; LHV = Lower heating value of gas
E_{ffgas}= Production gas conversion efficiency

LHV values for CFD simulation with various ER are shown in Table 8.11. The LHV displayed values between 4.38 and 7.65. These results agree with the previous literature (Sharma et al. 2018; Yepes Maya et al. 2021) even though they used the 3D CFD model with Miscanthus briquettes. Also, the produced gas conversion efficiencies of the WSP gasification were between 51 and 80%. This study's results were close to the experimental gasification of hardwood pellets conducted by Brar et al. (2012). The authors used the same gasifier (GEK 10 kW) to gasify hardwood pellets and recorded a combustion temperature of roughly 1473K (1200°C). About 21% of the mixture was CO, while 11, 16, and 2% were CO_2, H_2, and CH_4. Overall, the efficacy of WSP gasification in the GEK 10 kW gasifier can be reasonably and accurately predicted using this model.

8.8.4.3. Effect of temperature on syngas species concentration

Theoretically, the devolatilisation rate, volatile decomposition scheme, oxidation reaction and reduction reaction were all included in the current CFD model (Pandey et al. 2015; Kumar & Paul 2019). Also, the gas phase and solid particle reaction happened due to the temperature variation in the gasifier (Table 8.5) (Di Blasi 2000).

This study estimated the downdraft gasifier's gas composition with an ER = 0.35. Using the CFD model, gas composition calculations were made in the temperature range of 1073~473K for WSPs on a dry basis. The N_2 content remained constant while CO concentration increased in high temperatures (Figure 8.20). Also, the H_2 and CO_2 concentrations declined as the temperature rose. Additionally, CH_4 concentration dropped to zero

beyond 1173k. These findings were also seen in the literature review of Gkouletsos (2011) and Mathieu & Dubuisson (2002).
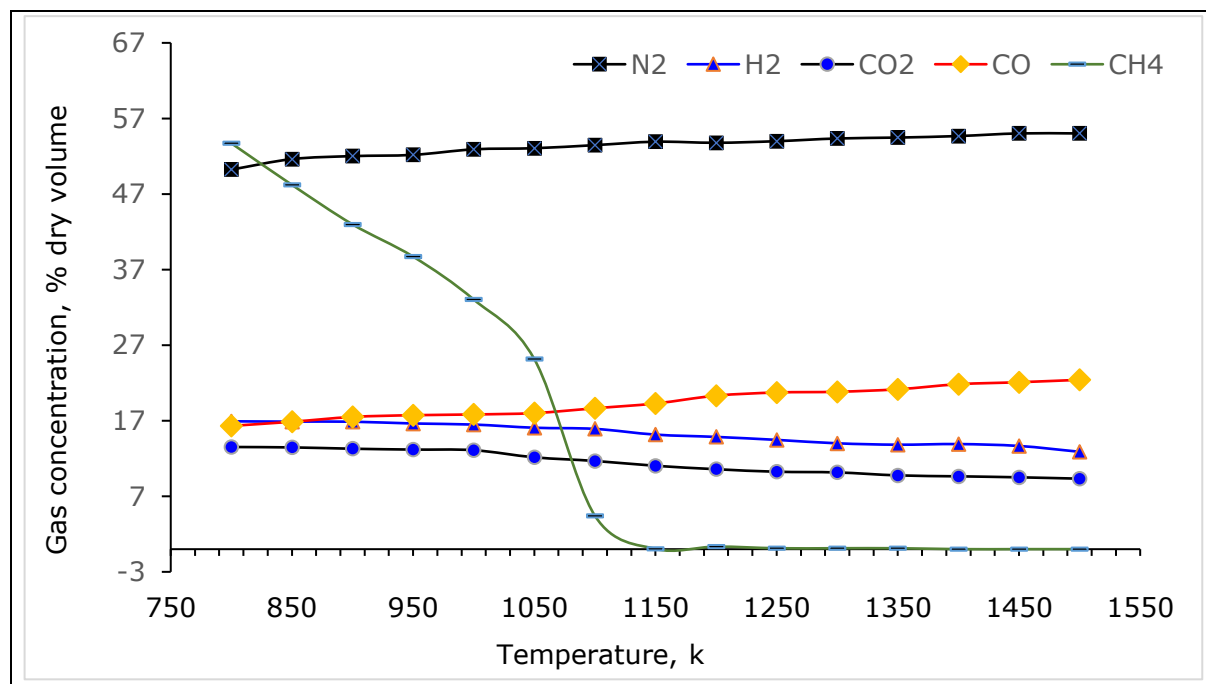
Figure 8.20: Effect of temperature on gas species

8.9. Conclusion

This work has presented the simulation results of a 2D CFD model to simulate the WSP gasification process in a fixed bed downdraft gasifier.

The prediction of temperature, pressure and velocity variation inside the reactor was studied. Based on the numerical prediction, the following conclusions were drawn:

- A higher temperature zone prevails beneath the air injection zone.

- A rise in the equivalence ratio increases or decreases the heating value of gas and gas production efficiency.

- ER = 0.35 seems to be the optimum for optimum syngas production (CO: 27.67% and H_2: 11.09%). Increased ER decreases the CO and H_2 composition in the product gas, followed by raising the CO_2 concentration.

- A higher equivalence ratio (0.25~0.6) is responsible for the high nitrogen content (42~67.3%) in producer gas.

- The proposed CFD model provides a preliminary estimate of producer gas composition, which would help control the operating parameters during actual experiments.

- Simulation work can help improve the gasifier's design parameters and performance.

CHAPTER 9: TECHNO-ECONOMICAL ANALYSIS OF WHEAT STRAW PELLET MAKING

Abstract

This chapter assesses WS pellet potential and its impact on energy generation. This study considers two simplified scenarios (T_1 and T_5 WS pellets). The input costs include electricity, material requirements and wages for pellets production in Australia. The estimated input energy was 0.1342 kWh/kg of pellets. The cost of producing one tonne of WS pellets varied from AU\$232.00 to 360.00. Compared with the current market price, the profit from pellet production was about 42%. The study determined that for drying one tonne of wheat crop and reducing its moisture content from 20% to 12%, a total of 19.741 kg of the T_5 pellets would be required. Overall, the WS pellet is a potentially good energy source for farming operations.

9.1. Introduction

Wheat is one of the major winter crops in Australia. Grain harvesting and drying are the major steps in the wheat postharvest system, while the straw remains a leftover residue (GummertCabardo, et al. 2020). Typically, the amount of WS residue is more than the grain itself (the typical grain-to-straw ratio is 1:1.3) (Liu, Q. et al. 2008). The straw comprises plant stems, leaves, pods and small grains (Akhtar et al. 2019). Of late, these residues are often used in energy systems and may offer a cost effective way to solve management and energy problems.

A pellet is a popular form of transforming solid biomass into biofuel for heating and energy generation purposes (Jiang et al. 2020; Gong et al. 2021). Demand for pellets is mainly driven by policies that promote greenhouse gas (GHG) mitigation and renewable energy generation (Yun et al. 2022). The conversion of biomass pellets into energy depends on various factors, including the type and quality of available biomass, conversion efficiency, the intended energy utilization, environmental conditions and economic factors (Czaplicka et al. 2021). Biomass pellet burning may also significantly impact human health and the environment (Bray, Battye & Aneja 2019). Therefore, it is important to examine the energy potential variables of pellet making.

Several studies reported on the techno-economic analysis of agricultural waste pellets for power generation (Chandrasekaran et al. 2013; Ozgen et al. 2014; Purohit & Chaturvedi 2016; Maj 2018; Pantaleo et al. 2020; Buss et al. 2022; Næss et al. 2023). Mani, Tabil and Sokhansanj (2006) reported that the production cost of SD pellets was 51 US\$/tonne at a plant capacity of 45 tonnes per year. A European pellet

production scenario (SD based) was reported by Obernberger and Thek (2004), who found pellet production costs of 95.56 US$/tonne at a plant capacity of 24 tonnes. Recently, Yuldashev et al. (2020) examined the techno-economic analysis for small scale pellet processing for the bioenergy market and reported that the solid biomass pellet has the most significant positive effect on profitability. In comparison, very few research studies have analysed cereal crop straw pellets (Greinert et al. 2020; König, Müller & Hartmann 2021; Shrivastava et al. 2021; Mohrmann & Otter 2022). For instance, Sultana, Kumar and Harfield (2010) reported that a straw pellet production cost was 132 US$/tonne with an annual pellet production capacity of 50,000 tonnes.

This study analysed the economic feasibility of WS pellets as a bioenergy feedstock. This chapter's specific objectives were to (a) assess the WS pellet production cost, (b) evaluate the return on investment into small scale pellet mills for processing biomass into pellets, and (c) estimate the reuse of WS pellets for on farm wheat grain drying.

9.2. Methods

Two types of WS pellets (T_1 and T_5) were manufactured using different additive combinations. In this study, the pellet production costs were first estimated. After that, the sensitivity of pellet production cost was assessed. In the end, the wheat grain on farm drying energy was estimated and compared to the pellet needed.

The methods for evaluating WS pellet utilisation as an energy source were as follows.

9.2.1. Net energy analyses

WS pellet production net energy requirement is the difference between the input energy used in the production process and the energy content of the final product (de Souza et al. 2020). This is also known as energy balance. The drying, chopping and mixing of WS pellet materials and manufacturing energy (electricity) consumed were considered for estimating total energy input. The heating value of pellets was the gained energy in this estimation. The following equation was used to calculate the energy needed to make the pellets:

$$E_p = E_c + E_m + E_p + E_d \quad \text{..}9.1$$

Where: E_p = energy required for pellet production, MJ/kg
E_c = energy for chopping of straw, MJ/kg
E_m = energy of mixing the WS additives, MJ/kg
E_d = energy of WS drying, MJ/kg
E_p = energy of pelletisation, MJ/kg

Table 9.1: Assumption inputs for economic calculation

Items		Average	Unit
Pellet mill capacity		500.00	kg/h
Electricity requirements for pellet mill operation		7.50	kW
Pellet machine operational time		2400.00	h/year
Straw chopping capacity		500.00	kg/h
Electricity requirement for chopper machine operation		10.00	kW
Operation of chopper		2400.00	h/year
Binder ratio	BioC	10%	weight
	SD	10%	Weight
	BC	10%	weight
WS proportion in pellets	T_1	100%	weight
	T_5	70%	weight

The main assumptions for this study are listed in Table 9.1. This study assumed that the pellet mill capacity was 500 kg/hour. Based on the available quantity of WS converted into pellets, the pellet mill operation was assumed to be about 2400 hours per year. The daily operation was 8 hours because it is standard working time. In Australia, wheat is a winter crop and grows once a year (seasonal), so the WS was collected and stored for year-round use; however, pellet mill operation was considered for ten months.

9.2.2. Economic analyses

This study compared the manufacturing costs of the T_1 and T_5 pellets. Economic analysis includes the input labour price, raw materials, equipment and energy (electricity) that are likely to be required in the production process (Agar 2017; Fu et al. 2022).

The cost estimation was based mainly on pellet production and electricity consumption and was calculated as follows (Elita 2018):

$$C_p = \frac{(I_m \times f) + (P_c + B_c + L_c)}{P_y}$$ ....….…….9.2

Where: C_p = cost of pellet production, $AU/kg
I_m = investment cost of purchasing machinery, $AU
f = years operation factor (1/year)
B_c = binder (BioC, SD, BC) cost, $AU/year
L_c = labour cost, $AU/year
P_y = pellet production, kg/year
P_c = electricity costs for dryer, chopper, mixer and pellet mill, $AU/year

Based on current market prices, this study estimates the materials cost. This cost estimation included the machinery (pellet mill, chopping mill, biomass dryer and mixing machine) purchasing cost as an investment budget. The primary assumptions for the economic analysis are listed in Table 9.2.

Table 9.2: Input data and projected cost for economic analysis

Items		Average	Unit
Investment cost	Pellet mill	419000.00	$/unit
	Biomass dryer	25000.00	$/unit
	Straw chopper	10000.00	$/unit
	Mixer machine	2000.00	$/unit
Electricity price		0.255	$/kWh
BioC price		0.425	$/kg
SD price		0.300	$/kg
BC price		0.550	$/kg
Labour costs		25.00	$/hour
Total labour required		4	person
Machine life		10	year

9.3. Results and discussions

9.3.1. Net energy analysis

The primary objective of pelletisation is to improve energy density. The energy density boost can significantly decrease handling, storage, packing and transportation costs. Energy input is necessary for palletisation (Anukam et al. 2021). Several studies on manufacturing pellet fuels have compared energy use to energy gain (Uslu, Faaij & Bergman 2008; Sultana & Kumar 2012; Shahrukh et al. 2016). Chapter 3 describes the size reduction, mixing, pelleting and drying steps in the pellet manufacturing process employed in this study (Figure 3.3).

The main purpose of biomass chopping is to reduce the size and create a uniform size of raw WS (Liashenko et al. 2019). This study used a high speed chopping mill with a 10 kW motor with 40% power efficiency. The chopping mill consumes 0.05 kWh of energy for one kilogram of WS chopping (Table 9.3).

This study also used a mixing machine with an energy requirement of 0.0108 kWh/kg straw to mix the binding materials (Levis & Barlaz 2013). The mixing was initially to combine the raw material (WS), water and binding materials (BioC, SD, BC). Here, BC holds the particle together and softens the pelleting materials. BioC has recently been used as a medium for heating value improvement (Arous et al. 2021), while SD is used as a structural material.

As mentioned in Chapter 3, this research used a 7.5 kW electric motor to drive a small commercial pellet mill. According to the manufacturer, the nominal pellet mill capacity is 1000 kg of wood pellets per hour (Table 9.3). This investigation repeatedly tried refeeding material due to the changing qualities of the pellets; however, the output was only about 500 kg per hour of WS pellets. Refeeding is required to obtain a dry and suitable quality pellet.

Table 9.3: Energy required for pellet production

Items		Value	Unit
Chopper mill	Electricity for operation	10	kW
	Capacity	500	kg/h
	Energy required	0.02	kWh/kg of straw
	Efficiency	40	%
	Actual straw chopping energy	0.05	kWh/kg of straw
Mixing machine	Energy requirement for operation	0.0065	kWh/kg of straw
	Efficiency	60	%
	Actual energy required	0.0108	kWh/kg of straw
Pellet mill	Electricity for operation	7.5	kW
	Capacity	500	Kg of pellet/h
	Energy requirement	0.015	kWh/kg of pellet
Dryer	Moisture reduction from WS	5	%
	Total moisture reduction	0.05	kg/kg moisture
	Energy required	0.7	kWh/kg of moisture
	Dryer efficiency	60	%
	Actual energy required	0.0583	kWh/kg of pellet
Total energy required (I+II+III+IV)		0.1342	kWh/ kg of pellet
Heating value of pellets	T_5	5.294	kWh/kg of pellet
	T_1	4.73	kWh/kg of pellet
Energy for pellet production as % of its heating value	T_5	2.5343	%
	T_1	2.8365	%

Typically, the raw biomass moisture content varies from 6 to 25% (wb) for cereal straw (Mani, Tabil & Sokhansanj 2006). Sometimes biomass was dried outdoors in clear weather. Sundried biomass may, however, be impractical and time consuming for commercial production. Thus, a mechanical dryer is required. The energy needed for biomass drying is around 0.7 kWh/kg moisture (Souza-Santos 2010). Therefore, a biomass dryer was considered for drying both the biomass and pellets. In this study, the energy necessary was about 0.0583 kWh/kg to dry pellets with an 18% moisture content down to 13% (Table 9.3).

The energy input and output analyses for manufacturing the WS pellets are shown in Table 9.3, where the overall energy needed for pellet production was 0.1342 kWh/kg of pellet. Also, the pellet without additives (T_1) used around 2.8365% energy in its heating value. In contrast, the additive pellet (T_5) needed 2.5343% of its energy content to be produced. Thus, the input energy for additive blended pellets (T_5) has an insignificant impact on the overall energy production.

9.3.2. Economic analysis of pellet making

This section examines the economic potential of WS pellet making. The production cost is related to electricity, materials, and labour for pellet manufacturing. The estimated costs for manufacturing WS pellets are shown in Table 9.4.

Table 9.4: WS pellet production cost

Item		Pellets		Unit
		T$_1$	T$_5$	
Amount of pelleting materials		1200000		kg/year
Operational (electricity) cost				
Electricity price		0.255		$/kWh
Pellet making (I)	Operation hour	2400		h/year
	Pellet production capacity	500		kg/h
		1200000		kg/year
	Electricity required for pellet production	0.015		kWh/ kg of pellet
		18000		kWh/year
	Electricity cost	4590.00		$/year
Straw chopping (II)	Operation hour	2400		h/year
	Chopping capacity	500		kg/h
		1200000		kg/year
	Electricity required for chopping straw	0.05		kWh/kg
		60000		kWh/year
	Electricity cost	15300.00		$/year
Pelleting materials mixing (III)	Operation hour	2400		h/year
	Chopping capacity	100		kg/h
	Mixing materials	240000		kg/year
	Electricity required for material mixing	0.0108		kWh/kg
		2600.00		kWh/year
	Electricity cost for mixing machine	663.00		$/year
Pellet drying (IV)	Drying pellets	1200000		kg/year
	Actual energy required	0.0583		kWh/kg
	Electricity per year	70000		kWh/year
	Electricity cost for pellet drying	17850.00		$/year
a.	Total operational cost (I+II+III+IV)	38403.00		$/year
Materials cost for pellet production				
BioC		-	51000.00	$/year
SD		-	36000.00	$/year
BC		-	66000.00	$/year
b.	Pelleting materials cost	0.0	153000.00	$/year
Worker cost				
c.	Labour cost*	240000.00		$/year
Total operational cost (a+b+c)		278403.00	431403.00	$/year
Pellet production cost per tonne		232.025	359.5025	$/tonne
Pellet heating value		17.02	19.06	GJ/tonne
Comparable energy production cost		13.631	21.122	$/GJ

Note; * Labour cost: 25 $/hr (https://au.talent.com/salary?job=labour)

Table 9.4 shows that the T$_1$ pellet production cost was 232.2 $/tonne, while the T$_5$ pellet cost was 359.5025 $/tonne. Shahrukh et al. (2016) reported that pellet production cost varies from 211~226 AU$/tonne (146 to 156 US$/tonne). The present study results were higher due to higher operating costs. T$_1$ pellet production was lower because no additive materials were used for manufacturing this type of pellet. In Chapter 3, it was reported that the T$_1$ pellet quality did not fit the ISO standard quality.

Sensitivity analyses were also presented in the present study to investigate the impact of pellet production materials price on pellet production cost. Here, only the T_5 pellets were considered for sensitivity analysis because this pellet quality fulfils the ISO/EN*plus* quality requirement. The results of the sensitivity analysis are shown in Table 9.5.

Table 9.5: Sensitivity analysis of production cost ($/tonnes)

Production cost increase, %	*Wholesale pellet cost	Pellet production cost	Profit compared to market price, %
0		359.5025	42.14
10%		395.4528	29.22
20%	511.0	431.403	18.45
30%		467.3533	9.34
40%		503.3035	1.53

* https://www.selinawamucii.com/insights/prices/australia/cereal-pellets/#:~:text=In%202022%2C%20the%20approximate%20price,352.29%20in%20Melbourne%20and%20Canberra

It can be found that the pellet production cost varies from 232~360 AU$/tonne, while the wholesale price for a straw pellet was about AU$ 511/tonne (US$ 352.29/tonne) in 2022. Hence, the pellet production profit was 42%.

9.3.3. Use of WS pellets for on farm crop drying

The biomass pellet is a promising alternative fuel for residential cooking (Sandro et al. 2019; Stančin et al. 2020). Table 9.6 presents the estimated results of the WS pellet utilisation scenario for on farm wheat crop drying. Three moisture settings (15%, 18% and 20%) were considered for this estimation for 1000 kg of wheat grain. Stored crops must maintain 12% moisture content for long term storage (Chen et al. 2002). It can be found that 1000 kg wheat grain drying needs 13 to 15 kg pellets when moisture is reduced from 18% to 12% (Scenario: S2) (Table 9.6). Overall, the T_5 pellet had the highest energy potential due to the smaller amount of pellet required for 1000 kg of grain (wheat) drying, irrespective of moisture content.

Table 9.6: Drying of 1000 kg wheat and cost

Particulars		Scenarios		
		S1	S2	S3
Wheat quantity, kg		1000	1000	1000
Wheat moisture content, %		15	18	20
Optimum moisture in wheat, %			12	
Moisture reduction, %		3	6	8
Water removed, kg		30	60	80
* The energy required to evaporate water, kWh		21	42	56
Heating value, kWh/kg	T_1		4.728	
	T_5		5.294	
Pellet requirement, kg	T_1	4.442	8.883	11.844
	T_5	3.967	7.934	10.578
**Actual pellet requirement, kg	T_1	7.403	14.805	19.741
	T_5	6.611	13.223	17.630
Drying cost, AU$	T_1	2.661	5.323	7.097
	T_5	2.377	4.754	6.338

Note; *Around 0.7kWh of energy is required to remove each kg of moisture
**Biomass dryer efficiency = 60%

9.4. Conclusion

Agricultural residue often poses disposal and storage cost issues and, at the same time, can be a potentially good source of bioenergy. Examination of the T_1 and T_5 pellets indicates that they have good energy properties. The following conclusions can be made:

- The pellet production energy required 0.1342 kWh/kg, while the production cost was calculated as AU$359.5 /tonne of T_5 pellet.

- The research showed that the manufacturing of WS pellets is profitable, and, at current market value, the profit was about 42%.

- The drying results showed that of the two pellets, T_5 had the highest energy potential. Overall, the amount of pellets needed was 6 to 20 kg for 1000 kg wheat grain drying, while the initial moisture varied from 15 to 20% in the crop.

CHAPTER 10: CONCLUSION AND RECOMMENDATIONS

10.1. General summary and conclusions

The main focus of this research project was to develop solid biofuel from herbaceous biomass straw for converting into bioenergy. The study used widely available and bulky wheat straw (WS). The investigation was broken down into four steps. Firstly, it investigated a suitable pellet making process and the improvement of pellet quality (Chapters 3 and 4). Secondly, it examined the transformation of solid pellets into bioenergy with laboratory scale fixed bed kiln experiments and thermogravimetric analyser (TGA) analyses (Chapters 5, 6 and 7). Thirdly, it developed a CFD model to predict gasification performance (Chapter 8). Finally, a techno-economic analysis was conducted (Chapter 9).

This research has investigated the process of manufacturing suitable pellets from WS. The densification process was performed with different pretreatment processes and additives. The study employed biomass sourced blending materials rather than non-renewable materials (coal, chemical, etc.), which had been used in most published studies. Chopping, sieving, additive mixing, conditioning, binding, compressing, and drying were all included in this pelleting process. It was found that the binding materials could change pellet quality traits such as bulk density (244 to 607 kg/m^3), tensile strength (0.36 to 1.09 MPa) and durability (83.0 to 98.0%) (Chapter 3). The additives were also found to reduce pellet fines content from 11.0 to 1.93%, which would be helpful for transport and storage. The study indicated that it was challenging to densify the WS to make pellets with sufficient density, homogeneity and hardness without mixing in additives.

Seven types of additive combinations were investigated for the improvement of pellet quality. The developed pellet quality was then compared with the ISO and EN*plus* standard requirements. It was found that additives significantly boost pellet quality. Except for ash content, most physiochemical characteristics of developed pellets fulfilled the relevant ISO standard (Chapter 4). In particular, mixing biochar could increase the heating value from 17.02 to 19.06 MJ/kg.

In Chapter 5, a slow pyrolysis of WS pellets was conducted on a laboratory scale fixed bed kiln. The pyrolysis of two types of WS pellets (T_1 and T_5) was performed under a nitrogen environment at 20 to 700°C. It was found that the pellet with additive (T_5) had a higher pyrolysis temperature at a particular time (60 minutes). In addition, the gas yield (43.52%), biomass conversion efficiency (75.67%) and syngas production (H_2+CO: 46%) were also higher than the pellet without additives (T_1) at a

pyrolysis temperature (600°C). Overall, the additives, especially biochar added to WS, changed the thermokinetic behaviour of the pellets considerably compared to pellets without additives (T_1). The overall results demonstrated that additives were often quite useful for pellet making.

The behaviour of all pellets in combustion (Chapter 6) and pyrolysis (Chapter 7) was determined with a thermogravimetric analyser (TGA). It was found that both pellets followed a multistage reaction and equilibrium chemical reaction behaviour. The performance of pyrolysis and combustion thermokinetic behaviour was analysed using model free and model-based assumptions. The TG/DTG profile demonstrated that thermogravimetric characteristics supported only the model-based assumptions. The WS pellets' thermokinetic properties in pyrolysis and combustion were very similar. The DTG curve peak or chemical reaction in pyrolysis followed the three stages, while the combustion process had four stages.

The TGA of combustion performance was measured in an air atmosphere range of 25~1200°C to investigate the activation energy, pre-exponential factor and the reaction model (Chapter 6). Based on the TG/DTG profile, the WS pellet's thermal decomposition occurred in four consecutive reaction steps: A→B→C→D→E→F. The kinetic reaction Cn (n^{th} order reaction with autocatalyst), Fn (n^{th} order phase interfacial reaction model), $F2$ (second order phase interfacial reaction mode) and $D3$ (diffusion control model) were best fitted with TGA combustion. The average $E\alpha$ for Fn, Cn, $D3$ and $F2$ models were 164.723, 189.782, 273.88 and 45.0 kJ/mole, respectively, for the T_1 pellets. For the T_5 pellets, the pre-exponential factor (*lnA*) was 4.764, 37.405, 54.666 and 7.006 (1/s) for the $F2$, $D3$, Cn and Fn models, respectively, at a heating rate of 20 °C/min. In addition, the ignition temperatures for the T_1 and T_5 pellets were 292 and 277°C, respectively, while the burnout point was similar (422°C) for both pellets at a heating rate of 10 °C/min.

The pyrolytic kinetic parameters and the reaction mechanism under a nitrogen environment were also determined using TGA, where the temperature varied from 31 to 800°C, and with three heating rates (5, 10 and 20 °C/min) (Chapter 7). The obtained result showed that temperature significantly impacted the mass loss and reaction rates. However, the influences on heating rates were not significant. Instead, a model-based reaction such as Fn and $F2$ was the most appropriate kinetic technique for explaining the thermal degradation of WS pellet pyrolysis and the three-phase consecutive reaction mechanism (A→B, C→D and D→E). The average $E\alpha$ for Phases 2 and 3 were 136.038 and 358.110 kJ/mole for the T_1 pellet. The *lnA* varied from 3.647 to 21.802 (1/s) for T_5 pellets at a 20 °C/min heating rate.

A two-dimensional CFD model was developed for GEK 10 kW downdraft Imbert gasifier and simulated using macadamia shells (Chapter 8). The model was created in ANSYS meshing and simulated in the ANSYS Fluent software package with in-house coding via the User-Defined Function (UDF). A steady state regime was considered for the non-premixed combustion and species transport models. The activation energy and pre-exponential factors were taken from the TGA experiments on pyrolysis and combustion to set the boundary conditions. Biomass and air flow rates were initially set as 9.0 kg/h and 37.78 Nm^3/h, respectively. The projected temperature agreed well with the macadamia experiments. Also, predicted values in CO and CO_2 were in reasonable agreement with the investigation. At the same time, it was found that the equivalence ratio (ER) could either negatively or positively impact gas production and lower heating value (LHV), where the suitable ER value was 0.35 for syngas (H_2+CO) production. The producer gas composition was CO~27.67%, CH_4~3.29%, CO_2~11.09%, H_2~11.09% and N_2~51%, respectively when the ER was 0.35. The reactor temperature positively affected the syngas quantity increase. The contour profile and centreline distribution of temperature, static pressure, velocity and density were not constant throughout the reactor due to the uneven shape and various thermal reactions. Also, the gas species distribution followed the same trend, but the volume was dissimilar.

This research found that the estimated energy requirement for pellet production was 0.134 kWh/kg, and the cost of producing one tonne of WS pellets varied from AU$232.0 to 360.0, depending on the additive used (Chapter 9). Moreover, pellet production profit was about 42% compared to the current market price. The energy from the WS pellet was adequate for wheat crop drying, indicating the circular use of biomass.

10.2. Research contribution

The PhD research has made significant contributions to knowledge in various ways, including:

- **Advancing the understanding of a specific bioenergy research field:**

The research is focused on exploring biomass-based energy from wheat straw and its circular utilisation in agricultural farms for crop drying to promote various dimensions of sustainable development. The research includes work on developing solid fuel, studying physio-chemical characteristics, exploring thermochemical traits, investigating pyrolysis, examining thermal combustion, and exploring on-farm crop drying techniques. One notable aspect of this PhD research is the development of a unique computational fluid dynamics (CFD) model that can be applied to different biomass gasifier designs and applications for syngas (CO, CO_2, CH_4, H_2) production. The developed a research protocol that can also be

replicated to convert other agricultural residues into bioenergy in an emission-neutral way.

- ▪ **PhD Research Contribution to the Australian Economy**

Wheat production is increasing in Australia, leading to a growing amount of waste that presents management challenges and energy generation opportunities. The PhD research goal aligns with the United Nation's "Sustainable Development Goal Target 7: Affordable and Clean Energy" agenda for sustainable development (https://tinyurl.com/8yyd48s3). Also, this objective aligns with Australia's bioenergy roadmap, especially theme 3, which aims to develop resources through projects such as assessing Australian biomass for bioenergy (https://arena.gov.au/renewable-energy/bioenergy/). This innovative research contributes to decarbonisation efforts by producing renewable energy (biomass to bioenergy) and energy efficiency through the circular use of waste. It helps mitigate climate change, particularly in Australia. Australia aims for net-zero emissions by 2050 and a 45% emissions reduction by 2030, demonstrating its commitment to combatting climate change through renewable energy development. The global community, including Australia, is actively transitioning from fossil fuels to renewable energy sources, and bioenergy derived from biomass plays a crucial role in this transition. Specifically focusing on agricultural waste, the PhD research effort directly addresses the potential to reduce global and Australian emissions while substituting fossil fuels in an emission-neutral system and promoting a greener future.

In Australia, the production of solid fuel, mainly pellets, historically relied on forest wood. However, pellet production from natural forest wood has been discontinued in Australia and is considered a non-renewable source (https://tinyurl.com/4c672t4z). This decision creates a strong rationale for shifting towards pellet production from agricultural residues, with wheat straw being a particularly attractive option. Alternatively, managing crop straw through windrow burning (weed seed destruction), landfilling, or decomposition can be costly, problematic, and contribute to emissions. Therefore, scientists have proposed biomass valorisation by producing solid fuel (pellets), biochar, biogas, and other forms of energy. It is worth highlighting that Australia's animal feed mill industry also heavily relies on wood pellets as the primary energy source for boiler heating. Utilising wheat straw pellets for feed production, farm-level heating, and grain drying is a justifiable application for the findings of my PhD research in Australia. This approach addresses the need for sustainable alternatives to forest wood pellets and provides practical solutions for the agricultural sector's energy demand.

Australia, the sixth largest country globally, has vast remote and regional areas, some far from urban centres. Additionally, Australia's

reputation as a migrant-welcoming country necessities infrastructure improvements and the establishment of settlements in these regions has been suggested. Still, access to energy is limiting the realisation of this. Overcoming energy shortages and promoting localised energy production can be achieved through renewable energy sources, including biomass-based energy. The findings of PhD research are relevant for implementation in Australian regional areas.

10.3. Recommendations for future research

Although the developed WS pellet was demonstrated to have a suitable quality and energy value, some issues remain to be investigated. Therefore, future research is needed to increase the effectiveness of WS pellet utilisation. These include:

- The developed pellet properties, except for ash content, fulfil the ISO and EN*plus* requirements. However, herbaceous straw biomass contains more ash than woody biomass, so further research on alternative additive use or methods for ash reduction is needed.

- Bio-oil is a primary component of the biomass pyrolysis process. However, this research has not been able to examine the pyrolysis process of WS pellets in depth, so the bio-oil amount is unknown. It is important to know the bio-oil composition to explore other valuable biomass products. There is thus a window of opportunity to develop future understandings in this regard.

- Ash compositional analysis allows an understanding of specific materials' contribution to the ash sintering behaviour. This helps to determine a particular biomass for a specific thermal conversion application. A pyrolysis solid product biochar ultimate analysis was conducted (Chapter 5), but more information on ash composition is needed, creating future research scope to analyse the ash components.

- The behaviour of pyrolysis and combustion concerning thermokinetics was analysed using model free and model-based assumptions. The TG/DTG profile showed that only the model-based hypotheses were supported by thermogravimetric properties (Chapters 6 and 7). Conversely, most published research considered both model and single-stage reactions for analysing the thermal behaviour of herbaceous biomass. Therefore, this new finding needs to be verified as it will have significant implications for gasification and combustion.

- The developed CFD model is quite good in temperature, pressure, velocity, and gas prediction. At the same time, there are many

possibilities for further research in this area. One of the concerns is regarding the design perspective on output. Typically, all gasification produces solid materials, such as ash and tar, but they were not considered in the currently developed model. For the determination of gas emission as well as solid product yields, the created CFD model would need further modification.

- Because of COVID, macadamia shell gasification data were used in this research to validate the developed CFD model due to a lack of data sources for WS pellets. The macadamia shell is physicochemically similar to woody biomass, which is different from herbaceous biomass. Thus, the WS pellet gasification requires actual data to compare with the theoretical CFD model. This could be a topic of future work. Also, the model needs to be validated for industrial scale combustion and gasification.

- This WS pellets techno-economic analysis considered production cost and energy potential. It also analysed the pellet reuse for wheat crop drying. However, an in-depth economic evaluation was not undertaken due to time limitations. Also, the whole system life cycle assessment of biomass to bioenergy production through pyrolysis, gasification and combustion needs to be studied.

References

ABARES 2019, 'Australia's place in global agriculture and food value chains, ABARES insights', no. 4, https://www.agriculture.gov.au/sites/default/files/abares/documents/AustraliaPlaceInGlobalAgriculture_v1.0.0.pdf>.

Abdelhady, S, Borello, D & Shaban, A 2018, 'Techno-economic assessment of biomass power plant fed with rice straw: Sensitivity and parametric analysis of the performance and the LCOE', *Renewable Energy*, vol. 115, pp. 1026-34.

Abele, E & Fujara, M 2010, 'Simulation-based twist drill design and geometry optimization', *CIRP annals*, vol. 59, no. 1, pp. 145-50.

Açıkalın, K 2021, 'Determination of kinetic triplet, thermal degradation behaviour and thermodynamic properties for pyrolysis of a lignocellulosic biomass', *Bioresource technology*, vol. 337, p. 125438.

Adams, P, Bridgwater, T, Lea-Langton, A, Ross, A & Watson, I 2018, 'Biomass conversion technologies', in *Greenhouse gas balances of bioenergy systems*, Elsevier, pp. 107-39.

Adapa, P, Tabil, L & Schoenau, G 2009, 'Compaction characteristics of barley, canola, oat and wheat straw', *Biosystems Engineering*, vol. 104, no. 3, pp. 335-44.

Adapa, P, Tabil, L, Schoenau, G & Opoku, A 2010, 'Pelleting characteristics of selected biomass with and without steam explosion pretreatment', *International Journal of Agricultural and Biological Engineering*, vol. 3, no. 3, pp. 62-79.

Adapa, P, Schoenau, G, Tabil, L, Arinze, E, Singh, A & Dalai, A 2007, 'Customized and value-added high quality Alfalfa products: A new concept'.

Agar, DA 2017, 'A comparative economic analysis of torrefied pellet production based on state-of-the-art pellets', *Biomass and bioenergy*, vol. 97, pp. 155-61.

Agbor, VB, Cicek, N, Sparling, R, Berlin, A & Levin, DB 2011, 'Biomass pretreatment: fundamentals toward application', *Biotechnology advances*, vol. 29, no. 6, pp. 675-85.

Aguilar, G, D. Muley, P, Henkel, C & Boldor, D 2015, 'Effects of biomass particle size on yield and composition of pyrolysis bio-oil derived from Chinese tallow tree (*Triadica Sebifera L.*) and energy cane (*Saccharum* *complex*) in an inductively heated reactor', *AIMS Energy*, vol. 3, no. 4, pp. 838-50.

Ahmad, AA, Zawawi, NA, Kasim, FH, Inayat, A & Khasri, A 2016, 'Assessing the gasification performance of biomass: A review on biomass gasification process conditions, optimization and economic evaluation', *Renewable and Sustainable Energy Reviews*, vol. 53, pp. 1333-47.

Ahmad, MS, Mehmood, MA, Liu, C-G, Tawab, A, Bai, F-W, Sakdaronnarong, C, Xu, J, Rahimuddin, SA & Gull, M 2018, 'Bioenergy potential of Wolffia arrhiza appraised through pyrolysis, kinetics, thermodynamics parameters and TG-FTIR-MS study of the evolved gases', *Bioresource technology*, vol. 253, pp. 297-303.

Ahmed, TY, Ahmad, MM, Yusup, S, Inayat, A & Khan, Z 2012, 'Mathematical and computational approaches for design of biomass gasification for hydrogen production: A review', *Renewable and Sustainable Energy Reviews*, vol. 16, no. 4, pp. 2304-15.

Ahmmad, F, Sohel, M, Islam, M, Ani, FN & Islam, T 2020, 'Development of a Pelletizing Process to Improve the Properties of Biomass Pellets', *International Seminar of Science and Applied Technology (ISSAT 2020)*, Atlantis Press, pp. 337-43.

Ahn, HK, Sauer, TJ, Richard, TL & Glanville, TD 2009, 'Determination of thermal properties of composting bulking materials', *Bioresour Technol*, vol. 100, no. 17, pp. 3974-81.

Ahrenfeldt, J, Thomsen, TP, Henriksen, U & Clausen, LR 2013, 'Biomass gasification cogeneration – A review of state of the art technology and near future perspectives', *Applied Thermal Engineering*, vol. 50, no. 2, pp. 1407-17.

Akhtar, A, Krepl, V & Ivanova, T 2018, 'A combined overview of combustion, pyrolysis, and gasification of biomass', *Energy & Fuels*, vol. 32, no. 7, pp. 7294-318.

Akhtar, K, Wang, W, Khan, A, Ren, G, Afridi, MZ, Feng, Y & Yang, G 2019, 'Wheat straw mulching offset soil moisture deficient for improving physiological and growth performance of summer sown soybean', *Agricultural water management*, vol. 211, pp. 16-25.

Al-Ayed, O & Saadeh, W 2021, 'Approaches to Biomass Kinetic Modelling: Thermochemical Biomass Conversion Processes', *Jordanian Journal of Engineering and Chemical Industries*, vol. 4, no. 1.

Al-Hamamre, Z, Saidan, M, Hararah, M, Rawajfeh, K, Alkhasawneh, HE & Al-Shannag, M 2017, 'Wastes and biomass materials as sustainable-renewable energy resources for Jordan', *Renewable and Sustainable Energy Reviews*, vol. 67, pp. 295-314.

Al-Mansour, F & Zuwala, J 2010, 'An evaluation of biomass co-firing in Europe', *Biomass and bioenergy*, vol. 34, no. 5, pp. 620-9.

Al-Moftah, AMS, Marsh, R & Steer, J 2021, 'Thermal decomposition kinetic study of non-recyclable paper and plastic waste by thermogravimetric analysis', *ChemEngineering*, vol. 5, no. 3, p. 54.

Al-Rumaihi, A, Shahbaz, M, Mckay, G, Mackey, H & Al-Ansari, T 2022, 'A review of pyrolysis technologies and feedstock: A blending approach for plastic and biomass towards optimum biochar yield', *Renewable and Sustainable Energy Reviews*, vol. 167, p. 112715.

Al–Widyan, MIaAJ, H. F. 2001, 'STRESS–DENSITY RELATIONSHIP AND ENERGY REQUIREMENT OF COMPRESSED OLIVE CAKE, ' *Applied Engineering in Agriculture*, vol. 17, no. 6, pp. 749-53.

Al Afif, R, Anayah, SS & Pfeifer, C 2020, 'Batch pyrolysis of cotton stalks for evaluation of biochar energy potential', *Renewable Energy*, vol. 147, pp. 2250-8.

Alam, MS & Tanveer, MS 2020, 'Conversion of biomass into biofuel: a cutting-edge technology', in *Bioreactors*, Elsevier, pp. 55-74.

Alauddin, ZABZ, Lahijani, P, Mohammadi, M & Mohamed, AR 2010, 'Gasification of lignocellulosic biomass in fluidized beds for renewable energy development: A review', *Renewable and Sustainable Energy Reviews*, vol. 14, no. 9, pp. 2852-62.

Albu, P, Bolcu, C, Vlase, G, Doca, N & Vlase, T 2011, 'Kinetics of degradation under non-isothermal conditions of a thermooxidative stabilized polyurethane', *Journal of thermal analysis and calorimetry*, vol. 105, no. 2, pp. 685-9.

Ali, I, Bahaitham, H & Naebulharam, R 2017, 'A comprehensive kinetics study of coconut shell waste pyrolysis', *Bioresource technology*, vol. 235, pp. 1-11.

Alvarez, A, Pizarro, C, Garcia, R, Bueno, JL & Lavin, AG 2016, 'Determination of kinetic parameters for biomass combustion', *Bioresour Technol*, vol. 216, pp. 36-43.

Alves, JLF, Da Silva, JCG, Costa, RL, Dos Santos Junior, SF, da Silva Filho, VF, Moreira, RDFPM & José, HJ 2019, 'Investigation of the bioenergy potential of microalgae Scenedesmus acuminatus by physicochemical characterization and kinetic analysis of pyrolysis', *Journal of thermal analysis and calorimetry*, vol. 135, no. 6, pp. 3269-80.

Amalina, F, Abd Razak, AS, Krishnan, S, Sulaiman, H, Zularisam, A & Nasrullah, M 2022, 'Advanced techniques in the production of biochar from lignocellulosic biomass and environmental applications', *Cleaner Materials*, p. 100137.

Amutio, M, Lopez, G, Artetxe, M, Elordi, G, Olazar, M & Bilbao, J 2012, 'Influence of temperature on biomass pyrolysis in a conical spouted bed reactor', *Resources, Conservation and Recycling*, vol. 59, pp. 23-31.

Anca-Couce, A 2016, 'Reaction mechanisms and multi-scale modelling of lignocellulosic biomass pyrolysis', *Progress in energy and combustion science*, vol. 53, pp. 41-79.

Anca-Couce, A, Tsekos, C, Retschitzegger, S, Zimbardi, F, Funke, A, Banks, S, Kraia, T, Marques, P, Scharler, R & de Jong, W 2020, 'Biomass pyrolysis TGA assessment with an international round robin', *Fuel*, vol. 276, p. 118002.

ANSYS, I 2015, *ANSYS fluent theory guide*, ANSYS, Inc., Southpointe, 2600 ANSYS Drive, Canonsburg, PA 15317.

ANSYS, I 2018, *ANSYS fluent theory guide*, ANSYS, Inc., Southpointe, 2600 ANSYS Drive, Canonsburg, PA 15317.

Antonopoulos, I-S, Karagiannidis, A, Gkouletsos, A & Perkoulidis, G 2012, 'Modelling of a downdraft gasifier fed by agricultural residues', *Waste management*, vol. 32, no. 4, pp. 710-8.

Antonopoulos, IS, Karagiannidis, A, Gkouletsos, A & Perkoulidis, G 2012, 'Modelling of a downdraft gasifier fed by agricultural residues', *Waste Manag*, vol. 32, no. 4, pp. 710-8.

Anukam, A, Berghel, J, Henrikson, G, Frodeson, S & Ståhl, M 2021, 'A review of the mechanism of bonding in densified biomass pellets', *Renewable and Sustainable Energy Reviews*, vol. 148, p. 111249.

Anwar, MR, Li Liu, D, Farquharson, R, Macadam, I, Abadi, A, Finlayson, J, Wang, B & Ramilan, T 2015, 'Climate change impacts on phenology and yields of five broadacre crops at four climatologically distinct locations in Australia', *Agricultural systems*, vol. 132, pp. 133-44.

AOAC 1990a, *AOAC method 992.16 – total dietary fiber - enzymatic gravimetric method. In: Official Methods of Analysis of Association of Official Analytical Chemists (Gaithersberg. ed) (18th ed.). Association of Official Analytic Chemists, MD, USA.*

AOAC 1990b, *AOAC method 973.18—fiber (acid detergent) and lignin in animal feeds. In: Helrick K, editor. Official method of analysis of the Association of Official Analytical Chemists, 15th ed., vol. 82. Arlington, VA: Association of Official Analytical Chemists; 1990.*

AOAC 1990c, 'AOAC Method 942.05 – ash in animal feeds. In official method of analysis of the association of official analytical chemists, 15th ed., 1990, Vol. 70. Gaithersburg, MD: Association of Official Analytic Chemists1990. '.

AOAC 2002, *Official Methods of Analysis of AOAC International, Seventeen, AOAC International, Gaithersburg, 2002. Hach, Water Analysis Handbook, Hach Company, Loveland, CO, USA, 2015*, https://www.hach.com/wah>.

AOAC 2006, *Official Method 990.03, Protein (Crude) in Animal Feed, Combustion Method, in Official Methods of Analysis of AOAC International, 18th edition Revision 1, 2006. Chapter 4, pp. 30-31, AOAC International, Gaithersburg, MD.*

Aqsha, A, Tijani, MM, Moghtaderi, B & Mahinpey, N 2017, 'Catalytic pyrolysis of straw biomasses (wheat, flax, oat and barley) and the comparison of their product yields', *Journal of Analytical and Applied Pyrolysis*, vol. 125, pp. 201-8.

Arias, B, Pevida, C, Rubiera, F & Pis, J 2008, 'Effect of biomass blending on coal ignition and burnout during oxy-fuel combustion', *Fuel*, vol. 87, no. 12, pp. 2753-9.

Arous, S, Koubaa, A, Bouafif, H, Bouslimi, B, Braghiroli, FL & Bradai, C 2021, 'Effect of pyrolysis temperature and wood species on the properties of biochar pellets', *Energies*, vol. 14, no. 20, p. 6529.

Asadieraghi, M & Daud, WMAW 2014, 'Characterization of lignocellulosic biomass thermal degradation and physiochemical structure: Effects of demineralization by diverse acid solutions', *Energy Conversion and Management*, vol. 82, pp. 71-82.

Aslan, DI, Özoğul, B, Ceylan, S & Geyikçi, F 2018, 'Thermokinetic analysis and product characterization of Medium Density Fiberboard pyrolysis', *Bioresource technology*, vol. 258, pp. 105-10.

ASTM 1998, *ASTM Standards D 3173-87 - standard test method for moisture in the analysis sample of coal and coke. In: Furcola NC, editor Annual book of ASTM standards, section 5, vol.05.05. West Conshohocken, PA, USA: American Society for Testing and Materials; 1998. p. 301–2.*

ASTM 2003, *D5865-03-standard test method for gross calorific value of coal and coke. In: Annual book of ASTM standards. West Conshohocken, PA, USA: American Society for Testing and Materials; 2003. p. 517-27. 05.06.*

ASTM 2004, *Standard Test Method for Designating the Size of RDF-3 From its Sieve Analysis*, Engineering 360, viewed 09/01/2022, <https://standards.globalspec.com/std/3817125/astm-e828-81-2004>.

ASTM 2008, *Standard D5373, Standard Test Methods for Instrumental Determination of Carbon, Hydrogen, and Nitrogen in Laboratory Samples of Coal. ASTM International, West Conshohocken*, http://dx.doi.org/10.1520/D5373-08>.

ASTM 2013, *ASTM E873-82: Standard Test Method For Bulk Density Of Densified Particulate Biomass Fuels*, ASTM International.

Ataei, A, Azimi, A, Kalhori, SB, Abari, MF & Radnezhad, H 2012, 'Performance analysis of a co-gasifier for organic waste in agriculture', *International Journal of Recycling of Organic Waste in Agriculture*, vol. 1, no. 1, pp. 1-10.

Auersvald, M, Shumeiko, B, Vrtiška, D, Straka, P, Staš, M, Šimáček, P, Blažek, J & Kubička, D 2019, 'Hydrotreatment of straw bio-oil from ablative fast pyrolysis to produce suitable refinery intermediates', *Fuel*, vol. 238, pp. 98-110.

Azocar, L, Hermosilla, N, Gay, A, Rocha, S, Díaz, J & Jara, P 2019, 'Brown pellet production using wheat straw from southern cities in Chile', *Fuel*, vol. 237, pp. 823-32.

Babler, MU, Phounglamcheik, A, Amovic, M, Ljunggren, R & Engvall, K 2017, 'Modeling and pilot plant runs of slow biomass pyrolysis in a rotary kiln', *Applied energy*, vol. 207, pp. 123-33.

Babu, BV & Sheth, PN 2006, 'Modeling and simulation of reduction zone of downdraft biomass gasifier: Effect of char reactivity factor', *Energy Conversion and Management*, vol. 47, no. 15-16, pp. 2602-11.

Bach, Q-V & Chen, W-H 2017, 'A comprehensive study on pyrolysis kinetics of microalgal biomass', *Energy Conversion and Management*, vol. 131, pp. 109-16.

Bahng, MK, Mukarakate, C, Robichaud, DJ & Nimlos, MR 2009, 'Current technologies for analysis of biomass thermochemical processing: a review', *Anal Chim Acta*, vol. 651, no. 2, pp. 117-38.

Bajwa, DS, Peterson, T, Sharma, N, Shojaeiarani, J & Bajwa, SG 2018, 'A review of densified solid biomass for energy production', *Renewable and Sustainable Energy Reviews*, vol. 96, pp. 296-305.

Balasundram, V, Alias, N, Ibrahim, N, Kasmani, RM, Isha, R, Hamid, MKA & Hasbullah, H 2018, 'Thermal characterization of Malaysian biomass via thermogravimetric analysis', *Journal of Energy and Safety Technology (JEST)*, vol. 1, no. 1.

Balat, M & Ayar, G 2005, 'Biomass energy in the world, use of biomass and potential trends', *Energy Sources*, vol. 27, no. 10, pp. 931-40.

Balsora, HK, Kartik, S, Rainey, TJ, Abbas, A, Joshi, JB, Sharma, A & Chakinala, AG 2021, 'Kinetic modelling for thermal decomposition of agricultural residues at different heating rates', *Biomass conversion and biorefinery*, pp. 1-15.

Banerjee, A, Vithusha, T, Krishna, BB, Kumar, J, Bhaskar, T & Ghosh, D 2021, 'Pyrolysis of de-oiled yeast biomass of Rhodotorula mucilaginosa IIPL32: Kinetics and thermodynamic parameters using thermogravimetric analysis', *Bioresource technology*, vol. 340, p. 125534.

Barco-Burgos, J, Carles-Bruno, J, Eicker, U, Saldana-Robles, A & Alcántar-Camarena, V 2021, 'Hydrogen-rich syngas production from palm kernel shells (PKS) biomass on a downdraft allothermal gasifier using steam as a gasifying agent', *Energy Conversion and Management*, vol. 245, p. 114592.

Barman, NS, Ghosh, S & De, S 2012, 'Gasification of biomass in a fixed bed downdraft gasifier–A realistic model including tar', *Bioresource technology*, vol. 107, pp. 505-11.

Barone, G & Martelli, D 2014, 'Validation of the coupled calculation between RELAP5 STH code and Ansys FLUENT CFD code'.

Baruah, B, Tiwari, P, Thakur, P & Kataki, R 2018, 'TGA-FTIR analysis of Upper Assam oil shale, optimization of lab-scale pyrolysis process parameters using RSM', *Journal of Analytical and Applied Pyrolysis*, vol. 135, pp. 397-405.

Baruah, D & Baruah, DC 2014, 'Modeling of biomass gasification: A review', *Renewable and Sustainable Energy Reviews*, vol. 39, pp. 806-15.

Baruah, D, Baruah, DC & Hazarika, MK 2017, 'Artificial neural network based modeling of biomass gasification in fixed bed downdraft gasifiers', *Biomass and bioenergy*, vol. 98, pp. 264-71.

Barud, HS, Ribeiro, CA, Capela, JM, Crespi, MS, Ribeiro, SJ & Messadeq, Y 2011, 'Kinetic parameters for thermal decomposition of microcrystalline, vegetal, and bacterial cellulose', *Journal of thermal analysis and calorimetry*, vol. 105, no. 2, pp. 421-6.

Barzegar, R, Yozgatligil, A, Olgun, H & Atimtay, AT 2020, 'TGA and kinetic study of different torrefaction conditions of wood biomass under air and oxy-fuel combustion atmospheres', *Journal of the Energy Institute*, vol. 93, no. 3, pp. 889-98.

Basu, P 2010, *Biomass gasification and pyrolysis: practical design and theory*, Academic press.

Basu, P 2018, *Biomass Gasification, Pyrolysis and Torrefaction - Practical Design and Theory*,

Academic Press, United State of America.

Beenackers, A 1999, 'Biomass gasification in moving beds, a review of European technologies', *Renewable Energy*, vol. 16, no. 1-4, pp. 1180-6.

Beohar, H, Gupta, B, Sethi, V & Pandey, M 2012, 'Parametric study of fixed bed biomass gasifier: a review', *International Journal of Thermal Technologies*, vol. 2, no. 1, pp. 134-40.

Berghel, J, Frodeson, S, Granström, K, Renström, R, Ståhl, M, Nordgren, D & Tomani, P 2013, 'The effects of kraft lignin additives on wood fuel pellet quality, energy use and shelf life', *Fuel processing technology*, vol. 112, pp. 64-9.

Bhatti, MM, Marin, M, Zeeshan, A & Abdelsalam, SI 2020, 'Recent trends in computational fluid dynamics', *Frontiers in Physics*, vol. 8, p. 593111.

Bhavanam, A & Sastry, R 2011, 'Biomass gasification processes in downd raft fixed bed reactors: a review', *International Journal of Chemical Engineering and Applications*, vol. 2, no. 6, p. 425.

Bhoi, PR, Huhnke, RL, Kumar, A, Thapa, S & Indrawan, N 2018, 'Scale-up of a downdraft gasifier system for commercial scale mobile power generation', *Renewable Energy*, vol. 118, pp. 25-33.

Biagini, E, Bardi, A, Pannocchia, G & Tognotti, L 2009, 'Development of an entrained flow gasifier model for process optimization study', *Industrial & Engineering Chemistry Research*, vol. 48, no. 19, pp. 9028-33.

Biederbeck, V, Campbell, C, Bowren, K, Schnitzer, M & McIver, R 1980, 'Effect of burning cereal straw on soil properties and grain yields in Saskatchewan', *Soil Science Society of America Journal*, vol. 44, no. 1, pp. 103-11.

Bilal, M, Asgher, M, Iqbal, HM, Hu, H & Zhang, X 2017, 'Biotransformation of lignocellulosic materials into value-added products—a review', *International Journal of Biological Macromolecules*, vol. 98, pp. 447-58.

Biswas, B, Pandey, N, Bisht, Y, Singh, R, Kumar, J & Bhaskar, T 2017, 'Pyrolysis of agricultural biomass residues: Comparative study of corn cob, wheat straw, rice straw and rice husk', *Bioresour Technol*, vol. 237, pp. 57-63.

Blaine, RL & Kissinger, HE 2012, 'Homer Kissinger and the Kissinger equation', *Thermochimica Acta*, vol. 540, pp. 1-6.

Boac, JM, Casada, ME & Maghirang, RG 2008, 'Feed pellet and corn durability and breakage during repeated elevator handling', *Applied Engineering in Agriculture*, vol. 24, no. 5, pp. 637-43.

Bockelie, MJ, Denison, MK, Chen, Z, Linjewile, T, Senior, CL, Sarofim, AF & Holt, N 2002, 'CFD modeling for entrained flow gasifiers', *Gasification technologies conference*, Citeseer.

Bonechi, C, Consumi, M, Donati, A, Leone, G, Magnani, A, Tamasi, G & Rossi, C 2017, 'Biomass: an overview', *Bioenergy systems for the future*, pp. 3-42.

Boukaous, N, Abdelouahed, L, Chikhi, M, Meniai, A-H, Mohabeer, C & Bechara, T 2018, 'Combustion of flax shives, beech wood, pure woody pseudo-components and their chars: a thermal and kinetic study', *Energies*, vol. 11, no. 8, p. 2146.

Brand, MA, Mariano Rodrigues, T, Peretti da Silva, J & de Oliveira, J 2021, 'Recovery of agricultural and wood wastes: The effect of biomass blends on the quality of pellets', *Fuel*, vol. 284.

Brar, JS, Singh, K, Zondlo, J & Wang, J 2012, 'Co-gasification of Coal and Hardwood Pellets: Syngas Composition, Carbon Efficiency and Energy Efficiency', *2012 Dallas, Texas, July 29-August 1, 2012*, American Society of Agricultural and Biological Engineers, p. 1.

Bray, CD, Battye, WH & Aneja, VP 2019, 'The role of biomass burning agricultural emissions in the Indo-Gangetic Plains on the air quality in New Delhi, India', *Atmospheric environment*, vol. 218, p. 116983.

Bridgeman, T, Jones, J, Shield, I & Williams, P 2008, 'Torrefaction of reed canary grass, wheat straw and willow to enhance solid fuel qualities and combustion properties', *Fuel*, vol. 87, no. 6, pp. 844-56.

Bridgeman, TG, Jones, JM, Shield, IF & Williams, PT 2008, 'Torrefaction of reed canary grass, wheat straw and willow to enhance solid fuel qualities and combustion properties', *Fuel*, vol. 87, pp. 844-56.

Bridgwater, A 1995, 'The technical and economic feasibility of biomass gasification for power generation', *Fuel*, vol. 74, no. 5, pp. 631-53.

Bridgwater, AV 2012, 'Review of fast pyrolysis of biomass and product upgrading', *Biomass and bioenergy*, vol. 38, pp. 68-94.

Brown, D 2013, *Using mobile distributed pyrolysis facilities to deliver a forest residue resource for bio-fuel production*, University of Victoria (Canada).

Bueno, S, Durán, E, Gámiz, B & Hermosín, MC 2021, 'Formulating low cost modified bentonite with natural binders to remove pesticides in a pilot water filter system', *Journal of Environmental Chemical Engineering*, vol. 9, no. 1, p. 104623.

Burhenne, L, Messmer, J, Aicher, T & Laborie, M-P 2013, 'The effect of the biomass components lignin, cellulose and hemicellulose on TGA and fixed bed pyrolysis', *Journal of Analytical and Applied Pyrolysis*, vol. 101, pp. 177-84.

Buss, J, Mansuy, N, Laganière, J & Persson, D 2022, 'Greenhouse gas mitigation potential of replacing diesel fuel with wood-based bioenergy in an artic Indigenous community: A pilot study in Fort McPherson, Canada', *Biomass and bioenergy*, vol. 159, p. 106367.

Cai, J, Wu, W, Liu, R & Huber, GW 2013, 'A distributed activation energy model for the pyrolysis of lignocellulosic biomass', *Green Chemistry*, vol. 15, no. 5, pp. 1331-40.

Cai, J, Xu, D, Dong, Z, Yu, X, Yang, Y, Banks, SW & Bridgwater, AV 2018, 'Processing thermogravimetric analysis data for isoconversional kinetic analysis of lignocellulosic biomass pyrolysis: Case study of corn stalk', *Renewable and Sustainable Energy Reviews*, vol. 82, pp. 2705-15.

Cai, W, Liu, P, Chen, B, Xu, H, Liu, Z, Zhou, Q, Yu, F, Liu, M, Chen, M & Liu, J 2019, 'Plastic waste fuelled solid oxide fuel cell system for power and carbon nanotube cogeneration', *International Journal of Hydrogen Energy*, vol. 44, no. 3, pp. 1867-76.

Calabi-Floody, M, Medina, J, Rumpel, C, Condron, LM, Hernandez, M, Dumont, M & de La Luz Mora, M 2018, 'Smart fertilizers as a strategy for sustainable agriculture', *Advances in agronomy*, vol. 147, pp. 119-57.

Cao, L, Yuan, X, Li, H, Li, C, Xiao, Z, Jiang, L, Huang, B, Xiao, Z, Chen, X & Wang, H 2015, 'Complementary effects of torrefaction and co-pelletization: Energy consumption and characteristics of pellets', *Bioresource technology*, vol. 185, pp. 254-62.

Cao, W, Li, J, Martí-Rosselló, T & Zhang, X 2019, 'Experimental study on the ignition characteristics of cellulose, hemicellulose, lignin and their mixtures', *Journal of the Energy Institute*, vol. 92, no. 5, pp. 1303-12.

Caputo, AC, Palumbo, M, Pelagagge, PM & Scacchia, F 2005, 'Economics of biomass energy utilization in combustion and gasification plants: effects of logistic variables', *Biomass and bioenergy*, vol. 28, no. 1, pp. 35-51.

Carone, MT, Pantaleo, A & Pellerano, A 2011, 'Influence of process parameters and biomass characteristics on the durability of pellets from the pruning residues of Olea europaea L', *Biomass and bioenergy*, vol. 35, no. 1, pp. 402-10.

Carpenter, D, Westover, TL, Czernik, S & Jablonski, W 2014, 'Biomass feedstocks for renewable fuel production: a review of the impacts of feedstock and pretreatment on the yield and product distribution of fast pyrolysis bio-oils and vapors', *Green Chemistry*, vol. 16, no. 2, pp. 384-406.

Carrier, M, Loppinet-Serani, A, Denux, D, Lasnier, J-M, Ham-Pichavant, F, Cansell, F & Aymonier, C 2011, 'Thermogravimetric analysis as a new method to determine the lignocellulosic composition of biomass', *Biomass and bioenergy*, vol. 35, no. 1, pp. 298-307.

Carvalho, L, Wopienka, E, Pointner, C, Lundgren, J, Verma, VK, Haslinger, W & Schmidl, C 2013, 'Performance of a pellet boiler fired with agricultural fuels', *Applied energy*, vol. 104, pp. 286-96.

CEN, D 2004, 'TS 14775: Solid biofuels. Method for the determination of ash content', *British Standards*, p. 12.

Cen, K, Zhang, J, Ma, Z, Chen, D, Zhou, J & Ma, H 2019, 'Investigation of the relevance between biomass pyrolysis polygeneration and washing pretreatment under different severities: Water, dilute acid solution and aqueous phase bio-oil', *Bioresource technology*, vol. 278, pp. 26-33.

Chan, YH, Cheah, KW, How, BS, Loy, ACM, Shahbaz, M, Singh, HKG, Shuhaili, AFA, Yusup, S, Ghani, WAWAK & Rambli, J 2019, 'An overview of biomass thermochemical conversion technologies in Malaysia', *Science of the Total Environment*, vol. 680, pp. 105-23.

Chandra, R, Takeuchi, H & Hasegawa, T 2012, 'Methane production from lignocellulosic agricultural crop wastes: A review in context to second generation of biofuel production', *Renewable and Sustainable Energy Reviews*, vol. 16, no. 3, pp. 1462-76.

Chandrasekaran, SR, Hopke, PK, Hurlbut, A & Newtown, M 2013, 'Characterization of emissions from grass pellet combustion', *Energy & Fuels*, vol. 27, no. 9, pp. 5298-306.

Channiwala, S & Parikh, P 2002, 'A unified correlation for estimating HHV of solid, liquid and gaseous fuels', *Fuel*, vol. 81, no. 8, pp. 1051-63.

Chelouche, S, Trache, D, Tarchoun, AF, Abdelaziz, A, Khimeche, K & Mezroua, A 2019, 'Organic eutectic mixture as efficient stabilizer for nitrocellulose: kinetic modeling and stability assessment', *Thermochimica Acta*, vol. 673, pp. 78-91.

Chen, G, Anderson, JA, Bannister, P & Carrington, CG 2002, 'Monitoring and performance of a commercial grain dryer', *Biosystems Engineering*, vol. 81, pp. 73-84.

Chen, G, Yao, J, Yang, H, Yan, B & Chen, H 2015, 'Steam gasification of acid-hydrolysis biomass CAHR for clean syngas production', *Bioresource technology*, vol. 179, pp. 323-30.

Chen, H 2014, 'Chemical composition and structure of natural lignocellulose', in *Biotechnology of lignocellulose*, Springer, pp. 25-71.

Chen, J, Wang, Y, Lang, X & Fan, S 2017, 'Comparative evaluation of thermal oxidative decomposition for oil-plant residues via thermogravimetric analysis: thermal conversion characteristics, kinetics, and thermodynamics', *Bioresource technology*, vol. 243, pp. 37-46.

Chen, J, Liu, J, He, Y, Huang, L, Sun, S, Sun, J, Chang, K, Kuo, J, Huang, S & Ning, X 2017, 'Investigation of co-combustion characteristics of sewage sludge and coffee grounds mixtures using thermogravimetric analysis coupled to artificial neural networks modeling', *Bioresource technology*, vol. 225, pp. 234-45.

Chen, W-H, Wang, C-W, Ong, HC, Show, PL & Hsieh, T-H 2019, 'Torrefaction, pyrolysis and two-stage thermodegradation of hemicellulose, cellulose and lignin', *Fuel*, vol. 258, p. 116168.

Chen, W-H, Lin, B-J, Lin, Y-Y, Chu, Y-S, Ubando, AT, Show, PL, Ong, HC, Chang, J-S, Ho, S-H & Culaba, AB 2021, 'Progress in biomass torrefaction: Principles, applications and challenges', *Progress in energy and combustion science*, vol. 82, p. 100887.

Chen, X, Che, Q, Li, S, Liu, Z, Yang, H, Chen, Y, Wang, X, Shao, J & Chen, H 2019, 'Recent developments in lignocellulosic biomass catalytic fast pyrolysis: Strategies for the optimization of bio-oil quality and yield', *Fuel processing technology*, vol. 196, p. 106180.

Cheng, K, Winter, WT & Stipanovic, AJ 2012, 'A modulated-TGA approach to the kinetics of lignocellulosic biomass pyrolysis/combustion', *Polymer degradation and stability*, vol. 97, no. 9, pp. 1606-15.

Cherubini, F & Ulgiati, S 2010, 'Crop residues as raw materials for biorefinery systems–A LCA case study', *Applied energy*, vol. 87, no. 1, pp. 47-57.

Chiang, W-F, Fang, H-Y, Wu, C-H, Huang, C-J, Chang, C-Y, Chang, Y-M & Chen, C-L 2009, 'The effect of oxygen on the kinetics of the thermal degradation for rice straw', *Journal of the Air & Waste Management Association*, vol. 59, no. 2, pp. 148-54.

Chogani, A, Moosavi, A, Sarvestani, AB & Shariat, M 2020, 'The effect of chemical functional groups and salt concentration on performance of single-layer graphene membrane in water desalination process: A molecular dynamics simulation study', *Journal of Molecular Liquids*, vol. 301, p. 112478.

Chong, CT, Mong, GR, Ng, J-H, Chong, WWF, Ani, FN, Lam, SS & Ong, HC 2019, 'Pyrolysis characteristics and kinetic studies of horse manure using thermogravimetric analysis', *Energy Conversion and Management*, vol. 180, pp. 1260-7.

Chrissafis, K, Roumeli, E, Paraskevopoulos, K, Nianias, N & Bikiaris, D 2012, 'Effect of different nanoparticles on thermal decomposition of poly (propylene sebacate)/nanocomposites: Evaluation of mechanisms using TGA and TG–FTIR–GC/MS', *Journal of Analytical and Applied Pyrolysis*, vol. 96, pp. 92-9.

Chun, Y, Sheng, G, Chiou, CT & Xing, B 2004, 'Compositions and Sorptive Properties of Crop Residue-Derived Chars', *Environmental Science & Technology*, vol. 38, pp. 4649-55.

Ciferno, JP & Marano, JJ 2002, 'Benchmarking biomass gasification technologies for fuels, chemicals and hydrogen production', *US Department of Energy. National Energy Technology Laboratory*.

Coker, A 2001, 'Introduction to reactor design fundamentals for ideal systems', *Modeling of chemical kinetics and reactor design*, pp. 371-2.

Collard, F-X & Blin, J 2014, 'A review on pyrolysis of biomass constituents: Mechanisms and composition of the products obtained from the conversion of cellulose, hemicelluloses and lignin', *Renewable and Sustainable Energy Reviews*, vol. 38, pp. 594-608.

Collot, A-G, Zhuo, Y, Dugwell, D & Kandiyoti, R 1999, 'Co-pyrolysis and co-gasification of coal and biomass in bench-scale fixed-bed and fluidised bed reactors', *Fuel*, vol. 78, no. 6, pp. 667-79.

Contreras-Andrade, I, Martínez-González, M, Figueroa-Casallas, L, Parra-Santiago, J & Guerrero-Fajardo, C 2014, 'Modeling of liquid-liquid extraction process for glycerol purification from biodiesel production', *J Chem Eng Mater Sci*, vol. 8, pp. 971-7.

Couto, N, Monteiro, E, Silva, V & Rouboa, A 2016, 'Hydrogen-rich gas from gasification of Portuguese municipal solid wastes', *International Journal of Hydrogen Energy*, vol. 41, no. 25, pp. 10619-30.

Cozzani, V, Lucchesi, A, Stoppato, G & Maschio, G 1997, 'A new method to determine the composition of biomass by thermogravimetric analysis', *The Canadian Journal of Chemical Engineering*, vol. 75, no. 1, pp. 127-33.

Craven, JM, Swithenbank, J, Sharifi, VN, Peralta-Solorio, D, Kelsall, G & Sage, P 2015, 'Hydrophobic coatings for moisture stable wood pellets', *Biomass and bioenergy*, vol. 80, pp. 278-85.

Cuadros, F, González-González, A, Ruiz-Celma, A, López-Rodríguez, F, García-Sanz-Calcedo, J, García, J & Mena, A 2013, 'Challenges of biomass in a development model based on renewable energies', in *Without Bounds: A Scientific Canvas of Nonlinearity and Complex Dynamics*, Springer, pp. 747-68.

Cui, L, Liu, Z, Si, C, Hui, L, Kang, N & Zhao, T 2012, 'Influence of steam explosion pretreatment on the composition and structure of wheat straw', *BioResources*, vol. 7, no. 3, pp. 4202-13.

Czaplicka, M, Klyta, J, Komosiński, B, Konieczny, T & Janoszka, K 2021, 'Comparison of Carbonaceous Compounds Emission from the Co-Combustion of Coal and Waste in Boilers Used in Residential Heating in Poland, Central Europe', *Energies*, vol. 14, no. 17, p. 5326.

Dahms, RNU 2018, *Modeling turbulence-chemistry interactions for multi-zone combustion techniques*, Sandia National Lab.(SNL-CA), Livermore, CA (United States).

Damartzis, T, Vamvuka, D, Sfakiotakis, S & Zabaniotou, A 2011, 'Thermal degradation studies and kinetic modeling of cardoon (Cynara cardunculus) pyrolysis using thermogravimetric analysis (TGA)', *Bioresource technology*, vol. 102, no. 10, pp. 6230-8.

Das, BJ, Das, S, Boro, R, Nath, BP & Basumatary, AK 2022, 'Study and fabrication on heat efficient stove of low smoke emission', *Journal of The Institution of Engineers (India): Series E*, vol. 103, no. 1, pp. 125-34.

Datta, A, Hossain, A & Roy, S 2019, 'An overview on biofuels and their advantages and disadvantages'.

Dayoub, EJ, Eberly, LA, Nathan, AS, Khatana, SAM, Adusumalli, S, Navar, AM, Giri, J & Groeneveld, PW 2021, 'Adoption of PCSK9 Inhibitors Among Patients With Atherosclerotic Disease', *J Am Heart Assoc*, vol. 10, no. 9, p. e019331.

De Conto, D, Silvestre, WP, Baldasso, C & Godinho, M 2016, 'Performance of rotary kiln reactor for the elephant grass pyrolysis', *Bioresour Technol*, vol. 218, pp. 153-60.

De Corato, U, De Bari, I, Viola, E & Pugliese, M 2018, 'Assessing the main opportunities of integrated biorefining from agro-bioenergy co/by-products and agroindustrial residues into high-value added products associated to some emerging markets: A review', *Renewable and Sustainable Energy Reviews*, vol. 88, pp. 326-46.

de Jesus, MS, Martinez, CLM, Costa, LJ, Pereira, EG & de Carneiro, ACO 2020, 'Thermal conversion of biomass: a comparative review of different pyrolysis processes', *Revista Ciência da Madeira (Brazilian Journal of Wood Science)*, vol. 11, no. 1.

De, S & Assadi, M 2009, 'Impact of cofiring biomass with coal in power plants–A techno-economic assessment', *Biomass and bioenergy*, vol. 33, no. 2, pp. 283-93.

de Souza, HJPL, Arantes, MDC, Vidaurre, GB, Andrade, CR, Carneiro, AdCO, de Souza, DPL & de Paula Protásio, T 2020, 'Pelletization of eucalyptus wood and coffee growing wastes: Strategies for biomass valorization and sustainable bioenergy production', *Renewable Energy*, vol. 149, pp. 128-40.

Demirbas, A 2004, 'Combustion characteristics of different biomass fuels', *Progress in energy and combustion science*, vol. 30, no. 2, pp. 219-30.

Demirbas, A 2009, 'Pyrolysis mechanisms of biomass materials', *Energy Sources, Part A*, vol. 31, no. 13, pp. 1186-93.

Demirbaş, A 1997, 'Calculation of higher heating values of biomass fuels', *Fuel*, vol. 76, no. 5, pp. 431-4.

Dhanavath, KN, Shah, K, Bhargava, SK, Bankupalli, S & Parthasarathy, R 2018, 'Oxygen–steam gasification of karanja press seed cake: Fixed bed experiments, ASPEN Plus process model development and benchmarking

with saw dust, rice husk and sunflower husk', *Journal of Environmental Chemical Engineering*, vol. 6, no. 2, pp. 3061-9.

Dhyani, V, Kumar, J & Bhaskar, T 2017, 'Thermal decomposition kinetics of sorghum straw via thermogravimetric analysis', *Bioresource technology*, vol. 245, pp. 1122-9.

Di Blasi, C 2000, '<Dynamic behaviour of stratified downdraft gasifiers.pdf>', *Chemical Engineering Science*, vol. 55, no. 15, pp. 2931-44.

Di Blasi, C & Branca, C 2013, 'Modeling a stratified downdraft wood gasifier with primary and secondary air entry', *Fuel*, vol. 104, pp. 847-60.

Di Blasi, C, Tanzi, V & Lanzetta, M 1997, 'A study on the production of agricultural residues in Italy', *Biomass and bioenergy*, vol. 12, no. 5, pp. 321-31.

Dick, E, Ryabov, G, Tugov, A & Soboleva, A 2007, 'Comparing properties of coal ash and alternative-fuel ash', *Thermal engineering*, vol. 54, no. 3, pp. 231-5.

Ding, Y, Ezekoye, OA, Lu, S, Wang, C & Zhou, R 2017, 'Comparative pyrolysis behaviors and reaction mechanisms of hardwood and softwood', *Energy Conversion and Management*, vol. 132, pp. 102-9.

Dobermann, A & Fairhurst, T 2002, 'Rice straw management', *Better Crops International*, vol. 16, no. 1, pp. 7-11.

Doherty, W, Reynolds, A & Kennedy, D 2009, 'The effect of air preheating in a biomass CFB gasifier using ASPEN Plus simulation', *Biomass and bioenergy*, vol. 33, no. 9, pp. 1158-67.

Dragutinovic, N, Nakomcic-Smaragdakis, B, Djuric, S & Djordjic, D 2019, 'Investigation of additives in combustion of wheat straw pellets in a small scale boiler', *Journal of Renewable and Sustainable Energy*, vol. 11, no. 4, p. 043101.

Du, S-W, Chen, W-H & Lucas, J 2007, 'Performances of pulverized coal injection in blowpipe and tuyere at various operational conditions', *Energy Conversion and Management*, vol. 48, no. 7, pp. 2069-76.

Du, S-W, Chen, W-H & Lucas, JA 2014, 'Pretreatment of biomass by torrefaction and carbonization for coal blend used in pulverized coal injection', *Bioresource technology*, vol. 161, pp. 333-9.

Duca, D, Riva, G, Pedretti, EF & Toscano, G 2014, 'Wood pellet quality with respect to EN 14961-2 standard and certifications', *Fuel*, vol. 135, pp. 9-14.

Duffin, R, Tran, L, Brown, D, Stone, V & Donaldson, K 2007, 'Proinflammogenic effects of low-toxicity and metal nanoparticles in vivo and in vitro: highlighting the role of particle surface area and surface reactivity', *Inhalation toxicology*, vol. 19, no. 10, pp. 849-56.

Dufour, A, Girods, P, Masson, E, Rogaume, Y & Zoulalian, A 2009, 'Synthesis gas production by biomass pyrolysis: Effect of reactor temperature on product distribution', *International Journal of Hydrogen Energy*, vol. 34, no. 4, pp. 1726-34.

Dupont, C, Boissonnet, G, Seiler, J-M, Gauthier, P & Schweich, D 2007, 'Study about the kinetic processes of biomass steam gasification', *Fuel*, vol. 86, no. 1-2, pp. 32-40.

Dwyer, S & Teske, S 2018, 'Renewables 2018 global status report', *Renewables 2018 Global Status Report*.

EBC 2012, *European Biochar Certificate - Guidelines for a Sustainable Production of Biochar*, Arbaz, Switzerland, <http://european-biochar.org>.

El-Emam, RS, Dincer, I & Naterer, GF 2012, 'Energy and exergy analyses of an integrated SOFC and coal gasification system', *International Journal of Hydrogen Energy*, vol. 37, no. 2, pp. 1689-97.

El-Sayed, SA & Khairy, M 2017, 'An Experimental Study of Combustion and Emissions of Wheat Straw Pellets in High-Temperature Air Flows', *Combustion Science and Technology*, pp. 1-30.

El-Sayed, SA & Elsaid Mohamed, MK 2018, 'Mechanical properties and characteristics of wheat straw and pellets', *Energy & Environment*, vol. 29, no. 7, pp. 1224-46.

El-Sayed, SA & Mostafa, ME 2020, 'Thermal pyrolysis and kinetic parameter determination of mango leaves using common and new proposed parallel kinetic models', *RSC Advances*, vol. 10, no. 31, pp. 18160-79.

El-Shafay, AS, Hegazi, AA, Zeidan, ESB, El-Emam, SH & Okasha, FM 2020, 'Experimental and numerical study of sawdust air-gasification', *Alexandria Engineering Journal*, vol. 59, no. 5, pp. 3665-79.

Elita, RW 2018, 'THERMOCHEMICAL CONVERSION OF NON-WOODY BIOMASS: UPGRADING COTTON GIN WASTE INTO SOLID FUEL', Thesis (PhD/Research) thesis, University of Southern Queensland, ePrints.

Emami, S, Tabil, LG & Adapa, P 2015, 'Effect of glycerol on densification of agricultural biomass', *International Journal of Agricultural and Biological Engineering*, vol. 8, no. 1, pp. 64-73.

Emami, S, Tabil, LG, Adapa, P, George, E, Tilay, A, Dalai, A, Drisdelle, M & Ketabi, L 2014, 'Effect of fuel additives on agricultural straw pellet quality', *International Journal of Agricultural and Biological Engineering*, vol. 7, no. 2, pp. 92-100.

Emiola-Sadiq, T, Zhang, L & Dalai, AK 2021, 'Thermal and kinetic studies on biomass degradation via thermogravimetric analysis: a combination of model-fitting and model-free approach', *ACS omega*, vol. 6, no. 34, pp. 22233-47.

ENplus 2015, *Quality Certification Scheme For Wood Pellets*, https://enplus-pellets.eu/en-in/?option=com_attachments&task=download&id=145:ENplusHandbook_part3_V3>.

EPC 2013, *European Pellet Council: Handbook for the certification of wood pellets for heating purposes. European Pellet Council; 2013.*

Erakhrumen, AA 2012, 'Biomass gasification: Documented information for adoption/adaptation and further improvements toward sustainable utilisation of renewable natural resources', *International Scholarly Research Notices*, vol. 2012.

Erlich, C & Fransson, TH 2011, 'Downdraft gasification of pellets made of wood, palm-oil residues respective bagasse: Experimental study', *Applied energy*, vol. 88, no. 3, pp. 899-908.

Ethaib, S, Omar, R, Kamal, SMM, Awang Biak, DR & Zubaidi, SL 2020, 'Microwave-assisted pyrolysis of biomass waste: a mini review', *Processes*, vol. 8, no. 9, p. 1190.

Faber, G, Mangin, C & Sick, V 2021, 'Life Cycle and Techno-Economic Assessment Templates for Emerging Carbon Management Technologies', *Front. Sustain. 2: 764057. doi: 10.3389/frsus*.

Fagbemi, L, Khezami, L & Capart, R 2001, 'Pyrolysis products from different biomasses: application to the thermal cracking of tar', *Applied energy*, vol. 69, no. 2001, pp. 293-306.

Fahmi, R, Bridgwater, AV, Donnison, IS, Yates, NE & Jones, JM 2008, 'The effect of lignin and inorganic species in biomass on pyrolysis oil yields, quality and stability', *Fuel*, vol. 87, pp. 1230-40.

Fahmy, TY, Fahmy, Y, Mobarak, F, El-Sakhawy, M & Abou-Zeid, RE 2020, 'Biomass pyrolysis: past, present, and future', *Environment, Development and Sustainability*, vol. 22, no. 1, pp. 17-32.

Fahmy, TYA, Fahmy, Y, Mobarak, F, El-Sakhawy, M & Abou-Zeid, RE 2018, 'Biomass pyrolysis: past, present, and future', *Environment, Development and Sustainability*, vol. 22, no. 1, pp. 17-32.

Fang, Y, Paul, MC, Varjani, S, Li, X, Park, Y-K & You, S 2021, 'Concentrated solar thermochemical gasification of biomass: Principles, applications, and development', *Renewable and Sustainable Energy Reviews*, vol. 150, p. 111484.

FAO 2017, 'The future of food and agriculture -Trends and challenges', https://www.fao.org/3/i6583e/i6583e.pdf>.

FAO 2022, *World Food Situation*, Food and Agriculture Organization of the United Nations, Roam, viewed 16 September 2022, <https://www.fao.org/worldfoodsituation/csdb/en/>.

Farooq, MZ, Zeeshan, M, Iqbal, S, Ahmed, N & Shah, SAY 2018, 'Influence of waste tire addition on wheat straw pyrolysis yield and oil quality', *Energy*, vol. 144, pp. 200-6.

Fatma, S, Hameed, A, Noman, M, Ahmed, T, Shahid, M, Tariq, M, Sohail, I & Tabassum, R 2018, 'Lignocellulosic biomass: a sustainable bioenergy source for the future', *Protein and peptide letters*, vol. 25, no. 2, pp. 148-63.

Fedunik-Hofman, L, Bayon, A & Donne, SW 2019, 'Kinetics of Solid-Gas Reactions and Their Application to Carbonate Looping Systems', *Energies*, vol. 12, no. 15.

Fernandez, A, Ortiz, LR, Asensio, D, Rodriguez, R & Mazza, G 2020, 'Kinetic analysis and thermodynamics properties of air/steam gasification of agricultural waste', *Journal of Environmental Chemical Engineering*, vol. 8, no. 4, p. 103829.

Fernando, N & Narayana, M 2016, 'A comprehensive two dimensional Computational Fluid Dynamics model for an updraft biomass gasifier', *Renewable Energy*, vol. 99, pp. 698-710.

Ferreira, S, Monteiro, E, Brito, P & Vilarinho, C 2019, 'A holistic review on biomass gasification modified equilibrium models', *Energies*, vol. 12, no. 1, p. 160.

Filbakk, T, Jirjis, R, Nurmi, J & Høibø, O 2011, 'The effect of bark content on quality parameters of Scots pine (Pinus sylvestris L.) pellets', *Biomass and Bioenergy*, vol. 35, no. 8, pp. 3342-9.

Fonseca, FG, Anca-Couce, A, Funke, A & Dahmen, N 2022, 'Challenges in Kinetic Parameter Determination for Wheat Straw Pyrolysis', *Energies*, vol. 15, no. 19, p. 7240.

Forbes, E, Easson, D, Lyons, G & McRoberts, W 2014, 'Physico-chemical characteristics of eight different biomass fuels and comparison of combustion and emission results in a small scale multi-fuel boiler', *Energy Conversion and Management*, vol. 87, pp. 1162-9.

Fouilland, T, Grace, JR & Ellis, N 2010, 'Recent advances in fluidized bed technology in biomass processes', *Biofuels*, vol. 1, no. 3, pp. 409-33.

Fromm, J, Rockel, B, Lautner, S, Windeisen, E & Wanner, G 2003, 'Lignin distribution in wood cell walls determined by TEM and backscattered SEM techniques', *Journal of structural biology*, vol. 143, no. 1, pp. 77-84.

Fu, J, Xie, G, Ji, C, Wang, W, Zhou, Y, Zhang, G, Zha, X & Abdeen, MA 2021, 'Study on the distribution pattern of threshed mixture by drum-shape bar-tooth longitudinal axial flow threshing and separating device', *Agriculture*, vol. 11, no. 8, p. 756.

Fu, R, Kang, L, Zhang, C & Fei, Q 2022, 'The application and progress of techno-economic analysis and life cycle assessment in biomanufacturing of fuels and chemicals', *Green Chemical Engineering*.

Fuertes, A, Arbestain, MC, Sevilla, M, Maciá-Agulló, JA, Fiol, S, López, R, Smernik, R, Aitkenhead, W, Arce, F & Macìas, F 2010, 'Chemical and structural properties of carbonaceous products obtained by pyrolysis and hydrothermal carbonisation of corn stover', *Soil Research*, vol. 48, no. 7, pp. 618-26.

Fusi, A, Bacenetti, J, Proto, AR, Tedesco, DE, Pessina, D & Facchinetti, D 2021, 'Pellet Production from Miscanthus: Energy and Environmental Assessment', *Energies*, vol. 14, no. 1, p. 73.

Gabriela, I & Cora, B 2018, 'Estimation of Energy Potential for Solid Pyrolysis By-Products Using Analytical Methods', in P Kusch (ed.), *Analytical Pyrolysis*, IntechOpen Limited, UNITED KINGDOM.

Gageanu, I, Cujbescu, D, Persu, C & Voicu, G 2018, 'Impact of using additives on quality of agricultural biomass pellets', *Eng. Rural Dev*, vol. 17, pp. 1632-8.

Gagliano, A, Nocera, F, Patania, F, Bruno, M & Castaldo, DG 2016, 'A robust numerical model for characterizing the syngas composition in a downdraft gasification process', *Comptes Rendus Chimie*, vol. 19, no. 4, pp. 441-9.

Gai, C, Dong, Y & Zhang, T 2013, 'The kinetic analysis of the pyrolysis of agricultural residue under non-isothermal conditions', *Bioresource technology*, vol. 127, pp. 298-305.

Gajera, B, Tyagi, U, Sarma, AK & Jha, MK 2022, 'Impact of torrefaction on thermal behavior of wheat straw and groundnut stalk biomass: Kinetic and thermodynamic study', *Fuel Communications*, vol. 12, p. 100073.

Gani, A & Naruse, I 2007, 'Effect of cellulose and lignin content on pyrolysis and combustion characteristics for several types of biomass', *Renewable Energy*, vol. 32, no. 4, pp. 649-61.

Gao, J, Zhao, Y, Sun, S, Che, H, Zhao, G & Wu, J 2012, 'Experiments and numerical simulation of sawdust gasification in an air cyclone gasifier', *Chemical Engineering Journal*, vol. 213, pp. 97-103.

Gao, W, Tabil, LG, Dumonceaux, T, Ríos, SE & Zhao, R 2017, 'Optimization of biological pretreatment to enhance the quality of wheat straw pellets', *Biomass and bioenergy*, vol. 97, pp. 77-89.

Gao, Y, Yang, Y, Qin, Z & Sun, Y 2016, 'Factors affecting the yield of bio-oil from the pyrolysis of coconut shell', *SpringerPlus*, vol. 5, no. 1, pp. 1-8.

García, R, Pizarro, C, Lavín, AG & Bueno, JL 2012, 'Characterization of Spanish biomass wastes for energy use', *Bioresource technology*, vol. 103, no. 1, pp. 249-58.

García, R, Pizarro, C, Lavín, AG & Bueno, JL 2013, 'Biomass proximate analysis using thermogravimetry', *Bioresource technology*, vol. 139, pp. 1-4.

García, R, Gil, M, Rubiera, F & Pevida, C 2019, 'Pelletization of wood and alternative residual biomass blends for producing industrial quality pellets', *Fuel*, vol. 251, pp. 739-53.

García, R, Gil, M, Fanjul, A, González, A, Majada, J, Rubiera, F & Pevida, C 2021, 'Residual pyrolysis biochar as additive to enhance wood pellets quality', *Renewable Energy*, vol. 180, pp. 850-9.

Gerun, L, Paraschiv, M, Vîjeu, R, Bellettre, J, Tazerout, M, Gøbel, B & Henriksen, U 2008, 'Numerical investigation of the partial oxidation in a two-stage downdraft gasifier', *Fuel*, vol. 87, no. 7, pp. 1383-93.

Ghaffar, SH & Fan, M 2013, 'Structural analysis for lignin characteristics in biomass straw', *Biomass and bioenergy*, vol. 57, pp. 264-79.

Ghiasi, B, Kumar, L, Furubayashi, T, Lim, CJ, Bi, X, Kim, CS & Sokhansanj, S 2014, 'Densified biocoal from woodchips: is it better to do torrefaction before or after densification?', *Applied Energy*, vol. 134, pp. 133-42.

Gil, J, Corella, J, Aznar, MaP & Caballero, MA 1999, 'Biomass gasification in atmospheric and bubbling fluidized bed: effect of the type of gasifying agent on the product distribution', *Biomass and bioenergy*, vol. 17, no. 5, pp. 389-403.

Gil, MV, Casal, D, Pevida, C, Pis, J & Rubiera, F 2010, 'Thermal behaviour and kinetics of coal/biomass blends during co-combustion', *Bioresource technology*, vol. 101, no. 14, pp. 5601-8.

Gil, MV, Oulego, P, Casal, MD, Pevida, C, Pis, JJ & Rubiera, F 2010, 'Mechanical durability and combustion characteristics of pellets from biomass blends', *Bioresour Technol*, vol. 101, no. 22, pp. 8859-67.

Gilbert, P, Ryu, C, Sharifi, V & Swithenbank, J 2009, 'Effect of process parameters on pelletisation of herbaceous crops', *Fuel*, vol. 88, no. 8, pp. 1491-7.

Giuntoli, J, Boulamanti, AK, Corrado, S, Motegh, M, Agostini, A & Baxter, D 2013, 'Environmental impacts of future bioenergy pathways: the case of electricity from wheat straw bales and pellets', *GCB Bioenergy*, vol. 5, no. 5, pp. 497-512.

Gómez-Barea, A, Leckner, B, Perales, AV, Nilsson, S & Cano, DF 2013, 'Improving the performance of fluidized bed biomass/waste gasifiers for distributed electricity: a new three-stage gasification system', *Applied Thermal Engineering*, vol. 50, no. 2, pp. 1453-62.

Gong, C, Bryant, N, Meng, X, Bhagia, S, Pu, Y, Xin, D, Koch, CB, Felby, C, Thygesen, LG & Ragauskas, A 2021, 'Double bonus: surfactant-assisted biomass pelleting benefits both the pelleting process and subsequent enzymatic saccharification of the pretreated pellets', *Green Chemistry*, vol. 23, no. 2, pp. 1050-61.

González, WA, Pérez, JF, Chapela, S & Porteiro, J 2018, 'Numerical analysis of wood biomass packing factor in a fixed-bed gasification process', *Renewable Energy*, vol. 121, pp. 579-89.

Grammelis, P 2010, *Solid biofuels for energy*, Springer.

Greenhalf, CE, Nowakowski, DJ, Harms, AB, Titiloye, JO & Bridgwater, AV 2013, 'A comparative study of straw, perennial grasses and hardwoods in terms of fast pyrolysis products', *Fuel*, vol. 108, pp. 216-30.

Greenhalf, CE, Nowakowski, DJ, Bridgwater, AV, Titiloye, J, Yates, N, Riche, A & Shield, I 2012, 'Thermochemical characterisation of straws and high yielding perennial grasses', *Industrial Crops and Products*, vol. 36, no. 1, pp. 449-59.

Greinert, A, Mrówczyńska, M, Grech, R & Szefner, W 2020, 'The use of plant biomass pellets for energy production by combustion in dedicated furnaces', *Energies*, vol. 13, no. 2, p. 463.

Grønli, M, Antal, MJ & Varhegyi, G 1999, 'A round-robin study of cellulose pyrolysis kinetics by thermogravimetry', *Industrial & Engineering Chemistry Research*, vol. 38, no. 6, pp. 2238-44.

Grønli, MG, Várhegyi, G & Di Blasi, C 2002, 'Thermogravimetric analysis and devolatilization kinetics of wood', *Industrial & Engineering Chemistry Research*, vol. 41, no. 17, pp. 4201-8.

Grundy, MJ, Bryan, BA, Nolan, M, Battaglia, M, Hatfield-Dodds, S, Connor, JD & Keating, BA 2016, 'Scenarios for Australian agricultural production and land use to 2050', *Agricultural systems*, vol. 142, pp. 70-83.

Gummert, M, Hung, NV, Chivenge, P & Douthwaite, B 2020, *Sustainable rice straw management*, Springer Nature.

Gummert, M, Cabardo, C, Quilloy, R, Aung, YL, Thant, AM, Kyaw, MA, Labios, R, Htwe, NM & Singleton, GR 2020, 'Assessment of post-harvest losses and carbon footprint in intensive lowland rice production in Myanmar', *Scientific reports*, vol. 10, no. 1, pp. 1-13.

Gungor, A & Yildirim, U 2013, 'Two dimensional numerical computation of a circulating fluidized bed biomass gasifier', *Computers & Chemical Engineering*, vol. 48, pp. 234-50.

Guo, F & Zhong, Z 2018, 'Optimization of the co-combustion of coal and composite biomass pellets', *Journal of Cleaner Production*, vol. 185, pp. 399-407.

Guo, S, Wei, X, Li, J, Che, D, Liu, H, Sun, B & Wang, Q 2020, 'Experimental study on product gas and tar removal in air–steam gasification of corn straw in a bench-scale internally circulating fluidized bed', *Energy & Fuels*, vol. 34, no. 2, pp. 1908-17.

Gupta, GK & Mondal, MK 2019, 'Kinetics and thermodynamic analysis of maize cob pyrolysis for its bioenergy potential using thermogravimetric analyzer', *Journal of thermal analysis and calorimetry*, vol. 137, no. 4, pp. 1431-41.

Gupta, R, Jain, P & Vyas, S 2017, 'CFD modeling and simulation of 10 kWe Biomass Downdraft gasifier', *International Journal of Current Engineering and Technolog*, vol. 7, no. 4.

Gupta, S, Agarwal, R & Mittal, SK 2016, 'Respiratory health concerns in children at some strategic locations from high PM levels during crop residue burning episodes', *Atmospheric environment*, vol. 137, pp. 127-34.

Gupta, S, Gupta, GK & Mondal, MK 2020, 'Thermal degradation characteristics, kinetics, thermodynamic, and reaction mechanism analysis of pistachio shell pyrolysis for its bioenergy potential', *Biomass conversion and biorefinery*, pp. 1-15.

Habibi, A, Merci, B & Heynderickx, GJ 2007, 'Impact of radiation models in CFD simulations of steam cracking furnaces', *Computers & Chemical Engineering*, vol. 31, no. 11, pp. 1389-406.

Habibi, R 2013, 'Co-gasification of biomass and non-biomass feedstocks'.

Habibollahzade, A, Ahmadi, P & Rosen, MA 2021, 'Biomass gasification using various gasification agents: Optimum feedstock selection, detailed numerical analyses and tri-objective grey wolf optimization', *Journal of Cleaner Production*, vol. 284, p. 124718.

Halder, P, Kundu, S, Patel, S, Parthasarathy, R, Pramanik, B, Paz-Ferreiro, J & Shah, K 2019, 'TGA-FTIR study on the slow pyrolysis of lignin and cellulose-rich fractions derived from imidazolium-based ionic liquid pre-treatment of sugarcane straw', *Energy Conversion and Management*, vol. 200, p. 112067.

Hameed, Z, Aman, Z, Naqvi, SR, Tariq, R, Ali, I & Makki, AA 2018, 'Kinetic and Thermodynamic Analyses of Sugar Cane Bagasse and Sewage Sludge Co-pyrolysis Process', *Energy & Fuels*, vol. 32, no. 9, pp. 9551-8.

Hamelinck, CN, Faaij, AP, den Uil, H & Boerrigter, H 2004, 'Production of FT transportation fuels from biomass; technical options, process analysis and optimisation, and development potential', *Energy*, vol. 29, no. 11, pp. 1743-71.

Hanafi, EM, El Khadrawy, H, Ahmed, W & Zaabal, M 2012, 'Some observations on rice straw with emphasis on updates of its management', *World Applied Sciences Journal*, vol. 16, no. 3, pp. 354-61.

Handbook, EP 2013, *European Pellet Council: Handbook for the Certification of Wood Pellets for Heating Purposes v. 2.0, based on EN 1496, 1–2*, April.

Harmsen, PF, Huijgen, W, Bermudez, L & Bakker, R 2010, *Literature review of physical and chemical pretreatment processes for lignocellulosic biomass*, Wageningen UR-Food & Biobased Research.

Haykiri-Acma, H & Yaman, S 2008, 'Effect of co-combustion on the burnout of lignite/biomass blends: a Turkish case study', *Waste Management*, vol. 28, no. 11, pp. 2077-84.

Haykiri-Acma, H, Yaman, S & Kucukbayrak, S 2006, 'Effect of heating rate on the pyrolysis yields of rapeseed', *Renewable Energy*, vol. 31, no. 6, pp. 803-10.

Higman, C, van der Burgt, M, Higman, C & Vanderburgt, M 2008, 'The thermodynamics of gasification', *Gasification. Amsterdam, Boston: Gulf Professional Pub./Elsevier Science*, pp. 11-31.

Hoang, AT, Ong, HC, Fattah, IR, Chong, CT, Cheng, CK, Sakthivel, R & Ok, YS 2021, 'Progress on the lignocellulosic biomass pyrolysis for biofuel production toward environmental sustainability', *Fuel processing technology*, vol. 223, p. 106997.

Holt, GA, Blodgett, T & Nakayama, F 2006, 'Physical and combustion characteristics of pellet fuel from cotton gin by-products produced by select processing treatments', *Industrial Crops and Products*, vol. 24, no. 3, pp. 204-13.

Holt, GA, Blodgett, TL & Nakayama, FS 2006, 'Physical and combustion characteristics of pellet fuel from cotton gin by-products produced by select processing treatments', *Industrial Crops and Products*, vol. 24, no. 3, pp. 204-13.

Holubcik, M, Jandacka, J, Palacka, M & Vician, P 2016, 'Additives application to wheat straw to increasing the ash fusion temperature', *Proceedings of the*.

Hong, Z, Zhong, F, Niu, W, Zhang, K, Su, J, Liu, J, Li, L & Wu, F 2020, 'Effects of temperature and particle size on the compositions, energy conversions and structural characteristics of pyrolysis products from different crop residues', *Energy*, vol. 190, p. 116413.

Hoque, ME, Rashid, F & Aziz, M 2021, 'Gasification and power generation characteristics of rice husk, sawdust, and coconut shell using a fixed-bed downdraft gasifier', *Sustainability*, vol. 13, no. 4, p. 2027.

Hossain, MA, Hasan, MR & Islam, MR 2014, 'Design, Fabrication and Performance Study of a Biomass Solid Waste Pyrolysis System for Alternative Liquid Fuel Production', *Global Journal of Researches in Engineering: A Mechanical and Mechanics Engineering*, vol. 14, no. 5, pp. 25 - 33.

Howaniec, N & Smoliński, A 2014, 'Effect of fuel blend composition on the efficiency of hydrogen-rich gas production in co-gasification of coal and biomass', *Fuel*, vol. 128, pp. 442-50.

Hsi, C-L & Kuo, J-T 2008, 'Estimation of fuel burning rate and heating value with highly variable properties for optimum combustion control', *Biomass and bioenergy*, vol. 32, no. 12, pp. 1255-62.

Hu, J, Yan, Y, Evrendilek, F, Buyukada, M & Liu, J 2019, 'Combustion behaviors of three bamboo residues: gas emission, kinetic, reaction mechanism and optimization patterns', *Journal of Cleaner Production*, vol. 235, pp. 549-61.

Huang, J, Zhang, J, Liu, J, Xie, W, Kuo, J, Chang, K, Buyukada, M, Evrendilek, F & Sun, S 2019, 'Thermal conversion behaviors and products of spent mushroom substrate in CO2 and N2 atmospheres: kinetic, thermodynamic, TG and Py-GC/MS analyses', *Journal of Analytical and Applied Pyrolysis*, vol. 139, pp. 177-86.

Huang, J, Liu, J, Chen, J, Xie, W, Kuo, J, Lu, X, Chang, K, Wen, S, Sun, G & Cai, H 2018, 'Combustion behaviors of spent mushroom substrate using TG-MS and TG-FTIR: thermal conversion, kinetic, thermodynamic and emission analyses', *Bioresource technology*, vol. 266, pp. 389-97.

Huang, Y, Kuan, W, Chiueh, P & Lo, S 2011, 'A sequential method to analyze the kinetics of biomass pyrolysis', *Bioresource technology*, vol. 102, no. 19, pp. 9241-6.

Huangfu, Y, Li, H, Chen, X, Xue, C, Chen, C & Liu, G 2014, 'Effects of moisture content in fuel on thermal performance and emission of biomass semi-gasified cookstove', *Energy for Sustainable Development*, vol. 21, pp. 60-5.

238

Huidobro, JA, Iglesias, I, Alfonso, BF, Espina, A, Trobajo, C & Garcia, JR 2016, 'Reducing the effects of noise in the calculation of activation energy by the Friedman method', *Chemometrics and Intelligent Laboratory Systems*, vol. 151, pp. 146-52.

Hussain, M, Zabiri, H, Tufa, LD, Yusup, S & Ali, I 2022, 'A kinetic study and thermal decomposition characteristics of palm kernel shell using model-fitting and model-free methods', *Biofuels*, vol. 13, no. 1, pp. 105-16.

Hwang, IS, Sohn, J, Do Lee, U & Hwang, J 2021, 'CFD-DEM simulation of air-blown gasification of biomass in a bubbling fluidized bed gasifier: Effects of equivalence ratio and fluidization number', *Energy*, vol. 219, p. 119533.

Ibrahim, H 2018, 'Bio-energy production from rice straw: A review', *Recent Adv. Petrochem. Sci*, vol. 5, pp. 1-7.

Idris, SS, Abd Rahman, N, Ismail, K, Alias, AB, Abd Rashid, Z & Aris, MJ 2010, 'Investigation on thermochemical behaviour of low rank Malaysian coal, oil palm biomass and their blends during pyrolysis via thermogravimetric analysis (TGA)', *Bioresource technology*, vol. 101, no. 12, pp. 4584-92.

IEA 2018, *Gasification of waste for energy carriers: A review*, <http://task33.ieabioenergy.com/>>.

Ilic, D, Williams, K, Farnish, R, Webb, E & Liu, G 2018, 'On the challenges facing the handling of solid biomass feedstocks', *Biofuels, Bioproducts and Biorefining*, vol. 12, no. 2, pp. 187-202.

Ingole, PM, Ranveer, AC, Deshmukh, SM & Deshmukh, SK 2016, 'Microwave assisted pyrolysis of biomass: a review', *Int. J. Adv. Technol. Eng. Sci*, vol. 4, no. 6, pp. 78-84.

Iroba, KL, Tabil, LG, Sokhansanj, S & Venkatesh, M 2014, 'Producing durable pellets from barley straw subjected to radio frequency-alkaline and steam explosion pretreatments', *International Journal of Agricultural and Biological Engineering*, vol. 7, no. 3, pp. 68-82.

Ismail, TM & El-Salam, MA 2017, 'Parametric studies on biomass gasification process on updraft gasifier high temperature air gasification', *Applied Thermal Engineering*, vol. 112, pp. 1460-73.

Ismail, TM, Abd El-Salam, M, Monteiro, E & Rouboa, A 2018, 'Fluid dynamics model on fluidized bed gasifier using agro-industrial biomass as fuel', *Waste management*, vol. 73, pp. 476-86.

ISO, E 2014, '17225-2: 2014-Solid Biofuels-Fuel Specifications and Classes Part 2: Graded Wood Pellets', *The British Standards Institution: London, UK*.

ISO/TS 2016, *ISO/TS 17225-8:2016 Solid biofuels - Fuel specifications and classes - Part 8: Graded thermally treated and densified biomass fuels*, , ISO/CD 17225-8, viewed 07/01/2022, <https://www.iso.org/standard/71915.html>.

ISO/TS 2016, *17225-8: Solid biofuels - Fuel specifications and classes - Part 8: Graded thermally treated and densified biomass fuels*, https://www.iso.org/standard/71915.html.>.

Jackson, J, Turner, A, Mark, T & Montross, M 2016, 'Densification of biomass using a pilot scale flat ring roller pellet mill', *Fuel processing technology*, vol. 148, pp. 43-9.

Jacob, GA, Prabhakaran, SPS, Swaminathan, G & Joseyphus, RJ 2022, 'Thermal kinetic analysis of mustard biomass with equiatomic iron-nickel catalyst and its predictive modeling', *Chemosphere*, vol. 286, no. Pt 3, p. 131901.

Jahromi, R, Rezaei, M, Hashem Samadi, S & Jahromi, H 2021, 'Biomass gasification in a downdraft fixed-bed gasifier: Optimization of operating conditions', *Chemical Engineering Science*, vol. 231.

Jakobs, T, Djordjevic, N, Fleck, S, Mancini, M, Weber, R & Kolb, T 2012, 'Gasification of high viscous slurry R&D on atomization and numerical simulation', *Applied energy*, vol. 93, pp. 449-56.

Janajreh, I & Al Shrah, M 2013, 'Numerical and experimental investigation of downdraft gasification of wood chips', *Energy Conversion and Management*, vol. 65, pp. 783-92.

Janajreh, I, Adeyemi, I, Raza, SS & Ghenai, C 2021, 'A review of recent developments and future prospects in gasification systems and their modeling', *Renewable and Sustainable Energy Reviews*, vol. 138, p. 110505.

Jangam, SV, Karthikeyan, M & Mujumdar, A 2011, 'A critical assessment of industrial coal drying technologies: Role of energy, emissions, risk and sustainability', *Drying Technology*, vol. 29, no. 4, pp. 395-407.

Janković, B 2015, 'Devolatilization kinetics of swine manure solid pyrolysis using deconvolution procedure. Determination of the bio-oil/liquid yields and char gasification', *Fuel processing technology*, vol. 138, pp. 1-13.

Janković, B, Manić, N, Radović, I, Janković, M & Rajačić, M 2019, 'Model-free and model-based kinetics of the combustion process of low rank coals with high ash contents using TGA-DTG-DTA-MS and FTIR techniques', *Thermochimica Acta*, vol. 679, p. 178337.

Jaojaruek, K 2014, 'Mathematical model to predict temperature profile and air–fuel equivalence ratio of a downdraft gasification process', *Energy Conversion and Management*, vol. 83, pp. 223-31.

Jarungthammachote, S & Dutta, A 2007, 'Thermodynamic equilibrium model and second law analysis of a downdraft waste gasifier', *Energy*, vol. 32, no. 9, pp. 1660-9.

Jayah, TH, Aye, L, Fuller, RJ & Stewart, DF 2003, 'Computer simulation of a downdraft wood gasifier for tea drying', *Biomass and bioenergy*, vol. 25, no. 4, pp. 459-69.

Jazini, R, Soleimani, M & Mirghaffari, N 2018, 'Characterization of barley straw biochar produced in various temperatures and its effect on lead and cadmium removal from aqueous solutions', *Water and Environment Journal*, vol. 32, no. 1, pp. 125-33.

Jeguirim, M & Trouvé, G 2009, 'Pyrolysis characteristics and kinetics of Arundo donax using thermogravimetric analysis', *Bioresource technology*, vol. 100, no. 17, pp. 4026-31.

Jeguirim, M, Bikai, J, Elmay, Y, Limousy, L & Njeugna, E 2014, 'Thermal characterization and pyrolysis kinetics of tropical biomass feedstocks for energy recovery', *Energy for Sustainable Development*, vol. 23, pp. 188-93.

Jelonek, Z, Drobniak, A, Mastalerz, M & Jelonek, I 2020, 'Assessing pellet fuels quality: A novel application for reflected light microscopy', *International Journal of Coal Geology*, vol. 222, p. 103433.

Jenkins, BM, Baxter, LL & Koppejan, J 2019, 'Biomass combustion', *Thermochemical processing of biomass: conversion into fuels, chemicals and power*, pp. 49-83.

Jezerska, L, Zajonc, O, Rozbroj, J, Vyletělek, J & Zegzulka, J 2014, 'Research on effect of spruce sawdust with added starch on flowability and pelletization of the material', *IERI Procedia*, vol. 8, pp. 154-63.

Jia, G 2021, 'Combustion characteristics and kinetic analysis of biomass pellet fuel using thermogravimetric analysis', *Processes*, vol. 9, no. 5, p. 868.

Jiang, L-b, Yuan, X-z, Li, H, Chen, X-h, Xiao, Z-h, Liang, J, Leng, L-j, Guo, Z & Zeng, G-m 2016, 'Co-pelletization of sewage sludge and biomass: Thermogravimetric analysis and ash deposits', *Fuel Processing Technology*, vol. 145, pp. 109-15.

Jiang, L, Xue, B, Ma, Z, Yu, L, Huang, B & Chen, X 2020, 'A life-cycle based co-benefits analysis of biomass pellet production in China', *Renewable Energy*, vol. 154, pp. 445-52.

Jiang, L, Liu, C, Hu, S, Wang, Y, Xu, K, Su, S & Xiang, J 2018, 'Catalytic behaviors of alkali metal salt involved in homogeneous volatile and heterogeneous char reforming in steam gasification of cellulose', *Energy Conversion and Management*, vol. 158, pp. 147-55.

Jiang, L, Yuan, X, Li, H, Xiao, Z, Liang, J, Wang, H, Wu, Z, Chen, X & Zeng, G 2015, 'Pyrolysis and combustion kinetics of sludge–camphor pellet thermal decomposition using thermogravimetric analysis', *Energy Conversion and Management*, vol. 106, pp. 282-9.

Jiang, L, Yuan, X, Xiao, Z, Liang, J, Li, H, Cao, L, Wang, H, Chen, X & Zeng, G 2016, 'A comparative study of biomass pellet and biomass-sludge mixed pellet: Energy input and pellet properties', *Energy Conversion and Management*, vol. 126, pp. 509-15.

Jiang, TL, Chen, WS, Tsai, MJ & Chiu, HH 1995, 'A numerical investigation of multiple flame configurations in convective droplet gasification', *Combustion and flame*, vol. 103, no. 3, pp. 221-38.

Jin, Q, Wang, X, Li, S, Mikulčić, H, Bešenić, T, Deng, S, Vujanović, M, Tan, H & Kumfer, BM 2019, 'Synergistic effects during co-pyrolysis of biomass and plastic: Gas, tar, soot, char products and thermogravimetric study', *Journal of the Energy Institute*, vol. 92, no. 1, pp. 108-17.

Johnson, DT & Taconi, KA 2007, 'The glycerin glut: Options for the value-added conversion of crude glycerol resulting from biodiesel production', *Environmental Progress*, vol. 26, no. 4, pp. 338-48.

Kabir, M, Chowdhury, A & Rasul, M 2015, 'Pyrolysis of Municipal Green Waste: A Modelling, Simulation and Experimental Analysis', *Energies*, vol. 8, no. 8, pp. 7522-41.

Kaknics, J, Michel, R & Poirier, J 2016, 'Miscanthus ash transformation and interaction with bed materials at high temperature', *Fuel processing technology*, vol. 141, pp. 178-84.

Kaliyan, N & Morey, RV 2009, 'Factors affecting strength and durability of densified biomass products', *Biomass and bioenergy*, vol. 33, no. 3, pp. 337-59.

Kaliyan, N & Vance Morey, R 2009, 'Factors affecting strength and durability of densified biomass products', *Biomass and Bioenergy*, vol. 33, no. 3, pp. 337-59.

Kaliyan, N & Morey, RV 2010, 'Natural binders and solid bridge type binding mechanisms in briquettes and pellets made from corn stover and switchgrass', *Bioresource technology*, vol. 101, no. 3, pp. 1082-90.

Kan, T, Strezov, V & Evans, TJ 2016, 'Lignocellulosic biomass pyrolysis: A review of product properties and effects of pyrolysis parameters', *Renewable and Sustainable Energy Reviews*, vol. 57, pp. 1126-40.

Kandasamy, S, Bhuvanendran, N, Narayanan, M & He, Z 2022, 'Thermochemical conversion of algal biomass', in *Handbook of Algal Biofuels*, Elsevier, pp. 281-302.

Karaeva, JV, Timofeeva, SS, Islamova, SI & Gerasimov, AV 2022, 'Pyrolysis kinetics of new bioenergy feedstock from anaerobic digestate of agro-waste by thermogravimetric analysis', *Journal of Environmental Chemical Engineering*, vol. 10, no. 3, p. 107850.

Karkania, V, Fanara, E & Zabaniotou, A 2012, 'Review of sustainable biomass pellets production–A study for agricultural residues pellets' market in Greece', *Renewable and Sustainable Energy Reviews*, vol. 16, no. 3, pp. 1426-36.

Karl, J & Pröll, T 2018, 'Steam gasification of biomass in dual fluidized bed gasifiers: A review', *Renewable and Sustainable Energy Reviews*, vol. 98, pp. 64-78.

Kashaninejad, M & Tabil, LG 2011, 'Effect of microwave–chemical pre-treatment on compression characteristics of biomass grinds', *Biosystems Engineering*, vol. 108, no. 1, pp. 36-45.

Kaur, R, Gera, P, Jha, MK & Bhaskar, T 2018, 'Pyrolysis kinetics and thermodynamic parameters of castor (Ricinus communis) residue using thermogravimetric analysis', *Bioresource technology*, vol. 250, pp. 422-8.

Kaushal, P, Abedi, J & Mahinpey, N 2010, 'A comprehensive mathematical model for biomass gasification in a bubbling fluidized bed reactor', *Fuel*, vol. 89, no. 12, pp. 3650-61.

Kazawadi, D, Ntalikwa, J & Kombe, G 2021, 'A review of intermediate pyrolysis as a technology of biomass conversion for coproduction of biooil and adsorption biochar', *Journal of Renewable Energy*, vol. 2021.

Kern, S, Halwachs, M, Kampichler, G, Pfeifer, C, Pröll, T & Hofbauer, H 2012, 'Rotary kiln pyrolysis of straw and fermentation residues in a 3MW pilot plant – Influence of pyrolysis temperature on pyrolysis product performance', *Journal of Analytical and Applied Pyrolysis*, vol. 97, pp. 1-10.

Keshtkar, M, Eslami, M & Jafarpur, K 2020, 'A novel procedure for transient CFD modeling of basin solar stills: Coupling of species and energy equations', *Desalination*, vol. 481, p. 114350.

Khawam, A & Flanagan, DR 2006, 'Solid-state kinetic models: basics and mathematical fundamentals', *The journal of physical chemistry B*, vol. 110, no. 35, pp. 17315-28.

Khosravanipour Mostafazadeh, A, Solomatnikova, O, Drogui, P & Tyagi, RD 2018, 'A review of recent research and developments in fast pyrolysis and bio-oil upgrading', *Biomass conversion and biorefinery*, vol. 8, no. 3, pp. 739-73.

Kim, S & Dale, BE 2004, 'Global potential bioethanol production from wasted crops and crop residues', *Biomass and bioenergy*, vol. 26, no. 4, pp. 361-75.

Kimber, R 1973, 'Phytotoxicity from plant residues: III. The relative effect of toxins and nitrogen immobilization on the germination and growth of wheat', *Plant and Soil*, pp. 543-55.

Kingwell, R & Abadi, A 2014, 'Cereal straw for bioenergy production in an Australian region affected by climate change', *Biomass and bioenergy*, vol. 61, pp. 58-65.

Kirubakaran, V, Sivaramakrishnan, V, Nalini, R, Sekar, T, Premalatha, M & Subramanian, P 2009, 'A review on gasification of biomass', *Renewable and Sustainable Energy Reviews*, vol. 13, no. 1, pp. 179-86.

Kizuka, R, Ishii, K, Sato, M & Fujiyama, A 2019, 'Characteristics of wood pellets mixed with torrefied rice straw as a biomass fuel', *International Journal of Energy and Environmental Engineering*, vol. 10, no. 3, pp. 357-65.

Klimova, I, Kaljuvee, T, Mikli, V & Trikkel, A 2013, 'Influence of some lime-containing additives on the thermal behavior of urea', *Journal of thermal analysis and calorimetry*, vol. 111, no. 1, pp. 253-8.

Kloss, S, Zehetner, F, Dellantonio, A, Hamid, R, Ottner, F, Liedtke, V, Schwanninger, M, Gerzabek, MH & Soja, G 2012, 'Characterization of slow pyrolysis biochars: effects of feedstocks and pyrolysis temperature on biochar properties', *J Environ Qual*, vol. 41, no. 4, pp. 990-1000.

Knoef, H 2005, 'Handbook of biomass gasification, BTG', *See www. btgworld. com.[Google Scholar]*.

Koga, N, Vyazovkin, S, Burnham, AK, Favergeon, L, Muravyev, NV, Perez-Maqueda, LA, Saggese, C & Sánchez-Jiménez, PE 2022, 'ICTAC Kinetics Committee recommendations for analysis of thermal decomposition kinetics', *Thermochimica Acta*, p. 179384.

König, M, Müller, M & Hartmann, I 2021, 'Emission reduction process for the energetic use of biogenic residues', *IOP Conference Series: Earth and Environmental Science*, IOP Publishing, p. 012006.

Krishna, BB, Biswas, B, Ohri, P, Kumar, J, Singh, R & Bhaskar, T 2016, 'Pyrolysis of Cedrus deodara saw mill shavings in hydrogen and nitrogen atmosphere for the production of bio-oil', *Renewable Energy*, vol. 98, pp. 238-44.

Krishnamoorthy, V, Krishnamurthy, N & Pisupati, SV 2019, 'Intrinsic gasification kinetics of coal chars generated in a high-pressure, high-temperature flow reactor', *Chemical Engineering Journal*, vol. 375.

Kubojima, Y & Yoshida, T 2015, 'Testing method for determining water resistance of wood pellets', *European Journal of Wood and Wood Products*, vol. 73, no. 2, pp. 193-8.

Kulokas, M, Praspaliauskas, M & Pedišius, N 2021, 'Investigation of buckwheat hulls as additives in the production of solid biomass fuel from straw', *Energies*, vol. 14, no. 2, p. 265.

Kumabe, K, Hanaoka, T, Fujimoto, S, Minowa, T & Sakanishi, K 2007, 'Co-gasification of woody biomass and coal with air and steam', *Fuel*, vol. 86, no. 5-6, pp. 684-9.

Kumar, A, Jones, D & Hanna, M 2009, 'Thermochemical Biomass Gasification: A Review of the Current Status of the Technology', *Energies*, vol. 2, no. 3, pp. 556-81.

Kumar, A, Wang, L, Dzenis, YA, Jones, DD & Hanna, MA 2008, 'Thermogravimetric characterization of corn stover as gasification and pyrolysis feedstock', *Biomass and bioenergy*, vol. 32, no. 5, pp. 460-7.

Kumar, AA, Kumar, R, Ansari, A & Kumar, R 2021, 'Non-isothermal Degradation Analysis of Plywood and Determination of Kinetic Parameters Using Coats–Redfern Method', *Journal of The Institution of Engineers (India): Series E*, vol. 102, no. 2, pp. 249-55.

Kumar, M, Mishra, P & Upadhyay, S 2020, 'Thermal degradation of rice husk: effect of pre-treatment on kinetic and thermodynamic parameters', *Fuel*, vol. 268, p. 117164.

Kumar, P & Nandi, BK 2021, 'Combustion characteristics of high ash Indian coal, wheat straw, wheat husk and their blends', *Materials Science for Energy Technologies*, vol. 4, pp. 274-81.

Kumar, U & Paul, MC 2019, 'CFD modelling of biomass gasification with a volatile break-up approach', *Chemical Engineering Science*, vol. 195, pp. 413-22.

Kundu, K, Chatterjee, A, Bhattacharyya, T, Roy, M & Kaur, A 2018, 'Thermochemical conversion of biomass to bioenergy: a review', *Prospects of alternative transportation fuels*, pp. 235-68.

Kuokkanen, MJ, Vilppo, T, Kuokkanen, T, Stoor, T & Niinimäki, J 2011, 'Additives in wood pellet production–A pilot-scale study of binding agent usage', *BioResources*, vol. 6, no. 4, pp. 4331-55.

Kupka, T, Mancini, M, Irmer, M & Weber, R 2008, 'Investigation of ash deposit formation during co-firing of coal with sewage sludge, saw-dust and refuse derived fuel', *Fuel*, vol. 87, no. 12, pp. 2824-37.

Kuranc, A, Stoma, M, Rydzak, L & Pilipiuk, M 2020, 'Durability Assessment of Wooden Pellets in Relation with Vibrations Occurring in a Logistic Process of the Final Product', *Energies*, vol. 13, no. 22, p. 5890.

Kwan, TH, Hu, Y & Lin, CSK 2018, 'Techno-economic analysis of a food waste valorisation process for lactic acid, lactide and poly (lactic acid) production', *Journal of Cleaner Production*, vol. 181, pp. 72-87.

Kwon, EE, Kim, S & Lee, J 2019, 'Pyrolysis of waste feedstocks in CO2 for effective energy recovery and waste treatment', *Journal of CO2 utilization*, vol. 31, pp. 173-80.

La Villetta, M, Costa, M & Massarotti, N 2017, 'Modelling approaches to biomass gasification: A review with emphasis on the stoichiometric method', *Renewable and Sustainable Energy Reviews*, vol. 74, pp. 71-88.

Laouge, ZB & Merdun, H 2020, 'Kinetic analysis of Pearl Millet (Penissetum glaucum (L.) R. Br.) under pyrolysis and combustion to investigate its bioenergy potential', *Fuel*, vol. 267, p. 117172.

Lapuerta, M, Hernández, JJ, Pazo, A & López, J 2008, 'Gasification and co-gasification of biomass wastes: Effect of the biomass origin and the gasifier operating conditions', *Fuel processing technology*, vol. 89, no. 9, pp. 828-37.

Larsson, S, Lockneus, O, Xiong, S & Samuelsson, R 2015, 'Cassava stem powder as an additive in biomass fuel pellet production', *Energy & Fuels*, vol. 29, no. 9, pp. 5902-8.

Launder, B & Spalding, D 1972, ' Lectures in mathematical models of turbulence', Academic Press, London, England.

Leal-Quirós, E 2004, 'Plasma processing of municipal solid waste', *Brazilian Journal of Physics*, vol. 34, pp. 1587-93.

Lee, JM, Kim, YJ, Lee, WJ & Kim, SD 1998, 'Coal-gasification kinetics derived from pyrolysis in a fluidized-bed reactor', *Energy*, vol. 23, no. 6, pp. 475-88.

Lehmann, B, Schröder, H-W, Wollenberg, R & Repke, J-U 2012, 'Effect of miscanthus addition and different grinding processes on the quality of wood pellets', *Biomass and bioenergy*, vol. 44, pp. 150-9.

Lehtikangas, P 2001, 'Quality properties of pelletised sawdust, logging residues and bark', *Biomass and bioenergy*, vol. 20, no. 5, pp. 351-60.

Leroy-Cancellieri, V, Leoni, E, Simeoni, A, Kuzin, AY, Filkov, AI, Rein, G & Cancellieri, D 2012, 'Kinetic investigation on the smouldering combustion of boreal peat'.

Levis, JW & Barlaz, MA 2013, 'Composting process model documentation', *Retrieved May*, vol. 16, p. 2015.

Li, AM, Li, XD, Li, SQ, Ren, Y, Chi, Y, Yan, JH & Cen, KF 1999, 'Pyrolysis of Solid Waste in a Rotary Kiln: Influence of Final Pyrolysis Temperature on the Pyrolysis Products', *Journal of Analytical and Applied Pyrolysis*, vol. 50, pp. 149-62.

Li, J, Yin, Y, Zhang, X, Liu, J & Yan, R 2009, 'Hydrogen-rich gas production by steam gasification of palm oil wastes over supported tri-metallic catalyst', *International Journal of Hydrogen Energy*, vol. 34, no. 22, pp. 9108-15.

Li, S, Li, Y, Li, X, Tian, X, Zhao, A, Wang, S, Wang, S & Shi, J 2016, 'Effect of straw management on carbon sequestration and grain production in a maize–wheat cropping system in Anthrosol of the Guanzhong Plain', *Soil and Tillage Research*, vol. 157, pp. 43-51.

Li, X, Zone, WFT & Guan, Z 2009, 'Analysis of Permanent Gases and Light Hydrocarbons Using Agilent 7820A GC With 3-Valve System', *Beijing, China*, pp. 5990-4667.

Li, Y-H, Lin, H-T, Xiao, K-L & Lasek, J 2018, 'Combustion behavior of coal pellets blended with Miscanthus biochar', *Energy*, vol. 163, pp. 180-90.

Li, Y, Yan, L, Yang, B, Gao, W & Farahani, MR 2018, 'Simulation of biomass gasification in a fluidized bed by artificial neural network (ANN)', *Energy Sources, Part A: Recovery, Utilization, and Environmental Effects*, vol. 40, no. 5, pp. 544-8.

Li, Z, Xu, H, Yang, W, Zhou, A & Xu, M 2019, 'CFD simulation of a fluidized bed reactor for biomass chemical looping gasification with continuous feedstock', *Energy Conversion and Management*, vol. 201, p. 112143.

Lian, G & Zhong, W 2022, 'CFD–DEM modeling of oxy-char combustion in a fluidized bed', *Powder technology*, vol. 407, p. 117698.

Lian, Z, Wang, Y, Zhang, X, Yusuf, A, Famiyeh, L, Murindababisha, D, Jin, H, Liu, Y, He, J & Wang, Y 2021, *Hydrogen Production by Fluidized Bed Reactors: A Quantitative Perspective Using the Supervised Machine Learning Approach. J 2021, 4, 266–287*, s Note: MDPI stays neutral with regard to jurisdictional claims in published ….

Liang, W, Ning, X, Wang, G, Zhang, J, Li, R, Chang, W & Wang, C 2021, 'Influence mechanism and kinetic analysis of co-gasification of biomass char and semi-coke', *Renewable Energy*, vol. 163, pp. 331-41.

Liashenko, S, Sakalo, V, Minkova, O & Kalinichenko, A 2019, 'Justification of Construction Parameters of the Screen in the Small-Sized Household Biomass Chopper', *2019 IEEE International Conference on Modern Electrical and Energy Systems (MEES)*, IEEE, pp. 206-9.

Liavitskaya, T & Vyazovkin, S 2017, 'Delving into the kinetics of reversible thermal decomposition of solids measured on heating and cooling', *The Journal of Physical Chemistry C*, vol. 121, no. 28, pp. 15392-401.

Lin, Y-C, Cho, J, Tompsett, GA, Westmoreland, PR & Huber, GW 2009, 'Kinetics and mechanism of cellulose pyrolysis', *The Journal of Physical Chemistry C*, vol. 113, no. 46, pp. 20097-107.

Lindley, J & Vossoughi, M 1989, 'Physical properties of biomass briquets', *Transactions of the ASAE*, vol. 32, no. 2, pp. 361-0366.

Link, S, Yrjas, P & Hupa, L 2018, 'Ash melting behaviour of wheat straw blends with wood and reed', *Renewable Energy*, vol. 124, pp. 11-20.

Lipatnikov, AN & Sabelnikov, VA 2020, 'An extended flamelet-based presumed probability density function for predicting mean concentrations of various species in premixed turbulent flames', *International Journal of Hydrogen Energy*, vol. 45, no. 55, pp. 31162-78.

Lisowski, A, Pajor, M, Świętochowski, A, Dąbrowska, M, Klonowski, J, Mieszkalski, L, Ekielski, A, Stasiak, M & Piątek, M 2019, 'Effects of moisture content, temperature, and die thickness on the compaction process, and the density and strength of walnut shell pellets', *Renewable Energy*, vol. 141, pp. 770-81.

Lisowski, A, Olendzki, D, Świętochowski, A, Dąbrowska, M, Mieszkalski, L, Ostrowska-Ligęza, E, Stasiak, M, Klonowski, J & Piątek, M 2019, 'Spent coffee grounds compaction process: Its effects on the strength properties of biofuel pellets', *Renewable Energy*, vol. 142, pp. 173-83.

Liu, B, Papadikis, K, Gu, S, Fidalgo, B, Longhurst, P, Li, Z & Kolios, A 2017, 'CFD modelling of particle shrinkage in a fluidized bed for biomass fast pyrolysis with quadrature method of moment', *Fuel processing technology*, vol. 164, pp. 51-68.

Liu, H, Jiang, G, Zhuang, H & Wang, K 2008, 'Distribution, utilization structure and potential of biomass resources in rural China: With special references of crop residues', *Renewable and Sustainable Energy Reviews*, vol. 12, no. 5, pp. 1402-18.

Liu, H, Elkamel, A, Lohi, A & Biglari, M 2013, 'Computational Fluid Dynamics Modeling of Biomass Gasification in Circulating Fluidized-Bed Reactor Using the Eulerian–Eulerian Approach', *Industrial & Engineering Chemistry Research*, vol. 52, no. 51, pp. 18162-74.

Liu, H, Hong, R, Xiang, C, Wang, H, Li, Y, Xu, G, Chang, P & Zhu, K 2020, 'Thermal decomposition kinetics analysis of the oil sludge using model-based method and model-free method', *Process Safety and Environmental Protection*, vol. 141, pp. 167-77.

Liu, L, Pang, Y, Lv, D, Wang, K & Wang, Y 2021, 'Thermal and kinetic analyzing of pyrolysis and combustion of self-heating biomass particles', *Process Safety and Environmental Protection*, vol. 151, pp. 39-50.

Liu, Q, Wang, S, Zheng, Y, Luo, Z & Cen, K 2008, 'Mechanism study of wood lignin pyrolysis by using TG–FTIR analysis', *Journal of Analytical and Applied Pyrolysis*, vol. 82, no. 1, pp. 170-7.

Liu, Y, Li, X, Zhang, W, Ma, F, Zhang, Q & Gu, Q 2021, 'Pyrolysis of heavy hydrocarbons in weathered petroleum-contaminated soil enhanced with inexpensive additives at low temperatures', *Journal of Cleaner Production*, vol. 302, p. 127017.

Liu, Z, Hoekman, SK, Balasubramanian, R & Zhang, F-S 2015, 'Improvement of fuel qualities of solid fuel biochars by washing treatment', *Fuel processing technology*, vol. 134, pp. 130-5.

Liu, Z, Quek, A, Hoekman, SK, Srinivasan, M & Balasubramanian, R 2012, 'Thermogravimetric investigation of hydrochar-lignite co-combustion', *Bioresource technology*, vol. 123, pp. 646-52.

Liu, Z, Liu, Xe, Fei, B, Jiang, Z, Cai, Z & Yu, Y 2013, 'The properties of pellets from mixing bamboo and rice straw', *Renewable Energy*, vol. 55, pp. 1-5.

Liu, Z, Mi, B, Jiang, Z, Fei, B, Cai, Z & Liu, Xe 2016, 'Improved bulk density of bamboo pellets as biomass for energy production', *Renewable Energy*, vol. 86, pp. 1-7.

López-García, M, Lodeiro, P, Herrero, R, Barriada, JL, Rey-Castro, C, David, C & de Vicente, MES 2013, 'Experimental evidences for a new model in the description of the adsorption-coupled reduction of Cr (VI) by protonated banana skin', *Bioresource technology*, vol. 139, pp. 181-9.

Lu, D, Tabil, L, Wang, D & Wang, G 2013, 'Manufacturing wheat straw pellet with wood waste and binders', *CSBE Paper No. CSBE13-55*.

Lu, D, Yoshikawa, K, Ismail, TM & Abd El-Salam, M 2018, 'Assessment of the carbonized woody briquette gasification in an updraft fixed bed gasifier using the Euler-Euler model', *Applied energy*, vol. 220, pp. 70-86.

Lu, D, Tabil, LG, Wang, D, Wang, G & Emami, S 2014, 'Experimental trials to make wheat straw pellets with wood residue and binders', *Biomass and bioenergy*, vol. 69, pp. 287-96.

Lu, D, Tabil, L, Wang, D, Wang, G & Emami, S 2014a, 'Experimental trials to make wheat straw pellets with wood residue and binders', *Biomass and Bioenergy*, vol. 69, pp. 287-96.

Lu, D, Tabil, L, Wang, D, Wang, G & Wang, Z 2014b, 'Optimization of binder addition and compression load for pelletization of wheat straw using response surface methodology', *Int J Agric & Biol Eng*, vol. 7, no. 6, pp. 67-78.

Lu, F, Wang, C, Chen, M, Yue, F & Ralph, J 2021, 'A facile spectroscopic method for measuring lignin content in lignocellulosic biomass', *Green Chemistry*, vol. 23, no. 14, pp. 5106-12.

Lu, J-J & Chen, W-H 2015, 'Investigation on the ignition and burnout temperatures of bamboo and sugarcane bagasse by thermogravimetric analysis', *Applied energy*, vol. 160, pp. 49-57.

Lü, P, Kong, X, Wu, C, Yuan, Z, Ma, L & Chang, J 2008, 'Modeling and simulation of biomass air-steam gasification in a fluidized bed', *Frontiers of Chemical Engineering in China*, vol. 2, no. 2, pp. 209-13.

Luan, Y-T, Chyou, Y-P & Wang, T 2013, 'Numerical analysis of gasification performance via finite-rate model in a cross-type two-stage gasifier', *International Journal of Heat and Mass Transfer*, vol. 57, no. 2, pp. 558-66.

Lucas, C 2005, 'High temperature air/steam gasification of biomass in an updraft fixed bed batch type gasifier', KTH.

Luo, X, Wu, T, Shi, K, Song, M & Rao, Y 2018, 'Biomass Gasification: An Overview of Technological Barriers and Socio-Environmental Impact', in *Gasification for Low-grade Feedstock*, ch Chapter 1.

Luo, Z & Zhou, J 2022, 'Thermal conversion of biomass', in *Handbook of Climate Change Mitigation and Adaptation*, Springer, pp. 965-1021.

Lv, P, Xiong, Z, Chang, J, Wu, C, Chen, Y & Zhu, J 2004, 'An experimental study on biomass air–steam gasification in a fluidized bed', *Bioresource technology*, vol. 95, no. 1, pp. 95-101.

Mack, R, Kuptz, D, Schön, C & Hartmann, H 2019, 'Combustion behavior and slagging tendencies of kaolin additivated agricultural pellets and of wood-straw pellet blends in a small-scale boiler', *Biomass and bioenergy*, vol. 125, pp. 50-62.

Magdziarz, A, Wilk, M & Wądrzyk, M 2020, 'Pyrolysis of hydrochar derived from biomass – Experimental investigation', *Fuel*, vol. 267.

Magnussen, BF & Hjertager, BH 1977, 'On mathematical modeling of turbulent combustion with special emphasis on soot formation and combustion'.

Mahapatra, AK, Harris, DL, Durham, DL, Lucas, S, Terrill, TH, Kouakou, B & Kannan, G 2010, 'Effects of moisture change on the physical and thermal properties of sericea lespedeza pellets'.

Mahapatro, A, Kumar, A & Mahanta, P 2020, 'Parametric study and exergy analysis of the gasification of sugarcane bagasse in a pressurized circulating fluidized bed gasifier', *Journal of thermal analysis and calorimetry*, vol. 141, no. 6, pp. 2635-45.

Mahdavi, S 2020, 'Comparison of non-woody biomass properties for energy generation', *Iranian Journal of Wood and Paper Industries*, vol. 10, no. 4, pp. 617-28.

Mahinpey, N & Gomez, A 2016, 'Review of gasification fundamentals and new findings: Reactors, feedstock, and kinetic studies', *Chemical Engineering Science*, vol. 148, pp. 14-31.

Maia, A, Cavalca, DF, Tomita, JT, Costa, F & Bringhenti, C 2022, 'Evaluation of an effective and robust implicit time-integration numerical scheme for Navier-Stokes equations in a CFD solver for compressible flows', *Applied Mathematics and Computation*, vol. 413, p. 126612.

Maia, AAD & de Morais, LC 2016, 'Kinetic parameters of red pepper waste as biomass to solid biofuel', *Bioresource technology*, vol. 204, pp. 157-63.

Maj, G 2018, 'Emission factors and energy properties of agro and forest biomass in aspect of sustainability of energy sector', *Energies*, vol. 11, no. 6, p. 1516.

Mandal, S, Mohalik, NK, Ray, SK, Khan, AM, Mishra, D & Pandey, JK 2022, 'A comparative kinetic study between TGA & DSC techniques using model-free and model-based analyses to assess spontaneous combustion propensity of Indian coals', *Process Safety and Environmental Protection*, vol. 159, pp. 1113-26.

Mandapati, RN & Ghodke, PK 2021, 'Kinetics of pyrolysis of cotton stalk using model-fitting and model-free methods', *Fuel*, vol. 303, p. 121285.

Mani, S 2005, 'A systems analysis of biomass densification process', University of British Columbia.

Mani, S, Tabil, LG & Sokhansanj, S 2006, 'Effects of compressive force, particle size and moisture content on mechanical properties of biomass pellets from grasses', *Biomass and bioenergy*, vol. 30, no. 7, pp. 648-54.

Mani, T, Murugan, P & Mahinpey, N 2011, 'Pyrolysis of oat straw and the comparison of the product yield to wheat and flax straw pyrolysis', *Energy & Fuels*, vol. 25, no. 7, pp. 2803-7.

Manić, N, Janković, B & Dodevski, V 2021, 'Model-free and model-based kinetic analysis of Poplar fluff (Populus alba) pyrolysis process under dynamic conditions', *Journal of thermal analysis and calorimetry*, vol. 143, no. 5, pp. 3419-38.

Manić, NG, Janković, BŽ, Stojiljković, DD, Jovanović, VV & Radojević, MB 2019, 'TGA-DSC-MS analysis of pyrolysis process of various agricultural residues', *Thermal Science*, vol. 23, no. Suppl. 5, pp. 1457-72.

Mansaray, K, Ghaly, A, Al-Taweel, A, Hamdullahpur, F & Ugursal, V 1999, 'Air gasification of rice husk in a dual distributor type fluidized bed gasifier', *Biomass and bioenergy*, vol. 17, no. 4, pp. 315-32.

Martinez-Hernandez, E, Amezcua-Allieri, MA & Aburto, J 2021, 'Assessing the cost of biomass and bioenergy production in agroindustrial processes', *Energies*, vol. 14, no. 14, p. 4181.

Martínez, JD, Mahkamov, K, Andrade, RV & Silva Lora, EE 2012, 'Syngas production in downdraft biomass gasifiers and its application using internal combustion engines', *Renewable Energy*, vol. 38, no. 1, pp. 1-9.

Martínez, LV, Rubiano, JE, Figueredo, M & Gómez, MF 2020, 'Experimental study on the performance of gasification of corncobs in a downdraft fixed bed gasifier at various conditions', *Renewable Energy*, vol. 148, pp. 1216-26.

Masiá, AT, Buhre, B, Gupta, R & Wall, T 2007, 'Characterising ash of biomass and waste', *Fuel processing technology*, vol. 88, no. 11-12, pp. 1071-81.

Masmoudi, MA, Sahraoui, M, Grioui, N & Halouani, K 2014, '2-D Modeling of thermo-kinetics coupled with heat and mass transfer in the reduction zone of a fixed bed downdraft biomass gasifier', *Renewable Energy*, vol. 66, pp. 288-98.

Masnadi, MS, Habibi, R, Kopyscinski, J, Hill, JM, Bi, X, Lim, CJ, Ellis, N & Grace, JR 2014, 'Fuel characterization and co-pyrolysis kinetics of biomass and fossil fuels', *Fuel*, vol. 117, pp. 1204-14.

McBeath, AV, Wurster, CM & Bird, MI 2015, 'Influence of feedstock properties and pyrolysis conditions on biochar carbon stability as determined by hydrogen pyrolysis', *Biomass and bioenergy*, vol. 73, pp. 155-73.

McCaffrey, Z, Thy, P, Long, M, Oliveira, M, Wang, L, Torres, L, Aktas, T, Chiou, B-S, Orts, W & Jenkins, BM 2019, 'Air and steam gasification of almond biomass', *Frontiers in Energy Research*, vol. 7, p. 84.

McKendry, P 2002, 'Energy production from biomass (part 1): overview of biomass', *Bioresource technology*, vol. 83, no. 1, pp. 37-46.

Mediavilla, I, Esteban, L & Fernández, M 2012, 'Optimisation of pelletisation conditions for poplar energy crop', *Fuel processing technology*, vol. 104, pp. 7-15.

Medic, D, Darr, M, Potter, B & Shah, A 2010, 'Effect of torrefaction process parameters on biomass feedstock upgrading', *2010 Pittsburgh, Pennsylvania, June 20-June 23, 2010*, American Society of Agricultural and Biological Engineers, p. 1.

Meenaroch, P, Kerdsuwan, S & Laohalidanond, K 2015, 'Development of kinetics models in each zone of a 10 kg/hr downdraft gasifier using computational fluid dynamics', *Energy Procedia*, vol. 79, pp. 278-83.

Mendiburu, AZ, Carvalho, JA & Coronado, CJR 2014, 'Thermochemical equilibrium modeling of biomass downdraft gasifier: Stoichiometric models', *Energy*, vol. 66, pp. 189-201.

Mendonça, M, Mantilla, V, Patela, J, Silva, V & Resende, F 2022, 'Design and experimental tests of an Imbert type downdraft gasifier prototype and clean-up system for small-scale biomass-based power generation', *Renewable Energy and Environmental Sustainability*, vol. 7, p. 10.

Meng, F, Meng, J & Zhang, D 2018, 'Influence of higher equivalence ratio on the biomass oxygen gasification in a pilot scale fixed bed gasifier', *Journal of Renewable and Sustainable Energy*, vol. 10, no. 5, p. 053101.

Mevissen, N, Schulzke, T, Unger, CA & an Bhaird, SM 2009, 'Thermodynamics of autothermal wood gasification', *Environmental Progress & Sustainable Energy*, vol. 28, no. 3, pp. 347-54.

Mian, I, Li, X, Dacres, OD, Wang, J, Wei, B, Jian, Y, Zhong, M, Liu, J, Ma, F & Rahman, N 2020, 'Combustion kinetics and mechanism of biomass pellet', *Energy*, vol. 205, p. 117909.

Miladinovic, DD, Storebakken, T, Lekang, OI & Salas-Bringas, C 2021, 'The effect of feed enzymes phytase, protease and xylanase on pelleting of microalgal biomass', *Heliyon*, vol. 7, no. 12, p. e08598.

MILES, T, BAXTER, L, BRYERS, R, JENKINS, B & ODEN, L 1995, 'Alkali deposits found in biomass power plants: A preliminary investigation of their extent and nature'.

Min, F, Zhang, M, Zhang, Y, Cao, Y & Pan, W-P 2011, 'An experimental investigation into the gasification reactivity and structure of agricultural waste chars', *Journal of Analytical and Applied Pyrolysis*, vol. 92, no. 1, pp. 250-7.

Mishra, G & Bhaskar, T 2014, 'Non isothermal model free kinetics for pyrolysis of rice straw', *Bioresource technology*, vol. 169, pp. 614-21.

Mishra, RK & Mohanty, K 2018, 'Pyrolysis kinetics and thermal behavior of waste sawdust biomass using thermogravimetric analysis', *Bioresource technology*, vol. 251, pp. 63-74.

Mishra, RK & Mohanty, K 2020, 'Kinetic analysis and pyrolysis behaviour of waste biomass towards its bioenergy potential', *Bioresource technology*, vol. 311, p. 123480.

Mišljenović, N, Čolović, R, Vukmirović, Đ, Brlek, T & Bringas, CS 2016, 'The effects of sugar beet molasses on wheat straw pelleting and pellet quality. A comparative study of pelleting by using a single pellet press and a pilot-scale pellet press', *Fuel processing technology*, vol. 144, pp. 220-9.

Mohammadi, A 2021, 'Overview of the benefits and challenges associated with pelletizing biochar', *Processes*, vol. 9, no. 9, p. 1591.

Mohammed, IY, Abakr, YA, Kazi, FK, Yusup, S, Alshareef, I & Chin, SA 2015, 'Comprehensive characterization of Napier grass as a feedstock for thermochemical conversion', *Energies*, vol. 8, no. 5, pp. 3403-17.

Mohammed, M, Salmiaton, A, Azlina, WW & Amran, MM 2012, 'Gasification of oil palm empty fruit bunches: A characterization and kinetic study', *Bioresource technology*, vol. 110, pp. 628-36.

Mohammed, M, Salmiaton, A, Azlina, WW, Amran, MM & Fakhru'l-Razi, A 2011, 'Air gasification of empty fruit bunch for hydrogen-rich gas production in a fluidized-bed reactor', *Energy Conversion and Management*, vol. 52, no. 2, pp. 1555-61.

Mohan, D, Pittman Jr, CU & Steele, PH 2006, 'Pyrolysis of wood/biomass for bio-oil: a critical review', *Energy & Fuels*, vol. 20, no. 3, pp. 848-89.

Mohrmann, S & Otter, V 2022, 'Categorisation of Biogas Plant Operators in Germany with Regards to Their Intention to Use Straw Pellets as Innovative and Sustainable Substrate Alternative', *Energies*, vol. 16, no. 1, p. 5.

Moilanen, A 2006, *Thermogravimetric characterisations of biomass and waste for gasification processes*, VTT Technical Research Centre of Finland.

Molino, A, Chianese, S & Musmarra, D 2016, 'Biomass gasification technology: The state of the art overview', *Journal of Energy Chemistry*, vol. 25, no. 1, pp. 10-25.

Molino, A, Larocca, V, Chianese, S & Musmarra, D 2018, 'Biofuels Production by Biomass Gasification: A Review', *Energies*, vol. 11, no. 4.

Monteiro, E, Ismail, TM, Ramos, A, Abd El-Salam, M, Brito, PSD & Rouboa, A 2017, 'Assessment of the miscanthus gasification in a semi-industrial gasifier using a CFD model', *Applied Thermal Engineering*, vol. 123, pp. 448-57.

Montero, G, Coronado, MA, García, C, Campbell, HE, Montes, DG, Torres, R, Pérez, L, León, JA & Ayala, JR 2018, 'Wheat Straw Open Burning: Emissions and Impact on Climate Change', in *Global Wheat Production*, IntechOpen London, UK.

Morais, LCd, Maia, AA, Resende, PR, Rosa, AH & Nunes, LJ 2022, 'Thermochemical Conversion of Sugarcane Bagasse: A Comprehensive Analysis of Ignition and Burnout Temperatures', *Clean Technologies*, vol. 4, no. 4, pp. 1127-37.

Motta, IL, Miranda, NT, Maciel Filho, R & Maciel, MRW 2018, 'Biomass gasification in fluidized beds: A review of biomass moisture content and operating pressure effects', *Renewable and Sustainable Energy Reviews*, vol. 94, pp. 998-1023.

Moukhina, E 2012, 'Determination of kinetic mechanisms for reactions measured with thermoanalytical instruments', *Journal of thermal analysis and calorimetry*, vol. 109, no. 3, pp. 1203-14.

Mountouris, A, Voutsas, E & Tassios, D 2008, 'Plasma gasification of sewage sludge: Process development and energy optimization', *Energy Conversion and Management*, vol. 49, no. 8, pp. 2264-71.

Muilenburg, M, Shi, Y & Ratner, A 2011, 'Computational Modeling of the Combustion and Gasification Zones in a Downdraft Gasifier', *ASME 2011 International Mechanical Engineering Congress and Exposition*, pp. 151-8, viewed 6/8/2022, <https://doi.org/10.1115/IMECE2011-64009>.

Mulligan, CJ, Strezov, L & Strezov, V 2010, 'Thermal Decomposition of Wheat Straw and Mallee Residue Under Pyrolysis Conditions†', *Energy & Fuels*, vol. 24, no. 1, pp. 46-52.

Mundi, I 2020, *Agricultural production, supply, and distribution*.

Munir, S, Daood, S, Nimmo, W, Cunliffe, A & Gibbs, B 2009, 'Thermal analysis and devolatilization kinetics of cotton stalk, sugar cane bagasse and shea meal under nitrogen and air atmospheres', *Bioresource technology*, vol. 100, no. 3, pp. 1413-8.

Muravyev, NV, Pivkina, AN & Koga, N 2019, 'Critical appraisal of kinetic calculation methods applied to overlapping multistep reactions', *Molecules*, vol. 24, no. 12, p. 2298.

Mureddu, M, Dessì, F, Orsini, A, Ferrara, F & Pettinau, A 2018, 'Air-and oxygen-blown characterization of coal and biomass by thermogravimetric analysis', *Fuel*, vol. 212, pp. 626-37.

Murgia, S, Vascellari, M & Cau, G 2010, 'Comprehensive CFD model of an air-blown coal-fired updraft gasifier', *Fuel*, vol. 101, pp. 129-38.

Murugan, P & Sekhar, SJ 2017, 'Species - Transport CFD model for the gasification of rice husk (Oryza Sativa) using downdraft gasifier', *Comput. Electron. Agric.*, vol. 139, pp. 33-40.

Næss, JS, Hu, X, Gvein, MH, Iordan, C-M, Cavalett, O, Dorber, M, Giroux, B & Cherubini, F 2023, 'Climate change mitigation potentials of biofuels produced from perennial crops and natural regrowth on abandoned and degraded cropland in Nordic countries', *Journal of Environmental Management*, vol. 325, p. 116474.

Naimi, LJ & Sokhansanj, S 2018, 'Data-based equation to predict power and energy input for grinding wheat straw, corn stover, switchgrass, miscanthus, and canola straw', *Fuel processing technology*, vol. 173, pp. 81-8.

Nanda, S, Reddy, SN, Vo, D-VN, Sahoo, BN & Kozinski, JA 2018, 'Catalytic gasification of wheat straw in hot compressed (subcritical and supercritical) water for hydrogen production', *Energy Science & Engineering*, vol. 6, no. 5, pp. 448-59.

Naqvi, SR, Ali, I, Nasir, S, Ali Ammar Taqvi, S, Atabani, AE & Chen, W-H 2020, 'Assessment of agro-industrial residues for bioenergy potential by investigating thermo-kinetic behavior in a slow pyrolysis process', *Fuel*, vol. 278.

Naqvi, SR, Tariq, R, Hameed, Z, Ali, I, Taqvi, SA, Naqvi, M, Niazi, M, Noor, T & Farooq, W 2018, 'Pyrolysis of high-ash sewage sludge: Thermo-kinetic study using TGA and artificial neural networks', *Fuel*, vol. 233, pp. 529-38.

Naqvi, SR, Hameed, Z, Tariq, R, Taqvi, SA, Ali, I, Niazi, MBK, Noor, T, Hussain, A, Iqbal, N & Shahbaz, M 2019, 'Synergistic effect on co-pyrolysis of rice husk and sewage sludge by thermal behavior, kinetics, thermodynamic parameters and artificial neural network', *Waste Manag*, vol. 85, pp. 131-40.

Narnaware, SL & Panwar, N 2022a, 'Biomass gasification for climate change mitigation and policy framework in India: A review', *Bioresource Technology Reports*, vol. 17, p. 100892.

Narnaware, SL & Panwar, N 2022b, 'Kinetic study on pyrolysis of mustard stalk using thermogravimetric analysis', *Bioresource Technology Reports*, vol. 17, p. 100942.

Natarajan, E, Nordin, A & Rao, A 1998, 'Overview of combustion and gasification of rice husk in fluidized bed reactors', *Biomass and bioenergy*, vol. 14, no. 5-6, pp. 533-46.

Nebojša, P, Marija, I & Kristina, Č 2020, 'ORGANIZATIONAL CULTURE AND JOB SATISFACTION AMONG UNIVERSITY PROFESSORS IN THE SELECTED CENTRAL AND EASTERN EUROPEAN COUNTRIES', *Studies in Business & Economics*, vol. 15, no. 3.

Nelson, PF, Shah, P, Strezov, V, Halliburton, B & Carras, JN 2010, 'Environmental impacts of coal combustion: A risk approach to assessment of emissions', *Fuel*, vol. 89, no. 4, pp. 810-6.

NETZSCH 2021, 'Kinetics Neo Software, Version 2.5.3, Kinetic Analysis Software for Thermal Measurements of Chemical Reactions. Model-Free and Model-Based Methods.'.

Neves, D, Thunman, H, Matos, A, Tarelho, L & Gómez-Barea, A 2011, 'Characterization and prediction of biomass pyrolysis products', *Progress in energy and combustion science*, vol. 37, no. 5, pp. 611-30.

Ngadi, Z & Lahlaouti, M 2021, 'CFD modeling of petcoke co-combustion in a real cement kiln: The effect of the turbulence-chemistry interaction model applied with K-ϵ variations', *International Review of Applied Sciences and Engineering*.

Ngo, SI, Nguyen, TD, Lim, Y-I, Song, B-H, Lee, U-D, Choi, Y-T & Song, J-H 2011, 'Performance evaluation for dual circulating fluidized-bed steam gasifier of biomass using quasi-equilibrium three-stage gasification model', *Applied energy*, vol. 88, no. 12, pp. 5208-20.

Nhuchhen, D, Basu, P & Acharya, B 2014, 'A Comprehensive Review on Biomass Torrefaction', *International Journal of Renewable Energy & Biofuels*, pp. 1-56.

Nikoo, MB & Mahinpey, N 2008, 'Simulation of biomass gasification in fluidized bed reactor using ASPEN PLUS', *Biomass and bioenergy*, vol. 32, no. 12, pp. 1245-54.

Nilsson, D, Bernesson, S & Hansson, P-A 2011, 'Pellet production from agricultural raw materials – A systems study', *Biomass and bioenergy*, vol. 35, no. 1, pp. 679-89.

Ningbo, G, Baoling, L, Aimin, L & Juanjuan, L 2015, 'Continuous pyrolysis of pine sawdust at different pyrolysis temperatures and solid residence times', *Journal of Analytical and Applied Pyrolysis*, vol. 114, pp. 155-62.

Nirmale, TC, Kale, BB & Varma, AJ 2017, 'A review on cellulose and lignin based binders and electrodes: Small steps towards a sustainable lithium ion battery', *International journal of biological macromolecules*, vol. 103, pp. 1032-43.

Njenga, M, Iiyama, M, Jamnadass, R, Helander, H, Larsson, L, de Leeuw, J, Neufeldt, H, Röing de Nowina, K & Sundberg, C 2016, 'Gasifier as a cleaner cooking system in rural Kenya', *Journal of Cleaner Production*, vol. 121, pp. 208-17.

Nørregaard, A, Bach, C, Krühne, U, Borgbjerg, U & Gernaey, KV 2019, 'Hypothesis-driven compartment model for stirred bioreactors utilizing computational fluid dynamics and multiple pH sensors', *Chemical Engineering Journal*, vol. 356, pp. 161-9.

Nunes, L, Matias, J & Catalão, J 2016, 'Biomass combustion systems: A review on the physical and chemical properties of the ashes', *Renewable and Sustainable Energy Reviews*, vol. 53, pp. 235-42.

Nutalapati, D, Gupta, R, Moghtaderi, B & Wall, T 2007, 'Assessing slagging and fouling during biomass combustion: A thermodynamic approach allowing for alkali/ash reactions', *Fuel processing technology*, vol. 88, no. 11-12, pp. 1044-52.

Nzihou, A, Stanmore, B, Lyczko, N & Minh, DP 2019, 'The catalytic effect of inherent and adsorbed metals on the fast/flash pyrolysis of biomass: A review', *Energy*, vol. 170, pp. 326-37.

Obernberger, I & Thek, G 2004, 'Physical characterisation and chemical composition of densified biomass fuels with regard to their combustion behaviour', *Biomass and bioenergy*, vol. 27, no. 6, pp. 653-69.

Ogi, T, Nakanishi, M, Fukuda, Y & Matsumoto, K 2013, 'Gasification of oil palm residues (empty fruit bunch) in an entrained-flow gasifier', *Fuel*, vol. 104, pp. 28-35.

Oh, S, Lee, J, Lam, SS, Kwon, EE, Ha, J-M, Tsang, DC, Ok, YS, Chen, W-H & Park, Y-K 2021, 'Fast hydropyrolysis of biomass Conversion: A comparative review', *Bioresource technology*, vol. 342, p. 126067.

Okoroigwe, EC, Enibe, S & Onyegegbu, S 2016, 'Determination of oxidation characteristics and decomposition kinetics of some Nigerian biomass', *Journal of Energy in Southern Africa*, vol. 27, no. 3, pp. 39-49.

Olatunji, O, Akinlabi, S, Mashinini, M, Fatoba, S & Ajayi, O 2018, 'Thermo-gravimetric characterization of biomass properties: A review', *IOP Conference Series: Materials Science and Engineering*, IOP Publishing, p. 012175.

Olgun, H, Ozdogan, S & Yinesor, G 2011, 'Results with a bench scale downdraft biomass gasifier for agricultural and forestry residues', *Biomass and bioenergy*, vol. 35, no. 1, pp. 572-80.

Olsson, A-M & Salmén, L 1997, 'The effect of lignin composition on the viscoelastic properties of wood', *Nordic Pulp & Paper Research Journal*, vol. 12, no. 3, pp. 140-4.

Olsson, M 2006, 'Wheat straw and peat for fuel pellets—organic compounds from combustion', *Biomass and bioenergy*, vol. 30, no. 6, pp. 555-64.

Onay, O, Beis, SH & Kockar, OM 2000, 'Fast pyrolysis of rape seed in a well-swept fixed-bed reactor', *Journal of Analytical and Applied Pyrolysis*, vol. 58-59, no. 2001, pp. 995 - 1007.

Ong, HC, Chen, W-H, Singh, Y, Gan, YY, Chen, C-Y & Show, PL 2020, 'A state-of-the-art review on thermochemical conversion of biomass for biofuel production: A TG-FTIR approach', *Energy Conversion and Management*, vol. 209, p. 112634.

Opfermann, J, Kaisersberger, E & Flammersheim, H 2002, 'Model-free analysis of thermoanalytical data-advantages and limitations', *Thermochimica Acta*, vol. 391, no. 1-2, pp. 119-27.

Osman, AI, Abdelkader, A, Farrell, C, Rooney, D & Morgan, K 2019, 'Reusing, recycling and up-cycling of biomass: A review of practical and kinetic modelling approaches', *Fuel processing technology*, vol. 192, pp. 179-202.

Osman, AI, Mehta, N, Elgarahy, AM, Al-Hinai, A, Al-Muhtaseb, AaH & Rooney, DW 2021, 'Conversion of biomass to biofuels and life cycle assessment: a review', *Environmental Chemistry Letters*, vol. 19, no. 6, pp. 4075-118.

Otchere, P, Pan, J, Fan, B, Chen, W, Lu, Y & Jianxing, L 2020, 'Mixture formation and combustion process of a biodiesel fueled direct injection rotary engine (DIRE) considering injection timing, spark timing and equivalence ratio–CFD study', *Energy Conversion and Management*, vol. 217, p. 112948.

Oveisi, E, Lau, A, Sokhansanj, S, Lim, CJ, Bi, X, Larsson, SH & Melin, S 2013, 'Breakage behavior of wood pellets due to free fall', *Powder technology*, vol. 235, pp. 493-9.

Ozgen, S, Caserini, S, Galante, S, Giugliano, M, Angelino, E, Marongiu, A, Hugony, F, Migliavacca, G & Morreale, C 2014, 'Emission factors from small scale appliances burning wood and pellets', *Atmospheric environment*, vol. 94, pp. 144-53.

Ozsin, G & Putun, AE 2019, 'TGA/MS/FT-IR study for kinetic evaluation and evolved gas analysis of a biomass/PVC co-pyrolysis process', *Energy Conversion and Management*, vol. 182, pp. 143-53.

Pagliaro, M, Ciriminna, R, Kimura, H, Rossi, M & Della Pina, C 2007, 'From glycerol to value-added products', *Angewandte Chemie International Edition*, vol. 46, no. 24, pp. 4434-40.

Pampuro, N, Busato, P & Cavallo, E 2018, 'Effect of Densification Conditions on Specific Energy Requirements and Physical Properties of Compacts Made from Hop Cone', *Energies*, vol. 11, no. 9.

Pan, X & Sano, Y 2005, 'Fractionation of wheat straw by atmospheric acetic acid process', *Bioresource technology*, vol. 96, no. 11, pp. 1256-63.

Pandey, A, Bhaskar, T, Stöcker, M & Sukumaran, R 2015, 'Recent advances in thermochemical conversion of biomass'.

Pandey, B, Prajapati, YK & Sheth, PN 2021, 'CFD analysis of biomass gasification using downdraft gasifier', *Materials Today: Proceedings*, vol. 44, pp. 4107-11.

Paniagua, S, García-Pérez, AI & Calvo, LF 2019, 'Biofuel consisting of wheat straw–poplar wood blends: Thermogravimetric studies and combustion characteristic indexes estimation', *Biomass conversion and biorefinery*, vol. 9, no. 2, pp. 433-43.

Pantaleo, A, Villarini, M, Colantoni, A, Carlini, M, Santoro, F & Rajabi Hamedani, S 2020, 'Techno-economic modeling of biomass pellet routes: Feasibility in Italy', *Energies*, vol. 13, no. 7, p. 1636.

Papandrea, SF, Cataldo, MF, Palma, A, Gallucci, F, Zimbalatti, G & Proto, AR 2021, 'Pelletization of Compost from Different Mixtures with the Addition of Exhausted Extinguishing Powders', *Agronomy*, vol. 11, no. 7.

Parajuli, R, Løkke, S, Østergaard, PA, Knudsen, MT, Schmidt, JH & Dalgaard, T 2014, 'Life Cycle Assessment of district heat production in a straw fired CHP plant', *Biomass and bioenergy*, vol. 68, pp. 115-34.

Parcheta, P, Koltsov, I & Datta, J 2018, 'Fully bio-based poly (propylene succinate) synthesis and investigation of thermal degradation kinetics with released gases analysis', *Polymer degradation and stability*, vol. 151, pp. 90-9.

Paredes, IJ, Yohannes, B, Emady, H, Glasser, BJ, Borghard, WG, Muzzio, F, Cuitiño, AM, Beeckman, J, Ilias, S, Podsiadlo, P, Jezek, E & Baumgartner, J 2017, 'The effect of operating conditions on the residence time distribution and axial dispersion coefficient of a cohesive powder in a rotary kiln', *Chemical Engineering Science*, vol. 158, pp. 50-7.

Parihar, MF, Kamil, M, Goyal, HB, Gupta, AK & Bhatnagar, AK 2007, 'An Experimental Study on Pyrolysis of Biomass', *Process Safety and Environmental Protection*, vol. 85, no. 5, pp. 458-65.

Parikh, J, Channiwala, S & Ghosal, G 2007, 'A correlation for calculating elemental composition from proximate analysis of biomass materials', *Fuel*, vol. 86, no. 12-13, pp. 1710-9.

Park, KY, Lee, K & Kim, D 2018, 'Characterized hydrochar of algal biomass for producing solid fuel through hydrothermal carbonization', *Bioresource technology*, vol. 258, pp. 119-24.

Park, S-W, Lee, J-S, Yang, W-S, Alam, MT & Seo, Y-C 2020, 'A comparative study of the gasification of solid refuse fuel in downdraft fixed bed and bubbling fluidized bed reactors', *Waste and Biomass Valorization*, vol. 11, no. 5, pp. 2345-56.

Parthasarathy, P & Sheeba, KN 2015, 'Combined slow pyrolysis and steam gasification of biomass for hydrogen generation-a review', *International Journal of Energy Research*, vol. 39, no. 2, pp. 147-64.

Pasangulapati, V, Ramachandriya, KD, Kumar, A, Wilkins, MR, Jones, CL & Huhnke, RL 2012, 'Effects of cellulose, hemicellulose and lignin on thermochemical conversion characteristics of the selected biomass', *Bioresource technology*, vol. 114, pp. 663-9.

Patel, KD, Shah, NK & Patel, RN 2013, 'CFD Analysis of Spatial Distribution of Various Parameters in Downdraft Gasifier', *Procedia Engineering*, vol. 51, pp. 764-9.

Patra, TK & Sheth, PN 2015, 'Biomass gasification models for downdraft gasifier: A state-of-the-art review', *Renewable and Sustainable Energy Reviews*, vol. 50, pp. 583-93.

Paul, AS, Panwar, NL, Salvi, BL, Jain, S & Sharma, D 2020, 'Experimental investigation on the production of bio-oil from wheat straw', *Energy Sources, Part A: Recovery, Utilization, and Environmental Effects*, pp. 1-16.

Peacocke, G & Bridgwater, AV 2001, 'Transport, handling and storage of biomass derived fast pyrolysis liquid', *Progress in Thermochemical Biomass Conversion*, vol. 2, pp. 1482-99.

Pedroso, DT, Machin, EB, Cabrera-Barjas, G, Farias, O, Loyola, AP, Quilodrán, CP, Machín, AB, Pérez, NP & de Carvalho Junior, JA 2022, 'A Study of Bioenergy Production from Chilean Tessaria absinthioides', *BioEnergy Research*, vol. 15, no. 1, pp. 385-98.

Peng, J, Bi, XT, Lim, CJ, Peng, H, Kim, CS, Jia, D & Zuo, H 2015, 'Sawdust as an effective binder for making torrefied pellets', *Applied energy*, vol. 157, pp. 491-8.

Pepiot, P, Dibble, CJ & Foust, TD 2010, 'Computational Fluid Dynamics Modeling of Biomass Gasification and Pyrolysis', in *Computational Modeling in Lignocellulosic Biofuel Production*, pp. 273-98.

Pérez-Maqueda, LA, Sánchez-Jiménez, PE, Perejón, A, García-Garrido, C, Criado, JM & Benítez-Guerrero, M 2014, 'Scission kinetic model for the prediction of polymer pyrolysis curves from chain structure', *Polymer testing*, vol. 37, pp. 1-5.

Pešenjanski, I, Miljković, B & Vićević, M 2016, 'Pyrolysis Kinetic Modelling of Wheat Straw from the Pannonian Region', *Journal of Combustion*, vol. 2016, pp. 1-10.

Pfeifer, C, Koppatz, S & Hofbauer, H 2011, *Steam gasification of various feedstocks at a dual fluidized bed gasifier: impacts of operation conditions and bed materials. Biomass Conv. Bioref. 1: 39–53*.

Pham, X-H, Piriou, B, Salvador, S, Valette, J & Van de Steene, L 2018, 'Oxidative pyrolysis of pine wood, wheat straw and miscanthus pellets in a fixed bed', *Fuel processing technology*, vol. 178, pp. 226-35.

Phapatarinan, S, Bumrungthaichaichan, E & Wattananusorn, S 2018, 'A suitable k-epsilon model for CFD simulation of pump-around jet mixing tank with moderate jet reynolds number', *MATEC Web of Conferences*, EDP Sciences, p. 03010.

Phounglamcheik, A, Babler, MU, Donaj, P, Amovic, M, Ljunggren, R & Engvall, K 2017, 'Pyrolysis of Wood in a Rotary Kiln Pyrolyzer: Modeling and Pilot Plant Trials', *Energy Procedia*, vol. 105, pp. 908-13.

Picchio, R, Latterini, F, Venanzi, R, Stefanoni, W, Suardi, A, Tocci, D & Pari, L 2020, 'Pellet production from woody and non-woody feedstocks: A review on biomass quality evaluation', *Energies*, vol. 13, no. 11, p. 2937.

Pichler, M, Haddadi, B, Jordan, C, Norouzi, H & Harasek, M 2021, 'Influence of particle residence time distribution on the biomass pyrolysis in a rotary kiln', *Journal of Analytical and Applied Pyrolysis*, vol. 158.

Pieratti, E 2011, 'Biomass gasification in small scale plants', University of Trento, Trento, Italy.

Pinto, F, Franco, C, Andre, RN, Tavares, C, Dias, M, Gulyurtlu, I & Cabrita, I 2003, 'Effect of experimental conditions on co-gasification of coal, biomass and plastics wastes with air/steam mixtures in a fluidized bed system', *Fuel*, vol. 82, no. 15-17, pp. 1967-76.

Pis, J, de La Puente, G, Fuente, E, Morán, A & Rubiera, F 1996, 'A study of the self-heating of fresh and oxidized coals by differential thermal analysis', *Thermochimica Acta*, vol. 279, pp. 93-101.

Pokhrel, G, Han, Y & Gardner, DJ 2021, 'Comparative Study of the Properties of Wood Flour and Wood Pellets Manufactured from Secondary Processing Mill Residues', *Polymers (Basel)*, vol. 13, no. 15.

Poletto, M, Dettenborn, J, Pistor, V, Zeni, M & Zattera, AJ 2010, 'Materials produced from plant biomass: Part I: evaluation of thermal stability and pyrolysis of wood', *Materials Research*, vol. 13, pp. 375-9.

Portarapillo, M, Di Sarli, V, Sanchirico, R & Di Benedetto, A 2020, 'CFD simulation of the dispersion of binary dust mixtures in the 20 L vessel', *Journal of Loss Prevention in the Process Industries*, vol. 67, p. 104231.

Pradana, YS & Budiman, A 2015, 'Bio-syngas derived from Indonesian oil palm empty fruit bunch (EFB) using middle-scale gasification', *Journal of Engineering Science and Technology*, vol. 10, no. 8, pp. 1-8.

Pradhan, P, Arora, A & Mahajani, SM 2018, 'Pilot scale evaluation of fuel pellets production from garden waste biomass', *Energy for Sustainable Development*, vol. 43, pp. 1-14.

Pradhan, P, Mahajani, SM & Arora, A 2018, 'Production and utilization of fuel pellets from biomass: A review', *Fuel processing technology*, vol. 181, pp. 215-32.

Prins, MJ, Ptasinski, KJ & Janssen, FJ 2007, 'From coal to biomass gasification: Comparison of thermodynamic efficiency', *Energy*, vol. 32, no. 7, pp. 1248-59.

Puig-Arnavat, M, Bruno, JC & Coronas, A 2010, 'Review and analysis of biomass gasification models', *Renewable and Sustainable Energy Reviews*, vol. 14, no. 9, pp. 2841-51.

Puig-Arnavat, M, Shang, L, Sárossy, Z, Ahrenfeldt, J & Henriksen, UB 2016, 'From a single pellet press to a bench scale pellet mill—Pelletizing six different biomass feedstocks', *Fuel processing technology*, vol. 142, pp. 27-33.

Puig-Gamero, M, Pio, D, Tarelho, L, Sánchez, P & Sanchez-Silva, L 2021, 'Simulation of biomass gasification in bubbling fluidized bed reactor using aspen plus®', *Energy Conversion and Management*, vol. 235, p. 113981.

Punsuwan, N & Tangsathitkulchai, C 2014, 'Product characterization and kinetics of biomass pyrolysis in a three-zone free-fall reactor', *International Journal of Chemical Engineering*, vol. 2014.

Purohit, P & Chaturvedi, V 2016, 'Techno-economic assessment of biomass pellets for power generation in India'.

Quayle, WC 2016, 'Alternative management of rice straw'.

Quesada, L, Pérez, A, Calero, M, Blázquez, G & Martín-Lara, M 2018, 'Reaction schemes for estimating kinetic parameters of thermal decomposition of native and metal-loaded almond shell', *Process Safety and Environmental Protection*, vol. 118, pp. 234-44.

Rafiq, MK, Bachmann, RT, Rafiq, MT, Shang, Z, Joseph, S & Long, R 2016, 'Influence of pyrolysis temperature on physico-chemical properties of corn stover (Zea mays L.) biochar and feasibility for carbon capture and energy balance', *PLoS One*, vol. 11, no. 6, p. e0156894.

Rahib, Y, Elorf, A, Sarh, B, Ezahri, M, Rahib, Y & Bonnamy, S 2019, 'Experimental analysis on thermal characteristics of argan nut shell (ANS) biomass as a green energy resource', *International Journal of Renewable Energy Research*, vol. 9, no. 4, pp. 1606-15.

Rahmani, AM, Gahlot, P, Moustakas, K, Kazmi, A, Ojha, CSP & Tyagi, VK 2022, 'Pretreatment methods to enhance solubilization and anaerobic biodegradability of lignocellulosic biomass (wheat straw): Progress and challenges', *Fuel*, vol. 319, p. 123726.

Rahn, D, Riedmann, H, Behr, R & Haidn, OJ 2018, 'Non-adiabatic flamelet modeling for the numerical simulation of methane combustion in rocket thrust chambers', *2018 Joint Propulsion Conference*, p. 4869.

Ramírez-Gómez, Á 2016, 'Research needs on biomass characterization to prevent handling problems and hazards in industry', *Particulate Science and Technology*, vol. 34, no. 4, pp. 432-41.

Rasool, T & Kumar, S 2020, 'Kinetic and thermodynamic evaluation of pyrolysis of plant biomass using TGA', *Materials Today: Proceedings*, vol. 21, pp. 2087-95.

Raveendran, K, Ganesh, A & Khilar, KC 1995, 'Influence of mineral matter on biomass pyrolysis characteristics', *Fuel*, vol. 74, no. 12, pp. 1812-22.

Ravindranath, NH & Hall, DO 1995, *Biomass, energy and environment: a developing country perspective from India*, Oxford University Press.

Raza, M, Abu-Jdayil, B, Al-Marzouqi, AH & Inayat, A 2022, 'Kinetic and thermodynamic analyses of date palm surface fibers pyrolysis using Coats-Redfern method', *Renewable Energy*, vol. 183, pp. 67-77.

Reed, TB & Das, A 1988, *Handbook of biomass downdraft gasifier engine systems*, Biomass Energy Foundation.

Relova, I, Vignote, S, León, M & Ambrosio, Y 2009, 'Optimisation of the manufacturing variables of sawdust pellets from the bark of Pinus caribaea Morelet: Particle size, moisture and pressure', *Biomass and bioenergy*, vol. 33, no. 10, pp. 1351-7.

Ren, J, Yu, P & Xu, X 2019, 'Straw utilization in China—status and recommendations', *Sustainability*, vol. 11, no. 6, p. 1762.

Ren, Q, Zhao, C, Duan, L & Chen, X 2011, 'NO formation during agricultural straw combustion', *Bioresource technology*, vol. 102, no. 14, pp. 7211-7.

Rex, P & Miranda, LR 2020, 'Catalytic activity of acid-treated biomass for the degradation of expanded polystyrene waste', *Environmental Science and Pollution Research*, vol. 27, no. 1, pp. 438-55.

Ríos-Badrán, IM, Luzardo-Ocampo, I, García-Trejo, JF, Santos-Cruz, J & Gutiérrez-Antonio, C 2020, 'Production and characterization of fuel pellets from rice husk and wheat straw', *Renewable Energy*, vol. 145, pp. 500-7.

Rioux, R, Song, H, Hoefelmeyer, J, Yang, P & Somorjai, G 2005, 'High-surface-area catalyst design: synthesis, characterization, and reaction studies of platinum nanoparticles in mesoporous SBA-15 silica', *The journal of physical chemistry B*, vol. 109, no. 6, pp. 2192-202.

Rizkiana, J, Guan, G, Widayatno, WB, Hao, X, Huang, W, Tsutsumi, A & Abudula, A 2014, 'Effect of biomass type on the performance of cogasification of low rank coal with biomass at relatively low temperatures', *Fuel*, vol. 134, pp. 414-9.

Robbins, MP, Evans, G, Valentine, J, Donnison, IS & Allison, GG 2012, 'New opportunities for the exploitation of energy crops by thermochemical conversion in Northern Europe and the UK', *Progress in energy and combustion science*, vol. 38, no. 2, pp. 138-55.

Roberts, DG & Harris, DJ 2015, 'A numerical model for understanding the behaviour of coals in an entrained-flow gasifier', *Fuel processing technology*, vol. 134, pp. 424-40.

Ronsse, F, van Hecke, S, Dickinson, D & Prins, W 2013, 'Production and characterization of slow pyrolysis biochar: influence of feedstock type and pyrolysis conditions', *GCB Bioenergy*, vol. 5, no. 2, pp. 104-15.

Rupar-Gadd, K & Forss, J 2018, 'Self-heating properties of softwood samples investigated by using isothermal calorimetry', *Biomass and bioenergy*, vol. 111, pp. 206-12.

Sadaka, SS 2013, 'Gasification of raw and torrefied cotton gin wastes in an auger system', *Applied Engineering in Agriculture*, vol. 29, no. 3, pp. 405-14.

Saddawi, A, Jones, J, Williams, A & Wojtowicz, M 2010, 'Kinetics of the thermal decomposition of biomass', *Energy & Fuels*, vol. 24, no. 2, pp. 1274-82.

Sadhukhan, AK, Gupta, P, Goyal, T & Saha, RK 2008, 'Modelling of pyrolysis of coal–biomass blends using thermogravimetric analysis', *Bioresource technology*, vol. 99, no. 17, pp. 8022-6.

Safarian, S, Unnthorsson, R & Richter, C 2020, 'The equivalence of stoichiometric and non-stoichiometric methods for modeling gasification and other reaction equilibria', *Renewable and Sustainable Energy Reviews*, vol. 131, p. 109982.

Safiullina, AS, Buzyurov, AV, Ziganshina, SA, Gerasimov, AV, Schick, C, Gorbatchuk, VV & Ziganshin, MA 2020, 'Using fast scanning calorimetry to study solid-state cyclization of dipeptide L-leucyl-L-leucine', *Thermochimica Acta*, vol. 692, p. 178748.

Sahoo, SS, Vijay, VK, Chandra, R & Kumar, H 2021, 'Production and characterization of biochar produced from slow pyrolysis of pigeon pea stalk and bamboo', *Cleaner Engineering and Technology*, vol. 3, p. 100101.

Sait, HH, Hussain, A, Salema, AA & Ani, FN 2012, 'Pyrolysis and combustion kinetics of date palm biomass using thermogravimetric analysis', *Bioresource technology*, vol. 118, pp. 382-9.

Sandro, N, Agis, P, Gojmir, R, Vlasta, Z & Müslüm, A 2019, 'Using pellet fuels for residential heating: A field study on its efficiency and the users' satisfaction', *Energy and Buildings*, vol. 184, pp. 193-204.

Sannigrahi, P, Ragauskas, AJ & Tuskan, GA 2010, 'Poplar as a feedstock for biofuels: a review of compositional characteristics', *Biofuels, Bioproducts and Biorefining*, vol. 4, no. 2, pp. 209-26.

Sarafraz, M, Jafarian, M, Arjomandi, M & Nathan, G 2017, 'Potential use of liquid metal oxides for chemical looping gasification: A thermodynamic assessment', *Applied energy*, vol. 195, pp. 702-12.

Sarkar, M, Kumar, A, Tumuluru, JS, Patil, KN & Bellmer, D 2014, 'Thermal devolatilization kinetics of switchgrass pretreated with torrefaction and densification', *Transactions of the ASABE*, vol. 57, no. 4, pp. 1199-210.

Sarker, S 2016, 'Thermochemical gasification of local lignocellulosic biomass via fixed-bed and fluidized-bed reactors'.

Sarker, S, Arauzo, J & Nielsen, HK 2015, 'Semi-continuous feeding and gasification of alfalfa and wheat straw pellets in a lab-scale fluidized bed reactor', *Energy Conversion and Management*, vol. 99, pp. 50-61.

Schluckner, C, Gaber, C, Landfahrer, M, Demuth, M & Hochenauer, C 2020, 'Fast and accurate CFD-model for NOx emission prediction during oxy-fuel combustion of natural gas using detailed chemical kinetics', *Fuel*, vol. 264, p. 116841.

Sedighi, M & Salarian, H 2017, 'A comprehensive review of technical aspects of biomass cookstoves', *Renewable and Sustainable Energy Reviews*, vol. 70, pp. 656-65.

Sedmihradská, A, Pohořelý, M, Jevič, P, Skoblia, S, Beňo, Z, Farták, J, Čech, B & Hartman, M 2020a, 'Pyrolysis of wheat and barley straw', *Research in Agricultural Engineering*, vol. 66, no. No. 1, pp. 8-17.

Sedmihradská, A, Pohořelý, M, Jevič, P, Skoblia, S, Beňo, Z, Farták, J, Čech, B & Hartman, M 2020b, 'Pyrolysis of wheat and barley straw', *Research in Agricultural Engineering*, vol. 66, no. 1, pp. 8-17.

Serapiglia, MJ, Cameron, KD, Stipanovic, AJ, Abrahamson, LP, Volk, TA & Smart, LB 2013, 'Yield and woody biomass traits of novel shrub willow hybrids at two contrasting sites', *BioEnergy Research*, vol. 6, no. 2, pp. 533-46.

Serrano, C, Monedero, E, Lapuerta, M & Portero, H 2011, 'Effect of moisture content, particle size and pine addition on quality parameters of barley straw pellets', *Fuel processing technology*, vol. 92, no. 3, pp. 699-706.

Sezer, S & Özveren, U 2021, 'Investigation of syngas exergy value and hydrogen concentration in syngas from biomass gasification in a bubbling fluidized bed gasifier by using machine learning', *International Journal of Hydrogen Energy*, vol. 46, no. 39, pp. 20377-96.

Shaaban, A, Se, S-M, Dimin, M, Juoi, JM, Husin, MHM & Mitan, NMM 2014, 'Influence of heating temperature and holding time on biochars derived from rubber wood sawdust via slow pyrolysis', *Journal of Analytical and Applied Pyrolysis*, vol. 107, pp. 31-9.

Shabbar, S & Janajreh, I 2013, 'Thermodynamic equilibrium analysis of coal gasification using Gibbs energy minimization method', *Energy Conversion and Management*, vol. 65, pp. 755-63.

Shadangi, KP & Mohanty, K 2014, 'Kinetic study and thermal analysis of the pyrolysis of non-edible oilseed powders by thermogravimetric and differential scanning calorimetric analysis', *Renewable Energy*, vol. 63, pp. 337-44.

Shagali, AA, Hu, S, Li, H, Chi, H, Qing, H, Xu, J, Jiang, L, Wang, Y, Su, S & Xiang, J 2023, 'Thermal behavior, synergistic effect and thermodynamic parameter evaluations of biomass/plastics co–pyrolysis in a concentrating photothermal TGA', *Fuel*, vol. 331, p. 125724.

Shah, IA, Gou, X, Zhang, Q, Wu, J, Wang, E & Liu, Y 2018, 'Experimental study on NOx emission characteristics of oxy-biomass combustion', *Journal of Cleaner Production*, vol. 199, pp. 400-10.

Shah, MA, Khan, MNS & Kumar, V 2018, 'Biomass residue characterization for their potential application as biofuels', *Journal of thermal analysis and calorimetry*, vol. 134, no. 3, pp. 2137-45.

Shahram Emami, LGT, Phani Adapa, Elizabeth George, Ashwini Tilay, Ajay Dalai, Mark Drisdelle, Lily Ketabi 2014, 'Effect of Fuel Additives on Agricultural Straw Pellet Quality, ' *Int J Agric & Biol Eng*, vol. 7, no. 2, pp. 92-100.

Shahrukh, H, Oyedun, AO, Kumar, A, Ghiasi, B, Kumar, L & Sokhansanj, S 2016, 'Comparative net energy ratio analysis of pellet produced from steam pretreated biomass from agricultural residues and energy crops', *Biomass and bioenergy*, vol. 90, pp. 50-9.

Sharma, P, Pandey, O & Diwan, P 2019, 'Non-isothermal kinetics of pseudo-components of waste biomass', *Fuel*, vol. 253, pp. 1149-61.

Sharma, P, Gupta, B, Pandey, M, Bisen, KS & Baredar, P 2021, 'Downdraft biomass gasification: A review on concepts, designs analysis, modelling and recent advances', *Materials Today: Proceedings*, vol. 46, pp. 5333-41.

Sharma, T, Yepes Maya, DM, M. Nascimento, FR, Shi, Y, Ratner, A, Silva Lora, EE, Mendes Neto, LJ, Escobar Palacios, JC & Vieira Andrade, R 2018, 'An experimental and theoretical study of the gasification of miscanthus briquettes in a double-stage downdraft gasifier: syngas, tar, and biochar characterization', *Energies*, vol. 11, no. 11, p. 3225.

Shaw, M, Karunakaran, C & Tabil, L 2009, 'Physicochemical characteristics of densified untreated and steam exploded poplar wood and wheat straw grinds', *Biosystems Engineering*, vol. 103, no. 2, pp. 198-207.

Shaw, MD 2008, 'Feedstock and process variables influencing biomass densification'.

Shen, D, Xiao, R, Gu, S & Zhang, H 2013, 'The overview of thermal decomposition of cellulose in lignocellulosic biomass', *Cellulose-biomass conversion*, pp. 193-226.

Sher, F, Iqbal, SZ, Liu, H, Imran, M & Snape, CE 2020, 'Thermal and kinetic analysis of diverse biomass fuels under different reaction environment: A way forward to renewable energy sources', *Energy Conversion and Management*, vol. 203.

Sheth, PN & Babu, B 2009, 'Experimental studies on producer gas generation from wood waste in a downdraft biomass gasifier', *Bioresource technology*, vol. 100, no. 12, pp. 3127-33.

Shi, L, Gong, J & Zhai, C 2022, 'Application of a hybrid PSO-GA optimization algorithm in determining pyrolysis kinetics of biomass', *Fuel*, vol. 323, p. 124344.

Shiehnejadhesar, A, Mehrabian, R, Hochenauer, C & Scharler, R 2017, 'The virtual biomass grate furnace-an overall CFD model for biomass combustion plants', *Energy Procedia*, vol. 120, pp. 516-23.

Shrivastava, P, Kumar, A, Tekasakul, P, Lam, SS & Palamanit, A 2021, 'Comparative investigation of yield and quality of bio-oil and biochar from pyrolysis of woody and non-woody biomasses', *Energies*, vol. 14, no. 4, p. 1092.

Siedlecki, M, De Jong, W & Verkooijen, AH 2011, 'Fluidized bed gasification as a mature and reliable technology for the production of bio-syngas and applied in the production of liquid transportation fuels—a review', *Energies*, vol. 4, no. 3, pp. 389-434.

Siegel, R & Howell, J 1992, *Thermal Radiation Heat Transfer*, Hemisphere, New York.

Siemons, RV 2001, 'Identifying a role for biomass gasification in rural electrification in developing countries: the economic perspective', *Biomass and bioenergy*, vol. 20, no. 4, pp. 271-85.

Simone, M, Barontini, F, Nicolella, C & Tognotti, L 2013, 'Assessment of syngas composition variability in a pilot-scale downdraft biomass gasifier by an extended equilibrium model', *Bioresource technology*, vol. 140, pp. 43-52.

Singh, R, Krishna, BB, Mishra, G, Kumar, J & Bhaskar, T 2016, 'Strategies for selection of thermo-chemical processes for the valorisation of biomass', *Renewable Energy*, vol. 98, pp. 226-37.

Singh, RK, Patil, T & Sawarkar, AN 2020, 'Pyrolysis of garlic husk biomass: Physico-chemical characterization, thermodynamic and kinetic analyses', *Bioresource Technology Reports*, vol. 12.

Singh, RK, Pandey, D, Patil, T & Sawarkar, AN 2020, 'Pyrolysis of banana leaves biomass: Physico-chemical characterization, thermal decomposition behavior, kinetic and thermodynamic analyses', *Bioresour Technol*, vol. 310, p. 123464.

Singh, S, Chakraborty, JP & Mondal, MK 2020, 'Intrinsic kinetics, thermodynamic parameters and reaction mechanism of non-isothermal degradation of torrefied Acacia nilotica using isoconversional methods', *Fuel*, vol. 259, p. 116263.

Singh, Y & Sidhu, H 2014, 'Management of cereal crop residues for sustainable rice-wheat production system in the Indo-Gangetic plains of India', *Proceedings of the Indian National Science Academy*, vol. 80, no. 1, pp. 95-114.

Siripaiboon, C, Sarabhorn, P & Areeprasert, C 2020, 'Two-dimensional CFD simulation and pilot-scale experimental verification of a downdraft gasifier: effect of reactor aspect ratios on temperature and syngas composition during gasification', *International Journal of Coal Science & Technology*, vol. 7, no. 3, pp. 536-50.

Siriwardane, R, Riley, J, Tian, H & Richards, G 2016, 'Chemical looping coal gasification with calcium ferrite and barium ferrite via solid–solid reactions', *Applied energy*, vol. 165, pp. 952-66.

Sivabalan, K, Hassan, S, Ya, H & Pasupuleti, J 2021, 'A review on the characteristic of biomass and classification of bioenergy through direct combustion and gasification as an alternative power supply', *Journal of Physics: Conference Series*, IOP Publishing, p. 012033.

Skoulou, V, Swiderski, A, Yang, W & Zabaniotou, A 2009, 'Process characteristics and products of olive kernel high temperature steam gasification (HTSG)', *Bioresource technology*, vol. 100, no. 8, pp. 2444-51.

Slopiecka, K, Bartocci, P & Fantozzi, F 2012, 'Thermogravimetric analysis and kinetic study of poplar wood pyrolysis', *Applied energy*, vol. 97, pp. 491-7.

Smith, JD, Alembath, A, Al-Rubaye, H, Yu, J, Gao, X & Golpour, H 2019, 'Validation and application of a kinetic model for downdraft biomass gasification simulation', *Chemical Engineering & Technology*, vol. 42, no. 12, pp. 2505-19.

Snelders, J, Dornez, E, Benjelloun-Mlayah, B, Huijgen, WJ, de Wild, PJ, Gosselink, RJ, Gerritsma, J & Courtin, CM 2014, 'Biorefining of wheat straw using an acetic and formic acid based organosolv fractionation process', *Bioresour Technol*, vol. 156, pp. 275-82.

Snyder, BF 2019, 'Costs of biomass pyrolysis as a negative emission technology: A case study', *International Journal of Energy Research*, vol. 43, no. 3, pp. 1232-44.

Soh, M, Chew, JJ, Liu, S & Sunarso, J 2019, 'Comprehensive kinetic study on the pyrolysis and combustion behaviours of five oil palm biomass by thermogravimetric-mass spectrometry (TG-MS) analyses', *BioEnergy Research*, vol. 12, no. 2, pp. 370-87.

Sohi, SP, Krull, E, Lopez-Capel, E & Bol, R 2010, 'A review of biochar and its use and function in soil', *Advances in agronomy*, vol. 105, pp. 47-82.

Solar, J, de Marco, I, Caballero, BM, Lopez-Urionabarrenechea, A, Rodriguez, N, Agirre, I & Adrados, A 2016, 'Influence of temperature and residence time in the pyrolysis of woody biomass waste in a continuous screw reactor', *Biomass and bioenergy*, vol. 95, pp. 416-23.

Solarin, SA 2017, 'The role of urbanisation in the economic development process: evidence from Nigeria', *Margin: The Journal of Applied Economic Research*, vol. 11, no. 3, pp. 223-55.

Solarin, SA, Al-Mulali, U, Gan, GGG & Shahbaz, M 2018, 'The impact of biomass energy consumption on pollution: evidence from 80 developed and developing countries', *Environmental Science and Pollution Research*, vol. 25, no. 23, pp. 22641-57.

Soleimani, M, Tabil, XL, Grewal, R & Tabil, LG 2017, 'Carbohydrates as binders in biomass densification for biochemical and thermochemical processes', *Fuel*, vol. 193, pp. 134-41.

Sommer, S & Møller, H 2000, 'Emission of greenhouse gases during composting of deep litter from pig production–effect of straw content', *The Journal of Agricultural Science*, vol. 134, no. 3, pp. 327-35.

Soomro, A, Chen, S, Ma, S & Xiang, W 2018, 'Catalytic activities of nickel, dolomite, and olivine for tar removal and H2-enriched gas production in biomass gasification process', *Energy & Environment*, vol. 29, no. 6, pp. 839-67.

Soria-Verdugo, A, Rubio-Rubio, M, Goos, E & Riedel, U 2018, 'Combining the lumped capacitance method and the simplified distributed activation energy model to describe the pyrolysis of thermally small biomass particles', *Energy Conversion and Management*, vol. 175, pp. 164-72.

Souza-Santos, MLd 2010, 'Solid Fuels Combustion and Gasification: Modeling, Simulation, and Equipment Operations Second Edition'.

Sriram, A & Swaminathan, G 2018, 'Pyrolysis of Musa balbisiana flower petal using thermogravimetric studies', *Bioresource technology*, vol. 265, pp. 236-46.

Ståhl, M & Berghel, J 2011, 'Energy efficient pilot-scale production of wood fuel pellets made from a raw material mix including sawdust and rapeseed cake', *Biomass and bioenergy*, vol. 35, no. 12, pp. 4849-54.

Ståhl, M, Berghel, J & Williams, H 2016, 'Energy efficiency, greenhouse gas emissions and durability when using additives in the wood fuel pellet chain', *Fuel processing technology*, vol. 152, pp. 350-5.

Ståhl, M, Granström, K, Berghel, J & Renström, R 2004, 'Industrial processes for biomass drying and their effects on the quality properties of wood pellets', *Biomass and bioenergy*, vol. 27, no. 6, pp. 621-8.

Stančin, H, Mikulčić, H, Wang, X & Duić, N 2020, 'A review on alternative fuels in future energy system', *Renewable and Sustainable Energy Reviews*, vol. 128, p. 109927.

Stelte, W, Holm, JK, Sanadi, AR, Barsberg, S, Ahrenfeldt, J & Henriksen, UB 2011, 'Fuel pellets from biomass: The importance of the pelletizing pressure and its dependency on the processing conditions', *Fuel*, vol. 90, no. 11, pp. 3285-90.

Stelte, W, Clemons, C, Holm, JK, Ahrenfeldt, J, Henriksen, UB & Sanadi, AR 2011, 'Fuel Pellets from Wheat Straw: The Effect of Lignin Glass Transition and Surface Waxes on Pelletizing Properties', *BioEnergy Research*, vol. 5, no. 2, pp. 450-8.

Sultana, A & Kumar, A 2012, 'Ranking of biomass pellets by integration of economic, environmental and technical factors', *Biomass and bioenergy*, vol. 39, pp. 344-55.

Sultana, A, Kumar, A & Harfield, D 2010, 'Development of agri-pellet production cost and optimum size', *Bioresource technology*, vol. 101, no. 14, pp. 5609-21.

Sun, Y, Nakano, J, Liu, L, Wang, X & Zhang, Z 2015, 'Achieving waste to energy through sewage sludge gasification using hot slags: syngas production', *Sci Rep*, vol. 5, p. 11436.

Sun, Y, Gao, B, Yao, Y, Fang, J, Zhang, M, Zhou, Y, Chen, H & Yang, L 2014, 'Effects of feedstock type, production method, and pyrolysis temperature on biochar and hydrochar properties', *Chemical Engineering Journal*, vol. 240, pp. 574-8.

Surono, UB & Saptoadi, H 2022, 'Pellet combustion characteristics and emission of cocoa pod shell and coal blends', *Biomass conversion and biorefinery*, pp. 1-9.

Susastriawan, AAP, Saptoadi, H & Purnomo 2017, 'Small-scale downdraft gasifiers for biomass gasification: A review', *Renewable and Sustainable Energy Reviews*, vol. 76, pp. 989-1003.

Szufa, S, Dzikuć, M, Adrian, Ł, Piersa, P, Romanowska-Duda, Z, Lewandowska, W, Marcza, M, Błaszczuk, A & Piwowar, A 2020, 'Torrefaction of oat straw to use as solid biofuel, an additive to organic fertilizers for agriculture purposes and activated carbon–TGA analysis, kinetics', *E3S web of conferences*.

Tabil, L 1996, 'Pelleting and binding characteristics of alfalfa', *Unpublished Ph. D. thesis, Department of Agricultural and Bioresource Engineering, Saskatoon, SK Canada: University of Saskatchewan*.

Tag, AT, Duman, G, Ucar, S & Yanik, J 2016, 'Effects of feedstock type and pyrolysis temperature on potential applications of biochar', *Journal of Analytical and Applied Pyrolysis*, vol. 120, pp. 200-6.

Talebnia, F, Karakashev, D & Angelidaki, I 2010, 'Production of bioethanol from wheat straw: An overview on pretreatment, hydrolysis and fermentation', *Bioresour Technol*, vol. 101, no. 13, pp. 4744-53.

Tanoh, TS, Ait Oumeziane, A, Lemonon, J, Escudero Sanz, FJ & Salvador, S 2020, 'Green Waste/Wood Pellet Pyrolysis in a Pilot-Scale Rotary Kiln: Effect of Temperature on Product Distribution and Characteristics', *Energy & Fuels*, vol. 34, no. 3, pp. 3336-45.

Tarasov, D, Shahi, C & Leitch, M 2013, 'Effect of additives on wood pellet physical and thermal characteristics: A review', *International Scholarly Research Notices*, vol. 2013.

Tarchoun, AF, Trache, D, Klapötke, TM, Chelouche, S, Derradji, M, Bessa, W & Mezroua, A 2019, 'A promising energetic polymer from Posidonia oceanica brown algae: synthesis, characterization, and kinetic modeling', *Macromolecular Chemistry and Physics*, vol. 220, no. 22, p. 1900358.

Tauqir, W, Zubair, M & Nazir, H 2019, 'Parametric analysis of a steady state equilibrium-based biomass gasification model for syngas and biochar production and heat generation', *Energy Conversion and Management*, vol. 199, p. 111954.

Teh, JS, Teoh, YH, How, HG & Sher, F 2021, 'Thermal Analysis Technologies for Biomass Feedstocks: A State-of-the-Art Review', *Processes*, vol. 9, no. 9.

Telmo, C & Lousada, J 2011, 'Heating values of wood pellets from different species', *Biomass and bioenergy*, vol. 35, no. 7, pp. 2634-9.

Tezer, Ö, Karabağ, N, Öngen, A, Çolpan, CÖ & Ayol, A 2022, 'Biomass gasification for sustainable energy production: A review', *International Journal of Hydrogen Energy*, vol. 47, no. 34, pp. 15419-33.

Theerarattananoon, K, Xu, F, Wilson, J, Ballard, R, Mckinney, L, Staggenborg, S, Vadlani, P, Pei, Z & Wang, D 2011, 'Physical properties of pellets made from sorghum stalk, corn stover, wheat straw, and big bluestem', *Industrial Crops and Products*, vol. 33, no. 2, pp. 325-32.

Thomas, M, Van Vliet, T & Van der Poel, A 1998, 'Physical quality of pelleted animal feed 3. Contribution of feedstuff components', *Animal Feed Science and Technology*, vol. 70, no. 1-2, pp. 59-78.

Tilay, A, Azargohar, R, Drisdelle, M, Dalai, A & Kozinski, J 2015, 'Canola meal moisture-resistant fuel pellets: Study on the effects of process variables and additives on the pellet quality and compression characteristics', *Industrial Crops and Products*, vol. 63, pp. 337-48.

Tinaut, FV, Melgar, A, Perez, JF & Horrillo, A 2008, 'Effect of biomass particle size and air superficial velocity on the gasification process in a downdraft fixed bed gasifier. An experimental and modelling study', *Fuel processing technology*, vol. 89, no. 11, pp. 1076-89.

Tognotti, L, Malotti, A, Petarca, L & Zanelli, S 1985, 'Measurement of ignition temperature of coal particles using a thermogravimetric technique', *Combustion Science and Technology*, vol. 44, no. 1-2, pp. 15-28.

Tomczyk, A, Sokołowska, Z & Boguta, P 2020, 'Biochar physicochemical properties: pyrolysis temperature and feedstock kind effects', *Reviews in Environmental Science and Bio/Technology*, vol. 19, no. 1, pp. 191-215.

Torres, C, Urvina, L & de Lasa, H 2019, 'A chemical equilibrium model for biomass gasification. Application to Costa Rican coffee pulp transformation unit', *Biomass and bioenergy*, vol. 123, pp. 89-103.

Toscano, G, Riva, G, Pedretti, EF, Corinaldesi, F, Mengarelli, C & Duca, D 2013, 'Investigation on wood pellet quality and relationship between ash content and the most important chemical elements', *Biomass and bioenergy*, vol. 56, pp. 317-22.

Tripathi, M, Sahu, JN & Ganesan, P 2016, 'Effect of process parameters on production of biochar from biomass waste through pyrolysis: A review', *Renewable and Sustainable Energy Reviews*, vol. 55, pp. 467-81.

Tumuluru, JS & Wright, CT 2010, 'A review on biomass densification technologie for energy application'.

Tumuluru, JS, Wright, CT, Hess, JR & Kenney, KL 2011, 'A review of biomass densification systems to develop uniform feedstock commodities for bioenergy application', *Biofuels, Bioproducts and Biorefining*, vol. 5, no. 6, pp. 683-707.

Tursunov, O, Zubek, K, Czerski, G & Dobrowolski, J 2019, 'Studies of CO2 gasification of the Miscanthus giganteus biomass over Ni/Al2O3-SiO2 and Ni/Al2O3-SiO2 with K2O promoter as catalysts', *Journal of thermal analysis and calorimetry*, vol. 139, no. 6, pp. 3481-92.

Udeigwe, TK, Teboh, JM, Eze, PN, Stietiya, MH, Kumar, V, Hendrix, J, Mascagni Jr, HJ, Ying, T & Kandakji, T 2015, 'Implications of leading crop production practices on environmental quality and human health', *Journal of Environmental Management*, vol. 151, pp. 267-79.

Udomsirichakorn, J & Salam, PA 2014, 'Review of hydrogen-enriched gas production from steam gasification of biomass: the prospect of CaO-based chemical looping gasification', *Renewable and Sustainable Energy Reviews*, vol. 30, pp. 565-79.

Ullah, K, Ahmad, M, Sharma, VK, Lu, P, Harvey, A, Zafar, M & Sultana, S 2015, 'Assessing the potential of algal biomass opportunities for bioenergy industry: a review', *Fuel*, vol. 143, pp. 414-23.

Urbanovici, E, Popescu, C & Segal, E 1999, 'Improved iterative version of the Coats-Redfern method to evaluate non-isothermal kinetic parameters', *Journal of thermal analysis and calorimetry*, vol. 58, no. 3, pp. 683-700.

Uslu, A, Faaij, AP & Bergman, PC 2008, 'Pre-treatment technologies, and their effect on international bioenergy supply chain logistics. Techno-economic evaluation of torrefaction, fast pyrolysis and pelletisation', *Energy*, vol. 33, no. 8, pp. 1206-23.

Vaezi, M, Passandideh-Fard, M, Moghiman, M & Charmchi, M 2012, 'On a methodology for selecting biomass materials for gasification purposes', *Fuel processing technology*, vol. 98, pp. 74-81.

Valdés, CF, Marrugo, G, Chejne, F, Cogollo, K & Vallejos, D 2018, 'Pelletization of agroindustrial biomasses from the tropics as an energy resource: implications of pellet quality', *Energy & Fuels*, vol. 32, no. 11, pp. 11489-501.

Valdés, JP, Becerra, D, Rozo, D, Cediel, A, Torres, F, Asuaje, M & Ratkovich, N 2020, 'Comparative analysis of an electrical submersible pump's performance handling viscous Newtonian and non-Newtonian fluids through experimental and CFD approaches', *Journal of Petroleum Science and Engineering*, vol. 187, p. 106749.

Valente, G 2021, 'Taking up statistical thermodynamics: Equilibrium fluctuations and irreversibility', *Studies in History and Philosophy of Science Part A*, vol. 85, pp. 176-84.

Valero, A & Uson, S 2006, 'Oxy-co-gasification of coal and biomass in an integrated gasification combined cycle (IGCC) power plant', *Energy*, vol. 31, no. 10-11, pp. 1643-55.

Vamvuka, D & Sfakiotakis, S 2011, 'Effects of heating rate and water leaching of perennial energy crops on pyrolysis characteristics and kinetics', *Renewable Energy*, vol. 36, no. 9, pp. 2433-9.

Van der Drift, A, Van Doorn, J & Vermeulen, J 2001, 'Ten residual biomass fuels for circulating fluidized-bed gasification', *Biomass and bioenergy*, vol. 20, no. 1, pp. 45-56.

Van der Drift, A, Boerrigter, H, Coda, B, Cieplik, M & Hemmes, K 2004, 'Entrained flow gasification of biomass. Ash behaviour, feeding issues, system analyses'.

Várhegyi, G, Chen, H & Godoy, S 2009, 'Thermal decomposition of wheat, oat, barley, and Brassica carinata straws. A kinetic study', *Energy & Fuels*, vol. 23, no. 2, pp. 646-52.

Varma, AK & Mondal, P 2016, 'Physicochemical characterization and pyrolysis kinetic study of sugarcane bagasse using thermogravimetric analysis', *Journal of Energy Resources Technology*, vol. 138, no. 5.

Varma, AK, Lal, N, Rathore, AK, Katiyar, R, Thakur, LS, Shankar, R & Mondal, P 2021, 'Thermal, kinetic and thermodynamic study for co-pyrolysis of pine needles and styrofoam using thermogravimetric analysis', *Energy*, vol. 218, p. 119404.

Vassilev, SV & Vassileva, CG 2019, 'Water-soluble fractions of biomass and biomass ash and their significance for biofuel application', *Energy & Fuels*, vol. 33, no. 4, pp. 2763-77.

Vassilev, SV, Baxter, D, Andersen, LK & Vassileva, CG 2010, 'An overview of the chemical composition of biomass', *Fuel*, vol. 89, no. 5, pp. 913-33.

Vhathvarothai, N, Ness, J & Yu, QJ 2014, 'An investigation of thermal behaviour of biomass and coal during copyrolysis using thermogravimetric analysis', *International Journal of Energy Research*, vol. 38, no. 9, pp. 1145-54.

Vhathvarothai, N, Ness, J & Yu, J 2014, 'An investigation of thermal behaviour of biomass and coal during co-combustion using thermogravimetric analysis (TGA)', *International Journal of Energy Research*, vol. 38, no. 6, pp. 804-12.

Vidian, F, Dwi Sampurno, R & ail, I 2018, 'Cfd Simulation of Sawdust Gasification on Open Top Throatless Downdraft Gasifier', *Journal of Mechanical Engineering Research & Developments*, vol. 41, no. 2, pp. 106-10.

Vithanage, M, Herath, I, Joseph, S, Bundschuh, J, Bolan, N, Ok, YS, Kirkham, MB & Rinklebe, J 2017, 'Interaction of arsenic with biochar in soil and water: A critical review', *Carbon*, vol. 113, pp. 219-30.

Vuppaladadiyam, AK, Antunes, E, Sanchez, PB, Duan, H & Zhao, M 2021, 'Influence of microalgae on synergism during co-pyrolysis with organic waste biomass: A thermogravimetric and kinetic analysis', *Renewable Energy*, vol. 167, pp. 42-55.

Vuthaluru, H 2004, 'Thermal behaviour of coal/biomass blends during co-pyrolysis', *Fuel processing technology*, vol. 85, no. 2-3, pp. 141-55.

Vyazovkin, S 2000, 'Computational aspects of kinetic analysis.: Part C. The ICTAC Kinetics Project—the light at the end of the tunnel?', *Thermochimica Acta*, vol. 355, no. 1-2, pp. 155-63.

Vyazovkin, S 2006, 'Model-freeKinetics', *Journal of thermal analysis and calorimetry*, vol. 83, no. 1, pp. 45-51.

Vyazovkin, S, Burnham, AK, Criado, JM, Pérez-Maqueda, LA, Popescu, C & Sbirrazzuoli, N 2011, 'ICTAC Kinetics Committee recommendations for performing kinetic computations on thermal analysis data', *Thermochimica Acta*, vol. 520, no. 1-2, pp. 1-19.

Vyazovkin, S, Burnham, AK, Favergeon, L, Koga, N, Moukhina, E, Pérez-Maqueda, LA & Sbirrazzuoli, N 2020, 'ICTAC Kinetics Committee recommendations for analysis of multi-step kinetics', *Thermochimica Acta*, vol. 689.

Wahab, A, Sattar, H, Ashraf, A, Hussain, SN, Saleem, M & Munir, S 2020, 'Thermochemical, kinetic and ash characteristics behaviour of Thar Lignite, agricultural residues and synthetic polymer waste (EVA)', *Fuel*, vol. 266.

Walsh, M & Newman, P 2007, 'Burning narrow windrows for weed seed destruction', *Field Crops Research*, vol. 104, no. 1-3, pp. 24-30.

Wang, B, Liu, L, O'Leary, GJ, Asseng, S, Macadam, I, Lines-Kelly, R, Yang, X, Clark, A, Crean, J, Sides, T, Xing, H, Mi, C & Yu, Q 2018, 'Australian wheat production expected to decrease by the late 21st century', *Glob Chang Biol*, vol. 24, no. 6, pp. 2403-15.

Wang, C, Wang, F, Yang, Q & Liang, R 2009, 'Thermogravimetric studies of the behavior of wheat straw with added coal during combustion', *Biomass and bioenergy*, vol. 33, no. 1, pp. 50-6.

Wang, C, Wang, X, Jiang, X, Li, F, Lei, Y & Lin, Q 2019, 'The thermal behavior and kinetics of co-combustion between sewage sludge and wheat straw', *Fuel processing technology*, vol. 189, pp. 1-14.

Wang, L, Skreiberg, Ø, Becidan, M & Li, H 2016, 'Investigation of rye straw ash sintering characteristics and the effect of additives', *Applied energy*, vol. 162, pp. 1195-204.

Wang, L, Qin, T, Liu, T, Guo, L, Li, C & Zhai, Z 2020, 'Inclusion of microbial inoculants with straw mulch enhances grain yields from rice fields in central China', *Food and Energy Security*, vol. 9, no. 4, p. e230.

Wang, S, Dai, G, Yang, H & Luo, Z 2017, 'Lignocellulosic biomass pyrolysis mechanism: a state-of-the-art review', *Progress in energy and combustion science*, vol. 62, pp. 33-86.

Wang, S, Uzoejinwa, BB, Abomohra, AE-F, Wang, Q, He, Z, Feng, Y, Zhang, B & Hui, C-W 2018, 'Characterization and pyrolysis behavior of the green microalga Micractinium conductrix grown in lab-scale tubular photobioreactor using Py-GC/MS and TGA/MS', *Journal of Analytical and Applied Pyrolysis*, vol. 135, pp. 340-9.

Wang, T, Fu, T, Chen, K, Cheng, R, Chen, S, Liu, J, Mei, M, Li, J & Xue, Y 2020, 'Co-combustion behavior of dyeing sludge and rice husk by using TG-MS: Thermal conversion, gas evolution, and kinetic analyses', *Bioresource technology*, vol. 311, p. 123527.

Wang, X, Deng, S, Tan, H, Adeosun, A, Vujanović, M, Yang, F & Duić, N 2016, 'Synergetic effect of sewage sludge and biomass co-pyrolysis: a combined study in thermogravimetric analyzer and a fixed bed reactor', *Energy Conversion and Management*, vol. 118, pp. 399-405.

Wang, X, Hu, M, Hu, W, Chen, Z, Liu, S, Hu, Z & Xiao, B 2016, 'Thermogravimetric kinetic study of agricultural residue biomass pyrolysis based on combined kinetics', *Bioresource technology*, vol. 219, pp. 510-20.

Wang, Y & Yan, L 2008, 'CFD studies on biomass thermochemical conversion', *Int J Mol Sci*, vol. 9, no. 6, pp. 1108-30.

Wang, Y, Hu, Y, Zhao, X, Wang, S & Xing, G 2013, 'Comparisons of Biochar Properties from Wood Material and Crop Residues at Different Temperatures and Residence Times', *Energy & Fuels*, vol. 27, no. 10, pp. 5890-9.

Warnecke, R 2000, 'Gasification of biomass: comparison of fixed bed and fluidized bed gasifier', *Biomass and bioenergy*, vol. 18, no. 6, pp. 489-97.

Watson, J, Zhang, Y, Si, B, Chen, W-T & de Souza, R 2018, 'Gasification of biowaste: A critical review and outlooks', *Renewable and Sustainable Energy Reviews*, vol. 83, pp. 1-17.

Wei, H, Liu, W, Chen, X, Yang, Q, Li, J & Chen, H 2019, 'Renewable bio-jet fuel production for aviation: A review', *Fuel*, vol. 254.

Wei, J, Gong, Y, Guo, Q, Ding, L, Wang, F & Yu, G 2017, 'Physicochemical evolution during rice straw and coal co-pyrolysis and its effect on co-gasification reactivity', *Bioresource technology*, vol. 227, pp. 345-52.

Weidenkaff, A, Reller, A, Wokaun, A & Steinfeld, A 2000, 'Thermogravimetric analysis of the ZnO/Zn water splitting cycle', *Thermochimica Acta*, vol. 359, no. 1, pp. 69-75.

Weiser, C, Zeller, V, Reinicke, F, Wagner, B, Majer, S, Vetter, A & Thraen, D 2014, 'Integrated assessment of sustainable cereal straw potential and different straw-based energy applications in Germany', *Applied energy*, vol. 114, pp. 749-62.

White, JE, Catallo, WJ & Legendre, BL 2011, 'Biomass pyrolysis kinetics: a comparative critical review with relevant agricultural residue case studies', *Journal of Analytical and Applied Pyrolysis*, vol. 91, no. 1, pp. 1-33.

Widjaya, ER, Chen, G, Bowtell, L & Hills, C 2018, 'Gasification of non-woody biomass: A literature review', *Renewable and Sustainable Energy Reviews*, vol. 89, pp. 184-93.

Wilk, V, Kitzler, H, Koppatz, S, Pfeifer, C & Hofbauer, H 2011, 'Gasification of waste wood and bark in a dual fluidized bed steam gasifier', *Biomass conversion and biorefinery*, vol. 1, no. 2, pp. 91-7.

Winarno, OT, Alwendra, Y & Mujiyanto, S 2016, 'Policies and strategies for renewable energy development in Indonesia', *2016 IEEE International Conference on Renewable Energy Research and Applications (ICRERA)*, IEEE, pp. 270-2.

Wong, F & Gunawardena, J 2020, 'Gene regulation in and out of equilibrium', *Annual review of biophysics*, pp. 199-226.

Woolf, D, Amonette, JE, Street-Perrott, FA, Lehmann, J & Joseph, S 2010, 'Sustainable biochar to mitigate global climate change', *Nat Commun*, vol. 1, p. 56.

Wu, C-C, Völker, D, Weisbrich, S & Neitzel, F 2022, 'The finite volume method in the context of the finite element method', *Materials Today: Proceedings*.

Wu, X, Gong, Y, Guo, Q, Xue, Z & Yu, G 2019, 'Experimental study on the atomization and particle evolution characteristics in an impinging entrained-flow gasifier', *Chemical Engineering Science*, vol. 207, pp. 542-55.

Wu, Y, Zhang, Q, Yang, W & Blasiak, W 2013, 'Two-Dimensional Computational Fluid Dynamics Simulation of Biomass Gasification in a Downdraft Fixed-Bed Gasifier with Highly Preheated Air and Steam', *Energy & Fuels*, vol. 27, no. 6, pp. 3274-82.

Xiao, R, Yang, W, Cong, X, Dong, K, Xu, J, Wang, D & Yang, X 2020, 'Thermogravimetric analysis and reaction kinetics of lignocellulosic biomass pyrolysis', *Energy*, vol. 201.

Xie, J, Zhong, W, Jin, B, Shao, Y & Liu, H 2012, 'Simulation on gasification of forestry residues in fluidized beds by Eulerian–Lagrangian approach', *Bioresource technology*, vol. 121, pp. 36-46.

Xie, T, Wei, R, Wang, Z & Wang, J 2020, 'Comparative analysis of thermal oxidative decomposition and fire characteristics for different straw powders via thermogravimetry and cone calorimetry', *Process Safety and Environmental Protection*, vol. 134, pp. 121-30.

Xing, X, Fan, F & Jiang, W 2018, 'Characteristics of biochar pellets from corn straw under different pyrolysis temperatures', *Royal Society open science*, vol. 5, no. 8, p. 172346.

Xinjie, L, Singh, S, Yang, H, Wu, C & Zhang, S 2021, 'A thermogravimetric assessment of the tri-combustion process for coal, biomass and polyethylene', *Fuel*, vol. 287, p. 119355.

Xiong, Q, Zhang, J, Xu, F, Wiggins, G & Daw, CS 2016, 'Coupling DAEM and CFD for simulating biomass fast pyrolysis in fluidized beds', *Journal of Analytical and Applied Pyrolysis*, vol. 117, pp. 176-81.

Xu, F, Ming, X, Jia, R, Zhao, M, Wang, B, Qiao, Y & Tian, Y 2020, 'Effects of operating parameters on products yield and volatiles composition during fast pyrolysis of food waste in the presence of hydrogen', *Fuel processing technology*, vol. 210, p. 106558.

Xu, G, Lv, Y, Sun, J, Shao, H & Wei, L 2012, 'Recent Advances in Biochar Applications in Agricultural Soils: Benefits and Environmental Implications', *CLEAN - Soil, Air, Water*, vol. 40, no. 10, pp. 1093-8.

Xu, Q 2013, 'Investigation of co-gasification characteristics of biomass and coal in fluidized bed gasifiers'.

Xu, Q, Pang, S & Levi, T 2011, 'Reaction kinetics and producer gas compositions of steam gasification of coal and biomass blend chars, part 1: Experimental investigation', *Chemical Engineering Science*, vol. 66, no. 10, pp. 2141-8.

Xu, Q, Tang, S, Wang, J & Ko, JH 2018, 'Pyrolysis kinetics of sewage sludge and its biochar characteristics', *Process Safety and Environmental Protection*, vol. 115, pp. 49-56.

Xu, Y & Chen, B 2013, 'Investigation of thermodynamic parameters in the pyrolysis conversion of biomass and manure to biochars using thermogravimetric analysis', *Bioresource technology*, vol. 146, pp. 485-93.

Xue, Z, Zhong, Z & Zhang, B 2019, 'Experimental studies on co-combustion of sludge and wheat straw', *Catalysts*, vol. 9, no. 2, p. 182.

Yacout, D, Yadav, P, Athanassiadis, D, Tysklind, M & Upadhyayula, VKK 2020, 'An evaluation of different climate matrices used in biomass energy research', in *Current Developments in Biotechnology and Bioengineering*, Elsevier, pp. 179-204.

Yan, F, Zhang, L, Hu, Z, Cheng, G, Jiang, C, Zhang, Y, Xu, T, He, P, Luo, S & Xiao, B 2010, 'Hydrogen-rich gas production by steam gasification of char derived from cyanobacterial blooms (CDCB) in a fixed-bed reactor: Influence of particle size and residence time on gas yield and syngas composition', *International Journal of Hydrogen Energy*, vol. 35, no. 19, pp. 10212-7.

Yandapalli, V & Mani, S 2014, 'Effect of lime pretreatment on granulation of switchgrass', *BioEnergy Research*, vol. 7, pp. 833-44.

Yang, F, Hanna, MA & Sun, R 2012, 'Value-added uses for crude glycerol--a byproduct of biodiesel production', *Biotechnology for biofuels*, vol. 5, no. 1, pp. 1-10.

Yang, Q, Cheng, K, Wang, Y & Ahmad, M 2019, 'Improvement of semi-resolved CFD-DEM model for seepage-induced fine-particle migration: Eliminate limitation on mesh refinement', *Computers and Geotechnics*, vol. 110, pp. 1-18.

Yang, S, Zhou, T, Wei, Y, Hu, J & Wang, H 2020, 'Dynamical and thermal property of rising bubbles in the bubbling fluidized biomass gasifier with wide particle size distribution', *Applied energy*, vol. 259, p. 114178.

Yang, W, Pudasainee, D, Gupta, R, Li, W, Wang, B & Sun, L 2021, 'An overview of inorganic particulate matter emission from coal/biomass/MSW combustion: Sampling and measurement, formation, distribution, inorganic composition and influencing factors', *Fuel processing technology*, vol. 213, p. 106657.

Yang, X, Liu, X, Li, R, Liu, C, Qing, T, Yue, X & Zhang, S 2018, 'Co-gasification of thermally pretreated wheat straw with Shengli lignite for hydrogen production', *Renewable Energy*, vol. 117, pp. 501-8.

Yang, Y, Liu, J & Wang, Z 2020, 'Reaction mechanisms and chemical kinetics of mercury transformation during coal combustion', *Progress in energy and combustion science*, vol. 79, p. 100844.

Yang, Y, Wang, J, Chong, K & Bridgwater, AV 2018, 'A techno-economic analysis of energy recovery from organic fraction of municipal solid waste (MSW) by an integrated intermediate pyrolysis and combined heat and power (CHP) plant', *Energy Conversion and Management*, vol. 174, pp. 406-16.

Yao, Z & Ma, X 2018, 'Characteristics of co-hydrothermal carbonization on polyvinyl chloride wastes with bamboo', *Bioresource technology*, vol. 247, pp. 302-9.

Yeo, JY, Chin, BLF, Tan, JK & Loh, YS 2019, 'Comparative studies on the pyrolysis of cellulose, hemicellulose, and lignin based on combined kinetics', *Journal of the Energy Institute*, vol. 92, no. 1, pp. 27-37.

Yepes Maya, DM, Silva Lora, EE, Andrade, RV, Ratner, A & Martínez Angel, JD 2021, 'Biomass gasification using mixtures of air, saturated steam, and oxygen in a two-stage downdraft gasifier. Assessment using a CFD modeling approach', *Renewable Energy*, vol. 177, pp. 1014-30.

Yi, J, Li, X, He, J & Duan, X 2020, 'Drying efficiency and product quality of biomass drying: a review', *Drying Technology*, vol. 38, no. 15, pp. 2039-54.

Yi, Q, Qi, F, Cheng, G, Zhang, Y, Xiao, B, Hu, Z, Liu, S, Cai, H & Xu, S 2013, 'Thermogravimetric analysis of co-combustion of biomass and biochar', *Journal of thermal analysis and calorimetry*, vol. 112, no. 3, pp. 1475-9.

Yılmaz, H, Çanakcı, M, Topakcı, M & Karayel, D 2021, 'The effect of raw material moisture and particle size on agri-pellet production parameters and physical properties: A case study for greenhouse melon residues', *Biomass and bioenergy*, vol. 150.

Yin, R, Liu, R, Mei, Y, Fei, W & Sun, X 2013, 'Characterization of bio-oil and bio-char obtained from sweet sorghum bagasse fast pyrolysis with fractional condensers', *Fuel*, vol. 112, pp. 96-104.

Yogalakshmi, K, Sivashanmugam, P, Kavitha, S, Kannah, Y, Varjani, S, AdishKumar, S & Kumar, G 2022, 'Lignocellulosic biomass-based pyrolysis: A comprehensive review', *Chemosphere*, vol. 286, p. 131824.

Yoshida, T, Kuroda, K, Kamikawa, D, Kubojima, Y, Nomura, T, Watada, H, Sano, T & Ohara, S 2021, 'Water Resistance of Torrefied Wood Pellets Prepared by Different Methods', *Energies*, vol. 14, no. 6.

Younis, M, Alnouri, SY, Abu Tarboush, BJ & Ahmad, MN 2018, 'Renewable biofuel production from biomass: A review for biomass pelletization, characterization, and thermal conversion techniques', *International Journal of Green Energy*, vol. 15, no. 13, pp. 837-63.

Yuan, Y, Zuo, H, Wang, J, Gao, Y, Xue, Q & Wang, J 2022, 'Co-combustion behavior, kinetic and ash melting characteristics analysis of clean coal and biomass pellet', *Fuel*, vol. 324, p. 124727.

Yuansheng, J, He, Y & Shenghua, L 2007, 'Mechanochemical additive-assisted reconditioning effects and mechanism on worn ferrous surfaces', *Journal of ASTM International*, vol. 4, no. 10, pp. 1-13.

Yucel, O & Hastaoglu, MA 2016, 'Kinetic modeling and simulation of throated downdraft gasifier', *Fuel processing technology*, vol. 144, pp. 145-54.

Yue, Y, Singh, H, Singh, B & Mani, S 2017, 'Torrefaction of sorghum biomass to improve fuel properties', *Bioresource technology*, vol. 232, pp. 372-9.

Yuldashev, F, Illukpitiya, P, Tegegne, F & Ekanem, E 2020, 'Techno-economic analysis of plantation biomass production and small-scale wood pellet processing for bioenergy market', *International Wood Products Journal*, vol. 11, no. 4, pp. 173-88.

Yun, H, Wang, H, Clift, R & Bi, X 2022, 'The role of torrefied wood pellets in the bio-economy: A case study from Western Canada', *Biomass and bioenergy*, vol. 163, p. 106523.

Yusuf, AA, Inambao, FL, Hassan, AS, Nura, SS & Karthickeyan, V 2020, 'Comparative study on pyrolysis and combustion behavior of untreated Matooke biomass wastes in East Africa via TGA, SEM, and EDXS', *International Journal of Energy and Environmental Engineering*, vol. 11, no. 2, pp. 265-73.

Yuzbasi, NS & Selçuk, N 2011, 'Air and oxy-fuel combustion characteristics of biomass/lignite blends in TGA-FTIR', *Fuel processing technology*, vol. 92, no. 5, pp. 1101-8.

Zafari, A & Kianmehr, MH 2014, 'Factors affecting mechanical properties of biomass pellet from compost', *Environ Technol*, vol. 35, no. 1-4, pp. 478-86.

Zainal, ZA, Ali, R, Lean, CH & Seetharamu, KN 2001, 'Prediction of performance of a downdraft gasifier using equilibrium modeling for different biomass materials', *Energy Conversion and Management*, vol. 42, no. 12, pp. 1499-515.

Zainal, ZA, Rifau, A, Quadir, GA & Seetharamu, KN 2002, 'Experimental investigation of a downdraft biomass gasifier', *Biomass and bioenergy*, vol. 23, no. 4, pp. 283-9.

Zaini, IN, Nurdiawati, A & Aziz, M 2017, 'Cogeneration of power and H2 by steam gasification and syngas chemical looping of macroalgae', *Applied Energy*, vol. 207, pp. 134-45.

Zanetti, M, Brandelet, B, Marini, D, Sgarbossa, A, Giorio, C, Badocco, D, Tapparo, A, Grigolato, S, Rogaume, C & Rogaume, Y 2017, 'Vineyard pruning residues pellets for use in domestic appliances: a quality assessment according to the EN ISO 17225', *Journal of Agricultural Engineering*, vol. 48, no. 2, pp. 99-108.

Zawawi, MH, Saleha, A, Salwa, A, Hassan, N, Zahari, NM, Ramli, MZ & Muda, ZC 2018, 'A review: Fundamentals of computational fluid dynamics (CFD)', *AIP conference proceedings*, AIP Publishing LLC, p. 020252.

Zeng, K, Gauthier, D, Soria, J, Mazza, G & Flamant, G 2017, 'Solar pyrolysis of carbonaceous feedstocks: A review', *Solar energy*, vol. 156, pp. 73-92.

Zeng, X, Ma, Y & Ma, L 2007, 'Utilization of straw in biomass energy in China', *Renewable and Sustainable Energy Reviews*, vol. 11, no. 5, pp. 976-87.

Zhai, M, Guo, L, Zhang, Y, Dong, P, Qi, G & Huang, Y 2016, 'Kinetic parameters of biomass pyrolysis by TGA', *BioResources*, vol. 11, no. 4, pp. 8548-57.

Zhang, B & Lu, GW 2013, 'Experimental study on combustion characteristics of biomass and coal blended', *Advanced Materials Research*, Trans Tech Publ, pp. 200-7.

Zhang, B, Zhang, J, Zhong, Z, Wang, W & Zhu, M 2019, 'Syngas production and trace element emissions from microwave-assisted chemical looping gasification of heavy metal hyperaccumulators', *Science of the Total Environment*, vol. 659, pp. 612-20.

Zhang, D, Cao, C-Y, Lu, S, Cheng, Y & Zhang, H-P 2019, 'Experimental insight into catalytic mechanism of transition metal oxide nanoparticles on combustion of 5-Amino-1H-Tetrazole energetic propellant by multi kinetics methods and TG-FTIR-MS analysis', *Fuel*, vol. 245, pp. 78-88.

Zhang, J, Li, T, Ström, H & Løvås, T 2020, 'Grid-independent Eulerian-Lagrangian approaches for simulations of solid fuel particle combustion', *Chemical Engineering Journal*, vol. 387, p. 123964.

Zhang, L, Xu, CC & Champagne, P 2010, 'Overview of recent advances in thermo-chemical conversion of biomass', *Energy Conversion and Management*, vol. 51, no. 5, pp. 969-82.

Zhang, Q, Zhou, D, Zhou, P & Ding, H 2013, 'Cost analysis of straw-based power generation in Jiangsu Province, China', *Applied energy*, vol. 102, pp. 785-93.

Zhang, Q, Dor, L, Zhang, L, Yang, W & Blasiak, W 2012, 'Performance analysis of municipal solid waste gasification with steam in a Plasma Gasification Melting reactor', *Applied energy*, vol. 98, pp. 219-29.

Zhang, R-J, Xia, G-F, Li, M-F, Yu, W, Hong, N & Li, D-D 2015, 'Effect of support on the performance of Ni-based catalyst in methane dry reforming', *Journal of Fuel Chemistry and Technology*, vol. 43, no. 11, pp. 1359-65.

Zhang, X & Ma, F 2015, 'Emergy Evaluation of Different Straw Reuse Technologies in Northeast China', *Sustainability*, vol. 7, no. 9, pp. 11360-77.

Zhang, X, Xu, M, Sun, R & Sun, L 2005, 'Study on biomass pyrolysis kinetics', *Turbo Expo: Power for Land, Sea, and Air*, pp. 401-5.

Zhang, X, Li, H, Liu, L, Bai, C, Wang, S, Zeng, J, Liu, X, Li, N & Zhang, G 2018, 'Thermodynamic and economic analysis of biomass partial gasification process', *Applied Thermal Engineering*, vol. 129, pp. 410-20.

Zhang, Y, Chen, F, Chen, D, Cen, K, Zhang, J & Cao, X 2020, 'Upgrading of biomass pellets by torrefaction and its influence on the hydrophobicity, mechanical property, and fuel quality', *Biomass conversion and biorefinery*, pp. 1-10.

Zhang, Y, Cui, Y, Chen, P, Liu, S, Zhou, N, Ding, K, Fan, L, Peng, P, Min, M & Cheng, Y 2019, 'Gasification technologies and their energy potentials', in *Sustainable resource recovery and zero waste approaches*, Elsevier, pp. 193-206.

Zhao, B, O'Connor, D, Zhang, J, Peng, T, Shen, Z, Tsang, DC & Hou, D 2018, 'Effect of pyrolysis temperature, heating rate, and residence time on rapeseed stem derived biochar', *Journal of Cleaner Production*, vol. 174, pp. 977-87.

Zhao, J, Deng, J, Wang, T, Song, J, Zhang, Y, Shu, C-M & Zeng, Q 2019, 'Assessing the effectiveness of a high-temperature-programmed experimental system for simulating the spontaneous combustion properties of bituminous coal through thermokinetic analysis of four oxidation stages', *Energy*, vol. 169, pp. 587-96.

Zhao, S-X, Ta, N & Wang, X-D 2017, 'Effect of temperature on the structural and physicochemical properties of biochar with apple tree branches as feedstock material', *Energies*, vol. 10, no. 9, p. 1293.

Zhaosheng, Y, Xiaoqian, M & Ao, L 2009, 'Thermogravimetric analysis of rice and wheat straw catalytic combustion in air-and oxygen-enriched atmospheres', *Energy Conversion and Management*, vol. 50, no. 3, pp. 561-6.

Zheng, S, Hu, Y, Wang, Z & Cheng, X 2020, 'Experimental investigation on ignition and burnout characteristics of semi-coke and bituminous coal blends', *Journal of the Energy Institute*, vol. 93, no. 4, pp. 1373-81.

Zhou, H, Jensen, A, Glarborg, P, Jensen, P & Kavaliauskas, A 2005, 'Numerical modeling of straw combustion in a fixed bed', *Fuel*, vol. 84, no. 4, pp. 389-403.

Zhou, L, Wang, Y, Huang, Q & Cai, J 2006, 'Thermogravimetric characteristics and kinetic of plastic and biomass blends co-pyrolysis', *Fuel processing technology*, vol. 87, no. 11, pp. 963-9.

Zhu, M, Chen, X, Zhou, C-s, Xu, J-s & Musa, O 2020, 'Numerical study of micron-scale aluminum particle combustion in an afterburner using two-way coupling CFD–DEM approach', *Flow, Turbulence and Combustion*, vol. 105, no. 1, pp. 191-212.

Zhu, S, Wu, Y, Yu, Z, Chen, Q, Wu, G, Yu, F, Wang, C & Jin, S 2006, 'Microwave-assisted alkali pre-treatment of wheat straw and its enzymatic hydrolysis', *Biosystems Engineering*, vol. 94, no. 3, pp. 437-42.

Zulkifli, AA, Mohd Yusoff, MZ, Abd Manaf, L, Zakaria, MR, Roslan, AM, Ariffin, H, Shirai, Y & Hassan, MA 2019, 'Assessment of municipal solid waste generation in Universiti Putra Malaysia and its potential for green energy production', *Sustainability*, vol. 11, no. 14, p. 3909.

APPENDIX A: KEY LITERATURE RELATED TO THIS WORK

Table A1: Additives used in pellet making from biomass

Types	Binders	Results	References
Structural	Sawdust	• Enhanced the quality of fuel pellets • Abundantly available and much cheaper than other binders such as lignin and starch	(Serrano et al. 2011; Peng et al. 2015; Brand et al. 2021)
	Lignosulfonates	• A by-product in cellulose production from pulp and paper industries • Improves process stability and decreases specific energy consumption during pelletization	(Mediavilla, Esteban & Fernández 2012)
Lubricant	Oil cake	• Co-pelletization of torrefied biomass and oil cake reduces energy consumption and improves pellet density and strength • Higher calorific value	(Nilsson, Bernesson & Hansson 2011; Cao et al. 2015)
	Phytase, protease, and xylanase enzymes	• Reduce the flow resistance in the die	(Miladinovic et al. 2021)
Energy	Biochar	• Synergistic effect and increase the heat	(Elita 2018)
	Glycerol	• Increase pellet heating value	(Lu et al. 2014)
	Sludge	• Sludge-mixed pellets reduce energy input, increase pellet quality, and improve combustion characteristics compared with pure	(Jiang, L. et al. 2016)
Binding	Bentonite clay	• Bentonite is a clay mineral, an aluminum silicate composed of montmorillonite • It has unique ion exchange property responsible for binding action bentonite is attractive because of its low price and good binding performance in small quantities	(Lu et al. 2014)
	Cassava stem powder	• Cassava stem is starch-rich (as high as 30%), cheap, and underutilized byproducts from food production.	(Larsson et al. 2015)
	Starch	• It acts as a glue that improves particle binding during pelletization • Potato peel residues (starch) as a binding agent improve the pellet durability • Maize starch as an additive improves the pellet quality during pelletization	(Kuokkanen et al. 2011; Pradhan, Arora & Mahajani 2018)
	Carbohydrates	• Molasses is an effective binder due to the presence of various materials such as sucrose, monosaccharides, protein, and minerals • Fructose is very effective due to its high hygroscopic properties resulting	(Soleimani et al. 2017)
Catalyst	NaOH, NaCl, CaO, ZnO, NiO, MgO	• Increase ash melting temperature	(Mohammed et al. 2012; Holubcik et al. 2016)

Table A2: Literature on the biomass pellet

Material	Objectives	Analysis	References
Wheat straw pellet bonded with wood residues, pre-treated wood residues, glycerol, lignosulfonate, and bentonite clay	▪ Investigate the binder effects on pellet quality ▪ Study of specific energy consumption and pellet properties	▪ Binders significantly decrease the specific energy consumption ▪ Additives increase the tensile strength, higher heating value, and reduce the ash content	(Lu et al. 2014)
Barley, canola, oat, and wheat straw	▪ Study the compaction characteristics ▪ Specific energy measured	▪ Mean density increase and specific energy decrease	(Adapa, Tabil & Schoenau 2009)
Wheat straw, barley straw, corn stover, and switchgrass pellet	▪ Mechanical properties determine based on compressive forces, particle sizes, and moisture contents	▪ Compressive strength, particle size, and moisture content significantly affected the pellet density. ▪ Asymptotic modulus has a relation to maximum compressive pressure ▪ The barley pellet is more rigid	(Mani, Tabil & Sokhansanj 2006)
Wheat straw pellet	▪ Effect of pelletisation process and densification parameters on the properties of the wheat straw powder and 40% epoxy 1092 mixture	▪ Increase the fixed carbon and heating value, bulk density ▪ Improved combustion characteristic	(El-Sayed & Elsaid Mohamed 2018)
Rice husk pellets Wheat straw pellets	▪ Physicochemical and energetic characterization	▪ Ric husks exhibit lower calorific value and higher ash content ▪ Moisture, ashes, and nitrogen content did not match ISO 17225-6 standard but diameter, length, and durability were compiled	(Ríos-Badrán et al. 2020)
Wheat straw pellet	▪ Identification of the key factors affecting the pelletizing pressure in biomass pelletization processes	▪ Pelletizing pressure increased the pellet length ▪ Increasing the temperature resulted in a decrease in the pelletizing pressure	(StelteClemons, et al. 2011)
Pellets made from sorghum stalk, corn stover, wheat straw, and big bluestem	▪ Physical properties of pellet ▪ Effect of moisture and particle size on bulk density, true density, and durability	▪ Biomass pelleting can significantly improve the bulk density ▪ High Moisture content and particle size decrease the density, durability	(Theerarattananoon et al. 2011)
Wheat straw pellet	▪ Investigation of the effects of molasses on wheat straw pellet physical quality	▪ Temperature is a key factor for good pellet quality ▪ Exceeding the lignin glass transition temperature leads to better pellet quality ▪ Molasses strengthens pellets production at temperatures below the lignin glass transition	(Mišljenović et al. 2016)
Wheat straw pellet	▪ Investigation of biological pretreatment to improve the pellet quality	▪ Temperature and biological pretreatment could improve the physical quality	(Gao et al. 2017)
Pellet from torrefied and raw wheat straw	▪ Thermo kinetic properties study	▪ The bulk density is higher in brown torrefied pellets ▪ Pellet properties satisfy the (ISO 17225-6) standards ▪ Temperature is the potential pretreatment application	(Azocar et al. 2019)
Wheat straw pellet Peat/wood pellet	▪ Study the emissions to air during combustion	▪ Wood pellets burned more efficiently and with lower emissions than straw and peat pellets	(Olsson 2006)

Table A3:Specification of non-woody pellets according to ISO 17225-8: 2016 (E) (ISO/TS, 2016 2016)

Types	Property Class/ analysis method	Units	A	B
Normative	Origin and source[s]		Herbaceous biomass/Fruit biomass/Aquatic biomass: Blends and mixtures	
	Diameter (D)[b] and Length (L)[c]	mm	D06 to D25, D±1: 3.15<L ≤ 40 (from D06 to D10) D±1: 3.15<L ≤50 (from D12 to D25)	
	Moisture, M	w % as the received, wet basis	M10 ≤10	M10 ≤ 10
	Ash, A	w % dry	A5.0 ≤5.0	A10.0 ≤10.0
	Mechanical durability, DU	w % as received	DU97.5≥97.5	DU96.5 ≥96.5
	Fines, F[d]	w % as received	F2.0 ≤ 2.0	F2.0 ≤ 2.0
	Additives	w % as received	Type and amount to be stated	Type and amount to be stated
	Net calorific value, Q	MJ/kg or kWh/kg as received	Q18 ≥18 or Q5 ≥ 5	Q17 ≥17 or Q4.7 ≥ 4.7
	Bulk density, BD	Kg/m^3 as received	BD600 ≥ 600	BD600 ≥ 600
	Carbon	w-% dry	Value to be stated	Value to be stated
	Nitrogen, N	w % dry	N1.5 ≤ 1.5	N2.0 ≤ 2.0
	Sulfur, S	w % dry	S0.1 ≤ 0.1	S0.20 ≤ 0.20
	Chlorine, Cl	w % dry	Cl0.1 ≤ 0.10	Cl0.2 ≤ 0.20
	Arsenic, As	mg/kg dry	≤ 2	
	Cadmium, Cd	mg/kg dry	≤ 1	
	Chromium, Cr	mg/kg dry	≤ 50	
	Copper, Cu	mg/kg dry	≤ 20	
	Lead, Pb	mg/kg dry	≤ 10	
	Mercury, Hg	mg/kg dry	≤ 0.1	
	Nickel, Ni	mg/kg dry	≤ 10	
	Zinc, Zn	mg/kg dry	≤ 200	
Informative	Ash melting behavior	°C	Should be stated	

[a] To be stated, the 4-digit classification (*Table 1 ISO 17225-1*). Blends and mixtures can also include woody biomass. If the blend composition is known, the w-% can be used to specify blends

[b] Selected size (e.g. D06, D08, D10, D12 or D25) of pellets to be stated

[c] Amount of pellets longer than 40 mm can be 1% w-% (from D06 to D10). Maximum length shall be ≤45 mm for pellets from D06 to D10

[d] At factory gate in bulk transport (at the time of loading) and in small (up to 20 kg) and large sacks (at the time of packing or when delivering to end-user)

[e] Type of additives to aid production, delivery or combustion (e.g. pressing aids, slagging inhibitors or any other additives like starch, corn flour, potato flour, vegetable oil, lignin)

[f] It is recommended that all characteristic temperatures (shrinkage starting temperature (SST), deformation temperature (DT), hemisphere temperature and flow temperature (FT) in oxidizing conditions should be stated

Table A4: EnPlus standard for pellet quality requirements (ENplus 2015)

Property	Unit	ENplus A1	ENplus A2	ENplus B
Diameter	mm	6–8		
Length	mm	3.15 < L ≤ 40		
Moisture Content	w % a.r	≤10		
Ash Content	w % d.b	≤0.7	≤1.2	≤2.0
Mechanical Durability	w % a.r	≥98.0	≥97.5	
Fines (<3.15 mm)	w % a.r	≤1.0		
Net calorific value	MJ/kg a.r	≥16.5		
Bulk density	Kg/m^3	≥600		
Additives	w % a.r	≤2.0		
Nitrogen	w % d.b	≤0.3	≤0.5	≤1.0
Sulphur	w % d.b	≤0.04	≤0.05	
Chlorine	w % d.b	≤0.02		≤0.03
Ash Deformation Temperature	°C	≥1200	≥1100	

Note: Symbols refer to a.r = as received, d.b = dry basis
   A1: Used in residential, small commercial, public buildings, and industrial energy generation
   A2: quality pellets are used in larger installations (> 50 kW)
   B: quality pellets in large CHP or district heating units

Table A5: TG analysis for biomass

Materials	Technology	Findings	Reference
Sawdust	Combustion (TGA)	Thermal stability and activation energy	(Poletto et al. 2010)
Rice husk	Pyrolysis (TGA)	Thermal stability and thermal degradation process	(Chiang et al. 2009)
Micactinium conductrix	Pyrolysis (TGA-MS)	Mass loss	(Wang, S. et al. 2018)
Napier grass	Combustion and Pyrolysis (TGA)	Thermal characteristics	(Mohammed et al. 2015)
Corn brakes, wheat straw, and hazelnut shell	Pyrolysis (TGA-MS)	Gas product with heating rate	(Manić et al. 2019)
Palm kernel shell, African bush mango wood, and shell	Combustion (TGA)	Oxidation characteristics	(Okoroigwe, Enibe & Onyegegbu 2016)
Biomass and coal	Pyrolysis (TGA)	Product yields	(Vhathvarothai, N., Ness, J. & Yu, J. 2014)
Sugarcane straw	Slow pyrolysis (TGA-FTIR)	Decomposition with heating rate	(Halder et al. 2019)
Corn stover	Combustion and Pyrolysis (TGA)	TGA characteristics	(Kumar et al. 2008)
Rice straw and pine sawdust	Combustion (TGA)	Pyrolysis kinetics characteristics	(Xiao et al. 2020)
Wheat straw and plastic	Combustion and Pyrolysis (TGA)	Pyrolysis yield	(Jin et al. 2019)
Mustard	Pyrolysis (TGA)	Biochar, bio-oil, and hydrocarbon gases	(Jacob et al. 2022)
Corn straw powder, poplar wood chip, and rice husk	Combustion and Pyrolysis (TGA)	Pyrolysis and combustion characteristics	(Liu, L. et al. 2021)
Barley straw, miscanthus, waste wood, wheat straw, willow, and wood pellet	Combustion (TGA)	Thermal and kinetic analysis	(Sher et al. 2020)
Sewage sludge and wheat straw	Pyrolysis (TGA)	Pyrolysis yield	(Wang, Xuebin et al. 2016)
Empty fruit bunch, rice husk, coconut pulp sawdust, coconut shell, and sugar cane bagasse	Pyrolysis (TGA)	Hating value and thermal degradation rate	(Balasundram et al. 2018)
Biomass wastes and digests biomass wastes	Co-pyrolysis (TGA)	Gas yield	(Vuppaladadiyam et al. 2021)
Wheat straw	Pyrolysis (TGA-FTIR)	Gasification rate changes with temperature	(Yang, X. et al. 2018)

Table A6: Different types of gasifier (Lian et al. 2021)

Type		Main characteristics	Photographic view
Fixed bed	Updraft	- Small to medium scale capacity (< 20 MW) - High tar and impurities 700-900 °C gasification temp - Small-chunk of the fuel particle size	
	Downdraft	- Small scale capacity (<5 MW) - Low tar 700-900 °C gasification temp - Small and uniform fuel particle size	
Fluidised bed	Bubbling	- Medium to big scale (10- 100 MW) - Medium tars <900 °C gasification temp - Small to fine fuel particle	
	Circulating	- Medium to big scale (20- 100 MW) - Medium tars 1450 °C gasification temp - Small to fine fuel particle	
Entrained bed		- Big scale (>100 MW) - Very low tar 1450 °C gasification temp - Fuel particles in the form of slurry	

Table A7. Advantages and disadvantages of commonly used gasifier

Type of gasifier		Advantage	Disadvantage	References
Fixed bed	Updraft	▪ High ash content tolerance ▪ High MC feedstock ▪ Less sensitive to feedstock size ▪ Exit gas temperature low ▪ High thermal efficiency	▪ Large quantities of tar ▪ Limited flexibility to load and process ▪ Action required for tar cracking ▪ Needed engine cleanup	*(Alauddin et al. 2010)* *(Pfeifer, Koppatz & Hofbauer 2011)* *(Erakhrumen 2012),* *(Ahmad et al. 2016)* *(Puig-Arnavat, Bruno & Coronas 2010)* *(Ngo et al. 2011)*
	Downdraft	▪ Simple and proven technology ▪ Marginal actor ▪ High carbon conversion ▪ Low tar accumulation ▪ Oldest and capacity 20-200kW ▪ Less gas cleanup needed	▪ Low and nonuniform heat and mass transfer ▪ Lower uses of bed materials as heat transfer medium and catalyst ▪ Lower quality of gas ▪ High concentration of CO_2 and CH_4	
	Counterflow	▪ Higher energy efficiency ▪ High moisture content feedstock quickly dried	▪ Limited feedstock selection ▪ Exit gas leaves with higher temperature	
Fluidized bed/ Rotary type	Bubbling fluidized Bed	▪ Over reactor ▪ Good mixes of solid-gas ▪ Efficient heat, mass transfer and conversion efficiencies	▪ Operation is complicated ▪ High tar and dust content in syngas ▪ Required higher gas flow velocities	*(Wilk et al. 2011)* *(Siedlecki, De Jong & Verkooijen 2011)*
	Circulating fluidized bed	▪ Easy ash removal system ▪ Useable large quantity, less quality feedstock ▪ Easily scale-up	▪ Highly cost involve ▪ Need special materials ▪ Security issue ▪ Technology is complex and difficult to control	
	Twin fluidized bed	▪ Good solid-gas contact and mixing ▪ Large scale capacity (up to 1 MW or above) ▪ In-bed catalytic conversions	▪ Relatively complex design and operation	*(Puig-Arnavat, Bruno & Coronas 2010)*
Modern	Entire flow	▪ Uniform reaction temperature ▪ Higher degree of feedstock flexibility ▪ Higher carbon conversion ▪ Short reactor residence time ▪ Not problem scale-up ▪ Ash removes as slag ▪ Low volume of tar production ▪ Good ability to control the parameter process	▪ High amount of oxidizing agent required ▪ Low cold gas efficiency ▪ Requires size reduction and preparation of feedstock ▪ High capital cost ▪ High level of producing gas ▪ Relatively complex operation ▪ High maintenance cost	*(Ogi et al. 2013)* *(Biagini et al. 2009) (Higman et al. 2008)*
	Plasma	▪ Suitable for all types hazardous and non-hazardous wastes ▪ Suitable for waste product ▪ Very little ash content ▪ Extremely short reaction times	▪ Large initial and operating costs ▪ Frequent maintenance required ▪ Negative net energy production ▪ Non continuous process ▪ Necessary of auxiliary fuel	*(Leal-Quirós 2004; Mountouris, Voutsas & Tassios 2008; Zhang et al. 2012)*
	Chemical looping	▪ Avoiding direct contact between biomass and air ▪ No need for syngas separation ▪ Syngas production with high quality ▪ Considerable catalytic surface for tar cracking	▪ High capital cost	*(Siriwardane et al. 2016; Sarafraz et al. 2017; Zhang, B. et al. 2019)*

Table A8: Typical gasification reactor characteristics (Pieratti 2011; IEA 2018)

Characteristics	Gasification types			
	Moving bed	Stationary fluidised bed	Circulating fluidised bed	Entrained flow
Suitable scale, MW Thermal	Downdraft< 5 Updraft < 20	10-100	20-150	>100
Typical operational pressure	atmospheric	atmospheric < 200 (< 3 MPa)	atmospheric	(1-3 MPa)
Bed material, particle size, mm	none	0.1-0.5	0.1-0.4	None
Particle size fuel, mm	10-100	1-100	1-100	< 1 mm
Operating temperature, °C	Downdraft, 700-1200 Updraft, 700-900	800, bottom, 200-300, top	800-1450	1400-1500
Control	Easy	Moderate	Moderate	Difficult
Feedstock preparation	Critical	Less critical	less critical	Only fine particles
Gas superficial velocity, m/s	0.1-0.5	0.5-1,5	4-8	15-25
Solids mixing	Very low	High, complex	High, complex	Low
Temperature gradients	High	Low	Low	High
Tar content in gas, g/Nm^3	Downdraft < 1 Updraft >>10	> 10	> 10	<<1
Particles in gas, g/Nm^3	0.1-0.2	0.1-1	2-20	1

Table A9: Typical performance indicators for different gasification technologies
(Bridgwater 1995; Mansaray et al. 1999; Van der Drift, Van Doorn & Vermeulen 2001; Puig-Arnavat, Bruno & Coronas 2010)

Performance indicators	Units	Updraft	Downdraft	BFB	CFB
SGP	Nm^3/kg$_{bio}$	-	2–3.3	1.9–2.46	2.50–2.65
CCE	%	93-97	91-91	76–98	86–97
CGE	%	40–60	52.2–65	50–60	46–66
LHV$_{syngas}$	MJ/Nm^3$_{gas}$	5.0–6.0	4.2–6.5	3.3–5.3	3.6–4.0
TAR	g/Nm^3$_{gas}$	20–100	0.1–6.0	1–15	1–15
Particulate matter (PM)	g/Nm^3$_{gas}$	0.1–10	0.1–0.2	2–20	10–35
Syngas with max tar	mg/Nm^3	-	45	-	50
Tar and PM	mg/Nm^3	50~100	10~50	-	-

Note; SGP: Specific gas production, CCE: Carbon conversion efficiency, CGE: Cold gas efficiency, LHV: Low heating value, BFB=Bubbling fluidised bed, CFB= Circulating fluidised bed

Table A10: Types of downdraft gasifiers
(Mendiburu, Carvalho & Coronado 2014)

| a. Imbert (Closed top/throated) | b. Stratified gasifier (Open top/throat less) |
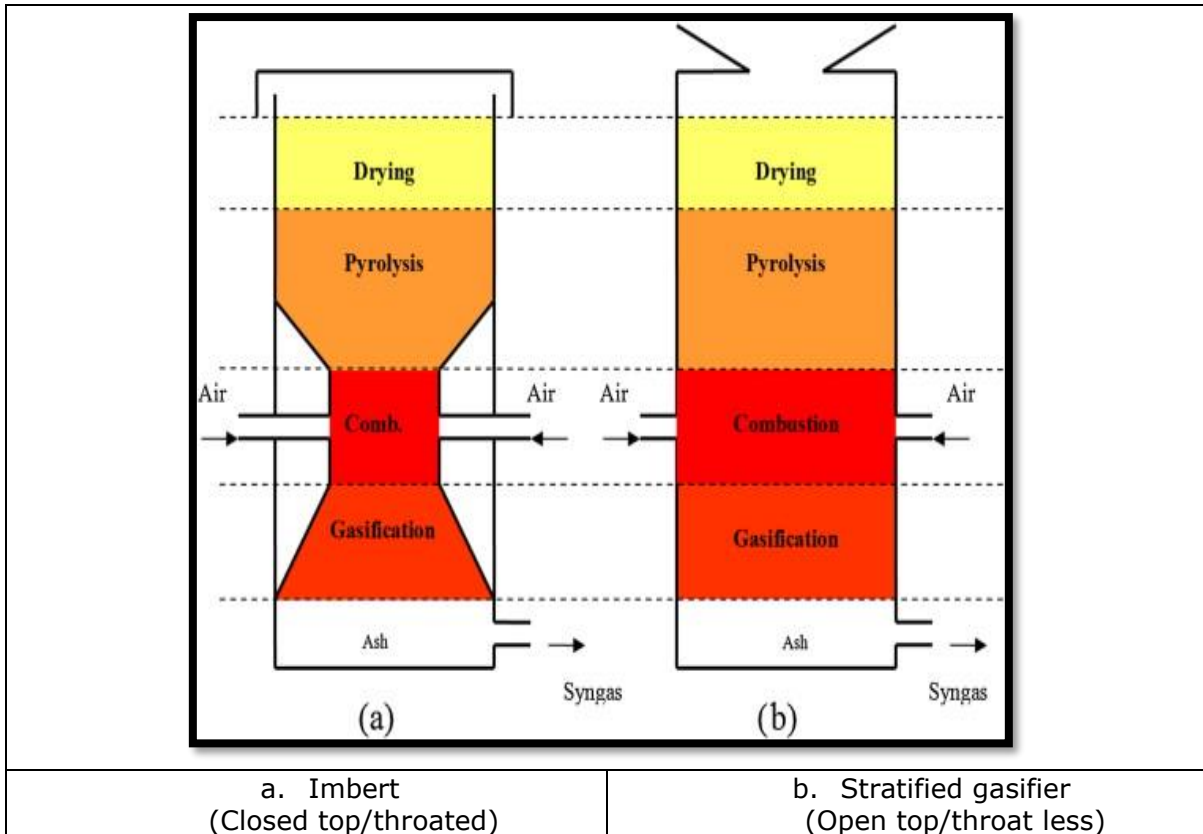
Table A11: Equilibrium models of gasification

Model	Type of gasifier	Objectives of studies	Reference/Authors
Stoichiometric equilibrium	Downdraft	✓ Prediction of syngas composition ✓ Simulation using the effect of initial moisture content and temperatures	(Zainal et al. 2001)
Stoichiometric equilibrium	Downdraft	✓ Incorporated Char Reactivity Factor (CRF) for prediction of temperature and its syngas composition profile	(Babu & Sheth 2006)
Stoichiometric equilibrium	Downdraft	✓ Determine the temperature of gasification at the equilibrium condition ✓ Modification of the model using a coefficient of correction to adjust methane composition	(Jarungthammachote & Dutta 2007)
Gibbs free energy	Downdraft	✓ Determined the best temperature in the reduction zone, which has an impact on the high gas heating value	(Antonopoulos, I. S. et al. 2012)
Stoichiometric Equilibrium	Downdraft	✓ Prediction of syngas composition by including the tar in reactions.	(Barman, Ghosh & De 2012)
Stoichiometric equilibrium	Entrained bed	✓ Study the gas composition of co-gasification petroleum coke and 10% of several biomass using oxygen as an oxidant ✓ Simulation using a variation of AF ratio and steam/fuel ratio for temperatures, efficiency, and syngas compositions prediction	(Valero & Uson 2006)
Gibbs free energy	Universal	✓ Prediction of syngas composition using Bituminous coal proximate & ultimate ✓ Simulation using air, air stream, and solar steam as oxidants	(Shabbar & Janajreh 2013)

Table A12: Kinetic models of gasification

Model	Type of gasifier	Objectives of studies	References
- Volumetric model - 0-dimensional	Stratified downdraft	✓ Prediction of gas composition and axial temperature profile ✓ The simulation described the effect of air to fuel ratio on the reaction rate in the reactor zones	(Di Blasi 2000)
- Exponential Char reactivity Factor - 2-dimensional	Fixed bed downdraft (Reduction zones)	✓ Prediction syngas compositions and temperature profiles at reduction zone both radially and longitudinally	(Masmoudi et al. 2014)
- Shrinking model - One dimensional	Bubbling fluidized bed Two-phase (bubble and emulsion), Two-zone (dense bottom bed and upper freeboard)	✓ Prediction temperatures, solid remained, and gas concentrations along the axis of reactor Simulation using wood pellet using air, oxygen, steam and a mix of oxygen and steam as oxidant	(Kaushal, Abedi & Mahinpey 2010)
- Random pore model	Universal	✓ Prediction of syngas compositions and carbon consumption of the biomass at times of gasification progress for single biomass and coal gasification and mixed biomass and coal co-gasification using steam as oxidant	(Xu, Pang & Levi 2011)

Table A13: CFD models of pyrolysis and gasification

Model	Type of gasifier	Objectives of studies	Reference/Authors
- 2D Axisymmetric - Discrete phase	2 Stage Downdraft	✓ To study the influence of air injection on tar cracking of steam and air as oxidant at the gasification stage ✓ To investigate the detail of the partial oxidation zone, which is crucial for tar cracking	(Gerun et al. 2008)
- 2D planar - Non-premixed combustion - Applied FLUENT software	Downdraft	✓ To investigate the flow pattern, temperature, turbulence, and product gas composition of lignite gasification	(Patel, Shah & Patel 2013)
- 2D Axisymmetric - Discrete phase model - Applied ANSYS FLUENT	Downdraft	✓ To investigate the temperature distribution and evolution of the species inside the reactor in the gasification of a wood particle using air as an oxidant	(Janajreh & Al Shrah 2013)
- 2D planar - Euler-Euler Multiphase - Applied ANSYS FLUENT	Downdraft	✓ To study the gasification process in the downdraft configuration considering drying, pyrolysis, combustion, and gasification reactions of wood pellet	(Wu et al. 2013)
- 2D Axisymmetric - Eulerian multiphase - Applied ANSYS FLUENT	Downdraft	✓ To study the temperature, syngas composition, and flow pattern inside the reactors using wood charcoal as feedstock and air as oxidant	(Contreras-Andrade et al. 2014)
- 2D planar - Euler-Euler Multiphase - Applied MFIX computer code	Updraft	✓ To simulate and evaluate the dynamics of the coal gasification process in an updraft gasifier using air as an oxidant	(Murgia, Vascellari & Cau 2010)
- 3D - Multiphase - Eulerian-Lagrangian	Fluidized bed	✓ To predict the performance of fluidized bed biomass gasification ✓ To simulate the effect of reactor temperature, ER, and steam to biomass (wood chip) ratio on product gas composition and carbon conversion efficiency	(Xie et al. 2012)
- 2D in-house code	Entrained Flow Gasifiers	To reaction kinetics of coal gasification at high pressure, high solids loading and slagging wall	(Bockelie et al. 2002)

APPENDIX B: EXPERIMENTAL RESULTS

Table B1: Pellet dimensional stability analysis

$B_1T_1\_a$: Raw data (before and after storage) for treatment T_1

Observation	Data measured before storage (1 day)				Data measured after storage (14 days storage)				Changed			
	Length, mm	Diameter, mm	Individual Weight, g	Innitial Apparent density, Kg/m³	Length, mm	Diameter, mm	Individual Weight, g	Apparent density, Kg/m³	Length, mm	Diameter, mm	Weight, g	Relax density, Kg/m³
1.	36.01	8.26	1.30	674.05	35.94	8.32	1.27	650.29	0.07	-0.06	0.03	23.75
2.	16.99	8.22	1.16	1287.22	16.92	8.25	1.15	1272.10	0.07	-0.03	0.01	15.12
3.	32.00	8.18	1.67	993.55	32.30	8.13	1.62	966.63	-0.30	0.05	0.05	26.92
4.	21.10	8.25	1.33	1179.75	20.90	8.28	1.23	1093.52	0.20	-0.03	0.10	86.23
5.	17.09	8.32	1.17	1259.88	17.32	8.35	1.13	1192.03	-0.23	-0.03	0.04	67.84
6.	18.06	8.00	1.32	1454.81	18.56	7.98	1.27	1368.83	-0.50	0.02	0.05	85.98
7.	29.00	8.26	1.53	985.06	28.56	8.29	1.51	980.03	0.44	-0.03	0.02	5.03
8.	31.98	8.29	1.77	1025.93	31.89	8.16	1.63	977.87	0.09	0.13	0.14	48.05
9.	24.35	8.34	1.65	1241.03	24.20	8.29	1.49	1141.28	0.15	0.05	0.16	99.75
10.	19.50	8.32	1.23	1160.79	19.04	8.35	1.22	1170.71	0.46	-0.03	0.01	-9.92
11.	22.26	8.26	1.36	1140.73	22.43	8.39	1.34	1081.14	-0.17	-0.13	0.02	59.59
12.	22.70	8.76	1.40	1023.82	22.68	8.75	1.35	990.39	0.02	0.01	0.05	33.43
13.	10.75	8.56	0.98	1584.89	10.63	8.58	0.95	1546.49	0.12	-0.02	0.03	38.41
14.	19.00	8.31	1.29	1252.46	18.89	8.26	1.25	1235.52	0.11	0.05	0.04	16.95
15.	34.70	8.12	1.88	1046.76	34.71	8.07	1.70	958.03	-0.01	0.05	0.18	88.73
16.	14.40	8.08	1.20	1626.02	14.43	8.01	1.17	1609.85	-0.03	0.07	0.03	16.17
17.	27.30	8.04	1.43	1032.27	27.30	8.07	1.40	1003.11	0.00	-0.03	0.03	29.16
18.	32.60	8.07	1.87	1122.04	32.64	8.10	1.84	1094.53	-0.04	-0.03	0.03	27.51
19.	17.70	8.30	1.26	1316.35	17.68	8.31	1.19	1241.63	0.02	-0.01	0.07	74.72
20.	11.90	8.19	1.02	1627.86	12.00	8.13	0.98	1573.96	-0.10	0.06	0.04	53.89
21.	22.00	8.12	1.47	1290.96	21.92	8.17	1.46	1271.16	0.08	-0.05	0.01	19.81
22.	18.60	8.21	1.30	1320.91	18.52	8.22	1.30	1323.39	0.08	-0.01	0.00	-2.48
23.	18.54	8.05	1.21	1282.96	18.56	8.01	1.20	1283.71	-0.02	0.04	0.01	-0.75
24.	25.88	8.21	1.68	1226.84	25.86	8.21	1.61	1176.63	0.02	0.00	0.07	50.21
25.	38.21	8.14	1.36	684.30	38.19	8.23	1.36	669.76	0.02	-0.09	0.00	14.53
26.	20.22	8.11	1.32	1264.39	20.24	8.13	1.30	1237.89	-0.02	-0.02	0.02	26.50
27.	21.12	8.01	1.50	1410.14	21.01	8.00	1.48	1402.12	0.11	0.01	0.02	8.02
28.	22.46	8.09	1.41	1221.92	22.43	8.10	1.37	1185.91	0.03	-0.01	0.04	36.01
29.	26.90	8.10	1.52	1097.11	26.82	8.14	1.50	1075.26	0.08	-0.04	0.02	21.85
30.	11.60	8.09	0.95	1594.04	11.62	8.12	0.95	1579.56	-0.02	-0.03	0.00	14.48
31.	18.96	8.20	1.38	1378.93	18.90	8.21	1.37	1369.94	0.06	-0.01	0.01	8.99
32.	31.49	8.16	1.61	978.15	31.47	8.11	1.60	984.72	0.02	0.05	0.01	-6.57
33.	13.50	8.11	0.89	1276.86	13.46	8.12	0.89	1277.51	0.04	-0.01	0.00	-0.64

$B_1T_1\_b$: Statistical analysis for T_1
Independent T-test of pellet dimension: *One sample (group) statistics*

Parameter	Storage	Observation, N	Mean	Standard deviation	Std. Error Mean
Length, mm	Before	33	22.6930	7.3563	1.2806
	After	33	22.6673	7.3479	1.2791
Diameter, mm	Before	33	8.2039	0.1540	0.0268
	After	33	8.2073	0.1619	0.0281
Weight, g	Before	33	1.3764	0.2467	0.0429
	After	33	1.3358	0.2259	0.0393
Density, kg/m³	Before (initial apparent)	33	1214.0236	229.7051	39.9865
	After (apparent)	33	1181.3788	229.2689	39.9106

Paired Samples Test for T_1

Parameter	Pair	Paired difference							
		T	df	Mean difference	Std. Deviation difference	Std. Error Mean	Sig. (2-tailed)	95% confidence interval of the difference	
								Lower	Upper
Length, mm	Before	0.85	32	0.02576	0.17367	0.03023	0.401	-0.035	0.0873
	After								
Diameter, mm	Before	-0.38	32	-0.00333	0.05029	0.00875	0.706	-0.021	0.01450
	After								
Weight, g	Before	5.21	32	0.04061	0.04472	0.00778	0.000	0.0247	0.05646
	After								
Density, kg/m³	Before (initial apparent)	6.24	32	32.6448	30.01638	5.22518	0.000	22.001	43.28819
	After (apparent)								

$B_1T_2\_a$: Raw data (before and after storage) for treatment T_2 pellet

Observation	Data measured before storage (1 day)				Data measured after storage (14 days storage)				Changed			
	Length, mm	Diameter, mm	Individual Weight, g	Innitial Apparent density, Kg/m³	Length, mm	Diameter, mm	Individual Weight, g	Apparent density, Kg/m³	Length, mm	Diameter, mm	Weight, g	Relax density, Kg/m³
1.	37.14	8.51	2.03	961.45	37.14	8.54	2.01	945.30	0.00	-0.03	0.02	16.15
2.	27.80	8.20	1.54	1049.49	27.81	8.19	1.51	1031.19	-0.01	0.01	0.03	18.30
3.	12.90	8.25	0.56	812.50	12.90	8.25	0.53	768.97	0.00	0.00	0.03	43.53
4.	8.10	8.16	0.35	826.67	8.06	8.18	0.35	826.72	0.04	-0.02	0.00	-0.05
5.	28.70	8.50	1.74	1068.96	28.70	8.51	1.68	1029.67	0.00	-0.01	0.06	39.28
6.	16.20	8.35	0.90	1015.04	16.19	8.37	0.84	943.43	0.01	-0.02	0.06	71.61
7.	25.55	8.30	1.44	1042.19	25.54	8.33	1.37	984.78	0.01	-0.03	0.07	57.41
8.	14.00	8.12	0.59	814.22	13.66	8.12	0.60	848.63	0.34	0.00	-0.01	-34.41
9.	25.88	8.34	1.40	990.75	25.87	8.44	1.38	953.96	0.01	-0.10	0.02	36.79
10.	37.85	8.16	1.90	960.37	37.84	8.22	1.89	941.67	0.01	-0.06	0.01	18.70
11.	38.68	8.08	1.85	933.24	38.68	8.09	1.85	930.93	0.00	-0.01	0.00	2.31
12.	17.30	8.76	0.83	796.44	17.30	8.82	0.79	747.78	0.00	-0.06	0.04	48.66
13.	35.30	8.20	2.00	1073.39	35.27	8.27	1.95	1029.79	0.03	-0.07	0.05	43.60
14.	26.18	8.30	1.38	974.73	26.18	8.32	1.37	963.02	0.00	-0.02	0.01	11.71
15.	20.65	8.40	1.20	1049.14	20.64	8.44	1.14	987.74	0.01	-0.04	0.06	61.40
16.	13.30	8.37	0.68	929.69	13.29	8.38	0.66	900.87	0.01	-0.01	0.02	28.82
17.	17.88	8.18	0.90	958.29	17.89	8.32	0.85	874.36	-0.01	-0.14	0.05	83.93
18.	14.67	8.37	0.80	991.61	14.67	8.42	0.76	930.87	0.00	-0.05	0.04	60.74
19.	15.33	8.30	0.78	940.86	15.32	8.30	0.70	844.92	0.01	0.00	0.08	95.95
20.	14.64	8.27	0.78	992.37	14.62	8.23	0.77	990.54	0.02	0.04	0.01	1.82
21.	8.10	8.12	0.40	954.10	8.10	8.18	0.38	893.15	0.00	-0.06	0.02	60.95
22.	26.78	8.39	1.73	1169.07	26.80	8.51	1.64	1076.42	-0.02	-0.12	0.09	92.66
23.	18.20	8.40	0.90	892.78	18.19	8.37	0.87	869.69	0.01	0.03	0.03	23.08
24.	26.54	8.21	1.45	1032.55	26.54	8.33	1.39	961.51	0.00	-0.12	0.06	71.04
25.	13.60	8.14	0.68	961.28	13.60	8.17	0.60	841.97	0.00	-0.03	0.08	119.31
26.	25.80	8.11	1.46	1096.03	25.80	8.42	1.38	961.09	0.00	-0.31	0.08	134.94
27.	36.61	8.20	1.74	900.43	35.94	8.22	1.85	970.47	0.67	-0.02	-0.11	-70.03
28.	35.61	8.09	1.52	830.82	35.61	8.09	1.78	972.93	0.00	0.00	-0.26	-142.11
29.	17.32	8.40	0.90	938.14	17.30	8.52	0.80	811.51	0.02	-0.12	0.10	126.63
30.	35.10	8.30	1.68	885.07	35.10	8.27	1.95	1034.78	0.00	0.03	-0.27	-149.71
31.	26.22	8.23	1.44	1032.91	26.18	8.23	1.34	962.64	0.04	0.00	0.10	70.26
32.	20.65	8.16	1.28	1185.88	20.64	8.19	1.13	1039.76	0.01	-0.03	0.15	146.12
33.	13.35	8.11	0.70	1015.56	13.29	8.16	0.68	978.89	0.06	-0.05	0.02	36.67

$B_1T_2\_b$: Statistical analysis for T_2
Independent T-test of pellet dimension: one sample (group) statistics

Parameter	Storage	Observation, N	Mean	Standard deviation	Std. Error Mean
Length, mm	Before	33	22.7858	9.19277	1.60026
	After	33	22.7473	9.17608	1.59735
Diameter, mm	Before	33	8.2721	0.14756	0.02569
	After	33	8.3152	0.15621	0.02719
Weight, g	Before	33	1.1979	0.49442	0.08607
	After	33	1.1755	0.51748	0.09008
Density, kg/m^3	Before (initial apparent)	33	972.0006	96.21828	16.74945
	After (apparent)	33	934.8470	80.87815	14.07908

Paired Samples Test for T_2

Parameter	Pair	Paired difference							
		T	df	Mean difference	Std. Deviation difference	Std. Error Mean	Sig. (2-tailed)	95% confidence interval of the difference	
								Lower	Upper
Length, mm	Before	1.725	32	0.03848	0.12816	.02231	0.094	-0.0069	0.08393
	After								
Diameter, mm	Before	-3.74	32	-0.0430	0.06593	.01148	0.001	-0.0664	-0.0196
	After								
Weight, g	Before	1.492	32	0.02242	0.08631	0.01503	0.145	-0.0081	0.05303
	After								
Density, kg/m^3	Before (initial apparent)	3.224	32	37.1535	66.2025	11.52438	0.003	13.6792	60.6279
	After (apparent)								

$B_1T_3\_a$: Raw data (before and after storage) for treatment T_3 pellet

Observation	Data measured before storage (1 day)				Data measured after storage (14 days storage)				Changed			
	Length, mm	Diameter, mm	Individual Weight, g	Innitial Apparent density, Kg/m³	Length, mm	Diameter, mm	Individual Weight, g	Apparent density, Kg/m³	Length, mm	Diameter, mm	Weight, g	Relax density, Kg/m³
1.	30.95	8.36	1.62	954.05	29.84	8.52	1.37	805.70	1.11	-0.16	0.25	148.35
2.	25.42	8.97	1.12	697.57	24.44	8.64	0.91	635.39	0.98	0.33	0.21	62.18
3.	38.75	8.69	1.96	853.25	37.83	8.56	1.76	808.83	0.92	0.13	0.20	44.41
4.	37.57	8.89	1.92	823.73	37.57	8.89	1.92	823.73	0.00	0.00	0.00	0.00
5.	24.07	8.80	1.05	717.59	22.38	8.40	0.83	669.56	1.69	0.40	0.22	48.03
6.	20.27	8.39	0.90	803.52	20.17	8.28	0.70	644.85	0.10	0.11	0.20	158.66
7.	24.78	8.90	1.10	713.91	24.82	8.24	0.86	650.09	-0.04	0.66	0.24	63.82
8.	27.50	8.69	1.20	736.10	17.45	8.21	0.62	671.49	10.05	0.48	0.58	64.61
9.	21.26	8.69	0.93	737.92	20.39	8.35	0.81	725.81	0.87	0.34	0.12	12.11
10.	19.41	8.93	0.93	765.39	19.41	8.93	0.93	765.39	0.00	0.00	0.00	0.00
11.	23.40	8.84	1.00	696.64	28.31	9.14	1.28	689.46	-4.91	-0.30	-0.28	7.18
12.	18.35	8.66	0.81	749.80	18.23	8.16	0.66	692.64	0.12	0.50	0.15	57.16
13.	23.95	8.92	1.88	1256.76	23.95	8.92	1.88	1256.76	0.00	0.00	0.00	0.00
14.	28.14	8.15	1.50	1022.31	28.00	8.16	1.42	970.24	0.14	-0.01	0.08	52.07
15.	28.02	8.30	1.96	1293.49	27.99	8.30	1.92	1268.45	0.03	0.00	0.04	25.04
16.	32.58	8.10	1.92	1144.22	32.51	8.20	1.92	1118.89	0.07	-0.10	0.00	25.33
17.	28.79	8.21	1.41	925.60	28.77	8.21	1.38	906.53	0.02	0.00	0.03	19.06
18.	39.73	8.06	2.62	1293.13	39.73	8.10	2.50	1221.75	0.00	-0.04	0.12	71.38
19.	19.95	8.11	1.23	1194.13	19.88	8.13	1.20	1163.36	0.07	-0.02	0.03	30.77
20.	22.76	8.08	1.80	1543.15	22.75	8.08	1.80	1543.83	0.01	0.00	0.00	-0.68
21.	24.13	8.11	1.51	1212.02	24.10	8.12	1.48	1186.49	0.03	-0.01	0.03	25.53
22.	33.51	8.12	2.00	1153.12	33.50	8.12	1.98	1141.93	0.01	0.00	0.02	11.19
23.	24.40	8.15	1.45	1139.71	24.50	8.15	1.40	1095.92	-0.10	0.00	0.05	43.79
24.	20.09	8.25	1.12	1043.42	20.00	8.24	1.10	1031.90	0.09	0.01	0.02	11.52
25.	27.19	8.28	2.01	1373.59	27.00	8.30	2.00	1369.75	0.19	-0.02	0.01	3.84
26.	26.64	8.10	1.72	1253.59	26.65	8.20	1.68	1194.30	-0.01	-0.10	0.04	59.28
27.	27.98	8.12	1.38	952.91	27.90	8.12	1.35	934.86	0.08	0.00	0.03	18.04
28.	37.93	8.16	2.60	1311.42	37.90	8.16	2.40	1211.50	0.03	0.00	0.20	99.92
29.	19.95	8.12	1.30	1258.98	19.81	8.15	1.28	1239.20	0.14	-0.03	0.02	19.78
30.	27.26	8.13	1.68	1187.77	27.26	8.13	1.68	1187.77	0.00	0.00	0.00	0.00
31.	21.43	8.11	1.56	1409.91	21.43	8.12	1.54	1388.41	0.00	-0.01	0.02	21.50
32.	35.33	8.12	1.86	1017.16	35.00	8.12	1.80	993.63	0.33	0.00	0.06	23.53
33.	26.00	8.15	1.54	1135.96	25.78	8.16	1.50	1113.16	0.22	-0.01	0.04	22.80

$B_1T_3\_b$: Statistical analysis for T_3
Independent T-test of pellet dimension: One sample (group) statistics

Parameter	Storage	Observation, N	Mean	Standard deviation	Std. Error Mean
Length, mm	Before	33	26.8936	6.01437	1.04697
	After	33	26.5227	6.19856	1.07903
Diameter, mm	Before	33	8.3836	0.32584	0.05672
	After	33	8.3185	0.28191	0.04908
Weight, g	Before	33	1.5330	0.46078	0.08021
	After	33	1.4503	0.49186	0.08562
Density, kg/m³	Before (initial apparent)	33	1041.5703	244.75067	42.60562
	After (apparent)	33	1003.6839	256.34404	44.62377

Paired Samples Test for T₃

Parameter	Pair	T	df	Mean difference	Std. Deviation difference	Std. Error Mean	Sig. (2-tailed)	95% confidence interval of the difference	
								Lower	Upper
Length, mm	Before	1.067	32	0.37091	1.99624	0.34750	0.294	-0.33693	1.07874
	After								
Diameter, mm	Before	1.837	32	.06515	0.20378	0.03547	0.076	-0.00711	0.13741
	After								
Weight, g	Before	3.484	32	0.08273	0.13641	0.02375	0.001	0.03436	0.13110
	After								
Density, kg/m³	Before (initial apparent)	5.581	32	37.88636	38.99351	6.78790	0.000	24.05987	51.71286
	After (apparent)								

$B_1T_4\_a$: Raw data (before and after storage) for treatment T₄ pellet

Observation	Data measured before storage (1 day)				Data measured after storage (14 days storage)				Changed			
	Length, mm	Diameter, mm	Individual Weight, g	Initial Apparent density, Kg/m³	Length, mm	Diameter, mm	Individual Weight, g	Apparent density, Kg/m³	Length, mm	Diameter, mm	Weight, g	Relax density, Kg/m³
1.	38.93	8.13	2.52	1247.57	38.33	8.11	2.37	1197.56	0.60	0.02	0.15	50.01
2.	41.27	8.07	2.28	1080.65	40.01	7.94	2.05	1035.32	1.26	0.13	0.23	45.33
3.	39.55	8.17	2.50	1206.37	39.55	8.17	2.50	1206.37	0.00	0.00	0.00	0.00
4.	35.33	8.02	2.17	1216.46	34.90	7.91	2.01	1172.59	0.43	0.11	0.16	43.86
5.	36.92	8.10	2.26	1188.52	35.97	8.06	2.16	1177.53	0.95	0.04	0.10	10.99
6.	39.48	8.33	2.62	1218.33	39.21	8.22	2.49	1197.26	0.27	0.11	0.13	21.07
7.	32.80	8.20	2.01	1160.98	32.92	8.15	1.94	1130.20	-0.12	0.05	0.07	30.78
8.	38.14	8.24	2.31	1136.34	38.24	8.14	2.16	1085.97	-0.10	0.10	0.15	50.37
9.	41.39	8.30	2.83	1264.34	41.15	8.24	2.63	1199.12	0.24	0.06	0.20	65.23
10.	41.22	8.08	2.48	1173.95	40.30	7.93	2.27	1141.05	0.92	0.15	0.21	32.90
11.	35.55	8.11	2.15	1171.35	34.86	7.94	1.93	1118.71	0.69	0.17	0.22	52.64
12.	29.96	8.15	1.89	1209.86	29.96	8.15	1.89	1209.86	0.00	0.00	0.00	0.00
13.	33.30	8.09	1.97	1151.48	32.64	7.98	1.83	1121.57	0.66	0.11	0.14	29.91
14.	40.93	8.12	2.60	1227.30	40.67	8.01	2.46	1200.95	0.26	0.11	0.14	26.34
15.	32.28	8.11	1.97	1182.01	32.41	8.01	1.81	1108.83	-0.13	0.10	0.16	73.18
16.	30.39	8.14	1.85	1170.37	30.16	8.08	1.77	1145.12	0.23	0.06	0.08	25.25
17.	38.39	8.23	1.52	744.66	37.94	8.12	1.40	712.93	0.45	0.11	0.12	31.72
18.	39.55	8.17	2.50	1206.37	38.75	8.06	2.32	1174.02	0.80	0.11	0.18	32.35
19.	37.13	8.23	1.44	729.40	35.66	8.30	1.35	700.05	1.47	-0.07	0.09	29.36
20.	33.35	8.02	2.20	1306.50	33.35	8.02	2.17	1288.68	0.00	0.00	0.03	17.82
21.	32.70	8.20	2.27	1315.17	32.50	8.20	2.26	1317.43	0.20	0.00	0.01	-2.26
22.	40.40	8.30	2.53	1158.01	39.48	8.33	2.50	1162.53	0.92	-0.03	0.03	-4.51
23.	38.20	8.20	2.43	1205.16	38.00	8.20	2.39	1191.56	0.20	0.00	0.04	13.60
24.	31.80	8.24	2.36	1392.39	31.70	8.24	2.31	1367.19	0.10	0.00	0.05	25.20
25.	40.40	8.30	2.78	1272.44	40.30	8.30	2.75	1261.83	0.10	0.00	0.03	10.61
26.	40.00	8.20	2.50	1184.08	40.00	8.22	2.48	1168.90	0.00	-0.02	0.02	15.18
27.	35.00	8.11	2.10	1162.09	35.10	8.11	2.10	1158.78	-0.10	0.00	0.00	3.31
28.	33.37	8.15	2.00	1149.45	33.36	8.15	1.98	1138.29	0.01	0.00	0.02	11.15
29.	33.30	8.18	1.98	1132.00	33.30	8.18	1.97	1126.28	0.00	0.00	0.01	5.72
30.	30.40	8.12	2.10	1334.64	30.00	8.15	2.00	1278.57	0.40	-0.03	0.10	56.07
31.	28.90	8.11	2.00	1340.36	28.80	8.18	1.97	1302.26	0.10	-0.07	0.03	38.10
32.	21.40	8.14	1.70	1527.27	21.10	8.14	1.70	1548.99	0.30	0.00	0.00	-21.71
33.	40.38	8.20	2.30	1079.11	39.39	8.23	2.20	1050.43	0.99	-0.03	0.10	28.68

$B_1T_4\_b$: Statistical analysis for T_4 pellet
Independent T-test of pellet dimension: *One sample (group) statistics*

Parameter	Storage	Observation, N	Mean	Standard deviation	Std. Error Mean
Length, mm	Before	33	35.8215	4.64371	0.80837
	After	33	35.4548	4.50495	0.78421
Diameter, mm	Before	33	8.1655	0.07811	0.01360
	After	33	8.1264	0.11224	0.01954
Weight, g	Before	33	2.2158	0.33256	0.05789
	After	33	2.1248	0.32601	0.05675
Density, kg/m³	Before (initial apparent)	33	1189.2418	147.37236	25.65424
	After (apparent)	33	1163.5373	152.63906	26.57105

Paired samples test for T_4

Parameter	Pair	Paired difference							
		T	df	Mean difference	Std. Deviation difference	Std. Error Mean	Sig. (2-tailed)	95% confidence interval of the difference	
								Lower	Upper
Length, mm	Before	4.927	32	0.36667	0.42752	0.07442	0.000	0.21507	0.51826
	After								
Diameter, mm	Before	3.456	32	0.03909	0.06497	0.01131	0.002	0.01605	0.06213
	After								
Weight, g	Before	7.168	32	0.09091	0.07286	0.01268	0.000	0.06507	0.11674
	After								
Density, kg/m³	Before (initial apparent)	6.845	32	25.70447	21.57357	3.75548	0.000	18.05481	33.35412
	After (apparent)								

$B_1T_5\_a$: Raw data (before and after storage) for treatment T_5 pellet

Observation	Data measured before storage (1 day)				Data measured after storage (14 days storage)				Changed			
	Length, mm	Diameter, mm	Individual Weight, g	Innitial Apparent density, Kg/m³	Length, mm	Diameter, mm	Individual Weight, g	Apparent density, Kg/m³	Length, mm	Diameter, mm	Weight, g	Relax density, Kg/m³
1.	35.82	8.50	1.62	797.41	35.53	8.48	1.66	827.66	0.29	0.02	-0.04	-30.25
2.	38.59	8.29	1.18	566.80	38.07	8.07	1.22	626.85	0.52	0.22	-0.04	-60.05
3.	37.76	7.97	1.18	626.71	37.52	7.98	1.10	586.48	0.24	-0.01	0.08	40.22
4.	41.63	8.16	1.80	827.21	41.32	8.14	1.80	837.52	0.31	0.02	0.00	-10.31
5.	41.32	8.09	1.57	739.56	41.33	8.12	1.64	766.65	-0.01	-0.03	-0.07	-27.09
6.	38.83	8.13	1.18	585.68	39.00	8.04	1.20	606.37	-0.17	0.09	-0.02	-20.68
7.	38.43	8.25	1.19	579.56	38.36	8.23	1.18	578.54	0.07	0.02	0.01	1.02
8.	36.89	8.05	1.19	634.13	36.88	8.03	1.21	648.18	0.01	0.02	-0.02	-14.05
9.	39.83	8.36	1.16	530.84	39.41	8.06	1.36	676.69	0.42	0.30	-0.20	-145.85
10.	41.14	8.22	1.64	751.56	39.79	8.04	1.23	609.19	1.35	0.18	0.41	142.38
11.	37.76	8.19	1.40	704.14	37.29	8.32	1.51	745.19	0.47	-0.13	-0.11	-41.05
12.	38.30	7.91	1.26	669.81	39.10	7.99	1.35	688.96	-0.80	-0.08	-0.09	-19.15
13.	34.19	8.04	1.43	824.24	33.86	8.04	1.51	878.84	0.33	0.00	-0.08	-54.59
14.	41.59	8.20	1.46	665.07	40.85	8.08	1.52	726.04	0.74	0.12	-0.06	-60.97
15.	37.35	8.18	1.17	596.37	37.08	8.10	1.20	628.35	0.27	0.08	-0.03	-31.98
16.	40.92	8.04	1.35	650.15	41.29	8.23	1.67	760.68	-0.37	-0.19	-0.32	-110.53
17.	35.33	8.01	1.22	685.62	36.02	7.97	1.28	712.66	-0.69	0.04	-0.06	-27.04
18.	34.86	8.24	1.18	635.08	41.52	8.04	1.35	640.76	-6.66	0.20	-0.17	-5.68
19.	37.69	8.03	1.19	623.76	37.00	8.09	1.25	657.57	0.69	-0.06	-0.06	-33.81
20.	37.58	8.19	1.19	601.39	38.20	8.07	1.24	634.95	-0.62	0.12	-0.05	-33.57
21.	35.98	8.22	1.24	649.75	35.84	8.11	1.30	702.53	0.14	0.11	-0.06	-52.78
22.	41.62	8.03	1.47	697.77	42.17	8.17	1.59	719.58	-0.55	-0.14	-0.12	-21.81
23.	34.65	8.05	1.42	805.61	33.65	8.08	1.45	840.80	1.00	-0.03	-0.03	-35.19
24.	37.72	8.10	1.10	566.21	37.67	8.16	1.14	578.97	0.05	-0.06	-0.04	-12.76
25.	30.78	8.18	1.32	816.45	29.80	8.20	1.37	870.98	0.98	-0.02	-0.05	-54.53
26.	30.25	8.08	1.48	954.65	30.07	8.09	1.55	1003.30	0.18	-0.01	-0.07	-48.65
27.	29.55	8.06	1.18	783.04	28.74	8.06	1.28	873.34	0.81	0.00	-0.10	-90.30
28.	33.76	8.14	1.21	689.07	34.23	8.13	1.28	720.70	-0.47	0.01	-0.07	-31.62
29.	42.41	8.08	1.33	611.91	42.13	8.05	1.35	629.91	0.28	0.03	-0.02	-18.00
30.	41.02	8.15	1.59	743.39	41.25	8.09	1.65	778.56	-0.23	0.06	-0.06	-35.17
31.	41.47	8.24	1.27	574.57	41.38	8.01	1.27	609.37	0.09	0.23	0.00	-34.79
32.	30.93	8.00	1.09	701.45	31.58	8.04	1.15	717.64	-0.65	-0.04	-0.06	-16.19
33.	37.70	7.99	1.23	651.03	37.64	8.05	1.26	658.05	0.06	-0.06	-0.03	-7.02

$B_1T_5\_b$: Statistical Analysis for T_5 pellet
Independent T-test of pellet dimension: *One sample (group) statistics*

Parameter	Storage	Observation, N	Mean	Standard deviation	Std. Error Mean
Length, mm	Before	33	37..3833	3.56469	0.62053
	After	33	37.4415	3.67971	0.64056
Diameter, mm	Before	33	8.1324	0.12181	0.02120
	After	33	8.1018	0.10209	0.01777
Weight, g	Before	33	1.3179	0.17792	0.03097
	After	33	1.3673	0.18360	0.03196
Density, kg/m³	Before (initial apparent)	33	683.0300	96.75693	16.84322
	After (apparent)	33	713.3897	104.31948	18.15969

Paired samples test for T_5

Parameter	Pair	Paired difference							
		t	df	Mean difference	Std. Deviation difference	Std. Error Mean	Sig. (2-tailed)	95% confidence interval of the difference	
								Lower	Upper
Length, mm	Before	-0.258	32	-0.05818	1.29432	0.2253	0.798	-0.51713	0.40077
	After								
Diameter, mm	Before	1.593	32	0.03061	0.11037	0.0192	0.121	-0.00853	0.06974
	After								
Weight, g	Before	-2.652	32	-0.04939	0.10700	0.0186	0.012	-0.08734	-0.01145
	After								
Density, kg/m³	Before (initial apparent)	-3.840	32	-30.3597	45.41294	7.9053	0.001	-46.46243	-14.2569
	After (apparent)								

Table B2: Durability measured from a single drop test

Observation	T₁			T₂			T₃			T₄			T₅		
	Pallet initial weight, g	Pellet weight after dropped, g	Durability as Single Drop Test, (%)	Pallet initial weight, g	Pellet weight after dropped, g	Durability as Single Drop Test, (%)	Pallet initial weight, g	Pellet weight after dropped, g	Durability as Single Drop Test, (%)	Pallet initial weight, g	Pellet weight after dropped, g	Durability as Single Drop Test, (%)	Pallet initial weight, g	Pellet weight after dropped, g	Durability as Single Drop Test, (%)
1	0.85	0.69	81.18	0.96	0.95	98.96	1.50	1.47	98.00	2.40	2.33	97.08	2.63	2.57	97.72
2	1.02	0.8	78.43	0.92	0.9	97.83	1.96	1.94	98.98	2.08	1.51	72.60	2.47	1.36	55.06
3	1.04	0.57	54.81	1.21	0.93	76.86	1.92	1.72	89.58	2.07	1.97	95.17	1.88	1.24	65.96
4	1.1	0.94	85.45	1.22	1.22	100.00	1.41	0.78	55.32	2.17	2.08	95.85	2.31	1.98	85.71
5	0.87	0.85	97.70	1.21	1.21	100.00	2.62	2.6	99.24	2.48	2.06	83.06	1.77	1.64	92.66
6	0.65	0.63	96.92	1.37	1.36	99.27	1.23	1.21	98.37	1.98	1.17	59.09	2.24	2.15	95.98
7	0.78	0.77	98.72	2.5	1.44	57.60	1.80	1.3	72.22	2.15	1.47	68.37	2.14	2.09	97.66
8	0.6	0.55	91.67	1.37	0.61	44.53	1.51	0.71	47.02	1.44	1.2	83.33	1.36	1.31	96.32
9	1.09	0.72	66.06	0.89	0.61	68.54	2.00	1.88	94.00	2.24	2.2	98.21	1.89	1.79	94.71
10	0.79	0.49	62.03	0.7	0.69	98.57	1.45	1.36	93.79	2.00	1.83	91.50	1.84	1.49	80.98
11	0.94	0.94	100.00	1.41	1.41	100.00	1.12	0.73	65.18	1.86	1.8	96.77	1.96	1.2	61.22
12	0.7	0.69	98.57	2.12	2.12	100.00	2.01	1.25	62.19	2.50	2.4	96.00	1.33	0.85	63.91
13	0.82	0.62	75.61	1.14	1.14	100.00	1.72	1.35	78.49	1.89	1.73	91.53	1.98	1.89	95.45
14	1.05	0.81	77.14	1.38	0.93	67.39	1.92	1.4	72.92	1.79	1.72	96.09	1.88	1.08	57.45
15	0.94	0.79	84.04	2.15	1.97	91.63	2.08	1.82	87.50	1.33	0.56	42.11	1.92	1.86	96.88

One way ANOVA Test and PostHoc Test for durability-single drop method

		Descriptives							
		Observation N	Mean	Std. Deviation	Std. Error	95% Confidence Interval for Mean		Minimum	Maximum
						Lower Bound	Upper Bound		
Weight, g	T1	15	.8827	.16038	.04141	.7939	.9715	.60	1.10
	T2	15	1.3700	.50892	.13140	1.0882	1.6518	.70	2.50
	T3	15	1.7500	.38676	.09986	1.5358	1.9642	1.12	2.62
	T4	15	2.0253	.33698	.08701	1.8387	2.2119	1.33	2.50
	T5	15	1.9733	.35524	.09172	1.7766	2.1701	1.33	2.63
	Total	75	1.6003	.55860	.06450	1.4717	1.7288	.60	2.63
Durability, %	T1	15	83.2220	14.40348	3.71896	75.2456	91.1984	54.81	100.00
	T2	15	86.7453	18.72053	4.83362	76.3782	97.1124	44.53	100.00
	T3	15	80.8533	17.44724	4.50486	71.1914	90.5153	47.02	99.24
	T4	15	84.4507	16.80182	4.33821	75.1461	93.7552	42.11	98.21
	T5	15	82.5113	16.74609	4.32382	73.2377	91.7850	55.06	97.72
	Total	75	83.5565	16.53947	1.90981	79.7511	87.3619	42.11	100.00

ANOVA						
		Sum of Squares	df	Mean Square	F	Sig.
Weight, g	Between Groups	13.654	4	3.413	25.320	.000
	Within Groups	9.437	70	.135		
	Total	23.091	74			
Durability, %	Between Groups	292.193	4	73.048	.256	.905
	Within Groups	19950.806	70	285.012		
	Total	20242.999	74			

Table B3: Tensile strength

Treatment	Observation	Thickness, mm	Diameter, mm	Minimum fracture load, N	Tensile strength (KPa/m^3)
T_1	1	8.41	2.89	15.12	0.40
	2	8.22	3.21	7.06	0.17
	3	8.37	1.57	11.50	0.56
	4	8.20	4.18	12.00	0.22
	5	8.32	2.92	20.91	0.55
	6	8.16	3.63	21.75	0.47
	7	8.21	2.52	5.74	0.18
	8	8.53	2.67	7.43	0.21
	9	8.52	2.91	14.32	0.37
	10	8.17	3.04	17.90	0.46
T_2	1	8.21	4.90	22.65	0.36
	2	8.24	2.77	19.16	0.53
	3	8.40	4.81	29.77	0.47
	4	8.27	2.17	19.84	0.70
	5	8.56	2.99	18.32	0.46
	6	8.26	2.97	28.08	0.73
	7	8.09	2.86	18.00	0.50
	8	8.24	3.52	19.95	0.44
	9	8.52	3.25	18.36	0.42
	10	8.47	2.77	22.31	0.61
T_3	1	8.18	3.30	44.21	1.04
	2	8.23	3.10	34.87	0.87
	3	8.15	2.84	49.43	1.36
	4	8.41	1.93	28.64	1.12
	5	8.17	2.31	41.00	1.38
	6	8.24	2.18	39.60	1.40
	7	8.10	2.54	39.80	1.23
	8	8.13	1.95	29.15	1.17
	9	8.15	1.90	38.69	1.59
	10	8.20	2.06	26.86	1.01
T_4	1	8.18	2.28	41.90	1.43
	2	8.16	3.14	32.50	0.81
	3	8.23	2.58	29.30	0.88
	4	8.20	2.15	41.80	1.51
	5	8.31	2.16	43.00	1.53
	6	8.21	2.82	35.60	0.98
	7	8.11	2.32	43.20	1.46
	8	8.16	1.93	26.20	1.06
	9	8.08	1.95	27.11	1.10
	10	8.05	2.17	31.98	1.17
T_5	1	8.13	2.08	35.68	1.34
	2	7.96	1.98	22.3	0.90
	3	8.28	2.72	48.24	1.36
	4	8.34	2.39	32.33	1.03
	5	7.99	2.71	27.42	0.81
	6	8.11	2.14	38.3	1.41
	7	8.03	2.05	29.47	1.14
	8	8.13	3.06	38.84	0.99
	9	8.11	2.78	37.65	1.06
	10	8.1	1.88	21.33	0.89

One way ANOVA Test and PostHoc Test for Tensile Strength

Descriptive								
Treatment	N	Mean	Std. Deviation	Std. Error	95% Confidence Interval for Mean		Minimum	Maximum
					Lower Bound	Upper Bound		
T_1	10	.3590	.15293	.04836	.2496	.4684	.17	.56
T_5	10	.5220	.12164	.03846	.4350	.6090	.36	.73
T_3	10	1.2170	.21756	.06880	1.0614	1.3726	.87	1.59
T_4	10	1.1930	.27047	.08553	.9995	1.3865	.81	1.53
T_2	10	1.0930	.21323	.06743	.9405	1.2455	.81	1.41
Total	50	.8768	.41409	.05856	.7591	.9945	.17	1.59

ANOVA					
	Sum of Squares	df	Mean Square	F	Sig.
Between Groups	6.565	4	1.641	40.196	.000
Within Groups	1.837	45	.041		
Total	8.402	49			

Table B4: Fineness test

Small particles

Treatment	Observation	Initial weight, g	Final weight, g	Amount of dust, g	Dust percentage, %	Average, (%)
T1	1	225.00	116.98	108.02	48.01	44.32
	2	225.00	131.60	93.40	41.51	
	3	225.00	127.29	97.71	43.43	
T2	1	225.00	148.37	76.63	34.06	34.96
	2	225.00	152.90	72.10	32.04	
	3	225.00	137.77	87.23	38.77	
T3	1	225.00	201.88	23.12	10.28	9.76
	2	225.00	207.39	17.61	7.83	
	3	225.00	199.87	25.13	11.17	
T4	1	225.00	178.20	46.80	20.80	17.03
	2	225.00	185.34	39.66	17.63	
	3	225.00	196.52	28.48	12.66	
T5	1	225.00	213.60	11.40	5.07	7.52
	2	225.00	207.68	17.32	7.70	
	3	225.00	202.97	22.03	9.79	

One-way ANOVA Test and PostHoc Test for small particles

		Observation N	Mean	Std. Deviation	Std. Error	95% Confidence Interval for Mean		Minimum	Maximum
						Lower Bound	Upper Bound		
Fines	T1	3	44.3167	3.33948	1.92805	36.0209	52.6124	41.51	48.01
	T2	3	34.9567	3.45344	1.99384	26.3779	43.5355	32.04	38.77
	T3	3	9.7600	1.72965	.99862	5.4633	14.0567	7.83	11.17
	T4	3	17.0300	4.10304	2.36889	6.8375	27.2225	12.66	20.80
	T5	3	7.5200	2.36514	1.36552	1.6447	13.3953	5.07	9.79
	Total	15	22.7167	15.21181	3.92767	14.2926	31.1407	5.07	48.01
Lumps	T1	3	30.8767	1.49948	.86572	27.1518	34.6016	29.87	32.60
	T2	3	26.7500	3.69187	2.13150	17.5789	35.9211	23.77	30.88
	T3	3	6.8900	1.44696	.83540	3.2955	10.4845	5.32	8.17
	T4	3	14.3933	2.33024	1.34537	8.6047	20.1820	12.65	17.04
	T5	3	4.5167	2.39174	1.38087	-1.4248	10.4581	2.00	6.76
	Total	15	16.6853	11.06524	2.85703	10.5576	22.8131	2.00	32.60
Fines	T1	3	8.5800	2.56988	1.48372	2.1961	14.9639	6.37	11.40
	T2	3	5.4600	.48042	.27737	4.2666	6.6534	5.08	6.00
	T3	3	1.9233	.08327	.04807	1.7165	2.1302	1.83	1.99
	T4	3	1.9733	.30665	.17704	1.2116	2.7351	1.71	2.31
	T5	3	1.9333	.04726	.02728	1.8159	2.0507	1.88	1.97
	Total	15	3.9740	2.94307	.75990	2.3442	5.6038	1.71	11.40
Dust	T1	3	4.8600	.73627	.42509	3.0310	6.6890	4.01	5.30
	T2	3	2.7467	2.16602	1.25055	-2.6340	8.1274	1.14	5.21
	T3	3	.9467	.24132	.13932	.3472	1.5461	.68	1.15
	T4	3	.6300	.62522	.36097	-.9231	2.1831	.08	1.31
	T5	3	1.0700	.11358	.06557	.7879	1.3521	.94	1.15
	Total	15	2.0507	1.87309	.48363	1.0134	3.0879	.08	5.30

Table B5: Wettability index

Treatment	Observation	Weight before submerged, g	Final weight after submerged, g	Wetted index, %	Mean	Std. Deviation
T$_1$	1	20.00	37.46	87.30	78.64	8.03
	2	20.00	36.91	84.55		
	3	20.13	34.07	69.25		
	4	22.26	38.11	71.20		
	5	19.89	35.98	80.89		
T$_2$	1	29.91	62.09	107.59	115.68	10.19
	2	30.20	61.00	101.99		
	3	24.30	54.30	123.46		
	4	27.08	60.70	124.15		
	5	21.69	47.98	121.21		
T$_3$	1	28.85	35.31	22.39	26.29	4.82
	2	20.36	24.31	19.40		
	3	25.61	32.55	27.10		
	4	24.31	29.77	22.46		
	5	25.08	31.44	25.36		
T$_4$	1	30.53	37.01	28.94	24.07	6.36
	2	21.36	26.49	26.44		
	3	27.38	33.64	23.10		
	4	22.66	27.61	22.04		
	5	27.32	35.24	31.23		
T$_5$	1	22.92	26.81	16.97	28.17	7.13
	2	20.31	23.53	15.85		
	3	22.55	26.34	16.81		
	4	25.71	30.06	16.92		
	5	21.56	25.34	17.53		